METABOLOMICS IN CROP RESEARCH – CURRENT AND EMERGING METHODOLOGIES

EDITED BY: Marta Sousa Silva, Andreia Figueiredo, Ute Roessner and Carlos Cordeiro

PUBLISHED IN: Frontiers in Plant Science

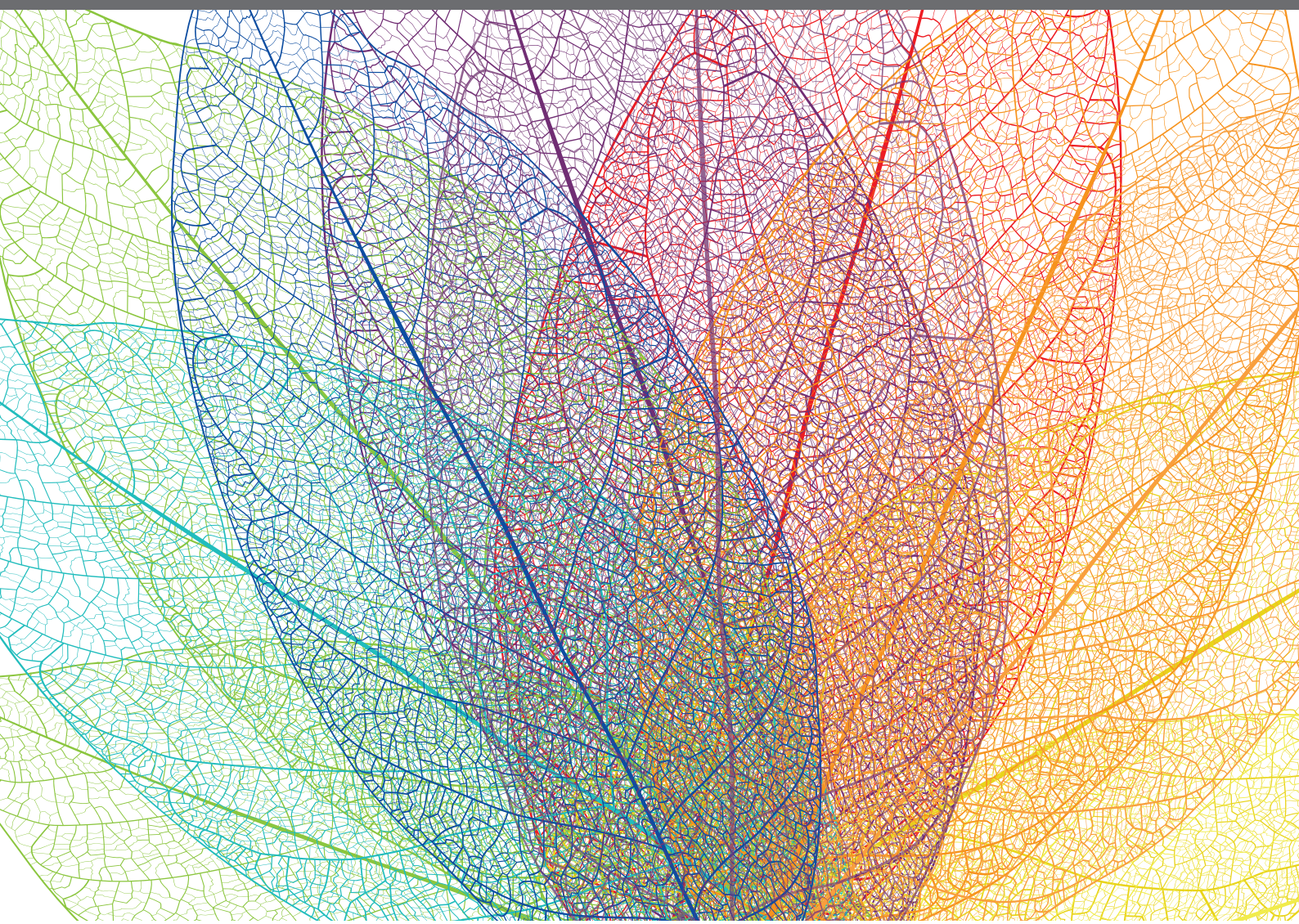

frontiers Research Topics

frontiers

ISSN 1664-8714
ISBN 978-2-88963-158-2
DOI 10.3389/978-2-88963-158-2

About Frontiers

Frontiers is more than just an open-access publisher of scholarly articles: it is a pioneering approach to the world of academia, radically improving the way scholarly research is managed. The grand vision of Frontiers is a world where all people have an equal opportunity to seek, share and generate knowledge. Frontiers provides immediate and permanent online open access to all its publications, but this alone is not enough to realize our grand goals.

Frontiers Journal Series

The Frontiers Journal Series is a multi-tier and interdisciplinary set of open-access, online journals, promising a paradigm shift from the current review, selection and dissemination processes in academic publishing. All Frontiers journals are driven by researchers for researchers; therefore, they constitute a service to the scholarly community. At the same time, the Frontiers Journal Series operates on a revolutionary invention, the tiered publishing system, initially addressing specific communities of scholars, and gradually climbing up to broader public understanding, thus serving the interests of the lay society, too.

Dedication to Quality

Each Frontiers article is a landmark of the highest quality, thanks to genuinely collaborative interactions between authors and review editors, who include some of the world's best academicians. Research must be certified by peers before entering a stream of knowledge that may eventually reach the public - and shape society; therefore, Frontiers only applies the most rigorous and unbiased reviews.
Frontiers revolutionizes research publishing by freely delivering the most outstanding research, evaluated with no bias from both the academic and social point of view. By applying the most advanced information technologies, Frontiers is catapulting scholarly publishing into a new generation.

What are Frontiers Research Topics?

Frontiers Research Topics are very popular trademarks of the Frontiers Journals Series: they are collections of at least ten articles, all centered on a particular subject. With their unique mix of varied contributions from Original Research to Review Articles, Frontiers Research Topics unify the most influential researchers, the latest key findings and historical advances in a hot research area! Find out more on how to host your own Frontiers Research Topic or contribute to one as an author by contacting the Frontiers Editorial Office: researchtopics@frontiersin.org

METABOLOMICS IN CROP RESEARCH – CURRENT AND EMERGING METHODOLOGIES

Topic Editors:
Marta Sousa Silva, Faculdade de Ciências da Universidade de Lisboa, Portugal
Andreia Figueiredo, Faculdade de Ciências da Universidade de Lisboa, Portugal
Ute Roessner, The University of Melbourne, Australia
Carlos Cordeiro, Faculdade de Ciências da Universidade de Lisboa, Portugal

Image created by Marta Sousa Silva

The plant metabolome is highly complex, being composed of over 200,000 metabolites. The characterization of these small molecules has been crucial to study plant growth and development as well as their response to environmental changes. The potential of metabolomics in plant research, particularly if applied to crop plants, is also extremely valuable in the discovery of biomarkers and in the improvement of crop yield and quality. This Frontiers Research Topic addresses many applications of metabolomics to crop research, based on different analytical platforms, including mass spectrometry, and nuclear magnetic resonance. It comprises 13 articles from

109 authors that show the importance and the contribution of metabolomics in the analysis of crop's traceability and genetic variation, in the study of fruit development, and in the understanding of the plant's response to the environment and to different biotic and abiotic stresses.

Citation: Sousa Silva, M., Figueiredo, A., Roessner, U., Cordeiro, C., eds. (2019). Metabolomics in Crop Research – Current and Emerging Methodologies. Lausanne: Frontiers Media SA. doi: 10.3389/978-2-88963-158-2

Table of Contents

METABOLOMICS IN THE STUDY OF BIOTIC STRESSES

frontiers in Plant Science

EDITORIAL
published: 02 August 2019
doi: 10.3389/fpls.2019.01013

Editorial: Metabolomics in Crop Research—Current and Emerging Methodologies

Marta Sousa Silva[1,2]*, *Carlos Cordeiro*[1,2], *Ute Roessner*[3] and *Andreia Figueiredo*[4]*

[1] Laboratório de FTICR e Espectrometria de Massa Estrutural, Faculdade de Ciências, Universidade de Lisboa, Lisbon, Portugal, [2] Centro de Química e Bioquímica, Faculdade de Ciências, Universidade de Lisboa, Lisbon, Portugal, [3] School of BioSciences, The University of Melbourne, Melbourne, VIC, Australia, [4] Biosystems and Integrative Sciences Institute, Faculdade de Ciências, Universidade de Lisboa, Lisbon, Portugal

Keywords: metabolomics, mass spectrometry, nuclear magnetic resonance, metabolic profiling, crop development

Editorial on the Research Topic

Metabolomics in Crop Research—Current and Emerging Methodologies

The plant metabolome is highly complex, being composed of over 200,000 metabolites (Fiehn, 2002). The characterization of these small molecules has been crucial to study plant growth and development as well as their response to environmental changes. The potential of metabolomics in plant research, particularly if applied to crop plants, is immense. Besides the aforementioned applications, it is extremely valuable in the discovery of biomarkers and in the improvement of crop yield and quality (Alseekh et al., 2018). This Frontiers Research Topic addresses many applications of metabolomics to crop research, based on different analytical platforms, including mass spectrometry, and nuclear magnetic resonance (NMR). It comprises 13 articles from 109 authors that show the importance and the contribution of metabolomics in the analysis of crop's traceability and genetic variation, in the study of fruit development, and in the understanding of the plant's response to the environment and to different biotic and abiotic stresses.

Numerous agricultural and food products are recognized by their qualities that result mainly from their geographical origin (Vandecandelaere et al., 2009). An unequivocal traceability of a crop guarantees, not only its origin, but also its quality and safety. Busconi et al. followed a targeted metabolomics approach to specifically analyse the phenolic profile of *Vanilla* × *tahitensis* and its relation to plant traceability. The phenolic compound profile of different *Vanilla* × *tahitensis* clearly discriminated the Papua New Guinea samples from the Tahitian ones from French Polynesia. Additionally, it was possible to separate the *Vanilla* cultivars that comprised the two Tahitian samples: one exclusively from "Haapape" cultivar and the other from a mixture of both "Haapape" and "Tahiti" cultivars. Within the same region, latitude, and altitude also influence the metabolic composition of a plant. Demasi et al. analyzed different populations of *Lavandula angustifolia* (lavender) grown in nine peripheral alpine regions for future selection of higher quality flowers and essential oils. A targeted strategy based on the analysis of volatile compounds and essential oils revealed that latitude significatively influenced phytochemical composition, while altitude didn't affect the phytochemical profile of *L. angustifolia*. These results can be explored for the future ranking of lavender cultivation sites, thus promoting quality and value linked to geographical origin.

OPEN ACCESS

Edited and reviewed by:
Kazuki Saito,
RIKEN Center for Sustainable Resource Science (CSRS), Japan

***Correspondence:**
Marta Sousa Silva
mfsilva@fc.ul.pt
Andreia Figueiredo
aafigueiredo@fc.ul.pt

Specialty section:
This article was submitted to Plant Metabolism and Chemodiversity, a section of the journal Frontiers in Plant Science

Received: *17 July 2019*
Accepted: *19 July 2019*
Published: *02 August 2019*

Citation:
Sousa Silva M, Cordeiro C, Roessner U and Figueiredo A (2019) Editorial: Metabolomics in Crop Research—Current and Emerging Methodologies. Front. Plant Sci. 10:1013. doi: 10.3389/fpls.2019.01013

In the search for quality traits within crops, untargeted metabolomics approaches have been also very useful. Ellis et al. performed untargeted metabolic profiling of *Pisum sativum* (pea) mature seeds from genetically marked lines to identify which genotypes were enriched in specific compounds related to end-use quality traits. Indeed, there were sets of compounds in mature seeds associated with their genetic variation, and this information can be used to assist future breeding programmes. Seed quality can be compromised by the occurrence of pests and diseases in the crop. *Pisum sativum* plants can be affected by the pea aphid *Acyrthosiphon pisum*, a phloem-feeding insect comprised of different biotypes (or host races), each specialized on a specific crop legume species, including *Medicago sativa* (alfalfa) and *Trifolium pratense* (red clover), besides *P. sativum* (Peccoud et al., 2009). Interestingly, all the host races of this insect can develop on *Vicia faba* (faba bean). Sanchez-Arcos et al. studied these four plant-herbivorous insect systems using an untargeted metabolomics strategy to identify the metabolites involved in the specificity of pea aphid interaction with the different host plants. All these crop legumes are also affected by other pathogens, including the *Aphanomyces euteiches*, a soil-borne oomycete that causes Aphanomyces root rot (ARR) (Gaulin et al., 2007). Bazghaleh et al. followed a targeted metabolomics approach focused on polyphenolic profiling, to study the resistance of several lentil genotypes (*Lens* sp.) to *A. euteiches* infection. Several differences were found within the root polyphenolic profiles from the wild and the different cultivars of lentils, and between healthy and infected roots. The observed relationship between polyphenol composition and tolerance to *A. euteiches* will be valuable for future selection of resistant plants. Similar results were obtained by Bernardi et al. while studying the susceptibility of *Zea mays* (maize) cultivars to the fungus *Fusarium verticillioides*. Again, a targeted strategy was chosen, focusing on the screening of phenolic compounds from pigmented and non-pigmented maize cultivars. The maize cultivar with highest phenolic content showed highest resistance to *Fusarium* infection, a promising result toward the selection of more resilient maize plants.

Studying another plant-pathogen system, Chitarrini et al.'s work also showed a great potential for future application for the development of resistant varieties. Using different analytical methods, they identified biomarkers in a resistant grapevine associated with the defense against the biotrophic oomycete *Plasmopara viticola*, the causative agent of downy mildew. This study contributes for a better understanding of the mechanisms of grapevine interaction and resistance to downy mildew. Negrel et al. took a further step in elucidating this grapevine-*P. viticola* interaction and characterized *P. viticola*'s metabolome using an untargeted metabolomics approach. These pathogen biomarkers can be used to in the development of a monitoring assay for the early detection of *P. viticola* in grapevine.

While analyzing both compatible and incompatible interactions between tomato (*Solanum lycopersicum*) and *Pseudomonas syringae*, López-Gresa et al. characterized the profile of volatile organic compounds associated with the tomato immune response to this bacteria. These results can be used in the future development of resistant tomato plants, thus preventing this agricultural problem and contributing to a more sustainable production. Another concern regarding stable fruit development is the availability of an optimal light environment. This has been a problem in several countries with fewer daylight hours. For tomato, a supplementary light system is often used in plants grown in greenhouses. However, an adequate plant growth and fruit development depends on the correct implementation of lightning strategies. Fukushima et al. performed an integrative omics strategy to investigate the metabolic changes in early fruit development of single-leaf tomato plants, with only one fruit truss, exposed to different intensities of red LED (light-emitting diode) light. The compounds that responded to the LED treatment and most contributed to the increase of fruit size of tomato plants were metabolites mainly involved in carbohydrate metabolism and the biosynthesis of several amino acids. This is quite relevant given the importance of carbon allocation for fruits during their development, for which a balanced source-sink relationship is essential to ensure adequate fruit nutritional quality and yield (Smith et al., 2018). Following this line of research, Beshir et al. used isotopically labeled substrates and metabolomics to investigate carbon re-allocation changes throughout the development of apple fruit. For the first time it was possible to create a thorough understanding of the metabolic changes' dynamics occurring during the different growth stages of fruit development using dynamic isotope labeling experiments.

Productivity increase in a crop and the efficient use of resources has been achieved through controlled growth in plant factories. Although not a natural environment, these closed production systems, with controlled lightning strategies and reduced environmental pollutants, became more sustainable and attractive to the food industry (Kosai, 2013). Tamura et al. analyzed the metabolite profiles of lettuce leaves grown under hydroponic conditions or fertilized soil, to investigate how cultivation conditions affected leaf metabolic composition. The results showed that the metabolic profile of both lettuce cultivars analyzed was greatly influenced by the cultivation method. Among the affected metabolites are the ones responsible for taste and functional ingredients, like amino acids, and phenolic compounds. Neugart et al. also analyzed the effect of soil fertilization with biological waste compost in the metabolic composition of *Brassica rapa* ssp. *Chinensis* (pak choi) sprouts. Indeed, the addition of biological waste from food production (coffee, aronia, and hop) strongly affected sprout metabolic profile, by increasing the concentration of carotenoids and decreasing the glucosinolates and phenolic compounds. The studies from Tamura et al., Fukushima et al., and Neugart et al. show that a detailed assessment of the effect of alternative cultivation systems, like greenhouses, and plant factories, is crucial in the quality and nutritional value of crop products, particularly the evaluation of the light, soil, and fertilization conditions.

Metabolomics has a huge potential in crop plant research. This Research Topic presents current and emerging approaches in metabolomics applied to crop research that we believe will be a future reference in the field and contribute to improve plant productivity and quality. The currently

available analytical platforms provide different strategies for metabolomics studies, from targeted, quantitative metabolite profiling, to global untargeted metabolic fingerprinting. In the field of quantitative metabolomics analysis, NMR and mass spectrometry coupled to liquid chromatography (LC-MS) or gas chromatography (GC-MS) are the techniques of choice (Lei et al., 2011). However, currently, Fourier-Transform Ion-Cyclotron-Resonance mass spectrometry (FT-ICR-MS) offers the greatest potential for untargeted metabolomics, being able to simultaneously detect and identify thousands of metabolites in very high-throughput assays, providing extreme-resolution and ultra-high-mass accuracy, and successfully used in crop metabolomics (Aliferis and Jabaji, 2012; Adrian et al., 2017; Maia et al., 2019).

AUTHOR CONTRIBUTIONS

This manuscript was written by MS and AF. It was revised and edited by all authors prior to submission.

FUNDING

This work was supported by projects UID/MULTI/00612/2013, PEst-OE/QUI/UI0612/2013, PEst-OE/BIA/UI4046/2014, PTDC/BAA-MOL/28675/2017, and by IF 00819/2015 to AF and CEECIND/02246/2017 to MS, all from Fundação para a Ciência e Tecnologia (Portugal). We also acknowledge the support from the Portuguese Mass Spectrometry Network (LISBOA-01-0145-FEDER-022125) and the Project EU_FT-ICR_MS, funded by the Europe and Union's Horizon 2020 research and innovation programme under grant agreement no. 731077.

ACKNOWLEDGMENTS

As Editors of this topic, we wish to thank all the colleagues, authors, reviewers, and support staff who contributed to the success of this Frontiers Research topic. We also acknowledge the Frontiers Editorial Office and the Chief Editors for their technical support.

REFERENCES

Adrian, M., Lucio, M., Roullier-Gall, C., Heloir, M. C., Trouvelot, S., Daire, X., et al. (2017). Metabolic fingerprint of PS3-induced resistance of grapevine leaves against *Plasmopara viticola* revealed differences in elicitor-triggered defenses. *Front. Plant Sci.* 8:101. doi: 10.3389/fpls.2017.00101

Aliferis, K. A., and Jabaji, S. (2012). FT-ICR/MS and GC-EI/MS metabolomics networking unravels global potato sprout's responses to *Rhizoctonia solani* infection. *PLoS ONE* 7:e42576. doi: 10.1371/journal.pone.0042576

Alseekh, S., Bermudez, L., de Haro, L. A., Fernie, A. R., and Carrari, F. (2018). Crop metabolomics: from diagnostics to assisted breeding. *Metabolomics* 14:148. doi: 10.1007/s11306-018-1446-5

Fiehn, O. (2002). Metabolomics - the link between genotypes and phenotypes. *Plant Mol. Biol.* 48, 155–171. doi: 10.1023/A:1013713905833

Gaulin, E., Jacquet, C., Bottin, A., and Dumas, B. (2007). Root rot disease of legumes caused by *Aphanomyces euteiches*. *Mol. Plant Pathol.* 8, 539–548. doi: 10.1111/j.1364-3703.2007.00413.x

Kosai, T. (2013). Sustainable plant factory: closed plant production systems with artificial light for high resource use efficiencies and quality produce. *Acta Hortic.* 1004, 27–40. doi: 10.17660/ActaHortic.2013.1004.2

Lei, Z., Huhman, D. V., and Sumner, L. W. (2011). Mass spectrometry strategies in metabolomics. *J. Biol. Chem.* 286, 25435–25442. doi: 10.1074/jbc.R111.238691

Maia, M., Ferreira, A. E. N., Laureano, G., Marques, A. P., Torres, V. M., Silva, A. B., et al. (2019). *Vitis vinifera* 'Pinot Noir' leaves as a source of bioactive nutraceutical compounds. *Food Funct.* 10, 3822–3827. doi: 10.1039/C8FO02328J

Peccoud, J., Ollivier, A., Plantegenest, M., and Simon, J. C. (2009). A continuum of genetic divergence from sympatric host races to species in the pea aphid complex. *Proc. Natl. Acad. Sci. U.S.A.* 106, 7495–7500. doi: 10.1073/pnas.0811117106

Smith, M. R., Rao, I. M., and Merchant, A. (2018). Source-sink relationships in crop plants and their influence on yield development and nutritional quality. *Front. Plant Sci.* 9:1889. doi: 10.3389/fpls.2018.01889

Vandecandelaere, E., Arfini, F., Belletti, G., and Marescotti, A. (eds.). (2009). "Linking people, places and products," in *A Guide for Promoting Quality Linked to Geographical Origin and Sustainable Geographical Indications, 2nd Edn* (Rome: FAO/SINER-GI), 194.

Conflict of Interest Statement: The authors declare that the research was conducted in the absence of any commercial or financial relationships that could be construed as a potential conflict of interest.

frontiers in Plant Science

ORIGINAL RESEARCH
published: 12 October 2017
doi: 10.3389/fpls.2017.01746

Phenolic Profiling for Traceability of *Vanilla ×tahitensis*

Matteo Busconi[1†], Luigi Lucini[2†], Giovanna Soffritti[1], Jamila Bernardi[1], Letizia Bernardo[2], Christel Brunschwig[3,4], Sandra Lepers-Andrzejewski[4], Phila Raharivelomanana[3*] and Jose A. Fernandez[5]*

[1] Department of Sustainable Crop Production, Università Cattolica del Sacro Cuore, Piacenza, Italy, [2] Institute of Environmental and Agricultural Chemistry, Università Cattolica del Sacro Cuore, Piacenza, Italy, [3] Equipe EIMS (Etude Intégrée des Métabolites Secondaires), UMR 241 EIO Université de la Polynésie Française, Tahiti, French Polynesia, [4] Département Recherche et Développement, Etablissement Vanille de Tahiti, Raiatea, French Polynesia, [5] IDR- Laboratorio de Biotecnología y Recursos Naturales, Universidad de Castilla-La Mancha, Albacete, Spain

OPEN ACCESS

Edited by:
Andreia Figueiredo, Universidade de Lisboa, Portugal

Reviewed by:
Ibrahim M. Abu-Reidah, An-Najah National University, Palestine
Gonçalo Graça, Imperial College London, United Kingdom

***Correspondence:**
Matteo Busconi
matteo.busconi@unicatt.it
Phila Raharivelomanana
phila.raharivelomanana@upf.pf

†These authors have contributed equally to this work.

Specialty section:
This article was submitted to Plant Metabolism and Chemodiversity, a section of the journal Frontiers in Plant Science

Received: *17 July 2017*
Accepted: *25 September 2017*
Published: *12 October 2017*

Citation:
Busconi M, Lucini L, Soffritti G, Bernardi J, Bernardo L, Brunschwig C, Lepers-Andrzejewski S, Raharivelomanana P and Fernandez JA (2017) Phenolic Profiling for Traceability of Vanilla ×tahitensis. Front. Plant Sci. 8:1746. doi: 10.3389/fpls.2017.01746

Vanilla is a flavoring recovered from the cured beans of the orchid genus *Vanilla*. *Vanilla ×tahitensis* is traditionally cultivated on the islands of French Polynesia, where vanilla vines were first introduced during the nineteenth century and, since the 1960s, have been introduced to other Pacific countries such as Papua New Guinea (PNG), cultivated and sold as "Tahitian vanilla," although both sensory properties and aspect are different. From an economic point of view, it is important to ensure *V. ×tahitensis* traceability and to guarantee that the marketed product is part of the future protected designation of the origin "Tahitian vanilla" (PDO), currently in progress in French Polynesia. The application of metabolomics, allowing the detection and simultaneous analysis of hundreds or thousands of metabolites from different matrices, has recently gained high interest in food traceability. Here, metabolomics analysis of phenolic compounds profiles was successfully applied for the first time to *V. ×tahitensis* to deepen our knowledge of vanilla metabolome, focusing on phenolics compounds, for traceability purposes. Phenolics were screened through a quadrupole-time-of-flight mass spectrometer coupled to a UHPLC liquid chromatography system, and 260 different compounds were clearly evidenced and subjected to different statistical analysis in order to enable the discrimination of the samples based on their origin. Eighty-eight and twenty three compounds, with a prevalence of flavonoids, resulted to be highly discriminant through ANOVA and Orthogonal Projections to Latent Structures Discriminant Analysis (OPLS-DA) respectively. Volcano plot analysis and pairwise comparisons were carried out to determine those compounds, mainly responsible for the differences among samples as a consequence of either origin or cultivar. The samples from PNG were clearly different from the Tahitian samples that were further divided in two different groups based on the different phenolic patterns. Among the 260 compounds, metabolomics analysis enabled the detection of previously unreported phenolics in vanilla (such as flavonoids, lignans, stilbenes and other polyphenols).

Keywords: *Vanilla ×tahitensis*, food metabolomics, phenolics, traceability, authenticity

INTRODUCTION

Vanilla is a flavoring traditionally recovered from the cured beans of the orchid genus *Vanilla*. It is also one of the three most expensive spices in the world, along with saffron and cardamom (Hondrogiannis et al., 2013). Other than as a fragrance, in traditional Mexican medicine vanilla was considered as a medicinal plant with multiple positive effects on men's health (Rain and Lubinsky, 2011). In eighteenth and nineteenth centuries, vanilla was included in the European and American pharmacopeia for its medicinal uses (King et al., 1898; Bythrow, 2005). Anti-inflammatory, antiviral, analgesic, antiseptic and aesthetic properties of vanilla have been recently reported (Duke et al., 2003). Antioxidant properties of vanilla and vanilla constituents (essential oil or extract) have been reported by different authors (Kumar et al., 2002; Teuscher et al., 2005; Maurya et al., 2007). The genus *Vanilla* is indigenous of Central America, and in particular of Mexico, and comprises over 100 different species (Soto Arenas, 2003; Soto Arenas and Dressler, 2010), of which only two are currently cultivated for commercial purposes, *Vanilla planifolia* Jacks. ex Andrews and *Vanilla* ×*tahitensis* (previously *V. tahitensis* Moore). Vanilla plants are grown in hot-humid tropical climates and have certain agro-ecological requirements in terms of temperature (20–32°C), precipitation (average from 2,000 to 3,000 mm per year), altitude (from sea level to 600 m), shade (50–70%), well-drained soil rich in humus, support trees (as they are hemi-epiphytic orchids). Optimal flowering, and, consequently, pod production, requires specific climatic conditions of a dry and cool season of at least 2 months (Hernandez and Lubinsky, 2011). The hybrid nature of Tahitian vanilla was recently determined (Lubinsky et al., 2008). Analysis of cpDNA and nuclear ITS sequences provided evidence that Tahitian vanilla is a hybrid between *V. planifolia* and *V. odorata* C. Presl, with *V. planifolia* being the female parent. *Vanilla* ×*tahitensis* is traditionally cultivated on French Polynesian islands, where vanilla vines were first introduced during the nineteenth century (Costantin and Bois, 1915; Bouriquet, 1954; Florence and Guérin, 1996; Lepers-Andrzejewski et al., 2012), currently, vanilla production is mainly carried out in the Leeward Islands (high islands: Raiatea, Tahaa, Huahine), Society archipelago (Lepers-Andrzejewski and Dron, 2010). Subsequently, within a short period of time, diversification resulted in the origination of about 14 cultivars identified over the years by local producers (Lepers-Andrzejewski et al., 2010). Among the isolated cultivars, two of them, "Haapape" and "Tahiti," which are morphologically and genetically differentiated (Lepers-Andrzejewski et al., 2011), became the most widespread and most commercialized cultivars in French Polynesia. Since the 1960s, *V.* ×*tahitensis* has been introduced into other Pacific countries such as Papua New Guinea (PNG), cultivated and sold as "Tahitian vanilla," although both sensory properties and aspect are different. These differences depend more on factors such as genetic traits, environment and technology (curing method and storage conditions). Actually, *V.* ×*tahitensis*, being less restrictive to humidity and supporting better rainfall, was found to be more suitable to the climate of PNG than *V. planifolia* and the Sepik area (well-drained alluvial plains) is the main vanilla production region (Mac Gregor, 2005). The volatile composition of vanilla in general and of *V.* ×*tahitensis* in particular has recently been investigated and the results were reported in the literature (Pérez-Silva et al., 2006; Brunschwig et al., 2009; Lepers-Andrzejewski et al., 2010; Brunschwig et al., 2012; Takahashi et al., 2013; Brunschwig et al., 2016).

According to official data (http://www.fao.org/faostat), in 2014, global vanilla production was over 7,000 t, with French Polynesia ranking ninth among the vanilla producers in the world. Considering the high economic value of vanilla, in the last years, several publications have dealt with the development of reliable methods to trace vanilla production according to the species or the different geographic origin. Tracing the genetic and/or the geographic origin of vanilla is crucial because the species, the variety, the environment (in particular climatic conditions) and the production method (curing methods and storage) imply characteristic different flavors that could be reflected in the quality and the price of the product. From an economic point of view, it is important to ensure *V.* ×*tahitensis* traceability and to guarantee that the product which is marketed is part of the future protected designation of the origin "Tahitian vanilla" (PDO) (Journal Officiel de la Polynésie Française, 2014, 2016). *Vanilla* ×*tahitensis* traceability has already been carried out via different analytical techniques, such as gas chromatography–flame ionization detection (GC-FID) and gas chromatography–mass spectrometry (GC-MS), to analyse the volatile compounds for quality control (Brunschwig et al., 2016); analysis of the stable isotopes of carbon and hydrogen evidencing that *V.* ×*tahitensis* has more heavy carbon than *V. planifolia* and that isotopes can be used to discriminate the geographic origin of the samples (Sølvbjerg Hansen et al., 2014); wavelength dispersive X-ray fluorescence to identify the elemental composition and the geographic origin of vanilla samples (Hondrogiannis et al., 2013). The use of metabolomics, allowing the detection and simultaneous analysis of hundreds or thousands of metabolites from different matrices, has recently gained high interest in food traceability (Oms-Oliu et al., 2013). Metabolomic techniques have been applied for the analysis of raw food material (cultivar identification, study of different metabolites that accumulate during plant growth, ripening and postharvest) and processed plant-derived food (food classification, authenticity assessment, food control) (Oms-Oliu et al., 2013). Up to now, the study of vanilla metabolome was applied to *V. planifolia*, albeit not for traceability purposes. Some studies concerning the metabolome of *V. planifolia* green pods from La Réunion (Palama et al., 2011) and the changes in metabolome composition in leaves (Palama et al., 2010) and pods (Palama et al., 2009) in different developmental stages have recently been published. Recently, Gu et al. (2017) carried out a comparative metabolomics analysis by using high-performance liquid chromatography–mass spectrometry (LC–MS) to analyse vanilla metabolome before and after curing to study the biosynthesis of vanillin during the curing process of vanilla. They evidenced the presence of at least seven different putative pathways of vanillin biosynthesis some of them possibly correlated with microbial activity.

In other species, metabolomics analysis was applied successfully to assess, among others, the authenticity of processed plant-derived food such as fruit juices (Vardin et al., 2008), coffee (Oliveira et al., 2009), vegetable oils (Rohman and Man, 2012; Ruiz-Samblás et al., 2012), and tomatoes (Lucini et al., 2017).

In the present work, we applied, for the first time, the comprehensive profile of the phenolic compounds for traceability purposes in *V.* ×*tahitensis*. Samples from two different areas, French Polynesia (FP) and PNG, were surveyed and the profile of the phenolic compounds investigated by UHPLC-ESI/QTOF-MS.

MATERIALS AND METHODS

Vanilla Samples

Two commercial samples of *Vanilla* ×*tahitensis* pods were obtained from two commercial providers ("Pacific Natural Product" and "Tahiti vanille" Brand); both of these samples were grown on the Leeward Islands and harvested in 2013. The pods have been cured following the traditional Polynesian method (Lepers-Andrzejewski et al., 2010). A sample of *V.* ×*tahitensis* pods (250 g) from PNG was provided by the NARI organization (PNG's National Agricultural Research Institute, donation from Dr. Sergie Bang) from the East Sepik region and collected from the 2013 harvest. It was used as reference for a comparison with *V.* ×*tahitensis* from French Polynesia. The pods have been cured according to the methods currently used in PNG (see discussion). At the end, three batches were available: batch1, pods of Tahitian vanilla, belonging to the "Haapape" cultivar, Vanille de Tahiti Brand from Pacific Natural Product, grown on the Leeward Islands (French Polynesia FP); batch2, mixture of pods of Tahitian vanilla, cultivars "Haapape" and "Tahiti," "Tahiti vanille" Brand, from the Leeward Islands (FP); batch3, pods of *V.*×*tahitensis* from PNG.

Profiling of Phenolic Compounds

Ten independent pods per treatment were analyzed as individual samples. The phenolic compounds were screened through a quadrupole-time-of-flight mass spectrometer coupled to a UHPLC liquid chromatography system (UHPLC-ESI/QTOF-MS), on the basis of the approach described by Lucini et al. (2015). Samples were extracted in 10 volumes of 50 mM HCOOH in 80% methanol, using an IKA T10 Ultra-Turrax to comminute samples (3 min at 30,000 rpm). The extracts were then centrifuged at +4°C and filtered through a 0.22-μm cellulose membrane, diluted five times in 50% methanol and transferred to an amber vial for LC-ESI/Q-TOF-MS analysis. A 1290 UHPLC liquid chromatograph, equipped with a binary pump and coupled to a G6550 iFunnel QTOF mass spectrometer through a Dual Electrospray JetStream ionization system (all from Agilent Technologies Santa Clara, CA, USA), was used to profile phenolic compounds. The mass spectrometer was operated in positive MS-only (SCAN) mode to acquire spectra in the range 50–1,000 m/z. Extracts were injected (6 μL) and chromatographed under a water-methanol gradient elution (from 6% methanol to 92% methanol in 35 min), using an Agilent Zorbax Eclipse Plus C18 column (50 × 2.1 mm, 1.8 μm). Lock masses and source conditions were optimized for phenolic compounds in previous experiments (Lucini et al., 2017). Briefly, nitrogen was used as drying gas (8 L min^{-1} and 330°C), nebulizer pressure was 60 psig and capillary voltage was 3,500 V. Blanks were analyzed between samples and lock masses (m/z 121.0509 and 922.0098) were continuously infused during chromatographic runs to achieve higher accuracies.

Raw data were processed via the Agilent Profinder B.0700 software using the "find-by-formula" algorithm. With this purpose, features mass and retention time were aligned and then the whole isotopic profile (isotopic spacing and isotopic ratio) was used for compounds' annotation, together with the monoisotopic accurate mass, against the database exported from Phenol-Explorer 3.6 (Rothwell et al., 2013). In addition, recursive analysis (using retention time as mandatory in the second ID step, with a tolerance of 0.1 min) and frequency filter were applied (only those compounds being in at least 80% of replications within at least one condition were retained). Therefore, based on the strategy applied, identification was carried out according to Level 2 (putatively annotated compounds) as set out by the COSMOS Metabolomics Standards Initiative (http://cosmos-fp7.eu/msi).

Statistical Analysis

The abundance value for each compound in the dataset was log2-transformed, normalized at 75th percentile and baselined to the median in the dataset. One-way analysis of variance (ANOVA) ($p < 0.05$, Benjamini-Hochberg multiple testing correction) has been carried out on the starting data set of metabolites. Unpaired *t*-test ($p < 0.05$, Benjamini-Hochberg FDR multiple testing correction) and fold-change analysis (cut-off = 2) were combined into Volcano plot analysis. Subsequently, unsupervised hierarchical cluster analysis (Euclidean similarity measure and Wards linkage rule) was generated on the basis of fold-change heatmaps.

Finally, the raw dataset was exported in SIMCA 14 (Umetrics, Malmo, Sweden), Pareto scaled (to reduce the relative importance of larger values and partially preserve data structure) and elaborated for orthogonal partial least squares discriminant analysis (OPLS-DA) prediction modeling. Herein, the variation between the three batches was separated into predictive and orthogonal (technical and biological variation) components. The presence of outliers was investigated according to Hotelling's T2 (i.e., the distance from the origin in the model plane), using 95 and 99% confidence limits for suspect and strong outliers, respectively. Method validity was next tested using CV-ANOVA ($P < 0.01$) and permutation testing after inspecting model parameters (goodness-of-fit R^2Y and goodness-of-prediction Q^2Y). Regarding Q^2Y prediction ability, a value > 0.5 indicates good model quality (Rombouts et al., 2017). Variable importance in projection (VIP analysis) was used to evaluate the importance of metabolites and select the most discriminant ones (VIP score > 1).

RESULTS

Ten single cured pods were recovered from each of the three vanilla batches and analyzed independently from the others. The use of an informative approach, such as UHPLC-ESI/QTOF-MS together with a comprehensive database (Phenol-Explorer), allowed the annotation of 260 phenolic compounds. All these phenolics belonged to a small number of main classes: flavonoids (120 compounds), phenolic acids (53 compounds), lignans (18 compounds), stilbenes (6 compounds) and one last group labeled as "other polyphenols" (63 compounds) (**Supplementary Table 1**). To the best of our knowledge, we report for the first time the occurrence of phenolic compounds from *V.* ×*tahitensis*, which do not belong to flavoring components (mainly composed by volatile components), such as flavonoids, lignans, stilbenes and other classes of polyphenols (curcuminoids). Based on the fold-change analysis, a heat map was developed and subsequently, an unsupervised hierarchical cluster analysis was carried out (**Figure 1**). It is important to underline that with the applied method we did not obtain an absolute quantification of the compounds but an indication of the relative abundance, based on the area of the peaks, of the different phenolics in the samples under comparison. Three main clusters could be identified: (1) all the pods from PNG batch3 (brown cluster); (2) eight pods from FP batch2 (blue cluster); (3) all the pods from FP batch1 (red cluster) plus two pods from FP batch2. Samples from PNG presented a characteristic phenolic profile, differing from that of the Tahitian ones, thus indicating that samples could be discriminated in terms of their geographic origin. Within the Tahitian pods, the metabolic profiles were quite similar, but still sufficiently different to allow two further sub-clusters to separate the Tahitian sample sets.

Two approaches were then applied to investigate the most differential compounds within the sample set. Initially, the data set was analyzed by using a one-way ANOVA ($P < 0.05$) that resulted in 88 differential compounds out of the 260 phenolics identified (**Supplementary Table 2**). Flavonoids were the most represented compounds (39 compounds), followed by "other polyphenols" and phenolic acids (21 and 20 compounds, respectively), stilbenes and lignans (four compounds per class). Among the phenolic acids, hydroxycinnamic acids were the most represented subclass (13 compounds) while within the flavonoids, flavonols (nine compounds), flavones (eight compounds) and anthocyanins (eight compounds) were more represented. Vanillin (4-Hydroxy-3-methoxybenzaldehyde) content was significantly different between the three samples according to one-way ANOVA, but the fold change was not high enough to be recognized as discriminant with the Volcano plot analysis in the pairwise comparison (see later). Among the 260 compounds, only one anisyl derivative (anisaldehyde) was detected, but not selected among the most discriminant compounds with ANOVA nor with the subsequent analyses (OPLS-DA and Volcano plot). This highlights that such metabolomics analysis was more powerful to detect, in *V.* × *tahitensis,* compounds even more discriminant than the characteristic odor-active anisyl compounds (Brunschwig et al., 2012, 2016).

The results of OPLS-DA agreed with the unsupervised cluster analysis being able to separate the samples according to their origin and, possibly, the cultivar of origin (**Figure 2**). Indeed, the characteristics of the model were excellent: $R^2Y = 0.969$ and $Q^2Y = 0.877$. No outlier samples could be observed by Hotelling's T2, whereas both CV-ANOVA ($P = 4.3\ 10^{-14}$ for regression) and permutation test (Supplementary Figure 2) showed a more than adequate degree of validation.

Overall, all these results evidenced that differences among the three samples were included in the compounds data set, thus driving the need for a more detailed assessment of which compounds these differences could be ascribed too. The VIP analysis from OPLS-DA allowed to select a small number of discriminant compounds, reducing the data set to only 23 highly discriminant compounds. Individual VIP scores are reported in **Table 1**, together with the discriminant compounds grouped in phenolic classes. Flavonoids (12 different compounds), other polyphenols and phenolic acids (four different compounds each one) were the most represented subclasses of phenolics (**Table 1**). Among the most discriminant compounds, two stilbenes (resveratrol and pterostilbene) have been detected.

Volcano plot analysis (unpaired *t*-test; $p \leq 0.01$; fold-change cut off = 2) was carried out to determine those compounds mainly responsible for the differences among samples as a consequence of either origin or cultivar. Three different pairwise comparisons were carried out: (1) between the two Tahitian batch samples; (2) between FP batch2 and PNG; (3) between FP batch1 and PNG. The discriminant compounds for all the three different comparisons have been reported in **Supplementary Table 3**, in three active sheets, along with the corresponding fold change (an estimate of the relative abundance of the compounds in the samples under pairwise comparison) and regulation. The volcano plot graphic output of the comparisons FP batch1 and PNG and FP batch2 and PNG is reported in Supplementary Figure 1.

Twenty-one compounds (**Table 2**) were discriminant between the samples from the same geographic location (French Polynesia): flavonoids (10 compounds, highly represented by flavonols) and phenolic acids (five compounds, almost exclusively hydroxycinnamic acids) were the most frequent classes of phenolics. Discriminant hydroxycinnamic acids were derivatives of coumaric and caffeic acid. Six compounds were grouped under a class named, in phenol-explorer (Rothwell et al., 2013), as "other polyphenols." Twelve compounds were up-regulated, while nine were down-regulated in FP batch1 with respect to the mixture (batch2). Fifty percent of flavonoids were respectively up- and down-regulated. Among other classes of phenolics, the up-regulated compounds in FP batch1 prevailed. Those compounds identified as discriminant through both the *t*-test and OPLS-DA are marked in **Table 2** with an asterisk.

Contrary to what was observed between the Tahitian samples, the other comparisons evidenced a higher number of differential compounds, respectively, 82 (FP batch2 vs. PNG) and 57 (FP batch1 vs. PNG). Checking these differential compounds through Venn analysis (Supplementary Figure 1), 46 metabolites were found in both the comparisons, while 36 and 11, respectively, were exclusive of the single comparisons for the two Tahitian batches when compared to

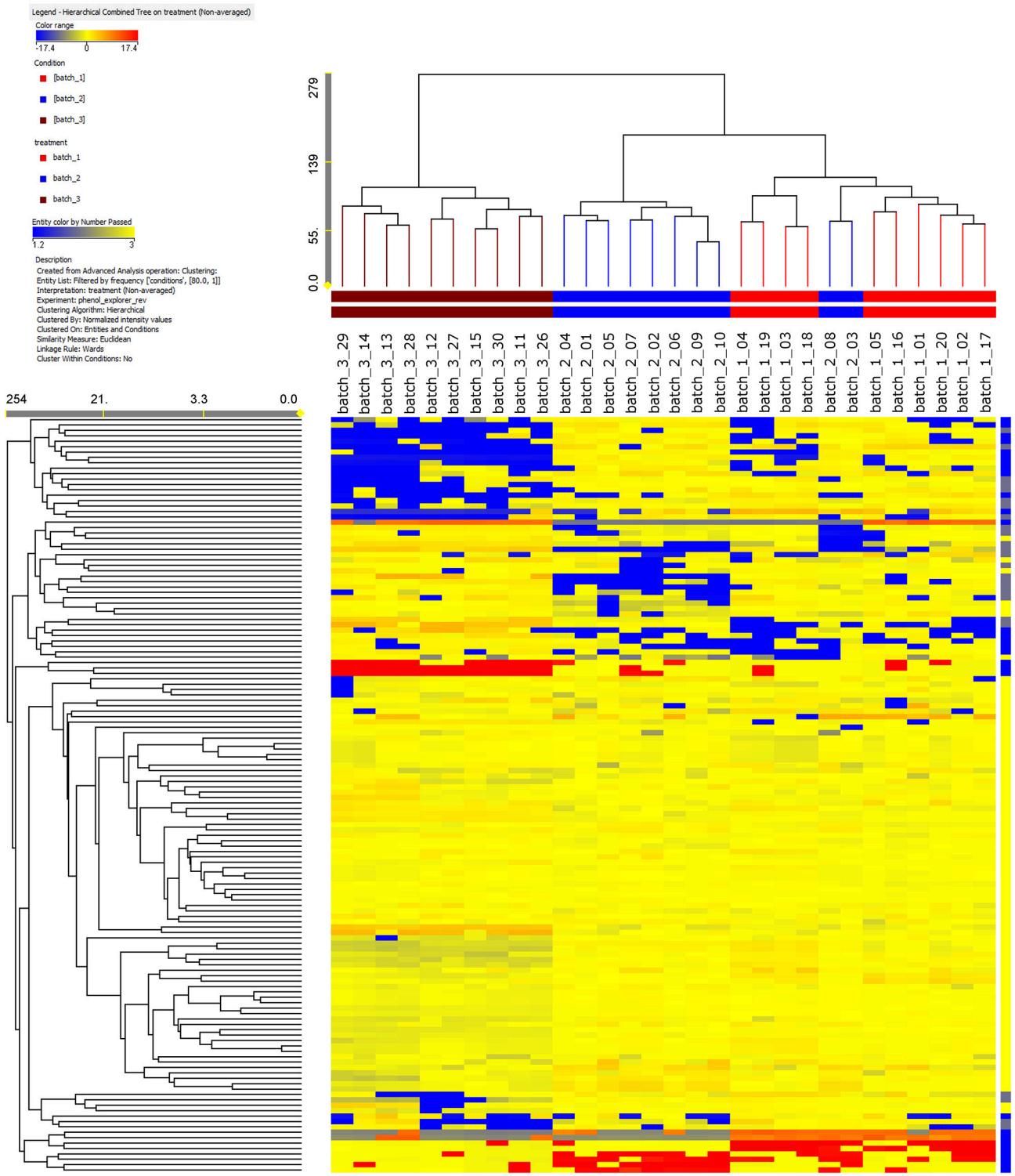

FIGURE 1 | Results of a not averaged, unsupervised hierarchical cluster analysis on the phenolic profile in the vanilla pods analyzed. The intensity of the compounds was used to build the heat maps on which the clusters were generated. Samples from PNG (brown) are clearly different with respect to Tahitian samples (red, batch1, and blue, batch2) in regards to the phenolic composition. Among the Tahitian samples, two patterns can be distinguished.

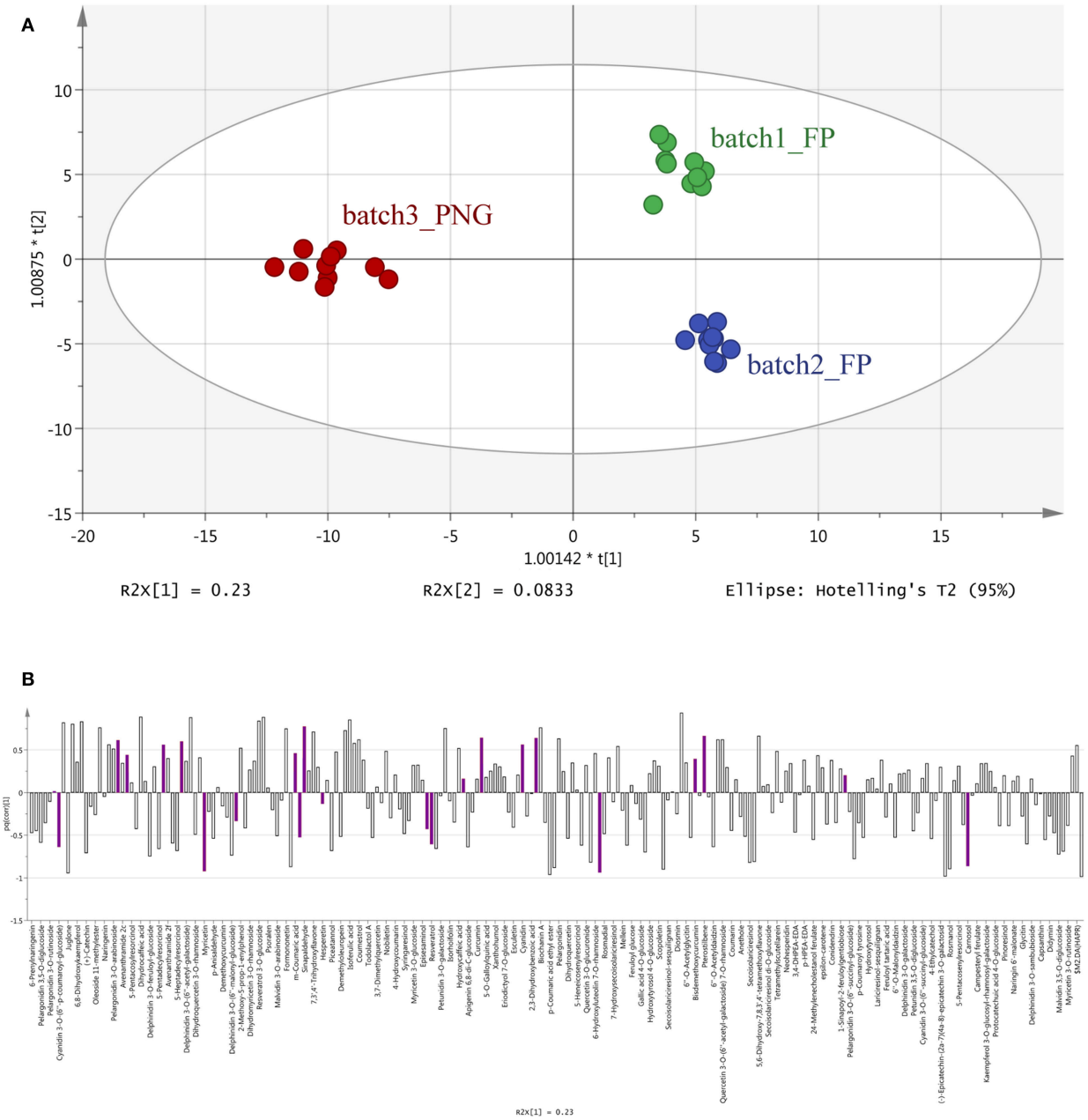

FIGURE 2 | Orthogonal Projections to Latent Structures Discriminant Analysis (OPLS-DA) on vanilla sample phenolic profiles. Individual replications are given in the model score plot **(A)**, whereas loadings column plot is reported in the **(B)**. Compounds selected by VIP analysis are reported in color in the loadings column plot. PNG samples (red samples) are clustered on the left whereas Tahitian samples (green and blue samples) on the right side of the plot. Both geographic origin and cultivars were responsible for the actual phenolic signature of the samples.

PNG (**Tables 3**, **4**). The common metabolites showed always the same kind of regulation in Tahitian samples, up or down, respectively, with respect to PNG samples; no compounds showing different regulations in the two comparisons could be observed (**Table 3**). The *p*-values of the common metabolites, as resulted from the two different pairwise comparisons, have been reported in **Table 3**. As an example, focusing on stilbenes, pterostilbene and resveratrol 3-*O*-glucoside were highly up-regulated, while piceatannol was down-regulated, both in batch2 vs. PNG and in batch1 vs. PNG. Among these compounds responsible for discrimination between the two different locations, flavonoids were the most represented ones (20 compounds), followed by phenolic acids (nine compounds). Within flavonoids, anthocyanins and flavonols were the most abundant compounds and glycosylated forms (e.g., malvidin 3-*O*-galactoside, petunidin 3-*O*-galactoside, petunidin

TABLE 1 | Compounds discriminating between the three vanilla samples, as obtained from VIP analysis from Orthogonal Projections to Latent Structures Discriminant Analysis (OPLS-DA).

Class	Sub class	Compound	VIP score
Flavonoids	Anthocyanins	Cyanidin 3-*O*-(6″-*p*-coumaroyl-glucoside)	1.2655
		Cyanidin	1.5515
		Peonidin	1.6544
		Kaempferol	1.5474
	Flavanols	(-)-Epigallocatechin	1.1652
	Flavanones	6-Geranylnaringenin	1.6041
		Hesperetin	1.2650
		Naringenin 7-O-glucoside	1.5636
	Flavones	Cirsilineol	1.5881
		7,4′-Dihydroxyflavone	1.6009
	Flavonols	Myricetin	1.4220
		Kaempferide	1.6410
Lignans	Lignans	Dimethylmatairesinol	1.4705
Other polyphenols	Curcuminoids	Bisdemethoxycurcumin	1.6693
	Hydroxybenzoketones	2,3-Dihydroxy-1-guaiacylpropanone	1.0357
		3-Methoxyacetophenone	1.6664
	Phenolic terpenes	Carnosol	1.3296
Phenolic acids	Hydroxycinnamic acids	*m*-Coumaric acid	1.7628
		Sinapic acid	1.3886
	Hydroxycinnamaldehydes	Sinapaldehyde	1.5979
	Hydroxyphenylpropanoic acids	3,4-dihydroxyphenyl-2-oxypropanoic acid	1.4280
Stilbenes	Stilbenes	Resveratrol	1.4601
		Pterostilbene	1.4923

3-*O*-rutinoside) were highly represented. Globally, 31 and 15 compounds, respectively, were significantly up- and down-regulated in Tahitian samples. In more detail, flavonoids (17 out of 20) and phenolic acids (6 out of 9) were mainly up-regulated, while within other polyphenols, more or less the same number of compounds were up- or down-regulated (5 and 6 out of 11, respectively). Eight of the compounds reported in **Table 3** were also selected by OPLS-DA as differential molecules able to discriminate samples based on both the geographic origin and genotype (five out of eight were up-regulated in Tahitian samples).

Focusing on the exclusive metabolites (**Table 4**), the number of differential compounds was lower between FP batch1 (11) vs. PNG than between FP batch2 vs. PNG (36). Furthermore, up-regulated compounds were more abundant than the down-accumulated ones, the corresponding *p*-values are reported in **Table 4**. Among the exclusive compounds of batch1 and of batch2, flavonoids were predominant: 7 out of 11 for batch1 and 19 out of 36 for batch2 (flavones and flavonols were particularly abundant). Exclusive compounds of batch2 were also phenolic acids (9 out of 36) and, despite the small number, stilbenes (**Table 4**). Among the stilbenes, both pinosylvin and delta-viniferin were up-regulated in batch2 with respect to PNG. Overall, out of five differential stilbenes (**Tables 3**, **4**), four were up-regulated and just one was down-regulated in Tahitian samples. Nine compounds among the exclusive metabolites were also recognized by OPLS-DA analysis; seven out of nine were up-regulated in Tahitian samples.

DISCUSSION

While traceability is usually most relevant when it concerns public health, the possibility to discover the origin of products, ingredients and their attributes from the farm throughout the whole food chain to the consumer is gaining more importance. Regarding plant-derived products, being able to trace the origin is extremely important. This is because the characteristics of these products are strongly influenced, other than by the genetic constitution of the cultivated varieties, by environmental conditions and by local traditional curing methods, both able to influence the final metabolic profile of the product (Brunschwig et al., 2016). Genetic bases being equal, the origin of the products, considered as the sum of environment and production technologies, implies characteristic flavors, subsequently reflected in premium prices that can represent a target for falsifications and frauds. This is particularly true in the case of *V.* ×*tahitensis*. Therefore, the development

TABLE 2 | Discriminant metabolites differentiating pods of batch1 from those of batch2.

Class	Sub class	Compound	Regulation	*p*-Value
Flavonoids	Flavones	Cirsilineol *	Down	2.65E-07
	Flavanones	6-Geranylnaringenin *	Up	0.002808
	Flavonols	Kaempferide *	Down	9.43E-08
		3,7-Dimethylquercetin	Down	6.97E-06
		Quercetin 3-O-acetyl-rhamnoside	Down	4.68E-04
		Myricetin *	Up	5.46E-03
		Isorhamnetin 3-O-glucuronide	Up	1.06E-05
		(-)-Epigallocatechin *	Up	1.59E-03
	Dihydroflavonols	Dihydroquercetin 3-O-rhamnoside	Up	0.007018
	Anthocyanins	Peonidin *	Down	1.99E-08
Phenolic acids	Hydroxycinnamic acids	Hydroxycaffeic acid	Down	0.003478
		m-Coumaric acid *	Up	3.63E-08
		Caffeoyl tartaric acid	Up	6.63E-03
		p-Coumaroyl tartaric acid	Up	1.19E-05
	Hydroxyphenylpropanoic acids	3,4-dihydroxyphenyl-2-oxypropanoic acid *	Up	1.82E-05
Other polyphenols	Alkylphenols	5-Heneicosylresorcinol	Down	6.88E-03
		5-Pentadecylresorcinol	Up	2.05E-03
	Hydroxybenzoketones	2,3-Dihydroxy-1-guaiacylpropanone *	Down	6.45E-06
	Phenolic terpenes	Carnosol *	Down	5.74E-04
	Hydroxycoumarins	Esculin	Up	2.81E-04
	Curcuminoids	Bisdemethoxycurcumin *	Up	7.42E-06

The compounds were grouped in their chemical classes and sub-classes. The up- and down-regulation and the corresponding p values, as a result of the Volcano analysis ($p \leq 0.05$, fold-change cut-off = 2.0), are reported.

** Compounds also recognized as discriminant via OPLS-DA analysis.*

of control procedures to protect the high-quality Tahitian production is of great interest and scientifically supported by the results of recent papers (Brunschwig et al., 2009, 2016; Takahashi et al., 2013). Among them, Brunschwig et al. (2016) have analyzed the volatile composition and the sensory properties of *V.* ×*tahitensis* from different geographic origins (French Polynesia and PNG), evidencing a clear difference in the composition of these compounds between the two different geographic locations. *V.* ×*tahitensis* from PNG was clearly different from *V.* ×*tahitensis* from French Polynesia. According to the authors, these differences were mainly a consequence of the curing technology. Our study could be considered as a prosecution of Brunschwig et al. (2016), although a different analytical approach was applied, to increase the knowledge on vanilla chemical composition toward the development of a traceability procedure for this product. Along with the analysis of chemical composition, the development of traceability methods based on DNA might be a topic of great interest. On this basis, we also tried to recover DNA from the cured pods. However, the techniques employed for DNA isolation from pods, both commercial kits and customized protocols, were not efficient and no DNA, or no PCR grade DNA, could be recovered (data not shown). Although further research is required to implement DNA-based approaches, these results strongly drive the analysis of secondary metabolites for traceability purposes. In the present study, we applied for the first time metabolomics, focused on the phenolic compounds, to *V.* ×*tahitensis* traceability. Ten pods for each one of the three samples (batch1 – cultivar "Haapape" FP; batch2 – "Haapape + Tahiti" FP; batch3 – PNG) were analyzed evidencing a quali-quantitative phenolic profile involving 260 compounds. The decision to focus our attention on phenolics has been driven by the fact that: (1) these secondary metabolites are highly associated to different environmental conditions, curing methods and genotypes, thus showing high discriminant capacity (Klockmann et al., 2016); (2) such an in-depth analysis of these chemically diverse compounds was not previously carried out for this species; (3) with respect to volatiles, phenolics are expected to be more stable during storage.

Pods from FP were softer than pods from PNG and this is very likely a direct consequence of the two different curing methods adopted: in the traditional FP method, the pods are harvested when fully mature, exposed in the shade for a natural browning (no high-temperature scalding step to stop maturation), alternatively dried in the sun and wrapped in cotton material overnight; they are then finally air-dried to stabilize the flavor and keep the water content at about 50%; in the PNG method it is included a high-temperature scalding step to stop maturation and drying to about 40% water content. Using ten individual pods for each samples increases the number of independent replicates strongly supporting the reliability of the results. Flavonoids were the most abundant phenolics, followed

TABLE 3 | Common metabolites, differentiating Tahitian and PNG samples, evidenced by matching the results of the two Volcano analyses: batch2 vs. PNG (b2-PNG) and batch1 vs. PNG (b1-PNG).

Class	Sub class	Compound	Regulation	*p*-value	
				b2-PNG	b1-PNG
Flavonoids	Flavones	7,4′-Dihydroxyflavone *	Up	3.32E-05	6.72E-09
		7,3′,4′-Trihydroxyflavone	Up	1.11E-11	2.75E-07
	Flavanones	Sakuranetin	Up	0.003981	0.002101
		Eriodictyol	Up	2.41E-05	4.88E-05
	Flavonols	Myricetin *	Down	3.57E-04	6.00E-04
		Isorhamnetin	Up	2.86E-07	1.51E-04
		Isorhamnetin 3-O-glucoside 7-O-rhamnoside	Up	1.49E-08	5.36E-04
		Quercetin 3-O-(6″-acetyl-galactoside) 7-O-rhamnoside	Up	1.41E-08	0.01372
	Anthocyanins	Malvidin 3-O-galactoside	Down	0.001473	0.004629
		Peonidin *	Up	2.25E-08	2.34E-03
		Pelargonidin	Up	2.56E-12	1.33E-07
		Pelargonidin 3-O-arabinoside	Up	2.50E-05	1.61E-05
		Petunidin 3-O-galactoside	Up	0.006946	0.005985
		Petunidin 3-O-rutinoside	Up	2.01E-24	1.35E-04
	Dihydrochalcones	Phloretin	Down	9.83E-08	4.36E-06
		Phloretin 2′-O-xylosyl-glucoside	Up	0.012373	3.56E-04
	Isoflavonoids	Formononetin	Up	3.38E-05	6.28E-04
		6″-O-Acetylgenistin	Up	0.015696	1.19E-05
		Genistin	Up	0.001106	0.005498
		6″-O-Acetylglycitin	Up	0.003609	1.62E-04
Stilbenes	Stilbenes	Piceatannol	Down	3.67E-06	0.00864
		Pterostilbene *	Up	6.17E-06	1.21E-06
		Resveratrol 3-O-glucoside	Up	3.20E-06	4.27E-06
Phenolic acids	Hydroxycinnamic acids	p-Coumaric acid ethyl ester	Down	5.97E-11	1.00E-07
		3-p-Coumaroylquinic acid	Down	5.51E-04	0.003488
		p-Coumaroyl tartaric acid	Down	5.22E-27	0.01277
		m-Coumaric acid *	Up	1.68E-05	2.95E-10
		Cinnamic acid	Up	0.010233	0.002471
		3-Sinapoylquinic acid	Up	1.13E-05	1.31E-05
	Hydroxyphenylpropanoic acids	Dihydrocaffeic acid	Up	3.14E-08	6.46E-07
	Hydroxyphenylacetic acids	Homoveratric acid	Up	1.42E-09	2.94E-09
	Hydroxybenzoic acids	Ellagic acid arabinoside	Up	8.98E-10	0.001704
Other polyphenols	Other polyphenols	Phlorin	Down	1.08E-05	4.22E-06
		3,4-Dihydroxyphenylglycol	Down	0.006922	0.002482
		Coumestrol	Up	1.30E-07	6.04E-08
	Naphtoquinones	Juglone	Down	1.47E-09	5.67E-14
	Phenolic terpenes	Carnosol *	Down	0.005197	5.86E-07
		Rosmanol	Down	8.77E-07	4.42E-09
	Hydroxyphenylpropenes	Acetyl eugenol	Down	1.35E-09	4.54E-07
	Hydroxycinnamaldehydes	Sinapaldehyde	Up	1.03E-09	3.54E-11
	Hydroxybenzoketones	3-Methoxyacetophenone *	Up	0.020033	0.010019
	Furanocoumarins	Xanthotoxin	Up	0.001288	0.001383
	Tyrosols	p-HPEA-EDA	Up	0.003026	0.01469
Lignans	Lignans	Dimethylmatairesinol *	Down	0.004767	3.32E-07
		Cyclolariciresinol	Down	0.003949	0.003149
		1-Acetoxypinoresinol	Up	0.002295	0.001418

Metabolites are reported according to the chemical class and sub-class of the compounds. The up- and down-regulation with the corresponding p values, as a result of the Volcano analysis ($p \leq 0.05$, fold-change cut-off = 2.0), are reported. Each compound reported in the Table had the same regulation (up or down) in Tahitian samples in both comparisons. The fold change of up and down regulation and other statistics have been reported in ***Supplementary Table 3****.*

** Compounds also recognized as discriminant via OPLS-DA analysis.*

TABLE 4 | Exclusive metabolites differentiating Tahitian and PNG samples.

Class	Sub class	Compound	Regulation	*p*-value
FP BATCH1 vs. PNG: EXCLUSIVE COMPOUNDS				
Flavonoids	Flavones	Apigenin 6,8-di-C-glucoside	Down	0.005157
	Flavanones	6-Geranylnaringenin *	Up	1.46E-08
	Flavanols	(+)-Catechin	Down	1.23E-02
		(+)-Catechin 3-O-glucose	Up	1.08E-05
	Flavonols	Kaempferol *	Up	1.00E-05
		Isorhamnetin 3-O-glucuronide	Up	5.36E-04
	Anthocyanins	Cyanidin *	Up	8.94E-06
Phenolic acids	Hydroxycinnamic acids	3-Feruloylquinic acid	Up	2.81E-04
Other polyphenols	Hydroxybenzoketones	3,4-dihydroxyphenyl-2-oxypropanoic acid *	Up	9.65E-05
	Curcuminoids	Bisdemethoxycurcumin *	Up	1.26E-08
Lignans	Lignans	Arctigenin	Up	0.011521
FP BATCH2 vs. PNG: EXCLUSIVE COMPOUNDS				
Flavonoids	Flavones	Cirsimaritin	Down	0.001366
		5,6-Dihydroxy-7,8,3′,4′-tetramethoxyflavone	Up	2.21E-07
		Chrysoeriol 7-O-glucoside	Down	0.001481
		Tetramethylscutellarein	Up	0.01319
		Nobiletin	Up	1.30E-04
		6-Hydroxyluteolin 7-O-rhamnoside	Up	6.57E-06
	Flavanones	Pinocembrin	Down	7.65E-07
		Naringenin 7-O-glucoside *	Down	0.015904
		Naringin 6′-malonate	Up	0.016008
	Flavanols	(-)-Epigallocatechin *	Down	2.67E-08
	Flavonols	Kaempferide *	Up	3.09E-09
		Isorhamnetin 3-O-galactoside	Up	0.022369
		Spinacetin 3-O-glucosyl-(1-6)-glucoside	Up	0.001063
		3,7-Dimethylquercetin	Up	0,00106
		Quercetin 3-O-acetyl-rhamnoside	Up	1.41E-08
	Anthocyanins	Malvidin 3-O-arabinoside	Down	0.001473
	Dihydroflavonols	Dihydroquercetin	Down	0.024123
	Isoflavonoids	6″-O-Malonyldaidzin	Down	0.009957
	Chalcones	Xanthohumol	Up	4.56E-04
Stilbenes	Stilbenes	Pinosylvin	Up	0.021468
		d-Viniferin	Up	0.016183
Phenolic acids	Hydroxycinnamic acids	Rosmarinic acid	Down	2.39E-04
		Caffeoyl tartaric acid	Down	2.65E-04
		Hydroxycaffeic acid	Up	1.80E-07
		Avenanthramide 2c	Up	0.012336
		Avenanthramide 2f	Up	0.010568
		Feruloyl glucose	Up	1.60E-05
	Hydroxyphenylpropanoic acids	Dihydro-p-coumaric acid	Up	3.94E-07
	Hydroxyphenylacetic acids	3,4-Dihydroxyphenylacetic acid	Up	0.001156
	Hydroxybenzoic acids	Gallic acid ethyl ester	Up	1.07E-04
Other polyphenols	Other polyphenols	Pyrogallol	Up	1.68E-04
	Alkylphenols	5-Pentadecylresorcinol	Down	5.06E-05
		5-Heneicosylresorcinol	Up	0.006515
	Hydroxycoumarins	Esculin	Down	9.51E-07
	Hydroxybenzoketones	2,3-Dihydroxy-1-guaiacylpropanone *	Up	0.003059
	Alkylmethoxyphenols	4-Vinylsyringol	Up	0.013802

By matching the differential metabolites from the two Volcano analyses, these metabolites were present only in the pods of batch1 or only in batch2. Metabolites are reported according to the chemical class and sub-class of the compounds. The up- and down-regulation and the corresponding p values, as a result of the Volcano analysis ($p \leq 0.05$, fold-change cut-off = 2.0), are reported. The fold change of up and down regulation and other statistics have been reported in ***Supplementary Table 3****.*

**Compounds also recognized as discriminant via OPLS-DA analysis.*

by phenolic acids and by a high number of compounds classified as other polyphenols. Small, albeit significant was the presence of stilbenes, such as resveratrol, molecules that have recently been widely studied, mainly in grapevine, for their role in protecting plants against diseases (Bavaresco et al., 2016) and for their health benefits because of a potent antioxidant activity (Marques et al., 2009). It was noted that out of five differential stilbenes, four were highly up-regulated in Tahitian samples.

Unsupervised cluster analysis (**Figure 1**) clearly evidenced that the whole phenolic profile was able to separate the three batches in different clusters based on the origin: PNG vanilla was clearly different from FP vanilla. Likely, the differences between Tahitian and PNG phenolic profiles were a consequence of the combination of the environment and the adopted curing technologies between FP and PNG. Indeed, being the exact composition of the *V.* ×*tahitensis* sample from PNG unknown, in principle, we cannot completely exclude also a possible effect of genotype. According to us, the genetic effect, in this case, should be less probable considering that cultivars "Haapape" and "Tahiti," the two mainly produced cultivars in FP (being "Haapape" the first and "Tahiti" the second most frequently grown cultivars) are also the most widespread cultivars out of FP and in particular in PNG. Further, two phenolic patterns could be distinguished, within the Tahitian main cluster, basically separating the pods from FP batches 1 and 2, and in this case the differences could be mainly a consequence of the different genotypes (Haapape and Tahiti) being the curing method the same and the environmental conditions more similar and uniform. Considering the whole data set, two pods of batch2 were placed within the batch1 cluster. These results confirmed that the pods of FP batch1 have a uniform phenolic profile strongly supporting their belonging to the single cultivar "Haapape." On the other hand, the FP batch2 was confirmed as a mixture of cultivars and, considering that the 10 pods representing batch2 were randomly selected for the analysis, the most likely scenario is that eight out of ten analyzed pods belong to "Tahiti" and two out of ten belong to "Haapape."

The OPLS-DA analysis confirmed the results of the cluster analysis, clearly separating the three batches according to their origin (**Figure 2**), and evidenced that 23 differential metabolites (mainly flavonoids, 12 out of 23 compounds, **Table 1** and **Figure 2**) can provide the same separation power as the cluster analysis. Taken together, these results support the utility of metabolomics in: separating pods based on a different origin and eventually on the different cultivars, even if vines were cultivated in the same area and the pods were processed using the same method; finding the most discriminant metabolites on which eventually base the development of traceability procedures.

Pairwise comparisons were carried out through Volcano plot analysis in order to identify the up- and down-accumulated compounds that can be more interesting in discriminating the different samples. A first comparison was carried out between the two Tahitian samples (**Table 2**). In this case, 21 compounds were detected to be highly up- or down-accumulated between the two groups (the fold change and the relative abundance of the compounds in the samples is reported in **Supplementary Table 3**). About half of these compounds were up-regulated in "Haapape" with respect to the mixture. The main differences were among flavonoids (particularly flavonols) and phenolic acids (mainly hydroxycinnamic acids). Amongst flavonols, three compounds were respectively up- and down-regulated in "Haapape"; among cinnamic acids, three and one compounds were respectively up- and down-regulated in the same treatment. These differences can be a consequence of genetic differences between the two cultivars. Indeed, the "Haapape" and "Tahiti" genotypes share common genetic markers, but they differ in their ploidy level, with "Tahiti" being diploid and "Haapape" tetraploid (Lepers-Andrzejewski et al., 2011). This difference can be reflected in a different metabolomics composition of the pods.

By matching the two pairwise comparisons, FP batch1 vs. PNG and FP batch2 vs. PNG, the differential metabolites could be separated in two categories: compounds common between the two comparisons (46 metabolites, **Table 3**) and compounds exclusive of the single comparisons (7 and 36 metabolites, respectively, **Table 4**). Among the metabolites reported in **Table 3**, generally, flavonoids and phenolic acids were the most abundant classes of compounds. Being shared in both pairwise comparisons, we can postulate that these metabolites were independent of the genotype and mainly related to the different origin. This hypothesis is strengthened by the fact that, in both comparisons, the trend of accumulation was always the same for all the compounds reported in **Table 3**. Furthermore, most of the discriminant metabolites were up-regulated in "Tahitian" batches as compared to the PNG group.

As reported before, the particular cultivar(s) of the PNG sample was/were unknown; nevertheless between batch1 and PNG and between batch2 vs. PNG there were, respectively, 7 and 36 differential molecules. Considering this, the phenolic profile of the PNG sample was more similar to that of batch1 (cultivar "Haapape"), supporting a hypothesis that PNG pods can belong to the cultivar "Haapape" and that the main differences between the two batches are mainly a consequence of the different origin.

Regardless of the cultivar(s) considered, a significantly higher number of differential metabolites was pointed out when geographical origin was adopted as classification criterion under all statistics applied. Similarly, unsupervised hierarchical clustering evidenced that origin was the principal classification parameter. Although discrimination of origin via metabolomics was effective, specific markers could not be pointed out. Indeed, the discrimination potential is related to the actual profile of a wide variety of phenolic compounds, both in terms of their identity and abundance, with flavonoids and hydroxycinnamic acids playing a major role.

Considering our phenolic profiling approach has not been described previously, it becomes difficult to compare our results with markers previously reported in the literature. Nonetheless, most of the markers are aroma-related compounds that are likely more informative regarding vanilla quality rather than its origin. Vanillin is a phenolic aldehyde and one of the most important compounds in the primary extracts from vanilla beans as well as the principal flavor and aroma compound in vanilla. Brunschwig et al. (2016) have reported a significant difference in vanillin content between *V.* ×*tahitensis* grown and processed in PNG and

in Tahiti, with a higher concentration in samples from PNG. In this case, vanillin values were significantly different among the three batches by ANOVA, but vanillin was not identified as one of the most differential compounds evidenced by Volcano analysis. This meant that, while a significantly different content of vanillin was present, the fold change value was lower than 2.0 (cut-off value adopted in the Volcano analysis) and that vanillin was not among the compounds mainly influenced by the origin under the present condition of analysis. This difference with respect to Brunschwig et al. (2016) can be a consequence of the different extraction method and of the different analytical technique. On the other hand, it is important to stress out that having several markers is expected to strengthen the discrimination capability of the analytical approach. With this regard, metabolomics followed by multivariate chemometrics is among the approaches gaining most of the popularity in traceability. Important characteristic constituents of *V.* ×*tahitensis* anisyl derivatives (anisyl alcohol, anisaldehyde, methyl anisate, anisyl formate, and anisyl acetate), which were previously detected by HPLC analysis (Brunschwig et al., 2009), were not found as discriminant in this study. However, this can be easily ascribed to their volatility that hampered their ionization efficiency at the electrospray interface. On the other hand, although these compounds are known to play an important role in the vanilla aroma, the whole phenolic profile was wide and differed under both a qualitative and quantitative point of view. With this regard, the latter appeared to be more informative for traceability purposes.

As a conclusion, in the present study, metabolomics focused on the phenolic profile was successfully applied for the first time to *V.* ×*tahitensis* in order to increase our knowledge of vanilla metabolome for traceability purposes. Among the results, the most significant were: (1) the discrimination of the samples based on their origin: PNG samples were clearly different from Tahitian samples; this variation could be mainly related to the different origin (i.e., a combination of pedo-climatic conditions and curing methods adopted in the two countries); (2) the grouping of the Tahitian samples based on the two patterns, which could be explained considering that the first sample corresponded to only one cultivar ("Haapape") while the second one was a mix of 2 cultivars ("Haapape" and "Tahiti"). These findings evidenced the utility of the metabolomics analysis to detect a high number of discriminating compounds; this possibility, in combination with robust multivariate chemometrics, might open to the possibility to develop a standard procedure for traceability and authentication based on the metabolic profile of the pods. Of course, further studies are necessary to deepen our vision on vanilla metabolome and on the metabolic variations correlated with the cultivars and the origins, in order to detect and then validate selected highly discriminant compounds suitable for authentication. Finally, our deep profiling approach allowed the annotation of unexpected phenolic components, not yet reported, whose presence could be linked to the medicinal properties of vanilla. Polyphenols, such as those identified in this study, significantly benefit human health (Del Rio et al., 2013) and they can deserve further perspective assessments for an up-dated pharmaceutical valuation of vanilla.

AUTHOR CONTRIBUTIONS

MB designed the study, in cooperation with PR and JF. CB, SL, LB, GS, and JB carried out the plant experiments, contributed to interpretation of data and drafted the manuscript. LL developed the mass spectrometric method, performed statistics and helped to draft the manuscript. MB, PR, and JF draft and critically revise the manuscript. All authors read and approved the final manuscript.

ACKNOWLEDGMENTS

We are grateful to Dr. Sergie Bang (NARI) for providing *V.* ×*tahitensis* pods from Papua New Guinea.

SUPPLEMENTARY MATERIAL

The Supplementary Material for this article can be found online at: https://www.frontiersin.org/articles/10.3389/fpls.2017.01746/full#supplementary-material

Supplementary Table 1 | A full list of the 260 phenolic compounds is provided.

Supplementary Table 2 | The compounds, significantly different among the three samples (one-way ANOVA, multiple testing correction, *p*-value 0.05), are reported with the corresponding *P*-value.

Supplementary Table 3 | The results of the volcano plot analysis reporting, for each pairwise comparison, the compounds characterized by a fold change higher than 2.

REFERENCES

Bavaresco, L., Lucini, L., Busconi, M., Flamini, R., and De Rosso, M. (2016). Wine resveratrol: from the ground up. *Nutrients* 8:222. doi: 10.3390/nu8040222

Bouriquet, G. (1954). *Le vanillier et la vanille dans le monde*. Paris: Paul Lechevalier.

Brunschwig, C., Collard, F. X., Bianchini, J. P., and Raharivelomanana, P. (2009). Evaluation of chemical variability of cured vanilla beans (*Vanilla tahitensis* and *Vanilla planifolia*). *Nat. Prod. Commun.* 4, 1393–1400.

Brunschwig, C., Rochard, S., Pierrat, A., Rouger, A., Senger-Emonnot, P., George, G., et al. (2016). Volatile composition and sensory properties of *Vanilla* ×*tahitensis* bring new insights for vanilla quality control. *J. Sci. Food Agric.* 96, 848–858. doi: 10.1002/jsfa.7157

Brunschwig, C., Senger-Emonnot, P., Aubanel, M. L., Pierrat, A., George, G., Rochard, S., et al. (2012). Odor-active compounds of Tahitian vanilla flavor. *Food Res. Int.* 46, 148–157. doi: 10.1016/j.foodres.2011.12.006

Bythrow, J. D. (2005). Historical perspective: vanilla as a medicinal plant. *Semin. Integr. Med.* 3, 129–131. doi: 10.1016/j.sigm.2006.03.001

Costantin, J., and Bois, D. (1915). Sur trois types de vanilles commerciales de Tahiti. *Comp. Rend. Acad. Sci.* 161, 196–202.

Del Rio, D., Rodriguez-Mateos, A., Spencer, J. P. E., Tognolini, M., Borges, G., and Crozier, A. (2013). Dietary (Poly)phenolics in human health: structures, bioavailability, and evidence of protective effects against chronic diseases. *Antioxid. Redox Signal.* 18, 1818–1892. doi: 10.1089/ars.2012.4581

Duke, J. A., Bogenschutz-Gowin, M. J., Du Cellier, J., and Duke, P. K. (2003). *CRC Handbook of Medicinal Spice*. Boca Raton, FL: CRC Press.

Florence, J., and Guérin, M. (1996). A propos de la vanille à Tahiti. *L'orchidée* 13, 84–87.

Gu, F., Chen, Y., Hong, Y., Fang, Y., and Tan, L. (2017). Comparative metabolomics in vanilla pod and vanilla bean revealing the biosynthesis of vanillin during the curing process of vanilla. *AMB Express* 7:116. doi: 10.1186/s13568-017-0413-2

Hernandez, J., and Lubinsky, P. (2011). "Cultivation systems," in *Vanilla: Medicinal and Aromatic Plants – Industrial* Profiles, eds M. Grisoni and E. Odoux (Boca Raton, FL: CRC Press/Taylor and Francis), 75–96.

Hondrogiannis, E., Rotta, K., and Zapf, C. M. (2013). The use of wavelength dispersive X-ray fluorescence in the identification of the elemental composition of vanilla samples and the determination of the geographic origin by discriminant function analysis. *J. Food Sci.* 78, C395–C401. doi: 10.1111/1750-3841.12050

Journal Officiel de la Polynésie Française (2014). *Arrêté no 960 CM du 26 juin 2014 portant définition de l'appellation d'origine "Vanille de Tahiti"*. 8210–8214.

Journal Officiel de la Polynésie Française (2016). *Arrêté no 1111 CM du 10 août 2016 portant définition de l'appellation d'origine "Vanille de Tahiti"*. 9169–9175

King, J., Felter, H. W., and Lloyd, J. U. (1898). *King's American Dispensary*. Cincinnati: Ohio Valley Co.

Klockmann, S., Reiner, E., Bachmann, R., Hackl, T., and Fischer, M. (2016). Food fingerprinting: metabolomic approaches for geographical origin discrimination of hazelnuts (*Corylus avellana*) by UPLC-QTOFMS. *J. Agric. Food Chem.* 64, 9253–9262. doi: 10.1021/acs.jafc.6b04433.

Kumar, S. S., Priyadarsini, K. I., and Sainis, K. B. (2002). Free radical scavenging activity of vanillin and o-vanillin using 1,1-diphenyl-2-picrylhydrazyl (DPPH) radical. *Redox Rep.* 7, 35–40. doi: 10.1179/135100002125000163

Lepers-Andrzejewski, S., Brunschwig, C., Collard, F. X., and Dron, M. (2010). "Morphological, chemical, sensory and genetic specificities of Tahitian vanilla", in *Vanilla: Medicinal and Aromatic Plants – Industrial Profiles,* eds M. Grisoni and E. Odoux (Boca Raton, FL: CRC Press/Taylor and Francis), 205–228.

Lepers-Andrzejewski, S., Causse, S., Caromel, B., Wong, M., and Dron, M. (2012). Genetic linkage map and diversity analysis of Tahitian vanilla (*Vanilla ×tahitensis*, *Orchidaceae*). *Crop Sci.* 52, 795–806. doi: 10.2135/cropsci2010.11.0634

Lepers-Andrzejewski, S., and Dron, M. (2010). "Vanilla production in French Polynesia," in *Vanilla: Medicinal and Aromatic Plants - Industrial Profiles*, eds M. Grisoni and E. Odoux (Boca Raton, FL: CRC Press/Taylor and Francis), 205–228.

Lepers-Andrzejewski, S., Siljak-Yakovlev, S., Brown, S. C., Wong, M., and Dron, M. (2011). Diversity and dynamics of plant genome size: an example of polysomaty from a cytogenetic study of Tahitian vanilla (*Vanilla ×tahitensis*, Orchidaceae). *Am. J. Bot.* 98, 1–12. doi: 10.3732/ajb.1000415

Lubinsky, P., Cameron, K. M., Molina, M. C., Wong, M., Lepers-Andrzejewski, S., Gómez-Pompa, A., et al. (2008). Neotropical roots of a Polynesian spice: the hybrid origin of tahitian vanilla, *Vanilla tahitensis* (*Orchidaceae*). *Am. J. Bot.* 95, 1040–1047. doi: 10.3732/ajb.0800067

Lucini, L., Pellizzoni, M., Pellegrino, R., Molinari, G. P., and Colla, G. (2015). Phytochemical constituents and *in vitro* radical scavenging activity of different *Aloe* species. *Food Chem.* 170, 501–507. doi: 10.1016/j.foodchem.2014.08.034

Lucini, L., Rocchetti, G., Kane, D., and Trevisan, M. (2017). Phenolic fingerprint allows discriminating processed tomato products and tracing different processing sites. *Food Control* 73, 696–703. doi: 10.1016/j.foodcont.2016.09.020

Mac Gregor, A. (2005). *Diversification into High Value Export Product: Case Study of the Papua New Guinea Vanilla Industry. Agricultural Management, Marketing and FINANCE Service (AGSF Working Document 2*). Rome: Agricultural Support Systems Division, Food and Agricultural Organization of the United Nations.

Marques, F. Z., Markus, M. A., and Morris, B. J. (2009). Resveratrol: cellular actions of a potent natural chemical that confers a diversity of health benefits. *Int. J. Biochem. Cell Biol.* 41, 2125–2128. doi: 10.1016/j.biocel.2009.06.003

Maurya, D. K., Adikari, S., Nair, C. K. K., and Devasagayam, T. P. A. (2007). DNA protective properties of vanillin against gamma-radiation under different conditions: possible mechanisms. *Mutat. Res. Genet. Toxicol. Environ. Mutagen.* 634, 69–80. doi: 10.1016/j.mrgentox.2007.06.003

Oliveira, R. C. S., Oliveira, L. S., Franca, A. S., and Augusti, R. (2009). Evaluation of the potential of SPME–GC–MS and chemometrics to detect adulteration of ground roasted coffee with roasted barley. *J. Food Comp. Anal.* 22, 257–261. doi: 10.1016/j.jfca.2008.10.015

Oms-Oliu, G., Odriozola-Serrano, I., and Martin-Belloso, O. (2013). Metabolomics for assessing safety and quality of plant-derived food. *Food Res. Int.* 54, 1172–1183. doi: 10.1016/j.foodres.2013.04.005

Palama, T. L., Fock, I., Choi, Y. H., Verpoorte, R., and Kodja, H. (2010). Biological variation of *Vanilla planifolia* leaf metabolome. *Phytochemistry* 71, 567–573. doi: 10.1016/j.phytochem.2009.12.011

Palama, T. L., Khatib, A., Choi, Y. H., Côme, B., Fock, I., Verpoorte, R., et al. (2011). Metabolic characterization of green pods from *Vanilla planifolia* accessions grown in La Réunion. *Environ. Exp. Bot.* 72, 258–265. doi: 10.1016/j.envexpbot.2011.03.015

Palama, T. L., Khatib, A., Choi, Y. H., Payet, B., Fock, I., Verpoorte, R., et al. (2009). Metabolic changes in different developmental stages of *Vanilla planifolia* pods. *J. Agric. Food Chem.* 57, 7651–7658. doi: 10.1021/jf901508f

Pérez-Silva, A., Odoux, E., Brat, P., Ribeyre, F., Rodriguez-Jimenes, G., Robles-Olvera, V., et al. (2006). GC-MS and GC-olfactometry analysis of aroma compounds in a representative organic aroma extract from cured vanilla (*Vanilla planifolia* G. Jackson) beans. *Food Chem.* 99, 728–735. doi: 10.1016/j.foodchem.2005.08.050

Rain, P., and Lubinsky, P. (2011). "Vanilla use in colonial Mexico and traditional Totonac vanilla farming," in *Vanilla: Medicinal and Aromatic Plants – Industrial Profile*, eds M. Grisoni and E. Odoux (Boca Raton, FL: CRC Press/Taylor and Francis), 251–260.

Rohman, A., and Man, Y. B. C. (2012). The chemometrics approach applied to FTIR spectral data for analysis of rice bran oil in extra virgin olive oil. *Chemometr. Intell. Lab.* 110, 129–134. doi: 10.1016/j.chemolab.2011.10.010

Rombouts, C., Hemeryck, L. Y., Van Hecke, T., De Smet, S., De Vos, W. H., and Vanhaecke, L. (2017). Untargeted metabolomics of colonic digests reveals kynurenine pathway metabolites, dityrosine and 3-dehydroxycarnitine as red versus white meat discriminating metabolites. *Sci. Rep.* 7:42514. doi: 10.1038/srep42514

Rothwell, J. A., Perez-Jimenez, J., Neveu, V., Medina-Remón, A., M'hiri, N., García-Lobato, P., et al. (2013). Phenol-Explorer 3.0: a major update of the Phenol-Explorer database to incorporate data on the effects of food processing on polyphenol content. *Database (Oxford)* 2013:bat070. doi: 10.1093/database/bat070

Ruiz-Samblás, C., Tres, A., Koot, A., Van de Ruth, S. M., González-Casado, A., and Cuadros-Rodríguez, L. (2012). Proton transfer reaction-mass spectrometry volatile organic compound fingerprinting for monovarietal extra virgin olive oil identification. *Food Chem.* 134, 589–596. doi: 10.1016/j.foodchem.2012.02.135

Sølvbjerg Hansen, A. M., Fromberg, A., and Frandsen, H. L. (2014). Authenticity and traceability of vanilla flavors by analysis of stable isotopes of carbon and hydrogen. *J. Agric. Food Chem.* 62, 10326–10331. doi: 10.1021/jf503055k

Soto Arenas, M. A. (2003). "Vanilla (generic treatment)," in *Genera Orchidacearum, Vol. 3, Orchidoideae (Part two), Vanilloideae*, eds A. M. Pridgeon, P. J. Cribb, M. W. Chase, and F. N. Rasmussen (Oxford: Oxford University Press), 321–334.

Soto Arenas, M. A., and Dressler, R. L. (2010). A revision of the mexican and central American species of *Vanilla Plumier* ex Miller with a characterisation of their ITS region of the nuclear ribosoma DNA. *Lankesteriana* 9, 285–354. doi: 10.15517/lank.v0i0.12065

Takahashi, M., Inai, Y., Miyazawa, N., Kurobayashi, Y., and Fujita, A. (2013). Identification of the key odorants in Tahitian cured vanilla beans (*Vanilla tahitensis*) by GC-MS and an aroma extract dilution analysis. *Biosci. Biotechnol. Biochem.* 77, 601–605. doi: 10.1271/bbb.120840

Teuscher, E., Anton, R., and Lobstein, A. (2005). *Plantes Aromatiques: Épices, Aromates, Condiments et Huiles Essentielles.* Paris: Tec & Doc Lavoisier.

Vardin, H., Tay, A., Ozen, B., and Mauer, L. (2008). Authentication of pomegranate concentrate using FTIR spectroscopy and chemometrics. *Food Chem.* 108, 742–748. doi: 10.1016/j.foodchem.2007.11.027

Conflict of Interest Statement: The authors declare that the research was conducted in the absence of any commercial or financial relationships that could be construed as a potential conflict of interest.

frontiers in Plant Science

ORIGINAL RESEARCH
published: 05 July 2018
doi: 10.3389/fpls.2018.00983

Latitude and Altitude Influence Secondary Metabolite Production in Peripheral Alpine Populations of the Mediterranean Species *Lavandula angustifolia* Mill.

*Sonia Demasi[1], Matteo Caser[1], Michele Lonati[1], Pier L. Cioni[2], Luisa Pistelli[2], Basma Najar[2] and Valentina Scariot[1]**

[1] Department of Agricultural, Forest and Food Sciences, University of Torino, Grugliasco, Italy, [2] Department of Pharmacy, University of Pisa, Pisa, Italy

OPEN ACCESS

Edited by:
Marta Sousa Silva, Universidade de Lisboa, Portugal

Reviewed by:
Ligia Salgueiro, University of Coimbra, Portugal
Inger Martinussen, Norwegian Institute of Bioeconomy Research (NIBIO), Norway

***Correspondence:**
Valentina Scariot
valentina.scariot@unito.it

Specialty section:
This article was submitted to Plant Metabolism and Chemodiversity, a section of the journal Frontiers in Plant Science

Received: *20 April 2018*
Accepted: *18 June 2018*
Published: *05 July 2018*

Citation:
Demasi S, Caser M, Lonati M, Cioni PL, Pistelli L, Najar B and Scariot V (2018) Latitude and Altitude Influence Secondary Metabolite Production in Peripheral Alpine Populations of the Mediterranean Species Lavandula angustifolia Mill. Front. Plant Sci. 9:983. doi: 10.3389/fpls.2018.00983

Lavandula angustifolia Mill. has a great economic importance in perfumery, cosmetics, food manufacturing, aromatherapy, and pharmaceutical industry. This species finds its phytosociological optimum in the sub-Mediterranean region. Latitudinal and altitudinal gradients are expected to affect species diversification in peripheral alpine populations. In this study, phenotypic traits including morphometric parameters, volatile organic compounds (VOCs) and essential oils (EOs) were analyzed in lavender peripheral populations selected in order to explore different ecological conditions. Plants were cultivated under uniform conditions to observe variations due to the genetic adaptation to native environments and to exclude the short-term response to environmental factors. Results showed qualitatively and quantitatively intra-specific variations in secondary metabolites, mainly along the latitudinal gradient, while minor effect was attributable to the altitude. This latter affected more the morphometric parameters. As the latitude augmented, VOCs showed lower content of monoterpene hydrocarbon (mh) and higher content of oxygenated monoterpenes (om); whereas EOs showed higher content of mh and non-terpene derivatives (nt) and lower content of sesquiterpene hydrocarbons (sh). Lavender aroma and EO composition varied in every population, for a total of 88 and 104 compounds identified, respectively. Eleven and 13 compounds were responsible for 95% of the dissimilarity, with linalool, linalyl acetate and 1,8-cineole as major contributors. As the latitude augmented, linalool decreased and 1,8-cineole increased while linalyl acetate content was unaffected. These results are discussed with regards to the potential adoption of the lavender peripheral alpine populations for the improvement of quality and productivity of lavender cultivations, especially in mountainous areas.

Keywords: lavender, Lamiaceae, volatile organic compounds, essential oils, ecological gradient

INTRODUCTION

The genus *Lavandula* (Lamiaceae family) comprises approximately 39 species, with a natural occurrence in the Mediterranean region, to the Arabian Peninsula, South West Asia and India (Lis-Balchin, 2003). This genus is constituted by small evergreen shrubs, with aromatic foliage and flowers, and due to its great economic importance this genus was the subject of several studies. Indeed, 1,000 tons of lavandin essential oil (*L.* × *intermedia* Emeric ex Loisel., EO) are produced worldwide every year, while only 200 tons of EO from lavender (*L. angustifolia* Mill.) together with 200 tons of EO from spike lavender (*L. latifolia* Medik.) are produced (Lesage-Meessen et al., 2015). Lavender dried flowers and EOs are commonly employed in perfumery and cosmetics, food manufacturing and aromatherapy (Cavanagh and Wilkinson, 2002; Gonçalves and Romano, 2013; Prusinowska and Smigielski, 2014). Biological and antioxidant properties of lavender EO have been extensively assessed (Cavanagh and Wilkinson, 2002; Raut and Karuppayil, 2014; Shahdadi et al., 2017). Numerous therapeutic activities have been reported, such as convulsion relief, anxiety and depression improvement, along with a positive effect to treat several neurological disorders (Cavanagh and Wilkinson, 2002; Caputo et al., 2016; López et al., 2017; Rahmati et al., 2017). The highest quality lavender oil comes from *L. angustifolia* (syn. *L. spica* L., *L. officinalis* Chaix., *L. vera* DC.) inflorescences, which contain high levels of linalyl acetate and linalool and low amount of camphor, considered positive features by both cosmetic and pharmaceutical industry (Cavanagh and Wilkinson, 2002; Kim and Lee, 2002; Shellie et al., 2002). Although the genus *Lavandula* has been widely studied in wild and controlled environment (Da Porto and Decorti, 2008; Da Porto et al., 2009; González-Coloma et al., 2011; Gonçalves and Romano, 2013; Pistelli et al., 2013, 2017; Hassiotis et al., 2014; Lesage-Meessen et al., 2015; Caputo et al., 2016; Kirimer et al., 2017; López et al., 2017; Rahmati et al., 2017), lavender aroma profile and its EO composition are continuously subjected to many investigations (Prusinowska and Smigielski, 2014).

Secondary metabolites from plants are involved in several functions such as attraction for pollinators, signaling between plants, defense and protection against biotic and abiotic stresses (Knudsen et al., 2006; Bakkali et al., 2008; Dudareva et al., 2013; Raut and Karuppayil, 2014; Nogués et al., 2015; Caser et al., 2016, 2017). The plant-environment interaction largely contributes to the phytochemicals expression (Kesselmeier and Staudt, 1999; Binns et al., 2002; Dudareva et al., 2013; Holopainen et al., 2013; Selmar and Kleinwächter, 2013; Loreto et al., 2014), and has already been proved to affect the chemical composition of lavender (Prusinowska and Smigielski, 2014). However, the variability in the emission of volatile organic compounds (VOCs) and in the EO biosynthesis is also evidently regulated by genetics, even though the mechanisms involved still need clarifications (Kesselmeier and Staudt, 1999; Sangwan et al., 2001; Brahmkshatriya and Brahmkshatriya, 2013). The intra-specific variation in secondary metabolite production in plants has been reviewed and explained by genetic drift, relaxed selective pressure, introgression of traits through hybridization, gene pleiotropic effects, and phenotypic plasticity (Eckert et al., 2008; Raguso, 2008; Dicke and Loreto, 2010). For instance, qualitatively and quantitatively differences in secondary metabolites have been reported not only between wild and cultivated plants (*L. luisieri*, González-Coloma et al., 2011), but also among plants of the same wild population, as described in lavandin of northwest Italy (Maffei and Peracino, 1993; Peracino et al., 1994) and in *L. latifolia* (Muñoz-Bertomeu et al., 2007).

The populations of plants that are geographically situated at the peripheral limit of a species distribution range are usually expected to exhibit lower abundance and intra-genetic diversity, according to the widely accepted "abundant center model." Moreover, a higher genetic differentiation than populations at the center is likely to occur (Eckert et al., 2008). Altitudinal gradient was also proved to affect species diversification in peripheral populations of *L. latifolia* (Herrera and Bazaga, 2008). Unfortunately, intra-specific studies on secondary metabolites production performed in plants in different environmental conditions do not inform whether the observed variations represent the genetic adaptation to specific environments, or the short-term response to environmental factors (Spitaler et al., 2006). Thus, trials under uniform cultivation practices are preferable to limit environmental influence on plant secondary metabolite production.

This study aimed to investigate if the environment differences, such as latitude and altitude, affected peripheral population diversification of *L. angustifolia*. Morphology, VOCs, and EOs were analyzed in lavender plants collected along both latitudinal and altitudinal gradients in West Alps (Italy), and grown in pots under uniform conditions, looking for traits of productive interest.

MATERIALS AND METHODS

Native Environment

Lavender (*L. angustifolia*) is widespread throughout Italy (Pignatti, 1982), where it is a common component of low-growing shrub vegetation on calcareous soils. *Lavandula angustifolia* finds its phytosociological optimum in the sub-Mediterranean region within the order *Ononidetalia*, that describes meso-xerophile, basophile, supra-oromediterranean vegetation communities (Theurillat et al., 1995). It is the only species naturally occurring in the West Italian Alps (Piedmont region). Nine peripheral populations (**Figure 1**) were selected according to the natural range of distribution of the species (Pignatti, 1982), in order to explore different ecological conditions (**Table 1**, Supplementary Figure 1) in terms of latitude (Susa Valley in the northern range, Stura Valley in the core areas, and Tanaro Valley in the southern part of the Piedmont region) and altitude (low, medium and high altitude). Susa Valley represents the highest latitudinal range of distribution of the

Abbreviations: AC, Apocarotenoids; EO, Essential Oils; GC-MS, Gas Cromatography-Mass Spectrometry; GI, Growth Index; MH, Monoterpene Hydrocarbons; NT, Non Terpene Derivatives; OM, Oxygenated Monoterpenes; OS, Oxygenated Sesquiterpenes; SH, Sesquiterpene Hydrocarbons; SPME, Solid Phase Micro Extraction; VOCs, Volatile Organic Compounds.

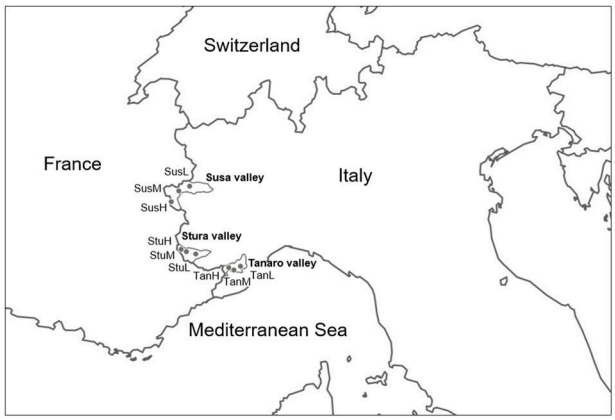

FIGURE 1 | Geographical origin of the nine *L. angustifolia* populations analyzed in this study. For the significance of the population codes, see **Table 1**.

species in the Alps (Aeschimann et al., 2004). As the latitude decreases (from Susa to Tanaro Valley), the annual rainfalls decrease and yearly temperatures increase, thus there is a clear ecological gradient moving toward the typical Mediterranean conditions (Fick and Hijmans, 2017).

Plant Material and Pot Cultivation

Portions of lavender branches were collected from wild plants during the flowering season of 2014, from August to September. In each of the nine selected sites, the main area of lavender distribution was identified as a central point and from there, an area with a radius of 10 m was plotted. Inside that area, 10 individuals were randomly chosen and twenty cuttings were immediately prepared from each individual. Specimens are currently available and cultivated in the DISAFA facilities (45°03′58.5″N; 7°35′29.1″E, WGS84 System). Cuttings were allowed to root in peat substrate under plastic tunnels in an organic nursery, specialized in medicinal and aromatic plants (Frat.lli Gramaglia, Collegno, Italy; 45°05′22.4″N, 7°34′26.4″E, 302 m. a.s.l.). In spring 2015, the percentage of successful rooting was calculated and the rooted plants were transplanted in pots, with a mixture of peat and green compost (70-30, % v/v) and transferred outdoors. Irrigation was provided when needed and manual weed control was performed. Plants were fertigated with NPK fertilizer (1:2:2) three times during spring and once during autumn. The cultivation cycle lasted two years and during the first one (Summer 2015), non-destructive VOC analysis was performed *in vivo* on flowered pot plants to characterize lavender aroma and evaluate their potential differences. As ecological characteristics of the sampling site did have an influence on lavender performance, during the second year (Summer 2016), biometric parameters and EOs were analyzed.

Plant Performance Evaluation

Biometric and morphological characteristics of 123 rooted flowered plants were evaluated once a week from the beginning of blooming, according to and implementing the guidelines of the International Union for the Protection of New Varieties of Plants (UPOV) proposed for lavenders. The selected parameters were: number of spikes per plant (n), spike length (cm), flowering time (% of flowered plants in each population per week), together with plant height (cm) and width (cm), used to calculate the Growth Index (i.e., the plant volume; cm^3) according to Demasi et al. (2017). The survival percentage was evaluated at the end of the second cultivation cycle.

VOCs Detection and Analysis

Emitted volatiles were analyzed using a Supelco (Bellofonte, USA) SPME device coated with polydimethylsiloxane (PDMS, 100 μm) in order to sample the headspace of each living/flowering plant. Plants of StuM population did not bloom, thus data on VOCs concerned eight populations, for a total of 33 plants. Sample was introduced individually into a 30 ml glass conical flask and allowed to equilibrate for 30 min. After the equilibration time, the fiber was exposed to the headspace for 15 min at room temperature; once sampling was finished, the fiber was withdrawn into the needle and transferred to the injector of the GC system, where the fiber was desorbed. GC-FID and GC-MS analyses were performed according to Pistelli et al. (2017) using a Varian CP-3800 apparatus (Paolo Alto, California, USA) equipped with a DB-5 capillary column (30 m × 0.25 mm i.d., film thickness 0.25 μm) and a Varian Saturn 2000 ion-trap mass detector. The oven temperature was programmed rising from 60°C to 240°C at 3°C/min; injector temperature, 220°C; transfer-line temperature, 240°C; carrier gas, He (1 ml/min).

Essential Oil Extraction and Analysis

Essential oil of lavender plants was obtained by hydro distillation of dried aerial parts of each sample using a Clevenger-type apparatus according to the Italian Pharmacopoeia (Helrich, 1990). Flowered plants of StuM population did not produce enough material to obtain EO, thus data on EOs concerned eight populations, for a total of 122 plants. The obtained EOs were immediately injected in GC-FID and GC-MS according to the method described in Pistelli et al. (2017). Identification of the constituents was based on the comparison of the retention times with those of authentic samples in comparing their linear retention indices (*LRI*) relative to a series of n-hydrocarbons, and on computer matching against commercial (Adams, 2007; NIST/EPA/NIH Mass Spectral Library, 2014) and home-made mass spectra library built up from pure substances and components of known EOs as well as MS literature data.

Statistical Analyses

Data were tested for the homogeneity of variance, then one-way ANOVA was performed to analyze latitude and altitude effect on biometric parameters and means were separated according to Ryan-Einot-Gabriel-Welsch-F post-hoc test (REGW-F). Statistically significant differences induced by latitude on chemical classes and compounds of VOCs and EO were assessed with the one-way ANOSIM with Euclidean-based similarity. The percentage contribution of each compound to the observed dissimilarity was assessed through the similarity percentage analysis (SIMPER, Euclidean distance). For each

TABLE 1 | Geographical characteristics and climatic conditions of *L. angustifolia* sampling sites in Piedmont region (West Italian Alps).

Code	Valley	Latitude (WGS84/32N)	Longitude (WGS84/32N)	Altitude (m a.s.l.)	Mean yearly temperature (°C)	Annual rainfall (mm year^{-1})	Precipitation of warmest quarter (mm June, July, August)
SusL	Susa	5001086	349052	910	9.8	859	202
SusM		4994234	334172	1260	7.7	976	213
SusH		4979650	323991	1570	4.8	1,208	232
StuL	Stura	4908484	357570	890	9.8	857	153
StuM		4914856	337635	1360	6.3	1,015	175
StuH		4911955	344807	1810	3.8	1,107	185
TanL	Tanaro	4891985	418508	600	10.4	867	136
TanM		4882887	406442	1240	7.8	969	154
TanH		4890065	402171	1710	5.8	1,036	170

compound the difference between valleys were tested with Mann-Whitney pairwise test. Besides, VOC and EO chemical classes were subjected to the regression analysis to investigate their eventual link to altitude or latitude of native environment. The value for statistical significance was $P < 0.05$. The ANOVA analysis was performed with SPSS software (version 22), while all other analyses were performed with Past software (version 3).

RESULTS AND DISCUSSION

Morphology and Performance of Cultivated Lavender

Lavenders of West Alps differently performed under cultivation, and influence of sea distance (latitude) or altitude of the native environment was observed in some biometric parameters (**Table 2**). Rooting percentage after 3 months in seed cells was generally below 40% and ranged among populations (SusH 23.9%, SusM 17.0%, SusL 38.0%; StuH 15.8%, StuM 9.6%, StuL 35.3%; TanH 37.5%, TanM 23.0%, TanL 39.5%). Rooting ability was therefore generally low, especially considering that selected lavender cultivars often reach 95% of successful rooting (Lis-Balchin, 2003). However, the propagation of wild adult plants by cutting is needed to produce genetically homogeneous individuals and the rooting percentage achieved in this study on *L. angustifolia* is considered of interest by local nurseries. Significant effects were observed due to both altitude and latitude of native environment, with a more successful rooting in plants evolved closer to the Mediterranean conditions (Tanaro) and from lower altitudes. The survival rate of rooted cuttings after 2 years of cultivation ranged between 54% (SusL) and 83% (StuL), but was independent from the geographical origin of the plants (**Table 2**). During the first cultivation cycle, 9% of pot lavenders bloomed, while in the second year, all plants bloomed (**Figure 2**); the first flowered plants were recorded on June 6th 2016 and the last on August 19th 2016. Interestingly, almost all lavenders of high populations flowered simultaneously in 1 week (SusH 100%, StuH 100%, and TanH 96%) regardless the latitude, followed by medium and low altitude populations, with the latter group defining a more gradual trend during summer. Knowledge of flowering times is essential to plan nursery activities (Lis-Balchin, 2003) or harvesting time for the production of EOs or dried flowers. Indeed, the nurseries can exploit lavenders with a flower production concentrated in a short period, since higher number of plants are available per sale. Furthermore, producers can optimize flower harvesting in the field when a simultaneous blooming occurs. Nonetheless, a gradual blooming can ensure flowered plants availability in the nursery and gardens for a longer period.

Altitude affected also morphological parameters and flower yield (**Table 2**). Contrariwise to low altitude groups, plants from higher elevation developed a more compact shrub (GI = 2,003 cm^3), with higher number (11.26) and longer spikes (37.8 cm) during cultivation, but producing lower yield of inflorescences (1.16 gDW/plant), attributable to a less number of flowers per spike. Altitudinal gradient effect has been previously observed in other Lamiaceae species, displaying lower height at high altitudes, to avoid wind damages and improve photosynthetic conditions (Kofidis and Bosabalidis, 2008 and references in it). However, compact plants can facilitate field operations, especially harvesting. Growth and number of flower spikes were influenced also by the population distance from the sea. Plants from Susa Valley showed a compact growth (GI = 1,886 cm^3) and a low number of flower spikes (5.4), contrary to what observed in Stura plants (GI = 3,706 cm^3 and 10.6). Tanaro plants were compact (GI = 2,470 cm^3) and produced a high number of spikes (8.8), showing an interesting habit for ornamental and field cultivation purposes. A latitudinal gradient in spike length and flower yield were not detected in the second cultivation cycle. These data could be helpful in the selection of alpine peripheral *L. angustifolia* populations with interesting traits for nurseries both for ornamental and production purposes.

Influence of Native Environment on Volatile Emission

The aroma profile represents the volatiles spontaneous emitted from the living plants and is a highly complex component of floral phenotype (Raguso, 2008). High intra and inter-specific variations in secondary metabolite production and aroma composition were reported in *Lavandula* genus, including *L. latifolia* and *L. luisieri* (Sanz et al., 2004; Muñoz-Bertomeu

TABLE 2 | Differences in rooting percentage, survival rate, growth index (GI), spike number and spike length recorded in the cultivated lavenders, according to altitude (High, Medium, and Low) and latitude (Susa, Stura, and Tanaro) of the native environment.

	Rooting (%)	Survival (%)	GI (cm^3)	Spike (n)	Spike length (cm)	Flower yield (g DW $plant^{-1}$)
ALTITUDE						
High	25.7 b[§]	67	2003 b	11.26 a	37.8 a	1.16 b
Medium	16.5 c	64	2125 ab	6.19 b	28.9 b	1.84 a
Low	37.6 a	69	3005 a	8.53 b	24.9 b	1.92 a
P	***	ns	*	**	***	*
LATITUDE						
Susa	26.3 b	66	1886 b	5.4 b	27.5	1.38
Stura	20.2 b	73	3706 a	10.6 a	30.5	1.84
Tanaro	33.3 a	61	2470 b	8.8 a	30.4	1.79
P	*	ns	**	**	ns	ns

[§]*Means followed by the same letter in the same column denote no significant differences according to REGW-F test ($P < 0.05$). ns,*,** or *** indicates non-significant differences or significant at $P \leq 0.05$, 0.01, or 0.001, respectively.*

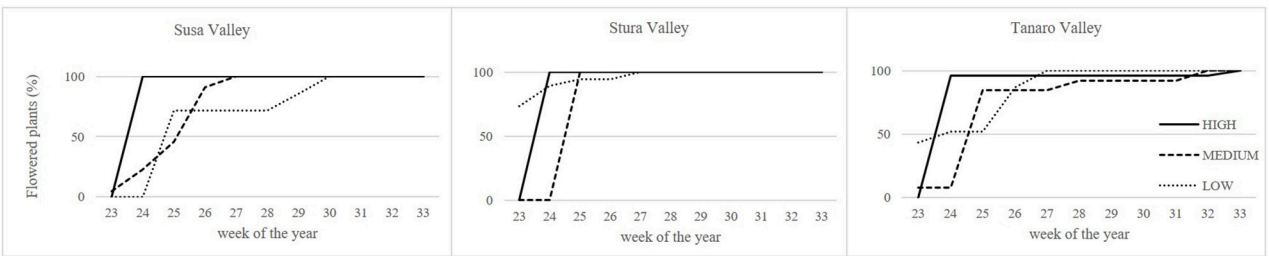

FIGURE 2 | Blooming trend of lavender plants during the second cultivation cycle under uniform conditions. Solid lines, higher altitudes; dashed lines, medium altitudes; dotted lines, lower altitudes.

et al., 2007; González-Coloma et al., 2011) and other ornamental plants, such as rose, magnolia, and butterfly bush (Azuma et al., 2001; Raguso, 2008; Gong et al., 2014).

The volatile chemical classes of lavender fragrance were mainly represented by terpenes, with low amount of non-terpene derivatives (NT, 1.1–6.1%) and apocarotenoids (AC, 0.1–0.5%) (**Figure 3**, Supplementary Table 1). Oxygenated monoterpenes were the most abundant VOCs in all the populations (OM, 61.2–78.1%), followed by monoterpene hydrocarbons (MH, 8.9–22.4%), sesquiterpene hydrocarbons (SH, 4.8–20.5%), and oxygenated sesquiterpenes (OS, 0.1–1.9%). Interestingly, SH were generally present in higher amounts in the aroma of the lowest-altitude populations (SusL 15.6%, StuL 18.3%, TanL 20.5%), and AC were not detected in SusM, SusL, and in TanM populations. One-way ANOSIM performed on chemical classes showed that populations far from the sea (Susa) significantly differed from the closest ones (Tanaro) in their phytochemical composition ($p = 0.038$), indicating a clear distinction of aroma profiles. Moreover, a linear negative regression fitted between latitude and MH and a positive with OM (**Figures 4A,B**), whereas a negative regression model fitted between SH and altitude (**Figure 4C**). Monoterpenes are high volatile terpenoids emitted with warm temperature (>20°C). Their amount in flower fragrance is variable and often exceeds 50% of the total flower emission (Holopainen et al., 2013), as found in our study. Sesquiterpenes are the most diverse class of terpenoids (Holopainen et al., 2013); they are more abundant in plant volatiles than oils and are effectively used in aromatherapy (Cavanagh and Wilkinson, 2002), giving a sweet aromatic note (Prusinowska and Smigielski, 2014). Therefore, altitude influence

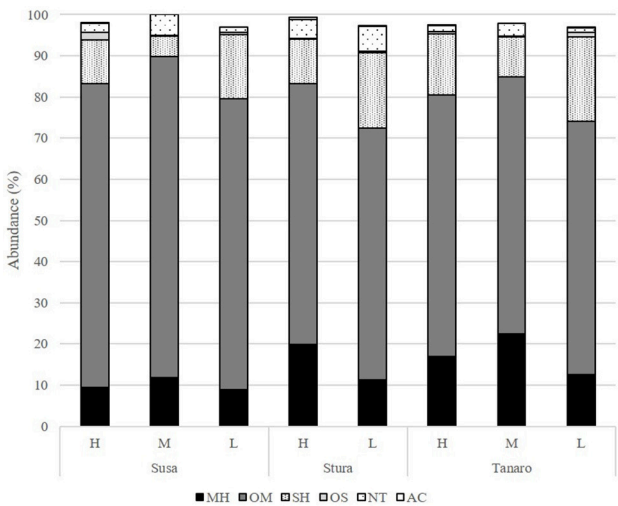

FIGURE 3 | Chemical classes composition (%) of the *L. angustifolia* aroma after one cultivation cycle in uniform conditions. H, high altitude; M, medium altitude; L, low altitude; MH, monoterpene hydrocarbons; OM, oxygenated monoterpenes; SH, sesquiterpene hydrocarbons; OS, oxygenated sesquiterpenes; NT, non terpene derivatives; AC, apocarotenoids.

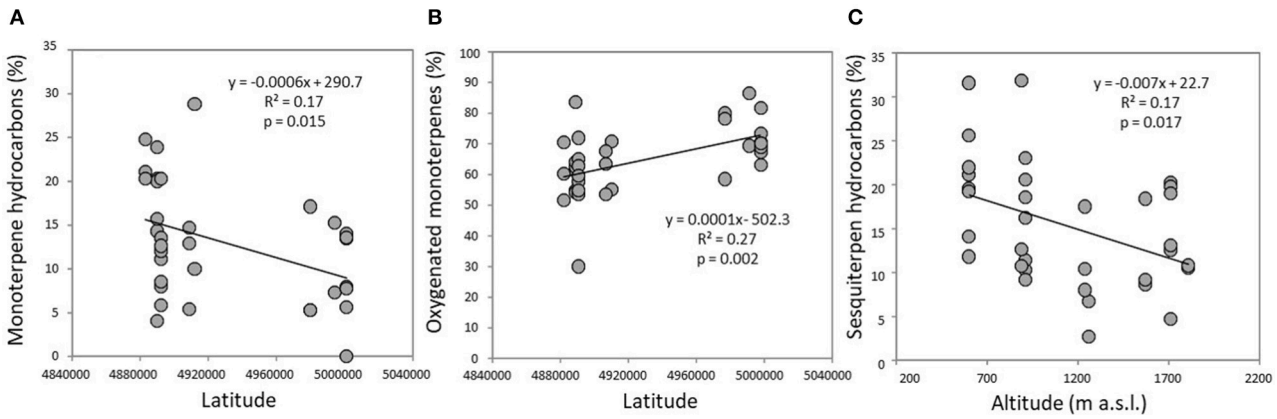

FIGURE 4 | Significant linear regressions detected in the headspace of flowering lavender plants between **(A)** monoterpene hydrocarbons and latitude; **(B)** oxygenated monoterpenes and altitude; **(C)** sesquiterpene hydrocarbons and altitude.

on sesquiterpenes content found in this study could be an interesting starting point to explore the selection of fragrance characteristics.

Considering single compounds, 88 VOCs were identified in lavender aroma profile (Supplementary Table 1). The identified compounds accounted for more than 97% of the total composition. The number of compounds in each population varied from 42 (TanM) to 62 (StuL). Interestingly, every population had a peculiar aroma composition and all populations shared only 27 compounds. Among these compounds, the sum of linalyl acetate, linalool and 1,8-cineole were present more than 50% in SusM and SusL populations and more than 40% in the others; 1,8-cineole was less abundant in TanM and TanL; 4-terpineol and (E)-β-ocimene occurred in high percentages only in TanM lavender (7.7% and 7.5%, respectively), which showed also higher amount of lavandulyl acetate (4.5%). Linalool (22.9%), β-caryophyllene (13.9%), as well as borneol (6.7%) evidenced the highest amount in TanL. Da Porto and Decorti (2008) found a different arrangement in VOCs of lavender cultivated in Northeast Italy, in particular with 1,8-cineole, linalool, camphor, linalyl acetate, and β-caryophyllene being the 70% of the total aroma. Moreover, (E)-β-ocimene was present in smaller amounts (0.2–0.7%) compared to our study (1.6–7.5%).

The one-way ANOSIM performed using VOCs composition showed a similar trend to what observed in chemical classes, with a clear differentiation between Susa and Tanaro populations ($p = 0.018$), respectively the farthest and the closest sites to Mediterranean conditions. According to the SIMPER analysis, 11 compounds were responsible for the 95% of this dissimilarity in lavender fragrance (**Table 3**), with 1,8-cineole, linalyl acetate and linalool as major contributors (50.65, 16.33, and 13.16% of the contribution, respectively). The effect of sea distance was particularly seen on five out of 11 compounds. In detail, linalool, (E)-β-ocimene and 4-terpineol increased in the populations closer to the Mediterranean Sea, whereas 1,8-cineole and bornyl acetate had an opposite behavior. These latter constituents usually adversely affect lavender fragrance (Prusinowska and Smigielski, 2014), while linalool is responsible for the fresh and floral smell (Chizzola, 2013; Prusinowska and Smigielski, 2014). It is one of the best-examined and most often reported monoterpene in flowers (Buchbauer and Ilic, 2013; Holopainen et al., 2013). Moreover, there are evidences that linalool acts synergistically with linalyl-acetate and both compounds are required for the anxiolytic effect of the inhaled EOs (Buchbauer and Ilic, 2013). Thereof peripheral populations adapted to Mediterranean ecological conditions (Tanaro) appear more interesting for the selection of fragrance genotypes.

Both isomers of β-ocimene, together with linalool, are frequently found in species pollinated by butterflies, bees, and moths (Andersson, 2003; Dötterl and Schäffler, 2007; Gong et al., 2014). TanM population emitted the highest quantity of both isomers [(Z)-β-ocimene, 6.4% and (E)-β-ocimene, 7.5%] and could have therefore differentiated its VOC emission to attract its peculiar type of pollinators (Dudareva et al., 2013).

Qualitative and quantitative variation was found in this study in the fragrance composition of *L. angustifolia* species according to its distance from the sea, while Stark et al. (2008) found only qualitative differences concerning other secondary metabolites (flavonoids and tannins). Several phenological events and environmental parameters may drive intra-specific floral scent variation, as observed also between and within *Phlox* cultivars (Majetic et al., 2014), highlighting that species contain a great potential of variation. Nonetheless, the uniform cultivation conditions adopted in our trial pointed out that variation in lavender fragrance composition could be partly attributed to its genetic adaptation to ecological conditions of peripheral alpine sites.

Influence of Native Environment on EO Composition

Generally, EO yields were consistent with previous studies on *L. angustifolia* (Da Porto et al., 2009; Prusinowska and Smigielski, 2014) which are very low in SusH and TanM to reach 0.69% in SusL (Supplementary Table 2). Plants from the lowest altitudes

TABLE 3 | List of VOCs responsible for dissimilarity induced by latitude in lavender aroma according to the SIMPER analysis.

Compound	Contribution (%)	Cumulative (%)	Susa	Stura	Tanaro	Sign
1,8-cineole	50.7	50.7	22.26a[§]	15.38ab	9.84b	*
Linalyl acetate	16.3	67.0	21.12	17.14	16.30	ns
Linalool	13.2	80.2	9.85b	11.62ab	16.35a	*
β-caryophyllene	4.4	84.6	9.16	8.90	10.98	ns
Borneol	2.5	87.1	4.86	3.66	5.83	ns
(E)-β-ocimene	1.8	88.9	2.18b	4.28ab	4.72a	*
(E)-β-farnesene	1.5	90.4	0.80	3.04	1.61	ns
(Z)-β-ocimene	1.5	91.9	2.34	4.84	4.08	ns
4-terpineol	1.5	93.4	1.11b	3.38ab	3.55a	*
Bornyl acetate	1.1	94.5	3.36*a*	0.80ab	0.36b	**
Lavandulyl acetate	0.8	95.3	1.72	2.48	2.50	ns

[§]*Data followed by the same letter in the same line are not significantly different according to Mann-Whitney test. ns, *, ** or *** indicates non-significant differences or significant at P ≤ 0.05, 0.01 or 0.001, respectively.*

showed higher yields in Susa and Tanaro valley (0.69 and 0.37%, respectively). Previous studies highlighted the same behavior in other aromatic plants such as *Origanum vulgare* (Vokou et al., 1993; Giuliani et al., 2013), *Coriandrum sativum* (Shams et al., 2016), and *Rosmarinus officinalis* (Tuttolomondo et al., 2015). Giuliani et al. (2013) found a correlation between higher yields at decreasing altitudes and, but not limited to, an increased presence of glandular peltate trichomes, the structures responsible for the accumulation of EOs. Considering distance from Mediterranean conditions, Susa lavenders were the most productive in terms of EO, followed by Tanaro and Stura plants.

The mean of the relative abundance of chemical classes was distributed as follows (**Figure 5**, Supplementary Table 2): OM (71.2%), OS (13.7%), SH (6.1%), NT (4.9%), MH (3.2%), and AC (0.3%). A different distribution was recorded by Pistelli et al. (2017) in *L. angustifolia* 'Maillette', where the amount of OS and SH were lower than that observed in this study (0.5 and 1.8%, respectively). Commonly, monoterpenes represent the major class in the oil of *Lavandula* species (Lis-Balchin, 2003) and our data are consistent with values reviewed by Prusinowska and Smigielski (2014). In this study, significant positive linear regression fitted between MH and NT concentration with latitude (**Figures 6A,B**) and AC content with altitude (**Figure 6D**); instead, a negative linear regression fitted between SH and latitude (**Figure 6C**), an opposite behavior than that observed in *Teucrium polium* EO by Sadeghi et al. (2014).

One-hundred-four compounds were identified in lavender EO (Supplementary Table 2), accounting for more than 99% of the total EO composition. The number of compounds in each population varied from 63 (SusH) to 83 (StuL). These numbers were higher than those previously reported in *L. angustifolia* species and cultivars cultivated in the Tyrrhenian coast (Venskutonis et al., 1997; Pistelli et al., 2017). Interestingly, each EO was a mixture of different compounds, but all populations shared at least 40 constituents. The EO composition of *L. angustifolia* is reported to be the most variable inside the genus (Lis-Balchin, 2003). However, the characteristic compounds found in *Lavandula* oil usually are

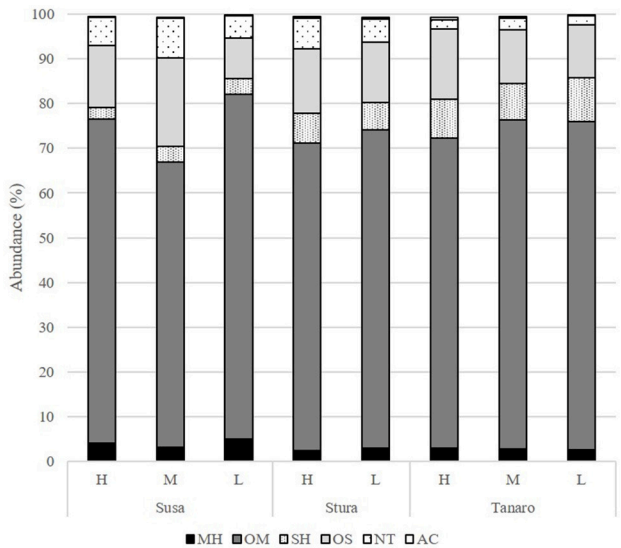

FIGURE 5 | Chemical classes composition (%) of the *L. angustifolia* essential oils after two cultivation cycle in uniform conditions. H, high altitude; M, medium altitude; L, low altitude; MH, monoterpene hydrocarbons; OM, oxygenated monoterpenes; SH, sesquiterpene hydrocarbons; OS, oxygenated sesquiterpenes; NT, non terpene derivatives; AC, apocarotenoids.

linalool, linalyl acetate, 1,8-cineole, β-ocimene, 4-terpineol, and camphor (Cavanagh and Wilkinson, 2002). Accordingly, in the present study linalool and linalyl acetate were the most abundant in all the EOs analyzed, with the highest amount recorded in TanL (linalool 35.0%) and StuH (linalyl acetate 26.3%). However, linalool content was present in lower percentage than in previous studies on lavender (Venskutonis et al., 1997; Pistelli et al., 2013, 2017). In fact, linalool production in *L. angustifolia* varies widely (Prusinowska and Smigielski, 2014) depending on temperature, flower development, and rainfall (Hassiotis et al., 2014). Linalyl acetate content registered in this work is in accordance with that reported for lavender 'Maillette'

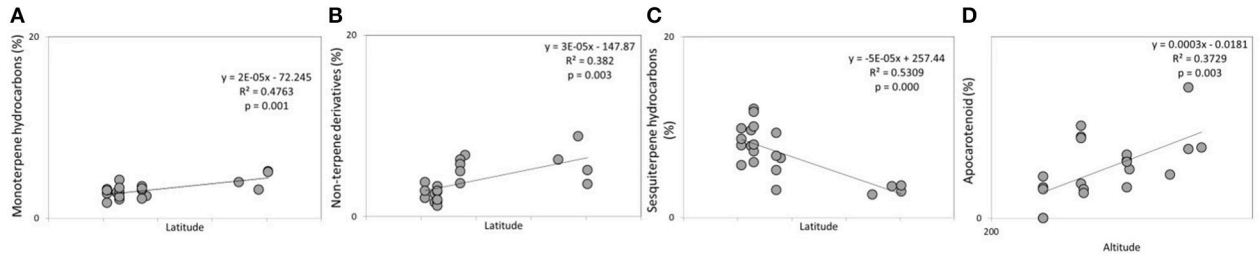

FIGURE 6 | Significant linear regressions detected in lavender EOs between **(A)** monoterpene hydrocarbons and latitude; **(B)** non-terpene derivatives and latitude; **(C)** sesquiterpene hydrocarbons and latitude; **(D)** apocarotenoids and altitude.

TABLE 4 | List of compounds responsible for dissimilarity induced in lavender EO by latitude according to the SIMPER analysis.

Compound	Contribution %	Cumulative %	Susa	Stura	Tanaro	Sign.
Linalool	46.0	46.0	20.97b[§]	23.95ab	29.50a	*
Linalyl acetate	17.7	63.7	17.67	15.27	14.88	ns
1,8-cineole	9.2	72.8	6.29a	1.50b	1.01b	***
Lavandulyl acetate	3.7	76.5	3.29	3.93	3.82	ns
Caryophyllene oxide	3.5	80.0	6.09	7.39	6.58	ns
T-cadinol (=epi-α-cadinol)	3.5	83.5	3.03a	0.65b	0.16b	**
Borneol	3.2	86.7	4.38	5.28	4.61	ns
4-terpinenol	2.3	89.0	0.87b	1.43ab	3.01a	*
1-octen-3-yl acetate	2.2	91.2	3.01a	2.38a	0.60b	***
β-caryophyllene	1.4	92.6	1.31b	1.83b	3.16a	**
Thujapsan-2-α-ol	0.8	93.4	0.03b	1.40a	1.49a	**
(Z)-γ-bisabolene	0.7	94.2	0.53b	1.89a	1.89a	**
α-terpineol	0.6	94.8	4.10a	3.05ab	2.90b	**

[§]*Data followed by the same letter in the same line are not significantly different according to Mann-Whitney test. ns,*,** or*** indicates non-significant differences or significant at P ≤ 0.05, 0.01 or 0.001, respectively.*

(Pistelli et al., 2017), but lower than in lavender species grow in Lithuania (Venskutonis et al., 1997). According to the percentage content of the characteristic compounds of lavender essential oil reported in the European Pharmacopoeia 6.0 (Ph. Eur.) none of the analyzed EOs completely fulfill the expected limits. StuH and TanL were closely related to the established ranges except for linalool (less than 20%) in StuH and linalyl acetate (less than 25%) in TanL. The percentages of 4-terpineol, 3-octanone, limonene, and lavandulyl acetate were in the range fixed by Ph. Eur. for all the tested EOs. Among the compounds reported in ISO 3515:2002 for lavender EO[1] only 3-octanone, limonene and lavandulyl acetate respected the fixed limits in all the analyzed EOs. The analysis of flower fragrance has been suggested as a good indicator of the EO composition (An et al., 2001). However, EO composition frequently differed from the aroma profiles (see section Influence of Native Environment on Volatile Emission), as already highlighted in several studies on lavenders (Cavanagh and Wilkinson, 2002). These differences were caused by processes such as hydrolysis, thermal degradation, and molecular rearrangements that are promoted during the hydro distillation method (Da Porto and Decorti, 2008).

The one-way ANOSIM performed on EO compounds revealed significant differences among populations at different latitudes ($p = 0.009$), likewise to what observed in lavender aroma (see section Influence of Native Environment on Volatile Emission), with a clear separation between populations with more (Tanaro) and less (Susa) Mediterranean ecological conditions. According to the SIMPER analysis, thirteen compounds were responsible for 95% of this difference (**Table 4**), with linalool being the major contributor (45.98%). The effect of sea distance was seen on nine out of the 13 compounds. In particular, linalool, 4-terpinenol, β-caryophyllene, thujapsan-2-α-ol, and (Z)-γ-bisabolene were higher in populations closer to the Mediterranean Sea (Tanaro), while 1,8-cineole, τ-cadinol, 1-octen-3-yl acetate and α-terpineol where higher in the furthest populations (Susa). Linalool and terpineol are of great interest for medicinal industry due to their positive effects on the central nervous system (Prusinowska and Smigielski, 2014). β-caryophyllene, with its woody and spicy aroma, is commonly used in the fragrance and cosmetic industry. However, it has also antibiotic, anesthetic, anti-inflammatory, antioxidant, and anti-spasmodic activity (Buchbauer and Ilic, 2013). Therefore,

[1]ISO 3515:2002 Oil of Lavender (*Lavandula angustifolia* Mill.).

similarly to results on fragrance, the populations closer to Mediterranean conditions (Tanaro) could be considered valuable germplasm for selection and breeding purposes, aimed to the production of EO, despite the low yields obtained. Indeed it is needed to consider that the cultivation occurred in pot. In proper open field conditions higher biomass and EO yields are expected. No significant differences were detected in EO compounds according to altitude, likewise to VOCs composition (see Section Influence of Native Environment on Volatile Emission), despite there are evidence that altitude significantly affected chemical composition of EO in other Lamiaceae plants (Giuliani et al., 2013; Sadeghi et al., 2015). Chograni et al. (2010) observed also a phytochemical variation in the leaf EO of wild *L. multifida* belonging to the same bioclimatic zone, possibly explained by genetic factors. Similarly, in the present study, the ecological conditions of peripheral sites may have induced different adaptation mechanisms in lavender, leading to different phytochemical compositions. Since the EO obtained in this work did not respect the limit established by Ph. Eur., they can be used for other industrial application, or for cosmetic purposes.

CONCLUSIONS

We hereby provide the first phytochemical description of secondary metabolites in *L. angustifolia* peripheral populations of the West Italian Alps. The influence of sea distance (latitude) and altitude on VOC and EO composition was analyzed in plants grown under uniform cultivation conditions. Interestingly, results showed that the ecological gradient created germplasm heterogeneity. Compared to other studies, altitude seemed to affect mainly biometric parameters, and to a low extent the phytochemical composition of *L. angustifolia*, while sea distance had an influence on both morphological and phytochemical traits. Lavenders of West Italian Alps disclosed a great potential for the development of a valuable local product, where the cultivation of the thermophilous species *L.* × *intermedia* cannot be applied due to the lower average temperature of the studied alpine areas. Among the studied alpine peripheral populations, plants of Tanaro Valley, which have evolved in almost Mediterranean ecological conditions, generally performed better in both morphological and phytochemical characteristics. To obtain uniform productions, the study of the phytochemical variation and the selection and propagation of interesting genotypes must be promoted, together with the improvement of cultivation protocols.

AUTHOR CONTRIBUTIONS

SD and MC equally contributed to this work in the acquisition of data, analysis and interpretation of data, and drafting of manuscript. BN and PC carried out phytochemical analyses. ML contributed to lavender population selection and data analysis. LP and BN contributed to data interpretation and discussion. VS conceived, designed and coordinated the work. LP and VS critically revised and approved the manuscript.

FUNDING

This work was partially supported by Fondazione Cassa di Risparmio di Torino (Project Le colture officinali: un approccio di filiera per aumentare la competitività delle aziende piemontesi e valorizzare il territorio, grant number 2014.0976) and by the program Interreg V-A Francia Italia Alcotra Attività innovative per lo sviluppo della filiera transfrontaliera del fiore edule–Antea n. 1139.

ACKNOWLEDGMENTS

The authors thank Walter Gaino and Paolo Lo Turco for their contribution in the collection and propagation of lavender plants; and Frat.lli Gramaglia nursery for hosting cultivation.

SUPPLEMENTARY MATERIAL

The Supplementary Material for this article can be found online at: https://www.frontiersin.org/articles/10.3389/fpls.2018.00983/full#supplementary-material

REFERENCES

Adams, R. P. (2007). *Identification of Essential Oil Components by Gas Chromatography/Mass Spectrometry*. Carol Stream, IL: Allured Publishign Corp.

Aeschimann, D., Lauber, K., Martin Moser, D., and Theurillat, J. P. (2004). *Flora Alpina*. Bologna: Zanichelli.

An, M., Haig, T., and Hatfield, P. (2001). On-site field sampling and analysis of fragrance from living Lavender (*Lavandula angustifolia* L.) flowers by solid-phase microextraction coupled to gas chromatography and ion-trap mass spectrometry. *J. Chromatogr. A* 917, 245–250. doi: 10.1016/S0021-9673(01)00657-4

Andersson, S. (2003). Antennal responses to floral scents in the butterflies Inachis io, *Aglais urticae* (Nymphalidae), and *Gonepteryx rhamni* (Pieridae). *Chemoecology* 13, 13–20. doi: 10.1007/s000490300001

Azuma, H., Toyota, M., and Asakawa, Y. (2001). Intraspecific variation of floral scent chemistry in *Magnolia kobus* DC.(Magnoliaceae). *J. Plant Res.* 114, 411–422. doi: 10.1007/PL00014006

Bakkali, F., Averbeck, S., Averbeck, D., and Idaomar, M. (2008). Biological effects of essential oils–a review. *Food Chem. Toxicol.* 46, 446–475. doi: 10.1016/j.fct.2007.09.106

Binns, S. E., Arnason, J. T., and Baum, B. R. (2002). Phytochemical variation within populations of *Echinacea angustifolia* (Asteraceae). *Biochem. Syst. Ecol.* 30, 837–854. doi: 10.1016/S0305-1978(02)00029-7

Brahmkshatriya, P. P., and Brahmkshatriya, P. S. (2013). "Terpenes: Chemistry, biological role, and therapeutic applications," in *Natural Products* eds K. G. Ramawat and J.-M. Mérillon (Berlin: Springer), 2665–2691.

Buchbauer, G., and Ilic, A. (2013). "Biological activities of selected mono-and sesquiterpenes: possible uses in medicine," in *Natural Products* eds K. G. Ramawat and J.-M. Mérillon (Berlin: Springer), 4109–4159.

Caputo, L., Souza, L. F., Alloisio, S., Cornara, L., and De Feo, V. (2016). *Coriandrum sativum* and *Lavandula angustifolia* essential oils: chemical composition and activity on central nervous system. *Int. J. Mol. Sci.* 17:1999. doi: 10.3390/ijms17121999

Caser, M., D'Angiolillo, F., Chitarra, W., Lovisolo, C., Ruffoni, B., Pistelli, L., et al. (2016). Water deficit regimes trigger changes in valuable physiological and

phytochemical parameters in *Helichrysum petiolare* Hilliard and BL Burtt. *Ind. Crops Prod.* 83, 680–692. doi: 10.1016/j.indcrop.2015.12.053

Caser, M., D'Angiolillo, F., Chitarra, W., Lovisolo, C., Ruffoni, B., Pistelli, L., et al. (2017). Ecophysiological and phytochemical responses of *Salvia sinaloensis Fern*. to drought stress. *Plant Growth Regul.* 84, 383–394. doi: 10.1007/s10725-017-0349-1

Cavanagh, H. M. A., and Wilkinson, J. M. (2002). Biological activities of lavender essential oil. *Phyther. Res.* 16, 301–308. doi: 10.1002/ptr.1103

Chizzola, R. (2013). "Regular monoterpenes and sesquiterpenes (Essential oils)," in *Natural products* eds K. G. Ramawat and J.-M. Mérillon (Berlin: Springer), 2973–3008.

Chograni, H., Zaouali, Y., Rajeb, C., and Boussaid, M. (2010). Essential oil variation among natural populations of *Lavandula multifida* L.(Lamiaceae). *Chem. Biodivers.* 7, 933–942. doi: 10.1002/cbdv.200900201

Da Porto, C., and Decorti, D. (2008). Analysis of the volatile compounds of flowers and essential oils from *Lavandula angustifolia* cultivated in northeastern Italy by headspace solid-phase microextraction coupled to gas chromatography-mass spectrometry. *Planta Med.* 74, 182–187. doi: 10.1055/s-2008-1034295

Da Porto, C., Decorti, D., and Kikic, I. (2009). Flavour compounds of Lavandula angustifolia L. to use in food manufacturing: comparison of three different extraction methods. *Food Chem.* 112, 1072–1078. doi: 10.1016/j.foodchem.2008.07.015

Demasi, S., Caser, M., Handa, T., Kobayashi, N., De Pascale, S., and Scariot, V. (2017). Adaptation to iron deficiency and high pH in evergreen azaleas (*Rhododendron* spp.): potential resources for breeding. *Euphytica* 213, 148–162. doi: 10.1007/s10681-017-1931-3

Dicke, M., and Loreto, F. (2010). Induced plant volatiles: from genes to climate change. *Trends Plant Sci.* 15, 115–117. doi: 10.1016/j.tplants.2010.01.007

Dötterl, S., and Schäffler, I. (2007). Flower scent of floral oil-producing *Lysimachia punctata* as attractant for the oil-bee Macropis fulvipes. *J. Chem. Ecol.* 33, 441–445. doi: 10.1007/s10886-006-9237-2

Dudareva, N., Klempien, A., Muhlemann, J. K., and Kaplan, I. (2013). Biosynthesis, function and metabolic engineering of plant volatile organic compounds. *New Phytol.* 198, 16–32. doi: 10.1111/nph.12145

Eckert, C. G., Samis, K. E., and Lougheed, S. C. (2008). Genetic variation across species' geographical ranges: The central-marginal hypothesis and beyond. *Mol. Ecol.* 17, 1170–1188. doi: 10.1111/j.1365-294X.2007.03659.x

Fick, S. E., and Hijmans, R. J. (2017). WorldClim 2: new 1-km spatial resolution climate surfaces for global land areas. *Int. J. Climatol.* 37, 4302–4315. doi: 10.1002/joc.5086

Giuliani, C., Maggi, F., Papa, F., and Maleci Bini, L. (2013). Congruence of phytochemical and morphological profiles along an altitudinal gradient in *Origanum vulgare* ssp. vulgare from Venetian region (NE Italy). *Chem. Biodivers.* 10, 569–583. doi: 10.1002/cbdv.201300019

Gonçalves, S., and Romano, A. (2013). *In vitro* culture of lavenders (*Lavandula* spp.) and the production of secondary metabolites. *Biotechnol. Adv.* 31, 166–174. doi: 10.1016/j.biotechadv.2012.09.006

Gong, W. C., ,Chen, G., Liu, C.-Q., Dunn, B. L., and Sun, W.-B. (2014). Comparison of floral scent between and within *Buddleja fallowiana* and *Buddleja officinalis* (Scrophulariaceae). *Biochem. Syst. Ecol.* 55, 322–328. doi: 10.1016/j.bse.2014.03.029

González-Coloma, A., Delgado, F., Rodilla, J. M., Silva, L., Sanz, J., and Burillo, J. (2011). Chemical and biological profiles of *Lavandula luisieri* essential oils from western Iberia Peninsula populations. *Biochem. Syst. Ecol.* 39, 1–8. doi: 10.1016/j.bse.2010.08.010

Hassiotis, C. N., Ntana, F., Lazari, D. M., Poulios, S., and Vlachonasios, K. E. (2014). Environmental and developmental factors affect essential oil production and quality of *Lavandula angustifolia* during flowering period. *Ind. Crops Prod.* 62, 359–366. doi: 10.1016/j.indcrop.2014.08.048

Helrich, K. (1990). *Official Methods of Analysis. 15th Edn.* Arlington, VA: AOAC Intl.

Herrera, C. M., and Bazaga, P. (2008). Adding a third dimension to the edge of a species' range: altitude and genetic structuring in mountainous landscapes. *Heredity* 100, 275–285. doi: 10.1038/sj.hdy.6801072

Holopainen, J. K., Himanen, S. J., Yuan, J. S., Chen, F., and Stewart Jr, C. N. (2013). "Ecological functions of terpenoids in changing climates," in *Natural Products* eds K. G. Ramawat and J.-M. Mérillon (Berlin: Springer), 2913–2940.

Kesselmeier, J., and Staudt, M. (1999). Biogenic volatile organic compounds (VOC): An overview on emission, physiology and ecology. *J. Atmos. Chem.* 33, 23–88. doi: 10.1023/A:1006127516791

Kim, N. S., and Lee, D. S. (2002). Comparison of different extraction methods for the analysis of fragrances from *Lavandula* species by gas chromatography-mass spectrometry. *J. Chromatogr. A* 982, 31–47. doi: 10.1016/S0021-9673(02)01445-0

Kirimer, N., Mokhtarzadeh, S., Demirci, B., Goger, F., Khawar, K. M., and Demirci, F. (2017). Phytochemical profiling of volatile components of *Lavandula angustifolia* Miller propagated under *in vitro* conditions. *Ind. Crops Prod.* 96, 120–125. doi: 10.1016/j.indcrop.2016.11.061

Knudsen, J. T., Eriksson, R., Gershenzon, J., and Ståhl, B. (2006). Diversity and distribution of floral scent. *Bot. Rev.* 72, 1–120. doi: 10.1663/0006-8101(2006)72[1:DADOFS]2.0.CO;2

Kofidis, G., and Bosabalidis, A. M. (2008). Effects of altitude and season on glandular hairs and leaf structural traits of *Nepeta nuda* L. *Bot. Stud.* 49, 363–372. Available online at: https://ejournal.sinica.edu.tw/bbas/content/2008/4/Bot494-08.pdf

Lesage-Meessen, L., Bou, M., Sigoillot, J.-C., Faulds, C. B., and Lomascolo, A. (2015). Essential oils and distilled straws of lavender and lavandin: a review of current use and potential application in white biotechnology. *Appl. Microbiol. Biotechnol.* 99, 3375–3385. doi: 10.1007/s00253-015-6511-7

Lis-Balchin, M. (2003). *Lavender: The Genus Lavandula*. London: CRC Press.

López, V., Nielsen, B., Solas, M., Ramírez, M. J., and Jäger, A. K. (2017). Exploring pharmacological mechanisms of lavender (*Lavandula angustifolia*) essential oil on central nervous system targets. *Front. Pharmacol.* 8:280. doi: 10.3389/fphar.2017.00280

Loreto, F., Dicke, M., Schnitzler, J., and Turlings, T. C. J. (2014). Plant volatiles and the environment. *Plant. Cell Environ.* 37, 1905–1908. doi: 10.1111/pce.12369

Maffei, M., and Peracino, V. (1993). Fatty acids from some *Lavandula* hybrids growing spontaneously in north west italy. *Phytochemistry* 33, 373–376. doi: 10.1016/0031-9422(93)85521-R

Majetic, C. J., Levin, D. A., and Raguso, R. A. (2014). Divergence in floral scent profiles among and within cultivated species of *Phlox*. *Sci. Hortic.* 172, 285–291. doi: 10.1016/j.scienta.2014.04.024

Muñoz-Bertomeu, J., Arrillaga, I., and Segura, J. (2007). Essential oil variation within and among natural populations of *Lavandula latifolia* and its relation to their ecological areas. *Biochem. Syst. Ecol.* 35, 479–488. doi: 10.1016/j.bse.2007.03.006

Nogués, I., Muzzini, V., Loreto, F., and Bustamante, M. A. (2015). Drought and soil amendment effects on monoterpene emission in rosemary plants. *Sci. Total Environ.* 538, 768–778. doi: 10.1016/j.scitotenv.2015.08.080

Peracino, V., Caramiello, R., and Maffei, M. (1994). Essential oils from some lavandula hybrids growing spontaneously in north west italy. *Flavour Fragr. J.* 9, 11–17. doi: 10.1002/ffj.2730090104

Pignatti, A. (1982). *Flora d'Italia.* Bologna: Edagricole.

Pistelli, L., Najar, B., Giovanelli, S., Lorenzini, L., Tavarini, S., and Angelini, L. G. (2017). Agronomic and phytochemical evaluation of lavandin and lavender cultivars cultivated in the Tyrrhenian area of Tuscany (Italy). *Ind. Crops Prod.* 109, 37–44. doi: 10.1016/j.indcrop.2017.07.041

Pistelli, L., Noccioli, C., D'Angiolillo, F., and Pistelli, L. (2013). Composition of volatile in micropropagated and field grown aromatic plants from tuscany islands. *Acta Biochim. Pol.* 60, 43–50. Available online at: http://www.actabp.pl/pdf/1_2013/43.pdf

Prusinowska, R., and Smigielski, K. B. (2014). Composition, biological properties and therapeutic effects of lavender (*Lavandula angustifolia* L). A review. *Herba Pol.* 60, 56–66. doi: 10.2478/hepo-2014-0010

Raguso, R. A. (2008). Wake up and smell the roses: the ecology and evolution of floral scent. *Annu. Rev. Ecol. Evol. Syst.* 39, 549–569. doi: 10.1146/annurev.ecolsys.38.091206.095601

Rahmati, B., Kiasalari, Z., Roghani, M., Khalili, M., and Ansari, F. (2017). Antidepressant and anxiolytic activity of *Lavandula officinalis* aerial parts hydroalcoholic extract in scopolamine-treated rats. *Pharm. Biol.* 55, 958–965. doi: 10.1080/13880209.2017.1285320

Raut, J. S., and Karuppayil, S. M. (2014). A status review on the medicinal properties of essential oils. *Ind. Crops Prod.* 62, 250–264. doi: 10.1016/j.indcrop.2014.05.055

Sadeghi, H., Jamalpoor, S., and Shirzadi, M. H. (2014). Variability in essential oil of *Teucrium polium* L. of different latitudinal populations. *Ind. Crops Prod.* 54, 130–134. doi: 10.1016/j.indcrop.2014.01.015

Sadeghi, H., Robati, Z., and Saharkhiz, M. J. (2015). Variability in *Zataria multiflora* Bioss. essential oil of twelve populations from Fars province. *Iran. Ind. Crops Prod.* 67, 221–226. doi: 10.1016/j.indcrop.2015.01.021

Sangwan, N. S., Farooqi, A. H. A., Shabih, F., and Sangwan, R. S. (2001). Regulation of essential oil production in plants. *Plant Growth Regul.* 34, 3–21. doi: 10.1023/A:1013386921596

Sanz, J., Soria, A. C., and Garcia-Vallejo, M. C. (2004). Analysis of volatile components of *Lavandula luisieri* L. by direct thermal desorption–gas chromatography–mass spectrometry. *J. Chromatogr. A* 1024, 139–146. doi: 10.1016/j.chroma.2003.10.024

Selmar, D., and Kleinwächter, M. (2013). Influencing the product quality by deliberately applying drought stress during the cultivation of medicinal plants. *Ind. Crops Prod.* 42, 558–566. doi: 10.1016/j.indcrop.2012.06.020

Shahdadi, H., Bahador, R. S., Eteghadi, A., and Boraiinejad, S. (2017). Lavender a plant for medical uses: a literature review. *Indian J. Public Heal. Res. Dev.* 8, 328–332. doi: 10.5958/0976-5506.2017.00065.1

Shams, M., Esfahan, S. Z., Esfahan, E. Z., Dashtaki, H. N., Dursun, A., and Yildirim, E. (2016). Effects of climatic factors on the quantity of essential oil and dry matter yield of coriander (*Coriandrum sativum* L.). *Indian J. Sci. Technol.* 9, 1–4. doi: 10.17485/ijst/2016/v9i6/61301

Shellie, R., Mondello, L., Marriott, P., and Dugo, G. (2002). Characterisation of lavender essential oils by using gas chromatography-mass spectrometry with correlation of linear retention indices and comparison with comprehensive two-dimensional gas chromatography. *J. Chromatogr. A* 970, 225–234. doi: 10.1016/S0021-9673(02)00653-2

Spitaler, R., Schlorhaufer, P. D., Ellmerer, E. P., Merfort, I., Bortenschlager, S., Stuppner, H., et al. (2006). Altitudinal variation of secondary metabolite profiles in flowering heads of *Arnica montana* cv. *ARBO Phytochemistry* 67, 409–417. doi: 10.1016/j.phytochem.2005.11.018

Stark, S., Julkunen-Tiitto, R., Holappa, E., Mikkola, K., and Nikula, A. (2008). Concentrations of foliar quercetin in natural populations of white birch (*Betula pubescens*) increase with latitude. *J. Chem. Ecol.* 34, 1382–1391. doi: 10.1007/s10886-008-9554-8

Theurillat, J.-P., Aeschimann, D., Küpfer, P., and Spichiger, R. (1995). "The higher vegetation units of the Alps," in *Colloques Phytosociologiques*, 23, 189–239.

Tuttolomondo, T., Dugo, G., Ruberto, G., Leto, C., Napoli, E. M., Cicero, N., et al. (2015). Study of quantitative and qualitative variations in essential oils of Sicilian *Rosmarinus officinalis* L. *Nat. Prod. Res.* 29, 1928–1934. doi: 10.1080/14786419.2015.1010084

Venskutonis, P. R., Dapkevicius, A., and Baranauskiene, M. (1997). Composition of the essential oil of Lavender (*Lavandula angustifolia* Mill.) from Lithuania. *J. Essent. Oil Res.* 9, 107–110. doi: 10.1080/10412905.1997.9700727

Vokou, D., Kokkini, S., and Bessiere, J.-M. (1993). Geographic variation of Greek oregano (*Origanum vulgare* ssp. hirtum*)* essential oils. *Biochem. Syst. Ecol.* 21, 287–295. doi: 10.1016/0305-1978(93)90047-U

Conflict of Interest Statement: The authors declare that the research was conducted in the absence of any commercial or financial relationships that could be construed as a potential conflict of interest.

frontiers in Plant Science

ORIGINAL RESEARCH
published: 17 July 2018
doi: 10.3389/fpls.2018.01022

NMR Metabolomics Defining Genetic Variation in Pea Seed Metabolites

*Noel Ellis[1,2,3], Chie Hattori[1], Jitender Cheema[1], James Donarski[4], Adrian Charlton[4], Michael Dickinson[4], Giampaolo Venditti[4], Péter Kaló[5], Zoltán Szabó[5], György B. Kiss[6] and Claire Domoney[1]**

[1] John Innes Centre, Norwich, United Kingdom, [2] IBERS, Aberystwyth University, Aberystwyth, United Kingdom, [3] Faculty of Science, School of Biological Sciences, University of Auckland, Auckland, New Zealand, [4] Fera Science Ltd., York, United Kingdom, [5] National Agricultural Research and Innovation Centre, Agricultural Biotechnology Institute, Gödöllő, Hungary, [6] AMBIS Biotechnology Ltd., Budapest, Hungary

Nuclear magnetic resonance (NMR) spectroscopy profiling was used to provide an unbiased assessment of changes to the metabolite composition of seeds and to define genetic variation for a range of pea seed metabolites. Mature seeds from recombinant inbred lines, derived from three mapping populations for which there is substantial genetic marker linkage information, were grown in two environments/years and analyzed by non-targeted NMR. Adaptive binning of the NMR metabolite data, followed by analysis of quantitative variation among lines for individual bins, identified the main genomic regions determining this metabolic variability and the variability for selected compounds was investigated. Analysis by *t*-tests identified a set of bins with highly significant associations to genetic map regions, based on probability (*p*) values that were appreciably lower than those determined for randomized data. The correlation between bins showing high mean absolute deviation and those showing low *p*-values for marker association provided an indication of the extent to which the genetics of bin variation might be explained by one or a few loci. Variation in compounds related to aromatic amino acids, branched-chain amino acids, sucrose-derived metabolites, secondary metabolites and some unidentified compounds was associated with one or more genetic loci. The combined analysis shows that there are multiple loci throughout the genome that together impact on the abundance of many compounds through a network of interactions, where individual loci may affect more than one compound and *vice versa*. This work therefore provides a framework for the genetic analysis of the seed metabolome, and the use of genetic marker data in the breeding and selection of seeds for specific seed quality traits and compounds that have high commercial value.

Keywords: genetic map, genetic variation, pea, seed, metabolite, nuclear magnetic resonance

OPEN ACCESS

Edited by:
Marta Sousa Silva,
Universidade de Lisboa, Portugal

Reviewed by:
Fabio Sciubba,
Sapienza Università di Roma, Italy
Matthew Paul,
Rothamsted Research (BBSRC),
United Kingdom

***Correspondence:**
Claire Domoney
claire.domoney@jic.ac.uk

Specialty section:
This article was submitted to Plant Metabolism and Chemodiversity, a section of the journal Frontiers in Plant Science

Received: *27 February 2018*
Accepted: *25 June 2018*
Published: *17 July 2018*

Citation:
Ellis N, Hattori C, Cheema J, Donarski J, Charlton A, Dickinson M, Venditti G, Kaló P, Szabó Z, Kiss GB and Domoney C (2018) NMR Metabolomics Defining Genetic Variation in Pea Seed Metabolites. Front. Plant Sci. 9:1022. doi: 10.3389/fpls.2018.01022

INTRODUCTION

Metabolite profiling, based on chemical fingerprints provided by nuclear magnetic resonance (NMR) spectroscopy, provides an approach for the unbiased assessment of changes in the content of small molecules in response to genetic and/or environmental factors. Such profiles provide a useful and rapid method for assessing the changes that occur in the metabolome as a consequence

of plant genotype and/or the interaction between genotype and environment (Messerli et al., 2007). The use of NMR spectroscopy for holistic studies of plant metabolism predates the term "metabolomics" (Fiehn et al., 2000) by some years (Moore et al., 1983; Belton and Ratcliffe, 1985; Ratcliffe, 1987; Fan, 1996).

NMR spectroscopy provides a method of choice to facilitate the efficient analysis of the large number of samples that is necessary to deal with the expected intrinsic variability of plant, or equivalent, biological materials particularly where these need to be grown or cultured under field or similar "near-natural" conditions. Such has been the case for the study of "substantial equivalence" in genetically modified plants, where NMR has been used in the analysis of field samples of wheat (Baker et al., 2006). Higher amounts of maltose and/or sucrose and differences in free amino acids were apparent in a transgenic line, and these observations were followed by more detailed studies of the amino acid composition using gas chromatography-mass spectrometry (GC-MS). NMR has also been employed to evaluate the effects of genetic modification and assess the effect of drought-stress on the *Pisum sativum* L. (pea) leaf metabolome (Charlton et al., 2004, 2008). Significant changes in resonances under drought-stress conditions were attributed to a range of compounds, both primary and secondary metabolites, including proline, valine, threonine, homoserine, myoinositol, γ -aminobutyrate (GABA) and trigonelline (nicotinic acid betaine). Some of these changes translated to alterations in the seed metabolome in the same experiments (unpublished data).

It has been shown, using GC/MS analyses of Arabidopsis developing seeds, that the seed desiccation period is associated with a major increase in the levels of free metabolites; these include the nitrogen-rich amino acids (asparagine, lysine, and arginine), the aromatic amino acids (tryptophan, phenylalanine, tyrosine), serine, alanine, the non-proteinogenic amino acid GABA, TCA-cycle intermediates, fumarate and succinate, and the levels of sucrose, galactose, arabinose, trehalose, sorbitol, galactitol, gluconate-6-phosphate and glycerate (Fait et al., 2006). Few studies have been carried out to investigate the effects of genetic variation on the metabolite composition of seeds. For the seeds of many crops, quality traits may be defined in terms of the synthesis of a number of key metabolites, for example the concentration of 2-acetyl-1-pyrroline (2AP) in rice linked to fragrance quality (Shi et al., 2008). An alternative to the expensive and time-consuming GC/MS method for assaying 2AP content in breeding programmes is offered by the demonstration that the metabolite is controlled by a gene, betaine aldehyde dehydrogenase, for which allelic variation has been described (Shi et al., 2008).

In pea, the molecular basis for many seed quality traits is largely unknown. An exception to this is the understanding of the control of sucrose content at a gross level, where naturally occurring mutants with defects in starch biosynthesis have elevated sucrose contents in their seeds. Mutations at two genetic loci (*r* and *rb*) have been exploited in the development of some of the varied food uses of pea seeds (Wang et al., 1998). Studies have shown the many pleiotropic effects that mutations at *r* and *rb* exert on seed metabolism overall; these include changes to nitrogen/protein accumulation, water content and seed shape when compared with wild-type lines (Perez et al., 1993; Casey et al., 1998; Lyall et al., 2003). These alterations to seed composition can be mimicked to similar or greater extents in mutants induced either through chemical mutagenesis or transgenesis, where additional genes of starch biosynthesis have been targeted (Wang and Hedley, 1991; Wang et al., 1998; Weigelt et al., 2009). While the *r* and *rb* loci are determined by mutations in a starch-branching enzyme and the large subunit of ADP-glucose pyrophosphorylase (AGPase), respectively, (Bhattacharyya et al., 1990; Hylton and Smith, 1992), transgenic lines of pea expressing RNAi constructs targeting the small subunit(s) of AGPase have shown a very similar phenotype, when compared with wild-type lines (Weigelt et al., 2009).

In many legume species, oligosaccharides derived from galactinol and sucrose are synthesized in seeds. In pea, these comprise the raffinose oligosaccharide (RFO) group of compounds, which include stachyose and verbascose in addition to raffinose. Quantitative and qualitative variation for these compounds has been described for pea, lentil and *Medicago* (Frias et al., 1994, 1999; Karner et al., 2004; Vandecasteele et al., 2011). Although RFOs are generally regarded as anti-nutrients in seeds, research in Medicago suggests that these compounds are related to seed vigor (Vandecasteele et al., 2011), while additional studies highlight their role in plant stress responses (Nakabayashi and Kazuki, 2015).

The aim of this study was to determine the extent to which variation in the metabolome of mature seeds was under genetic control and to investigate the main types of compounds involved in such regulation. This information could be used further to identify genotypes that are enriched in particular seed components, some of which may be associated positively or negatively with quality and/or health-promoting traits. Given the knowledge of the impact of the allelic state at the *r* and *rb* loci (above) and the variation that exists within these genotypes with respect to seed maturation, we sought to assess the extent of metabolome variation within *r* and *rb* genotypes of pea. In this paper, we define a metabolite phenotype for seeds from genetically marked recombinant inbred *r* and *rb* mutant lines. We describe variation within the metabolome of mature seeds from the recombinant inbred lines, for which we provide substantial genetic marker information and a framework for the analysis of metabolite data in relation to genetic loci and markers. Furthermore, for some of the identified metabolites, candidate genes have been identified for the control of metabolite content.

MATERIALS AND METHODS

Plant Materials

A selection of recombinant inbred lines (RILs) from three mapping populations (JI 281 × JI 399, 32 lines; JI 15 × JI 399, 38 lines; JI 15 × JI 1194, 26 lines) and their parent lines (all available from the JIC *Pisum* germplasm collection; https://www.seedstor.ac.uk/search-browseaccessions.php?idCollection=6) were grown in microplots (1 m^2) at two locations, John Innes Centre, Norwich (JIC) and at the Processors & Growers Research Organization, Peterborough (PGRO), over two consecutive seasons (Year 1, 2011 and Year 2, 2012). The lines comprise 100

variant vining seed genotypes (either *r* or *rb* mutants), derived from crosses that have integrated genetic maps and are densely populated with genetic markers (Supplementary File S1). The JI 1194 parent is *r*, JI 399 is *rb*, and JI 281 and JI 15 are wild type for both *r* and *rb*.

Seeds were treated with Wakil seed treatment and sown directly into plots in bird-proof cages in the spring (March). Plants were irrigated and sprayed for protection against aphids as necessary. Mature (senesced) plants and their seeds were harvested together in July. Seeds were threshed and hand-picked to remove any foreign objects, while phenotype checks ensured the identity, integrity and purity of the genetic stock. From these, seed aliquots (approximately 6g) were prepared for NMR metabolite analysis.

NMR Analysis

The NMR profiles of Year 1 and Year 2 samples (mature seeds from *r* and *rb* RILs grown at two sites) were analyzed by ^{1}H high resolution NMR spectroscopy. Dried pea samples were ground into a fine powder and extracted with 1:1 methanol: water (150 mg per 1.5 mL). Samples were vortexed for 30 min before centrifugation (20,817g for 10 min). Methanol was removed from 900 μL of every supernatant by passing a stream of nitrogen over the sample for approximately 1 h. Samples were lyophilized overnight and then re-constituted in 700 μL NMR sample buffer (250 mM sodium phosphate, pH 7.0; 0.5 mM trimethylsilyl propanoic acid, TSP, dissolved in D_2O), centrifuged (20,917g for 10 min) and 540 μL transferred to a labeled NMR tube. Sodium azide (60 μL aliquot of 10 mM, dissolved in D_2O) was added to every sample to prevent microbial growth before NMR analysis. Extracts were also produced from the seed material using deuterated chloroform to ensure that metabolites which were not soluble in deuterated phosphate buffer solution were analyzed.

All spectra were acquired using an 11.7 T Bruker 500 MHz NMR spectrometer equipped with a 5 mm TCI cryoprobe. Acquisition and processing of the raw data were performed by using Topspin 2.13 patch level 6 (Bruker, Germany). NMR parameters and the magnetic field homogeneity were optimized using a control pea seed extract. The magnetic field was locked on the deuterium signal of the D_2O and the homogeneity was optimized. The free induction decay (FID) was recorded using a 30° ^{1}H flip angle determined from a 90° pulse length of 11.25 μs. A relaxation delay of 3 s was inserted into the pulse sequence to ensure that quantitative data were acquired. Repetitions (256) of 65,536 complex points were collected over a spectral width of 7002.8 Hz, with the center of the spectrum at 500.1323546 MHz. The NMR probe head was maintained at a temperature of 300 K and the sample remained static during data collection. These parameters resulted in a total experiment time of approximately 45 min per sample.

NMR Data Processing

The data were Fourier transformed and an interactive phase correction applied to the spectrum. A baseline correction was applied and the spectrum referenced to the TSP peak at 0 ppm, the area of which was set to unity for all processed spectra using FELIX software (Accelrys, San Diego, CA, USA). Spectral binning of the resonances was performed using bespoke software, Metabolab, a graphical user interface developed using the Matlab platform. Adaptive binning was applied to the data by using the undecimated wavelet transform at a predefined level to reduce the number of variables and limit the effect of the variation of chemical shifts (Davis et al., 2007). Using this approach on the data acquired for different experiments (2 years) resulted in a difference in the total bin number determined for the two data sets. However, the bin identities could be compared, based on their defined limits.

NMR Compound Identification

The identification of metabolites was performed by comparing resonances in the bins with the resonances of spectral data available either from a list of standards present in an internal database or from literature. As a literature source, the following on-line NMR databases were used:

1. Madison Metabolomic Database: http://mmcd.nmrfam.wisc.edu
2. Human Metabolomics Database: http://www.hmdb.ca
3. Database of organic compounds: http://sdbs.db.aist.go.jp/

To assign the binned data, the profiles of all acquired spectra were superimposed to determine the range of chemical shifts of all resonances included in the binned area. Following identification of chemical shift values, the listed databases were interrogated and a list of the most likely candidate metabolites was formed. The spectrum of the candidate metabolite was compared with the spectra acquired from the samples either directly, by using the spectra of the compounds in the internal database, or indirectly, using the on-line NMR databases (1–3 above). One-dimensional ^{1}H and two-dimensional homonuclear and heteronuclear correlation NMR experiments (^{1}H –^{1}H TOCSY and ^{13}C – ^{1}H HSQC) were also used to aid the assignment. The acquisition parameters for the TOCSY and HSQC experiments are given in Supplementary Table 1. A set of resonances was attributed to aglycone derivatives of anthocyanins, based on the study of Kirby et al. (2013).

Normalization of NMR Bin Data and Determination of the Mean of Absolute Deviation (MAD)

The analysis of variation within any one bin across RILs was carried out following normalization of the bin values to a mean of 100 and standard deviation of 1, which resulted in all values being positive. Binned NMR data were normalized according to the formula below to facilitate further data processing.

A'_L is the normalized bin area for the line L calculated as follows:
a_L = NMR peak area
mu_a = mean of the peak area for the RILs and the parents of the mapping population
SD_a = standard deviation of the peak area for the RILs and the parents of the mapping population
$A'_L = 100 + ((a_L - mu_a)/ SD_a)$

As a result, each bin has a mean of 100 and a standard deviation of 1.

Due to the number of data points to be analyzed (968 NMR bins for year 1, 990 NMR bins for year 2), an initial prioritization of bins for mapping analysis was achieved, using Mean of Absolute Deviation from the mean (MAD) values as a measure of the variation within any given bin. MAD values provide a measure of the absolute deviations of a set of data about the data's mean, that is, it is the average distance of the data set from its mean. Although high MAD values indicate bins with high variation across the population, this variation in phenotype does not necessarily indicate genetic variation. However, analysis of bins which have higher MAD values increases the possibility of detecting those bins for which quantitative trait loci (QTL) could be mapped. Due to the normalization carried out (as above), MAD values for the normalized data ranged between 0 and 1. Heat maps were generated to visualize MAD value distributions along the NMR spectrum and to compare relative MAD values among datasets (Supplementary Figure 1).

Linkage map analysis (see below) was performed for bins of interest, whereby quantitative variation within NMR bins was shown to be associated with genetic loci, if the two groups of lines carrying one or the other parent marker at that locus showed significant difference in NMR signal strength. Analysis by *t*-tests identified a set of bins with highly significant associations to genetic map regions. The correlation between MAD value and probability of genetic association for each bin was examined, using Pearson's correlation coefficient, in order to validate the usefulness of MAD values as a method of prioritization.

Genetic Analysis of Quantitative Data Derived for NMR Bins

The genetic marker data and associated genetic maps for seven linkage groups (LG) of the three recombinant inbred pea populations (JI 281 × JI 399; JI 15 × JI 399; JI 15 × JI 1194) which formed the basis for this study are available as Supplementary Data (Supplementary File S1, with the genetic map data available as Supplementary File S1–Figures M1–M9). Briefly, the genetic markers determined were based on gene-specific polymorphisms, as well as sequence-specific amplified polymorphic markers based on the retroelement PDR1 (Knox et al., 2009). Linkage analysis was carried out for three sets of RILs, and genetic maps obtained by ordering all available markers and determining their relative positions using THREaD MAPPER, a web-based software developed at JIC (Cheema et al., 2010), which can be accessed at http://threadmapper.org/threadmapper. The linkage maps generated were used to draw genetic map charts for assessing genetic loci associated with quantitative variation in NMR signals, which can be visualized across the NMR spectrum for all datasets as movies at http://www.threadmapper.org/qdips. Additionally, genetic markers associated with groups of NMR signals were analyzed in Excel, based on *p*-values as described below.

For high-throughput genetic analysis of quantitative trait data, single marker analyses were performed for 12 data sets (RIL population, year and location), using the linkage maps generated and the NMR bin quantitative signals as phenotypic data (968 and 990 bins for year 1 and year 2, respectively). A programme (available on request) was developed in house to generate *p*-values from Student's *t*-tests between RIL and maternal/paternal alleles. For most subsequent analyses, *p*-values were transformed to $-\log_{10}$ to enable map charts to be plotted for visual investigation.

Significance thresholds were determined for all datasets. To minimize the impact of false positive signals generated by multiple *t*-tests, the significance threshold for each dataset was determined individually. First, the frequency distribution of all *p*-values associated with markers for all bins within a dataset was plotted within the range of $0 < p \leq 0.05$ with intervals of 0.0001 (**Figure 1**, blue line) and the average of ten successive intervals generated to remove noise from raw data (**Figure 1**, black line). The data were subjected to randomization (100 times resampled) and the mean *p*-value frequency derived from the randomized data (**Figure 1**, red line) plotted, with error bars of ± 3 standard deviations (**Figure 1**, yellow shadow). A significance threshold for *p*-value was determined where the plot of the experimental dataset crossed over the upper error bar of the resampled (randomized) dataset as indicated (**Figure 1**, green shadow).

RESULTS

Metabolite Analysis

NMR spectra were acquired and peaks identified by adaptive binning (see section Materials and Methods, Davis et al., 2007) which allowed clear separation of peaks, and therefore calculation of peak areas, but with the consequence that the peaks did not coincide exactly between years. Some resonance frequencies included within a peak were known and thus bonds and compounds that contributed to the peak area could be identified. A list of correspondences and potential contributing compounds are given in Supplementary Tables 2, 3.

Peak areas were imported to Microsoft Excel Worksheets and, for a given data set (year and RIL population), the data were normalized so that each peak had an area of 100 and a standard deviation of 1. This meant that all peak areas were positive and that statistical analyses did not unduly emphasize variation in intense peaks and thus global analyses could be applied to the whole data set.

For a given population of RILs, the peak areas for each individual were available and the difference between the mean score for the lines with contrasting alleles was calculated. The expectation for each genotype is that the mean is 100 and the standard deviation is 1. The expected value of the difference between the two means is therefore 0 and given the number of individuals of each genotype a Student's *t*-test statistic can be generated. A related test calculated the mean absolute difference (Mean of Absolute Deviation from the mean, MAD) of the peak areas; this is greatest if there are two data subsets, one greater than 100 and the other less than 100. Example heat maps of MAD values in relation to the NMR spectrum are shown in Supplementary Figure 1, where regions of the spectrum showing

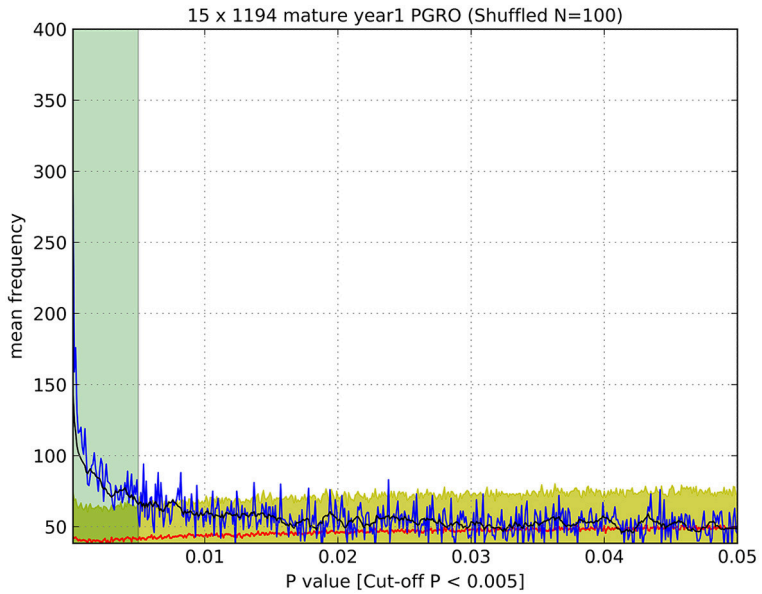

FIGURE 1 | Determination of significance values (as listed in **Table 1**). An example of a plot of the observed number of *p*-values (blue line) of a given value (<0.05) compared to the number of *p*-values of that magnitude from randomized data (red line), which enabled the estimation of a cut-off value above which *p*-values were indistinguishable from random values. Black line: average of ten successive intervals, Yellow shadow: error (±3 S.D.) of 100 times resampled data, Green shadow: cut off point of *p*-values above the significance threshold. Data were determined for JI 15 × JI 1194 RILs, mature seeds, year 1, PGRO location.

consistently high variation are apparent. MAD values and the *t* statistic were well-correlated (Supplementary Figure 1).

The *t*-tests performed provided a probability value (*p*) for the two means being different from each other, but this is seriously confounded by multiple testing (ca. 1,000 bins and 790 markers). We therefore examined the frequency distribution of *p* as compared to randomized data in order to identify a threshold significance value for *p* (**Figure 1**).

Genetic Map Based Analysis

The determination of cut-off *p*-values generated large numbers of "significant" associations (**Table 1**). This suggested that, for most NMR bins, some genetic marker(s) could explain a component of their variation. While this is of theoretical interest, it does not focus attention on specific marker/metabolite associations. An alternative approach was taken where the minimum *p*-value for each marker was plotted against the genetic map of each RIL population (**Figure 2**). This identified those regions of the genetic map with the most significant effect on the metabolite profile and, once these had been identified, the NMR bin most affected by that marker could be identified.

The plot identifies regions of the genetic map that have important effects on the metabolite profile. It should be realized that these are regions of relative importance because the low *p*-values are included in the estimation of the standard deviations. If one of the most extreme peaks was missing, then the standard deviations used to estimate significance would be of a lower value. Those associations that are consistent between years are symmetrically reflected about the genetic map and equivalent positions on the genetic maps can be seen. The seven regions identified as peaks on the map (**Figure 2**) are discussed below.

TABLE 1 | Summary of pea recombinant inbred populations for which metabolite data were collected for mature seeds in 2 years and two locations.

Dataset	Significance threshold (*p*-value)	Number of significant marker bin associations
JI 281 × JI 399, Y1, JIC	0.0073	18,040
JI 281 × JI 399, Y1, PGRO	0.0136	36,549
JI 281 × JI 399, Y2, JIC	0.0215	54,849
JI 281 × JI 399, Y2, PGRO	0.0071	19,261
JI 15 × JI 399, Y1, JIC	0.016	25,721
JI 15 × JI 399, Y1, PGRO	0.0168	27,136
JI 15 × JI 399, Y2, JIC	0.0001	398
JI 15 × JI 399, Y2, PGRO	0.0023	4,002
JI 15 × JI 1194, Y1, JIC	0.0035	3,012
JI 15 × JI 1194, Y1, PGRO	0.005	4,636
JI 15 × JI 1194, Y2, JIC	0.0018	1,392
JI 15 × JI 1194, Y2, PGRO	0.0003	401

*The significance threshold (see **Figure 1**) determined for every dataset [population identity, year (Y1 or Y2) and location of plant growth (JIC or PGRO)] is listed, together with the number of markers for which significant quantitative variation in NMR bin signal intensities was determined.*

Peak 1 and Peak 6

These peaks are associated with a segment at the top of linkage group (LG) I characterized by the microsatellite marker PC20 and the gene encoding a small subunit of AGPase (Aubert

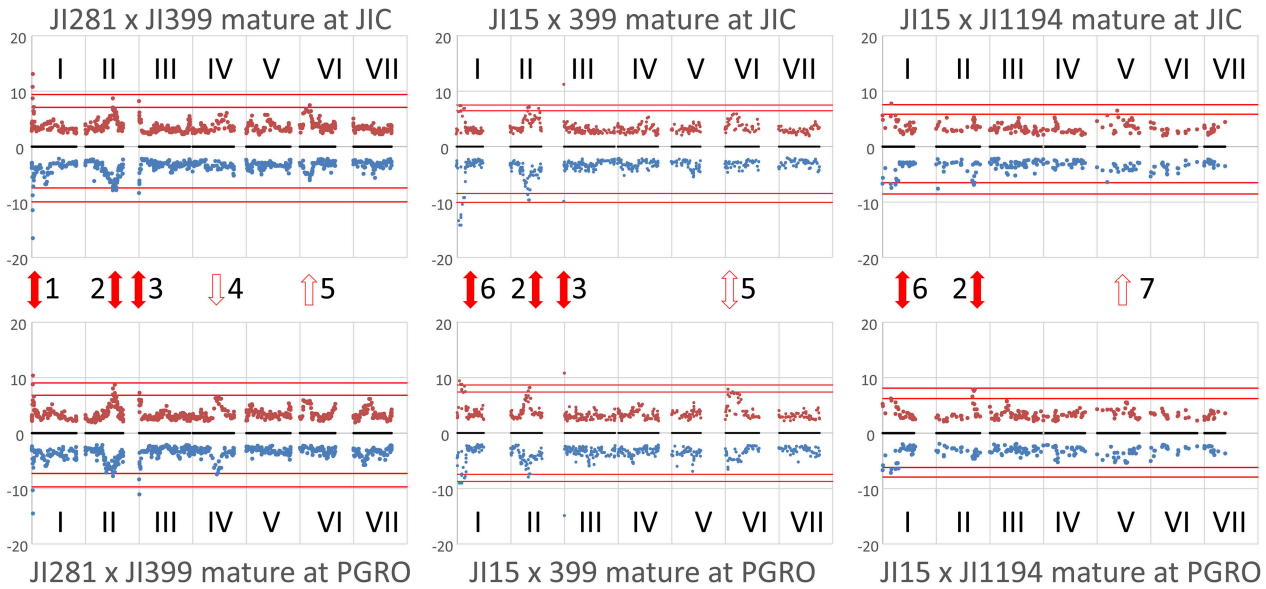

FIGURE 2 | Locating the genomic regions with the most contrasting alleles. Genetic maps (linkage groups identified by roman numerals, I–VII) of the three populations analyzed (left to right JI 281 × JI399, JI 15 × JI 399, JI 15 × JI 1194) grown at JIC **(Top)** and PGRO **(Bottom)** are shown and the common logarithm of minimum *p*-value [$-\log_{10}$ (*p*)] for each marker is plotted (in blue, below the map for year 1 data, and −1 times this value in brown above the map for year 2 data). The red lines correspond to +3 and +5 standard deviations of all *p*-values for that population and location. Solid red arrows indicate marker-NMR resonance associations that are consistent between years, open arrows indicate those that reach the threshold value in 1 year, all numbered for reference in the text.

et al., 2006). The classical locus *D* also maps in this region (Ellis and Poyser, 2002) and this locus is known to regulate the pattern of anthocyanin deposition. The resolution of the map is insufficient to identify a single causative allelic difference. However, although the peak assignments for this region (peaks 1 and 6) in the three populations at the two sites do not coincide exactly (**Figure 2**), the region includes some common genetic markers; the associated compounds are listed in **Table 2**. Note that these markers identify only the most significant associations, so a lack of replication does not mean that a shared association does not occur. One peak, and compound, implicated more than once is the flavanone glycoside hesperidin. The *p*-value data for the additional peaks identified for hesperidin, as shown in Supplementary Figure 2 for the JI 281 × JI 399 population (JIC, years 1 and 2), illustrate the consistency of this association. All but one of the bins that include a resonance assigned to hesperidin behave co-ordinately across the genetic map. This is consistent with the signals being derived from variation in the abundance of hesperidin or a closely related compound. The lack of significance for one bin (and an equivalent resonant range in both years) could be explained by a contribution from an additional signal in that bin from a compound that does not co-vary in abundance with hesperidin. Here, additional resonances are associated with aromatic compounds, tryptophan and its catabolite tyramine. Taken together, these signals suggest that there is allelic variation in this LG I region that alters the regulation of compounds closely related to the anthocyanin pathway, and the *D* locus may therefore be implicated.

Peak 2

This is a broad peak on LG II (**Figure 2**) and has its highest significance value in the population JI 281 × JI 399 associated with the classical gene *A*, which regulates anthocyanin biosynthesis and corresponds to a gene encoding a bHLH transcription factor (Hellens et al., 2010). The peak resonances are listed in **Table 3**; most of the bins are in the aromatic region of the spectrum, two in the sugar range and one in the expected range for aliphatic amino acids. The distribution of year 1 and year 2 *p*-values for the bin tentatively assigned as the flavonoid naringin in the JI 281 × JI 399 RILs (JIC location) are shown in Supplementary Figure 3 and show no significant *p*-value associated with *A*. Surprisingly although *A* and *a* segregate in all three populations analyzed, no signal for an anthocyanin was detected in this analysis. Kirby et al. (2013) have undertaken an NMR analysis of anthocyanins in *Rhus typhina*, identifying profiles with multiple resonances, and so it was expected that signals from pea anthocyanins might be similarly scattered throughout the NMR spectrum. The resonances identified by these authors as corresponding to aglycones can be aligned with the bins we defined in this group. These results are shown in Supplementary Figure 4, and suggest that it is likely that some *A*-regulated anthocyanins are detected by this analysis of mature seeds.

Peak 3

Peak 3 corresponded to the top region of LG III in two of the three populations analyzed (**Figure 2**). This peak, close to the *rb* locus, may be considered an artefact due to there being very few *RbRb* genotypes within these two populations, where the vining genotypes selected for analysis were *rb* mutant lines (see section Materials and Methods). The *rb* mutation is a consequence of a nine-base pair deletion in the gene encoding the large subunit of AGPase (Rayner et al., 2017),

TABLE 2 | Peak 1 and Peak 6 resonances and associated NMR bin data.

Population	Location	Year	Bin	ID comment	Bin range ppm	Compound ppm
JI 281 × JI 399	JIC	1	**196**	**Hesperidin**	7.106494107–7.096238809	7.106494
			199	Aromatic	7.09111116–7.085983511	7.085984
		2	209	Aromatic, unknown	7.139396521–7.130850439	7.13726
			210	Unknown	7.130850439–7.125722791	7.084702
			216	Aromatic, unknown	7.089829248–7.077010126	
	PGRO	1	**196**	**Hesperidin**	7.106494107–7.096238809	7.106494
		2	214	**Hesperidin**	7.107776019–7.09111116	7.106494
JI 15 × JI 399	JIC	1	**166**	Aromatic, tentative **Naringin**	7.359458121–7.347066302	7.359458
			182	Aromatic, tentative **Tyramine**	7.237249155–7.224002728	7.224003
			184	**Tyrosine multiplet 3,5**	7.219729688–7.209474390	7.2127
			206	Unassigned	7.050089969–7.041543887	7.031716
			207	Aromatic, tentative **Chlorogenic acid**	7.041543887–7.031715894	
		2	243	Unknown		6.9415
	PGRO	1	**166**	Aromatic, tentative **Naringin**	7.359458121–7.347066302	7.359458
			182	Aromatic, tentative **Tyramine**	7.237249155–7.224002728	7.224003
			219	Unassigned	6.945400467–6.932581348	6.9415
		2	200	**Tyrosine multiplet 3,5**	7.198791788–7.186399969	7.1898
			201	Aromatic, unknown	7.186399969–7.178708496	7.183409
			228	Unassigned	7.042398495–7.03342511	
JI 15 × JI 1194	JIC	1	166	Aromatic, tentative **Naringin**	7.359458121–7.347066302	7.359458
			183	Tyrosine	7.224002728–7.219729688	7.21973
			192	**Unassigned**	7.126150095–7.122304358	
		2	196	Aromatic, unknown	7.237676459–7.226993857	7.237249
	PGRO	1	**182**	Aromatic, tentative **Tyramine**	7.237249155–7.224002728	7.224003
			194	Unassigned	7.110339844–7.108203323	
			217	Unassigned	6.966765674–6.948818903	
		2	**228**	**Unassigned**	7.042398495–7.03342511	

Summary provides the population identity, year and location of plant growth (JIC or PGRO), NMR bin number and range, and compound information. In bold are the bin numbers and/or compound data that were identified consistently.

which maps close to the top of LG III. It is noteworthy that this peak is missing from the JI 15 × JI 1194 population where all individuals are *RbRb*. Nevertheless, it is of interest that variation in metabolite profiles reflected the status of the *rb* locus.

Peak 4

A peak in the JI 281 × JI 399 population in the middle of LG IV for plants grown at PGRO is seen for both years (**Figure 2**). The peak of this value corresponding to bin 681 in JI 281 × JI 399 (Y1, PGRO) was not assigned to a known compound.

Peak 5

For both the JI 281 × JI 399 and JI 15 × JI 399 populations a peak can be seen in LG VI (**Figure 2**). The significant signals are for bin 490 in year 2 in JI 281 × JI 399 (JIC) and in JI 15 × JI 399 (PGRO), which was not assigned to a known compound but there is a resonance noted at 5.1052 ppm.

Peak 7

This corresponds to bin 879 in year 1 in the JI 15 × JI 1194 population and corresponds to an unidentified compound with a resonance at 1.1974 ppm.

Compound Based Analyses

Using the genetic map as a way of identifying interesting compound/marker associations identified those regions of the map which had the most profound effect on the metabolite pool. However, this approach was limited because the association between NMR bins and known compounds within those bins was poorly established. It did suggest, however, that there are regions of the genome that have a major impact on the seed metabolome and which require further characterization, for example using 2D NMR or complementary analytical methods. The extent of this genetically controlled variation was revealed to be greater than initially expected, compared to analysis of leaf metabolomes (Charlton et al., 2008). A complementary approach was to examine variation associated with priority compounds, or classes of compounds, for which NMR resonances have been established.

TABLE 3 | Peak 2 resonances and associated NMR bin data.

Population	Location	Year	Bin	Comment	Bin range ppm	Compound ppm
JI 281 × JI 399	JIC	1	309	Unassigned	6.252740561–6.231375357	
			910	Unassigned	0.881101007–0.869136493	
		2	432	Unassigned	5.709637079–5.698527173	
	PGRO	1	250	Unassigned	6.720211221–6.706110187	
		2	249	Unassigned	6.891560156–6.883868683	
			569	Unknown	4.319616916–4.312780051	4.3151
			570	Unknown	4.312780051–4.304661273	4.3089
JI 15 × JI 299	JIC	1	299	Aromatic, unknown	6.371958398–6.34589285	6.371958
		2	**354**	**Unassigned**	6.289488712–6.271969244	
	PGRO	1	157	Unassigned	7.450046585–7.448337369	
		2	336	Aromatic, unknown	6.372385703–6.354866235	6.371958
JI 15 × JI 1194	JIC	1	307	Aromatic, tentative chlorogenic acid	7.450046585–7.448337369	
		2	n/a	n/a	n/a	
	PGRO	1	n/a	n/a	n/a	
		2	**354**	**Unassigned**	6.289488712–6.271969244	

Summary provides the population identity, year (Y1 or Y2), location of plant growth (JIC or PGRO), NMR bin number and range, and compound information. In bold is the bin number identified more than once.

Here we need to consider two problems. The first is that any bin contains more than one resonance frequency and so the signal intensity may reflect the abundance of more than one compound. The second problem is that any particular resonance may derive from more than one molecule, for example if the molecules differ at remote positions. One way to overcome this is to consider the behavior of the signals from molecules with many assigned resonances which might be expected to behave co-ordinately. Several amino acids fulfil these criteria and are discussed below.

Isoleucine

There are 23 bins that report the intensity of resonances from isoleucine in year 1 and year 2 data (see Supplementary Table 3). If these all report variation in the abundance of the same compound, then the *p*-values for each marker should be strongly correlated. Comparing the year 1 and year 2 data for JI 281 × JI 399 grown at JIC (Supplementary Table 4A), this is clearly not the case. The highest correlation coefficient is 0.344 (year 1 bins 795 and 904 vs. year 2 bin 977), and the lowest is −0.377 (year 1 bin 848 vs. year 2 bin 915). In contrast, comparison of the *p*-values for bins assigned to isoleucine within either year 1 or year 2 were highly correlated, with correlation coefficients reaching 0.97 in year 1 and 0.99 in year 2 (Supplementary Table 4B). This suggests that different bins are in fact reporting on co-varying determinants of the NMR signal, consistent with reporting on the same compound (or set of compounds). However, not all correlations were high even within an assignment class (defined in terms of the source of the NMR resonance in Supplementary Table 3). This is consistent with some bins reporting on resonance due to similar bonds in related (but different) compounds, or interference from resonances generated from different compounds that fall within the same bin.

The corresponding bins have different ppm ranges in different years; this may mean that the partitioning of signals is different between the data sets from the 2 years which may be more important than environmental effects on the biological samples. Indeed, the average of the correlation coefficients comparing overlapping bins between years is -0.024 ± 0.140 ($n = 21$), while the average of the correlation coefficient comparing non-overlapping bins between years is -0.027 ± 0.110 ($n = 209$), which would be consistent with the interpretation that overlapping bins are no more closely related than different bins that contain a resonance from the same compound; in other words, there are confounding signals within a bin. Partitioning these signals along the genetic map is therefore a useful way of dissecting out commonalities across the bins as shown in **Figure 3**. Although some peaks are consistent between **Figures 3A,B**, no peaks are consistent between years in **Figure 3B**, consistent with the suggestion that the bins are not comparable between years.

Leucine

Three bins were assigned to leucine in the year 1 and year 2 data, with details provided in Supplementary Table 5 and Supplementary Figure 5. These bins are close to one another and illustrate the way bins correspond between years. The data also highlight how adaptive binning can result in differences in the distribution of resonances among bins between the year 1 and year 2 datasets. (For example, the year 1 bin 903 includes the leucine resonance at 0.9494 ppm and the isoleucine resonance at 0.9584 ppm, but these are in separate bins in the year 2 data).

The distribution of $-\log_{10}(p)$ values for leucine is shown on the genetic linkage map in **Figure 4**. Here the reflection of the pattern above and below the map shows the consistency of the data between years and sites, which is particularly noticeable

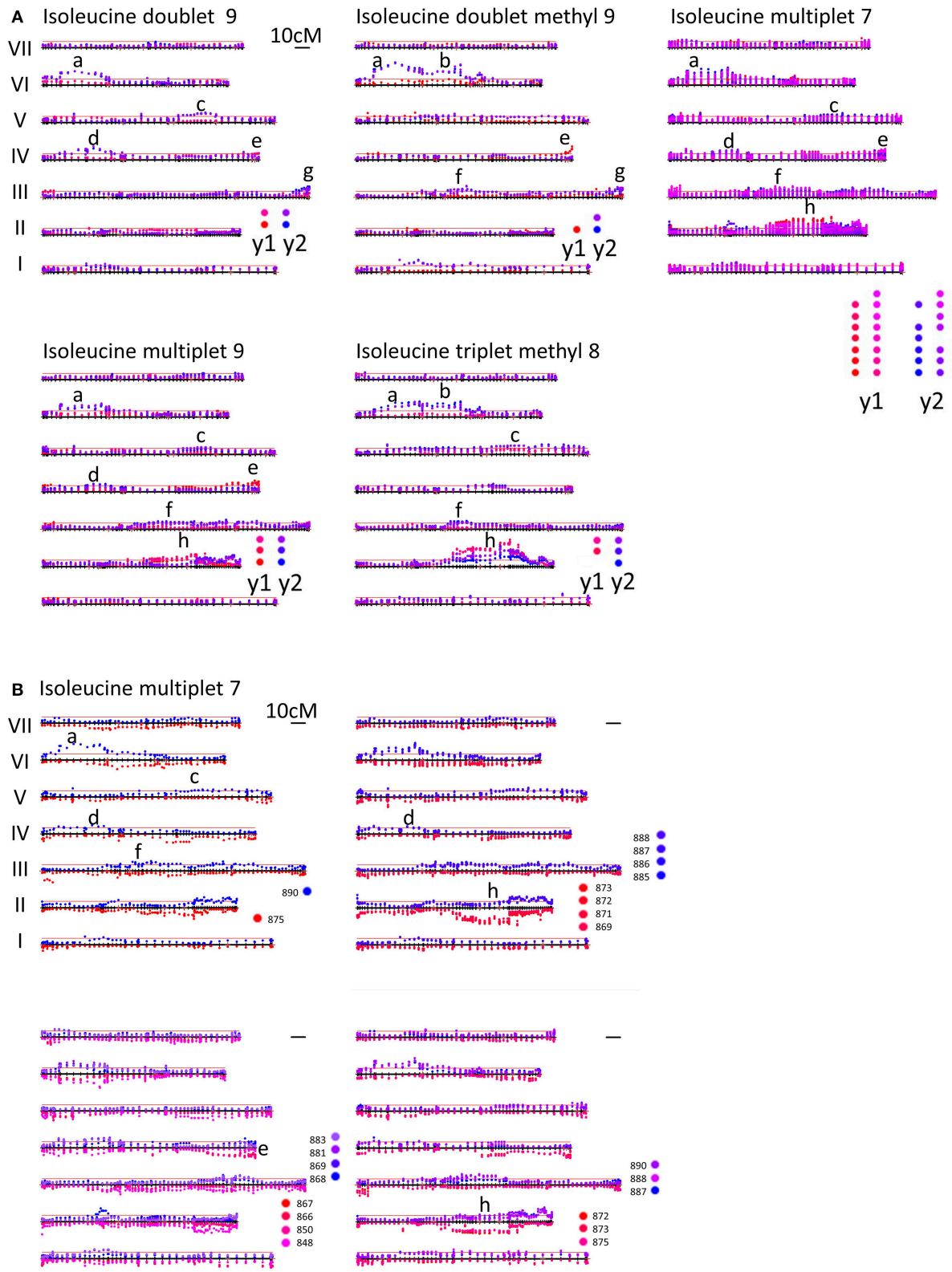

FIGURE 3 | (A) Mapping variation attributed to isoleucine. LG I–VII of the genetic map of the JI 281 × JI 399 RIL population are displayed horizontally from bottom to top for each isoleucine signal. The $-\log_{10}$ (p)-values for each marker are plotted above the genetic map for NMR resonances associated with different parts of the isoleucine molecule. Different bins are plotted with a slightly different color, those from year 1 in red and those in year 2 in blue. Overall, the identified peaks (labeled a–h)

(Continued)

FIGURE 3 | are different between years, with the exception of peak h. The multiple bins assigned to isoleucine multiplet 7 are deconvoluted in **(B)**. Mapping variation attributed to isoleucine multiplet 7. LG I–VII of the genetic map of the JI 281 × JI 399 RIL population are displayed horizontally from bottom to top. The $-\log_{10}$ (*p*)-values for each marker are plotted above the genetic map for year 2 data and below the genetic map for year 1 data. The color coding for the various bins is indicated adjacent to the relevant map. The bin groupings are according to the correlations given in Supplementary Table 4. The peaks (labeled a–h) correspond to those identified in **(A)** for isoleucine multiplet 7. The red lines above the map correspond to 3 SD units for the variation in *p*-values.

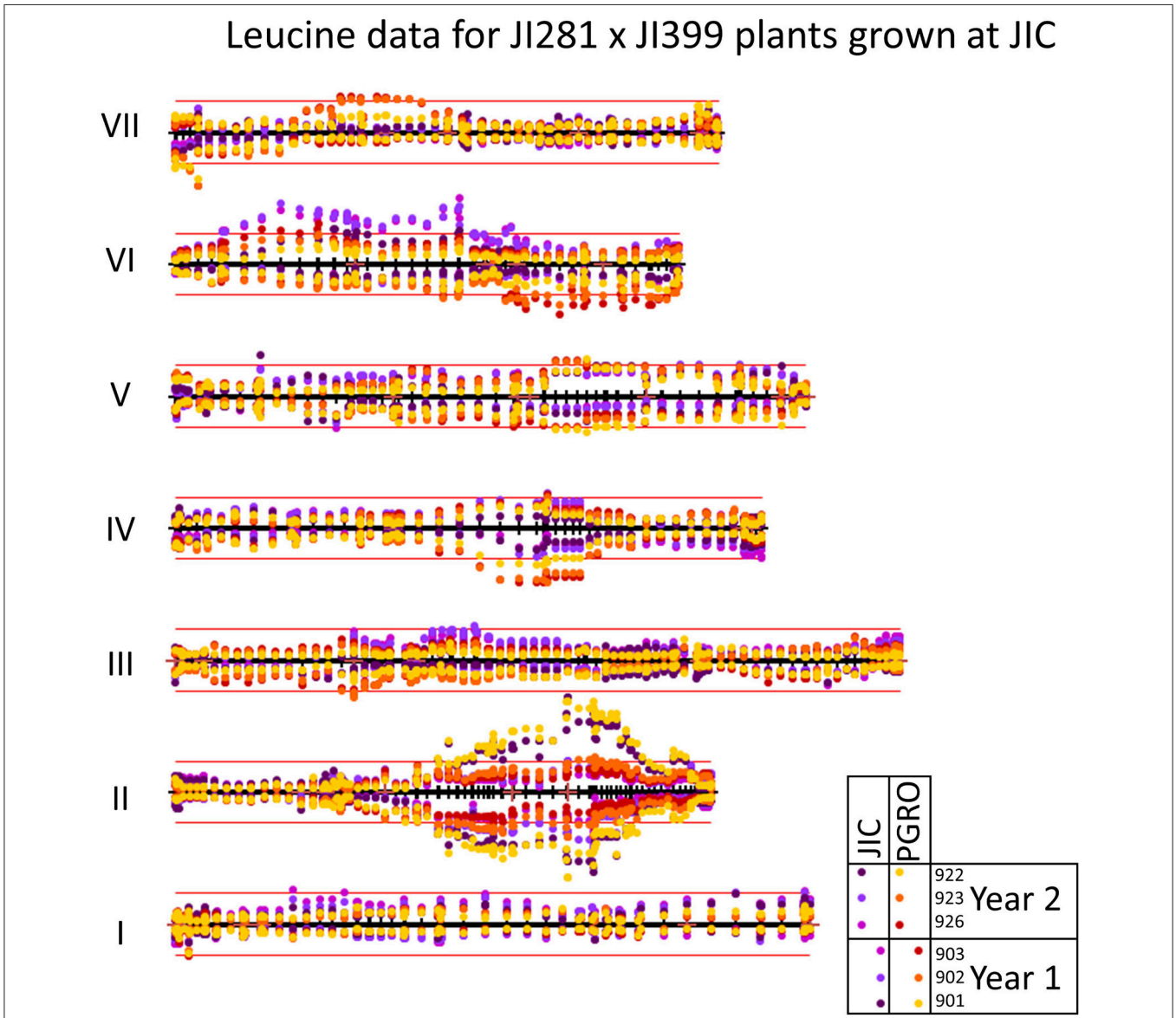

FIGURE 4 | Mapping variation attributed to leucine. The seven linkage groups (I–VII) of the JI 281 × JI 399 genetic map are displayed horizontally from bottom to top. The $-\log_{10}$ (*p*) values for each marker are plotted above the genetic map for year 2 data and below the genetic map for year 1 data. The color coding for the various bins is indicated adjacent in the boxed section. The bins that contain the same resonance in year 1 and year 2 are given the same color. The red lines above and below the map correspond to 3 SD units for the variation in *p*-values for year 2 and year 1, respectively.

on LG II in the region of the classical genetic marker *A*. The correlations among leucine associated bins for two years are given in Supplementary Table 6. The correlations between sites and years for LG II are given in **Table 4**, where the most different site/year combination is JIC in year 2. Remarkably, the strongest and most consistent signal is coincident with the *A* locus. The direction of this effect shows that the allele *a* is associated with an increase in signal intensity (Supplementary Figure 6), implying a role for this locus in regulating compounds beyond anthocyanins.

TABLE 4 | Linkage group II correlation coefficients of *p*-values among sites and years for leucine related NMR signals in the JI 281 × JI 399 RILs (Year 1, Year 2) across two sites (JIC, PGRO).

	JIC Y1	JIC Y2	PGRO Y1	PGRO Y2
JIC Y1		0.481	0.692	0.711
JIC Y2	0.481		0.580	0.680
PGRO Y1	0.692	0.580		0.719
PGRO Y2	0.711	0.680	0.719	

Shading intensity is proportional to the value of the correlation coefficient.

The JI 281 × JI 399 Recombinant Inbred Population

Focussing on a single RIL population limits the analysis to a pair of alternative alleles, and we have shown above that the least correlated pair is the year 1 and year 2 data for the population JI 281 × JI 399 grown at JIC. We therefore examined these data sets and filtered according to the $-\log_{10}$ (p) values, selecting only marker/bin associations having a $-\log_{10}$ (p) value greater than 5 standard deviations from the mean of all values. For both years, this is a more stringent selection than using the p-values obtained using data randomization (see above). These data are summarized in **Figure 5**. Where there is correspondence in the identification of a marker/bin association at this level of stringency, the two types of symbol are coincident, whereas regions unique to a given year are indicated by the presence of a single symbol type (**Figure 5**). The resonance signals for all the bins where a compound has been identified are listed in Supplementary Table 7 and the compounds affected are listed in **Table 5**.

Raffinose and Related Oligosaccharides in the JI 281 × JI 399 Population

The raffinose family of oligosaccharides (RFOs) are among the list of compounds in **Table 5**. These three (raffinose, stachyose, verbascose) are related in terms of their biosynthesis (Peterbauer et al., 2002). One of the enzymes involved (raffinose synthase, Rfs) shows genetic variation that maps approximately centrally on LG III (close to PSAB124, PSAA491 and PSAC18 markers in the JI 281 × JI 399 population; close to agpS1_SNP3 on LG III in Iglesias-García et al., 2015). The gene encoding a second enzyme of this pathway, stachyose synthase (Sts), has been mapped to LG V in another cross (cv. Princess × JI 185, not used in this study). It is therefore of interest to describe how allelic variation for those bins, which contribute to the set displayed in **Figure 5** and are associated with only one of these compounds, is distributed on the genetic map. This is illustrated in **Figure 6**.

The graph (**Figure 6**) includes an association between one of the verbascose-related bins (566) and the location of stachyose synthase on linkage group V. Overall, the correlation between the two verbascose bins (566, 544) is low, likely due to additional resonance signals. However, the correlations of bin 566 with the others assigned uniquely to RFOs suggests that this set of bins is reporting on related compounds. The slight elevation of $-\log_{10}$ (p) values near the location of the raffinose synthase gene does not reach the threshold level. This is notable, as there are eight amino acid differences between the deduced raffinose synthases of JI 281 and JI 399, four of which are predicted to lie within the mature protein (Q216K, R253W, G329V, and M379V for JI 281 and JI 399, respectively). The most significant associations for this group of compounds are with regions of LG II (stachyose, verbascose) and LG IV (raffinose, stachyose) (**Figure 6**).

Genetic loci on different linkage groups are associated with effects on raffinose concentration (**Figure 6**). The three raffinose bins (591, 589, and 587) are generally well correlated for the whole map, where the lowest correlation is for bins 589 and 587 with $r = 0.729$. However, the analysis for individual linkage groups has a range of correlation values, as would be expected if there is some interference from additional resonances that are under distinct genetic control. The most variable pair is 589 and 587 and their minimum correlation (for LG II) is 0.298 and maximum is 0.980 (for LG IV). Nevertheless, the strong correlation among these three bins is consistent with them reporting reasonably well on the same or a related compound. The most striking feature of these correlations according to linkage group is the contrast between LG II and LG IV. For LG II most correlations are positive; three negative pairwise combinations involve bin 587, with the other raffinose related bins having a positive correlation to both stachyose and verbascose bins. Linkage group II is the least differentiated in terms of these bins (measured as the mean average deviation of the non-self-correlations. For LG I–VII, these are: I, 0.331; II, 0.254; III, 0.351; IV, 0.616; V, 0.307; VI, 0.301; VII, 0.420, and overall 0.299). In contrast, LG IV is the most differentiated, with raffinose and stachyose positively correlated, but these are negatively correlated with verbascose, consistent with an allelic difference in the final step of the pathway. This is also seen on the $-\log_{10}$ (p) plot toward the right-hand side of LG IV (**Figure 6**), where the color symbols are well separated, suggesting a difference in control of the early and late steps in the RFO pathway. Within this group of compounds, the most intense NMR signal was from stachyose (bin 585) and this showed the largest actual difference in signal intensity between the contrasting allelic states (higher with the JI 399 allele); the greatest percentage difference between the allelic classes was for bin 544 (verbascose) which was higher when associated with the JI 281 allele.

DISCUSSION

In this paper, we investigate the genetic control of significant metabolites in pea seeds and provide a framework for their analysis in association with genetic maker data. Two approaches were adopted to examine the extent to which genetic, rather than environmental, control was important in determining the metabolome of seeds derived from three mapping populations: a map-based and a compound-based analysis. Despite the difficulties in associating NMR bin resonances exclusively with specific compounds, the screens have identified classes of compounds that should be investigated further as well as regions of the genetic map that warrant further investigation in relation to the compounds that are affected. We conclude that:

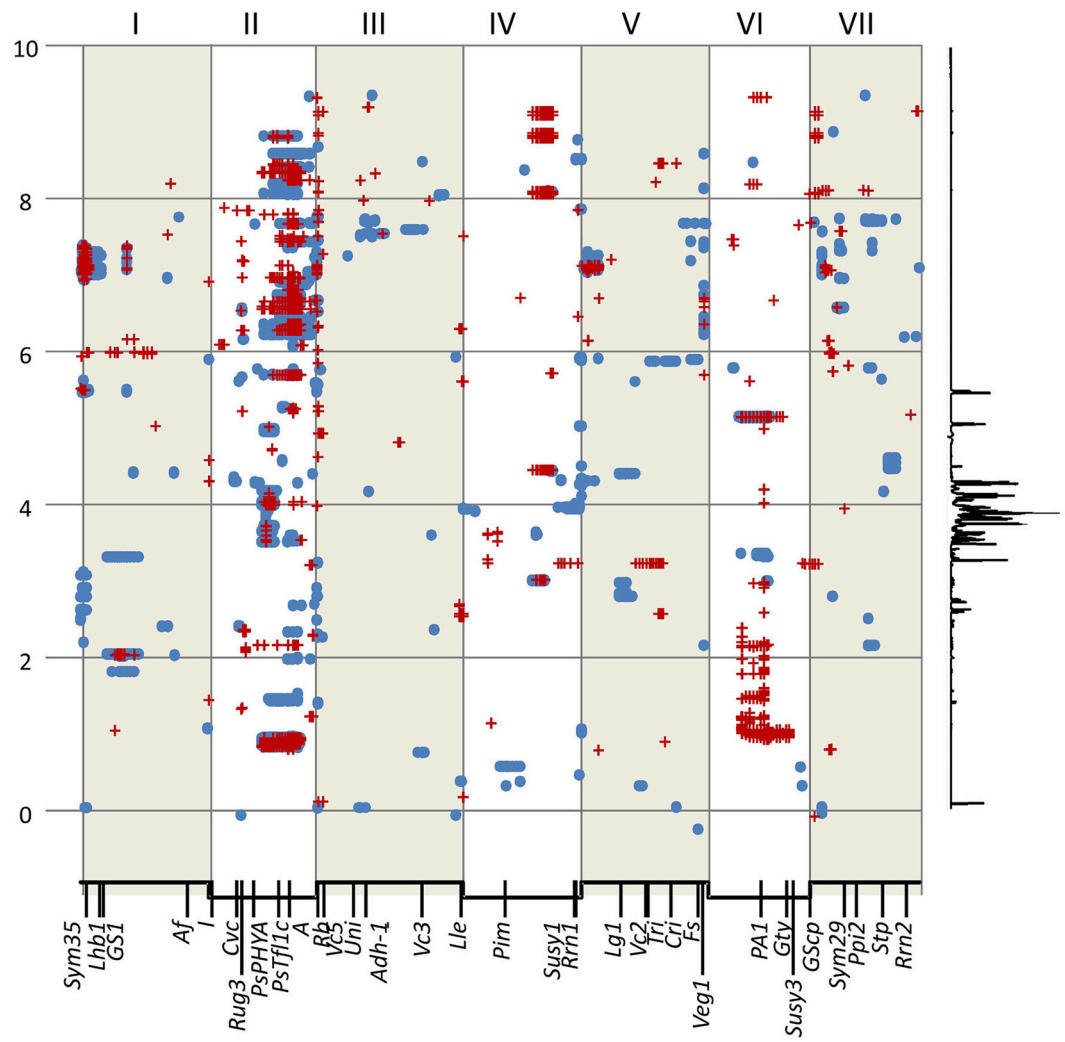

FIGURE 5 | Significant genetic marker-NMR bin associations in the JI 281 × JI 399 RILs. The x axis represents a concatenated genetic map for LG I–VII in numerical order. Below the axis several reference genetic loci are indicated. The y axis represents the NMR spectrum in ppm. To the right of the graph a representative trace of the NMR spectrum is shown vertically to indicate relative signal intensity. The blue spots represent the upper and lower bounds of a selected year 1 bin and the red crosses are the upper and lower bounds of selected year 2 bins (both JIC location). Bins were selected that had $-\log_{10}(p)$ values greater than the mean plus 5 SD units.

TABLE 5 | Summary of compounds identified which differed in JI 281 × JI 399 RILs with high significance.

Compounds identified in Years 1 and 2			Year 1 only	Year 2 only
Alanine	Isoleucine	Sucrose	Aspartic acid	Phenylacetic acid
Arginine	Leucine	Trigonelline	Delphinidin	
Chlorogenic acid	Myoinositol	Tyramine	(or hesperidin)	
Folic acid	Naringin	Tyrosine	Dodecenic acid	
GABA	*p*-coumarate	Valine	Glutamine	
Glutamate	Phenylalanine	Verbascose	Methyl maleic acid	
Glutathione	Raffinose			
Hesperidin	Rutin			
Homoserine	Stachyose			

1) There are many different metabolites for which their abundance, within seeds of the RILs studied, varies under genetic control.
2) The genetic control of these compounds is distributed throughout the genetic map, with some regions implicated in the control of diverse metabolites.

An association between anthocyanin/phenylpropanoid derivatives and the nature of the allele at the *A* locus on LG II provides an example where the associated gene is a strong candidate for the observed effect, based on knowledge of flower color and seed trait differences associated with *A*/*a*. However, the highly significant differences in the branched chain amino acids (leucine, isoleucine) also associated with this locus suggests a wider impact on amino acid metabolism. This may be explained by considering that the anthocyanins

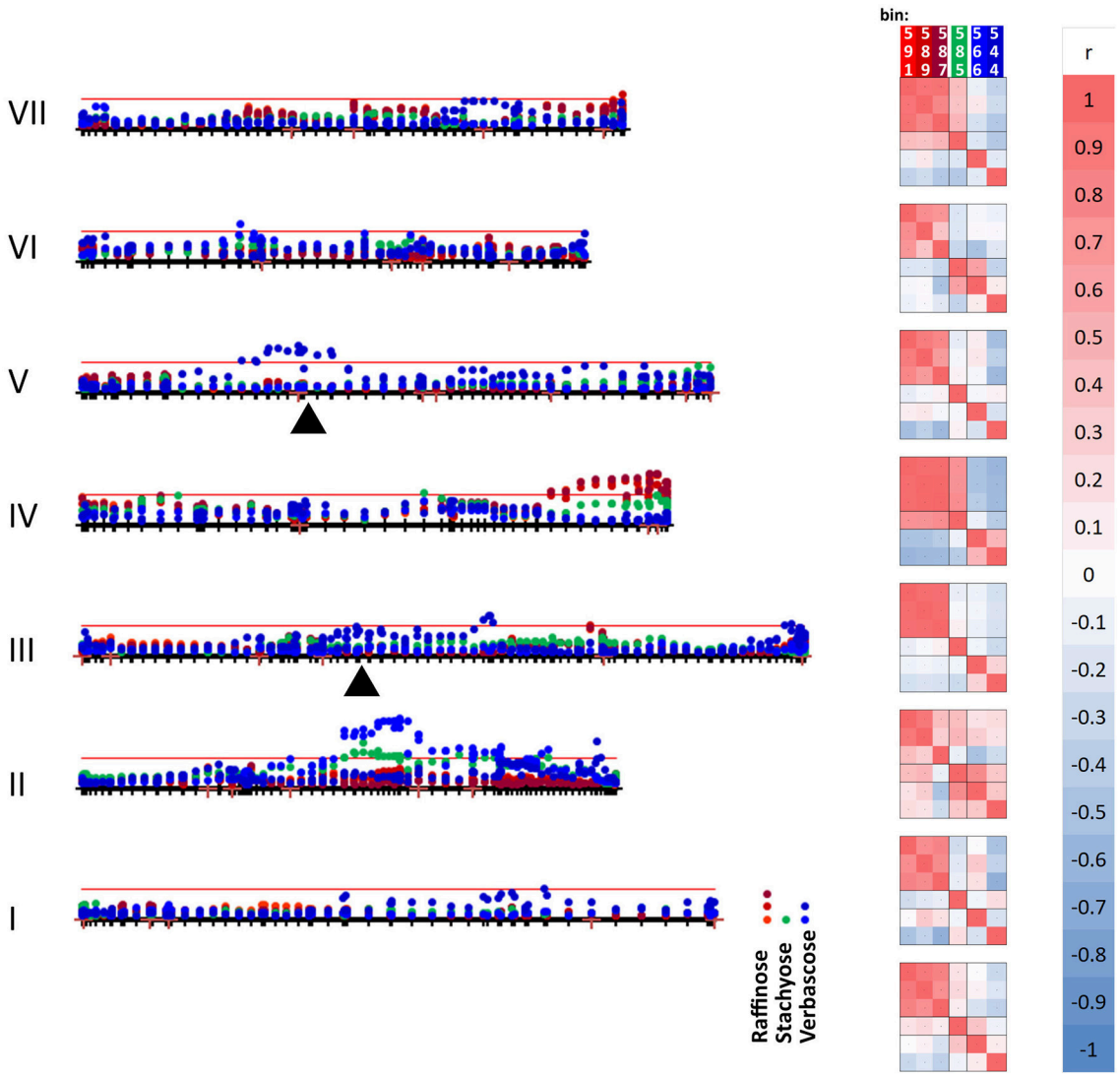

FIGURE 6 | Mapping variation attributed to oligosaccharides. The seven linkage groups (I–VII) of the JI 281 × JI 399 genetic map are displayed horizontally from bottom to top. The –log10 (*p*) values for each oligosaccharide bin/marker are plotted above the genetic map (year 1, JIC). The threshold value for *p* determined from the randomization and *t*-test is indicated by the red horizontal line. The positions of raffinose synthase and stachyose synthase genes on linkage groups III and V are indicated by black triangles. The three bins assigned to raffinose (591, 589, and 587) are indicated in shades of red, stachyose (585) in green, and the two verbascose bins (566 and 544) in blue. On the right of the genetic map, a correlation analysis of the *p*-values for each bin within each linkage group is indicated, together with a color scale for the correlation range −1 to +1. At the bottom of the correlation scores, the correlation between the bins for the whole linkage map is given.

are derived from phenylalanine/ phosphoenolpyruvate, while leucine/isoleucine are derived from pyruvate. Therefore, a reduced flux from phosphoenolpyruvate to phenylpropanoids in *a* mutants may generate a higher flux from pyruvate and hence more leucine/ isoleucine. This hypothesis is in agreement with the directional change in these amino acids (Supplementary Figure 6). Although the pool of free amino acids is relatively small in mature seeds, in comparison with protein-derived amino acids, it is likely to represent a component of the seed metabolome which is significant to seed storage and early germination. Fait et al. (2006) showed that the metabolic preparation for germination and efficient seedling establishment is initiated during seed desiccation. Understanding the genetic control of such variation is therefore of academic as well as economic interest. Other work has highlighted the impact of single gene changes on the seed metabolome; metabolomic profiling of pea lines down-regulated for AGPase has demonstrated the widespread consequences for metabolism of changes to this single gene (Weigelt et al., 2009). Significant variation in relative amounts of amino acids and in polyamine metabolism was reported in a study of seeds from wild type and mutant pea lines, differing by the presence or absence of pea

albumin 2 genes, normally expressed in seeds (Vigeolas et al., 2008).

The genetic loci associated with variation in RFOs are equally of interest, with some genetic control possibly attributed to genes encoding the major synthetic enzymes of the pathway (LG III and LG V), but a much higher level of significance implicating control by genetic loci on LG II and IV. The below threshold variation associated with the different *Rfs* genes in JI 281 and JI 399 is in agreement with the different *Rfs* alleles encoding proteins that do not differ greatly in functionality. Certainly, none of the variant Rfs regions are predicted to be of high relevance to protein function (using CODDLE and PARSESNP programmes). The association of verbascose variation with LG V and the *Sts* gene may be consistent with the JI 281 *Sts* allele progressing the galactosylation of RFOs further than its JI 399 counterpart. Transfer of a further galactinol residue to stachyose gives verbascose, a reaction which is probably catalyzed by a bifunctional stachyose synthase (Peterbauer et al., 2001). In combination, these loci (**Figure 6**) may be important for determining seedling vigor. In *Medicago truncatula*, seven of the 12 QTL for germination rate or post-germinative growth parameters co-located with sucrose/RFO QTL (Vandecasteele et al., 2011). A significant negative correlation was also found between seed vigor traits and sucrose: RFO ratio and, in addition, 80% of the variation in the stachyose: verbascose ratio co-located with a stachyose synthase gene. The genetic control of RFOs is of additional interest, given their involvement more generally in abiotic and biotic stress responses (Cao et al., 2013; Nakabayashi and Kazuki, 2015).

Further development of the framework presented here for association of NMR resonances and genetic variation could include two-dimensional NMR on the contrasting genotypes, focussing on the resonances identified as being significant. Additionally, HPLC and/or GC-MS could supplement these analyses. The identification of candidate genes implicated in the genetic regions highlighted by this work could be accelerated by using the fast neutron mutant population, which has been developed for pea in one of the genetic backgrounds studied here (*rb* mutant) and where large genomic regions have been shown to be deleted (Domoney et al., 2013). Deletions could be positioned with respect to the genetic map and (when available) the genome sequence of pea to identify a subset of fast neutron mutants in which the NMR signals could be compared. Mutants affected in the relevant signal would presumably carry a deletion in the gene of interest and therefore it could be identified. These approaches would be complementary to those presented by Luo (2015) for metabolite-based genome-wide association studies in plants.

CONCLUSION

NMR analysis of genetically marked lines of pea has revealed genetic variation associated with sets of metabolites present in mature seeds. Some of this variation may be explained by few genetic loci, including variation in compounds related to aromatic amino acids, branched-chain amino acids, sucrose-derived metabolites, secondary metabolites and some unidentified compounds. Overall there is extensive variation within *r* or *rb* genotypes that has major implications for seed quality traits and may impact nutritional and/or organoleptic parameters. This variation is under the control of multiple loci distributed throughout the genome, presenting an array of possibilities for breeders. Our approach shows how the major genetic determinants of such variation can be identified and therefore managed within a breeding programme. The combined analysis thus presented provides a framework for the genetic analysis of the seed metabolome. The genetic marker datasets provided may be used in the further analysis of seed components that relate directly to seed storage and end-use quality traits.

AUTHOR CONTRIBUTIONS

NE, CH, and CD conceptualized the research. NE, PK, ZS, GK, and CH performed genetic mapping and analyzed genetic map data. JD, MD, AC, and GV carried out the NMR and data analysis. CH, JC, and NE devised and performed the bioinformatic analysis of the NMR and genetic data; NE and CD drafted and finalized the paper.

ACKNOWLEDGMENTS

This work was supported by: Biotechnology and Biological Sciences Research Council (BBSRC) (BB/J004561/1, BB/P012523/1) and the John Innes Foundation, The Department for Environment, Food and Rural Affairs (Defra) (CH0103, Pulse Crop Genetic Improvement Network), a BBSRC/Defra LINK project (BBSRC: BB/H009787/1; Defra: LK09126; AHDB: FV 351), and the European Union (Grain Legumes Integrated Project, GLIP, a Framework Programme 6 project, FOOD–CT−2004–506223). We thank Carol Moreau, Lorelei Bilham, and Catherine Chinoy (John Innes Centre) for technical assistance with parts of this work.

SUPPLEMENTARY MATERIAL

The Supplementary Material for this article can be found online at: https://www.frontiersin.org/articles/10.3389/fpls.2018.01022/full#supplementary-material

REFERENCES

Aubert, G., Morin, J., Jacquin, F., Loridon, K., Quillet, M. C., Petit, A., et al. (2006). Functional mapping in pea, as an aid to the candidate gene selection and for investigating synteny with the model legume *Medicago truncatula*. *Theor. Appl. Genet.* 112, 1024–1041. doi: 10.1007/s00122-005-0205-y

Baker, J. M., Hawkins, N. D., Ward, J. L., Lovegrove, A., Napier, J. A., Shewry, P. R., et al. (2006). A metabolomic study of substantial equivalence of field-grown genetically modified wheat. *Plant Biotechnol. J.* 4, 381–392. doi: 10.1111/j.1467-7652.2006.00197.x

Belton, P. S., and Ratcliffe, R. G. (1985). NMR and compartmentation in biological tissues. *Prog. Nucl. Mag. Res. Sp.* 17, 241–279. doi: 10.1016/0079-6565(85)80010-8

Bhattacharyya, M. K., Smith, A. M., Ellis, T. H. N., Hedley, C., and Martin, C. (1990). The wrinkled-seed character of pea described by Mendel is caused by a transposon-like insertion in a gene encoding starch-branching enzyme. *Cell* 60, 115–122. doi: 10.1016/0092-8674(90)90721-P

Cao, T., Lahiri, I., Vingh, V., Louis, J., Shah, J., and Ayre, B. G. (2013). Metabolic engineering of raffinose-family oligosaccharides in the phloem reveals alterations in carbon partitioning and enhances resistance to green peach aphid. *Front. Plant Sci.* 4:263. doi: 10.3389/fpls.2013.00263

Casey, R., Domoney, C., Forster, C., Hedley, C., Hitchin, E., and Wang, T. (1998). The effect of modifying carbohydrate metabolism on seed protein gene expression in peas. *J. Plant Physiol.* 152, 636–640. doi: 10.1016/S0176-1617(98)80023-0

Charlton, A., Allnutt, T., Holmes, S., Chisholm, J., Bean, S., Ellis, N., et al. (2004). NMR profiling of transgenic peas. *Plant Biotechnol. J.* 2, 27–36. doi: 10.1046/j.1467-7652.2003.00045.x

Charlton, A. J., Donarski, J. A., Harrison, M., Jones, S. A., Godward, J., Oehlschlager, S., et al. (2008). Responses of the pea (*Pisum sativum* L.) leaf metabolome to drought stress assessed by nuclear magnetic resonance spectroscopy. *Metabolomics* 4, 312–327. doi: 10.1007/s11306-008-0128-0

Cheema, J., Ellis, T. H. N., and Dicks, J. (2010). THREaD Mapper Studio: a novel, visual web server form the estimation of genetic linkage maps. *Nucleic Acids Res.* 38, W188–W193. doi: 10.1093/nar/gkq430

Davis, R. A., Charlton, A. J., Godward, J., Jones, S. A., Harrison, M., and Wilson, J. C. (2007). Adaptive binning: an improved binning method for metabolomics data using the undecimated wavelet transform. *Chemometr. Intell. Lab. Syst.* 85, 144–154. doi: 10.1016/j.chemolab.2006.08.014

Domoney, C., Knox, M., Moreau, C., Ambrose, M., Palmer, S., Smith, P., et al. (2013). Exploiting a fast neutron mutant genetic resource in *Pisum sativum* (pea) for functional genomics. *Funct. Plant Biol.* 40, 1261–1270. doi: 10.1071/FP13147

Ellis, T. H. N., and Poyser, S. J. (2002). An integrated and comparative view of pea genetic and cytogenetic maps. *New Phytol.* 153, 17–25. doi: 10.1046/j.0028-646X.2001.00302.x

Fait, A., Angelovici, R., Less, H., Ohad, I., Urbanczyk-Wochniak, E., Fernie, A. R., et al. (2006). Arabidopsis seed development and germination is associated with temporally distinct metabolic switches. *Plant Physiol.* 142, 839–854. doi: 10.1104/pp.106.086694

Fan, W. M. T. (1996). Metabolite profiling by one- and two-dimensional NMR analysis of complex mixtures. *Prog. Nucl. Mag. Res. Sp.* 28, 161–219. doi: 10.1016/0079-6565(95)01017-3

Fiehn, O., Kopka, J., Dörmann, P., Altmann, T., Trethewey, R. N., and Willmitzer, L. (2000). Metabolite profiling for plant functional genomics. *Nat. Biotechnol.* 18, 1157–1161. doi: 10.1038/81137

Frias, J., Bakhsh, A., Jones, D. A., Arthur, A. E., Vidal-Valverde, C., Rhodes, M. J. C., et al. (1999). Genetic analysis of the raffinose oligosaccharide pathway in lentil seeds. *J. Exp. Bot.* 50, 469–476. doi: 10.1093/jxb/50.333.469

Frias, J., Vidal-Valverde, C., Bakhsh, A., Arthur, A. E., and Hedley, C. L. (1994). An assessment of variation for nutritional and non-nutritional carbohydrates in lentil (*Lens culinaris*) seeds. *Plant Breed.* 113, 170–173. doi: 10.1111/j.1439-0523.1994.tb00719.x

Hellens, R. P., Moreau, C., Lin-Wang, K., Schwinn, K. E., Thomson, S. J., Fiers, M. W. E. J., et al. (2010). Identification of Mendel's white flower character. *PLoS ONE* 5:e13230. doi: 10.1371/journal.pone.0013230

Hylton, C., and Smith, A. M. (1992). The *rb* mutation of peas causes structural and regulatory changes in ADP glucose pyrophosphorylase from developing embryos. *Plant Physiol.* 99, 1626–1634. doi: 10.1104/pp.99.4.1626

Iglesias-García, R., Prats, E., Fondevilla, S., Satovic, Z., and Rubiales, D. (2015). Quantitative trait loci associated to drought adaptation in pea (*Pisum sativum* L.) *Plant Mol. Biol. Rep.* 33, 1768–1778. doi: 10.1007/s11105-015-0872-z

Karner, U., Peterbauer,. T., Raboy, V., Jones, D. A., Hedley, C. L., and Richter, A. (2004). *myo*-Inositol and sucrose concentrations affect the accumulation of raffinose family oligosaccharides in seeds. *J. Exp. Bot.* 55, 1981–1987. doi: 10.1093/jxb/erh216

Kirby, C. W., Wu, T., Tsao, R., and McCallum, J. L. (2013). Isolation and structural characterization of unusual pyranoanthocyanins and related anthocyanins from Staghorn sumac (*Rhus typhina L.*) via UPLC–ESI-MS, ^{1}H, ^{13}C, and 2D NMR spectroscopy. *Phytochem.* 94, 284–293. doi: 10.1016/j.phytochem.2013.06.017

Knox, M. R., Moreau, C., Lipscombe, J., and Ellis, T. H. N. (2009). High-throughput retrotransposon-based fluorescent markers: improved information content and allele discrimination. *Plant Meths.* 5:10. doi: 10.1186/1746-4811-5-10

Luo, J. (2015). Metabolite-based genome-wide association studies in plants. *Current Op. Plant Biol.* 24, 31–38. doi: 10.1016/j.pbi.2015.01.006

Lyall, T. W., Ellis, R. H., John, P., Hedley, C. L., and Wang, T. L. (2003). Mutant alleles at the *rugosus* loci in pea affect seed moisture sorption isotherms and the relations between seed longevity and moisture content. *J. Exp. Bot.* 54, 445–450. doi: 10.1093/jxb/erg059

Messerli, G., Partovi Nia, V., Trevisan, M., Kolbe, A., Schauer, N., Geigenberger, P., et al. (2007). Rapid classification of phenotypic mutants of Arabidopsis via metabolite fingerprinting. *Plant Physiol.* 143, 1484–1492. doi: 10.1104/pp.106.090795

Moore, G. R., Ratcliffe, R. G., and Williams, R. J. (1983). NMR and the biochemist. *Essays. Biochem.* 19, 142–195.

Nakabayashi, R., and Kazuki, S. (2015). Integrated metabolomics for abiotic stress responses in plants. *Curr. Op. Plant Biol.* 24, 10–16. doi: 10.1016/j.pbi.2015.01.003

Perez, M. D., Chambers, S. J., Bacon, J. R., Lambert, N., Hedley, C. L., and Wang, T. (1993). Seed protein content and composition of near-isogenic and induced mutant pea lines. *Seed Sci. Res.* 3, 187–194. doi: 10.1017/S096025850000177X

Peterbauer, T., Lahuta, L. B., Blöchl, A., Mucha, J., Jones, D. A., Hedley, C. L., et al. (2001). Analysis of the raffinose family oligosaccharide pathway in pea seeds with contrasting carbohydrate composition. *Plant Physiol.* 127, 1764–1772. doi: 10.1104/pp.010534

Peterbauer, T., Mucha, J., Mach, L., and Richter, A. (2002). Chain elongation of raffinose in pea seeds. Isolation, characterization, and molecular cloning of mutifunctional enzyme catalyzing the synthesis of stachyose and verbascose. *J. Biol. Chem.* 277, 194–200. doi: 10.1074/jbc.M109734200

Ratcliffe, R. G. (1987). Application of nuclear magnetic resonance methods to plant-tissues. *Meth. Enzymol.* 148, 683–700. doi: 10.1016/0076-6879(87)48065-8

Rayner, T., Moreau, C., Ambrose, M., Isaac, P. G., Ellis, N., and Domoney, C. (2017). Genetic variation controlling wrinkled seed phenotypes in *Pisum*: how lucky was Mendel? *Int. J. Mol. Sci.* 18:1205. doi: 10.3390/ijms18061205

Shi, W., Yang, Y., Chen, S., and Xu, M. (2008). Discovery of a new fragrance allele and the development of functional markers for the breeding of fragrant rice varieties. *Mol. Breed.* 22, 185–192. doi: 10.1007/s11032-008-9165-7

Vandecasteele, C., Teulat-Merah, B., Morère-Le Paven, M.-C., Leprince, O., Vu, B. L., Viau, L., et al. (2011). Quantitative trait loci analysis reveals a correlation between the ratio of sucrose/raffinose family oligosaccharides and seed vigour in *Medicago truncatula*. *Plant Cell Env.* 34, 1473–1487. doi: 10.1111/j.1365-3040.2011.02346.x

Vigeolas, H., Chinoy, C., Zuther, E., Blessington, B., Geigenberger, P., and Domoney, C. (2008). Combined metabolomic and genetic approaches reveal a link between the polyamine pathway and albumin 2 in developing pea seeds. *Plant Physiol.* 146, 74–82. doi: 10.1104/pp.107.111369

Wang, T. L., Bogracheva, T. Y., and Hedley, C. L. (1998). Starch: as simple as A, B, C? *J. Exp. Bot.* 49, 481–502. doi: 10.1093/jxb/49.320.481

Wang, T. L., and Hedley, C. L. (1991). Seed development in peas: knowing your three "r's" (or four, or five). *Seed Sci. Res.* 1, 3–14.

Weigelt, K., Küster, H., Rutten, T., Fait, A., Fernie, A. R., Miersch, O., et al. (2009). ADP-glucose pyrophosphorylase-deficient pea embryos reveal specific transcriptional and metabolic changes of carbon-nitrogen metabolism and stress responses. *Plant Physiol.* 149, 395–411. doi: 10.1104/pp.108.129940

Conflict of Interest Statement: JD, AC, MD, and GV were employed by The Food & Environment Research Agency, a government agency (now the company Fera Science Ltd.). GK is employed by the company AMBIS Biotechnology Ltd.

The remaining authors declare that the research was conducted in the absence of any commercial or financial relationships that could be construed as a potential conflict of interest.

frontiers in Plant Science

ORIGINAL RESEARCH
published: 27 June 2018
doi: 10.3389/fpls.2018.00665

Metabolomic Evaluation of the Quality of Leaf Lettuce Grown in Practical Plant Factory to Capture Metabolite Signature

*Yoshio Tamura[1,2], Tetsuya Mori[3], Ryo Nakabayashi[3], Makoto Kobayashi[3], Kazuki Saito[3,4], Seiichi Okazaki[5,6], Ning Wang[1] and Miyako Kusano[1,3]**

[1] Graduate School of Life and Environmental Sciences, University of Tsukuba, Tsukuba, Japan, [2] Central Research Institute for Feed and Livestock, National Federation of Agricultural Co-operative Associations, Tsukuba, Japan, [3] RIKEN Center for Sustainable Resource Science, Yokohama, Japan, [4] Graduate School of Pharmaceutical Sciences, Chiba University, Chiba, Japan, [5] Keystone Technology, Yokohama, Japan, [6] Graduate School of Environment and Information Sciences, Yokohama National University, Yokohama, Japan

OPEN ACCESS

Edited by:
Andreia Figueiredo, Universidade de Lisboa, Portugal

Reviewed by:
Francisco A. Tomas-Barberan, Consejo Superior de Investigaciones Científicas (CSIC), Spain
Josep Maria Bayona, Consejo Superior de Investigaciones Científicas (CSIC), Spain
Luigi Lucini, Università Cattolica del Sacro Cuore, Italy

***Correspondence:**
Miyako Kusano
kusano.miyako.fp@u.tsukuba.ac.jp

Specialty section:
This article was submitted to Plant Metabolism and Chemodiversity, a section of the journal Frontiers in Plant Science

Received: *15 February 2018*
Accepted: *30 April 2018*
Published: *27 June 2018*

Citation:
Tamura Y, Mori T, Nakabayashi R, Kobayashi M, Saito K, Okazaki S, Wang N and Kusano M (2018) Metabolomic Evaluation of the Quality of Leaf Lettuce Grown in Practical Plant Factory to Capture Metabolite Signature. Front. Plant Sci. 9:665. doi: 10.3389/fpls.2018.00665

Vegetables produce metabolites that affect their taste and nutritional value and compounds that contribute to human health. The quality of vegetables grown in plant factories under hydroponic cultivation, e.g., their sweetness and softness, can be improved by controlling growth factors including the temperature, humidity, light source, and fertilizer. However, soil is cheaper than hydroponic cultivation and the visual phenotype of vegetables grown under the two conditions is different. As it is not clear whether their metabolite composition is also different, we studied leaf lettuce raised under the hydroponic condition in practical plant factory and strictly controlled soil condition. We chose two representative cultivars, "black rose" (BR) and "red fire" (RF) because they are of high economic value. Metabolite profiling by comprehensive gas chromatography-mass spectrometry (GC-MS) and liquid chromatography-mass spectrometry (LC-MS) resulted in the annotation of 101 metabolites from 223 peaks detected by GC-MS; LC-MS yielded 95 peaks. The principal component analysis (PCA) scatter plot showed that the most distinct separation patterns on the first principal component (PC1) coincided with differences in the cultivation methods. There were no clear separations related to cultivar differences in the plot. PC1 loading revealed the discriminant metabolites for each cultivation method. The level of amino acids such as lysine, phenylalanine, tryptophan, and valine was significantly increased in hydroponically grown leaf lettuce, while soil-cultivation derived leaf lettuce samples contained significantly higher levels of fatty-acid derived alcohols (tetracosanol and hexacosanol) and lettuce-specific sesquiterpene lactones (lactucopicrin-15-oxalate and 15-deoxylactucin-8-sulfate). These findings suggest that the metabolite composition of leaf lettuce is primarily affected by its cultivation condition. As the discriminant metabolites reveal important factors that contribute to the nutritional value and taste characteristics of leaf lettuce, we performed comprehensive metabolite profiling to identify metabolite compositions, i.e., metabolite signature, that directly improve its quality and value.

Keywords: leaf lettuce, plant factory, hydroponic system, soil cultivation, metabolomics

INTRODUCTION

For the stable supply of vegetables, plant factories use hydroponic cultivation that controls vegetable growth and development under closed environments by regulating important factors for plant growth such as the temperature, humidity, light, growing medium, and plant nutrition (Kozai, 2013). Many use artificial lighting for the cultivation of leafy vegetables and herbs. Because light-emitting diodes (LEDs) suppress heat, their energy requirement is lower than of other light sources such as fluorescent lamps. As plant factories involve higher initial financial investments and running costs than soil cultivation (Tokimasa and Nishiura, 2015), their cultivation conditions must be optimized to yield economically viable horticultural outputs.

Leaf lettuce (*Lactuca sativa* L. var crispa) is a popular leafy vegetable grown in plant factories. Optimization of hydroponic cultivation conditions has focused on increasing its yield (Touliatos et al., 2016) and on the accumulation of functional nutrients (Miyagi et al., 2017). Different light intensities influence the composition of important phytochemicals such as anthocyanins, carotenoids, chlorophylls, phenolics, and ascorbic acid in baby leaf lettuce (Li and Kubota, 2009; Samuoliene et al., 2013). Moreover, the soilless cultivation can be more efficient in term of nutrient requirements for vegetables growth than that of soil culture (Rouphael et al., 2004; Palermo et al., 2012). Although the metabolite composition of leaf lettuce grown under hydroponic cultivation has been investigated, a comparison of the primary and secondary metabolite profiles in lettuce grown under hydroponic- and soil cultivation conditions is still needed.

Metabolomics has been used to identify the effect of different cultivation environments on plants and for the quality evaluation of agricultural products (Kusano et al., 2011b; Zeng et al., 2014; Sung et al., 2015; Garcia et al., 2016; Ya-Qin et al., 2017). According to Lisec et al. (2006), plants can produce approximately 200,000 metabolites and specific metabolites are produced in different plant species (Kusano et al., 2011b, 2014a,b), even in cultivars and ecotypes (Sulpice et al., 2009). As mass spectrometry (MS)-based metabolomics yields highly sensitive results and facilitates high-throughput data acquisition, it has been combined with various types of analytical separation techniques, including gas chromatography (GC), liquid chromatography (LC), and capillary electrophoresis (CE) (Gowda and Djukovic, 2014). Since primary metabolites contribute to taste, integrated comprehensive GC-MS analysis and sensory evaluation were applied to determine the taste characteristics of green tea grown under various artificial light conditions, and bidimensional GC could provide extended metabolic phenotyping of natural variants in rice (Kusano et al., 2007; Miyauchi et al., 2017). LC-MS-based metabolite profiling aimed at detecting secondary metabolites including functional ingredients in foods and plants (Xie et al., 2008; Ma et al., 2013) revealed that environmental factors affected the accumulation of flavonoids in tea (Zhang et al., 2014). Comprehensive LC-MS analysis combined with ultra-high-performance LC (UHPLC) and quadrupole high-resolution time-of-flight MS (qTOF-MS) was used for secondary metabolite profiling to evaluate the quality of three artichoke cultivars and their commercial products (Farag et al., 2013). Furthermore, CE-MS-based metabolomics to analyze charged metabolites, i.e., amino acids and organic acids, has been utilized for quality control of agricultural products such as edamame beans, pork meat, and sake (rice spirit) (Sugimoto et al., 2010, 2012; Muroya et al., 2014). Additionally, the use of nuclear magnetic resonance (NMR) spectroscopy in plant metabolomics study also complements analytical technique choices in providing robust and reproducible metabolic data (Sobolev et al., 2005; Pereira et al., 2014; Sekiyama et al., 2017).

Metabolite profiling is a promising analytical method for the elucidation of taste characteristics and for the functional evaluation of agricultural products because unlike targeted analysis, it returns a variety of component profiles for many samples. Moreover, multi-MS-based metabolite profiling yields wider coverage for the detection of a large variety of metabolites than single chromatographic techniques combined with MS (Arbona et al., 2009; Lee et al., 2014; Sung et al., 2015). It not only detects variations in taste-related metabolites elicited by differences in cultivation conditions, but also contributes to the identification of quantitative changes in specialized metabolites in vegetables. Taken together, collection of metabolite alterations data of leaf lettuce from different cultivation systems is very important for clarifying their quality.

We performed GC-MS- and LC-MS analysis for the comprehensive capture of cultivation-specific- and taste-related metabolites in leaf lettuce (**Figure 1**). To differentiate the metabolite composition, including primary and secondary metabolites, of two leaf lettuce cultivars, black rose (BR) and red fire (RF), grown under hydroponic or fertilized soil conditions, including light sources and nutrient, we performed integrated MS-based metabolite profiling to capture metabolite signature for BR and RF, and thus to establish their quality indexes.

MATERIALS AND METHODS

Plant Materials and Growth Condition

Two cultivars of *L. sativa* L. cv. BR and RF were grown for 33 days under hydroponic or soil conditions. The soil was treated with optimized concentrations of liquid fertilizer. The BR and RF seeds were purchased from Kaneko Seed Co. (Japan) and Takii Seed Co., Ltd. (Japan), respectively.

For hydroponic cultivation of BR and RF lettuce we applied the methods used by Keystone Technology Inc. (Japan). The conditions were: temperature, 22°C; 16 h light/8 h dark cycle (16 l/8 days); photosynthetic photon flux density (PPFD), 150 μmol $m^{-2}s^{-1}$ from light-emitting diode (LED) light (peak wavelength: blue = 460 nm, green = 525 nm, red = 660 nm). For soil cultivation the growth-chamber (LPH-350S, Nippon Medical and Chemical Instruments Co., Ltd., Japan) conditions were: temperature, 24°C; 16 l/8 days; PPFD, 140 μmol m^{-2} s^{-1} from white LED light, 2–3 times per week watering (Tamoi et al., 2017). The leaves of each plant were counted starting with the smallest leaf and the leaf growth stages were recorded as "young," "middle" and "old" (Kusano et al., 2011a). The collected leaf samples were as follows: hydroponic cultivation; 2 cultivars × 2 sampling positions × 3 biological replicates, soil cultivation;

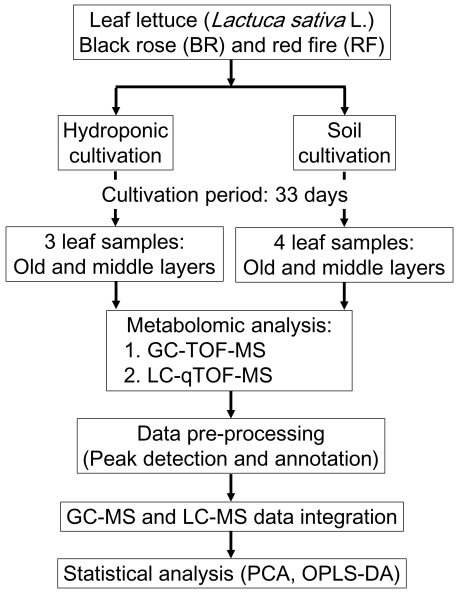

FIGURE 1 | Workflow for the metabolomic evaluation of leaf lettuce grown under hydroponic- and soil cultivation methods. The leaf samples from hydroponic and soil cultivations were 3 and 4 biological replicates, respectively.

2 cultivars × 2 sampling positions × 4 biological replicates. In total, there were 28 leaf samples (**Figure 1**). Leaf samples were collected in bulk from 4 sites on leaves in the middle- and old stage using an 8-mm leaf punch disk (Fujiwara Scientific Company Co., Ltd., Japan) and immediately frozen in liquid nitrogen. Samples were stored at −80°C until analysis.

Metabolite Profiling by GC-TOF-MS

For the extraction of 25-mg leaf samples (fresh weight) we used 1 ml methanol/chloroform/H_2O (3:1:1, v/v/v) containing 10 stable isotope references. The extraction was performed for 10 min at 15 Hz and 4°C using a mixer mill (Retsch MM301, Retsch GmbH, Germany) (Kusano et al., 2007). The mixture was then centrifuged, the supernatant was placed in a glass insert vial, and evaporated to dryness in a vacuum concentrator (Savant SPD2010 SpeedVac, Thermo Fisher Scientific Inc., United States). The dry extracts were derivatized using 30 μl of methoxylamine hydrochloride-HCl (20 mg/ml in pyridine) for 23 h at room temperature, then for 1 h in 30 μl of N-methyl-N-trimethylsilyltrifluoroacetamide (MSTFA) at 37°C with shaking; heptane (30 μl) was added to the extract mixture.

The extract (1 μl) was injected in into an Agilent 6890N GC instrument (Agilent Technologies, United States) via a CTC CombiPAL autosampler (CTC Analytics, Switzerland) for primary metabolite profiling. For separation we used an Rxi-5 Sil MS column [RESTEK, United States, inner diameter (ID), 30 m × 0.25 mm; film thickness, 0.25 μm]. Helium was the carrier gas delivered at a constant flow rate of 1 ml/min. The initial GC oven temperature was set at 80°C for 2 min, raised to 320°C at a rate of 30°C/min, and then held constant for 3.5 min. Data acquisition was performed on a Pegasus IV TOF MS instrument (LECO Corp., United States); the acquisition rate and range were 30 spectra/s and *m/z* 60–800, respectively. Alkane standard mixtures (C8–C20 and C21–C40, Sigma-Aldrich, Japan) were used for calculating the retention index (RI).

Metabolite Profiling by LC-TOF-MS

The dried samples were extracted (7 min, 18 Hz, 4°C) with 150 μl of 80% MeOH and zirconia beads containing 2.5 μM lidocaine and 10-Camphorsulfonic acid per mg dried weight using a mixer mill. Zirconia beads were used to increase extraction efficiency in particularly for cationic compounds, e.g., anthocyanins. After centrifugation, the supernatant was filtered using an Oasis HLB μElution plate (Waters Co., United States) (Nakabayashi et al., 2014). Extract (1 μl) was injected in into a Waters Acquity UPLC instrument coupled with a Waters Xevo G2 QTOF-MS instrument for metabolite profiling. The analytical conditions were LC column: Acquity-bridged ethyl hybrid (BEH) C18 (ID, 100 mm × 2.1 mm; 1.7 μm particle diameter; Waters); solvent system: solvent A (water including 0.1% formic acid); solvent B (acetonitrile including 0.1% formic acid); gradient program: 99.5% A/0.5% B, 0 min; 99.5% A/0.5% B, 0.1 min; 20% A/80% B, 10 min; 0.5% A/99.5% B, 10.1 min; 0.5% A/99.5% B, 12.0 min; 99.5% A/0.5% B, 12.1 min; 99.5% A/0.5% B, 15.0 min; flow rate: 0.3 ml/min at 0 min, 0.3 ml/min at 10 min, 0.4 ml/min at 10.1 min, 0.4 ml/min at 14.4 min, and 0.3 ml/min at 14.5 min; column temperature: 40°C; MS detection: capillary voltage, +3.0 keV; cone voltage, 25.0 V; source temperature, 120°C; desolvation temperature, 450°C; cone gas flow, 50 l/h; desolvation gas flow, 800 l/h; collision energy: 6 V; mass range: *m/z* 50–1500; scan duration: 0.1 s; interscan delay: 0.014 s; data acquisition: centroid mode; polarity: positive/negative; Lockspray (leucine enkephalin); scan duration: 1.0 s; interscan delay: 0.1 s. MS/MS data were acquired in ramp mode under the following analytical conditions: (1) MS: mass range, *m/z* 50–1500; scan duration, 0.1 s; inter-scan delay, 0.014 s; data acquisition, centroid mode; polarity, positive/negative; and (2) MS/MS: mass range, *m/z* 50–1500; scan duration, 0.02 s; inter-scan delay, 0.014 s; data acquisition, centroid mode; polarity, positive/negative; collision energy, ramped from 10–50 V. In this mode, MS/MS spectra of the top 10 ions (>1000 counts) in an MS scan were automatically obtained. If the ion intensity was below 1000, we did not perform MS/MS data acquisition but moved on to the next top 10 ions. Data acquisition was with Progenesis CoMet (Nonlinear Dynamics). Peak normalization was with lidocaine (positive mode) and 10-camphorsulfonic acid (negative mode).

Data Pre-processing

Non-processed data (NetCDF format) from GC-TOF-MS were exported to MATLAB (Mathworks, United States); custom scripts were used for data normalization, baseline correction, and subsequent analysis. Lastly, processed data obtained from hyphenated data analysis (HDA) were identified or annotated using an in-house metabolite library in PRIMe (Platform for RIKEN Metabolomics[1]), and the library in the Golm Metabolome

[1]http://prime.psc.riken.jp

Database (GMD) (Jonsson et al., 2005, 2006). Peaks were normalized with the cross-contribution compensating multiple standard normalization (CCMN) method (Redestig et al., 2009). Chemical assignment of data acquired from LC-TOF-MS was performed using reported MS- or MS/MS data (Wu and Prior, 2005; Abu-Reidah et al., 2013) and the KNApSAcK database (keyword: *Lactuca sativa*). The *m/z* values were set as monoisotopic masses [$(M+H)^+$ or $(M-H)^-$] under a tolerance match limit of 0.01 Da.

Statistical Analysis

To determine the effect of the different cultivation conditions on the metabolite profile of leaf lettuce we performed multivariate statistical analysis including principal component analysis (PCA) and orthogonal partial least square-discriminant analysis (OPLS-DA) of the unit variance scaled and $\log_{10}$-transformed data matrix obtained from GC- and UPLC-TOF-MS using SIMCA-P 14 (Umetrics, Sweden). Significant metabolites in leaf lettuce were evaluated based on their differing variable importance in projection (VIP) values calculated with OPLS-DA and *Q*-values adjusted via the false discovery rate (FDR) approach (Benjamini and Hochberg, 1995) using R package samr[2]. The effect of the different cultivation methods on the resulting common metabolites in the cultivars was visualized on the Venn diagram (VENNY ver.2.1[3]).

RESULTS

Experimental Design

To investigate the effect of different cultivation conditions, cultivars, and leaf positions on the metabolite composition of leaf lettuce, we studied BR and RF cultivars raised for 33 days under the strictly controlled soil and hydroponic conditions (**Table 1** and **Figure 1**). As metabolite profiles are largely affected the extent of visual phenotypes (Fiehn et al., 2000), we optimized soil condition for minimizing differences of visual phenotypes when compared to lettuce phenotypes harvested from the practical plat factory. The same type of liquid fertilizer was applied under both conditions and the light intensity was almost the same. Different concentration of the fertilizer was used for each cultivation because appearance and growth was different when we used the similar concentration for both cultivations (data not shown). Comparison of their phenotypes showed that the BR and RF lettuce leaves exposed to soil and hydroponic conditions were distinct (**Figure 2**). Soil-based cultivation yielded smaller colored leaves than hydroponic farming. Soil-grown BR and RF leaves were of the typical green color with dark- (BR) and bright-red pigments (RF) at the tip. For GC- and LC-MS, tissue samples from leaves in the old- and middle growth stage were collected from the same plant using an 8-mm leaf disk. The metabolites obtained by GC- and LC-MS were identified or annotated, and the metabolite profile data were then integrated for data interpretation by multivariate statistical analysis.

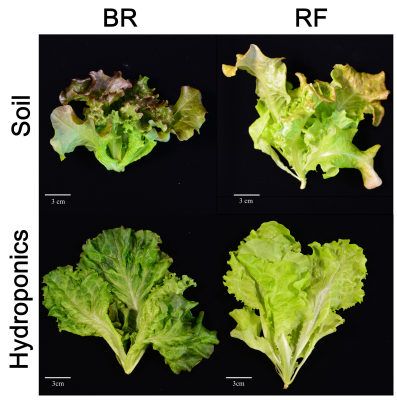

FIGURE 2 | Black rose (BR) and red fire (RF) lettuce leaves grown under the two cultivation conditions. White bar, 3 cm.

Metabolite Profiling of Leaf Lettuce Grown Under Different Cultivation Conditions

To investigate metabolite changes, including primary and secondary metabolites, in BR and RF lettuce grown under different cultivation conditions, we harvested 28 leaf samples from each cultivar for comprehensive GC- and LC-MS analyses. GC-MS detected 223 peaks; 101 were identified- or provisionally identified primary metabolites. Positive- and negative-ionization mode-LC-MS followed by an MS/MS library search made it possible to annotate 2 of 30- and 30 of 65-detected compounds, respectively (Supplementary Table 1). Unsupervised multivariate statistical analysis by PCA was then performed to visualize the extent of metabolite changes elicited in the cultivars, under the different cultivation conditions, and in the leaf position.

In detail, "cultivation conditions" could differentiate on the first principal component, PC1 (22.9%), in which soil-based cultivation was recorded in the positive quadrant and hydroponic in the negative (**Figure 3**). Except for samples obtained from old-layer BR leaves grown hydroponically (H-BR), the plots of the other leaves were not clearly separated. This observation suggests that there is little difference in the metabolite composition of the cultivars and of leaves sampled at different growth stages.

[2]https://cran.r-project.org/web/packages/samr/index.html

[3]http://bioinfogp.cnb.csic.es/tools/venny/

TABLE 1 | Soil- and hydroponic-cultivation conditions.

Parameter	Soil	Hydroponics
LED light source wavelength (nm)	White (400–800)	Blue (460), green (525), red (660)
Light intensity (PPFD)*	140	150 (blue, 23%; green, 5%; red, 72%)
Liquid fertilizer (ppm)	NH_3-N, 0.50; NO_3-N, 25.00; P, 9.00; K, 56.00; Mg, 11.00; Mn, 0.05; B, 0.20; trace (Cu, Zn, Mo, Fe, Ca)	NH_3-N, 1.67; NO_3-N, 83.33; P, 30.00; K, 186.67; Mg, 36.67; Mn, 0.17; B, 0.67; trace (Cu, Zn, Mo, Fe, Ca)

**PPFD, photosynthetic photon flux density (μmol $m^{-2}s^{-1}$).*

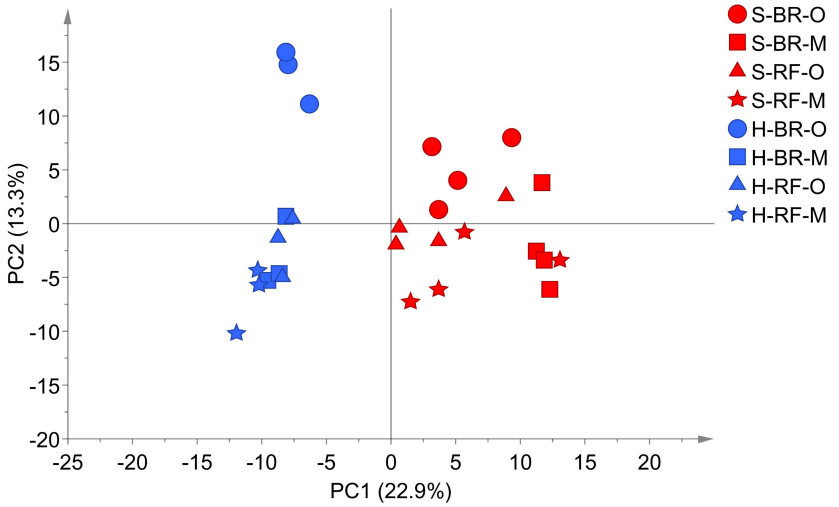

FIGURE 3 | PCA score scatter plot of metabolites derived from black rose (BR) and red fire (RF) lettuce leaves (O, old layer; M, middle layer) grown under hydroponic (H) and soil (S) cultivation conditions. The leaf samples from hydroponic and soil cultivations were 3 and 4 biological replicates, respectively. The normalized data matrix (318 peak areas × 28 leaf samples) obtained from GC and LC-MS was used.

We next identified the discriminant metabolites in leaf lettuce by OPLS-DA. The score scatter plot in **Figure 4A** shows that the samples were clearly separated by the cultivation condition [PredComp1 = 20.5%, overall predictive performance of the model = R2 (Y): 0.99%, Q2 (cum) = 0.92%]. Therefore, the cultivation conditions had more impact on metabolite changes than the cultivar-type or the leaf growth stage.

Discriminant Metabolites in Soil- and Hydroponic-Cultivated Leaf Lettuce

The discriminant metabolites for our quality index of leaf lettuce were screened from all 318 metabolites based on the selection criteria of VIP>1.0 and FDR<0.05 (**Figure 4B** and Supplementary Table 2). We then compared changes in the metabolite profiles of hydroponically- and soil-grown lettuce. Leaves harvested after soil cultivation contained more typical lettuce sesquiterpene lactones and fatty acid-derived alcohols [$\log_2$-fold change (FC) ranging from -3.37 to -1.45] than hydroponically grown leaf lettuce which contained more amino acids ($\log_2$-FC ranging from 0.84 to 4.25).

In both cultivars we looked for metabolites that differed when they were grown under the two different conditions. We extracted discriminant metabolites that showed FDR<0.05 and $|\log_2\text{-FC}| > 1$; our findings are presented in a Venn diagram (**Figure 5** and Supplementary Tables 3, 4). When GC-MS and LC-MS detected the same metabolite, we selected the metabolite peak with the higher VIP value. The Venn diagram of metabolites that accumulated under hydroponic conditions ($\log_2$-FC>1) shows that common metabolites in BR and RF were amino acids (lysine, phenylalanine, pyroglutamate, tryptophan, and tyrosine) and phosphoric acid (**Figure 5A**). Soil-specific metabolites ($\log_2$-FC<-1) were sugars, organic acids, sesquiterpenes, and fatty acid-derived alcohols. Common metabolites in soil-grown BR and RF were arabinose, sucrose, *myo*-inositol, β-sitosterol, 1-hexacosanol, 1-tetracosanol, cystine, galactonic acid, galacturonic acid, and hydroxybenzoic acid (**Figure 5B**). The cultivar-specific metabolites in BR leaves grown hydroponically were amino acids (isoleucine, leucine and valine), caffeoylmalic acid, and coniferoside; in RF leaves grown hydroponically they were 2-propenoic acid and glutamate (**Figure 5A**). BR-specific metabolites obtained from plants grown in soil were sugars (erythritol and raffinose), organic acids (2-oxoglutaric, glutaric, and shikimic acids), and sesquiterpenes (lactucopicrin-15-oxalate and 15-deoxylactucin-8-sulfate); RF-specific metabolites included organic acids (glyceric and suberic acids) and phenolics (caffeoyltartaric-*p*-coumaroyl and *p*-coumaroylquinic acids) (**Figure 5B**). The different cultivation systems did not significantly alter the content of pigment and flavonol compounds in leaf lettuce, while these compounds tended to be accumulated in BR leaves (**Figure 6**). The application of the two cultivation methods could significantly differentiate ($p < 0.05$) taste-related compounds that might influence the sensory acceptance of lettuce, including glutamate (umami) (Halpern, 2000; Hounsome et al., 2008; Kurihara, 2009), sucrose (sweetness), and lactucopicrin-15-oxalate (bitterness) (**Figure 6**). Thoroughly, RF leaves from hydroponic cultivation had significantly more glutamate content than that of soil-cultivated RF leaves. Then again, both BR and RF leaves grown hydroponically had significantly less sucrose and lactucopicrin-15-oxalate levels than leaves from soil cultivation.

DISCUSSION

Effect of Cultivation Conditions on Leaf Lettuce Growth

The leaves of BR and RF lettuce grown for 33 days in soil or under hydroponic conditions exhibited different morphological

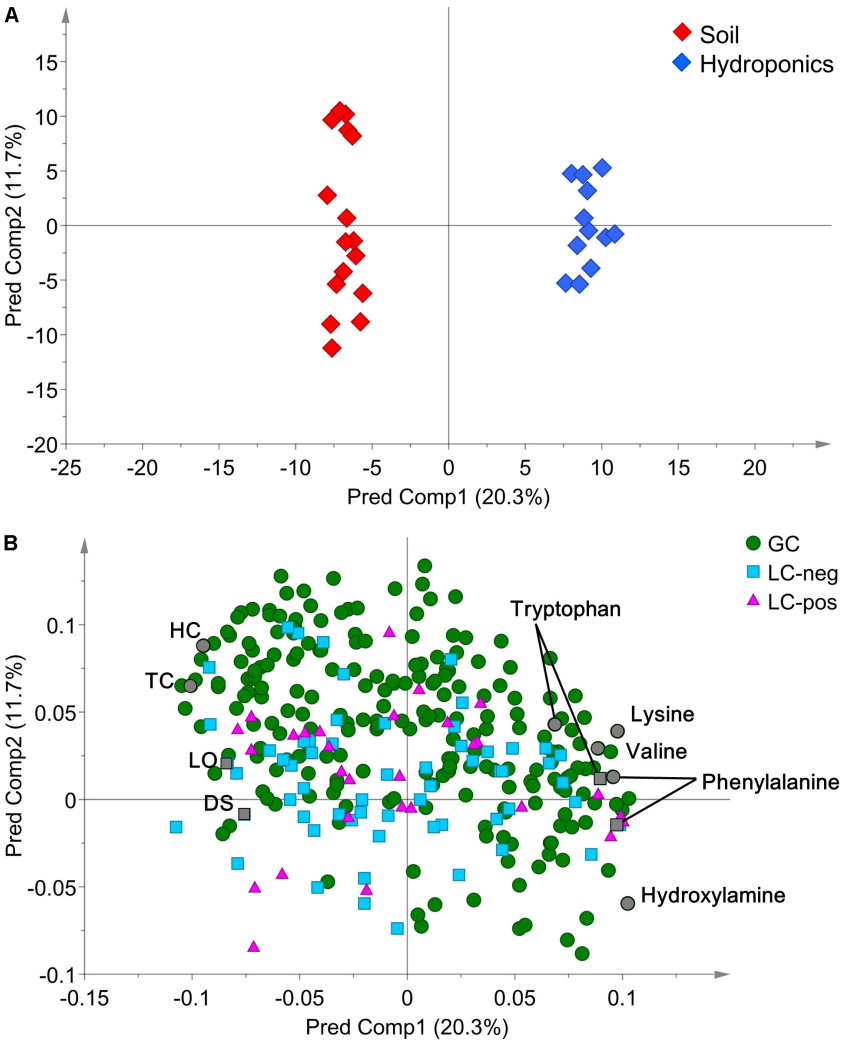

FIGURE 4 | (A) OPLS-DA score scatter- and **(B)** loading plots of metabolites derived from 12 hydroponically- and 16 soil-grown lettuce leaves (number of samples: hydroponic cultivation; 2 cultivars × 2 sampling positions × 3 biological replicates, soil cultivation; 2 cultivars × 2 sampling positions × 4 biological replicates). The normalized data matrix (318 peak areas × 28 leaf samples) obtained by GC and LS-MS was used. HC, 1-hexacosanol; TC, 1-tetracosanol; LO, lactucopicrin-15-oxalate; DS, 15-deoxylactucin-8-sulfate.

characteristics, i.e., their color and shape, but similar size (**Figure 2**). It has been reported that metabolite profiles largely affect from differences that is considered to be derived from difference of growth stages as well as visible phenotypes (Kusano et al., 2011a; Clevenger et al., 2015; Li et al., 2016). Soil-cultivated leaves had more reddish appearance than leaves grown hydroponically. Under both growth conditions the BR leaves were reddish and more darkly green than RF leaves, suggesting leaf pigmentation is affected by cultivar characteristics (Caldwell and Britz, 2006). According to Stutte et al. (2009) and Son and Oh (2013), the combination of red and blue LED light yields red leaf lettuce while the sole exposure to red LED light failed to yield pigmented leaves. These differences in appearance, including the leaf morphology and color, may influence sensorial preferences and the acceptance RF and BR lettuce (McWatters et al., 2002). As plant pigmentation reflects the level of chlorophyll and other secondary metabolites such as carotenoid and anthocyanin, we hypothesized that environmental- and cultivar-related factors impact the primary and secondary metabolite composition associated with metabolic pathways (Sass-Kiss et al., 2005; Caldwell and Britz, 2006). Therefore, we used comprehensive GC- and LC-MS-based metabolic profiling to identify specific metabolites related with the BR and RF lettuce phenotype except for chlorophylls and carotenoids. Because the MS-based metabolomics platform cannot detect these compounds.

Metabolomic Evaluation of the Quality of Leaf Lettuce Grown Under Different Cultivation Conditions

We demonstrate that the cultivation condition exerts greater influence on the metabolite composition of leaf lettuce than

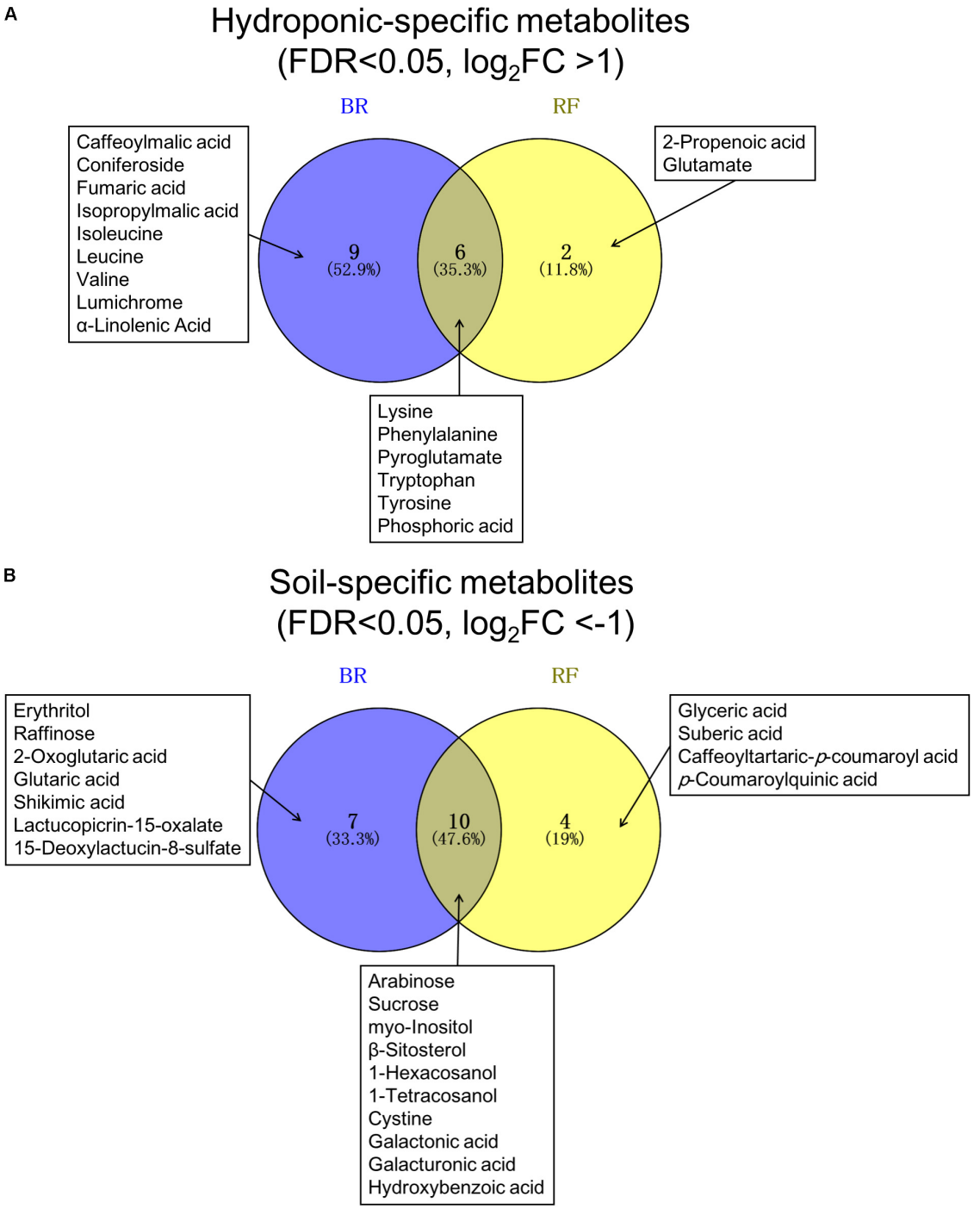

FIGURE 5 | Venn diagram of **(A)** hydroponic-specific- and **(B)** soil-specific metabolites in black rose (BR) and red fire (RF) lettuce leaves. The false discovery rate (FDR) and $\log_2$-fold changes (FC) were calculated with soil cultivation as the control condition. Significant metabolites of the two lettuce cultivars were identified using a threshold of FDR<0.05 and | log2-FC| > 1.

the cultivar type or the leaf position. Environmental factors of cultivation systems can contribute to the elicitation of taste- and nutrition-related compounds in various plants (Ohashi-Kaneko et al., 2007; Zhang et al., 2014). Okazaki et al. (2008), who examined the influence of the primary metabolite composition and of nitrogen availability in two spinach cultivars grown under different inorganic nitrogen concentrations, found that the efficiency of their nitrogen use was not the same.

We varied the light source intensity and the liquid fertilizer concentration in our study of RF and BR lettuce grown

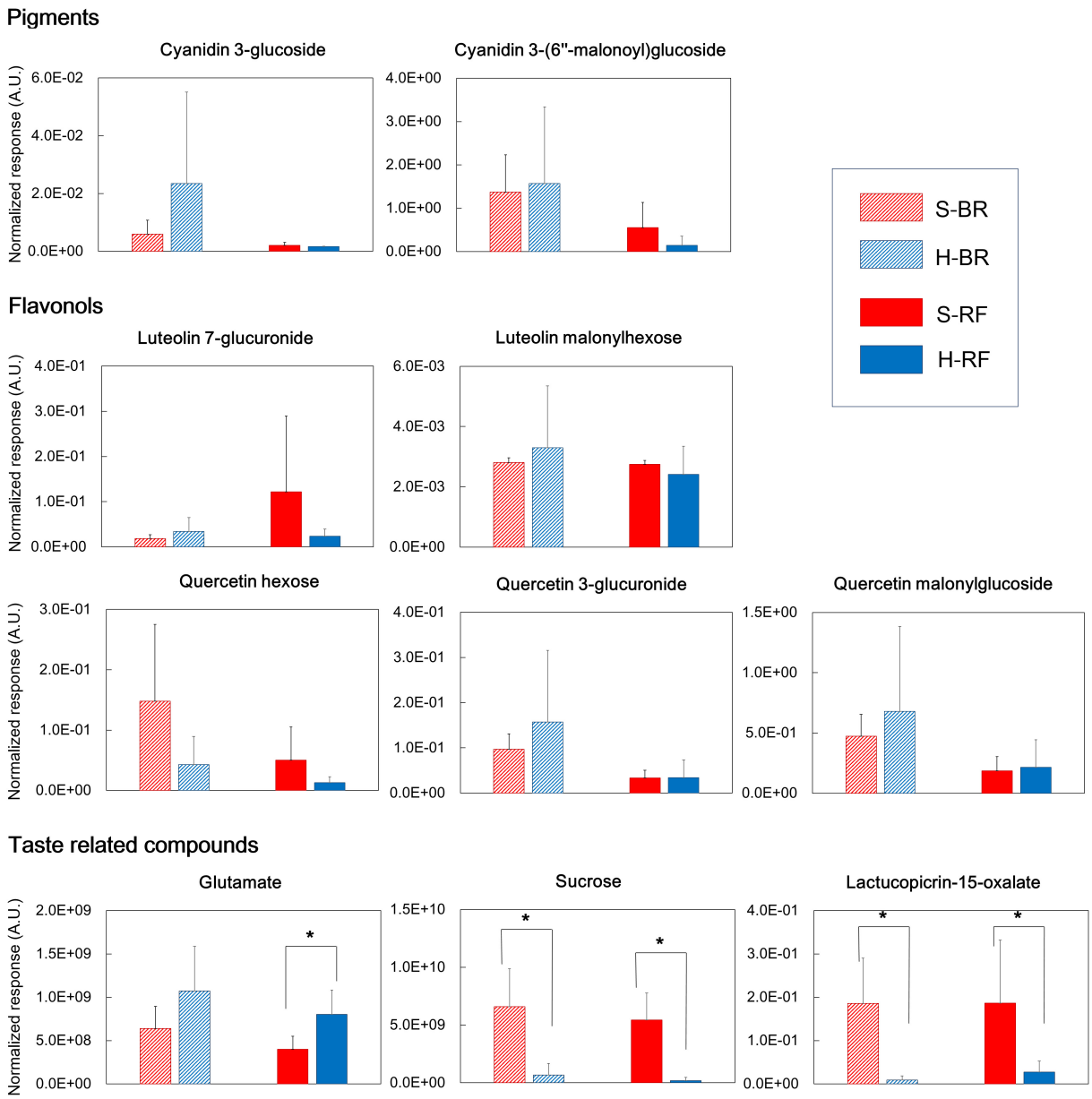

FIGURE 6 | Quality index metabolites, represented by pigments, flavonols, and taste-related compounds, of Black rose (BR) and red fire (RF) lettuce leaves grown under hydroponic (H) and soil (S) cultivation conditions (number of samples: 6 × H-BR, 6 × H-RF, 8 × S-BR and 8 × S-RF). (*indicates significant difference at $p < 0.05$ analyzed by Student's *t*-test).

hydroponically and in soil. Miyagi et al. (2017) reported that red LED radiation combined with high concentrations of carbon dioxide and liquid fertilizer increased the biomass and the level of some amino acids in head lettuce grown hydroponically. Nitrogen, the main component of liquid fertilizer, impacts the plant metabolism. We found higher concentrations of amino acids (leucine, isoleucine, tryptophan, tyrosine, and phenylalanine) in the leaves of hydroponically- than soil-grown BR and RF lettuce. This phenomenon might also be affected by the applied nutritional values in both cultivation systems wherein more nitrogen nutrition was provided for hydroponic condition than in soil cultivation (**Table 1**). Due to the elicitation of higher amino acid levels, hydroponic cultivation may result in stronger "umami" perception than soil cultivation (Morris et al., 2007; Wang et al., 2016). On the other hand, the accumulation of sugars, fatty acid-derived alcohols, and β-sitosterol was lower in hydroponically- than soil-grown lettuce leaves. Our findings agree with earlier reports that the accumulation of sugars may be affected by environmental factors or stress such as light- and nutrient-conditions (Okazaki et al., 2008; Rosa et al., 2009; Miyagi et al., 2017). The level of leaf epidermal wax compounds such fatty acid-derived alcohols and β-sitosterol might be decreased

in lettuce leaves grown in a hydroponic culture system (Baker et al., 1979). Also, the three-times shorter shelf life of hydroponically grown leaf lettuce may be attributable to lower dehydration (Manzocco et al., 2011), suggesting that the decreased level of fatty acids and sterols we observed in hydroponically grown lettuce contributed to the change in its leaf epidermal composition. Additionally, increased levels of fatty acids were considered to reflect stress of lettuce in soil (Yang and Ohlrogge, 2009).

To evaluate the effect of environmental growth conditions on RF and BR lettuces, we compared their metabolite profiles and extract metabolite signature for developing a quality index. Compared with hydroponically grown lettuce, the accumulation of sesquiterpene lactones and phenolics was markedly greater in BR- and RF-lettuce leaves harvested after soil cultivation. Seo et al. (2009) reported that the correlation between mineral nutrients intake and producing of sesquiterpene lactones in leaf lettuce. Exposure to short-wavelength light (blue LED and UV-B treatments) elicits an increase in phenolics, flavonoids, and the pigment content in lettuce leaves (Ouzounis et al., 2015) and in *Arabidopsis thaliana* (Kusano et al., 2011c) and our light conditions may have exerted a similar effect. Caldwell and Britz (2006) suggested that differences in the photosensitivity trait among cultivars changes the metabolite composition in leafy vegetables. The higher level of phenolics in soil- than hydroponically grown RF lettuce may increase its antioxidant and antimutagenic effects but render it more bitter-tasting and more astringent (Ren et al., 2001; Altunkaya et al., 2016; Filippo D'Antuono et al., 2016). BR-specific metabolites such as sesquiterpene lactones found in soil-grown plants may also enhance its bitter taste (Chadwick et al., 2016; Filippo D'Antuono et al., 2016). On the other hand, the sugar components in these soil-grown lettuces may mask their bitter taste and enrich their taste complexity (Beck et al., 2014; Chadwick et al., 2016).

CONCLUSION

Our study shows that the two cultivation methods greatly affect the metabolite profile of RF and BR leaf lettuce, including the metabolites responsible for their taste and their functional ingredients (e.g., amino acids and phenolic compounds). These metabolites may contribute to the overall quality and sensorial perception of leaf lettuce grown under hydroponic and soil cultivation methods (Manzocco et al., 2011; Mampholo et al., 2016). Metabolomic elucidations for lettuce have been conducted using various analytical techniques, including GC-MS, LC-MS, CE-MS, and NMR analyses (Pereira et al., 2014; Garcia et al., 2016; Zhao et al., 2016; Hurtado et al., 2017; Miyagi et al., 2017; Kitazaki et al., 2018). These techniques enabled to detect most of nutritional and pigment metabolites in the evaluated lettuce. Thus, metabolomic data can be used as an important basis for further detailed assessment of cultivation systems and horticulture products not only for lettuce, but for other vegetables. As the next step, it will be needed to evaluate which growth factor(s) are essential to affect phytochemical accumulation as well as yield in plant factories. We document that integrated metabolic profiling is a powerful tool for the comprehensively evaluation of the quality of leaf lettuce. Studies are underway to examine the effect of the light properties and of the liquid fertilizer concentration on the quality and nutritional value of leaf lettuce.

AUTHOR CONTRIBUTIONS

MK initiated the study conception. MK, KS, and SO designed the analysis. YT performed the statistical analysis and drafted the manuscript. TM, RN, and MKo worked on data acquisition and analysis. MK supervised the study. SO and NW created and provided the samples. YT and MK wrote the manuscript and interpreted biological meaning of the results.

FUNDING

This research was partly supported by the "Sustainable Food Security Research Project" in the form of an operational grant from the National University Corporation.

ACKNOWLEDGMENTS

We thank Drs. Thomas Moritz, Pär Jonsson, and Hans Stenlund (Umeå Plant Science Centre) for their assistance with data analysis and Dr. Yonathan Asikin (University of Tsukuba) for helpful comments on the manuscript.

SUPPLEMENTARY MATERIAL

The Supplementary Material for this article can be found online at: https://www.frontiersin.org/articles/10.3389/fpls.2018.00665/full#supplementary-material

REFERENCES

Abu-Reidah, I. M., Contreras, M. M., Arráez-Román, D., Segura-Carretero, A., and Fernández-Gutiérrez, A. (2013). Reversed-phase ultra-high-performance liquid chromatography coupled to electrospray ionization-quadrupole-time-of-flight mass spectrometry as a powerful tool for metabolic profiling of vegetables: *Lactuca sativa* as an example of its application. *J. Chromatogr. A* 1313, 212–227. doi: 10.1016/j.chroma.2013.07.020

Altunkaya, A., Gökmen, V., and Skibsted, L. H. (2016). pH dependent antioxidant activity of lettuce (*L. sativa*) and synergism with added phenolic antioxidants. *Food Chem.* 190, 25–32. doi: 10.1016/j.foodchem.2015.05.069

Arbona, V., Iglesias, D. J., Talón, M., and Gómez-Cadenas, A. (2009). Plant phenotype demarcation using nontargeted LC-MS and GC-MS metabolite profiling. *J. Agric. Food Chem.* 57, 7338–7347. doi: 10.1021/jf9009137

Baker, E. A., Bukovac, M. J., and Flore, J. A. (1979). Ontogenetic variations in the composition of peach leaf wax. *Phytochemistry* 18, 781–784. doi: 10.1016/0031-9422(79)80013-8

Beck, T. K., Jensen, S., Bjoern, G. K., and Kidmose, U. (2014). The masking effect of sucrose on perception of bitter compounds in brassica vegetables. *J. Sens. Stud.* 29, 190–200. doi: 10.1111/joss.12094

Benjamini, Y., and Hochberg, Y. (1995). Controlling the false discovery rate: a practical and powerful approach to multiple testing. *J. R. Stat. Soc. Series B Stat. Methodol.* 57, 289–300.

Caldwell, C. R., and Britz, S. J. (2006). Effect of supplemental ultraviolet radiation on the carotenoid and chlorophyll composition of green house-grown leaf lettuce (*Lactuca sativa* L.) cultivars. *J. Food Compost. Anal.* 19, 637–644. doi: 10.1016/j.jfca.2005.12.016

Chadwick, M., Gawthrop, F., Michelmore, R. W., Wagstaff, C., and Methven, L. (2016). Perception of bitterness, sweetness and liking of different genotypes of lettuce. *Food Chem.* 197, 66–74. doi: 10.1016/j.foodchem.2015.10.105

Clevenger, J. P., Van Houten, J., Blackwood, M., Rodríguez, G. R., Jikumaru, Y., Kamiya, Y., et al. (2015). Network analyses reveal shifts in transcript profiles and metabolites that accompany the expression of SUN and an elongated tomato fruit. *Plant Physiol.* 168, 1164–1178. doi: 10.1104/pp.15.00379

Farag, M. A., El-ahmady, S. H., Elian, F. S., and Wessjohann, L. A. (2013). Metabolomics driven analysis of artichoke leaf and its commercial products via UHPLC–q-TOF-MS and chemometrics. *Phytochemistry* 95, 177–187. doi: 10.1016/j.phytochem.2013.07.003

Fiehn, O., Kopka, J., Dormann, P., Altmann, T., Trethewey, R. N., and Willmitzer, L. (2000). Metabolite profiling for plant functional genomics. *Nat. Biotechnol.* 18, 1157–1161. doi: 10.1038/81137

Filippo D'Antuono, L., Ferioli, F., and Manco, M. A. (2016). The impact of sesquiterpene lactones and phenolics on sensory attributes: an investigation of a curly endive and escarole germplasm collection. *Food Chem.* 199, 238–245. doi: 10.1016/j.foodchem.2015.12.002

Garcia, C. J., García-Villalba, R., Garrido, Y., Gil, M. I., and Tomás-Barberán, F. A. (2016). Untargeted metabolomics approach using UPLC-ESI-QTOF-MS to explore the metabolome of fresh-cut iceberg lettuce. *Metabolomics* 12, 1–13. doi: 10.1007/s11306-016-1082-x

Gowda, G. A. N., and Djukovic, D. (2014). Overview of Mass spectrometry-based metabolomics: opportunities and challenges. *Methods Mol. Biol.* 1198, 3–12. doi: 10.1007/978-1-4939-1258-2

Halpern, B. P. (2000). Glutamate and the flavor of foods. *J. Nutr.* 130, 921–926. doi: 10.1093/jn/130.4.910S

Hounsome, N., Hounsome, B., Tomos, D., and Edwards-Jones, G. (2008). Plant metabolites and nutritional quality of vegetables. *J. Food Sci.* 73, 48–65. doi: 10.1111/j.1750-3841.2008.00716.x

Hurtado, C., Parastar, H., Matamoros, V., Piña, B., Tauler, R., and Bayona, J. M. (2017). Linking the morphological and metabolomic response of *Lactuca sativa* L exposed to emerging contaminants using GC × GC-MS and chemometric tools. *Sci. Rep.* 7, 18–26. doi: 10.1038/s41598-017-06773-0

Jonsson, P., Johansson, A. I., Gullberg, J., Trygg, J., Aa, J., Grung, B., et al. (2005). High-throughput data analysis for detecting and identifying differences between samples in GC/MS-based metabolomic analyses. *Anal. Chem.* 77, 5635–5642. doi: 10.1021/ac050601e

Jonsson, P., Johansson, E. S., Wuolikainen, A., Lindberg, J., Schuppe-Koistinen, I., Kusano, M., et al. (2006). Predictive metabolite profiling applying hierarchical multivariate curve resolution to GC-MS data - A potential tool for multi-parametric diagnosis. *J. Proteome Res.* 5, 1407–1414. doi: 10.1021/pr0600071

Kitazaki, K., Fukushima, A., Nakabayashi, R., Okazaki, Y., Kobayashi, M., Mori, T., et al. (2018). Metabolic reprogramming in leaf lettuce grown under different light quality and intensity conditions using narrow-band LEDs. *Sci. Rep.* 8:7914. doi: 10.1038/s41598-018-25686-0

Kozai, T. (2013). Resource use efficiency of closed plant production system with artificial light: concept, estimation and application to plant factory. *Proc. Jpn. Acad. Ser. B* 89, 447–461. doi: 10.2183/pjab.89.447

Kurihara, K. (2009). Glutamate: from discovery as a food flavor to role as a basic taste (umami). *Am. J. Clin. Nutr.* 90, 1–3. doi: 10.3945/ajcn.2009.27462D

Kusano, M., Baxter, I., Fukushima, A., Oikawa, A., Okazaki, Y., Nakabayashi, R., et al. (2014a). Assessing metabolomic and chemical diversity of a soybean lineage representing 35 years of breeding. *Metabolomics* 261–270. doi: 10.1007/s11306-014-0702-6

Kusano, M., Fukushima, A., Kobayashi, M., Hayashi, N., Jonsson, P., Moritz, T., et al. (2007). Application of a metabolomic method combining one-dimensional and two-dimensional gas chromatography-time-of-flight/mass spectrometry to metabolic phenotyping of natural variants in rice. *J. Chromatogr. B* 855, 71–79. doi: 10.1016/j.jchromb.2007.05.002

Kusano, M., Jonsson, P., Fukushima, A., Gullberg, J., Sjöström, M., Trygg, J., et al. (2011a). Metabolite signature during short-day induced growth cessation in populus. *Front. Plant Sci.* 2:29. doi: 10.3389/fpls.2011.00029

Kusano, M., Redestig, H., Hirai, T., Oikawa, A., and Matsuda, F. (2011b). Covering chemical diversity of genetically-modified tomatoes using metabolomics for objective substantial equivalence assessment. *PLoS One* 6:e16989. doi: 10.1371/journal.pone.0016989

Kusano, M., Tohge, T., Fukushima, A., Kobayashi, M., Hayashi, N., Otsuki, H., et al. (2011c). Metabolomics reveals comprehensive reprogramming involving two independent metabolic responses of Arabidopsis to UV-B light. *Plant J.* 67, 354–369. doi: 10.1111/j.1365-313X.2011.04599.x

Kusano, M., Yang, Z., Okazaki, Y., Nakabayashi, R., Fukushima, A., and Saito, K. (2014b). Using metabolomic approaches to explore chemical diversity in rice. *Mol. Plant* 8, 58–67. doi: 10.1016/j.molp.2014.11.010

Lee, J., Jung, Y., Shin, J. H., Kim, H. K., Moon, B. C., Ryu, D. H., et al. (2014). Secondary metabolite profiling of curcuma species grown at different locations using GC/TOF and UPLC/Q-TOF MS. *Molecules* 19, 9535–9551. doi: 10.3390/molecules19079535

Li, L., Zhao, J., Zhao, Y., Lu, X., Zhou, Z., Zhao, C., et al. (2016). Comprehensive investigation of tobacco leaves during natural early senescence via multi-platform metabolomics analyses. *Sci. Rep.* 6:37976. doi: 10.1038/srep37976

Li, Q., and Kubota, C. (2009). Effects of supplemental light quality on growth and phytochemicals of baby leaf lettuce. *Environ. Exp. Bot.* 67, 59–64. doi: 10.1016/j.envexpbot.2009.06.011

Lisec, J., Schauer, N., Kopka, J., Willmitzer, L., and Fernie, A. R. (2006). Gas chromatography mass spectrometry – based metabolite profiling in plants. *Nat. Protoc.* 1, 387–396. doi: 10.1038/nprot.2006.59

Ma, C., Dastmalchi, K., Flores, G., Wu, S. B., Pedraza-Peñalosa, P., Long, C., et al. (2013). Antioxidant and metabolite profiling of North American and neotropical blueberries using LC-TOF-MS and multivariate analyses. *J. Agric. Food Chem.* 61, 3548–3559. doi: 10.1021/jf400515g

Mampholo, B. M., Maboko, M. M., Soundy, P., and Sivakumar, D. (2016). Phytochemicals and overall quality of leafy lettuce (*Lactuca sativa* L.) varieties grown in closed hydroponic system. *J. Food Qual.* 39, 805–815. doi: 10.1111/jfq.12234

Manzocco, L., Foschia, M., Tomasi, N., Maifreni, M., Dalla Costa, L., Marino, M., et al. (2011). Influence of hydroponic and soil cultivation on quality and shelf life of ready-to-eat lamb's lettuce (*Valerianella locusta* L. Laterr). *J. Sci. Food Agric.* 91, 1373–1380. doi: 10.1002/jsfa.4313

McWatters, L. H., Chinnan, M. S., Walker, S. L., Doyle, M. P., and Lin, C. M. (2002). Consumer acceptance of fresh-cut iceberg lettuce treated with 2% hydrogen peroxide and mild heat. *J. Food Prot.* 65, 1221–1226.

Miyagi, A., Uchimiya, H., and Kawai-Yamada, M. (2017). Synergistic effects of light quality, carbon dioxide and nutrients on metabolite compositions of head lettuce under artificial growth conditions mimicking a plant factory. *Food Chem.* 218, 561–568. doi: 10.1016/j.foodchem.2016.09.102

Miyauchi, S., Yonetani, T., Yuki, T., Tomio, A., Bamba, T., and Fukusaki, E. (2017). Quality evaluation of green tea leaf cultured under artificial light condition using gas chromatography/mass spectrometry. *J. Biosci. Bioeng.* 123, 197–202. doi: 10.1016/j.jbiosc.2016.07.017

Morris, W. L., Ross, H. A., Ducreux, L. J. M., Bradshaw, J. E., Bryan, G. J., and Taylor, M. A. (2007). Umami compounds are a determinant of the flavor of potato (*Solanum tuberosum* L.). *J. Agric. Food Chem.* 55, 9627–9633. doi: 10.1021/jf0717900

Muroya, S., Oe, M., Nakajima, I., Ojima, K., and Chikuni, K. (2014). CE-TOF MS-based metabolomic profiling revealed characteristic metabolic pathways in postmortem porcine fast and slow type muscles. *Meat Sci.* 98, 726–735. doi: 10.1016/j.meatsci.2014.07.018

Nakabayashi, R., Yonekura-Sakakibara, K., Urano, K., Suzuki, M., Yamada, Y., Nishizawa, T., et al. (2014). Enhancement of oxidative and drought tolerance in Arabidopsis by overaccumulation of antioxidant flavonoids. *Plant J.* 77, 367–379. doi: 10.1111/tpj.12388

Ohashi-Kaneko, K., Takese, M., Kon, N., Fujiwara, K., and Kurata, K. (2007). Effect of light quality on growth and vegetable quality in leaf lettuce, spinach and komatsuna. *Environ. Control Biol.* 45, 189–198. doi: 10.2525/ecb.45.189

Okazaki, K., Oka, N., Shinano, T., Osaki, M., and Takebe, M. (2008). Differences in the metabolite profiles of spinach (*Spinacia oleracea* L.) leaf in different concentrations of nitrate in the culture solution. *Plant Cell Physiol.* 49, 170–177. doi: 10.1093/pcp/pcm173

Ouzounis, T., Razi Parjikolaei, B., Frette, X., Rosenqvist, E., and Ottosen, C. O. (2015). Predawn and high intensity application of supplemental blue light decreases the quantum yield of PSII and enhances the amount of phenolic acids, flavonoids, and pigments in *Lactuca sativa*. *Front. Plant Sci.* 6:19. doi: 10.3389/fpls.2015.00019

Palermo, M., Paradiso, R., Pascale, S., and Fogliano, V. (2012). Hydroponic cultivation improves the nutritional quality of soybean and its products. *J. Agric. Food Chem.* 55, 9627–9633. doi: 10.1021/jf203275m

Pereira, S. I., Figueiredo, P. I., Barros, A. S., Dias, M. C., Santos, C., Duarte, I. F., et al. (2014). Changes in the metabolome of lettuce leaves due to exposure to mancozeb pesticide. *Food Chem.* 154, 291–298. doi: 10.1016/j.foodchem.2014.01.019

Redestig, H., Fukushima, A., Stenlund, H., Moritz, T., Arita, M., Saito, K., et al. (2009). Compensation for systematic cross-contribution improves normalization of mass spectrometry based metabolomics data. *Anal. Chem.* 81, 7974–7980. doi: 10.1021/ac901143w

Ren, H., Endo, H., and Hayashi, T. (2001). Antioxidative and antimutagenic activities and polyphenol content of pesticide-free and organically cultivated green vegetables using water-soluble chitosan as a soil modifier and leaf surface spray. *J. Sci. Food Agric.* 81, 1426–1432. doi: 10.1002/jsfa.955

Rosa, M., Prado, C., Podazza, G., Interdonato, R., González, J. A., Hilal, M., et al. (2009). Soluble sugars-metabolism, sensing and abiotic stress a complex network in the life of plants. *Plant Signal. Behav.* 4, 388–393. doi: 10.4161/psb.4.5.8294

Rouphael, Y., Colla, G., Battistelli, A., Moscatello, S., Rea, E., Proietti, S., et al. (2004). Yield, water requirement, nutrient uptake and fruit quality of zucchini squash grown in soil and closed soilless culture. *J. Hort. Sci. Biotechnol.* 79, 423–431. doi: 10.1080/14620316.2004.11511784

Samuoliene, G., Brazaityte, A., Sirtautas, R., Viršile, A., Sakalauskaite, J., Sakalauskiene, S., et al. (2013). LED illumination affects bioactive compounds in romaine baby leaf lettuce. *J. Sci. Food Agric.* 93, 3286–3291. doi: 10.1002/jsfa.6173

Sass-Kiss, A., Kiss, J., Milotay, P., Kerek, M. M., and Toth-Markus, M. (2005). Differences in anthocyanin and carotenoid content of fruits and vegetables. *Food Res. Int.* 38, 1023–1029. doi: 10.1016/j.foodres.2005.03.014

Sekiyama, Y., Okazaki, K., Kikuchi, J., and Ikeda, S. (2017). NMR-based metabolic profiling of field-grown leaves from sugar beet plants harbouring different levels of resistance to cercospora leaf spot disease. *Metabolites* 7:4. doi: 10.3390/metabo7010004

Seo, M. W., Yang, D. S., Kays, S. J., Lee, G. P., and Park, K. W. (2009). Sesquiterpene lactones and bitterness in Korean leaf lettuce cultivars. *HortScience* 44, 246–249.

Sobolev, A. P., Brosio, E., Gianferri, R., and Segre, A. L. (2005). Metabolic profile of lettuce leaves by high-field NMR spectra. *Magn. Reson. Chem.* 43, 625–638. doi: 10.1002/mrc.1618

Son, K. H., and Oh, M. M. (2013). Leaf shape, growth, and antioxidant phenolic compounds of two lettuce cultivars grown under various combinations of blue and red light-emitting diodes. *HortScience* 48, 988–995.

Stutte, G. W., Edney, S., and Skerritt, T. (2009). Photoregulation of bioprotectant content of red leaf lettuce with light-emitting diodes. *HortScience* 44, 79–82.

Sugimoto, M., Goto, H., Otomo, K., Ito, M., Onuma, H., Suzuki, A., et al. (2010). Metabolomic profiles and sensory attributes of edamame under various storage duration and temperature conditions. *J. Agric. Food Chem.* 58, 8418–8425. doi: 10.1021/jf101471d

Sugimoto, M., Kaneko, M., Onuma, H., Sakaguchi, Y., Mori, M., Abe, S., et al. (2012). Changes in the charged metabolite and sugar profiles of pasteurized and unpasteurized Japanese sake with storage. *J. Agric. Food Chem.* 60, 2586–2593. doi: 10.1021/jf2048993

Sulpice, R., Pyl, E., Ishihara, H., Trenkamp, S., Steinfath, M., Witucka-wall, H., et al. (2009). Starch as a major integrator in the regulation of plant growth. *Proc. Natl. Acad. Sci. U.S.A.* 106, 10348–10353. doi: 10.1073/pnas.0903478106

Sung, J., Lee, S., Lee, Y., Ha, S., Song, B., Kim, T., et al. (2015). Metabolomic profiling from leaves and roots of tomato (*Solanum lycopersicum* L.) plants grown under nitrogen, phosphorus or potassium-deficient condition. *Plant Sci.* 241, 55–64. doi: 10.1016/j.plantsci.2015.09.027

Tamoi, M., Ishida, K., Eguchi, M., Harada, K., Kijihana, I., and Shigeoka, S. (2017). Growth and photosynthetic characteristics of arabidopsis and tobacco plants grown under LED lights "PLANT FLEC" (in Japanese with English summary). *Shokubutsu Kankyo Kogaku* 29, 96–103. doi: 10.2525/shita.29.96

Tokimasa, M., and Nishiura, Y. (2015). Automation in plant factory with labor-saving conveyance system. *Environ. Control Biol.* 53, 101–105. doi: 10.2525/ecb.53.101

Touliatos, D., Dodd, I. C., and Mcainsh, M. (2016). Vertical farming increases lettuce yield per unit area compared to conventional horizontal hydroponics. *Food Energy Secur.* 5, 184–191. doi: 10.1002/fes3.83

Wang, L., Xu, B., Li, L., Zhang, M., Feng, T., Wang, J., et al. (2016). Enhancement of umami taste of hydrolyzed protein from wheat gluten by β-cyclodextrin. *J. Sci. Food Agric.* 96, 4499–4504. doi: 10.1002/jsfa.7665

Wu, X., and Prior, R. L. (2005). Identification and characterization of anthocyanins by high-performance liquid chromatography-electrospray ionization-tandem mass spectrometry in common foods in the United States: vegetables, nuts, and grains. *J. Agric. Food Chem.* 53, 3101–3113. doi: 10.1021/jf0478861

Xie, G. X., Ni, Y., Su, M. M., Zhang, Y. Y., Zhao, A. H., Gao, X. F., et al. (2008). Application of ultra-performance LC-TOF MS metabolite profiling techniques to the analysis of medicinal Panax herbs. *Metabolomics* 4, 248–260. doi: 10.1007/s11306-008-0115-5

Yang, Z., and Ohlrogge, J. B. (2009). Turnover of fatty acids during natural senescence of *Arabidopsis*, brachypodium, and switchgrass and in arabidopsis -oxidation mutants. *Plant Physiol.* 150, 1981–1989. doi: 10.1104/pp.109.140491

Ya-Qin, W., Li-Ping, H., Guang-Min, L., De-Shuang, Z., and Hong-Ju, H. (2017). Evaluation of the nutritional quality of Chinese kale (*Brassica alboglabra* Bailey) using UHPLC-quadrupole-orbitrap MS/MS-based metabolomics. *Molecules* 22:E1262. doi: 10.3390/molecules22081262

Zeng, W., Hazebroek, J., Beatty, M., Hayes, K., Ponte, C., Maxwell, C., et al. (2014). Analytical method evaluation and discovery of variation within maize varieties in the context of food safety: transcript profiling and metabolomics. *J. Agric. Food Chem.* 62, 2997–3009. doi: 10.1021/jf405652j

Zhang, Q., Shi, Y., Ma, L., Yi, X., and Ruan, J. (2014). Metabolomic analysis using ultra-performance liquid chromatography-quadrupole-time of flight mass spectrometry (UPLC-Q-TOF MS) uncovers the effects of light intensity and temperature under shading treatments on the metabolites in tea. *PLoS One* 9:e112572. doi: 10.1371/journal.pone.0112572

Zhao, L., Ortiz, C., Adeleye, A. S., Hu, Q., Zhou, H., Huang, Y., et al. (2016). Metabolomics to detect response of lettuce (*Lactuca sativa*) to Cu(OH)2 nanopesticides: oxidative stress response and detoxification mechanisms. *Environ. Sci. Technol.* 50, 9697–9707. doi: 10.1021/acs.est.6b02763

Conflict of Interest Statement: The authors declare that the research was conducted in the absence of any commercial or financial relationships that could be construed as a potential conflict of interest.

frontiers in Plant Science

ORIGINAL RESEARCH
published: 16 March 2018
doi: 10.3389/fpls.2018.00305

Effect of Solid Biological Waste Compost on the Metabolite Profile of *Brassica rapa* ssp. *chinensis*

*Susanne Neugart[1†], Melanie Wiesner-Reinhold[1†], Katja Frede[1,2], Elisabeth Jander[2], Thomas Homann[2], Harshadrai M. Rawel[2], Monika Schreiner[1] and Susanne Baldermann[1,2]**

[1] Leibniz Institute of Vegetable and Ornamental Crops, Großbeeren, Germany, [2] Department of Food Chemistry, Institute of Nutritional Science, University of Potsdam, Nuthetal, Germany

Large quantities of biological waste are generated at various steps within the food production chain and a great utilization potential for this solid biological waste exists apart from the current main usage for the feedstuff sector. It remains unclear how the usage of biological waste as compost modulates plant metabolites. We investigated the effect of biological waste of the processing of coffee, aronia, and hop added to soil on the plant metabolite profile by means of liquid chromatography in pak choi sprouts. Here we demonstrate that the solid biological waste composts induced specific changes in the metabolite profiles and the changes are depending on the type of the organic residues and its concentration in soil. The targeted analysis of selected plant metabolites, associated with health beneficial properties of the Brassicaceae family, revealed increased concentrations of carotenoids (up to 3.2-fold) and decreased amounts of glucosinolates (up to 4.7-fold) as well as phenolic compounds (up to 1.5-fold).

Keywords: metabolite profiling, LC/MS, pak choi, carotenoids, phenolic compounds, glucosinolates

OPEN ACCESS

Edited by:
Marta Sousa Silva, Universidade de Lisboa, Portugal

Reviewed by:
Lachlan James Palmer, Flinders University, Australia
Bartosz Adamczyk, University of Helsinki, Finland

***Correspondence:**
Susanne Baldermann
baldermann@igzev.de

[†]*These authors have contributed equally to this work.*

Specialty section:
This article was submitted to Plant Metabolism and Chemodiversity, a section of the journal Frontiers in Plant Science

Received: *20 November 2017*
Accepted: *22 February 2018*
Published: *16 March 2018*

Citation:
Neugart S, Wiesner-Reinhold M, Frede K, Jander E, Homann T, Rawel HM, Schreiner M and Baldermann S (2018) Effect of Solid Biological Waste Compost on the Metabolite Profile of Brassica rapa ssp. chinensis. Front. Plant Sci. 9:305. doi: 10.3389/fpls.2018.00305

INTRODUCTION

Rising world population, globally changing climate, intensification and competition of biomass usage as source of bioenergy and urban horticultural practice are only a few examples which enhance people's concern about the efficient, multiple use of bio-mass and recycling of residues. Biological waste is generated at various steps within the food production chain, e.g., production of dairy products, oil industry, beverage producers including breweries, processing of fruits and vegetables, and coffee producers (e.g., Mahro et al., 2015). These industries generate large quantities of biological waste and 13 million tons are produced in Germany per annum (Mahro et al., 2015). Much of these wastes are either burnt or treated by oxygen-driven biological methods, such as composting, which serves a dual purpose, i.e., valorization *via* material value as well as decreasing the pollution potential (Murthy and Naidu, 2012; Shemekite et al., 2014). On the other hand biological food waste is a reservoir of complex carbohydrates, proteins, lipids, and nutraceuticals and can form the raw materials for commercially important metabolites. Different modes of pre-treatments, followed by recovery procedures have been applied to attain value-added products (natural antioxidants, vitamins, enzymes, cellulose, starch, lipids, proteins, and pigments) of spent coffee of high significance to pharmaceutical, cosmetic, and food industries (Murthy and Naidu, 2012). The valorization of the solid coffee by-products in the non-food sector is also gaining more importance (Murthy and Naidu, 2012). During the technological processing of fruits and berries, large amounts of solids remain containing pulp, skins, seeds etc. In Germany, industrial processing

produces around 7 million tons and in Europe ca. 30 million tons of such wastes. Aronia and hop wastes represent two of these potential wastes. In case of berries, such wastes have also been termed as "pomace." The major part of these residues is either used for animal feed or is more generally disposed–the disposal being costly. Aronia pomace and spent hops have been utilized to extract bioactive antioxidant phenolics (Baranowski et al., 2009; Yui et al., 2013; D'Alessandro et al., 2014; Brazdauskas et al., 2016; Takahashi and Osada, 2017; Xu et al., 2017). Furthermore, compost can enhance the organic content of soil. In this context, the use of organic soil amendments can influence soil fertility, microbial soil communities as well as plant growth and health. The use of compost is positively associated with higher plant available water holding capacity and lower bulk density and can foster beneficial microorganism populations (Grassi et al., 2015; Pan et al., 2016). Studies report the potential of using diverse cover crop green manure in field vegetable production; however the potential of organic waste as compost arising within the food production chain remains to be investigated. Green manures contribute to nitrogen, phosphorus, and potassium contents of soil (Thönnissen Michel, 1996; Diniz et al., 2007; De Neve, 2017; Verlinden et al., 2017). Moreover, eliminating synthetic fertilizers in agriculture is an issue of global concern, due to the associated decrease in soil fertility after its use, pollution, and contamination of produced horticultural products; all with possible relations to human health. The effect of organic production on the secondary metabolite profiles has been Investigated (Soltoft et al., 2011), however it remains unclear how the usage of residues of the food production chain modulates secondary plant metabolite profiles.

Apart from sustainable production and processing in recent years demands concerning the quality of foods is changing and consumers expect safe, high-quality plant foods. Quality is determined by a variety of aspects, including appearance, aroma, and taste, but increasingly also of value-giving plant metabolites. Secondary plant metabolites are defined as bioactive non-nutrients in fruits, vegetables and other plant foods and have been linked to reducing the risk of chronic diseases, i.e., cardiovascular or aging eye diseases (Hartley et al., 2013; Larsson et al., 2013). Secondary plant metabolites include carotenoids, glucosinolates, and phenolic compounds.

Here we report the effect of biological waste used as compost on the content of secondary plant metabolites in *Brassica rapa* ssp. *chinensis* (pak choi). Pak choi can be cultivated under a variety of agro-climatic conditions and is a fast growing green leafy vegetable, which is very frequently consumed in Asian countries and in steadily rising quantities in Europe. As with other species, the amount of bioactive substances is known to depend on several parameters, including genotype, growing conditions comprising also soil characteristics, and developmental stage.

Pak choi is rich in secondary plant metabolites and contains considerable amounts of β-carotene and lutein with average concentrations of around 4.5 and 8 mg/100 g edible fresh weight (FW), respectively (Reif et al., 2013). The concentration of β-carotene in other vegetables such as broccoli (0.8–2 mg/100 g FW), cauliflower (white, 0.01 mg/100 g FW), or Chinese cabbage (0.4–3 mg/100 g FW) is substantially lower (Harbaum et al., 2007).

As *Brassica* species pak choi is rich in glucosinolates, too. The concentrations of these valuable secondary metabolites are ranging from 100 to 300 mg/100 g FW (Wiesner et al., 2013b). The concentrations are comparable to other vegetables such as cabbage (90–200 mg/100 FW), kohlrabi (109 mg/100 g FW) and more than in cauliflower (60 mg/100 g FW) or broccoli (80 mg/100 g FW) (Sones et al., 1984; Kushad et al., 1999).

Moreover, *Brassica* vegetables are a rich source for phenolic compounds. Diverse phenolic compounds have been described in vegetables of the Brassicaceae family. These include the flavonoids kaempferol, quercetin, and isorhamnetin derivatives (Schmidt et al., 2010). As in other plants these core structures are glycosylated with sugar moieties and can be additionally acylated (Schmidt et al., 2010). Former studies presented a variety of kaempferol, quercetin, and isorhamnetin derivatives as well as various hydroxycinnamic acids in pak choi (Harbaum et al., 2007). The concentration of flavonoid derivatives in the leaf ranged from 4.68 to 16.67 mg/g and the concentration of hydroxycinnamic acid derivatives ranged from 1.48 mg/g of to 5.83 mg/g of dry matter (Rochfort et al., 2006).

We used solid biological waste as compost of the food production of coffee, aronia and hop and were particularly interested if these can modulate the phytochemical concentrations and profiles. We applied LC-ToF-MS to investigate the effect of the organic residues on metabolite profiles in pak choi. In addition, targeted analyses of carotenoids and chlorophylls, glucosinolates, and phenolic compounds were performed.

MATERIALS AND METHODS

Plant Material

Sprouts of pak choi (*Brassica rapa* ssp. *chinenesis*) cv. Black Behi were grown in green houses in Grossbeeren, Germany in summer 2015. The sprouts were grown on soil and mixtures of soil and compost. The soil used consisted of 35% vulcan clay, 50% turf, and 15% bark humus (Fruhstorfer Erde, Vechta, Germany, for further characterization see **Table 1).** Five or 10% of the soil was replaced by compost (percent by weight) since these quantities did not impact the plants' development. The biological waste used as compost was dried and grounded to a powder prior mixing with the soil. Spent coffee grounds were obtained from DEK Deutsche Extrakt Kaffee GmbH Berlin (Berlin, Germany) and the spent aronia organic material from Aronia Original Naturprodukte GmbH (Dresden, Germany). Hop production residue was provided by Hopsteiner HHV Hallertauer Hopfenveredlungsgesellschaft m.b.H. (Mainburg, Germany). The soil or soil compost mixtures were filled into aluminum foil trays (33 × 10 cm) and wetted with tap water if needed. Three grams of seeds (= about 1,100 seeds) was sown per replicate. The total aerial tissue of the sprouts with fully expanded cotyledons were harvested after 12 days above the surface, ∼2–3 cm long) and immediately frozen in liquid nitrogen and stored at −80°C until lyophylisation. Prior analysis the samples were

TABLE 1 | Composition of soil and soil compost mixtures.

	Soil	Soil compost mixtures					
		Coffee		Hop		Aronia	
		5%	10%	5%	10%	5%	10%
pH-Wert in $CaCl_2$	5.7	5.7	5.7	6.3	6.5	5.9	5.9
EC µs/cm	1666	1532	1385	2390	2615	1018	981
[mg/100 g]							
Mg in $CaCl_2$	49	50	46	57	57	44	43
Mg in DL*	89	94	88	131	141	87	87
K	148	127	133	498	668	193	229
P	91	75	71	131	141	76	57
Salt content	463	430	387	658	740	279	258
NO_3^-	91	75	71	92	104	76	57
NH_4^+	<0.2	0.4	0.7	3.7	7.4	0.3	0.6
[%]							
C	29.4	32.6	33.0	34.2	33.9	32.6	33.0
N	0.80	0.86	0.90	1.27	1.45	0.82	0.84
C/N	37	38	37	27	23	38	37
S	0.23	0.24	0.20	0.27	0.24	0.24	0.17

**double lactate extract.*

ground to a homogeneous, fine powder with a Retsch ball mill. All experiments were performed in triplicate.

Non-targeted Analysis of Non-volatile Metabolites

To assess differences in the composition of metabolites of sprouts grown on pure soil and compost soil mixtures non-volatile metabolites were analyzed by UHPLC-ToF-MS according to Errard et al. (2015, 2016). Ten milligrams of finely powdered tissue was extracted five times with 1.5 mL of 70% methanol acidified with 0.1% formic acid by shaking for 5 min. The volume of the combined supernatants was adjusted to a final volume of 10 mL. The extract was filtered through a 0.2 µm PTFE membrane prior to UPLC-ToF-MS (Agilent Technologies 6230 TOF LC/MS) analysis. Samples (5 µL) were injected into an Agilent Zorbax Extend—C18 Rapid resolution HT (50 × 2.1 mm, 1, 1.8 µm) column. Sample and column temperatures were maintained at 4° and 30°C, respectively. The metabolites were eluted at a flow rate of 0.4 ml min^{-1} using a chromatographic gradient [A: 0–3 min 98% (isocratic), 3–15 min 98–15%, 18 min 15–0%)] of the two mobile phases A; 0.01% aqueous formic acid and B; 0.01% formic acid in acetonitrile. The capillary voltage was set to 3.5 kV in the electrospray source. The source temperature was set to 320°C. The nebulizer gas flow was set to 8 L min^{-1} at 35 psi. Spectra were collected in negative or positive ionization mode at over the *m/z* range 70–1,200.

Analysis of Carotenoids

The carotenoids were extracted three times from 5 mg of freeze dried material using 0.5 ml methanol: tetrahydrofuran solution (1:1, v/v) according to Errard et al. (2015) and Mageney et al. (2016). The extracts were shaken at 1,000 rpm for 5 min at room temperature and centrifuged at 4,500 rpm for 5 min at 20°C. The combined extracts were evaporated in a stream of nitrogen. The extracts were dissolved in 0.02 ml dichloromethane and 0.18 ml of isopropyl alcohol. Prior analysis the solutions were filtered through a 0.2 µM PTFE membrane and kept at 4°C in the auto sampler during the analysis. The separation was performed on a C30-column (YMC Co. Ltd., Japan, YMC C30, 100 × 2.1 mm, 3 µm) on an Agilent Technologies 1290 Infinity UHPLC. Mixtures of methanol, methyl-tert-butyl-ether and water in different volume ratios (solvent A: 81/15/4 and solvent B: 6/90/4) were used as mobile phases at a flow rate of 0.2 ml min^{-1}. To enhance the ionization 20 mM ammonium acetate was added to the mobile phases. The pigments were analyzed on an Agilent Technologies 6230 TOF LC/MS equipped with an APCI ion source in positive ionization mode. The gas flow rate was set to 8 L min^{-1} and the temperature to 325°C, the vaporizer temperature to 350°C and the nebulizer pressure was set to 35 psi. The voltage was set to 3,500 V and a fragmentor voltage of 175 V was applied at a corona current of 6.5 µA. Stock solutions of the authentic standards were prepared individually and the concentrations were determined spectro-photometrically using the substance specific wavelengths and extinction coefficients. Identification was achieved by co-chromatography with references substances. External standard calibration curves were used for quantification by dose–response curves.

Analysis of Glucosinolates

Desulfo-glucosinolates were analyzed after a method reported by Witzel et al. (2015). Twenty milligrams of lyophilized sample material were extracted by shaking with 750 µL 70% hot methanol (70°C) for 10 min at 1,400 rpm. As internal standard 100 µL 2-propenyl glucosinolate (sinigrin) (1 mM) were added to the extraction mixture. The samples are centrifuged at 4,500 rpm at room temperature and the supernatant transferred to sample tube. The samples are re-extracted twice with 500 µl of hot methanol. The combined supernatants were applied to an acetic acid-activated DEAE Sephadex A-25 (0.5 mL bed volume) and desulfolated by 75 µL ß-glucuronidase/arylsulfatase over night at room temperature. Desulfo-glucosinolates were obtained by elution with 0.5 mL ultrapure water (2x) and the samples filtered through a SpinX (0.22 µMSpinX Costar Cellulose acetate, 3 min 3000 rpm) prior analysis by UHPLC-DAD (Agilent Technologies 1290 Infinity). The separation was performed on a Poroshell 120 EC-C18 (100 × 2.1 mm, 2.7 µm) column in gradient mode using water and 40% acetonitrile as mobile phases at a flow rate of 0.4 mL min^{-1}. The glucosinolate concentrations were calculated using 2-propenyl glucosinolate as an internal standard at a detection wavelength of 229 nm.

Analysis of Phenolic Compounds

The analyses were performed based on a modified method by Schmidt et al. (2010). Twenty milligrams of lyophilized sample material were extracted with 600 µL 60% methanol by ultra-sonication followed by 20 min shaking at 1,400 rpm. The sample was pelleted at 12,000 rpm at 20°C and re-extracted by 400 and 200 µL. The combined supernatant

was evaporated and re-dissolved in 500 μL of 20% methanol. Prior analysis the samples were filtered through a SpinX (0.22 μM SpinX Costar Cellulose Acetate, 3 min 3,000 rpm). The phenolics were analyzed on an Agilent Technologies 6230 TOF LC/MS equipped with an ESI ion source in positive ionization mode. The gas temperature was set to 350°C at a flow rate of 10 L min^{-1}, the vaporizer to 320°C and the nebulizer pressure was set to 35 psi. The voltage was set to 3,500 V and a fragmentor voltage of 350 V was applied. The separation was performed on a Prodigy ODS1 100 A (150 × 2.1 mm, 5 μm) column in gradient mode using 0.5% acetic acid and acetonitrile as mobile phases at a flow rate of 0.4 mL min^{-1}. Stock solutions of the authentic standards were prepared individually and identification was achieved by co-chromatography with references substances. External standard calibration curves were used for quantification by dose–response curves.

Analysis of Selected Soil Properties

The analyses have been performed by validated analytical methods of LUFA (Hoffmann, 1991). The analyses of the soil-pH (A 5.1.1), the EC value, salt content (A 10.1.1) as well as NO_3^- and NH_4^+ (A 6.1.4.1) have been described by Seck-Mbengue et al. (2017). The total C, N and S concentrations were determined by Dumas combustion using the Elementar Analyser Vario EL (Elementar, Elementar Analysensysteme GmbH, Langenselbold, Germany) according to LUFA A 2.2.5. Minerals have been determined after LUFA (A 6.2.4.1/A 6.2.4.2) using an ICP-OES iCAP 7400 instrument (Thermo Scientific GmbH, Dreieich, Germany) at the following detection wavelengths: P 213.618 nm, K 766.490 nm, and Mg 285.213 nm.

Data Pre-treatment and Data Analysis

The raw data from the UPLC-ToF-MS analysis were transformed and processed by Mass Profiler Professional (MPP; Version 12.1). The raw data were extracted by using the molecular feature extraction of Mass Hunter B.06.00 using the following settings: small molecules, min. 500 counts, ion species $[M+H]^+$, $[M-H]^-$, $[M+Na]^+$, $[M+NH_4]^+$, H_2O as neutral loss, peak spacing tolerance 0.025 ppm and a quality score based on mass accuracy, isotope abundance, and isotope spacing of 80%. Raw data files were imported to MPP for recursive workflow. Statistical analysis was carried out by MPP and included one-way-ANOVA followed by *post-hoc* Tukey's HSD test ($p \leq 0.05$). Compounds subjected to a minimum fold change of 2 were considered for identification. Afterwards, formulas were generated using the above mentioned ions and using a match tolerance of 10 ppm. Putative identification was obtained by using the Metlin database (Vers. 4.0, 24768 compounds). The statistical analysis of the results obtained from the targeted analysis of carotenoids, glucosinolates, and phenolic compounds was performed by Statistica 12. Shapiro–Wilk test has been used to test normal distribution. The means were compared by one-way-ANOVA followed by *post-hoc* Tukey's HSD test ($p \leq 0.05$).

RESULTS

Characteristics of Soil and Soil Compost Mixtures

Changes induced by addition of compost to the soil have been investigated and are summarized in **Table 1**. The pH of the soil compost mixtures was not affected by the addition of coffee, but increased from 5.7 to 5.9 using aronia and to 6.5 using hop compost. The EC value increased after addition of hop compost and was lower using aronia compost and coffee compost. Major changes have been detected after addition of hop compost. Mg, K, P, NO_3^-, and NH_4^+ increased in the hop compost soil mixtures as well as the total salt content. In aronia compost soil mixtures the total salt content was much lower compared to the common soil, however cannot be explained by the changes in Mg, K, P, or NO_3^- and NH_4^+ and further analyses are required to explain the changed salt contents. The total N was the highest in the hop compost soil mixtures which also yield in a changed C/N ratio compared to the other soils. The carbon contents were in general higher after addition of biological waste as compost, whereas the impact on the total S content was minimal.

Effects of Composts on Metabolite Profiles

LC-ToF-metabolomics was used to investigate the effect of biological waste as compost on non-volatile metabolites in pak choi. Therefore, metabolomic differences were combined with statistical analysis to determine the degree of metabolic differences caused by changing soil compositions. To evaluate the effect of organic residues on the metabolome, visualization of the altered metabolite profiles was done using principal component analysis (**Figure 1**). The first three principal components accounted for 28.6, 25.2, and 14.8% of the variance in pak choi samples, respectively. The samples could be clearly classified by soil conditions. We observed clusters for sprouts grown solely on soil and those grown on different soil-compost mixtures. There is a slightly different response in the sprouts depending on the amount of biological waste inside the soil. The overall composition was reflected by metabolic differences in the primary and secondary metabolite metabolism. We observed changes in the amino acid, energy, hormone, phenylpropanoid, and sugar metabolism (**Table 2**). For instance the amino acids isoleucine, leucine, methionine, and proline were all increased in sprouts grown on the different composts compared to the control group. Changes in other metabolites of the amino acid metabolism were related to the type and concentration of compost, e.g., threonine increased in sprouts grown on coffee or hop compost or 2-oxoglutarate and oxaloacetate in sprouts grown on coffee or aronia compost. Pyruvate was detected in higher concentration in sprouts grown on coffee compost and 4-hydroxyphenylpyruvate in those grown on hop compost. Glycerinaldehyde-3-phosphate, a metabolite of the sugar metabolism, decreased in any sample grown on compost, whereas galactose, galactose-1-phosphate, and glucose were found in higher concentrations in sprouts grown on coffee compost. Two metabolites of the energy metabolism have been tentatively identified. AMP strongly increased in sprouts grown on coffee or aronia compost, whereas dAMP decreased in

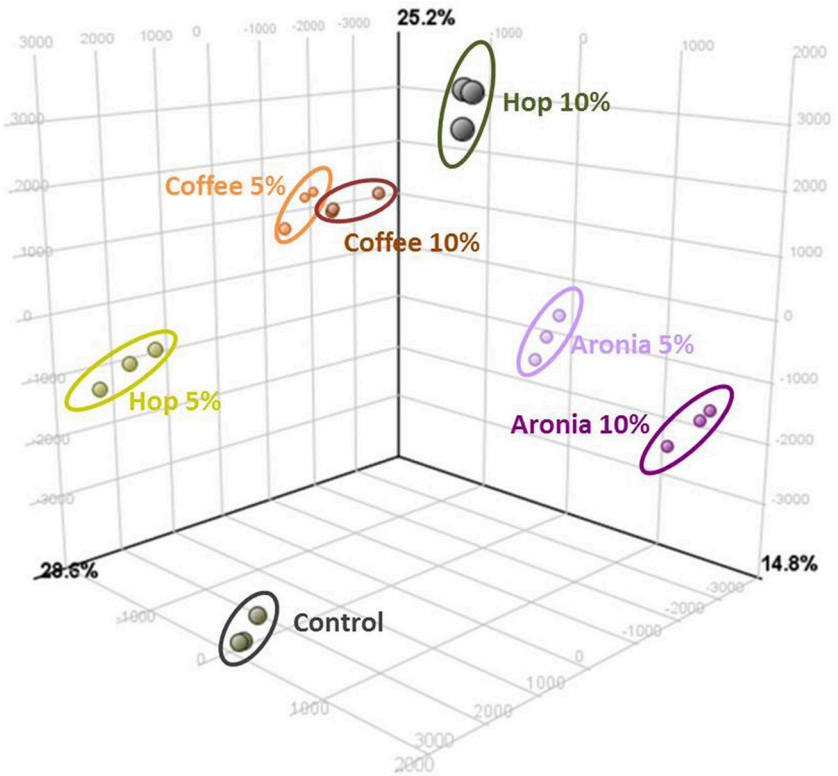

FIGURE 1 | Results of the principal component analysis (PCA) of significant differently abundant compounds (ANOVA $p \leq 0.05\%$, *post-hoc* Tukey HDS, min fold change 2) analyzed by UHPLC-ToF-MS$^{+/-}$.

samples grown on hop or aronia compost. Different pathways of the hormone metabolism were involved in the response to the usage of composts, such as salicylate, abscisic acid, and jasmonic acid. Salicylate and an epi-jasmonic acid derivative were reduced compared to the control, except for the sprouts grown on 10% coffee compost and cis-abscisate strongly induced by coffee and hop compost. An induction of the ascorbate levels have been found in samples grown on coffee or hop compost and for dehydroascorbate in those grown on coffee or aronia compost. Malate was detected in higher concentrations in sprouts grown on coffee or hop compost compared to the control group. Compounds of the phenylpropanoid metabolism were reduced compared to sprouts solely grown on soil, except for a tentatively identified isorhamnetin derivative which was accumulated in sprouts grown on coffee or hop compost.

Effect of Compost on Carotenoids, Glucosinolates, and Phenolic Compounds

On the basis of the putatively identified compounds we expected changes in valuable secondary plant metabolites and carried out a targeted analysis of carotenoids, glucosinolates, and phenolic compounds in the lyophilized sample material.

The factorial analysis of major carotenes, xanthophylls, glucosinolates, and phenolic compounds revealed that the different soil mixtures had noticeable impacts on the secondary plant metabolite profile (**Figure 2**).

The control group (sprouts grown on pure soil) and sprouts grown on soil mixtures with coffee, hop, or aronia composts show altered secondary plant metabolite profiles. Whereas slight differences were observed for the profiles of sprouts grown on coffee compost (5 and 10%) or aronia compost (5 and 10%), we observed higher variations among sprouts grown on hop compost (5 and 10%) (**Figure 2A**). Carotenoids contribute importantly to changes in sprouts grown on coffee and hop compost (5%), and glucosinolates in samples grown on aronia (5 and 10%) and hop compost (10%). The phenolic compounds show a more structure-specific response and contribute to the different metabolite profiles in sprouts grown on hop, aronia, or coffee compost (**Figure 2B**). More in detail, we estimated single carotenoid, glucosinolate, and phenolic compounds variability in sprouts of pak choi grown on pure soil (control) and compost-soil mixtures (**Table 3**).

Effect of Compost on Carotenoids

Highest changes were observed for the xanthophyll lutein (up to 3.2-fold), which is also the major carotenoid in pak choi sprouts. The concentration in the control group was 236 ± 46.6 μg/g and with all treatments showing a significant increase and the largest increase found in sprouts grown on 10% hop compost. The lutein concentration in this sample group was 966.9 ± 48.3 μg/g. In the treatments, the concentration of neoxanthin was found to increase by up to 3-fold. Major changes compared to the

TABLE 2 | Metabolites affected significantly by organic composts (coffee, hop, aronia) in soil (n.d. not detected; – reduced compared to the control; + increased compared to the control; level of change: weak (+)/(–) (0–1), moderate +/– (1–5), strong ++ (5–20), very strong +++ >100).

	Coffee		Hop		Aronia	
	5%	10%	5%	10%	5%	10%
AMINO ACIDS METABOLISM						
L-Isoleucine	+	+	+	+	+	+
Leucine	+	+	+	+	+	+
Methionine	+	+	+	+	(+)	+
Proline	+	+	+	++	+	+
Threonine	+	+	(+)	+	–	–
Tyrosine	–	–	++	+	–	–
Phenylalanine	–	–	–	+		(+)
4-Hydroxy-phenylpyruvate	–	–	++	+	–	–
2-Oxo-3-phenylpropanoate	+	+	–	+	+	+
2-Oxoglutarate	(+)	(+)	–	–	+	+
Oxalacetate	++	++	–	–	+++	+++
Pyruvate	+	(+)	–	–	–	–
ENERGY METABOLISM						
AMP	+++	+++	–	–	+++	+++
dADP			–	–	–	–
HORMONE METABOLISM						
Salicylate	–	–	–	–	–	–
Salicin	(+)	(+)	–	–	+	+
Benzoate	–	(+)	++	++	++	++
cis- Abscisate	+++	+++	+++	+++	–	–
epi-Jasmonic acid derivative	–	+	–	–	–	–
SUGAR METABOLISM						
Glycerinaldehyde-3-phosphate	–	–	–	–	–	–
Galactose	+	+	–	–	n.d	+
Galactose-1-phosphate	+++	+++	n.d.	n.d.	n.d.	
Glucose	+	+	–	–	n.d.	+
PHENYLPROPANOID METABOLISM						
Chrosmic acid	–	–	n.d.	n.d.		–
Galic acid	–	(–)		–	–	–
Chlorogenic acid derivative	–	–	(–)	–	–	–
Isorhamnetin derivative	+	+		+	–	–
OTHERS						
Ascorbate	+	+	+	+		–
Dehydroascorbate	(+)	(+)	–	–	+	+
Malate	+	+	+	+	–	–
Isocitrate	+	+	–	–	+	+
Citrate	+	+	–	–	+	+
Fumarate	+	(+)	–	–	–	–

control group (51.6 ± 7.5 μg/g) were detected again for sprouts grown on 10% hop compost (186.9 ± 9.3 μg/g). The changes in the xanthophyll zeaxanthin were less pronounced with max 1.7-fold change in case of sprouts grown on 10% hop compost (22.4 ± 1.1 μg/g control compared to 37.9 ± 1.9 μg/g 10% hop compost), too. The alterations in the β-carotene contents were minor compared to the variations observed for the xanthophylls. Slightly higher concentrations have been detected in all sprouts grown on compost, but significant effects were only found in the samples grown on hop compost or 5% aronia compost.

Effect of Compost on Glucosinolates

The total amount of the glucosinolates decreased in all sprouts except in the sample where 5% of the soil was replaced by compost derived from hop residue. In case of compost from coffee the reduction was from 13.62 ± 0.014 μg/g in the control to 12.19 ± 0.153 μg/g and 12.17 ± 0.118 μg/g in sprouts grown on 5 and 10% coffee compost, respectively. Higher losses have been found after addition of aronia (5.66 ± 0.105 μg/g 5% aronia and 4.36 ± 0.079 μg/g 10% aronia) or hop compost (2.94 ± 0.006 μg/g 10% hop) (**Table 3**). In all samples grown on soil-compost mixtures the aliphatic glucosinolates were reduced. Highest losses were found in those samples grown on aronia compost (5 and 10%) and on hop compost (10%). Using aronia compost the concentrations dropped by 0.59 (5% aronia compost) and 0.68 (10% aronia compost), from 12.29 ± 0.11 μg/g to 5.10 ± 0.11 μg/g and 3.94 ± 0.04 μg/g. In the pak choi sprouts grown on 10% hop compost the loss of aliphatic glucosinolates was 0.79 corresponding to 2.5 ± 0.01 μg/g. Interestingly, in sprouts grown on coffee compost, just the concentration of the aliphatic 4-methylthiobutyl glucosinolate was significantly reduced. The indole glucosinolates were significantly affected using coffee (5 and 10%), aronia (5 and 10%) or hop compost (10%). Noteworthy, in sprouts grown on the coffee compost the concentration of the methoxylated indole glucosinolates increased significantly. The 4-methoxyindole-3-ylmethyl glucosinolate was significantly affected by compost containing 5% coffee (0.30 ± 0.014 μg/g) residues compared to the control (0.14 ± 0.003 μg/g), whereas the 10% coffee compost affected more the 1-methoxyindole-3-ylmethyl glucosinolate (0.16 ± 0.068 – 0.74 ± 0.040 μg/g). The precursor of both, the indole-3-ylmethyl glucosinolates, kept almost unaffected compared to the concentration in sprouts grown on pure soil. In contrast, soils mixed with aronia (5 and 10%) and hop (10%) reduced significantly the concentration of all indole glucosinolates compared to the control. The aromatic 2-phenylethyl glucosinolate was significantly reduced in all samples grown on soil-compost mixtures compared to pure soil (**Table 3**).

Effect of Compost on Phenolic Compounds

The concentration in the phenolic compounds (2154.43 ± 93.70 μg/g) did not change (5 and 10% coffee compost, and 5% aronia compost) or were lower (5 and 10% hop compost, and 10% aronia compost compared to pure soil). In pak choi sprouts grown on 5% hop compost the concentration was reduced by 0.25 (1665.94 ± 76.36 μg/g), on 10% hop compost by 0.31 (1525.24 ± 33.01 μg/g, and on 10% aronia compost by 0.23 (1719.27 ± 7.23 μg/g).

More specifically, single phenolic compounds showed a particular response in respect of the various soil composts (**Table 3**); e.g., caffeoylmalate and kaempferol-3-*O*-caffeoyl-diglucoside-7-*O*-glucoside were reduced from control values of 28.39 ± 0.74 μg/g by up 100-fold and 18.23 ± 1.48 μg/g by 2-fold,

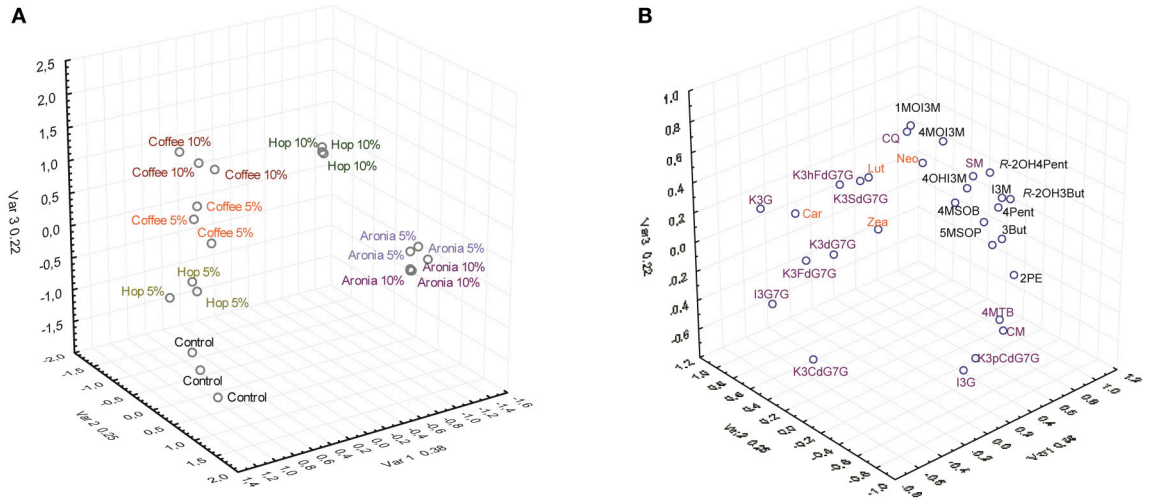

FIGURE 2 | Results of the factor analysis of the targeted analysis of glucosinolates, phenolic compounds, and carotenoids by treatment **(A)** and compound **(B)**. Abbreviations see **Table 3**.

respectively. The concentrations of isorhamnetin-3-*O*-glycoside-7-*O*-glycoside and kaempferol-3-*O*-sinapoyl-diglucoside-7-*O*-glucoside were higher in samples grown on coffee compost (7.63 ± 0.25 µg/g and 748.00 ± 41.73, respectively) and aronia compost (16.16 ± 0.33 µg/g and 664.7 ± 0.60 µg/g, respectively). To summarize, the addition of hop compost (5 and 10%) to the soil resulted in a decrease of malates and all kaempferol glycosides except for kaempferol-3-*O*-glucoside, whereas the use of aronia compost (5 and 10%) showed a decrease of malates but an increase of most kaempferol glycosides depending on the compost percentage added to the soil. However, the coffee composts (5 and 10%) were presented by decrease of caffeoylmalate to a minimum of 0.28 ± 0.13 µg/g, but only slight or no changes in the kampferol glycosides showing an increase of kaempferol-3-*O*-sinapoyl-diglucoside-7-*O*-glucoside to 787.18 ± 21.89 µg/g, kaempferol-3-*O*-glucoside to 7.83 ± 0.58 µg/g, and kaempferol-3-*O*-hydroxyferuloyl-diglucoside-7-*O*-glucoside to 188.85 ± 7.45 µg/g.

DISCUSSION

Effects of Composts on Metabolite Profiles

In this study profiling methods and targeted analyses have been used to explore the overall impact of biological waste of food chain production used as composts on the metabolite profile of pak choi sprouts. Metabolomic approaches for studying changes induced by biotic (Errard et al., 2015) and abiotic factors (Jorge et al., 2016) became an important analytical tool in plant science (Witzel et al., 2015). The metabolite profile differed when comparing sprouts grown composts and control plants grown solely on soil. The overall composition was reflected by metabolic differences in the primary and secondary metabolism.

Interestingly, changes in diverse hormone signaling pathways have been observed. It is well-known that abscisic acid (Taylor et al., 2000), salicylic acid (Janda et al., 2007), and jasmonic acid (Creelman and Mullet, 1995) act as signals in plants to response to biotic and abiotic challenges alone or in combination. These changes lead to alternation in primary and secondary metabolites of which the latter one will be discussed specifically in the following subchapters. Whereas, many amino acids were reduced in response to biotic stress (Errard et al., 2016), in the present study the application of composts increased their concentrations. This accounts also for some sugars. The changes in ascorbate might be also correlated with changes in the xanthophyll cycle, where one of the key enzymes, the violaxanthin de-epoxidase, requires ascorbate as co-substrate and the enzymatic activity is pH-depended (Arnoux et al., 2009). The glucosinolate levels also depend on ascorbate, because ascorbate influences the myrosinase activity—the enzyme responsible for the hydrolyzation of glucosinolates to the bioactive breakdown products (Hasapis and Macleod, 1982). But, in our experimental setup the myrosinase and glucosinolates kept separated from each other and further research is needed to evaluate the possible interaction between ascorbate and glucosinolate concentrations.

Responses to abiotic stress are dynamic and complex and to get a comprehensive understanding further systematic studies are required to understand the specific changes induced by the different composts.

Effect of Compost on Carotenoids, Glucosinolates, and Phenolic Compounds

We focused our recent study on the secondary metabolites because they are associated with health beneficial properties. Carotenoids are well-known antioxidants and they can lower the risk of chronic diseases, including cardiovascular diseases (Gammone et al., 2017) and type-2 diabetes mellitus (Akbaraly et al., 2008), and several types of cancer (Bolhassani, 2015). Lutein and zeaxanthin can prevent age-related eye diseases

TABLE 3 | Carotenoids, glucosinolates, and phenolic compounds in pak choi grown on soil and soil-organic compost mixtures.

	Control	Coffee		Hop		Aronia	
		5%	10%	5%	10%	5%	10%
CAROTENOIDS							
Car	27.4 ± 2.1a	53.1 ± 16.5ab	79.1 ± 23.5ab	**34.0 ± 1.7b**	**35.3 ± 1.8b**	**31.2 ± 2.4b**	60.2 ± 3.0ab
Lut	236.9 ± 46.6a	**753.9 ± 26.3b**	**703.9 ± 24.5cd**	**619.9 ± 31.0c**	**966.9 ± 48.3e**	**493.3 ± 32.5b**	**488.5 ± 24.4b**
Neo	51.6 ± 7.5a	**147.3 ± 4.8b**	**141.3 ± 17.7b**	**132.7 ± 6.6b**	**186.9 ± 9.3c**	59.5 ± 3.2a	55.3 ± 2.8a
Zea	22.4 ± 1.1a	**27.9 ± 1.5b**	21.8 ± 0.3a	**28.9 ± 1.4b**	**37.9 ± 1.9c**	**26.7 ± 0.5b**	20.1 ± 1.0a
GLUCOSINOLATES							
4MTB	0.34 ± 0.020e	**0.19 ± 0.001c**	**0.12 ± 0.049b**	**0.28 ± 0.011d**	**0.06 ± 0.004a**	**0.11 ± 0.010ab**	**0.19 ± 0.001c**
4MSOB	0.26 ± 0.019bc	0.32 ± 0.026c	0.27 ± 0.051bc	0.28 ± 0.060bc	**0.08 ± 0.008a**	0.19 ± 0.036b	0.20 ± 0.001b
5MSOP	0.55 ± 0.014c	0.56 ± 0.017c	0.52 ± 0.013c	**0.66 ± 0.077d**	**0.19 ± 0.003a**	**0.39 ± 0.031b**	**0.36 ± 0.004b**
3But	3.31 ± 0.096d	**2.71 ± 0.060c**	**2.53 ± 0.069c**	3.49 ± 0.162d	**0.76 ± 0.006a**	**1.71 ± 0.034b**	**1.51 ± 0.002b**
4Pent	2.95 ± 0.025f	**2.70 ± 0.069e**	**2.51 ± 0.082d**	2.86 ± 0.114ef	**0.53 ± 0.002a**	**1.27 ± 0.024c**	**0.96 ± 0.003b**
(*R*)-2OH3But	4.07 ± 0.186d	**3.59 ± 0.076c**	**3.50 ± 0.124c**	4.20 ± 0.203d	**0.81 ± 0.014a**	**1.19 ± 0.023b**	**0.6 ± 0.001a**
(*R*)-2OH4Pent	0.74 ± 0.030cd	0.71 ± 0.014cd	0.80 ± 0.078d	0.67 ± 0.022c	**0.13 ± 0.003a**	**0.25 ± 0.008b**	**0.11 ± 0.001a**
I3M	0.29 ± 0.073b	0.23 ± 0.006b	0.25 ± 0.038b	0.27 ± 0.018b	**0.07 ± 0.004a**	**0.11 ± 0.005a**	**0.06 ± 0.000a**
4OHI3M	0.31 ± 0.053bc	0.33 ± 0.031c	0.33 ± 0.120c	0.32 ± 0.059c	**0.09 ± 0.004a**	0.20 ± 0.044abc	0.16 ± 0.004ab
4MOI3M	0.14 ± 0.003d	**0.30 ± 0.014f**	**0.22 ± 0.030e**	**0.11 ± 0.009c**	**0.04 ± 0.001ab**	**0.06 ± 0.006b**	**0.02 ± 0.000a**
1MOI3M	0.16 ± 0.068b	0.22 ± 0.013b	**0.74 ± 0.040c**	0.16 ± 0.008b	**0.05 ± 0.002a**	**0.05 ± 0.002a**	**0.01 ± 0.000a**
2PE	0.43 ± 0.01f	**0.27 ± 0.01d**	**0.22 ± 0.03c**	**0.36 ± 0.01e**	**0.09 ± 0.00a**	**0.14 ± 0.01b**	**0.17 ± 0.00b**
Aliphatic GS	e	**d**	**d**	e	**a**	**c**	**b**
Indolic GS	b	b	**c**	b	**a**	**a**	**a**
Aromatic GS	f	**d**	**c**	**e**	**a**	**b**	**b**
PHENOLIC COMPOUNDS							
CM	28.39 ± 0.74e	**0.34 ± 0.07ab**	**0.28 ± 0.13a**	**16.36 ± 1.38d**	**13.85 ± 1.17c**	**2.58 ± 1.35b**	**0.06 ± 0.00a**
CQ	0.6 ± 0.06bc	0.57 ± 0.05b	**2.22 ± 0.11d**	0.59 ± 0.02b	**0.75 ± 0.03c**	**0.34 ± 0.01a**	**0.22 ± 0.01a**
SM	1105.67 ± 56.80cd	1117.34 ± 60.01d	984.15 ± 32.83c	**790.69 ± 33.62b**	**778.64 ± 19.96b**	**721.54 ± 6.64b**	**574.02 ± 3.99a**
I3G	1.22 ± 0.67b	**0.46 ± 0.01a**	**0.45 ± 0.06a**	2.07 ± 0.26b	1.39 ± 0.20b	**0.63 ± 0.01a**	1.52 ± 0.00b
I3G7G	0.82 ± 0.02a	**5.23 ± 0.49b**	**7.63 ± 0.25c**	0.87 ± 0.22a	0.73 ± 0.03a	**28.53 ± 1.91e**	**16.16 ± 0.33d**
K3G	2.10 ± 0.35a	4.97 ± 0.16a	**7.69 ± 0.05d**	3.59 ± 0.17a	**5.95 ± 0.11ab**	**8.32 ± 0.44d**	**6.07 ± 0.07c**
K3CdG7G	18.23 ± 1.48d	**8.41 ± 0.28a**	**7.83 ± 0.58a**	**15.05 ± 0.63c**	**9.38 ± 0.44ab**	**11.87 ± 2.54bc**	**9.69 ± 0.23ab**
K3dG7G	95.69 ± 4.28cd	91.52 ± 6.13c	102.59 ± 3.66d	**58.20 ± 1.99b**	**42.78 ± 1.48a**	**115.54 ± 2.21e**	84.45 ± 0.50c
K3FdG7G	130.28 ± 9.17b	161.17 ± 11.40bc	165.25 ± 7.12c	**105.08 ± 10.70a**	**80.81 ± 7.74a**	**191.13 ± 9.03d**	**164.87 ± 0.51c**
K3SdG7G	593.74 ± 31.83c	**748.00 ± 41.73ef**	**787.18 ± 21.89f**	**468.28 ± 19.73b**	**392.74 ± 2.85a**	**664.71 ± 0.60de**	619.07 ± 4.43cd
K3hFdG7G	151.28 ± 6.40c	168.23 ± 9.72c	**188.85 ± 7.42d**	**129.52 ± 6.17ab**	**131.01 ± 4.09b**	**183.58 ± 2.93d**	**108.85 ± 0.71a**
K3pCdG7G	113.03 ± 10.47b	**101.00 ± 6.92a**	**101.70 ± 5.08a**	**97.64 ± 9.48a**	**90.59 ± 3.74a**	160.92 ± 0.62b	**134.27 ± 2.29c**

Means [μg/g DW] were compared by one-way-ANOVA followed by post-hoc Tukey's HSD test ($p \leq 0.05$). Letters indicate significant differences within a group (in alphabetical order from the lowest to highest) and bold numbers show significant difference compared to the control group (post-hoc Dunnet's test, $p \leq 0.05$). Each value represents the mean of three samples ± S_E.

Carotene: Car, β-Carotene; Xanthophylls: Lut, Lutein; Neo, neoxanthin; Zea, Zeaxanthin; aliphatic Glucosinolates: (GS): 4MTB, 4-Methylthio-butyl GS; 4MSOB, 4-Methyltsulfinly-butyl GS; 5MSOP, 5-Methylsufinyl-pentyl GS; 3But, 3-Butenyl GS; 4Pent, 4-Pentenyl GS, (R)-2OH3But, (R)-2-Hydroxy-3-butenyl GS; (S)-2OH3But, (S)-2-Hydroxy-3-butenyl GS; 2OH4Pent, 2-Hydroxy-4-pentenyl GS; indolic GS: I3M, Indol-3-ylmethyl GS; 4OHI3M, 4-Hydroxyindol-3-ylmethyl GS; 4MOI3M, 4-Methoxyindol-3-ylmethyl GS; 1MOI3M, 1-Methoxyindol-3-ylmethyl GS; aromatic GS: 2PE, 2-Phenylethyl GS; Hydroxybenzoeic acids: CM, Caffeoylmalate; CQ, Caffeoylquinicacid; SM, Sinapoylmalate; Flavonoids: I3G, Isorhamnetin-3-O-glucoside; I3G7G, Isorhamnetin-3-O-glycoside-7-O-glycoside; K3G, Kaempferol-3-O-glucoside; K3CdG7G, Kaempferol-3-O-caffeoyl-diglucoside-7-O-glucoside; K3dG7G, Kaempferol-3-O-diglucoside-7-O-glucoside; K3FdG7G, Kaempferol-3-O-feruloyl-diglucoside-7-O-glucoside; K3SdG7G, Kaempferol-3-O-sinapoyl-diglucoside-7-O-glucoside; K3hFdG7G, Kaempferol-3-O-hydroxyferuloyl-diglucoside-7-O-glucoside; K3pCdG7G, Kaempferol-3-O-p-coumaroyl-diglucoside-7-O-glucoside.

such as macular degeneration (Mares, 2016; Frede et al., 2017). Crops have been bred or engineered to increase β-carotene as precursor of vitamin A (Bai et al., 2011). Glucosinolates, as characteristically secondary metabolites in *Brassica* vegetables, are of interest due to the wide range of health-promoting properties of their breakdown products, e.g., for anti-carcinogenic (Traka and Mithen, 2009; Wu et al., 2012), anti-diabetic (Waterman et al., 2015; Guzman-Perez et al., 2016), and anti-inflammatory effects (Bentley-Hewitt et al., 2014; Herz et al., 2016). For human health phenolic compounds are of special interest due to their antioxidant activity (Zietz et al., 2010), as well as anti-inflammatory and anti-cancerogenic effects (Pan et al., 2010; Chen and Chen, 2013).

Structure-specific responses of carotenoids, glucosinolates, and flavonoid glycosides, in *Brassica* species are also found in response to other eco-physiological conditions such as light or temperature (Schonhof et al., 2007; Neugart et al., 2012; Mageney et al., 2016). However, the sprouts were grown under the same environmental conditions and therefore interacting climatic effects are not expected.

Effect of Compost on Carotenoids

The structure-specific response of phenolic compounds as well as the variation in carotenoids and glucosinolates might be partly due to the various nitrogen contents of these composts. We measured the total nitrogen in the organic composts. The highest total nitrogen content was found in the hop compost and slightly higher values in the coffee and aronia compost soil mixtures. Plants response differently to changes of nitrogen concentration and form in soil. For instance, reduction in nitrogen fertilization yield in a reduction of carotenoids in lettuce (Becker et al., 2015), but carotenoid pigments increased in response to increasing nitrogen concentrations in kale (Kopsell et al., 2007) as they did in this study. In other studies, the carotenoid concentrations were not affected such as in leafy *Brassica* species (e.g., Fallovo et al., 2011). Under organic farming practices, higher concentrations of carotenoids were detected in cauliflower (Lo Scalzo et al., 2013). The content of carotenoids in carrot roots and human diets was not significantly affected by the agricultural production system (organic vs. conventional) or year, despite differences in fertilization strategy and levels (Soltoft et al., 2011), whereas β-carotene was found to be higher in organically grown *Brassica* species (Kapusta-Duch et al., 2014). This is in accordance to this study, where higher carotenoid concentrations were detected in sprouts grown on compost.

Carotenoids also react in response to stresses. In our study, neoxanthin increased in sprouts grown on soil containing composts from coffee and hop. Neoxanthin positively influences ABA accumulation in response to dehydration (North et al., 2007). However, ABA is only one plant hormone influenced by growing conditions and the metabolic profiling revealed that changes not only occurred in the abscisic acid signaling, but also in the salicylic acid, and jasmonate pathways (**Table 2**). Salicylic acid concentrations have been positively associated with carotenoid concentrations in maize and Indian mustard (Khodary, 2004; Thakur and Sohal, 2014), whereas methyl jasmonate either reduced the degradation of carotenoids in post-harvest lettuce (Kim et al., 2006) or increased β-carotene as well as mannitol in broccoli sprouts (Natella et al., 2016). The exogenous application of ABA, JA, and SA was positively correlated with photosynthetic pigment concentrations in turnip (Thiruvengadam et al., 2016). Therefore, the changes in plant hormones are one possible approach to explain the higher carotenoid concentrations in the present study. An additional factor might be the regulation of the violaxanthin de-epoxidase by ascorbate contributing to the accumulation of xanthophylls (Arnoux et al., 2009).

Effect of Compost on Glucosinolates

Glucosinolates are nitrogen containing compounds suggesting that nitrogen supply strongly affect glucosinolate concentration. The effect of nitrogen fertilization on changes in glucosinolates in kale has been reported recently. Increasing nitrogen concentrations in the soil results in reduction of aliphatic glucosinolates and an activation of the glucosinolate catabolic process was observed under ammonium nutrition (Groenbaek et al., 2014; Marino et al., 2016). However, increasing glucosinolate contents were found in broccoli and red cabbage grown on organic soil (Meyer and Adam, 2008). But, the effect of organic soil seems to be genotype-dependent. Picchi et al. (2012) found that the total glucosinolate content as well content of the major glucosinolates decreased in cauliflower grown on organic fields compared to cauliflower grown under conventional conditions. But, these effects were shown just for one cultivar; the glucosinolates in the cultivar Magnifico showed the opposite effect and were increased.

The factor analysis revealed that the aronia compost in both concentrations and hop compost (10%) had the strongest effect on the glucosinolates (**Figure 2**). In sprouts grown on these compost mixtures all individual glucosinolates decreased. This compost induced glucosinolate reduction could be due to a unbalanced ratio of nitrogen and sulfur in the soil: an optimal or high nitrogen supply combined with an insufficient sulfur supply leads to a decrease of aliphatic and increase of indole glucosinolates (Li et al., 2007). But, the optimal ratio of N/S is not only species-specific, but structure-specific, too. High N/S ratio promote the formation of aliphatic and indolic glucosinolates in broccoli florets (Schonhof et al., 2007), but in turnips a lower ratio of N/S lead to an increase of aromatic glucosinolates (Li et al., 2007). However, in our experiments the N/S ratio does not explain the decreases or increases of the individual glucosinolates. Furthermore, the ratio of alkenyl to hydroxyalkenyl glucosinolates is changed from about 1.3 to 2.1 (5%) and 3.5 (10%) in sprouts grown on aronia compost. It might be that aronia residues in the soil influence the conversion of alkenyl to hydroxyalkenyl glucosinolates due to the induction of the 2-oxo acid dependent dioxygenase (*BrGSL-OH*) as higher concentrations of 2-oxo acids have been detected in sprouts grown on aronia compost in this study. In contrast, in the coffee compost samples the aliphatic glucosinolates concentrations are slightly decreased or unchanged. Only the methoxylated indole glucosinolates (4-methoxyindole-3-ylmethyl and 1-methoxyindole-3-ylmethyl glucosinolate) increased significantly in pak choi sprouts grown on coffee compost mixtures, which might be due to the ammonium nutrition (Marino et al., 2016). The authors determined different expression levels depending on the nitrogen source: higher expression levels of *CYP79B2/B3* in the indole glucosinolate pathway under nitrate nutrition, and a higher expression of genes involved in the aliphatic glucosinolate pathway under ammonium nutrition. The paradox is that under ammonium nutrition the transcript levels for the genes of the indolic glucosinolate biosynthesis pathway were reduced, but at metabolite level the indolic glucosinolates were increased in *Arabidopsis* and broccoli (Marino et al., 2016). Furthermore, the gene expression of *CYP81F1/F2/F3/F4*, involved in the methoxylation of the indole-3-ylmethyl glucosinolate to the methoxylated indole glucosinolates, might be induced by

ammonium. Further investigations are needed to shed light on links between nitrogen and glucosinolate metabolism.

Previous experiments showed a regulation of the glucosinolate metabolism by the salicylic acid or jasmonate pathways. In pak choi sprouts an induction of glucosinolates was observed by methyl jasmonate treatment, but no changes were observed after treatment with methyl salicylate (Wiesner et al., 2013a). Other researchers observed an increase of aliphatic and indole glucosinolates after salicylic acid treatment (Kiddle et al., 1994). The interaction of signaling molecules is more complex and regulated by different positive and negative back loops. Also it could be demonstrated in that a drought-induced accumulation of aliphatic glucosinolates is related to ABA formation *B. juncea* (Tong et al., 2014).

Effect of Compost on Phenolic Compounds

The structure-specific response of phenolic compounds might be partly due to the various nitrogen contents of these composts. A negative correlation between specific flavonoid aglycones (kaempferol and quercetin) and nitrogen fertilization in *Brassica juncea* and between flavonoid glycosides and nitrogen fertilization in lettuce has been proven previously (Fallovo et al., 2011; Becker et al., 2015). Also in kale a species-specific response on changes in nitrogen content has been reported for phenolic compounds (Groenbaek et al., 2014). In the kale cv. Reflex the total flavonoid glucosides were significantly reduced, which was in this species genotype mainly related to the changes in quercetin glucosides while kaempferol and isorhamnetin glycosides were less susceptible to higher nitrogen fertilization. However, the main compounds in pak choi and kale are monoacylated kaempferol and quercetin tri- and tetraglycosides which were reduced in kale with higher dose of nitrogen fertilization (Groenbaek et al., 2014). For the pak choi sprouts in this study the monoacylated kaempferol glycosides were reduced with soil-hop compost mixtures assuming a negative correlation of nitrogen and flavonoid glycosides. However, the results were partly different for the three soil compost mixtures tested which leads to the conclusion that nitrogen is not the only influencing factor and the effect of soil coffee and soil aronia compost cannot be explained like this. Organically grown plants are considered to protect themselves better and form phytoalexins like flavonoids (Asami et al., 2003). Asami et al. (2003) found in organically grown plants (marionberry, strawberry and maize) higher total phenolic contents than in conventionally produced plants. In tomatoes quercetin, kaempferol, and narigenin were higher in organically grown plants compared to conventional grown plants in a 10 year trial (Mitchell et al., 2007). Biologically food waste can be considered as organically fertilization and the flavonoid glycosides in pak choi are mainly decreased. There is the need to study other underlying mechanisms that triggers the production of flavonoids. Apart from nitrogen supply, hormones, and other signaling compounds released as roots exudates could contribute to the modulated secondary plant metabolite profiles (Broeckling et al., 2008). Interestingly, we found specific reactions for sprouts grown on soil-aronia composts mixtures, e.g., kaempferol-3-*O*-feruloyl-diglucoside-7-*O*-glucoside increased significantly. It might be speculated that this is the result of higher concentrations in the root environment and lower active release rates by the roots. Further investigations should also include the analysis of modulated soil microorganism communities.

Moreover, jasmonate, salicylate, and abscisic acid are generally known to enhance flavonoids and hydroxycinnamic acids (Chen et al., 2006; Sandhu et al., 2011), but this cannot directly be linked to the present results.

CONCLUSION

Interestingly, addition of biological waste of the food production chain as compost had strong effects on plant metabolites profiles in sprouts of pak choi. Different composts of the food production chain impact differently the plant metabolite profile of pak choi sprouts. The usage of coffee, aronia or hop composts incorporated in soil increased the concentration of carotenoids and decreased the amount of glucosinolates and phenolic compounds being associated with health beneficial properties of vegetables. The usage of compost might be besides the application of chemical and physical elicitors another possibility to target the accumulation of specific metabolites e.g., for the production of carotenoids to prevent vitamin A deficiency or age-related macular degenerative diseases. However, taking into account the intrinsic quality and health effects of vegetables that is in large measure driven by the secondary plant metabolites unintentional changes such as observed for glucosinolates and phenolic compounds need further investigations. Further studies are necessary and would shed light on the metabolome dynamics and underlying mechanism responsible for the changes induced by composts.

AUTHOR CONTRIBUTIONS

SB designed the study in cooperation with MW-R, HR, and KF. MW-R, SN, and SB carried out the plant experiments, contributed to interpretation of data and drafted the manuscript. SB developed the mass spectrometric method for the non-targeted analyses and performed statistics. EJ contributed to the non-targeted analysis. KF analyzed the carotenoids and chlorophylls, SN analyzed the phenolic compounds and MW-R and MS the glucosinolates. TH, HR, and MS critically revised the manuscript. All authors read and approved the final manuscript.

ACKNOWLEDGMENTS

We thank E. Büsch, A. Jankowsky, A. Platalla, and M. Skoruppa, K. Schmidt for their assistance.

REFERENCES

Akbaraly, T. N., Fontbonne, A., Favier, A., and Berr, C. (2008). Plasma carotenoids and onset of dysglycemia in an elderly population. *Diabetes Care* 31, 1355–1359. doi: 10.2337/dc07-2113

Arnoux, P., Morosinotto, T., Saga, G., Bassi, R., and Pignol, D. (2009). A structural basis for the pH-dependent xanthophyll cycle in *Arabidopsis thaliana*. *Plant Cell* 21, 2036–2044. doi: 10.1105/tpc.109.068007

Asami, D. K., Hong, Y. J., Barrett, D. M., and Mitchell, A. E. (2003). Comparison of the total phenolic and ascorbic acid content of freeze-dried and air-dried marionberry, strawberry, and corn grown using conventional, organic, and sustainable agricultural practices. *J. Agric. Food Chem.* 51, 1237–1241. doi: 10.1021/jf020635c

Bai, C., Twyman, R. M., Farré, G., Sanahuja, G., Christou, P., Capell, T., et al. (2011). A golden era—pro-vitamin A enhancement in diverse crops. *In Vitro Cell. Dev. Biol. Plant* 47, 205–221. doi: 10.1007/s11627-011-9363-6

Baranowski, K., Baca, E., Salamon, A., Michalowska, D., Meller, D., and Karas, M. (2009). Possibilities of retrieving and making a practical use of phenolic compounds from the waste products: Blackcurrant and chokeberry pomace and spent hops. *Zywn-Nauk. Technol. Ja.* 16, 100–109. Available online at: http://pttz.org/zyw/wyd/czas/2009,%204(65)/13_Baranowski.pdf

Becker, C., Urlić, B., Jukić Špika, M., Kläring, H. P., Krumbein, A., Baldermann, S., et al. (2015). Nitrogen limited red and green leaf lettuce accumulate flavonoid glycosides, caffeic acid derivatives, and sucrose while losing chlorophylls, beta-carotene and xanthophylls. *PLoS ONE* 10:e0142867. doi: 10.1371/journal.pone.0142867

Bentley-Hewitt, K. L., De Guzman, C. E., Ansell, J., Mandimika, T., Narbad, A., and Lund, E. K. (2014). Polyunsaturated fatty acids modify expression of TGF-β in a co-culture model ultilising human colorectal cells and human peripheral blood mononuclear cells exposed to *Lactobacillus gasseri*, *Escherichia coli* and *Staphylococcus aureus*. *Eur. J. Lipid Sci. Tech.* 116, 505–513. doi: 10.1002/ejlt.201300337

Bolhassani, A. (2015). Cancer chemoprevention by natural carotenoids as an efficient strategy. *Anti Cancer Agents Med. Chem.* 15, 1026–1031. doi: 10.2174/1871520615666150302125707

Brazdauskas, T., Montero, L., Venskutonis, P. R., Ibañez, E., and Herrero, M. (2016). Downstream valorization and comprehensive two-dimensional liquid chromatography-based chemical characterization of bioactives from black chokeberries (*Aronia melanocarpa*) pomace. *J. Chromatogr. A* 1468, 126–135. doi: 10.1016/j.chroma.2016.09.033

Broeckling, C. D., Broz, A. K., Bergelson, J., Manter, D. K., and Vivanco, J. M. (2008). Root exudates regulate soil fungal community composition and diversity. *Appl. Environ. Microbiol.* 74, 738–744. doi: 10.1128/AEM.02188-07

Chen, A. Y., and Chen, Y. C. (2013). A review of the dietary flavonoid, kaempferol on human health and cancer chemoprevention. *Food Chem.* 138, 2099–2107. doi: 10.1016/j.foodchem.2012.11.139

Chen, J. Y., Wen, P. F., Kong, W. F., Pan, Q. H., Zhan, J. C., Li, J. M., et al. (2006). Effect of salicylic acid on phenylpropanoids and phenylalanine ammonia-lyase in harvested grape berries. *Postharvest Biol. Technol.* 40, 64–72. doi: 10.1016/j.postharvbio.2005.12.017

Creelman, R. A., and Mullet, J. E. (1995). Jasmonic acid distribution and action in plants: regulation during development and response to biotic and abiotic stress. *Proc. Natl. Acad. Sci. U.S.A.* 92, 4114–4119. doi: 10.1073/pnas.92.10.4114

D'Alessandro, L. G., Dimitrov, K., Vauchel, P., and Nikov, I. (2014). Kinetics of ultrasound assisted extraction of anthocyanins from Aronia melanocarpa (black chokeberry) wastes. *Chem. Eng. Res. Des.* 92, 1818–1826. doi: 10.1016/j.cherd.2013.11.020

De Neve, S. (2017). "Organic matter mineralization as a source of nitrogen," in *Advances in Research on Fertilization Management of Vegetable Crops*, eds F. Tei, S. Nicola, and P. Benincasa (Springer), 65–83. Available online at: http://www.bookmetrix.com/detail/book/e91205d3-d808-4895-ad4a-ded2ab6610b6#downloads

Diniz, E. R., Santos, R. H. S., Urquiaga, S. S., Peternelli, L. A., Barrella, T. P., and Freitas, G. B. D. (2007). Green manure incorporation timing for organically grown broccoli. *Pesqui. Agropecu. Bras.* 42, 199–206. doi: 10.1590/S0100-204X2007000200008

Errard, A., Ulrichs, C., Kühne, S., Mewis, I., Drungowski, M., Schreiner, M., et al. (2015). Single- versus multiple-pest infestation affects differently the biochemistry of tomato (*Solanum lycopersicum* 'Ailsa Craig'). *J. Agric. Food Chem.* 63, 10103–10111. doi: 10.1021/acs.jafc.5b03884

Errard, A., Ulrichs, C., Kühne, S., Mewis, I., Mishig, N., Maul, R., et al. (2016). Metabolite profiling reveals a specific response in tomato to predaceous *Chrysoperla carnea* harvae and herbivore(s)-predator interactions with the generalist pests *Tetranychus urticae* and *Myzus persicae*. *Front. Plant Sci.* 7:1256. doi: 10.3389/fpls.2016.01256

Fallovo, C., Schreiner, M., Schwarz, D., Colla, G., and Krumbein, A. (2011). Phytochemical changes induced by different nitrogen supply forms and radiation levels in two leafy Brassica species. *J. Agric. Food Chem.* 59, 4198–4207. doi: 10.1021/jf1048904

Frede, K., Ebert, F., Kipp, A. P., Schwerdtle, T., and Baldermann, S. (2017). Lutein activates the transcription factor Nrf2 in human retinal pigment epithelial cells. *J. Agric. Food Chem.* 65, 5944–5952. doi: 10.1021/acs.jafc.7b01929

Gammone, M. A., Pluchinotta, F. R., Bergante, S., Tettamanti, G., and D'orazio, N. (2017). Prevention of cardiovascular diseases with carotenoids. *Front. Biosci.* 9, 165–171. doi: 10.2741/s480

Grassi, F., Mastrorilli, M., Mininni, C., Parente, A., Santino, A., Scarcella, M., et al. (2015). Posidonia residues can be used as organic mulch and soil amendment for lettuce and tomato production. *Agron. Sustain. Dev.* 35, 679–689. doi: 10.1007/s13593-014-0268-8

Groenbaek, M., Jensen, S., Neugart, S., Schreiner, M., Kidmose, U., and Kristensen, H. L. (2014). Influence of cultivar and fertilizer approach on curly kale (*Brassica oleracea* L. var. *sabellica*). 1. Genetic diversity reflected in agronomic characteristics and phytochemical concentration. *J. Agric. Food Chem.* 62, 11393–11402. doi: 10.1021/jf503096p

Guzmán-Pérez, V., Bumke-Vogt, C., Schreiner, M., Mewis, I., Borchert, A., and Pfeiffer, A. F. (2016). Benzylglucosinolate derived isothiocyanate from tropaeolum majus reduces gluconeogenic gene and protein expression in human cells. *PLoS ONE* 11:e0162397. doi: 10.1371/journal.pone.0162397

Harbaum, B., Hubbermann, E. M., Wolff, C., Herges, R., Zhu, Z., and Schwarz, K. (2007). Identification of flavonoids and hydroxycinnamic acids in pak choi varieties (*Brassica campestris* L. ssp. *chinensis* var. communis) by HPLC–ESI-MSn and NMR and their quantification by HPLC–DAD. *J. Agric. Food. Chem.* 55, 8251–8260. doi: 10.1021/jf071314+

Hartley, L., Igbinedion, E., Holmes, J., Flowers, N., Thorogood, M., Clarke, A., et al. (2013). Increased consumption of fruit and vegetables for the primary prevention of cardiovascular diseases. *Cochrane Database Syst. Rev.* 4:CD009874. doi: 10.1002/14651858.CD009874.pub2

Hasapis, X., and Macleod, A. J. (1982). Effects of pH and ascorbate on benzylglucosinolate degradation in seed extracts of *Lepidium sativum*. *Phytochem* 21, 291–296. doi: 10.1016/S0031-9422(00)95253-1

Herz, C., Marton, M.-R., Tran, H. T. T., Gründemann, C., Schell, J., and Lamy, E. (2016). Benzyl isothiocyanate but not benzyl nitrile from Brassicales plants dually blocks the COX and LOX pathway in primary human immune cells. *J. Funct. Food* 23, 135–143. doi: 10.1016/j.jff.2016.02.034

Hoffmann, G. (1991). *VDLUFA—Methodenbuch - Die Untersuchung von Böden*, ISBN 978-3-9411273-13-9. Darmstadt: VDLUFA-Verlag.

Janda, T., Horváth, E., Szalai, G., and Paldi, E. (2007). "Role of salicylic acid in the induction of abiotic stress tolerance," in *Salicylic acid: A plant hormone*, eds S. Hayat and A. Ahmad (Springer), 91–150. Available online at: http://www.springer.com/de/book/9781402051838#otherversion=9789048173013

Jorge, T. F., Rodrigues, J. A., Caldana, C., Schmidt, R., Van Dongen, J. T., Thomas-Oates, J., et al. (2016). Mass spectrometry-based plant metabolomics: metabolite responses to abiotic stress. *Mass Spectrom. Rev.* 35, 620–649. doi: 10.1002/mas.21449

Kapusta-Duch, J., Borczak, B., Kopeć, A., Filipiak-Florkiewicz, A., and Leszczynska, T. (2014). The influence of packaging type and time of frozen storage on antioxidative properties of Brussels sprouts. *J. Food Process. Preserv.* 38, 1089–1096. doi: 10.1111/jfpp.12067

Khodary, S. E. A. (2004). Effect of salicylic acid on the growth, photosynthesis and carbohydrate metabolism in salt stressed maize plants. *Int. J. Agric. Biol.* 6, 5–8.

Kiddle, G. A., Doughty, K. J., and Wallsgrove, R. M. (1994). Salicylic acid-induced accumulation of glucosinolates in oilseed rape (*Brassica napus* l) leaves. *J. Exp. Bot.* 45, 1343–1346. doi: 10.1093/jxb/45.9.1343

Kim, H. J., Chen, F., Wang, X., and Rajapakse, N. C. (2006). Effect of methyl jasmonate on secondary metabolites of sweet basil (*Ocimum basilicum* L.). *J. Agric. Food Chem.* 54, 2327–2332. doi: 10.1021/jf051979g

Kopsell, D. A., Kopsell, D. E., and Curran-Celentano, J. (2007). Carotenoid pigments in kale are influenced by nitrogen concentration and form. *J. Sci. Food Agric.* 87, 900–907. doi: 10.1002/jsfa.2807

Kushad, M. M., Brown, A. F., Kurilich, A. C., Juvik, J. A., Klein, B. P., Wallig, M. A., et al. (1999). Variation of glucosinolates in vegetable crops of *Brassica oleracea*. *J. Agric. Food Chem.* 47, 1541–1548. doi: 10.1021/jf980985s

Larsson, S. C., Virtamo, J., and Wolk, A. (2013). Total and specific fruit and vegetable consumption and risk of stroke: a prospective study. *Atherosclerosis* 227, 147–152. doi: 10.1016/j.atherosclerosis.2012.12.022

Li, S., Schonhof, I., Krumbein, A., Li, L., Stützel, H., and Schreiner, M. (2007). Glucosinolate concentration in turnip (*Brassica rapa* ssp. *Rapifera* L.*)* roots as affected by nitrogen and sulfur supply. *J. Agric. Food. Chem.* 55, 8452–8457. doi: 10.1021/jf070816k

Lo Scalzo, R., Picchi, V., Migliori, C. A., Campanelli, G., Leteo, F., Ferrari, V., et al. (2013). Variations in the phytochemical contents and antioxidant capacity of organically and conventionally grown Italian cauliflower (*Brassica oleracea* L. subsp. *botrytis*): Results from a three-year field study. *J. Agric. Food Chem.* 61, 10335–10344. doi: 10.1021/jf4026844

Mageney, V., Baldermann, S., and Albach, D. C. (2016). Intraspecific variation in carotenoids of *Brassica oleracea* var. sabellica. *J. Agric. Food Chem.* 64, 3251–3257. doi: 10.1021/acs.jafc.6b00268

Mahro, B., Gaida, B., Schuettmann, I., and Zorn, H. (2015). Survey of the amount and use of biogenic residues of the German food and biotech industry. *Chem-Ing-Tech*. 87, 537–542. doi: 10.1002/cite.201400023

Mares, J. (2016). Lutein and zeaxanthin isomers in eye health and disease. *Annu. Rev. Nutr*. 36, 571–602. doi: 10.1146/annurev-nutr-071715-051110

Marino, D., Ariz, I., Lasa, B., Santamaría, E., Fernández-Irigoyen, J., González-Murua, C., et al. (2016). Quantitative proteomics reveals the importance of nitrogen source to control glucosinolate metabolism in *Arabidopsis thaliana* and *Brassica oleracea*. *J. Exp. Bot.* 67, 3313–3323. doi: 10.1093/jxb/erw147

Meyer, M., and Adam, S. T. (2008). Comparison of glucosinolate levels in commercial broccoli and red cabbage from conventional and ecological farming. *Eur. Food Res. Technol.* 226, 1429–1437. doi: 10.1007/s00217-007-0674-0

Mitchell, A. E., Hong, Y. J., Koh, E., Barrett, D. M., Bryant, D. E., Denison, R. F., et al. (2007). Ten-year comparison of the influence of organic and conventional crop management practices on the content of flavonoids in tomatoes. *J. Agric. Food Chem.* 55, 6154–6159. doi: 10.1021/jf070344+

Murthy, P. S., and Naidu, M. M. (2012). Sustainable management of coffee industry by-products and value addition-a review. *Resour. Conserv. Recycl.* 66, 45–58. doi: 10.1016/j.resconrec.2012.06.005

Natella, F., Maldini, M., Nardini, M., Azzini, E., Foddai, M. S., Giusti, A. M., et al. (2016). Improvement of the nutraceutical quality of broccoli sprouts by elicitation. *Food Chem.* 201, 101–109. doi: 10.1016/j.foodchem.2016.01.063

Neugart, S., Kläring, H.-P., Zietz, M., Schreiner, M., Rohn, S., Kroh, L. W., et al. (2012). The effect of temperature and radiation on flavonol aglycones and flavonol glycosides of kale (*Brassica oleracea* var. *sabellica). Food Chem.* 133, 1456–1465. doi: 10.1016/j.foodchem.2012.02.034

North, H. M., De Almeida, A., Boutin, J. P., Frey, A., To, A., Botran, L., et al. (2007). The Arabidopsis ABA-deficient mutant aba4 demonstrates that the major route for stress-induced ABA accumulation is *via* neoxanthin isomers. *Plant J.* 50, 810–824. doi: 10.1111/j.1365-313X.2007.03094.x

Pan, F., Li, Y., Chapman, S. J., Khan, S., and Yao, H. (2016). Microbial utilization of rice straw and its derived biochar in a paddy soil. *Sci. Total Environ.* 559, 15–23. doi: 10.1016/j.scitotenv.2016.03.122

Pan, M. H., Lai, C. S., and Ho, C. T. (2010). Anti-inflammatory activity of natural dietary flavonoids. *Food Funct.* 1, 15–31. doi: 10.1039/c0fo00103a

Picchi, V., Migliori, C., Scalzo, R. L., Campanelli, G., Ferrari, V., and Di Cesare, L. F. (2012). Phytochemical content in organic and conventionally grown Italian cauliflower. *Food Chem.* 130, 501–509. doi: 10.1016/j.foodchem.2011.07.036

Reif, C., Arrigoni, E., Berger, F., Baumgartner, D., and Nyström, L. (2013). Lutein and β-carotene content of green leafy Brassica species grown under different conditions. *LWT-Food Sci. Technol.* 53, 378–381. doi: 10.1016/j.lwt.2013.02.026

Rochfort, S. J., Imsic, M., Jones, R., Trenerry, V. C., and Tomkins, B. (2006). Characterization of flavonol conjugates in immature leaves of pak choi *[Brassica rapa* L. ssp. *chinensis* L. (Hanelt.)] by HPLC-DAD and LC-MS/MS. *J. Agric. Food. Chem.* 54, 4855–4860. doi: 10.1021/jf060154j

Sandhu, A. K., Gray, D. J., Lu, J., and Gu, L. (2011). Effects of exogenous abscisic acid on antioxidant capacities, anthocyanins, and flavonol contents of muscadine grape (*Vitis rotundifolia*) skins. *Food Chem.* 126, 982–988. doi: 10.1016/j.foodchem.2010.11.105

Schmidt, S., Zietz, M., Schreiner, M., Rohn, S., Kroh, L. W., and Krumbein, A. (2010). Identification of complex, naturally occurring flavonoid glycosides in kale (*Brassica oleracea* var. sabellica) by high-performance liquid chromatography diode-array detection/electrospray ionization multi-stage mass spectrometry. *Rapid Commun. Mass Spectrom.* 24, 2009–2022. doi: 10.1002/rcm.4605

Schonhof, I., Kläring, H.-P., Krumbein, A., Claußen, W., and Schreiner, M. (2007). Effect of temperature increase under low radiation conditions on phytochemicals and ascorbic acid in greenhouse grown broccoli. *Agric. Ecosyst. Environ.* 119, 103–111. doi: 10.1016/j.agee.2006.06.018

Seck-Mbengue, M. F., Müller, A., Ngwene, B., Neumann, E., and George, E. (2017). Transport of nitrogen and zinc to rhodes grass by arbuscular mycorrhiza and roots as affected by different nitrogen sources (NH_4^+-N and NO_3^--N). *Symbiosis* 73, 191–200. doi: 10.1007/s13199-017-0480-9

Shemekite, F., Gómez-Brandón, M., Franke-Whittle, I. H., Praehauser, B., Insam, H., and Assefa, F. (2014). Coffee husk composting: an investigation of the process using molecular and non-molecular tools. *Waste Manage.* 34, 642–652. doi: 10.1016/j.wasman.2013.11.010

Søltoft, M., Bysted, A., Madsen, K. H., Mark, A. B., Bügel, S. G., Nielsen, J., et al. (2011). Effects of organic and conventional growth systems on the content of carotenoids in carrot roots, and on intake and plasma status of carotenoids in humans. *J. Sci. Food Agric.* 91, 767–775. doi: 10.1002/jsfa.4248

Sones, K., Heaney, R. K., and Fenwick, G. R. (1984). The glucosinolate content of UK vegetables—cabbage (*Brassicae oleracea*), swede (*B. napus)* and turnip *(B. campestris). Food Addit. Contam.* 1, 289–296. doi: 10.1080/02652038409385856

Takahashi, K., and Osada, K. (2017). Effect of dietary purified xanthohumol from hop (H*umulus lupulus* L.) pomace on adipose tissue mass, fasting blood glucose level, and lipid metabolism in KK-Ay mice. *J. Oleo Sci.* 66, 531–541. doi: 10.5650/jos.ess16234

Taylor, I. B., Burbidge, A., and Thompson, A. J. (2000). Control of abscisic acid synthesis. *J. Exp.l Bot.* 51, 1563–1574. doi: 10.1093/jexbot/51.350.1563

Thakur, M., and Sohal, B. (2014). Biochemical defense induction in Indian mustard (*Brassica juncea* L.) and rapeseed (*B. napus* L.) by salicylic acid and benzothiadiazole. *Appl. Biol. Res.* 16, 199–208. doi: 10.5958/0974-4517.2014.00011.1

Thiruvengadam, M., Baskar, V., Kim, S.-H., and Chung, I.-M. (2016). Effects of abscisic acid, jasmonic acid and salicylic acid on the content of phytochemicals and their gene expression profiles and biological activity in turnip (*Brassica rapa* ssp. rapa). *Plant Growth Reg.* 80, 377–390. doi: 10.1007/s10725-016-0178-7

Thönnissen Michel, C. (1996). *Nitrogen Fertilizer Substitution for Tomato by Legume Green Manures in Tropical Vegetable Production Systems*. Zürich: ETH Zurich.

Tong, Y., Gabriel-Neumann, E., Ngwene, B. Krumbein, A., George, E., Platz, S., et al. (2014). Topsoil drying combined with increased sulfur supply leads to enhanced aliphatic glucosinolates in *Brassica juncea* leaves and roots. *Food Chem.* 152, 190–196. doi: 10.1016/j.foodchem.2013.11.099

Traka, M., and Mithen, R. (2009). Glucosinolates, isothiocyanates and human health. *Phytochem. Rev.* 8, 269–282. doi: 10.1007/s11101-008-9103-7

Verlinden, S., Mcdonald, L., Kotcon, J., and Childs, S. (2017). Long-term effect of manure application in a certified organic production system on soil physical and chemical parameters and vegetable yields. *Hort. Technol.* 27, 171–176. doi: 10.21273/HORTTECH03348-16

Waterman, C., Rojas-Silva, P., Tumer, T. B., Kuhn, P., Richard, A. J., Wicks, S., et al. (2015). Isothiocyanate-rich *Moringa oleifera* extract reduces weight gain, insulin resistance, and hepatic gluconeogenesis in mice. *Mol. Nutr. Food Res.* 59, 1013–1024. doi: 10.1002/mnfr.201400679

Wiesner, M., Hanschen, F. S., Schreiner, M., Glatt, H., and Zrenner, R. (2013a). Induced production of 1-methoxy-indol-3-ylmethyl glucosinolate by jasmonic acid and methyl jasmonate in sprouts and leaves of pak choi (*Brassica rapa* ssp. chinensis). *Int. J. Mol. Sci.* 14, 14996–15016. doi: 10.3390/ijms140714996

Wiesner, M., Zrenner, R., Krumbein, A., Glatt, H., and Schreiner, M. (2013b). Genotypic variation of the glucosinolate profile in pak choi (*Brassica rapa* ssp. chinensis). *J. Agric. Food. Chem.* 61, 1943–1953. doi: 10.1021/jf303970k

Witzel, K., Neugart, S., Ruppel, S., Schreiner, M., Wiesner, M., and Baldermann, S. (2015). Recent progress in the use of 'omics technologies in brassicaceous vegetables. *Front. Plant Sci.* 6:244. doi: 10.3389/fpls.2015.00244

Wu, Q. J., Yang, Y., Vogtmann, E., Wang, J., Han, L. H., Li, H. L., et al. (2012). Cruciferous vegetables intake and the risk of colorectal cancer: a meta-analysis of observational studies. *Ann. Oncol.* 24, 1079–1087. doi: 10.1093/annonc/mds601

Xu, Y. Y., Qiu, Y., Ren, H., Ju, D. H., and Jia, H. L. (2017). Optimization of ultrasound-assisted aqueous two-phase system extraction of polyphenolic compounds from Aronia melanocarpa pomace by response surface methodology. *Prep. Biochem. Biotechn.* 47, 312–321. doi: 10.1080/10826068.2016.1244684

Yui, K., Uematsu, H., Muroi, K., Ishii, K., Baba, M., and Osada, K. (2013). Effect of dietary polyphenols from hop (*Humulus lupulus* L.) pomace on adipose tissue mass, fasting blood glucose, hemoglobin A1c, and plasma monocyte chemotactic protein-1 levels in OLETF rats. *J. Oleo Sci.* 62, 283–292. doi: 10.5650/jos.62.283

Zietz, M., Weckmüller, A., Schmidt, S., Rohn, S., Schreiner, M., Krumbein, A., et al. (2010). Genotypic and climatic influence on the antioxidant activity of flavonoids in kale (*Brassica oleracea* var. sabellica). *J. Agric. Food. Chem.* 58, 2123–2130. doi: 10.1021/jf9033909

Conflict of Interest Statement: The authors declare that the research was conducted in the absence of any commercial or financial relationships that could be construed as a potential conflict of interest.

frontiers in Plant Science

ORIGINAL RESEARCH
published: 18 October 2017
doi: 10.3389/fpls.2017.01785

Dynamic Labeling Reveals Temporal Changes in Carbon Re-Allocation within the Central Metabolism of Developing Apple Fruit

*Wasiye F. Beshir[1], Victor B. M. Mbong[1], Maarten L. A. T. M. Hertog[1], Annemie H. Geeraerd[1], Wim Van den Ende[2] and Bart M. Nicolaï[1,3]**

[1] Division of Mechatronics, Biostatistics and Sensors, Department of Biosystems, KU Leuven, Leuven, Belgium, [2] Laboratory of Molecular Plant Biology, Department of Biology, KU Leuven, Leuven, Belgium, [3] Flanders Centre of Postharvest Technology, Leuven, Belgium

In recent years, the application of isotopically labeled substrates has received extensive attention in plant physiology. Measuring the propagation of the label through metabolic networks may provide information on carbon allocation in sink fruit during fruit development. In this research, gas chromatography coupled to mass spectrometry based metabolite profiling was used to characterize the changing metabolic pool sizes in developing apple fruit at five growth stages (30, 58, 93, 121, and 149 days after full bloom) using ^{13}C-isotope feeding experiments on hypanthium tissue discs. Following the feeding of [U-^{13}C]glucose, the ^{13}C-label was incorporated into the various metabolites to different degrees depending on incubation time, metabolic pathway activity, and growth stage. Evidence is presented that early in fruit development the utilization of the imported sugars was faster than in later developmental stages, likely to supply the energy and carbon skeletons required for cell division and fruit growth. The declined ^{13}C-incorporation into various metabolites during growth and maturation can be associated with the reduced metabolic activity, as mirrored by the respiratory rate. Moreover, the concentration of fructose and sucrose increased during fruit development, whereas concentrations of most amino and organic acids and polyphenols declined. In general, this study showed that the imported compounds play a central role not only in carbohydrate metabolism, but also in the biosynthesis of amino acid and related protein synthesis and secondary metabolites at the early stage of fruit development.

Keywords: ***Malus domestica*** **Borkh, Braeburn, fruit growth, GC-MS, metabolomics, ^{13}C-label accumulation**

OPEN ACCESS

Edited by:
Ute Roessner,
University of Melbourne, Australia

Reviewed by:
John A. Morgan,
Purdue University, United States
Shyam K. Masakapalli,
Indian Institute of Technology Mandi, India

***Correspondence:**
Bart M. Nicolaï
bart.nicolai@kuleuven.be

Specialty section:
This article was submitted to Plant Metabolism and Chemodiversity, a section of the journal Frontiers in Plant Science

Received: *12 July 2017*
Accepted: *02 October 2017*
Published: *18 October 2017*

Citation:
Beshir WF, Mbong VBM, Hertog MLATM, Geeraerd AH, Van den Ende W and Nicolaï BM (2017) Dynamic Labeling Reveals Temporal Changes in Carbon Re-Allocation within the Central Metabolism of Developing Apple Fruit. Front. Plant Sci. 8:1785. doi: 10.3389/fpls.2017.01785

INTRODUCTION

Apple (*Malus domestica* Borkh.) is a member of the *Rosaceae* family that includes many important fruit trees like pear, peach, cherry, apricot, and prune. Apple is the most important fruit in the world market followed by pear and peach (Brown, 2012). It is consumed widely for its flavor, health, and nutritional value. The composition of the mature apple fruit is the resultant of carbohydrate import and the metabolic processes occurring during fruit development.

In plants, carbon is usually exchanged between source and sink tissues as simple sugars, typically sucrose (White et al., 2015). However, in *Rosaceae*, sorbitol and sucrose are the two main

photosynthates, comprising, for instance, respectively 70 and 30% of the components collected from phloem exudate of apple fruit stalks (Klages et al., 2001). Phloem unloading of soluble sugars in developing apple and pear fruit follows an apoplastic route (Zhang et al., 2004, 2014) with sorbitol and sugar transporters being responsible for the uptake by the cells (Watari et al., 2004; Fan et al., 2009; Peng et al., 2011). Sorbitol is converted into fructose by different types of sorbitol dehydrogenase (SDH) enzymes (Loescher et al., 1982) showing different subcellular localizations in the different tissue types of apple (Wang et al., 2009), perhaps indicating its distinct role in the different tissues. Sucrose is either directly transported into parenchyma cells by sucrose transporters (SUT), or is converted into fructose and glucose in the apoplast by cell wall bound invertase (CWI) before being transported into the cells by hexose transporters (HT) (Büttner and Sauer, 2000; Williams et al., 2000). Subsequently, the imported compounds enter the fruit's respiration pathway to generate the energy to fuel metabolic processes (White et al., 2015) and to contribute to sucrose, fructose, glucose, malate, and starch pools (Berüter et al., 1997; Li et al., 2012) (see **Figure 1**).

In the field of systems biology there is a growing interest in using "omics" technologies, mainly genomics, transcriptomics, proteomics, and metabolomics for better understanding growth and ripening related changes of apple fruit (Janssen et al., 2008; Zhang et al., 2010; Henry-Kirk et al., 2012; Li et al., 2012). Metabolomics plays a central role in systems biology focusing on identification and quantification of low molecular weight metabolites, which are end products of cellular regulation, especially when encountering various stress conditions (Fiehn, 2002; Fernie et al., 2004b; Roessner and Beckles, 2009). Metabolomics studies are commonly used to characterize complex physiological and biochemical changes occurring during fruit development (Zhang et al., 2010; Li et al., 2013). Nonetheless, knowledge of metabolite levels by itself is insufficient to unravel intracellular fluxes related with activity levels in different pathway and regulatory mechanisms. For example, fluxes through a pathway can change without a significant change in the levels of intermediate metabolites (Fernie et al., 2005). The application of isotopically labeled substrates to reveal the *in vivo* carbon flow levels through metabolic networks in responses to physiological stimuli or genetic modification has, lately, received extensive attention (Schwender et al., 2004; Sauer, 2006; Ampofo-Asiama et al., 2014; Buescher et al., 2015; Heux et al., 2017; Mbong et al., 2017a,b). Previous isotope labeling studies in developing apple fruit were focused at a specific growth stage (Berüter et al., 1997; Berüter, 2004) rather than covering the journey from flowering to fully mature fruit. This has triggered the question of how the metabolite levels and metabolic pathway activity changed with the various stages of apple fruit development, covering cell division, cell expansion, and maturation.

Therefore, the aim of this study was to create a comprehensive understanding of the dynamics of metabolic changes occurring throughout apple fruit development by studying the changing uptake and distribution of ^{13}C-label through feeding experiments on hypanthium tissue discs taken at distinct stages of fruit development. It is the first time that dynamic isotope labeling experiments have been performed at various stages of apple fruit development to study changes in carbon re-allocation during fruit growth. A wide range of polar metabolites were analyzed using gas chromatography coupled to mass spectrometry (GC-MS) characterizing the metabolic pool sizes and the ^{13}C-label distribution in growing apple fruit at distinct stages of development covering all major events occurring during fruit development.

MATERIALS AND METHODS

Plant Materials and Chemicals

Apples (*Malus domestica* Borkh., cv. "Braeburn") collected from seven designated 2-year-old trees grown at the KU Leuven Research orchard at Rillaar, Belgium (50°57′48.8″N, 4°52′56.5″E) were used for this study. During the 2015–2016 growing season fruit samples were harvested at five growth stages (30, 58, 93, 121, and 149 days after full bloom, i.e., after the flowering is fully completed, see Figure S1). Fruits were harvested in the morning and immediately transported to the MeBioS lab, KU Leuven, where the experiments were carried out. At each stage, at least 45 replicate fruits were collected from the seven trees.

Previously published physiological and morphological data from apple fruit development (Janssen et al., 2008; Li et al., 2012) were used to select stages matching five major events occurring during fruit growth and development, i.e., 30 days (cell division), 58 days (peak rate of cell expansion and starch accumulation), 93 days (decline of cell expansion rate), 121 days (decline of starch levels), and 149 days (ripening) after full bloom.

Analytical grade chemicals were purchased from Sigma-Aldrich (Belgium) and stored according to the manufacturer's instructions.

Respiration, Ethylene Production, and Osmolality Measurements

The results used to characterize the physiological parameters of developing apple fruit were all expressed on a fresh weight basis. The respiration and ethylene production rates of developing apple fruit were measured based on the methods described in Bulens et al. (2011). With respect to the five growth stages, one or two fruits were placed in 1-liter air tight glass jars. The jars were flushed with regular air. After 2 h of flushing, the gas flow was stopped and the initial composition of the gases in the headspace was measured using a compact-GC (Interscience, Louvain La Neuve, Belgium). The final reading was taken after 24 h. Respiration and ethylene production rate were calculated from these data with respiration rate being expressed in terms of CO_2 production rate (nmol kg^{-1} s^{-1}).

The osmolality of the fruit was determined based on the freezing point depression of pressed juice extract of 10 fruits, as described previously (Berüter, 2004). After the water activity of the extracted juice was measured using aw-Kryometer (AWK-40; Nagy, Germany), the osmolality of the fruit was derived from a calibration curve prepared using $NaCl_2$ solutions of known osmolality.

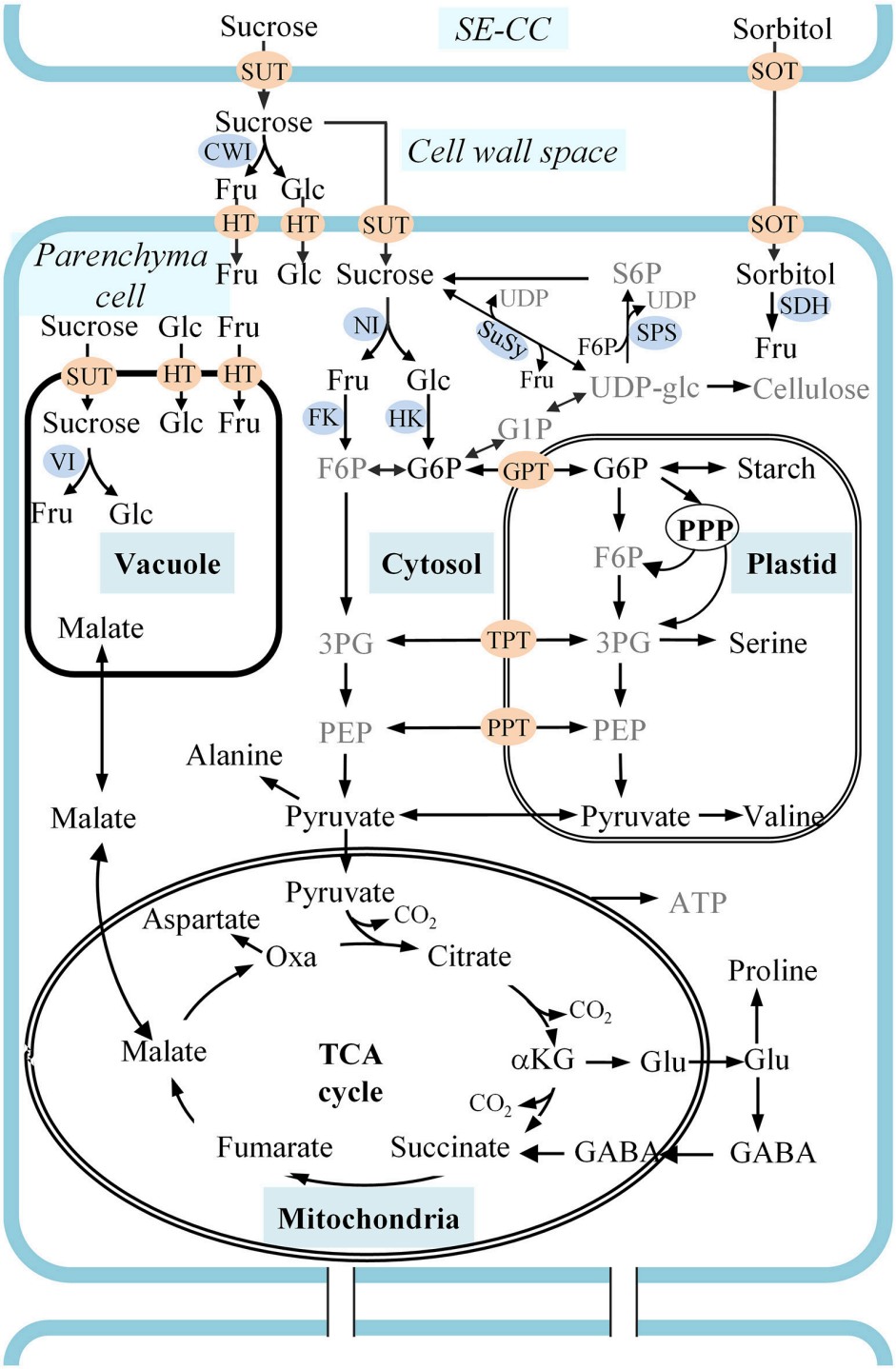

FIGURE 1 | A schematic representation of carbon metabolism in developing apple fruit. Sorbitol and sucrose are transported from the leaves to the fruit and unloaded in the cell wall space between sieve element-companion cell complexes (SE-CC) and parenchyma cells. Sorbitol is transported from the cell wall space into cells by sorbitol transporters (SOT). Sucrose is either directly transported into cells by sucrose transporters (SUT), or is converted into fructose and glucose in the cell wall space by cell wall bound invertase (CWI) before being transported into the cells by hexose transporters (HT). Metabolic pathways are described considering carbon metabolism in developing apple fruit and using the labeling of intermediates described in the text and information in the literature. Metabolites presented in gray text are those whose ^{13}C-labeling could not be reliably quantified in this study. αKG, α-ketoglutarate; 3PG, 3-phosphoglycerate; F6P, fructose 6-phosphate; Fru, fructose; G1P, Glucose 1-phosphate; G6P, Glucose 6-phosphate; GABA, γ-aminobutyrate; Glc, glucose; GPT, G6P/phosphate transporter; NI, neutral invertase; Oxa, oxaloacetate; PEP, phosphoenolpyruvate; PPP, pentose phosphate pathway; PPT, PEP/phosphate transporter; S6P, sucrose 6-phosphate; TCA cycle, tricarboxylic acid cycle; UDP-glc, uridine diphosphate-glucose; VI, vacuolar invertase; XPT, triose-phosphate transporter.

^{13}C-Isotope Labeling Experiments

In vivo ^{13}C labeling experiments were conducted using apple tissue discs cut from the harvested apple fruit, submerged in a liquid medium supplemented with 20 mM [U-^{13}C]glucose (Figure S1). The choice of [U-^{13}C]glucose was based on the assumption that glucose is transported into the parenchyma cells after sucrose being converted into glucose and fructose by apoplastic CWI. The fruit was sliced along the equatorial axis and tissue discs (∼10 mm diameter and ∼1 mm thickness) were collected from the hypanthium tissue using a cork borer. Excised tissue discs were washed three times in an isotonic solution containing 50 mM HEPES/KOH buffer (pH 7.0), 2 mM $CaCl_2$, 2 mM $MgCl_2$, 2 mM DTT (1,4-dithiothreitol) using betaine as an osmoticum, and while shaking at 90 rpm, to remove damaged cells. The osmotic strength of the solution was adjusted to the osmolality of the different growth stages to preserve the integrity of tissue discs submerged in liquid medium. As a result, the betaine concentration in the medium was increased from 160 mM at 30 days to 730 mM at 149 days. After washing thoroughly about 2.5 g of tissue discs was placed in a 50 ml flask containing 5 ml of buffer solution. This solution was identical to the one used to prepare the tissue discs, yet supplemented with 20 mM unlabeled glucose. After pre-incubation in unlabeled solution for 12 h the tissue discs were transferred to a solution containing [U-^{13}C]glucose (≥99% enrichment). The solution was continuously aerated with humidified air at 20°C in a controlled environment. Tissue discs were incubated for various time intervals (1, 2, 4, 6, 8, 10, or 24 h) after label introduction. Subsequently, samples were washed three times using 100 ml of a hypotonic solution of 50 mM HEPES/KOH buffer (pH 7.0) to remove the salt and excess of substrate from the tissue. After washing, excess medium was removed from the discs using paper tissue. The tissue samples were rapidly frozen in liquid N_2 and subsequently stored at −80°C prior to GC-MS analysis. Each ^{13}C labeling experiment was performed three times starting from independent biological plant material.

Primary Metabolite and Starch Analysis

Extraction and derivatization of polar metabolites were performed following the protocols described by Bekele et al. (2014). The frozen hypanthium tissue samples were homogenized using Mixer Mill (Retsch, MM 200, Haan, Germany) at a frequency of 30 Hz for 1 min. 200 mg of fresh weight of powdered frozen apple tissue material was extracted using 1 ml of methanol and incubated in a thermomixer (Eppendorf AG, Hamburg, Germany) at 70°C for 15 min, shaking at 1,400 rpm. The methanol extract was centrifuged at 22,000 g for 20 min at 4°C to separate the aliquot from the pellet. Next, the supernatant aliquot was dried at 50°C on a heating block (Stuart, sample concentrator (SBH CON/1), Bibby Scientific Limited Stone, and Staffordshire, UK) under a stream of nitrogen gas. Subsequently, metabolites were derivatized by methoxymation followed by silylation. Firstly, 120 µl of methoxyamine hydrochloride (20 mg methoxyamine hydrochloride (MEOX) in 1 ml pyridine) was added to each sample and incubated in the thermomixer for 60 min at 30°C. Secondly, 120 µl of BSTFA (N,O-Bis(trimethylsilyl(TMS))trifluoroacetamide) was added to each sample and incubated in the thermomixer for 120 min at 45°C. Finally, 100 µl of the derivatized sample was transferred into glass vials containing deactivated glass inserts. In addition, standard compounds were injected alongside the samples in order to allow for the calculation of absolute metabolite concentrations.

GC-MS analysis was performed on a GC 7890A coupled with 5975C MS (Agilent Technologies, Palo Alto, CA). Initially, the sample was volatilized at 230°C, inside the deactivated glass liner (SGE Analytical Science, Victoria, Australia). The chromatographic separation was performed on HP-5 ms column (30 m × 250 µm ID, 0.25 µm film thickness, Supelco, Bellefonte, CA) with programmed temperature ramp. Helium was used as a carrier gas applying a constant flow of 1 ml min^{-1}. Each sample was injected in two different split modes. One with split ratio of 5:1 injection, which was optimized for less abundant metabolites. For this injection, the oven temperature was set to 50°C for 2 min, ramped at 10°C min^{-1} to 325°C and held for 5 min at 325°C (34.5 min run time). Second, a high split ratio of 500:1 was used for most abundant metabolites corresponding to malate, asparagine, quinate, fructose, glucose, sorbitol, and sucrose. In 500:1 split mode, the oven temperature was set to 90°C for 2 min and ramped to 325°C switching between 50 and 10°C min^{-1} and held at 325°C for a further 5 min resulting in a run time of 17.3 min. The mass selective detector (MSD) was operated in the electron ionization (70 eV) mode with quadrupole and MS ion source temperatures maintained at 150 and 230°C, respectively. The detector was activated to record throughout the mass spectra range 35–500 *m/z*.

Starch extraction and determination was carried out using the method described by Hendriks et al. (2003). The pellet obtained after the extraction of polar metabolites was further extracted with 80% ethanol at 80°C for 15 min. The pellets were dried and homogenized in 0.2 mM KOH and incubated for 1 h by heating them at 95°C. After acidification to pH 4.9 with 1 M acetic acid/sodium-acetate buffer, the suspension was digested overnight with a mixture of amyloglucosidase and α-amylase. The glucose content of the supernatant was then used to assess the starch content of the sample.

Metabolite Annotation and ^{13}C-Label Enrichments

Metabolite annotation was performed using Agilent MSD Chemstation Software (Agilent Technologies, Santa Clara, USA) by comparing the acquired spectra with an in-house built library, with the Agilent Fiehn Metabolomics Library, and with the NIST2011 Library (National Institute of Standards and Technology, Gaithersburg, MD, USA) (Table S1). MS Correction Tool was used to correct isotopomer fractions of a particular metabolite fragment for the natural stable isotopes (Wahl et al., 2004). The percentage ^{13}C enrichment was calculated from the total abundance of ^{12}C and ^{13}C ions in a particular metabolite pool (Araújo et al., 2014).

Data Analysis

To reveal the correlation structure of the data principal component analysis (PCA) was conducted using the Unscrambler® X software (version 10.3, CAMO A/S, Trondheim, Norway). Heat maps were generated to compare the concentration of metabolites during fruit development (30, 58, 93, 121, and 149 days after full bloom) using the MultiExperiment Viewer software (MeV v4.9.0, http://www.tm4.org/, Saeed et al., 2003). A paired *t*-test analysis was used to compare the mean difference between the glucosyl and fructosyl moieties of sucrose with a significance level of p-value = 0.05 using JMP software, version 13.0 (SAS Institute Inc., Cary, NC, USA).

RESULTS

Experimental Setup and Physiological Parameters of Developing Apple Fruit

The results reported in this article were carried out at five stages of fruit development (30, 58, 93, 121, and 149 days after full bloom) throughout the 2015–2016 growing season. Preliminary ^{13}C labeling experiments were performed to test the uptake capacity of [U-^{13}C]glucose by tissue discs cut from developing apple fruit at three distinct growth stages (from the earlier growing season, 2014–2015) including fully ripe apple fruit. The latter showed little to no ^{13}C-label incorporation (Figure S2). In contrast, an appreciable amount of ^{13}C-label was incorporated into tissue from developing apple fruit with the percentage labeling varying with progressing fruit development (Figure S2). The percentage labeling of glucose increased with fruit development while fully ripe apple fruit showed the lowest uptake rate. In addition, the incorporation of ^{13}C-label into the various metabolites increased linearly with the concentration of [U-^{13}C]glucose increasing from 5 to 20 mM (Figure S3).

Physiological parameters of apple fruit were measured during fruit development. The changes in fruit osmolality, mass, diameter, respiration and ethylene production rate, and starch content during fruit growth are shown in **Figure 2**. The osmolality of the fruit increased from 30 days all the way to fruit maturation. Simultaneously, fruit mass and diameter increased approximately linearly from 30 to 149 days. During fruit growth, the respiration rate decreased from 460 nmol kg^{-1} s^{-1} in young fruit to 70 nmol kg^{-1} s^{-1} at 121 days followed by a slight increase at 149 days. In contrast, ethylene production rate remained relatively low until 121 days, showing a slight increase at 149 days. Starch content reached its peak level within 93 days and decreased throughout the later stages of fruit growth.

Metabolite Changes throughout Fruit Development

The metabolite changes of the developing apple fruit were analyzed using a GC-MS-based metabolite profiling approach. Typical chromatograms are shown in **Figure 3**. Two injections were realized in this study, one with a split ratio of 5:1 (**Figure 3A**), which was optimized for less abundant metabolites (34.5 min run time) and one with a split ratio of 500:1 (**Figure 3B**) used for the most abundant metabolites (17.3 min run time). To verify the identity of the metabolites individual standard compounds were injected. Detailed peak information for the metabolites identified are presented in Table S1.

Figure 4 shows the PCA bi-plot that reveals associations among sugars, sugar alcohols, organic and amino acids, and polyphenols observed in the ^{13}C labeling experiments executed at each of the five growth stages. The measured metabolites are represented by the open circles whereas the individual tissue samples are represented by their scores (closed symbols) and colored according to the five growth stages. The amount of variation covered by PC1 and PC2 was 48 and 13%, respectively,

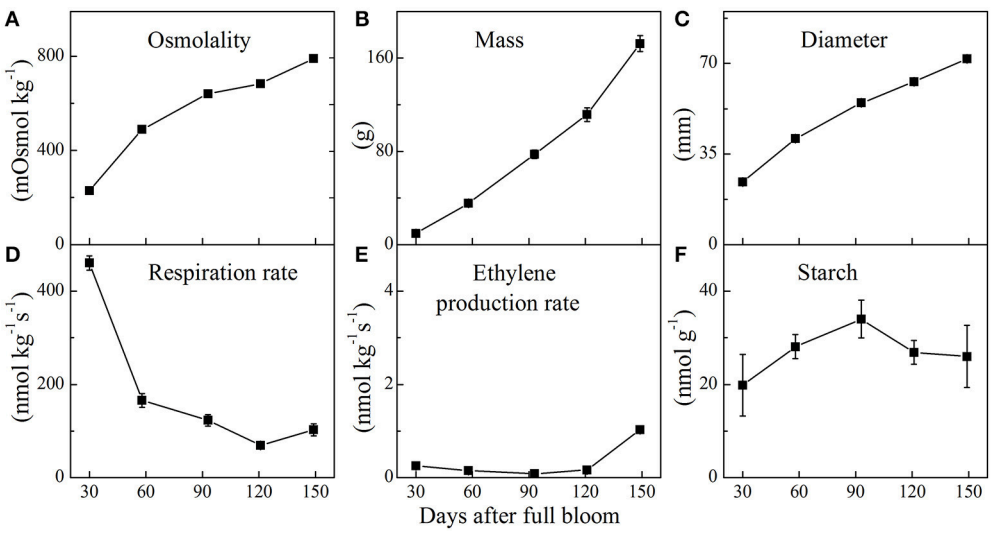

FIGURE 2 | Fruit osmolality **(A)**, mass **(B)**, diameter **(C)**, respiration rate **(D)**, ethylene production rate **(E)**, and starch content **(F)** of "Braeburn" apple throughout fruit development (mean ± SE; n = 15). The fruit was sampled at five growth stages throughout the 2015–2016 growing season.

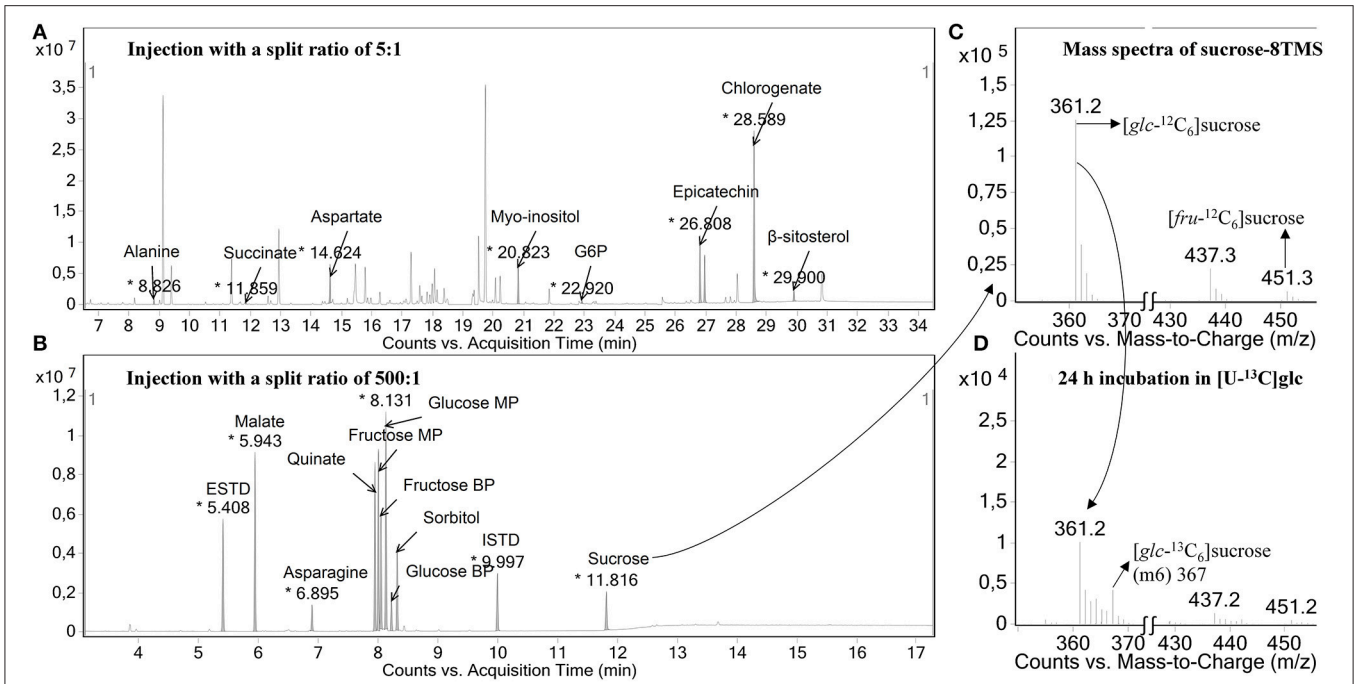

FIGURE 3 | Typical chromatographic results. **(A)** Example of a GC-chromatogram of samples injected with a split ratio of 5:1, which was optimized for less abundant metabolites (34.5 min run time) and **(B)** one with a split ratio of 500:1 used for most abundant metabolites in apple fruit (17.3 min run time). In the former injection mode, the detector was turned off during the time windows where highly abundant peaks were eluting so that those metabolites can be analyzed in a separate injection with a higher split ratio of 500:1 from the same sample. In addition, a mass spectrum generated for TMS-derivatized sucrose before **(C)** and after **(D)** the tissue discs were fed with 20 mM [U-^{13}C]glucose are shown. The fragments with *m/z* 361 and *m/z* 451 represent the mass isotopomers of the glucosyl and fructosyl moieties of sucrose, respectively. MP, main product; BP, by product.

covering 61% of the total variance. The scores showed a clear order according to growth stage. The largest variation was observed between the five growth stages (30, 58, 93, 121, and 149 days) whereas the effect of changes in incubation time was less pronounced (as indicated by the size of the closed symbols). Based on the PCA bi-plot some of the sugars, such as fructose and sucrose were positively associated with progressing growth stage. In contrast, most of the organic and amino acids and polyphenols were negatively correlated with growth stage.

To provide a more detailed representation of the results, heat maps were generated to show the metabolite changes during fruit growth (**Figure 5**). Fructose content increased significantly from 30 to 93 days and varied slightly later in development. The increase of fructose content was accompanied by a decrease of sorbitol level and starch degradation (**Figure 2F**) in the later growth stages. In contrast to the behavior observed in sorbitol, sucrose content increased from 30 to 149 days. Glucose reached its maximum level within 58 days and decreased throughout the later stages of fruit growth. G6P and F6P were high at 30 days and decreased gradually throughout fruit growth. Organic acids such as fumarate, succinate, pyruvate, quinate, glycerate, α-ketoglutarate, threonate, shikimate, and dehydroascorbate contents were high at 30 days and decreased substantially throughout fruit growth. In contrast, malate content increased up to 58 days and decreased considerably toward 149 days. Like most organic acids, the levels of most amino acids were very high in the early development and decreased gradually throughout fruit development. Most importantly, the major phenolic compounds present in apple (epicatechin, catechin, and chlorogenate) were very high at 30 days but strongly declined throughout fruit development (**Figure 5**, Figure S6C).

Validation of Isotopomers Analysis

Fragments used for isotopomer analysis were selected by comparing the experimental mass isotopomer of tissue discs incubated with unlabeled substrate with the theoretically expected values (Table S2). The extent of incorporation of ^{13}C-label into a certain metabolite was calculated using the molecular ion whenever available, otherwise, the average labeling of multiple fragments containing the carbon backbone of the molecular ion was considered. In some cases, when no suitable fragments could be found to represent the entire carbon skeleton, a single fragment was selected to represent the labeling of the metabolite in question (Roessner-Tunali et al., 2004). For example, *m/z* 218 of valine contains C1-C2, whereas *m/z* 144 contains C2-C5. However, *m/z* 144 seems to be superimposed with a minor peak from *m/z* 147, introducing about 9.3% error in m3, making its use for isotopomer analysis ambiguous (see Figure S4A). As a consequence, fragment *m/z* 218 was selected to represent the percentage labeling in valine. Similarly, fragment *m/z* 319 (C3-C6) of glucose was selected instead of taking into account *m/z* 160 that contains the first two carbons of glucose

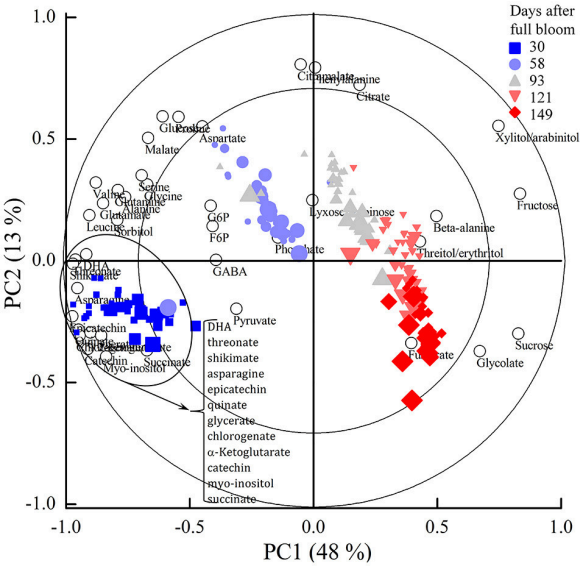

FIGURE 4 | PCA bi-plot showing variation in metabolite levels in relation to the five growth stages and 24 h incubation period with 20 mM [U-13C]glucose of "Braeburn" apple fruit. The loadings of the PCA (open circles) represent individual metabolites. The scores (closed symbols) represent individual samples from the five growth stages (indicated by different colors). The size of the closed symbols reflects the length of the ^{13}C-feeding period at each growth stage. The percentage of the explained variances are shown on the axes. PC, principal component.

(C1-C2) because *m/z* 160 contains around 5% error (Figure S4B). In addition, as shown in **Figure 3C**, *m/z* 361 and 451 corresponding to the mass spectra of sucrose were selected to represent the glucosyl and fructosyl moieties of sucrose, respectively, using fragmentation simulation available in the NIST library. After the incubation of the tissue discs for 24 h with 20 mM [U-^{13}C]glucose medium, a clear change in the mass isotopomer distributions of sucrose moieties were observed (**Figure 3D**). Koubaa et al. (2012) reported that the fructosyl moiety of sucrose contributes about 40% to the intensity of *m/z* 361, which, by the fragmentation simulation, is considered solely as the glucosyl moiety of sucrose. In contrast, the glucosyl moiety of sucrose contributes only a small amount (near 5%) to the intensity of *m/z* 451 (Koubaa et al., 2012), which implies that any dilution effect linked to the two moieties of sucrose could lead a different degree of labeling for each fragment. It is important to note that the fragments of sucrose at *m/z* 361, 437, and 451 gave the same isotopic enrichment (Table S2), as reported in previous studies (Alonso et al., 2005; Füzfai et al., 2008). In summary, we were able to estimate the natural stable istope abundance pattern in a range of fragments for each metabolite by selecting one or more representative fragments.

Analysis of the ^{13}C-Label Accumulation

^{13}C-isotope feeding experiments were performed to get a better insight into the metabolite changes and metabolic pathway activity during apple fruit development at five selected growth stages. Following the feeding of [U-^{13}C]glucose, the ^{13}C-label was incorporated into the various metabolites to different degrees of labeling depending on incubation time, metabolic pathway activity, and growth stage (**Figure 6**). The ^{13}C-label was incorporated considerably into glycolysis intermediates 1 h after the addition of exogenous [U-^{13}C]glucose. The labeling dynamics of metabolites in the glycolysis pathway was very fast and reached more or less a plateau within a few hours as indicated, for instance, by a nearly constant labeling of G6P (**Figure 6A**). Moreover, a higher percentage labeling of the majority of metabolites was observed at 30 days as compared to the later growth stages. In contrast, sorbitol, epicatechin, and catechin remained unlabeled during the 24 h incubation period, irrespective of the growth stages.

At 30 days, the enrichment of intracellular ^{13}C-glucose reached 2.2% within 6 h and increased to 4.8% after 24 h while G6P and pyruvate ramped to 54.5 and 24.1% within 6 h, respectively. Between 6 and 24 h, the labeling of G6P slightly decreased while a continuous increase or nearly constant labeling was observed in the labeling dynamics of downstream metabolites. The labeling of pyruvate, citrate, succinate, malate, GABA, isoleucine, phenylalanine, proline, and valine increased over the time course of the feeding experiment. The labeling of α-ketoglutarate, alanine, aspartate, glutamate, and serine appeared to be approaching isotopic steady state between 10 and 24 h of the incubation. The incorporation of ^{13}C-label into fructose and malate (the most abundant sugar and organic acid metabolite in apple, respectively) were quite similar and continuously increased during the time course of the experiment, except for fructose exhibiting a longer lag phase in ^{13}C-label accumulation than malate. As compared to fructose, a much larger proportion of label was directed to sucrose that strongly increased throughout the feeding experiment, reaching over 35% within 24 h. Moreover, there was no considerable difference between the labeling pattern of glucosyl and fructosyl moieties of sucrose (**Table 1**).

In the later growth stages (58–149 days), there was a much larger increase in the labeling of glucose in comparison with 30 days. The opposite was true for most of other metabolites, showing a decrease in percentage labeling throughout fruit development. It should be noted that GABA behaves differently. A decent amount of labeling of sucrose also took place at 58 days, exhibiting a gradual decrease in percentage labeling, whereas no considerable labeling of fructose could be found in the later growth stages.

Net ^{13}C-Incorporation in Contrast with Unlabeled Pools

Figure 7 shows the total ^{13}C-label incorporated into selected metabolites in comparison to the unlabeled pools of tissue discs retrieved from five growth stages during the feeding experiment with 20 mM [U-^{13}C]glucose. Interestingly, the net ^{13}C-incorporation into sucrose at 30 days reached a nearly constant value within a few hours (**Figure 7**) whilst the percentage ^{13}C enrichment strongly increased, reaching over 35% within 24 h (**Figure 6A**) as the pool size of sucrose was reduced (from 8.4 μmol g^{-1} at time zero to 4.02 μmol g^{-1} at 24 h). The percentage ^{13}C labeling of sucrose at 58 days was 11.9% at 24 h,

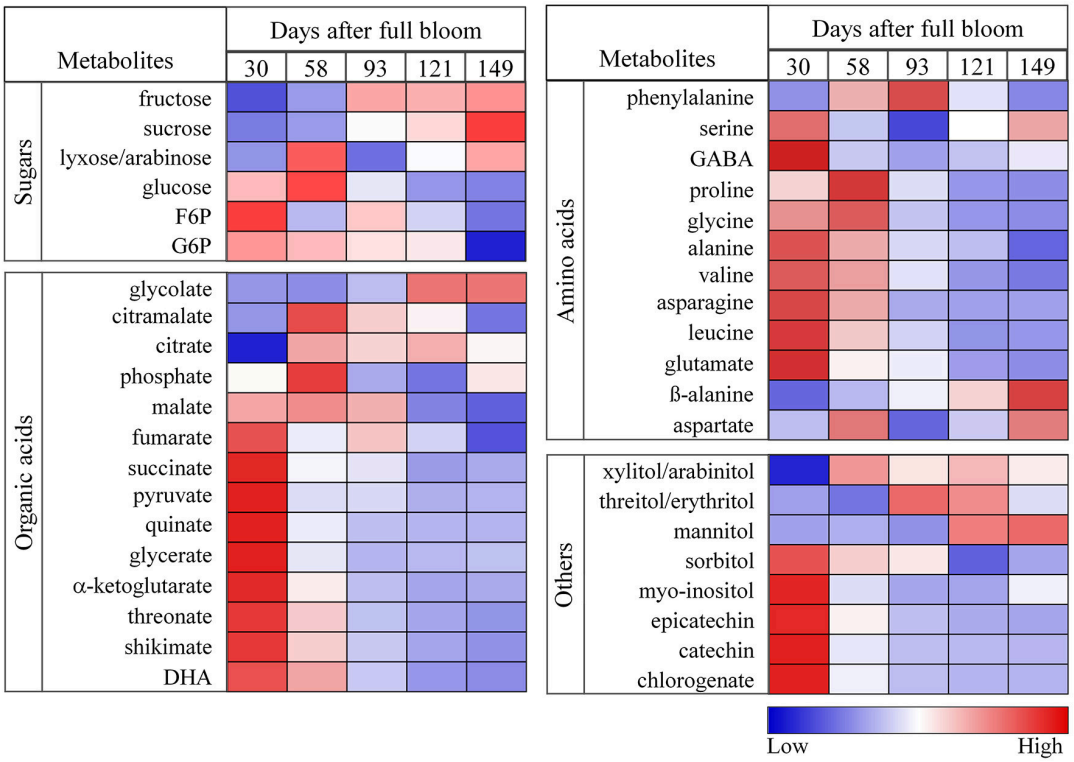

FIGURE 5 | Heat maps showing the changes in the concentrations of sugars, organic acids, amino acids, sugar alcohols, and polyphenols during fruit growth (30, 58, 93, 121, and 149 days after full bloom). The deep blue color (low) denoted lower concentration of metabolites whereas the deep red color (high) denoted higher concentration of metabolites. The colors were generated from GC-MS metabolite profiling raw data (relative value) using the MultiExperiment Viewer software (MeV v4.9.0) after mean center and scale transformation into comparable levels.

however, the net ^{13}C-incorporation (2.64 μmol g^{-1}) showed a 2 fold increase relative to the early growth stage (1.4 μmol g^{-1}; **Table 2**). This is because the total sucrose pool was smaller at 30 days (4.02 μmol g^{-1}) than 58 days (22 μmol g^{-1}).

Unlike most other metabolites, the total isotope accumulation in intracellular glucose was much more prominent in the later growth stage. For instance, after 24 h of incubation the absolute amount of the total isotope incorporated at 30 days in glucose reached 6.31 μmol g^{-1} whereas the value was considerably higher in the later growth stage (149 days), reaching 11.2 μmol g^{-1} although the total concentration of glucose was decreased at the later growth stage (**Figure 7**). Fructose labeling was high in young fruit and decreased over the growth stage. In addition, more label was incorporated into malate than in all other organic acids combined (**Table 2**).

DISCUSSION

Rationale for Developing ^{13}C-Labeling Experimental Setup for Developing Apple Fruit

In developing apple fruit, sorbitol and sucrose enter the fruit respiratory metabolism (Berüter et al., 1997) predominantly through the apoplastic pathway (Zhang et al., 2004), essentially after being converted into free fructose and glucose (Loescher et al., 1982; Büttner and Sauer, 2000; Williams et al., 2000). Several studies have been published using labeling with [U-^{13}C]glucose to study the central metabolic fluxes in many plant species (apple, Berüter, 2004; potato tubers, Roessner-Tunali et al., 2004; maize root tips, Alonso et al., 2007). To establish incorporation of ^{13}C labeled sugars within the central metabolism, we allowed tissue discs cut from growing fruit to take up uniformly ^{13}C labeled extracellular glucose from the medium. We therefore carried out an additional set of experiments to establish the rate of glucose uptake and the labeling kinetics of the various metabolite pools. The preliminary experiment was performed at three distinct growth stages: i.e., 30 days (cell division), 90 days (cell expansion), and 150 days (maturation) throughout the 2014–2015 growing season. These preliminary results indicated a fast labeling of the upstream metabolites resulting in saturating of the labeling within a few hours of incubation. The ^{13}C-label was incorporated into the various metabolites in just 1 h after the addition of labeled substrate. This rate of incorporation is similar to what was observed for the accumulation of [^{14}C]sorbitol in apple tissue discs (Zhang et al., 2004) but very fast when compared with the uptake of carboxyfluorescein (a common fluorescent marker of phloem transport) supplied to the intact apple fruit pedicel, which takes up to 4 h to reach the fruit flesh (Zhang et al., 2004). It must be

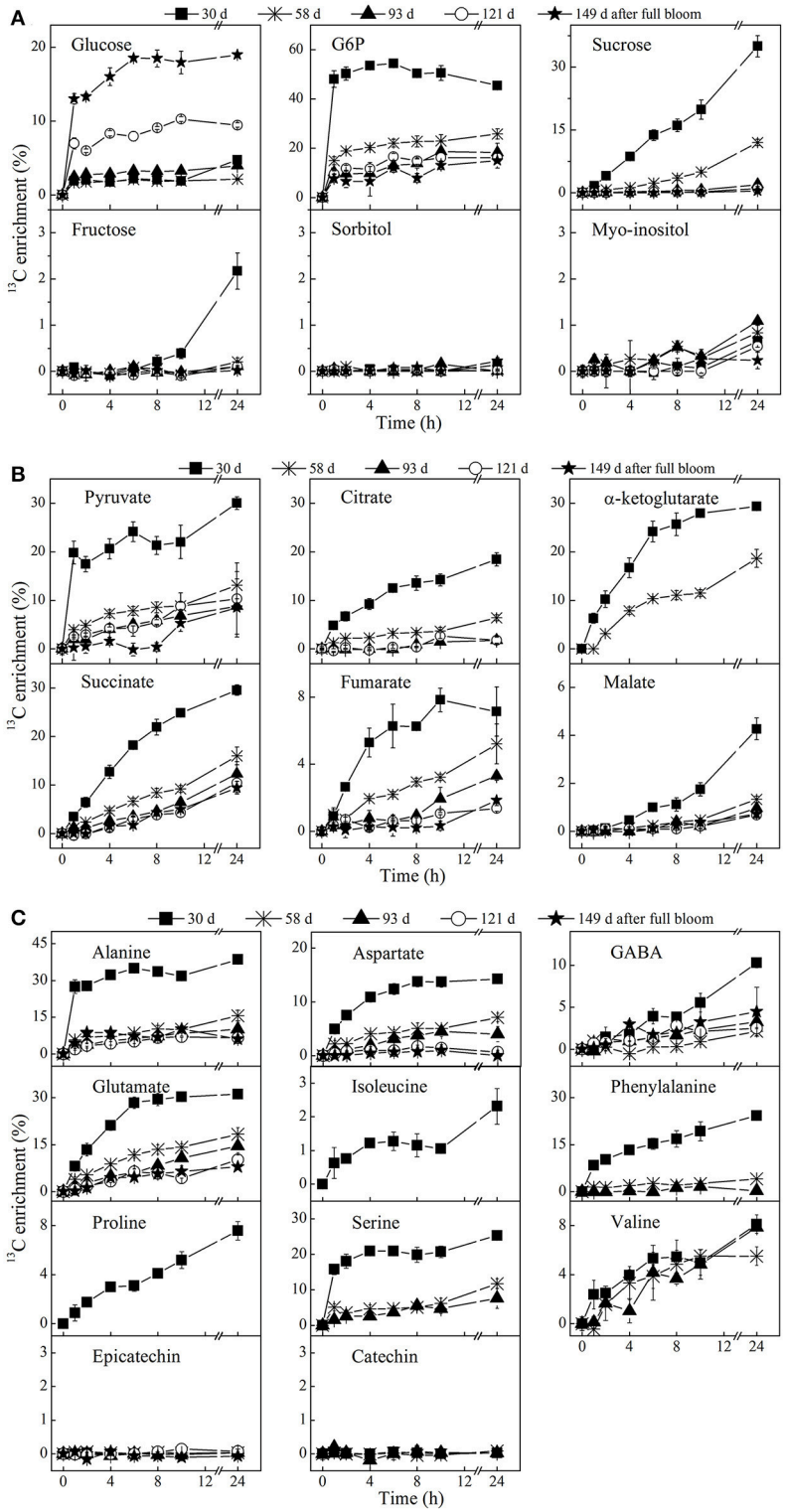

FIGURE 6 | Time course of ^{13}C-isotope enrichment of sugars **(A)**, organic acids (**B**), and amino acid and polyphenols **(C)** following [U-^{13}C]glucose loading. The enrichment values are different for each metabolite. The fruit were harvested at **five** growth stages, 30 days (■), 58 days (⁕), 93 days (▲), 121 days (○), and 149 days (★) after full bloom and incubated in 20 mM [U-^{13}C]glucose. Tissue discs were retrieved at 1, 2, 4, 6, 8, 10, and 24 h of incubation. The percentage labeling of isoleucine, proline, α-ketoglutarate, and phenylalanine were only calculated for the early growth stage(s), due to their very low concentrations as fruit growth advanced. Values are means of three independent replicates.

TABLE 1 | Percentage ^{13}C enrichments of sucrose moiety following incubation in 20 mM [U-^{13}C]glucose in apple tissue discs cut from 30 days (mean ± SE; n = 3).

Incubation time (h)	Percentage ^{13}C enrichment (sucrose moieties)		Mean difference	*p*-value
	Glucosyl (*m/z* 361)	Fructosyl (*m/z* 451)		
0	1.2 ± 0.1	1.0 ± 0.2	−0.4029	0.2018
1	3.2 ± 0.4	2.4 ± 0.1		
2	5.6 ± 0.9	4.7 ± 0.5		
4	9.6 ± 1.2	10.0 ± 0.7		
6	14.5 ± 2.1	15.1 ± 2.4		
8	17.0 ± 3.0	17.4 ± 2.2		
10	21.1 ± 4.3	20.8 ± 3.7		
24	37.4 ± 3.3	34.7 ± 5.5		

The glucosyl (fragment m/z 361) and fructosyl (fragment m/z 451) moieties were used for the calculation of ^{13}C-label enrichment, the average labeling reflects the labeling state of sucrose. Based on a paired t-test identifying the difference in labeling between the two sucrose moieties, the overall difference of the mean and the corresponding p-value was calculated.

pointed out that in the current experiments [U-^{13}C]glucose was supplied directly to tissue discs being a simplified model system whereas Zhang et al. (2004) supplied the carboxyfluorescein to the intact apple fruit pedicel so that it covered a longer transport distance to the fruit flesh.

An additional experiment showed that the incorporation of the ^{13}C-label into the various metabolites increased linearly with the concentration of [U-^{13}C]glucose in the range of 5–20 mM (Figure S3). This is in good agreement with the relationship between the source leave and sink fruit reported previously (Paul and Foyer, 2001; Morandi et al., 2008; Dash et al., 2013; White et al., 2015). These authors indicated that growth may be controlled by source and sink strength. For example, increasing carbohydrate availability through photosynthesis can increase growth to a certain extent. Also for sorbitol it has been demonstrated that its uptake by isolated tissue discs and in intact apple fruit is linear with respect to concentration (Berüter and Studer-Feusi, 1995). The final experiments were conducted using 20 mM [U-^{13}C]glucose to ensure excess amount of label in the medium to allow incorporation of decent amounts of label in a broad range of metabolites (see "Materials and Methods"). In addition, the osmotic strength of the medium was adjusted to the osmolality of the different growth stages in the range of 228–790 mOsmol kg^{-1} by using betaine (**Figure 2A**) – thus to preserve the integrity of tissue discs submerged in liquid medium – whilst the glucose concentration was kept the same for the different growth stages.

Dynamic Labeling Revealed Metabolite Features of Developing Apple Fruit

Reduction in Respiration Rate during Fruit Growth Can Be Related to Changing Label Incorporation

Like pear fruit (Zhang et al., 2005), apple is characterized by high respiration rate at the early growth stage which then generally decreases throughout the season until prior to initiation of fruit ripening (Bepete and Lakso, 1997). During the early stage (30 days) when cell division was most active (Janssen et al., 2008), fruit showed the highest respiration rate (**Figure 2D**), driving utilization of the imported labeled glucose into the wider metabolism (**Figure 6**). Given the expected high FK/HK (fructose- and hexose-kinase) enzyme activities at the early growth stage of the fruit (Li et al., 2012), rapid utilization of the imported sugars for cell division and fruit growth is facilitated (Berüter, 1985; Dash et al., 2013). With fruit development progressing respiration rate gradually declined and most of the labeled glucose taken up was no longer transferred to the other metabolites (**Figures 6**, **7**). This reduction might be associated with the decrease in HK activity during fruit growth (Li et al., 2012). Similarly, Beauvoit et al. (2014) reported a higher glycolytic flux during cell division and a sharp decline during cell expansion of tomato fruit.

In general, carbon accumulation in a sink fruit depends on sink characteristics such as uptake rate (sink size × sink activity), photosynthesis and respiration rate of the fruit, as well as acquisition of carbon via the peduncle (Henton et al., 1999; Paul and Foyer, 2001; White et al., 2015). As reported for tomato (Greve and Labavitch, 1991), the ^{13}C-label incorporation into actively growing tissue is much higher than into fully grown yet ripening tomato pericarp. Therefore, this data confirms the tight relationship between the fruit's respiration rate and its glycolytic capacity, both changing during fruit development (Figure S5). Moreover, the declining net isotope accumulation into various metabolites observed at 58 and 93 days growth stages showed a slightly higher accumulation in some of TCA cycle metabolites such as fumarate, succinate, and malate at the later growth stage of 149 days (**Table 2**), which was in parallel with a slight increase in respiration and ethylene production rate (**Figures 2D,E**). In addition, the ^{13}C-label incorporated into GABA was high at 149 days (1.5 μmol/g) as well as at 30 days (3 μmol/g), but lower at the intermediate growth stages (**Table 2** and **Figure 6C**). Thus, the observed increase in label accumulation in TCA cycle metabolites, as well as the slight increase in the respiration and ethylene measurements at final growth stage reflects the onset of the climacteric rise (Dilley, 1981). This suggested that around 149 days after full bloom the "Braeburn" apple fruit were sufficiently mature for commercial harvest, at least for the concerning orchard and growth season.

The percentage ^{13}C-label incorporated into glucose, especially in the early growth stages, was lower than the labeling of some other downstream intermediate metabolites such as G6P and pyruvate. This leads to the hypothesis that, early during development, tissue favors extracellular sugars over cellular sugars already stored in the vacuole as their main source of carbon, thus maximizing the fruit's net carbon loading. The fast glycolytic turnover of the imported labeled glucose only represents a small fraction against a large background of unlabeled glucose stored in the vacuole resulting in a low overall percentage of labeled glucose. This suggests a high carbon conversion efficiency in young fruit. The interfering effect of existing unlabeled pools of metabolites in interpreting labeling data has been recognized before (Alonso et al., 2005, 2007).

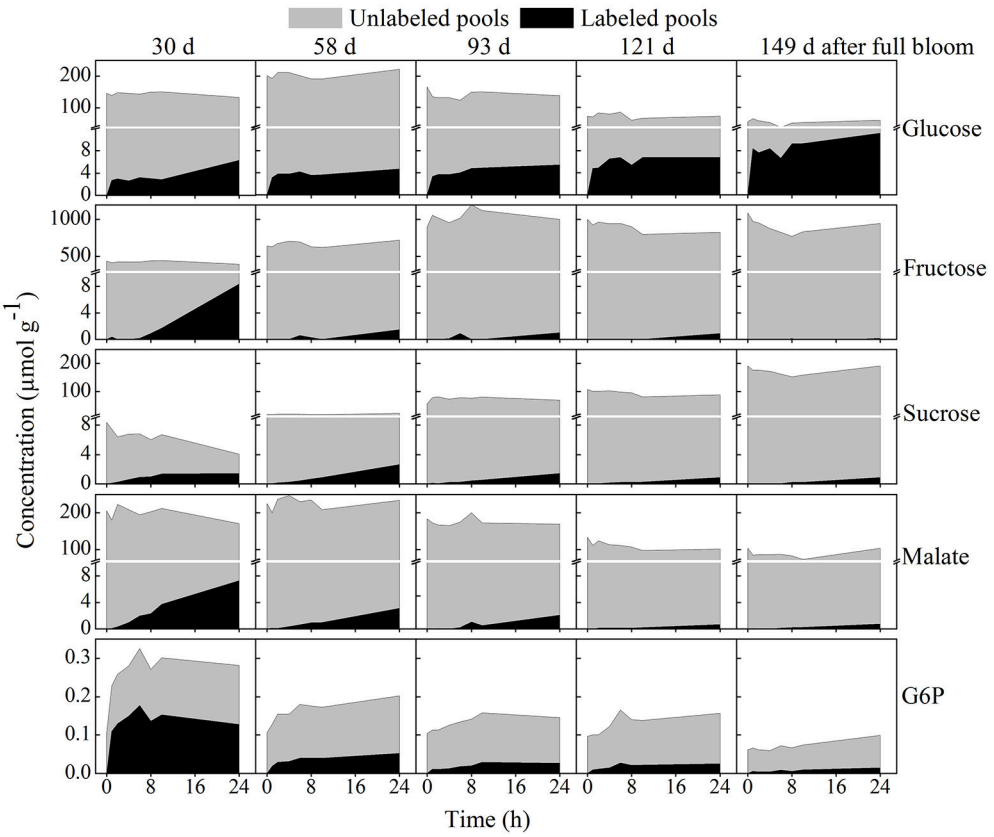

FIGURE 7 | Time course of net ^{13}C-incorporation in selected metabolites contrasted with unlabeled pools. The labeled pools are represented by the black area whereas the unlabeled pools are represented by the gray area. The five growth stages are ordered horizontally and similar scales were used for each metabolite across the five growth stages. Tissue discs were retrieved from five growth stages and incubated in 20 mM [U-^{13}C]glucose for 24 h. Values are means of three independent replicates.

The pool of the glycolysis intermediate G6P was high at 30 days and decreased gradually throughout fruit development. The higher concentration of G6P early in development can be related to the higher respiratory flux in young fruits, resulting in a high incorporation of label into G6P, reaching over 54% (**Figure 6A**). Likewise, facilitated entry of radioactive glucose into the hexose phosphate pools were reported for tissue discs retrieved from 50% fully grown apple fruit (Berüter et al., 1997). G6P could have been incorporated into sucrose, starch and cell wall polysaccharides (Alonso et al., 2005), as well as into the glycolytic pathway as indicated by the massive ^{13}C-label incorporation in the current experiments. G6P can also be used as a substrate for inositol synthesis in the cytosol, which can serve as a precursor for phytate synthesis (Mitsuhashi et al., 2008). During the cell expansion phase at 93 days, a slightly higher percentage labeling of myo-inositol was observed in the current study (**Figure 6A**) although it was evident that the net ^{13}C-incorporation showed a higher value at 30 days relative to the later growth stage. The decreased G6P labeling between 6 and 24 h in young fruit is quite similar to that previously observed in potato tuber discs (Roessner-Tunali et al., 2004). The decrease could be related to either the turnover of unlabeled starch or the cycling of unlabeled sucrose. However, starch degradation mainly occurs in mature fruit (Janssen et al., 2008; Li et al., 2012) thus, the most likely explanation is the regeneration of G6P through sucrose cycling (Berüter et al., 1997; Beauvoit et al., 2014). In agreement with our hypothesis, a decreasing sucrose level was observed during the 24 h incubation at 30 days (**Figure 7**).

Sucrose Cycles in Growing Fruit

As reported for potato tuber discs (Roessner-Tunali et al., 2004), a substantial labeling of sucrose took place during fruit development (**Figure 6A**). This suggests that in addition to the large flux of sucrose translocated from the leaves (Klages et al., 2001), the fruit is actively sustaining its sucrose synthesis apparatus, confirming that sucrose is the major product of sugar metabolism. Sucrose may be synthesized via conversion of F6P and uridine diphosphate-glucose (UDP-Glc) catalyzed by sucrose phosphate synthase (SPS) or from UDP-Glc and fructose as catalyzed by sucrose synthase (SuSy) which has higher activity in young fruit (Li et al., 2012) (see **Figure 1**). Given there was no significant difference between the labeling pattern of glucosyl and fructosyl moieties (**Table 1**), sucrose synthesis is most likely mediated by SPS with F6P inheriting the labeling directly from G6P through isomerization, suggesting that the hexose-phosphate isomerase reaction is at equilibrium.

TABLE 2 | Total isotope accumulating into selected metabolites of apple tissue discs retrieved from five growth stages and incubated in 20 mM [U-^{13}C]glucose for 24 h, at which most of the metabolites are reaching isotopic steady state.

Metabolites (nmol g^{-1})	Days after full bloom				
	30	58	93	121	149
SUGARS AND SUGAR PHOSPHATE					
Glucose	6,315 ± 12.3	4,848 ± 23.8	5,461 ± 3.08	6,816 ± 7.97	11,204 ± 32.4
Fructose	8,372 ± 91.8	1,457 ± 58.1	1,041 ± 82.4	891 ± 13.9	176.7 ± 81.1
Sucrose	1,403 ± 8.14	2,638 ± 18.3	1,414 ± 10.1	868 ± 4.87	882.2 ± 72.6
G6P	127 ± 0.13	51.9 ± 0.25	26.5 ± 0.1	25.3 ± 0.22	14.7 ± 0.39
ORGANIC ACIDS					
Pyruvate	34.4 ± 0.22	6.91 ± 0.13	10.3 ± 0.12	12.0 ± 1.72	8.1 ± 1.04
Citrate	55.8 ± 0.05	30.1 ± 0.09	8.95 ± 0.31	8.9 ± 0.27	nd
α-ketoglutarate	62.1 ± 0.18	15.7 ± 0.11	Nd	nd	nd
Succinate	69.5 ± 0.60	17.1 ± 0.18	19.8 ± 0.85	17.4 ± 0.25	26.8 ± 0.99
Fumarate	4.6 ± 0.00	4.4 ± 0.02	2.71 ± 0.03	2.1 ± 0.02	3.3 ± 0.00
Malate	7,250 ± 191	3,117 ± 33.3	1,636 ± 16.8	689 ± 6.7	736 ± 25.0
AMINO ACIDS					
Alanine	654 ± 2.48	110 ± 3.31	56.1 ± 3.28	7.2 ± 0.02	23.1 ± 4.53
Valine	12.7 ± 0.15	7.23 ± 0.02	8.34 ± 0.03	nd	nd
Serine	51.4 ± 0.10	11.5 ± 0.47	3.92 ± 0.45	nd	nd
GABA	3.50 ± 0.05	0.59 ± 0.01	1.09 ± 0.08	0.5 ± 0.07	1.6 ± 0.7
Aspartate	321 ± 0.79	113 ± 4.66	31.1 ± 5.48	1.66 ± 0.82	nd

Values are means ± SE (n = 3). nd, not detected, due to very low metabolite concentrations it was not possible to calculate reliably the relative distribution of mass isotopomers both in unlabeled and labeled ions.

Alonso et al. (2005) demonstrated that the labeling state of the glucosyl and fructosyl moieties in isotopic steady state conditions reflects the labeling state of G6P and F6P, respectively. At the same time, fructose labeling (**Figure 6A**) exhibited a longer lag phase as compared to G6P and sucrose. If sucrose was coming from fructose and UDP-Glc via the SuSy mediated reaction, the fructose moiety of sucrose would have been diluted by unlabeled fructose, at least in the first few hours of incubation when fructose labeling was not initiated. This means that sucrose synthesis via SuSy would lead to a higher labeling of the glucosyl moiety of sucrose, when labeled glucose was supplied (Geigenberger and Stitt, 1993). Altogether, equal labeling of the two moieties of sucrose can only be achieved through SPS and therefore, sucrose synthesis was most likely mediated by SPS.

In young fruit at 30 days, the overall sucrose content decreased by twofold (from 8.4 to 4.01 μmol g^{-1}) during 24 h of incubation. Its increased percentage labeling and its overall low and decreasing levels indicated sucrose was actively metabolized during early development in line with the high metabolic demand related to cell division and growth. Evidence for the rapid turnover of sucrose during the early growth stage of tomato fruit—after being transported into the vacuole, due to a higher vacuolar invertase (VI) activity—is reported by Beauvoit et al. (2014). Similarly, a high VI activity during the early growth stage of rapid cell division of apple and peach fruit has already been published (Li et al., 2012; Zhang et al., 2013). This implies that VI and SPS enzymes are recognized as the main players of sucrose cycling in many sink tissues.

At 58 days, where cell expansion rate reached its peak (Janssen et al., 2008; Li et al., 2012), there was a significant increase in total isotope accumulation in sucrose as compared to the early and the later growth stages (**Table 2** and **Figure 7**). The two fold increase in net ^{13}C-label incorporation into sucrose implies that ^{13}C allocation into reserves was high during cell expansion with limited conversion to intermediate metabolites. It underlines the importance of sucrose cycling in controlling the glucose level in the cell, regulating the glycolytic capacity of plant cells. This increased labeling of sucrose can be related to the peaking glucose phosphorylation activity and the higher glucose content during this period of apple fruit development as observed by Zhao et al. (2016). In line with their report, a higher glucose content was observed at 58 days (**Figure 5**, Figure S6).

SPS is known to play an important role in this as well but shows various behaviors for the different fruits. In developing peach fruit SPS activity was reported to increase during the most rapid sucrose accumulation phase (Lowell et al., 1989; Zhang et al., 2013), which is consistent with the higher sucrose labeling observed at 58 days. In apple fruit, SPS activity was shown to increase slightly with progressing fruit growth followed by a rapid increase during ripening, mirroring the reduction in starch level (Berüter and Studer-Feusi, 1997; Li et al., 2012), which is inconsistent with the currently decline in labeling of sucrose toward maturation. Similarly, an increase in SPS activity during kiwifruit ripening was reported (Nardozza et al., 2013). This concurrent high SPS activity and low labeling of G6P and sucrose currently observed in mature fruit (**Figure 6A**) leads to the hypothesis that G6P is more likely to originate from starch

degradation in the plastid than from exogenous [U-^{13}C]glucose. Nardozza et al. (2013) observed a positive correlation between starch accumulation in high starch kiwifruit genotypes and SPS activity which leads to sucrose accumulation during ripening.

Furthermore, the incorporation of label into fructose can be explained from sucrose hydrolysis into fructose catalyzed by invertase and/or SuSy; particularly VI and SuSy are known to be more active in the early growth stage of some *Rosaceae* fruit such as peach (Lo Bianco et al., 1999) and apple (Li et al., 2012). The observed slower and lower labeling of fructose at 30 days can be explained from the much larger pool of unlabeled fructose (**Figure 7**). Such slow labeling of fructose was already found for *Arabidopsis* indicating that the hydrolysis of sucrose into glucose and fructose is evidently a slow process (Szecowka et al., 2013). Moreover, the absence of fructose labeling in young fruit during the first few hours of incubation suggests the glucose-fructose isomerase activity might be negligible with fructose being mainly formed from sucrose. Berüter (2004) reported a lower labeling of fructose as compared to the labeling of sucrose after addition of ^{14}C-glucose. However, considering the absolute pool size of labeled carbon accumulated in fructose after 24 h (8.4 μmol g^{-1}, **Figure 7**), which was higher than the pool of labeled sucrose, shows that the actual flux into fructose was very high. The decline in fructose labeling with fruit development (**Figures 6A**, **7**) can be explained from the decreased activities of invertase and SuSy observed for apple (Li et al., 2012). In general, the labeling of fructose supports the hypothesis of sucrose cycling in apple (Berüter et al., 1997; Beauvoit et al., 2014). In contrast to sucrose and fructose, there was no ^{13}C-label incorporated into sorbitol at any growth stage (**Figure 6A**) suggesting the conversion of sorbitol into fructose is effectively irreversible in developing apple fruit (Berüter et al., 1997).

Besides the gradual decline in percentage labeling, fructose and sucrose both increased in their concentration with fruit growth, becoming the most abundant soluble sugars in mature fruit (Figure S6). Fructose accumulation can be explained coming from either sorbitol or sucrose. Both sorbitol and sucrose are being transported from the leaves to the sink tissue and either are stored as such or converted into fructose (Loescher et al., 1982; Büttner and Sauer, 2000; Williams et al., 2000; Klages et al., 2001). The decrease of sorbitol levels during fruit growth can be related to the observed increase of fructose levels, which for sucrose was not the case. The increasing sucrose content with progressing fruit development can be associated with a decrease in sucrose-cleaving enzymes, invertase and SuSy in addition to an increase in sucrose synthesizing enzyme, SPS (Berüter and Studer-Feusi, 1997; Li et al., 2012). Another comprehensive example in addition to sucrose synthesis via SPS is starch degradation sustaining the energy used to fuel metabolic processes, hence, accumulation of incoming sucrose (Berüter, 2004; Nardozza et al., 2013; Mesa et al., 2016; **Figure 2F**).

Young Fruits Are Characterized by High Levels of Organic and Amino Acids and Polyphenols

Extensive metabolic changes occurred during fruit growth (**Figure 5,** Figure S6). Organic acids, free amino acids, and phenolic compounds exhibited a significant higher concentration in the early growth stage. These large pools of organic and amino acid metabolites can serve as building blocks for cell growth at the early growth stage. In addition to the larger pools of these metabolites, the higher accumulation of large amount of label in organic acids (**Figure 6B**) and amino acids (**Figure 6C**) observed in the early growth stage can be associated with a higher rate of glycolysis/TCA cycle metabolism and subsequent contribution to protein synthesis (Fernie et al., 2004a; Li et al., 2012) related to cell division. This allows the fruit to grow to a bigger extend (Farinati et al., 2017). The decrease in level and labeling with growth stage can be explained from the shift in processes from mainly cell division toward mainly cell expansion and maturation. Similarly, Ishihara et al. (2015) reported a higher rate of protein synthesis in young leaves characterized by a gradual decline with leave maturation.

The amount of label incorporated into malate was considerably higher than the total amount of label in the other TCA cycle intermediates (**Table 2**) which can be understood from the fact that malate is one of the major storage compounds in apple (Berüter et al., 1997). Interestingly, it should be noted that in all of the growth stages, fumarate showed a substantial increase in its concentration during the feeding experiments (see Figure S6B). Pyruvate and alanine showed a consistent pattern in their dynamics of label enrichment. The labeling of alanine was slightly higher than its precursor pyruvate. However, MS measurements may have been biased as consequence of very low pyruvate concentrations, as well as the high turnover rate of pyruvate and its localization in multiple subcellular compartments, with unlabeled pyruvate present in the various cellular compartments diluting the labeled pyruvate mainly present in the cytosol (Buescher et al., 2015). Isoleucine and valine, which are synthesized from pyruvate were strongly labeled. Aspartate and glutamate, which are formed by transamination reaction from oxaloacetate and α-ketoglutarate (Szecowka et al., 2013), also showed a more rapid ^{13}C-label accumulation at 30 days.

The absence of label in epicatechin and catechin (**Figure 6C**) metabolites can be explained by their metabolic remoteness from the supplied ^{13}C substrate although the label, to a certain level, did reach phenylalanine, which serves as a bridge between the plant primary metabolism and the polyphenolic pathway. Like most organic acids in the TCA cycle, chlorogenate, catechin, and epicatechin were synthesized, to a large extent, early during development (30 days) and gradually decreased during fruit growth (**Figure 5**). However, the expression level of anthocyanidin reductase and leucoanthocyanidin reductase, which are responsible for the synthesis of catechin and epicatechin in apple, are known to increase toward maturity (Henry-Kirk et al., 2012). Previous studies have suggested that the decline in the content of phenolic compounds is associated with a dilution effect linked to fruit growth (vacuole expansion in mature apple fruit) (Renard et al., 2007). In general, the changes of metabolite levels were consistent with previous studies of apple fruit growth (Zhang et al., 2010; Li et al., 2013).

In conclusion, the novelty of the present work is in the dynamic labeling experiments performed at various stages of fruit growth to study carbon re-allocation metabolism during

apple fruit development. Interestingly, short time isotope feeding experiments showed a wide range of label distributions between the different growth stages, depending on the proximity of each metabolite to the substrate. Isotopic steady state labeling was achieved in the majority of metabolites within few hours of exogenous [U-^{13}C]glucose addition. It is important to remark that young fruit is characterized by a greater degree of label accumulation, related to the higher metabolite demand during cell division and fruit growth. Due to the reduced metabolic activity, as mirrored by respiratory rate, ^{13}C re-allocation into various metabolites gradually declined as the requirement for cell growth and carbon skeletons decrease with fruit development. The work presented here can serve as a platform for further studies to understand developmental changes associated with fruit growth. Positional isotope feeding experiments and metabolic modeling can be considered to furthermore quantify fluxes through the glycolysis and the pentose phosphate pathway.

AUTHOR CONTRIBUTIONS

WB, MH, AG, and BN designed the experiments. WB carried out the experiments, data analysis and prepared the figures. MH, AG, and BN guided the experimental work. WB interpreted the results and wrote the manuscript with contributions from all the authors (VM, MH, AG, WVdE, and BN).

FUNDING

This work was funded by the Research Council of the KU Leuven (OT 12/055 and C16/16/002) for financial support. This research was carried out in the context of the European COST Action FA1106 ("QualityFruit").

ACKNOWLEDGMENTS

The authors wish to thank the KU Leuven Research orchard staff (Johan Verheyen) for providing the apple fruit, Prof. John Lunn and Prof. Mark Stitt for useful discussions.

SUPPLEMENTARY MATERIAL

The Supplementary Material for this article can be found online at: https://www.frontiersin.org/articles/10.3389/fpls.2017.01785/full#supplementary-material

REFERENCES

Alonso, A. P., Raymond, P., Hernould, M., Rondeau-Mouro, C., de Graaf, A., Chourey, P., et al. (2007). A metabolic flux analysis to study the role of sucrose synthase in the regulation of the carbon partitioning in central metabolism in maize root tips. *Metab. Eng.* 9, 419–432. doi: 10.1016/j.ymben.2007.06.002

Alonso, A. P., Vigeolas, H., Raymond, P., Rolin, D., and Dieuaide-noubhani, M. (2005). A new substrate cycle in plants. Evidence for a high glucose-phosphate-to-glucose turnover from *in vivo* steady-state and pulse-labeling experiments with [^{13}C]glucose and [^{14}C]glucose. *Plant Physiol.* 138, 2220–2232. doi: 10.1104/pp.105.062083

Ampofo-Asiama, J., Baiye, V. M. M., Hertog, M. L. A. T. M., Waelkens, E., Geeraerd, A. H., and Nicolai, B. M. (2014). The metabolic response of cultured tomato cells to low oxygen stress. *Plant Biol.* 16, 594–606. doi: 10.1111/plb.12094

Araújo, W. L., Tohge, T., Nunes-nesi, A., Obata, T., and Fernie, A. R. (2014). "Analysis of kinetic labeling of amino acids and organic acids by GC-MS," in *Plant Metabolic Flux Analysis,* eds M. Dieuaide-noubhani and A. P. Alonso (New York, NY: Springer), 107–119.

Beauvoit, B. P., Colombie, S., Monier, A., Andrieu, M.-H., Biais, B., Benard, C., et al. (2014). Model-assisted analysis of sugar metabolism throughout tomato fruit development reveals enzyme and carrier properties in relation to vacuole expansion. *Plant Cell* 26, 3224–3242. doi: 10.1105/tpc.114.127761

Bekele, E. A., Annaratone, C. E. P., Hertog, M. L. A. T. M., Nicolai, B. M., and Geeraerd, A. H. (2014). Multi-response optimization of the extraction and derivatization protocol of selected polar metabolites from apple fruit tissue for GC-MS analysis. *Anal. Chim. Acta* 824, 42–56. doi: 10.1016/j.aca.2014.03.030

Bepete, M., and Lakso, A. (1997). Apple fruit respiration in the field: relationships to fruit growth rate, temperature, and light exposure. *Acta Hort.* 451, 319–326. doi: 10.17660/ActaHortic.1997.451.37

Berüter, J. (1985). Sugar accumulation and changes in the activities of related enzymes during development of the apple fruit. *J. Plant Physiol.* 121, 331–341. doi: 10.1016/S0176-1617(85)80026-2

Berüter, J. (2004). Carbohydrate metabolism in two apple genotypes that differ in malate accumulation. *J. Plant Physiol.* 161, 1011–1029. doi: 10.1016/j.jplph.2003.12.008

Berüter, J., and Studer-Feusi, M. E. (1995). Comparison of sorbitol transport in excised tissue discs and cortex tissue of intact apple fruit. *J. Plant Physiol.* 146, 95–102. doi: 10.1016/S0176-1617(11)81973-5

Berüter, J., and Studer-Feusi, M. E. (1997). The effect of girdling on carbohydrate partitioning in the growing apple fruit. *J. Plant Physiol.* 151, 277–285. doi: 10.1016/S0176-1617(97)80253-2

Berüter, J., Studer-Feusi, M. E., and Rüedi, P. (1997). Sorbitol and sucrose partitioning in the growing apple fruit. *J. Plant Physiol.* 151, 269–276. doi: 10.1016/S0176-1617(97)80252-0

Brown, S. (2012). "Apple," in *Fruit Breeding,* eds M. L. Badenes and D. H. Byrne (New York, NY: Springer), 329–367.

Buescher, J. M., Antoniewicz, M. R., Boros, L. G., Burgess, S. C., Brunengraber, H., Clish, C. B., et al. (2015). A roadmap for interpreting 13C metabolite labeling patterns from cells. *Curr. Opin. Biotechnol.* 34, 189–201. doi: 10.1016/j.copbio.2015.02.003

Bulens, I., Van de Poel, B., Hertog, M. L. A. T. M., De Proft, M. P., Geeraerd, A. H., and Nicola,ï, B. M. (2011). Protocol: an updated integrated methodology for analysis of metabolites and enzyme activities of ethylene biosynthesis. *Plant Methods* 7:17. doi: 10.1186/1746-4811-7-17

Büttner, M., and Sauer, N. (2000). Monosaccharide transporters in plants: structure, function and physiology. *Biochim. Biophys. Acta*1465, 263–274. doi: 10.1016/S0005-2736(00)00143-7

Dash, M., Johnson, L. K., and Malladi, A. (2013). Reduction of fruit load affects early fruit growth in apple by enhancing carbohydrate availability, altering the expression of cell production-related genes, and increasing cell production. *J. Am. Soc. Hortic. Sci.* 138, 253–262.

Dilley, D. R. (1981). Assessing fruit maturity and ripening and techniques to delay ripening in storage. *Proc. Michigan State Hortic. Soc.* 11, 132–146.

Fan, R.-C., Peng, C.-C., Xu, Y.-H., Wang, X.-F., Li, Y., Shang, Y., et al. (2009). Apple sucrose ransporter SUT1 and sorbitol transporter SOT6 interact with cytochrome b5 to regulate their affinity for substrate sugars. *Plant Physiol.* 150, 1880–1901. doi: 10.1104/pp.109.141374

Farinati, S., Rasori, A., Varotto, S., and Bonghi, C. (2017). Rosaceae fruit development, ripening and post-harvest: an epigenetic perspective. *Front. Plant Sci.* 8:1246. doi: 10.3389/fpls.2017.01247

Fernie, A. R., Carrari, F., and Sweetlove, L. J. (2004a). Respiratory metabolism: glycolysis, the TCA cycle and mitochondrial electron transport. *Curr. Opin. Plant Biol.* 7, 254–261. doi: 10.1016/j.pbi.2004.03.007

Fernie, A. R., Geigenberger, P., and Stitt, M. (2005). Flux an important, but neglected, component of functional genomics. *Curr. Opin. Plant Biol.* 8, 174–182. doi: 10.1016/j.pbi.2005.01.008

Fernie, A. R., Trethewey, R. N., Krotzky, A. J., and Willmitzer, L. (2004b). Metabolite profiling: from diagnostics to systems biology. *Nat. Rev. Mol. Cell Biol.* 5, 763–769. doi: 10.1038/nrm1451

Fiehn, O. (2002). Metabolomics – the link between genotypes and phenotypes. *Plant Mol. Biol.* 48, 155–171. doi: 10.1023/A:1013713905833

Füzfai, Z., Boldizsár, I., and Molnár-Perl, I. (2008). Characteristic fragmentation patterns of trimethylsilyl and trimethylsilyl-oxime derivatives of various saccharides as obtained by gas chromatography coupled to ion-trap mass spectrometry. *J. Chromatogr. A* 1177, 183–189. doi: 10.1016/j.chroma.2007.11.023

Geigenberger, P., and Stitt, M. (1993). Sucrose synthase catalyses a readily reversible reaction *in vivo* in developing potato tubers and other plant tissues. *Planta* 189, 329–339. doi: 10.1007/BF00194429

Greve, L. C., and Labavitch, J. M. (1991). Cell wall metabolism in ripening fruit: v. Analysis of cell wall synthesis in ripening tomato pericarp tissue using a d-[U-13C]glucose tracer and gas chromatography-mass spectrometry. *Plant Physiol.* 97, 1456–1461. doi: 10.1104/pp.97.4.1456

Hendriks, J. H. M., Kolbe, A., Gibon, Y., Stitt, M., and Geigenberger, P. (2003). ADP-glucose pyrophosphorylase is activated by posttranslational redox-modification in response to light and to sugars in leaves of Arabidopsis and other plant species. *Plant Physiol.* 133, 838–849. doi: 10.1104/pp.103.024513

Henry-Kirk, R. A., McGhie, T. K., Andre, C. M., Hellens, R. P., and Allan, A. C. (2012). Transcriptional analysis of apple fruit proanthocyanidin biosynthesis. *J. Exp. Bot.* 63, 695–709. doi: 10.1093/jxb/ers193

Henton, S. M., Piller, G. J., and Gandar, P. W. (1999). A fruit growth model dependent on both carbon supply and inherent fruit characteristics. *Ann. Bot.* 83, 509–514. doi: 10.1006/anbo.1999.0850

Heux, S., Bergès, C., Millard, P., Portais, J.-C., and Létisse, F. (2017). Recent advances in high-throughput 13C-fluxomics. *Curr. Opin. Biotechnol.* 43, 104–109. doi: 10.1016/j.copbio.2016.10.010

Ishihara, H., Obata, T., Sulpice, R., Fernie, A. R., and Stitt, M. (2015). Quantifying protein synthesis and degradation in arabidopsis by dynamic $13CO_2$ labeling and analysis of enrichment in individual amino acids in their free pools and in protein. *Plant Physiol.* 168, 74–93. doi: 10.1104/pp.15.00209

Janssen, B. J., Thodey, K., Schaffer, R. J., Alba, R., Balakrishnan, L., Bishop, R., et al. (2008). Global gene expression analysis of apple fruit development from the floral bud to ripe fruit. *BMC Plant Biol.* 8:16. doi: 10.1186/1471-2229-8-16

Klages, K., Donnison, H., Wünsche, J., and Boldingh, H. (2001). Diurnal changes in non-structural carbohydrates in leaves, phloem exudate and fruit in "Braeburn" apple. *Aust. J. Plant Physiol.* 28, 131–139. doi: 10.1071/PP00077

Koubaa, M., Mghaieth, S., Thomasset, B., and Roscher, A. (2012). Gas chromatography-mass spectrometry analysis of 13C labeling in sugars for metabolic flux analysis. *Anal. Biochem.* 425, 183–188. doi: 10.1016/j.ab.2012.03.020

Li, M., Feng, F., and Cheng, L. (2012). Expression patterns of genes involved in sugar metabolism and accumulation during apple fruit development. *PLoS ONE* 7:e33055. doi: 10.1371/journal.pone.0033055

Li, P., Ma, F., and Cheng, L. (2013). Primary and secondary metabolism in the sun-exposed peel and the shaded peel of apple fruit. *Physiol. Plant.* 148, 9–24. doi: 10.1111/j.1399-3054.2012.01692.x

Lo Bianco, R., Rieger, M., and Sung, S.-J. S. (1999). Carbohydrate metabolism of vegetative and reproductive sinks in the late-maturing peach cultivar "Encore." *Tree Physiol.* 19, 103–109. doi: 10.1093/treephys/19.2.103

Loescher, W. H., Marlow, G. C., and Kennedy, R. A. (1982). Sorbitol metabolism and sink-source interconversions in developing apple leaves. *Plant Physiol.* 70, 335–339. doi: 10.1104/pp.70.2.335

Lowell, C. A., Tomlinson, P. T., and Koch, K. E. (1989). Sucrose-metabolizing enzymes in transport tissues and adjacent sink structures in developing citrus fruit. *Plant Physiol.* 90, 1394–1402. doi: 10.1104/pp.90.4.1394

Mbong, V. B. M., Ampofo-Asiama, J., Hertog, M. L. A. T. M., Geeraerd, A. H., and Nicolai, B. M. (2017a). Metabolic profiling reveals a coordinated response of isolated lamb's (*Valerianella locusta*, L.) lettuce cells to sugar starvation and low oxygen stress. *Postharvest Biol. Technol.* 126, 23–33. doi: 10.1016/j.postharvbio.2016.12.004

Mbong, V. B. M., Ampofo-Asiama, J., Hertog, M. L. A. T. M., Geeraerd, A. H., and Nicolai, B. M. (2017b). The effect of temperature on the metabolic response of lamb's lettuce (*Valerianella locusta*, (L), Laterr.) cells to sugar starvation. *Postharvest Biol. Technol.* 125, 1–12. doi: 10.1016/j.postharvbio.2016.10.013

Mesa, K., Serra, S., Masia, A., Gagliardi, F., Bucci, D., and Musacchi, S. (2016). Seasonal trends of starch and soluble carbohydrates in fruits and leaves of "Abbé Fétel" pear trees and their relationship to fruit quality parameters. *Sci. Hortic.* 211, 60–69. doi: 10.1016/j.scienta.2016.08.008

Mitsuhashi, N., Kondo, M., Nakaune, S., Ohnishi, M., Hayashi, M., Hara-Nishimura, I., et al. (2008). Localization of myo-inositol-1-phosphate synthase to the endosperm in developing seeds of Arabidopsis. *J. Exp. Bot.* 59, 3069–3076. doi: 10.1093/jxb/ern161

Morandi, B., Corelli Grappadelli, L., Rieger, M., and Lo Bianco, R. (2008). Carbohydrate availability affects growth and metabolism in peach fruit. *Physiol. Plant.* 133, 229–241. doi: 10.1111/j.1399-3054.2008.01068.x

Nardozza, S., Boldingh, H. L., Osorio, S., Höhne, M., Wohlers, M., Gleave, A. P., et al. (2013). Metabolic analysis of kiwifruit (*Actinidia deliciosa*) berries from extreme genotypes reveals hallmarks for fruit starch metabolism. *J. Exp. Bot.* 64, 5049–5063. doi: 10.1093/jxb/ert293

Paul, M. J., and Foyer, C. H. (2001). Sink regulation of photosynthesis. *J. Exp. Bot.* 52, 1383–1400. doi: 10.1093/jexbot/52.360.1383

Peng, C. C., Xu, Y. H., Xi, R. C., and Zhao, X. L. (2011). Expression, subcellular localization and phytohormone stimulation of a functional sucrose transporter (MdSUT1) in apple fruit. *Sci. Hortic.* 128, 206–212. doi: 10.1016/j.scienta.2011.01.019

Renard, C. M. G. C., Dupont, N., and Guillermin, P. (2007). Concentrations and characteristics of procyanidins and other phenolics in apples during fruit growth. *Phytochemistry* 68, 1128–1138. doi: 10.1016/j.phytochem.2007.02.012

Roessner, U., and Beckles, D. M. (2009). "Metabolite measurements," in *Plant Metabolic Networks*, ed J. Schwender (New York, NY: Springer), 39–69.

Roessner-Tunali, U., Liu, J., Leisse, A., Balbo, I., Perez-Melis, A., Willmitzer, L., et al. (2004). Kinetics of labelling of organic and amino acids in potato tubers by gas chromatography-mass spectrometry following incubation in 13C labelled isotopes. *Plant J.* 39, 668–679. doi: 10.1111/j.1365-313X.2004.02157.x

Saeed, A. I., Sharov, V., White, J., Li, J., Liang, W., Bhagabati, N., et al. (2003). TM4: A free, open-source system for microarray data management and analysis. *Biotechniques* 34, 374–378.

Sauer, U. (2006). Metabolic networks in motion: 13C-based flux analysis. *Mol. Syst. Biol.* 2, 62. doi: 10.1038/msb4100109

Schwender, J., Ohlrogge, J., and Shachar-Hill, Y. (2004). Understanding flux in plant metabolic networks. *Curr. Opin. Plant Biol.* 7, 309–317. doi: 10.1016/j.pbi.2004.03.016

Szecowka, M., Heise, R., Tohge, T., Nunes-Nesi, A., Vosloh, D., Huege, J., et al. (2013). Metabolic fluxes in an illuminated *Arabidopsis rosette*. *Plant Cell* 25, 694–714. doi: 10.1105/tpc.112.106989

Wahl, S. A. A., Dauner, M., and Wiechert, W. (2004). New tools for mass isotopomer data evaluation in 13C flux analysis: mass isotope correction, data consistency checking, and precursor relationships. *Biotechnol. Bioeng.* 85, 259–268. doi: 10.1002/bit.10909

Wang, X.-L., Xu, Y.-H., Peng, C.-C., Fan, R.-C., and Gao, X.-Q. (2009). Ubiquitous distribution and different subcellular localization of sorbitol dehydrogenase in fruit and leaf of apple. *J. Exp. Bot.* 60, 1025–1034. doi: 10.1093/jxb/ern347

Watari, J., Kobae, Y., Yamaki, S., Yamada, K., Toyofuku, K., Tabuchi, T., et al. (2004). Identification of sorbitol transporters expressed in the phloem of apple source leaves. *Plant Cell Physiol.* 45, 1032–1041. doi: 10.1093/pcp/pch121

White, A. C., Rogers, A., Rees, M., and Osborne, C. P. (2015). How can we make plants grow faster? A source–sink perspective on growth rate.*J. Exp. Bot.* 67, 31–45. doi: 10.1093/jxb/erv447

Williams, L. E., Lemoine, R., and Sauer, N. (2000). Sugar transporters in higher plants–a diversity of roles and complex regulation. *Trends Plant Sci.* 5, 283–290. doi: 10.1016/S1360-1385(00)01681-2

Zhang, C., Shen, Z., Zhang, Y., Han, J., Ma, R., Korir, N. K., et al. (2013). Cloning and expression of genes related to the sucrose-metabolizing enzymes

and carbohydrate changes in peach. *Acta Physiol. Plant*. 35, 589–602. doi: 10.1007/s11738-012-1100-1

Zhang, C., Tanabe, K., Tamura, F., Itai, A., and Wang, S. (2005). Partitioning of 13C-photosynthate from spur leaves during fruit growth of three Japanese pear (*Pyrus pyrifolia*) cultivars differing in maturation date. *Ann. Bot.* 95, 685–693. doi: 10.1093/aob/mci070

Zhang, H., Wu, J., Tao, S., Wu, T., Qi, K., Zhang, S., et al. (2014). Evidence for apoplasmic phloem unloading in pear fruit. *Plant Mol. Biol. Report*. 32, 931–939. doi: 10.1007/s11105-013-0696-7

Zhang, L.-Y., Peng, Y.-B., Pelleschi-Travier, S., Fan, Y., Lu, Y.-F., Lu, Y.-M., et al. (2004). Evidence for apoplasmic phloem unloading in developing apple fruit. *Plant Physiol*. 135, 574–586. doi: 10.1104/pp.103.036632

Zhang, Y., Li, P., and Cheng, L. (2010). Developmental changes of carbohydrates, organic acids, amino acids, and phenolic compounds in "Honeycrisp" apple flesh. *Food Chem.* 123, 1013–1018. doi: 10.1016/j.foodchem.2010.05.053

Zhao, J., Sun, M., Hu, D., and Hao, Y. (2016). Molecular cloning and expression analysis of a hexokinase gene, MdHXK1 in Apple. *Hortic. Plant J.* 2, 67–74. doi: 10.1016/j.hpj.2016.06.005

Conflict of Interest Statement: The authors declare that the research was conducted in the absence of any commercial or financial relationships that could be construed as a potential conflict of interest.

frontiers in Plant Science

ORIGINAL RESEARCH
published: 09 October 2018
doi: 10.3389/fpls.2018.01439

A Systems Analysis With "Simplified Source-Sink Model" Reveals Metabolic Reprogramming in a Pair of Source-to-Sink Organs During Early Fruit Development in Tomato by LED Light Treatments

*Atsushi Fukushima[1], Shoko Hikosaka[2], Makoto Kobayashi[1], Tomoko Nishizawa[1], Kazuki Saito[1,3], Eiji Goto[2] and Miyako Kusano[1,4]**

[1] RIKEN Center for Sustainable Resource Science, Yokohama, Japan, [2] Graduate School of Horticulture, Chiba University, Chiba, Japan, [3] Graduate School of Pharmaceutical Sciences, Chiba University, Chiba, Japan, [4] Graduate School of Life and Environmental Sciences, University of Tsukuba, Tsukuba, Japan

OPEN ACCESS

Edited by:
Ute Roessner,
The University of Melbourne, Australia

Reviewed by:
Adriano Nunes-Nesi,
Universidade Federal de Viçosa, Brazil
Maria Valeria Lara,
Universidad Nacional de Rosario, Argentina

***Correspondence:**
Miyako Kusano
kusano.miyako.fp@u.tsukuba.ac.jp

Specialty section:
This article was submitted to Plant Metabolism and Chemodiversity, a section of the journal Frontiers in Plant Science

Received: *31 January 2018*
Accepted: *10 September 2018*
Published: *09 October 2018*

Citation:
Fukushima A, Hikosaka S, Kobayashi M, Nishizawa T, Saito K, Goto E and Kusano M (2018) A Systems Analysis With "Simplified Source-Sink Model" Reveals Metabolic Reprogramming in a Pair of Source-to-Sink Organs During Early Fruit Development in Tomato by LED Light Treatments. Front. Plant Sci. 9:1439. doi: 10.3389/fpls.2018.01439

Tomato (*Solanum lycopersicum*) is a model crop for studying development regulation and ripening in flesh fruits and vegetables. Supplementary light to maintain the optimal light environment can lead to the stable growth of tomatoes in greenhouses and areas without sufficient daily light integral. Technological advances in genome-wide molecular phenotyping have dramatically enhanced our understanding of metabolic shifts in the plant metabolism across tomato fruit development. However, comprehensive metabolic and transcriptional behaviors along the developmental process under supplementary light provided by light-emitting diodes (LEDs) remain to be fully elucidated. We present integrative omic approaches to identify the impact on the metabolism of a single tomato plant leaf exposed to monochromatic red LEDs of different intensities during the fruit development stage. Our special light delivery system, the "simplified source-sink model," involves the exposure of a single leaf below the second truss to red LED light of different intensities. We evaluated fruit-size- and fruit-shape variations elicited by different light intensities. Our findings suggest that more than high-light treatment (500 μmol m^{-2} s^{-1}) with the red LED light is required to accelerate fruit growth for 2 weeks after anthesis. To investigate transcriptomic and metabolomic changes in leaf- and fruit samples we used microarray-, RNA sequencing-, and gas chromatography-mass spectrometry techniques. We found that metabolic shifts in the carbohydrate metabolism and in several key pathways contributed to fruit development, including ripening and cell-wall modification. Our findings suggest that the proposed workflow aids in the identification of key metabolites in the central metabolism that respond to monochromatic red-LED treatment and contribute to increase the fruit size of tomato plants. This study expands our understanding of systems-level responses mediated by low-, appropriate-, and high levels of red light irradiation in the fruit growth of tomato plants.

Keywords: *Solanum lycopersicum*, light emitting diode, metabolite profiling, RNA sequencing, light stress, fruit development

INTRODUCTION

Tomato (*Solanum lycopersicum*), a member of the Solanaceae family, is the leading vegetable crop. Supplementary lighting [e.g., fluorescent- and high-pressure sodium lamps, and light-emitting diodes (LEDs)] is used for tomato production in Northern Europe and Canada (for example, see Heuvelink et al., 2006). It can compensate for low rates of photosynthesis and increases both the growth and yield of tomato plants when compared to natural light (Gosselin et al., 1996; Gunnlaugsson and Adalsteinsson, 2006). Most greenhouses and areas without sufficient daily light integral (DLI) require such supplementary lights to maintain the optimal light environment for the stable growth of tomato plants. A seasonal effect of supplementary light was observed throughout the year (except from June to August); it resulted in increases in the tomato yield (Heuvelink et al., 2006). Others documented that supplementary lighting had no- or negative effects (Gunnlaugsson and Adalsteinsson, 2006; Trouwborst et al., 2010). These observations suggest that DLI from natural and supplemental lighting per plant, the light source, and/or the cultivar play an important role in determining fruit growth rates and yield. Also, depending on the crop species and several growth factors (e.g., temperature, CO_2, and air humidity), the light intensity [photosynthetic photon flux (PPF in μmol m^{-2} s^{-1})] should be optimized to provide sufficient supplementary lighting without eliciting leaf stress and associated leaf disorders (Moe et al., 2006; Darko et al., 2014).

Several tomato fruit characteristics, mainly the result of dramatic metabolic shifts during development and ripening, result in a complex system (Carrari and Fernie, 2006; Bovy et al., 2007). Increasing the fruit yield per plant is important but challenging as the molecular mechanism of the source-to-sink balance, a key step toward fruit development, remains largely unclear. The translocation of carbohydrates like sucrose and other nutrients from source to sink is a major determinant of plant growth (Nguyen-Quoc and Foyer, 2001; Paul et al., 2001; Ruan, 2014). Plants strictly regulate the production of photoassimilates and the source-to-sink response to changing environments (Lemoine et al., 2013; Osorio et al., 2014). Of these, sucrose contributes to translocation as a main carbon source in phloem. Tomato plants overexpressing sucrose phosphate synthase (SPS), a key enzyme in the sucrose metabolism, exhibited substantially altered carbon allocation in photosynthetic leaves (Galtier et al., 1993, 1995; Micallef et al., 1995). A reduction in the activity of sucrose synthase (SuSy), which catalyzes the sucrose cleavage in tomato fruit, considerably reduced its sucrose unloading capacity (D'Aoust et al., 1999). A comprehensive and quantitative molecular understanding of the tightly coupled coordination of photosynthesis and sink capacity is important. With respect to the quality of tomato fruit, these systems are closely associated with the phloem loading of sucrose in the source and with unloading in sink tissues via the central carbon metabolism, although generally, photosynthesis in fruit is not essential (Kahlau and Bock, 2008; Lytovchenko et al., 2011).

Transcriptome analysis with microarrays and RNA-sequencing (RNA-Seq) revealed important key factors involved in fruit ripening (Lin et al., 2008; Chung et al., 2010; Nakano et al., 2012; Fujisawa et al., 2014; Nguyen et al., 2014). The integration of transcriptomic and metabolomic approaches demonstrated that the detected primary metabolites, cell wall-related metabolites, and pigments were not strongly correlated with known key genes involved in ripening, but implied a causal relationship between tricarboxylic acid (TCA) cycle intermediates and fruit ripening (Alba et al., 2005; Carrari et al., 2006; Mounet et al., 2009; Osorio et al., 2011). Despite the agricultural importance of the developmental process under supplementary lighting, the comprehensive metabolic and transcriptional behaviors along the developmental period remain to be fully elucidated. Also, their role under artificial supplementary lighting with LEDs (Goto, 2003; Darko et al., 2014) in the regulation of flowering and early fruit development (rather than fruit ripening) remains to be identified quantitatively and systematically.

We present integrative omics approaches to elucidate the metabolomic impact of red LED light of different intensities on single leaves during the early fruit development of tomato plants. We set up a special light-irradiation system, our "simplified source-sink model," which involves a single tomato leaf, a fruit truss, and monochromatic red-LED light delivered during early fruit development; red light is widely used for supplemental lighting. Our findings suggest that the proposed workflow promises to aid in the discovery of key pathways that contribute to increasing the fruit size of tomatoes.

MATERIALS AND METHODS

Plant Material and Growth Conditions

Seeds from tomato (*Solanum lycopersicum* 'Reiyo') were sown in 72-cell trays (Takii Seed, Kyoto, Japan) and grown in a soil mix (Napura Soil Mixes, Yanmar, Osaka, Japan) for 2 weeks in a growth chamber (MKV DREAM, Tokyo, Japan) at 25°C/20°C (light/dark, Japan) and 900 μL L^{-1} CO_2 concentration. The light/dark cycle was 16 h/8 h for 2 weeks. Then the seedlings were transferred to 2.4 l pots and grown in a growth chamber (Asahi Kogyosha, Tokyo, Japan); the PPF level was adjusted to 450–500 μmol m^{-2} s^{-1} when measurements were at the meristem of each tomato plant (light source: ceramic metal halide lamps). *S. lycopersicum* cv. 'Moneymaker' was also used and exposed to the same conditions of cv. 'Reiyo' for fruit measurements. The experiments were performed at Chiba University, Japan.

For LED irradiation, we exposed single leaves for 4 weeks to a red LED panel (23 cm × 12 cm, 18 W, Shibasaki, Saitama, Japan); the peak wavelength was 660 nm (Showa Denko K. K., Tokyo, Japan). To remove the effects of supplemental light from other factors, we removed all leaves and trusses except for the flowers on the second truss, the leaf just below the second truss, and the apical portions of the main shoot at the anthesis stage of the second truss (Hikosaka et al., 2013) (**Supplementary Figure S1**). Each plant was trimmed to bear a single leaf and a truss with three flowers

(**Supplementary Figure S1B**). We used four light intensities at PPF 0-, 200-, 500-, and 1,000 μmol m^{-2} s^{-1} (P0, P200, P500, P1000). Different PPFs were applied to post-anthesis tomato plants for 2 weeks after anthesis (WAA), corresponding to 14 days after anthesis (DAA). Leaf and fruit samples were harvested 0-, 1-, and 2 WAA at the same hour 1600 (JST, Japan Standard Time), corresponding to midday in the growth chamber.

Fruit Measurements

It is known that the fresh weight (FW, in g) of tomato fruit can be estimated from the fruit length, diameter, and height (for example, see Mutschler et al., 1986). Therefore, fruit measurements were taken every week with a digital caliper and recorded as the estimated FW of each fruit. Biological replicates, $n = 3$.

RNA Isolation

Total RNA was isolated using the RNeasy Plant Mini kit (Qiagen, Hilden, Germany) according to the manufacturer's instructions. The concentration, integrity, and extent of contamination by ribosomal RNA were monitored using an ND-1000 spectrophotometer (Thermo Fisher Scientific, Waltham, MA, United States) and a Bioanalyzer 2100 (Agilent Technologies, Santa Clara, CA, United States).

cDNA Library Construction and RNA-Sequencing

Beads with oligo(dT) were used to isolate poly(A) mRNA after total RNA was collected from tomato tissues, leaves, and fruits. Fragmentation buffer was added to cut mRNA into short fragments to serve as templates; random hexamer primer was used to synthesize first-strand cDNA. Second-strand cDNA was synthesized using buffer, dNTPs, RNaseH, and DNA polymerase I. Short fragments were purified with the QiaQuick PCR extraction kit and resolved with EB buffer for end repair and for adding poly(A). The short fragments were connected with sequencing adapters. After agarose gel electrophoresis, suitable fragments were selected as templates for polymerase chain reaction (PCR) amplification. Lastly, the library was sequenced using Illumina HiSeq^{TM} 2000. We complementary analyzed same samples used for microarray analysis per condition ($n = 1$ each).

Sequence Processing, Mapping Reads to a Reference, and Differential Expressions

After Illumina reads were quality-checked, demultiplexed and trimmed, they were clustered per library using RobiNA (Lohse et al., 2012). The remaining short reads used for assembly were aligned to the CDS sequences with Bowtie (Langmead et al., 2009) to identify rRNA contamination; two mismatches were allowed. The ribosomal filtered reads were then aligned against tomato genome sequence SL2.40 (ITAG2.3) (Tomato Genome, 2012). Differentially expressed genes (DEGs) were identified using the DESeq (Anders and Huber, 2010) with default parameters. The level of significance was set at a false discovery rate (FDR) < 0.05 (Benjamini and Hochberg, 1995). We used BiNGO (Maere et al., 2005) to analyze significantly over-represented gene ontology (GO) categories in the DEGs (FDR < 0.05).

Metabolite Profiling

Metabolite profiling by gas chromatography-time-of-flight mass spectrometry (GC-TOF-MS) was performed essentially as described (Kusano et al., 2007a,b, 2011a) but with tomato-specific modifications [see our meta-data (accession no. MTBLS699) in MetaboLights (Kale et al., 2016)]. Briefly, all raw data in netCDF format were pre-processed by hyphenated data analysis (HDA) (Jonsson et al., 2005, 2006) and the obtained data matrix was normalized and summarized using the cross-contribution compensating multiple standard normalization (CCMN) method (Redestig et al., 2009). For metabolite identification, we cross-referenced the obtained mass spectra with gas chromatography with electron impact mass spectrometry (GC-EI-MS) and retention index libraries (Schauer et al., 2005) in the Golm Metabolome database (Kopka et al., 2005) and our own in-house libraries. According to the recommendation (Fernie et al., 2011), detailed information on metabolite identification was shown in **Supplementary Tables S2A,B**. The metabolite profile data (processed data) with our experimental design (phenodata) are also included in **Supplementary Tables S2G,H**. We compared the metabolite responses: (1) treatment comparison, i.e., highlight vs. lowlight treatment and (2) developmental comparison, e.g., 2 WAA vs. 1 WAA under LED irradiation at P1000. The control condition of comparison (1) was P200 red light, whereas 1 WAA was used as control condition in the case of (2). Each sample point was analyzed with six biological replicates.

Statistical Data Analyses for Transcript Profiling by Microarrays and Metabolite Profiling

We used same microarray data that were analyzed in our previous study (Fukushima et al., 2012) [accession#: GSE35020 in NCBI GEO (Barrett et al., 2013)]. We re-analyzed the total of 18 samples (12 leaf- and 6 fruit samples); three biological replicates per sample were used. Data normalization, visualization, and correlation analysis based on Pearson's correlation were performed using R[1] and Bioconductor (Gentleman et al., 2004). DEGs and differentially accumulated metabolites were identified using the LIMMA method, which is based on linear model fitting (Smyth, 2004). The level of significance was set at FDR < 0.05 (Benjamini and Hochberg, 1995). Principal component analysis (PCA) was performed using the pcaMethods package (Stacklies et al., 2007), with log-transformation and unit variance scaling. To visualize the global transcript responses of gene regulatory networks and metabolic pathways of fruit- and leaf samples, we used MapMan software (v3.5.1R2) (Usadel et al., 2005). Genes were classified into different functional categories based on MapMan BIN from the ITAG2.4 annotation. We used BiNGO (Maere et al., 2005) to analyze significantly over-represented GO terms in the DEGs. The level of significance was set at FDR < 0.05 (Benjamini and Hochberg, 1995).

[1] http://www.r-project.org

RESULTS

Scope of the Study and Its Systematic Experimental Design

In preliminary experiments, we studied the fruit weight and leaf area of whole *Solanum lycopersicum* L., 'Reiyo' plants exposed or not exposed to red LED irradiation. We first recorded the fruit weight along the developmental stages 1-, 2-, 3-, and 4 WAA of plants grown without supplemental LED lighting (**Supplementary Figure S2A**). Under normal light (average P500, metal halide lamp without supplemental LED light), we observed a remarkable increase in the fruit weight between 1- and 2 WAA, suggesting that the period was critical for early fruit development and the time of cell expansion. When we recorded the fruit weight and leaf area of whole plants grown under supplemental red LED light (P1000), we detected no effect on the fruit biomass at 2 WAA (**Supplementary Figure S2B**).

Based on these preliminary findings we focused on 2 WAA and developed a custom LED light system to gain insights into molecular regulation governing early tomato fruit development and biologically relevant changes in the storage pattern and translocation under different light conditions. Our "simplified source-sink model" (Hikosaka et al., 2013) is comprised of a single tomato leaf and fruit truss (**Supplementary Figure S1**) and can be used to deliver red or other color light irradiation in greenhouses or under closed growth conditions, e.g., in climate chambers. Although we delivered 100% of red LED light to the plants, leaves exhibited few stress signs under the P200 condition. However, after P500 and P1000 high light (HL) exposure, they manifested stress signs and accompanying disorders, including leaf curling and senescence (**Supplementary Figure S3**), due mainly to high light intensity and seemingly enhancement of translocation.

Enhanced Light Intensity Strongly Affects Leaf and Fruit Growth in Tomato

Using our simplified source-sink model we next assessed variations in the fruit size and shape due to different light intensities. **Figure 1A** shows a representative fruit shape developed under red LED irradiation (P200, P500, and P1000) in 2 WAA. Although the tomato plants were grown simultaneously in a controlled growth chamber under artificial conditions, there were variations in the fruit morphology due to uncontrollable factors affecting fruit set (**Supplementary Table S1**). For example, the developmental stage at P1000 irradiation in 4 WAA can correspond to breaker (in some case, it corresponds to red ripe). In the case of P500 in 4 WAA, the stage corresponds to mature green. The mean weight, height, and width were statistically greater after HL- than P200 treatment ($p < 0.05$, Welch's t-test) (**Figure 1B**). We also evaluated variations in the fruit size and shape obtained under the same conditions in a different year (i.e., independent *S. lycopersicum* L. 'Reiyo' experiments) (**Supplementary Figure S4**). *S. lycopersicum* cv., 'Moneymaker,' exposed to the same conditions also exhibited this tendency (**Supplementary Figure S5**). Our findings suggest that treatment with red LED light exceeding P500 is sufficient for fruit growth in tomato plants grown under our artificial conditions.

Overview of Metabolite and Transcript Responses to High Light Irradiation

To study small-molecule metabolites and gene expressions during early fruit development under red LED light with different light intensities, we performed global metabolite and transcript profiling using the experimental designs of an established GC-MS method (Kusano et al., 2007a,b), Illumina-based RNA-Seq, and previously reported microarrays (Fukushima et al., 2012) (**Supplementary Figures S6–S8**). To visualize the extent of metabolomic and transcriptomic changes elicited by different light intensities, we performed PCA and applied the data matrices of the metabolite- and transcript profiles separately. The PCA score scatter plot revealed that the strong impact on metabolite levels in accordance with observance of the presence or absence of light along with PC1 (**Figures 2A,B**). RNA-Seq data (**Supplementary Figure S9**) also showed different clustering groups based on tissue-dependent differences in the PC1 axis, while growth stages with PC2 (**Figure 2C**). When we focused on light intensity-dependent metabolomic changes in fruits, we found that samples exposed to HL conditions were clustered, while samples with light treatments were clearly separated from dark samples (P0). These observations suggest that while our HL condition strongly affected the metabolite accumulation in tomato plants, its effect on developing fruit was not as large.

Comparative Analyses of Metabolite Profiling of Tomato Fruit- and Leaf Samples Under Different Light Intensities

Our broad-range metabolite analysis identified HL-responsive metabolites and revealed changes in metabolite levels throughout the early fruit-development stage (**Figure 3**). We first focused on metabolites that exhibited a statistically significant difference when the plants were grown under HL and under control conditions (**Table 1** and **Supplementary Table S2**). When we compared between P1000 and P200 light intensities, we found that at P1000, sugars including glucose, fructose, and trehalose and cell wall related metabolites like xylose and mannose markedly increased in 1 WAA fruits while aromatic amino acids such as phenylalanine, tryptophan, and tyrosine, were decreased. There were fewer HL-responsive metabolites in 2 WAA than 1 WAA fruits, resulting in 10 significantly changed metabolites. Inverse changes were observed in the metabolite levels, for example, phenylalanine and tyrosine were increased in response to HL.

Except at 2 WAA, the trend observed in P500 and P1000 fruits was similar. Fruits examined in 2 WAA did not show a significant increase in metabolites; mainly polyol and some hydroxyl acids were decreased. Sucrose, glucose, and xylose increased in response to HL. The significantly increased organic acids in 1- and 2 WAA leaves exposed to HL were citrate, malate, succinate, quinate, and glycerate. Methionine levels in young leaves dramatically decreased in response to HL. In 1 WAA leaves, P500 HL largely affected the metabolome; the number of

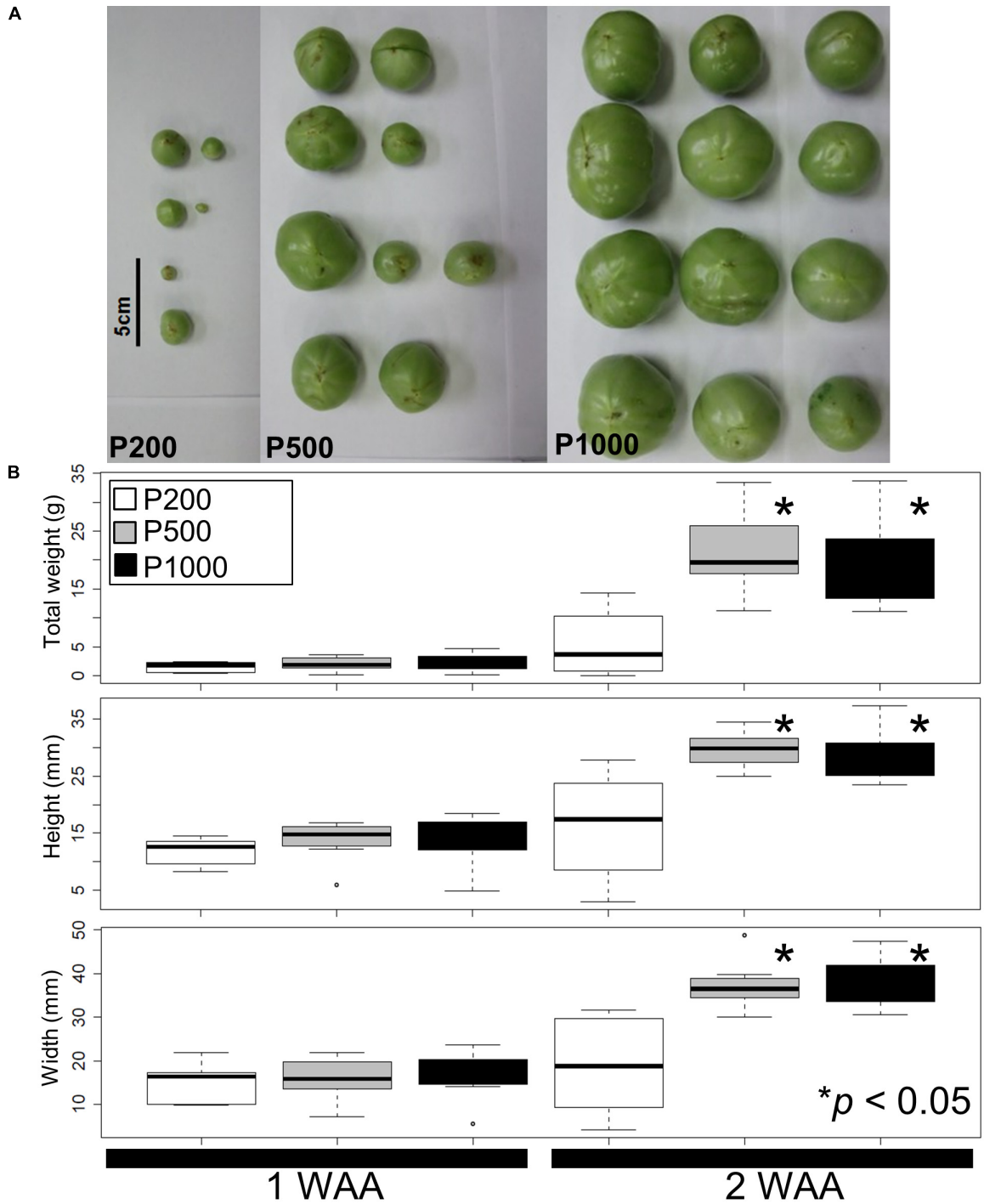

FIGURE 1 | Fruit size and shape variations elicited by different light intensities. **(A)** A representative fruit shape developed under red LED panels (P200, P500, and P1000) in 2 WAA. Scale bar: 5 cm. **(B)** Measured tomato fruit sizes. Statistically significant differences between fruits exposed to light intensities at P200, P500, and P1000. We used a box and whisker plot, a graphical summary of a distribution. This plot can visualize the minimum, lower and upper quartiles (25% and 75%), median, and maximum of data. Regarding extreme values, outliers may be displayed as open circles. Data show the mean of the total weight, height, and width calculated with the Welch *t*-test. Differences of $^*p < 0.05$ were considered statistically significant. The samples were used for metabolite profiling. The results indicate that treatment with higher than P500 red LEDs is sufficient for fruit growth under our artificial conditions. Biological replicates, $n = 3$. WAA, week after anthesis.

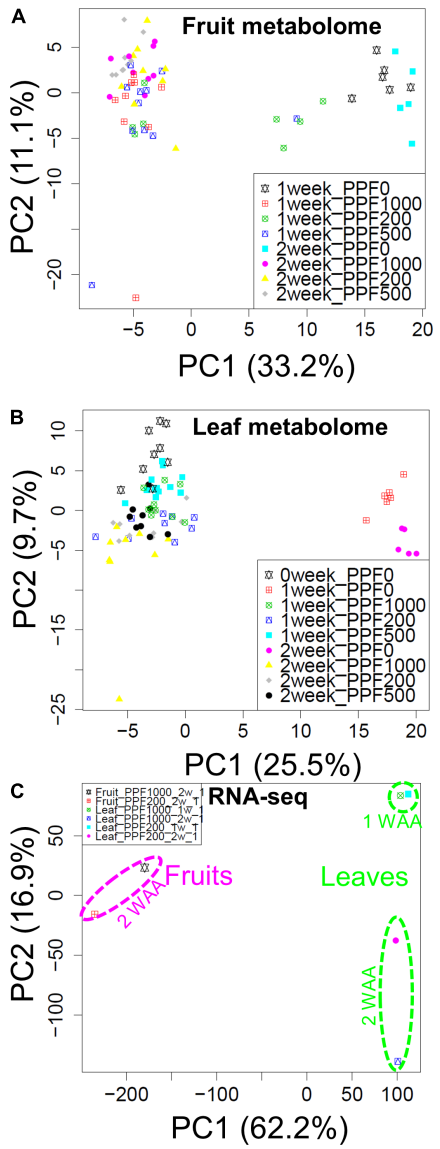

FIGURE 2 | Overview of the transcript and metabolite responses. Score scatter plots of the fruit metabolome **(A)**, and the leaf metabolome **(B)** obtained by GC-TOF-MS, and of the transcriptome obtained by Illumina-based RNA-Seq **(C)**. We observed changes in the metabolite composition of fruits and leaves in the presence or absence of light (PC1). RNA-Seq data also revealed different cluster groups according to tissue-dependent differences in the PC1 axis. The recorded changes in the growth stages were observed under PC2. Biological replicates, n = 5–6 for metabolite profiling and n = 1 for transcript profiling obtained by RNA-Seq analysis.

significantly accumulated metabolites was higher than at P1000 HL although we observed a similar tendency at P500 and P1000.

Comparison of 1- and 2 WAA fruits showed that sucrose decreased under HL while glucose and fructose increased in an essentially linear manner during fruit development and in response to HL (**Figure 3** and **Supplementary Table S2E**). Cell-wall related metabolites like xylose, mannose, and arabinose increased during fruit development. Irrespective of the light intensity, the level of most sugars, sugar phosphates, and some organic acids like citrate and aconitate was higher in fruits than leaves (**Supplementary Table S2F**). Most highly accumulated amino acids in fruits were γ-amino butyrate (GABA), glutamine, asparagine, branched chain amino acids (valine, leucine, and isoleucine), beta-alanine, and methionine.

Genome-Wide Transcript Profiling Revealed a Wide Range of Variations in Gene Expression and Reflected Changes in Regulatory Networks Under High Light Treatment

We assessed the comprehensive transcript abundance using microarrays and RNA-Seq (**Supplementary Tables S3**, **S4**). To mitigate issues associated with the coverage of gene annotation in microarrays we also performed RNA-Seq with the Illumina-based platform (**Supplementary Figure S9**). Using both datasets we identified DEGs. At P1000 and P200, microarray-based approaches detected 137 up- and 252 down-regulated genes, respectively, in fruits (**Figure 4A** and **Supplementary Table S5**). GO enrichment analysis in "Biological Process" showed that the 137 up-regulated genes were significantly enriched in "ripening (FDR = 3.2E-3)" and "cell wall modification (FDR = 3.2E-3)," whereas the 252 down-regulated genes were related to, for example, "cell division (FDR = 1.8E-2)" and "microtubule-based process (FDR = 1.4E-2)." Ripening-related genes encoded pectin methylesterase PME2.1 (probeset ID = Les.3630.1.S1_at), expansin 1 (probeset ID = Les.191.1.S1_at), and PME1.9 (3 probeset IDs: Les.3122.1.S1_a_at, Les.3122.2.A1_at, and Les.3122.2.A1_a_at). The RNA-Seq-based approach identified 60 up- and 340 down-regulated genes between P1000 and P200 treatments in tomato fruit (**Figure 4B** and **Supplementary Table S5B**). GO enrichment analysis using DEGs obtained by RNA-Seq indicated that the 60 up-regulated genes were involved in the "cell wall macromolecule catabolic and metabolic process (FDR = 5.1E-4)" and in lipid localization/transport (FDR = 0.047) (**Figure 4B**). The 340 down-regulates genes were related to "proteolysis (FDR = 1.1E-11)" and "negative regulation of molecular function (FDR = 9.3E-7)."

RNA-Seq of 1 WAA leaves also revealed that DEGs that were up-regulated at P1000 and were related to biological processes like "regulation of transcription (FDR = 1.2E-4)" included genes that encode MYB-related transcription factor, WRKY-like MYB-related transcription factor, and heat-shock factor protein. Our microarray data supported this observation (**Supplementary Table S5**). The number of down-regulated DEGs was larger than of up-regulated DEGs in P1000 2 WAA leaves; we only observed eight up-regulated DEGs. Our analysis for down-regulated genes significantly over-represented "glycerol metabolic process (FDR = 7.2E-4)," "alditol metabolic process (FDR = 7.2E-4)," and "polyol metabolic process (FDR = 1.3E-2)." Together, the results of our global transcript analysis suggest the presence of highly complex transcription dynamics in tomato fruits and leaves exposed to P1000 and P200 and examined at different

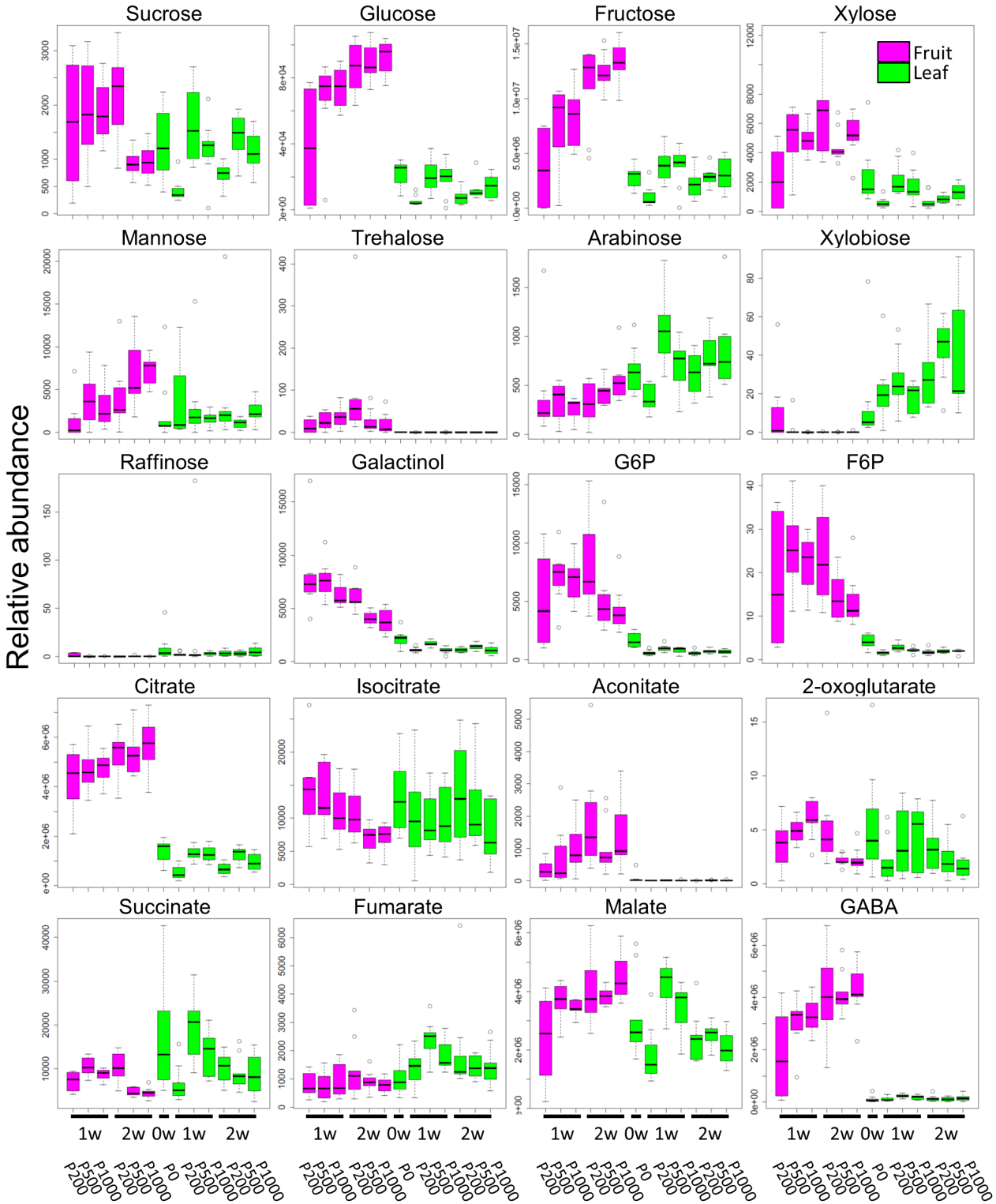

FIGURE 3 | Continued

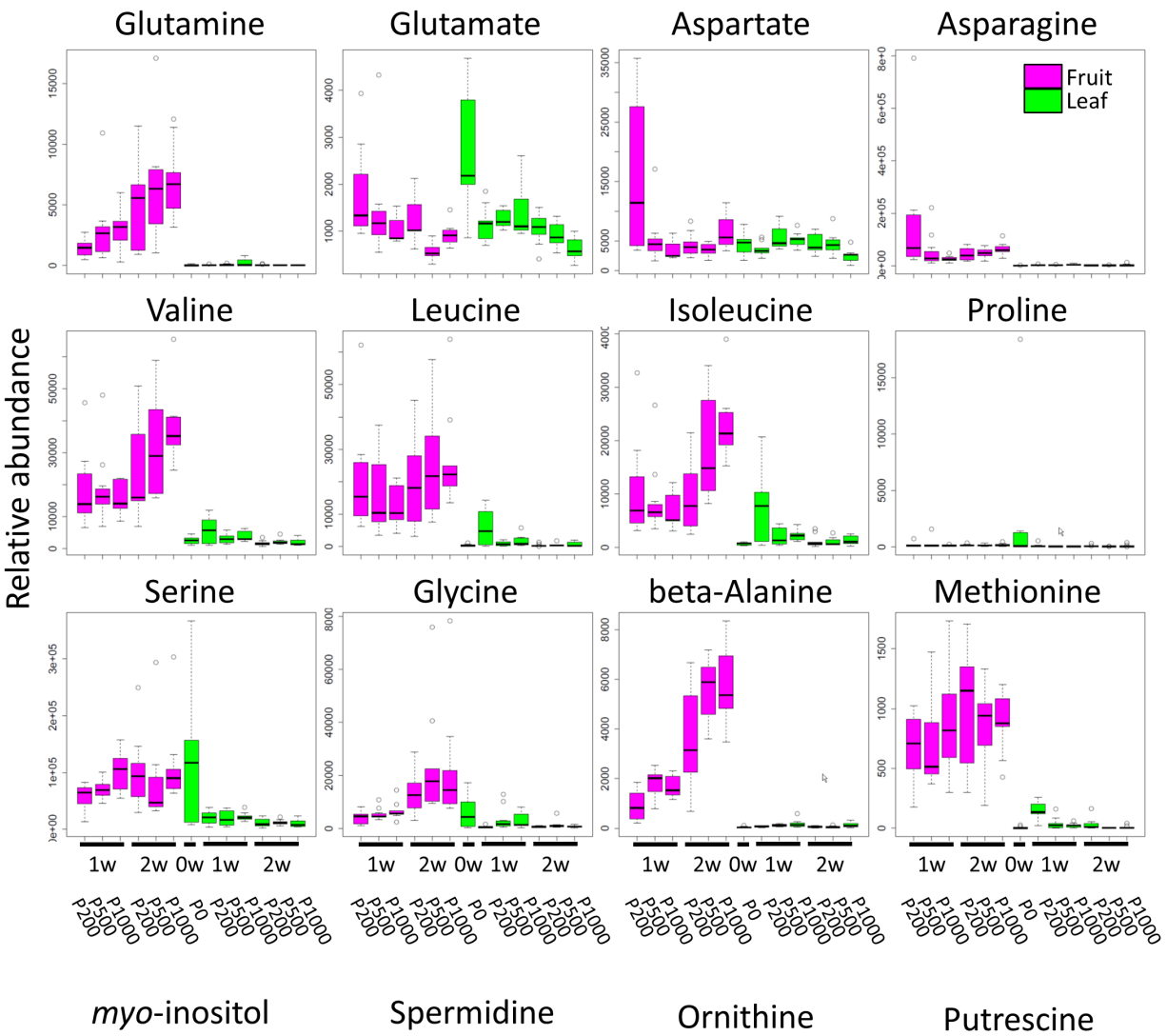

FIGURE 3 | Comparative analyses of metabolite profiling of fruit- and leaf samples of tomato plants grown under different light intensities (P0, P200, P500, and P1000). To summarize metabolite profile data, we used a box and whisker plot, a graphical summary of a distribution. This plot can visualize the minimum, lower and upper quartiles (25% and 75%), median, and maximum of each metabolite data. Regarding extreme values, outliers may be displayed as open circles. In each boxplot, the investigated time-points are 1 WAA and 2 WAA (*X*-axis). The relative abundance on the *Y*-axis shows the normalized responses of the metabolite peaks obtained by GC-TOF-MS. Typical metabolite classes such as sugars, sugar alcohols, and amino- and organic acids are shown. Magenta- and green boxes represent samples from fruit and leaves, respectively. Biological replicates, n = 5–6. WAA, week after anthesis.

developmental stages. These findings are reflected as the systems-level response to HL under artificial condition using red LEDs.

Tomato Leaf and Fruit Samples Exhibited Inverse Changes in the Expression Patterns Involved in Light Reactions, Secondary Metabolism, and Cell-Wall Biosynthesis

For a comprehensive study of transcript level changes in metabolic pathways, we visualized our RNA-Seq data using MAPMAN (Thimm et al., 2004; Usadel et al., 2005). **Figure 5** presents an overview of the transcript profiles of 2 WAA fruit- and leaf samples exposed to P1000- or P200 light treatment (**Supplementary Figure S10**). MapMan analysis demonstrated that, as a whole, changes in the expression patterns involved in light reactions, the secondary metabolism, and cell-wall biosynthesis exhibited an inverse tendency in fruit- and leaf samples. The marked up-regulation in the transcript level of P1000 fruits was associated with light reactions; in leaves those genes were down-regulated in response to HL. In leaves, genes involved in cell-wall biosynthesis and secondary metabolism were up-regulated, in fruits they were down-regulated.

To shift our focus onto dissecting the metabolic balance in fruit- and leaf samples as a whole plant system, we used Spearman's correlation ($p < 0.05$) to identify metabolites that

TABLE 1 | Metabolite responses of tomato fruits to high light treatment.

	Log_2FC	FDR
Fruit 1 WAA, P1000/P200		
Trehalose	4.8	1.10E-02
Mannose	4.3	2.90E-03
Fructose	3.8	8.70E-05
Glucose	2.5	2.30E-05
Xylose	2.2	3.10E-04
Butyro-1,4-lactam	2.1	9.70E-04
GABA	2	1.70E-03
Aconitate	1.9	2.70E-02
Dihydrouracil	1.5	7.90E-03
Threonate	1.4	2.90E-02
Aspartate	−1.7	7.50E-05
Lysine	−1.9	3.90E-02
Asparagine	−2.2	5.90E-04
Tryptophan	−2.4	4.60E-03
Alpha-tocopherol	−2.7	1.60E-02
Phenylalanine	−2.8	4.70E-04
Tyrosine	−3	2.70E-02
Xylobiose	−5.9	9.60E-04
Fruit 2 WAA, P1000/P200		
Tyrosine	3.3	2.50E-02
Phenylalanine	1.9	3.00E-02
Isoleucine	1.5	4.10E-02
Arabinose	1.4	3.00E-02
Threonine	1.1	4.10E-02
Succinate	−1.2	9.00E-03
Shikimate	−1.6	9.00E-03
Threonate	−2	6.20E-03
Dihydrouracil	−2.1	4.10E-04
Galacturonate	−6.3	2.00E-02

The listed metabolites exhibited a statistically significant difference under HL and control conditions at 1- and 2 WAA [LIMMA (Smyth, 2004); $|log_2FC| \geq 1$, false discovery rate (FDR) < 0.05]. Log_2FC means logarithmically transformed values of fold-changes (e.g., P1000/P200). See also ***Supplementary Table S1****. HL, high light; FC, fold-change.*

exhibited a significant correlation in fruit and leaf samples across time. We found that fumarate showed a negative correlation between fruit and leaf samples, while 2-oxoglutarate exhibited a positive correlation (**Figure 6**).

DISCUSSION

To enhance the growth/yield and to improve the fruit quality of tomato plants, a physiological understanding of their metabolic and transcriptional responses during fruit development under artificial supplementary LED light is necessary. In our "simplified source-sink model" (Hikosaka et al., 2013) (**Supplementary Figure S1**), each tomato plant is pruned to have a single leaf and one fruit truss. To gain insights into the storage patterns and translocation in developing tomato fruits in response to environmental perturbation by HL irradiation (**Figure 1**), we performed sophisticated molecular phenotyping of samples exposed to red-LED lighting (660 nm peak). Metabolite and transcript analysis using GC-MS and RNA-Seq/microarrays enhanced our understanding of the cellular response of the fruit storage metabolism associated with primed fruit ripening and cell-wall biosynthesis, the stress response, and photosynthesis in response to the light wavelength and to HL stress imposed by our artificial irradiation system (**Figure 2**). Our findings emphasize the tightly coupled coordination of photosynthesis and sink capacity and provide an important list of the candidate metabolites, transcripts, and key pathways that contribute to the cellular metabolic shift in the course of early fruit development.

Our "simplified source-sink model" is appropriable because it removes as many unwanted variations due to unstable greenhouse conditions as possible. We used this experimental system in our earlier co-expression network analysis to infer candidate functional genes in tomato plants (Fukushima et al., 2012). Applying the experimental system also enabled to compare the extent of changes of light intensity, the photosynthesis rate, and fruit growth in tomato plants grown under two types of supplementary LED lighting methods (Hikosaka et al., 2013). First, they assessed the effects of LED light intensity on the fruit set, dry weight, dry mass ratio of a tomato fruit, and the net photosynthetic rate of a center leaflet, i.e., by applying the same method presented in the study. The second experiments in the study assessed whether number of leaves irradiated by supplemental lighting made effects on the photosynthetic rate of a whole tomato plant. As the light irradiation per leaf could increase photosynthetic rate in both experiments, the present study performed comprehensive molecular phenotyping of samples collected under different light intensities by applying the simplified experimental design.

An artificial environment can cause plant developmental and morphological differences, and their responses can mask essential traits. The plant response to a combination of multiple abiotic stresses in the field condition cannot be directly extrapolated from that to each stress exposed individually (Mittler, 2006; Mishra et al., 2012). In addition, we notice an emerging area, so-called 'Field Omics' (Alexandersson et al., 2014), trying to monitor and analyze different molecular behavior of samples harvested from crop field trials. The current field-omics approaches face a difficult and fundamental problem causing from high variance influenced by temporal and spatial differences in field trials. Such intrinsic heterogeneity in each field overwhelms effect of the experimental perturbations. At least partially, our data can be used as one of references to learn about the differences in molecular mechanisms between field- and laboratory tests, although our system greatly differs from the field trials.

To increase and improve light distribution, supplementary lighting is widely used as it can promote a good photosynthetic response and fruit growth in the lower plant layers. Others (Gosselin et al., 1996; Hovi et al., 2004; Gunnlaugsson and Adalsteinsson, 2006; Hovi-Pekkanen and Tahvonen, 2008; Pettersen et al., 2010) reported the positive effects of supplemental lighting on fruit growth and yield. Based on our evaluation of the tomato fruit size and of shape variations, exposure to around P500 red LED light is sufficient for fruit

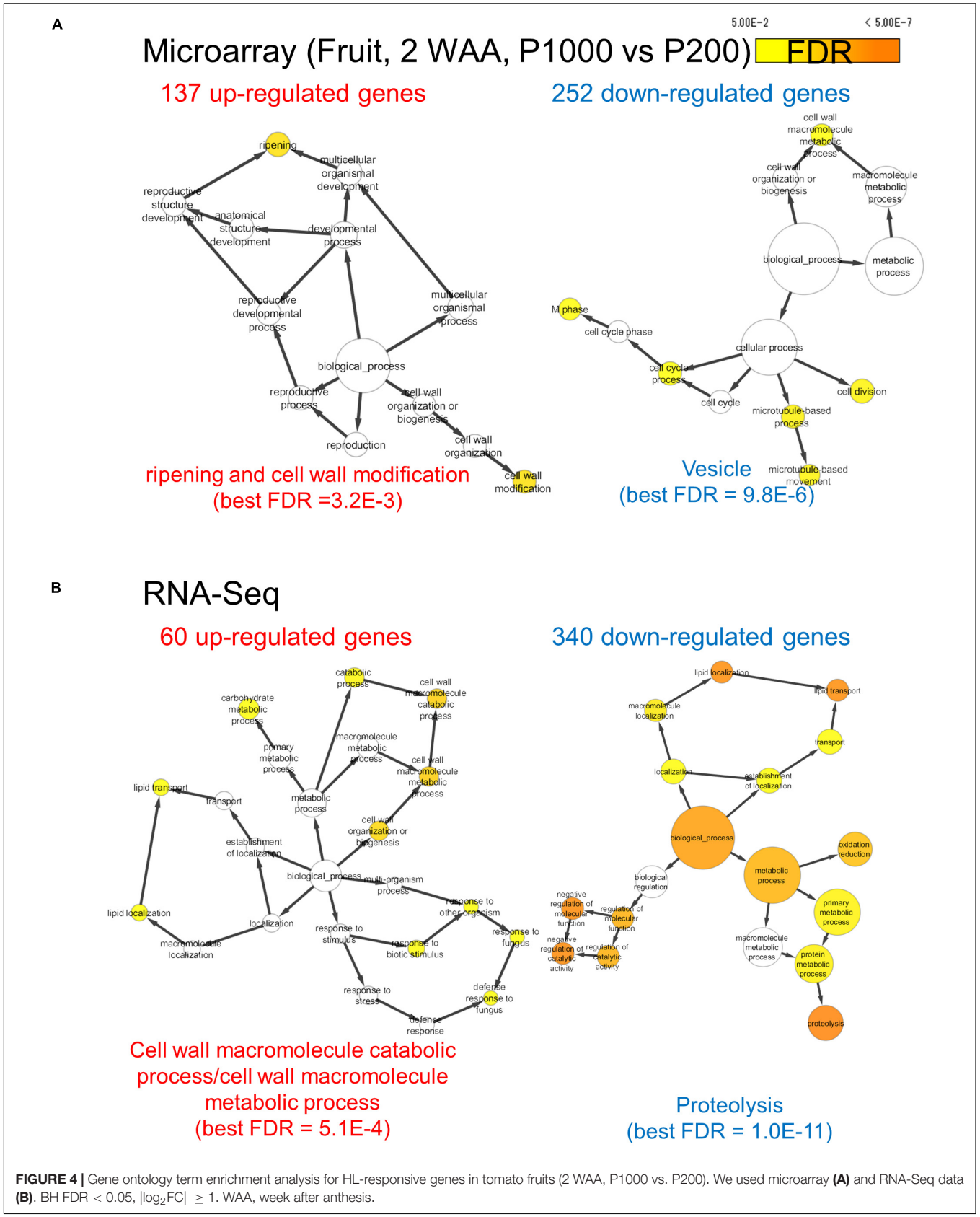

FIGURE 4 | Gene ontology term enrichment analysis for HL-responsive genes in tomato fruits (2 WAA, P1000 vs. P200). We used microarray **(A)** and RNA-Seq data **(B)**. BH FDR < 0.05, $|\log_2 FC| \geq 1$. WAA, week after anthesis.

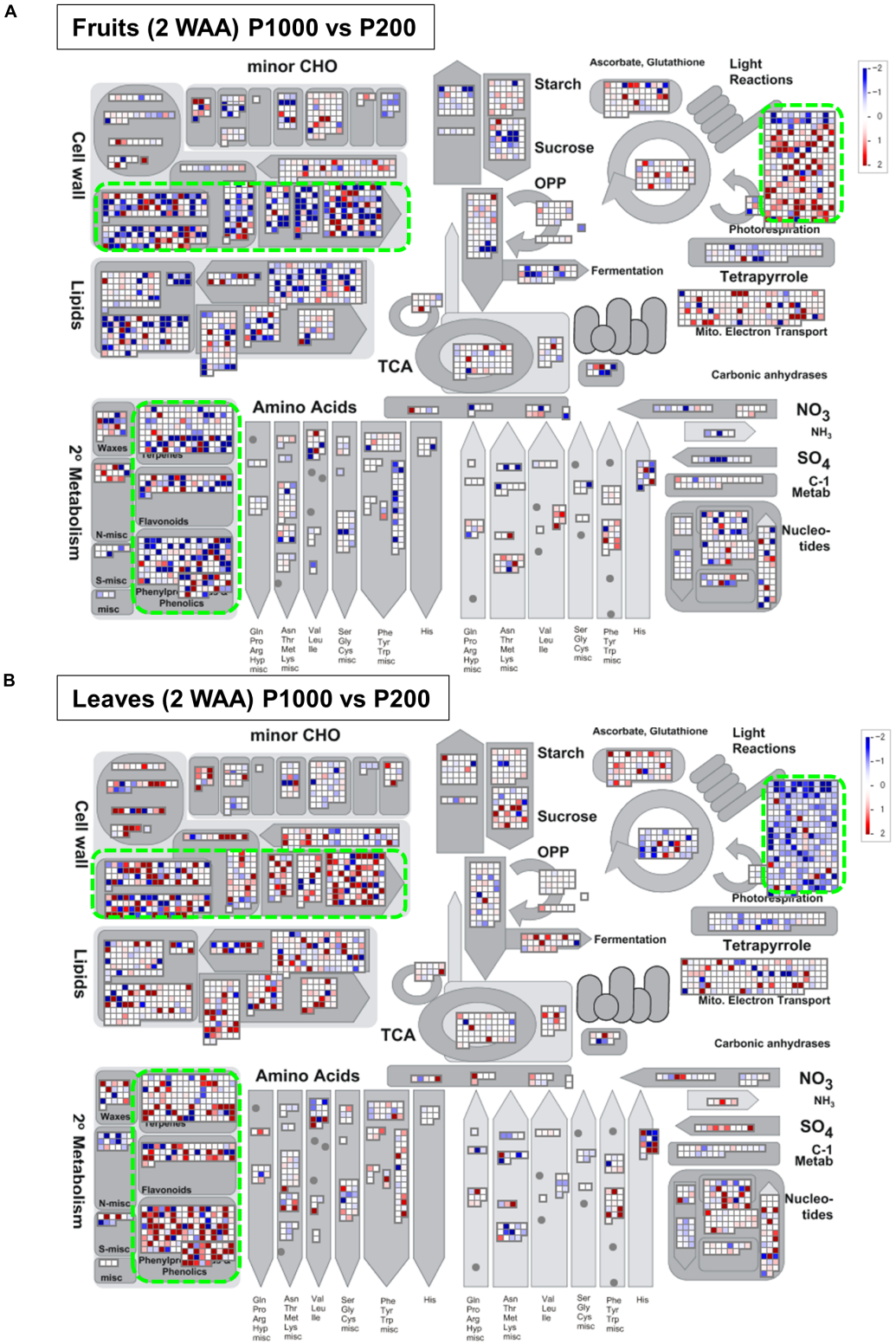

FIGURE 5 | Overview of the transcript profiles based on Illumina-based RNA-Seq. The RNA-Seq data from **(A)** fruit- and **(B)** leaf samples were obtained with MAPMAN software (http://mapman.gabipd.org/web/guest/mapman) (Thimm et al., 2004; Usadel et al., 2005). The fold-changes are presented in different colors where red = up-regulated and blue = down-regulated by P1000 treatment. The results show that the changes in the expression patterns involved in light reactions, the secondary metabolism, and in cell-wall biosynthesis were inverse in fruit- and leaf samples (green rectangles). WAA, weeks after anthesis.

growth not only with respect to *S. lycopersicum* L. 'Reiyo' but also *S. lycopersicum* cv. 'Moneymaker' (**Supplementary Figures S3–S5**). To confirm whether this observation is cultivar-dependent or independent, a larger number of samples and cultivars should be needed in a future study. As we used only monochromatic red LED panel in this study, future studies will also focus on other light quality treatments (e.g., blue and mixture of red and blue).

Our study highlighted metabolic shifts in the carbohydrate metabolism and in several key pathways that may contribute to early fruit development under HL condition (**Figures 2–4**). A wide range of plant metabolic responses to various stresses has been studied by metabolomic- and transcriptomic approaches (Shulaev et al., 2008; Urano et al., 2010; Obata and Fernie, 2012; Nakabayashi and Saito, 2015; Noctor et al., 2015). While plants need light for photosynthesis and their healthy growth, it can damage plant cells; strong light irradiance is an abiotic stress factor. Genome-wide analyses can be used to characterize plant stress responses to high (excess) light stress and it can contribute to enhancing our understanding of stress-signaling pathways and the central metabolism including glycolysis, the TCA cycle, and photorespiratory pathways (Obata and Fernie, 2012). Besides identifying HL stress-responsive metabolites like sucrose, inositol, and GABA in tomato leaves, we found that HL stress (both P1000 and P500) led to dramatic decreases in aromatic amino acids in fruits at the early developmental stage (**Table 1** and **Supplementary Table S1**). We also showed that the expression patterns associated with light reactions, the secondary metabolism, and cell-wall biosynthesis exhibited inverse changes when we compared fruit- and leaf samples (**Figure 5**). The coordinated expressions associated with light reactions indicate functional photosynthesis in immature green fruit of tomato plants, which is consistent with early reports (Piechulla et al., 1987; Wanner and Gruissem, 1991; Schaffer and Petreikov, 1997; Alba et al., 2004; Kahlau and Bock, 2008; Lytovchenko et al., 2011). In fruits, down-regulated genes were involved in cell wall degradation. For example, there were down-regulated genes encoding a polygalacturonase and a pectate lyase. Both genes are known to be up-regulated and their activities become dominant during tomato fruit ripening (Cheng and Huber, 1997). In leaves, the coordinated expressions involved in phenylpropanoid- and flavonoid biosynthesis included up-regulated genes encoding chalcone synthase (CHS) and dihydroflavonol 4-reductase (DFR). This implies that the both early flavonoid biosynthetic pathway- and the more anthocyanin-specific genes response to mitigate high light stress (Wulff-Zottele et al., 2010; Caldana et al., 2011; Kusano et al., 2011b).

We observed positive correlation relationships of 2-oxoglutarate between fruit and leaf samples (**Figure 6**). Recent works based on metabolite flux analysis and metabolic network models demonstrated that metabolite provision via TCA cycle has been operated in response to demand of physiological status in the cell (Sweetlove et al., 2010). Among the intermediates in TCA cycle, 2-oxoglutarate is a key compound relating to carbon-nitrogen metabolism (Hodges, 2002; Foyer et al., 2011; Araujo et al., 2014). Antisense of 2-oxoglutarate dehydrogenase complex, involving in enzyme reaction of 2-oxoglutarate as a substrate, exhibited reduction of tomato fruit biomass (Araujo et al., 2012). After inhibiting 2-oxoglutarate dehydrogenase complex in potato tuber, there was the significant decrease in the level of 2-oxoglutarate, while fumarate level was unchanged (Araujo et al., 2008). These observations imply that at least 2-oxoglutalate level and biomass of reproductive/storage organs are likely to be positively coordinated in *Solanaceae* such as tomato and potato.

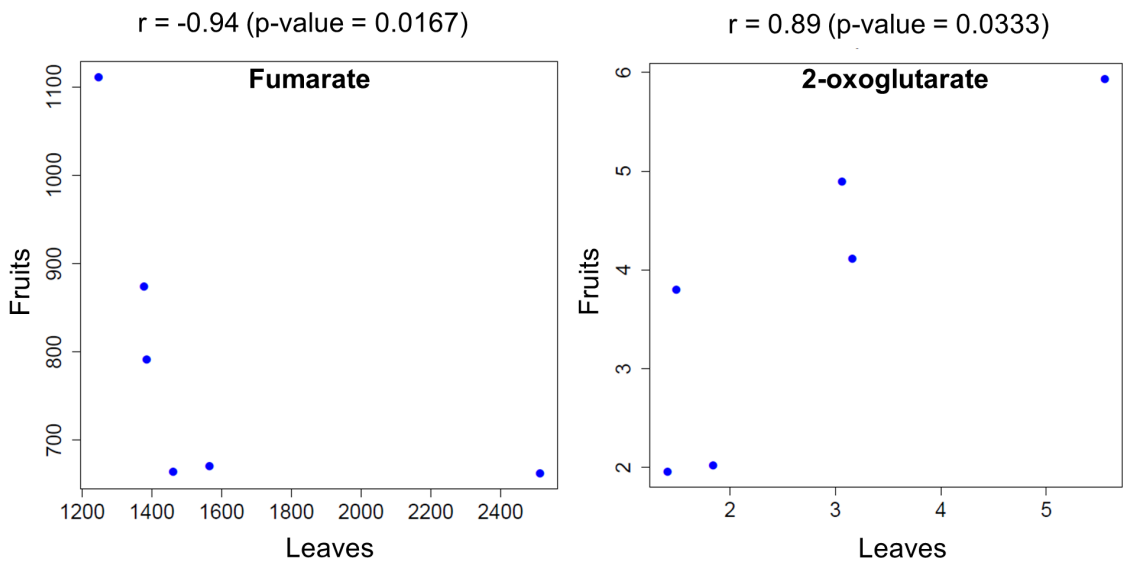

FIGURE 6 | Metabolites that were significantly correlated between fruit- and leaf samples across the examined time points. Circles represent the mean level of metabolites obtained at each time point for plants exposed to different light intensities.

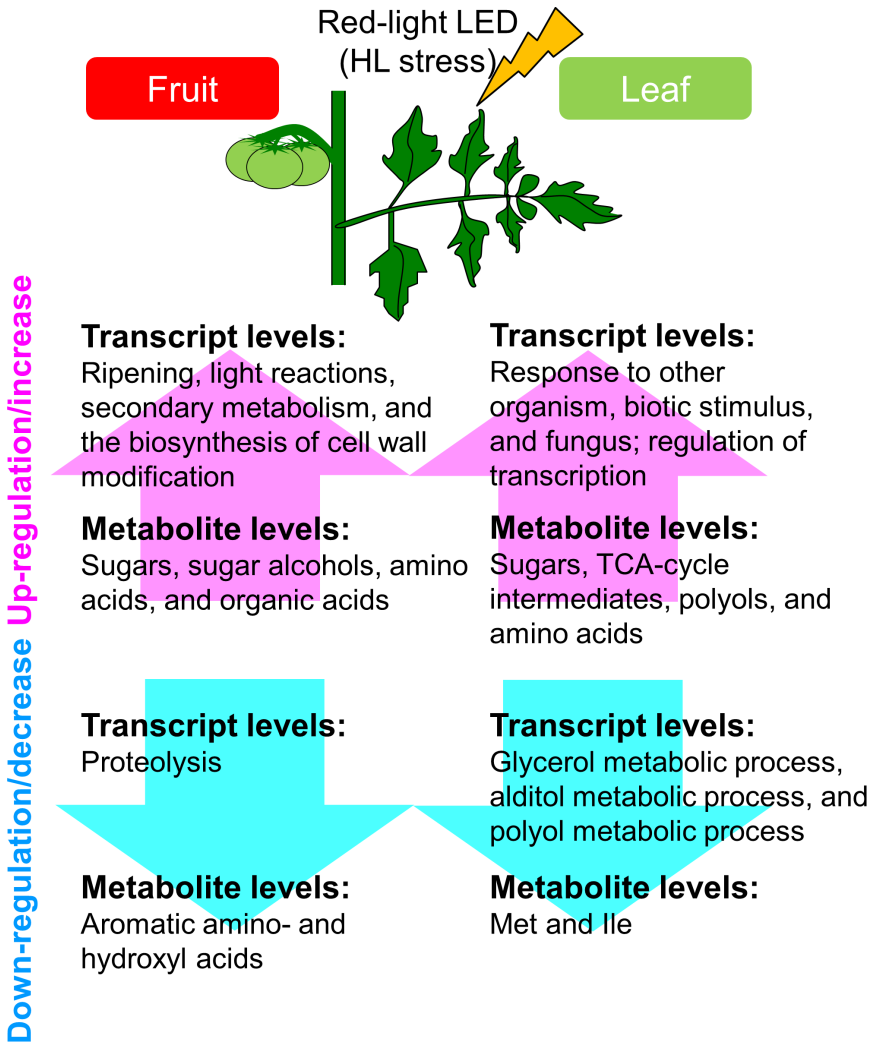

FIGURE 7 | Schematic summary of the metabolic and transcriptional responses to high light treatment in 'trimmed tomatoes' grown under artificial light. Transcript profiling performed with microarrays and RNA-Seq showed that the expression patterns involved in light reactions, the secondary metabolism, and in cell-wall biosynthesis exhibited changes that tended to be inverse between fruit- and leaf samples. Metabolite profiling revealed that sugars and some organic acids, citrate, aconitate, and malate increased along the developmental stages in fruits. Amino acids like Gln, Val, Leu, Ile, and beta-alanine were abundant in fruits and tended to increase in the course of fruit development.

Attention has long been focused on striking shifts in cell-wall composition and pigments (Rose et al., 2004), the strict control of climacteric fruit ripening by phytohormones (Alba et al., 2005; Barry et al., 2005), source-sink regulation (Do et al., 2010), and the physiological transition during the parallel differentiation of photosynthetically active chloroplasts into chromoplasts, (for example, see Klee and Giovannoni, 2011; Pesaresi et al., 2014) that occur during development and ripening of tomato plants. Comprehensive molecular phenotyping using transcript and metabolite profiling showed that *Aux/IAA* and *ARF* genes play an important role in triggering the fruit set program (Wang et al., 2005; Rohrmann et al., 2011). Critical aspects of metabolic regulatory mechanisms, especially the central metabolism that controls fruit development in tomato plants, have been studied (Carrari et al., 2006; Osorio et al., 2011). Steinhauser et al. (2010) used a near-isogenic line population derived from a cross between *S. lycopersicum* 'M82' and *S. pennellii* to compare changes in the enzyme activity levels that can affect the plant metabolism during fruit development. The studies stressed that the plant metabolism and source-sink interaction can be strongly affected by genetic and environmental perturbations and their interactions.

Broad metabolite profiling that combines the use of multiple analytical platforms and our proposed system is required for assessing the plant secondary or specialized metabolism because, in response to artificial LED, changes in the protectants, antioxidants, and other pigments/nutrients like lycopene are largely unclear. A significant difference between our- and earlier studies is the use of LEDs to inspect and capture the precise responses to HL treatment of tomato leaves and

fruits. Specific wavelengths and bandwidths generated by our red LEDs yield the specific red spectrum more efficiently than red filters combined with other light sources and elicit specific plant growth. The light spectrum strongly affects plant growth and development (Goto, 2003; Darko et al., 2014; Kitazaki et al., 2018) and the blue light spectrum near UV may increase the level of polyphenols such as anthocyanin as protectants and/or antioxidants (Seyoum et al., 2006). Massa (2008) suggested that certain light wavelengths may help to protect plants from attacks by insects and pathogens that elicit plant diseases.

Finally, under strictly controlled systems and LEDs, tomato plants exhibited system-level dynamic behaviors in the metabolism (**Figure 7**). This was a precise plant response to the supplemental light source, i.e., red LED light, we used, and yielded new insights that differed from findings made when conventional filters were applied to broad-spectrum light. Our approaches avoid direct, unwanted large-scale effects resulting from unstable greenhouse conditions and different light intensities. Our strategy helps to deepen our understanding of systems-level responses during the growth of tomato fruit and provides fundamental resources for further studies to investigate the molecular basis of the high plasticity of the plant metabolism.

DATA AVAILABILITY

Transcriptome datasets generated in this study are downloadable from the NCBI Sequence Read Archive (SRA) with the accession number DRA001843. Microarray GeneChip data are available at the NCBI GEO (GSE35020) as described in our previous study (Fukushima et al., 2012). All metabolite data (*.netCDF format) are also downloadable from MetaboLights (Kale et al., 2016) (accession no. MTBLS699).

AUTHOR CONTRIBUTIONS

AF, SH, and MiK designed and performed the statistical data analyses and interpreted the data, and wrote the manuscript with contributions from the other co-authors. MiK, MaK, TN, and KS performed the transcript and metabolite profiling. SH and EG conducted and analyzed the measurement of physiological data. All authors read and approved the final manuscript.

FUNDING

This work was supported by National Bioscience Database Center (NBDC) , Japan Science and Technology Agency (JST) (Project ID 18062862), Elucidation of biological mechanisms of photoresponse and development of advanced technologies using light sponsored by Ministry of Agriculture, Forestry and Fisheries (MAFF) and by the "Sustainable Food Security Research Project" in the form of an operational grant from the National University Corporation.

ACKNOWLEDGMENTS

We thank Drs. Thomas Moritz, Pär Jonsson, and Hans Stenlund from the Umeå Plant Science Centre (Umeå, Sweden) and Umeå University (Umeå, Sweden) for their assistance with the HDA and the raw-data analysis (RDA), Mr. Koji Takano and Ms. Miho Misawa (RIKEN Center for Sustainable Resource Science) for preparing the standard compounds, Ms. Ursula Petralia for editorial assistance, Ms. Mariko Hayakumo for experimental assistance, Dr. Tetsuya Sakurai, Mr. Yutaka Yamada, and Ms. Mikiko Takahashi (RIKEN Center for Sustainable Resource Science) for their computational assistance. Dr. Masahito Shikata helped to provide tomato cv. 'MoneyMaker' seeds from the National BioResource Project (NBRP), Ministry of Education, Culture, Sports, Science and Technology (MEXT), Japan.

SUPPLEMENTARY MATERIAL

The Supplementary Material for this article can be found online at: https://www.frontiersin.org/articles/10.3389/fpls.2018.01439/full#supplementary-material

FIGURE S1 | Simplified source-sink model and overall experimental design. **(A)** Schematic representation of red LED lighting in this study, named "simplified source-sink model." We removed all the leaves and trusses except for the flowers of the second truss, the leaf just below the second truss, and the apical portions of the main shoot at the anthesis stage of the second truss. **(B)** Tomato plant cultivation with our systems under three types of light intensities (P200, P500, and P1000).

FIGURE S2 | Fruit weight and leaf area under LED light irradiation in *Solanum lycopersicum* L., 'Reiyo' – a whole plant. **(A)** Fruit weight comparison along developmental stages under normal light condition (average PPF 500, metal halide lamp as 'Control') without supplemental LED lighting. Biological replicates, $n = 3$. **(B)** Measurement of fruit weight and leaf area under LED lighting (PPF 1000, red LED) at 14 days. A whole plant and a red LED panel were set in a semi-closed assimilation chamber. The leaf just below the second truss was irradiated by LED. The bar graph indicates mean and standard deviation. Biological replicates, $n = 6$. WAA, week after anthesis.

FIGURE S3 | Tomato plants and leaf morphology on exposure to different light intensities of red LED at 2 WAA. **(A)** Leaf and fruit growth of tomato plants. **(B)** Leaf morphology. Few stress signs in the leaf were visible under P200 condition. The leaves indicated stress signs and accompanying disorders after P500 and P1000 high light treatments. Scale bars represent 10 cm.

FIGURE S4 | Fruit size and shape variation under different light intensities in *Solanum lycopersicum* L., 'Reiyo' using "simplified source-sink model." Measurement of fruit sizes **(A)** and leaf area **(B)**. WAA, week after anthesis. The bar graph indicates mean and standard deviation. Biological replicates, $n = 1$–6 for fruits and $n = 3$–6 for leaves.

FIGURE S5 | Fruit size under different light intensities in *Solanum lycopersicum* L., 'Moneymaker' using "simplified source-sink model." Measurement of fruit fresh weight **(A)** and dry weight **(B)**. Three fruits per plant/treatment. We used a box and whisker plot, a graphical summary of a distribution. This plot can visualize the minimum, lower and upper quartiles (25% and 75%), median, and maximum of data. Regarding extreme values, outliers may be displayed as open circles. Biological replicates, $n = 3$.

FIGURE S6 | Experimental design for metabolite profiling. WAA, weeks after anthesis.

FIGURE S7 | Experimental design for RNA-Seq analysis. WAA, weeks after anthesis.

FIGURE S8 | Experimental design for microarray analysis. See in details, (Fukushima et al., 2012). WAA, weeks after anthesis.

FIGURE S9 | (A,B) Statistics for sequenced short reads and mapping results of Illumina-based RNA-Seq. WAA, weeks after anthesis.

FIGURE S10 | Overview of transcript profile based on Illumina-based RNA-Seq. The RNA-Seq data from leaf-samples (1 WAA) was described using MAPMAN software (http://mapman.gabipd.org/web/guest/mapman) (Thimm et al., 2004; Usadel et al., 2005). The fold change is visualized by pseudo-color: red, up-regulated by P1000 treatment; blue, down-regulated by P1000 treatment. The results show that expression patterns involved in light reactions, secondary metabolism, and the biosynthesis of cell wall exhibit opposite alteration tendency between fruit- and leaf samples (green rectangles). WAA, weeks after anthesis.

TABLE S1 | Fruit developmental stages used for the study.

TABLE S2 | Reporting metabolite data by GC-TOF-MS in this study. **(A)** Metabolite reporting checklist. **(B)** Summary of values for detected metabolites. This table is based on reporting suggestions (Fernie et al., 2011). Significantly changed metabolites, processed data matrix, and sample information are as follows. **(C)** Tomato fruits. Metabolite responses during the developmental stages. **(D)** Leaves. Metabolite responses to high light treatment. **(E)** Tomato fruits. Metabolite responses during the developmental stages. **(F)** Leaves. Metabolite responses during the developmental stages. **(G)** Summary of metabolome data matrix, and statistical data analysis. **(H)** Sample information.

TABLE S3 | Summarized transcriptome data matrix and significantly changed transcripts obtained by microarrays. FC, fold change; FDR, false discovery rate.

TABLE S4 | Summarized transcriptome data matrix and significantly changed transcripts obtained by RNA-Seq. FC, fold change; FDR, false discovery rate.

TABLE S5 | Results of enrichment analysis. The top five gene ontology (GO) terms (full) that were significantly enriched (hypergeometric test with Benjamini and Hochberg FDR correction, FDR < 0.05) among differentially expressed genes (DEGs) whose expression differed significantly in response to HL (LIMMA, FDR < 0.05 and $|\log_2 FC| \geq 1$) based on microarray **(A)** and RNA-Seq **(B)** analysis. FDR, false discovery rate; NS, not significant.

REFERENCES

Alba, R., Fei, Z., Payton, P., Liu, Y., Moore, S. L., Debbie, P., et al. (2004). ESTs, cDNA microarrays, and gene expression profiling: tools for dissecting plant physiology and development. *Plant J.* 39, 697–714. doi: 10.1111/j.1365-313X.2004.02178.x

Alba, R., Payton, P., Fei, Z., Mcquinn, R., Debbie, P., Martin, G. B., et al. (2005). Transcriptome and selected metabolite analyses reveal multiple points of ethylene control during tomato fruit development. *Plant Cell* 17, 2954–2965. doi: 10.1105/tpc.105.036053

Alexandersson, E., Jacobson, D., Vivier, M. A., Weckwerth, W., and Andreasson, E. (2014). Field-omics-understanding large-scale molecular data from field crops. *Front. Plant Sci.* 5:286. doi: 10.3389/fpls.2014.00286

Anders, S., and Huber, W. (2010). Differential expression analysis for sequence count data. *Genome Biol.* 11:R106. doi: 10.1186/gb-2010-11-10-r106

Araujo, W. L., Martins, A. O., Fernie, A. R., and Tohge, T. (2014). 2-Oxoglutarate: linking TCA cycle function with amino acid, glucosinolate, flavonoid, alkaloid, and gibberellin biosynthesis. *Front. Plant Sci.* 5:552. doi: 10.3389/fpls.2014.00552

Araujo, W. L., Nunes-Nesi, A., Trenkamp, S., Bunik, V. I., and Fernie, A. R. (2008). Inhibition of 2-oxoglutarate dehydrogenase in potato tuber suggests the enzyme is limiting for respiration and confirms its importance in nitrogen assimilation. *Plant Physiol.* 148, 1782–1796. doi: 10.1104/pp.108.126219

Araujo, W. L., Tohge, T., Osorio, S., Lohse, M., Balbo, I., Krahnert, I., et al. (2012). Antisense inhibition of the 2-oxoglutarate dehydrogenase complex in tomato demonstrates its importance for plant respiration and during leaf senescence and fruit maturation. *Plant Cell* 24, 2328–2351. doi: 10.1105/tpc.112.099002

Barrett, T., Wilhite, S. E., Ledoux, P., Evangelista, C., Kim, I. F., Tomashevsky, M., et al. (2013). NCBI GEO: archive for functional genomics data sets–update. *Nucleic Acids Res.* 41, D991–D995. doi: 10.1093/nar/gks1193

Barry, C. S., Mcquinn, R. P., Thompson, A. J., Seymour, G. B., Grierson, D., and Giovannoni, J. J. (2005). Ethylene insensitivity conferred by the *Green-ripe* and *Never-ripe 2* ripening mutants of tomato. *Plant Physiol.* 138, 267–275. doi: 10.1104/pp.104.057745

Benjamini, Y., and Hochberg, Y. (1995). Controlling the false discovery rate: a practical and powerful approach to multiple testing. *J. R. Statist. Soc. B* 57, 289–300.

Bovy, A., Schijlen, E., and Hall, R. D. (2007). Metabolic engineering of flavonoids in tomato (*Solanum lycopersicum*): the potential for metabolomics. *Metabolomics* 3, 399–412. doi: 10.1007/s11306-007-0074-2

Caldana, C., Degenkolbe, T., Cuadros-Inostroza, A., Klie, S., Sulpice, R., Leisse, A., et al. (2011). High-density kinetic analysis of the metabolomic and transcriptomic response of Arabidopsis to eight environmental conditions. *Plant J.* 67, 869–884. doi: 10.1111/j.1365-313X.2011.04640.x

Carrari, F., Baxter, C., Usadel, B., Urbanczyk-Wochniak, E., Zanor, M. I., Nunes-Nesi, A., et al. (2006). Integrated analysis of metabolite and transcript levels reveals the metabolic shifts that underlie tomato fruit development and highlight regulatory aspects of metabolic network behavior. *Plant Physiol.* 142, 1380–1396. doi: 10.1104/pp.106.088534

Carrari, F., and Fernie, A. R. (2006). Metabolic regulation underlying tomato fruit development. *J. Exp. Bot.* 57, 1883–1897. doi: 10.1093/jxb/erj020

Cheng, G. W., and Huber, D. J. (1997). Carbohydrate solutilization of tomato locule tissue cell walls: parallels with locule tissue liquefaction during ripening. *Physiol. Plant.* 101, 51–58. doi: 10.1111/j.1399-3054.1997.tb01819.x

Chung, M. Y., Vrebalov, J., Alba, R., Lee, J., Mcquinn, R., Chung, J. D., et al. (2010). A tomato (*Solanum lycopersicum*) *APETALA2/ERF* gene, *SlAP2a*, is a negative regulator of fruit ripening. *Plant J.* 64, 936–947. doi: 10.1111/j.1365-313X.2010.04384.x

D'Aoust, M. A., Yelle, S., and Nguyen-Quoc, B. (1999). Antisense inhibition of tomato fruit sucrose synthase decreases fruit setting and the sucrose unloading capacity of young fruit. *Plant Cell* 11, 2407–2418. doi: 10.1105/tpc.11.12.2407

Darko, E., Heydarizadeh, P., Schoefs, B., and Sabzalian, M. R. (2014). Photosynthesis under artificial light: the shift in primary and secondary metabolism. *Philos. Trans. R. Soc. Lond. B Biol. Sci.* 369:20130243. doi: 10.1098/rstb.2013.0243

Do, P. T., Prudent, M., Sulpice, R., Causse, M., and Fernie, A. R. (2010). The influence of fruit load on the tomato pericarp metabolome in a *Solanum chmielewskii* introgression line population. *Plant Physiol.* 154, 1128–1142. doi: 10.1104/pp.110.163030

Fernie, A. R., Aharoni, A., Willmitzer, L., Stitt, M., Tohge, T., Kopka, J., et al. (2011). Recommendations for reporting metabolite data. *Plant Cell* 23, 2477–2482. doi: 10.1105/tpc.111.086272

Foyer, C. H., Noctor, G., and Hodges, M. (2011). Respiration and nitrogen assimilation: targeting mitochondria-associated metabolism as a means to enhance nitrogen use efficiency. *J. Exp. Bot.* 62, 1467–1482. doi: 10.1093/jxb/erq453

Fujisawa, M., Shima, Y., Nakagawa, H., Kitagawa, M., Kimbara, J., Nakano, T., et al. (2014). Transcriptional regulation of fruit ripening by tomato FRUITFULL homologs and associated MADS box proteins. *Plant Cell* 26, 89–101. doi: 10.1105/tpc.113.119453

Fukushima, A., Nishizawa, T., Hayakumo, M., Hikosaka, S., Saito, K., Goto, E., et al. (2012). Exploring tomato gene functions based on coexpression modules using graph clustering and differential coexpression approaches. *Plant Physiol.* 158, 1487–1502. doi: 10.1104/pp.111.188367

Galtier, N., Foyer, C. H., Huber, J., Voelker, T. A., and Huber, S. C. (1993). Effects of elevated sucrose-phosphate synthase activity on photosynthesis, assimilate partitioning, and growth in tomato (*Lycopersicon esculentum* var UC82B). *Plant Physiol.* 101, 535–543. doi: 10.1104/pp.101.2.535

Galtier, N., Foyer, C. H., Murchie, E., Aired, R., Quick, P., Voelker, T. A., et al. (1995). Effects of light and atmospheric carbon dioxide enrichment on photosynthesis and carbon partitioning in the leaves of tomato (*Lycopersicon esculentum* L.) plants over-expressing sucrose phosphate synthase. *J. Exp. Bot.* 46, 1335–1344. doi: 10.1093/jxb/46.special_issue.1335

Gentleman, R. C., Carey, V. J., Bates, D. M., Bolstad, B., Dettling, M., Dudoit, S., et al. (2004). Bioconductor: open software development for computational biology and bioinformatics. *Genome Biol.* 5:R80. doi: 10.1186/gb-2004-5-10-r80

Gosselin, A., Xu, H. L., and Dafiri, N. (1996). Effects of supplemental lighting and fruit thinning on fruit yield and source-sink relations of greenhouse tomato plants. *J. Jpn. Soc. Hortic. Sci.* 65, 595–601. doi: 10.2503/jjshs.65.595

Goto, E. (2003). Effects of light quality on growth of crop plants under artificial lighting. *Environ. Control Biol.* 41, 121–132. doi: 10.2525/ecb1963.41.121

Gunnlaugsson, B., and Adalsteinsson, S. (2006). Interlight and plant density in year-round production of tomato at northern latitudes. *Acta Hortic.* 711, 71–75. doi: 10.17660/ActaHortic.2006.711.6

Heuvelink, E., Bakker, M. J., Hogendonk, L., Janse, J., Kaarsemaker, R. C., and Maaswinkel, R. H. M. (2006). Horticultural lighting in the Netherlands: new developments. *Acta Hortic.* 711, 25–33. doi: 10.17660/ActaHortic.2006.711.1

Hikosaka, S., Iyoki, S., Hayakumo, M., and Goto, E. (2013). Effects of light intensity and amount of supplemental LED lighting on photosynthesis and fruit growth of tomato plants under artificial conditions. *J. Agric. Meteorol.* 69, 93–100. doi: 10.2480/agrmet.69.2.5

Hodges, M. (2002). Enzyme redundancy and the importance of 2-oxoglutarate in plant ammonium assimilation. *J. Exp. Bot.* 53, 905–916. doi: 10.1093/jexbot/53.370.905

Hovi, T., Nakkila, J., and Tahvonen, R. (2004). Interlighting improves production of year-round cucumber. *Sci. Hortic.* 102, 283–294. doi: 10.1016/j.scienta.2004.04.003

Hovi-Pekkanen, T., and Tahvonen, R. (2008). Effects of interlighting on yield and external fruit quality in year-round cultivated cucumber. *Sci. Hortic.* 116, 152–161. doi: 10.1016/j.scienta.2007.11.010

Jonsson, P., Johansson, E. S., Wuolikainen, A., Lindberg, J., Schuppe-Koistinen, I., Kusano, M., et al. (2006). Predictive metabolite profiling applying hierarchical multivariate curve resolution to GC-MS data–a potential tool for multi-parametric diagnosis. *J. Proteome Res.* 5, 1407–1414. doi: 10.1021/pr0600071

Jonsson, P., Johansson, I., Gullberg, J., Trygg, J. A. J., Grung, B., Marklund, S., et al. (2005). High-throughput data analysis for detecting and identifying differences between samples in GC/MS-based metabolomic analyses. *Anal. Chem.* 77, 5635–5642. doi: 10.1021/ac050601e

Kahlau, S., and Bock, R. (2008). Plastid transcriptomics and translatomics of tomato fruit development and chloroplast-to-chromoplast differentiation: chromoplast gene expression largely serves the production of a single protein. *Plant Cell* 20, 856–874. doi: 10.1105/tpc.107.055202

Kale, N. S., Haug, K., Conesa, P., Jayseelan, K., Moreno, P., Rocca-Serra, P., et al. (2016). MetaboLights: an open-access database repository for metabolomics data. *Curr. Protoc. Bioinformatics* 53, 14.13.1–14.13.18. doi: 10.1002/0471250953.bi1413s53.

Kitazaki, K., Fukushima, A., Nakabayashi, R., Okazaki, Y., Kobayashi, M., Mori, T., et al. (2018). Metabolic reprogramming in leaf lettuce grown under different light quality and intensity conditions using narrow-band LEDs. *Sci. Rep.* 8:7914. doi: 10.1038/s41598-018-25686-0

Klee, H. J., and Giovannoni, J. J. (2011). Genetics and control of tomato fruit ripening and quality attributes. *Annu. Rev. Genet.* 45, 41–59. doi: 10.1146/annurev-genet-110410-132507

Kopka, J., Schauer, N., Krueger, S., Birkemeyer, C., Usadel, B., Bergmuller, E., et al. (2005). GMD@CSB.DB: the golm metabolome database. *Bioinformatics* 21, 1635–1638. doi: 10.1093/bioinformatics/bti236

Kusano, M., Fukushima, A., Arita, M., Jonsson, P., Moritz, T., Kobayashi, M., et al. (2007a). Unbiased characterization of genotype-dependent metabolic regulations by metabolomic approach in *Arabidopsis thaliana*. *BMC Syst. Biol.* 1:53. doi: 10.1186/1752-0509-1-53

Kusano, M., Fukushima, A., Kobayashi, M., Hayashi, N., Jonsson, P., Moritz, T., et al. (2007b). Application of a metabolomic method combining one-dimensional and two-dimensional gas chromatography-time-of-flight/mass spectrometry to metabolic phenotyping of natural variants in rice. *J. Chromatogr. B Analyt. Technol. Biomed. Life Sci.* 855, 71–79.

Kusano, M., Redestig, H., Hirai, T., Oikawa, A., Matsuda, F., Fukushima, A., et al. (2011a). Covering chemical diversity of genetically-modified tomatoes using metabolomics for objective substantial equivalence assessment. *PLoS One* 6:e16989. doi: 10.1371/journal.pone.0016989

Kusano, M., Tohge, T., Fukushima, A., Kobayashi, M., Hayashi, N., Otsuki, H., et al. (2011b). Metabolomics reveals comprehensive reprogramming involving two independent metabolic responses of Arabidopsis to UV-B light. *Plant J.* 67, 354–369. doi: 10.1111/j.1365-313X.2011.04599.x

Langmead, B., Trapnell, C., Pop, M., and Salzberg, S. L. (2009). Ultrafast and memory-efficient alignment of short DNA sequences to the human genome. *Genome Biol.* 10:R25. doi: 10.1186/gb-2009-10-3-r25

Lemoine, R., La Camera, S., Atanassova, R., Dedaldechamp, F., Allario, T., Pourtau, N., et al. (2013). Source-to-sink transport of sugar and regulation by environmental factors. *Front. Plant Sci.* 4:272. doi: 10.3389/fpls.2013.00272

Lin, Z., Hong, Y., Yin, M., Li, C., Zhang, K., and Grierson, D. (2008). A tomato HD-Zip homeobox protein, LeHB-1, plays an important role in floral organogenesis and ripening. *Plant J.* 55, 301–310. doi: 10.1111/j.1365-313X.2008.03505.x

Lohse, M., Bolger, A. M., Nagel, A., Fernie, A. R., Lunn, J. E., Stitt, M., et al. (2012). RobiNA: a user-friendly, integrated software solution for RNA-Seq-based transcriptomics. *Nucleic Acids Res.* 40, W622–W627. doi: 10.1093/nar/gks540

Lytovchenko, A., Eickmeier, I., Pons, C., Osorio, S., Szecowka, M., Lehmberg, K., et al. (2011). Tomato fruit photosynthesis is seemingly unimportant in primary metabolism and ripening but plays a considerable role in seed development. *Plant Physiol.* 157, 1650–1663. doi: 10.1104/pp.111.186874

Maere, S., Heymans, K., and Kuiper, M. (2005). BiNGO: a Cytoscape plugin to assess overrepresentation of gene ontology categories in biological networks. *Bioinformatics* 21, 3448–3449. doi: 10.1093/bioinformatics/bti551

Massa, G. D. (2008). Plant productivity in response to LED lighting. *HortScience* 43, 1951–1956.

Micallef, B. J., Haskins, K. A., Vanderveer, P. J., Roh, K. S., Shewmaker, C. K., and Sharkey, T. D. (1995). Altered photosynthesis, flowering, and fruiting in transgenic tomato plants that have an increased capacity for sucrose synthesis. *Planta* 196, 327–334. doi: 10.1007/BF00201392

Mishra, Y., Jankanpaa, H. J., Kiss, A. Z., Funk, C., Schroder, W. P., and Jansson, S. (2012). Arabidopsis plants grown in the field and climate chambers significantly differ in leaf morphology and photosystem components. *BMC Plant Biol.* 12:6. doi: 10.1186/1471-2229-12-6

Mittler, R. (2006). Abiotic stress, the field environment and stress combination. *Trends Plant Sci.* 11, 15–19. doi: 10.1016/j.tplants.2005.11.002

Moe, R., Grimstad, S. O., and Gislerod, H. R. (2006). The use of artificial light in year round production of greenhouse crops in Norway. *Acta Hortic.* 711, 35–42. doi: 10.17660/ActaHortic.2006.711.2

Mounet, F., Moing, A., Garcia, V., Petit, J., Maucourt, M., Deborde, C., et al. (2009). Gene and metabolite regulatory network analysis of early developing fruit tissues highlights new candidate genes for the control of tomato fruit composition and development. *Plant Physiol.* 149, 1505–1528. doi: 10.1104/pp.108.133967

Mutschler, M. A., Yasamura, L., and Sethna, J. (1986). Estimation of tomato fruit volume from fruit measurements. *Rep. Tomato Genet. Coop.* 36:10. doi: 10.1093/aob/mcp283

Nakabayashi, R., and Saito, K. (2015). Integrated metabolomics for abiotic stress responses in plants. *Curr. Opin. Plant Biol.* 24, 10–16. doi: 10.1016/j.pbi.2015.01.003

Nakano, T., Kimbara, J., Fujisawa, M., Kitagawa, M., Ihashi, N., Maeda, H., et al. (2012). MACROCALYX and JOINTLESS interact in the transcriptional regulation of tomato fruit abscission zone development. *Plant Physiol.* 158, 439–450. doi: 10.1104/pp.111.183731

Nguyen, C. V., Vrebalov, J. T., Gapper, N. E., Zheng, Y., Zhong, S., Fei, Z., et al. (2014). Tomato *GOLDEN2-LIKE* transcription factors reveal molecular gradients that function during fruit development and ripening. *Plant Cell* 26, 585–601. doi: 10.1105/tpc.113.118794

Nguyen-Quoc, B., and Foyer, C. H. (2001). A role for 'futile cycles' involving invertase and sucrose synthase in sucrose metabolism of tomato fruit. *J. Exp. Bot.* 52, 881–889. doi: 10.1093/jexbot/52.358.881

Noctor, G., Lelarge-Trouverie, C., and Mhamdi, A. (2015). The metabolomics of oxidative stress. *Phytochemistry* 112, 33–53. doi: 10.1016/j.phytochem.2014.09.002

Obata, T., and Fernie, A. R. (2012). The use of metabolomics to dissect plant responses to abiotic stresses. *Cell Mol. Life Sci.* 69, 3225–3243. doi: 10.1007/s00018-012-1091-5

Osorio, S., Alba, R., Damasceno, C. M., Lopez-Casado, G., Lohse, M., Zanor, M. I., et al. (2011). Systems biology of tomato fruit development: combined transcript, protein, and metabolite analysis of tomato transcription factor (*nor*, *rin*) and ethylene receptor (*Nr*) mutants reveals novel regulatory interactions. *Plant Physiol.* 157, 405–425. doi: 10.1104/pp.111.175463

Osorio, S., Ruan, Y. L., and Fernie, A. R. (2014). An update on source-to-sink carbon partitioning in tomato. *Front. Plant Sci.* 5:516. doi: 10.3389/fpls.2014.00516

Paul, M., Pellny, T., and Goddijn, O. (2001). Enhancing photosynthesis with sugar signals. *Trends Plant Sci.* 6, 197–200. doi: 10.1016/S1360-1385(01)01920-3

Pesaresi, P., Mizzotti, C., Colombo, M., and Masiero, S. (2014). Genetic regulation and structural changes during tomato fruit development and ripening. *Front. Plant Sci.* 5:124. doi: 10.3389/fpls.2014.00124

Pettersen, R. I., Torre, S., and Gislerød, H. R. (2010). Effects of intracanopy lighting on photosynthetic characteristics in cucumber. *Sci. Hortic.* 125, 77–81. doi: 10.1016/j.scienta.2010.02.006

Piechulla, B., Glick, R. E., Bahl, H., Melis, A., and Gruissem, W. (1987). Changes in photosynthetic capacity and photosynthetic protein pattern during tomato fruit ripening. *Plant Physiol.* 84, 911–917. doi: 10.1104/pp.84.3.911

Redestig, H., Fukushima, A., Stenlund, H., Moritz, T., Arita, M., Saito, K., et al. (2009). Compensation for systematic cross-contribution improves normalization of mass spectrometry based metabolomics data. *Anal. Chem.* 81, 7974–7980. doi: 10.1021/ac901143w

Rohrmann, J., Tohge, T., Alba, R., Osorio, S., Caldana, C., Mcquinn, R., et al. (2011). Combined transcription factor profiling, microarray analysis and metabolite profiling reveals the transcriptional control of metabolic shifts occurring during tomato fruit development. *Plant J.* 68, 999–1013. doi: 10.1111/j.1365-313X.2011.04750.x

Rose, J. K., Bashir, S., Giovannoni, J. J., Jahn, M. M., and Saravanan, R. S. (2004). Tackling the plant proteome: practical approaches, hurdles and experimental tools. *Plant J.* 39, 715–733. doi: 10.1111/j.1365-313X.2004.02182.x

Ruan, Y. L. (2014). Sucrose metabolism: gateway to diverse carbon use and sugar signaling. *Annu. Rev. Plant Biol.* 65, 33–67. doi: 10.1146/annurev-arplant-050213-040251

Schaffer, A. A., and Petreikov, M. (1997). Sucrose-to-starch metabolism in tomato fruit undergoing transient starch accumulation. *Plant Physiol.* 113, 739–746. doi: 10.1104/pp.113.3.739

Schauer, N., Steinhauser, D., Strelkov, S., Schomburg, D., Allison, G., Moritz, T., et al. (2005). GC-MS libraries for the rapid identification of metabolites in complex biological samples. *FEBS Lett.* 579, 1332–1337. doi: 10.1016/j.febslet.2005.01.029

Seyoum, A., Asres, K., and El-Fiky, F. K. (2006). Structure-radical scavenging activity relationships of flavonoids. *Phytochemistry* 67, 2058–2070. doi: 10.1016/j.phytochem.2006.07.002

Shulaev, V., Cortes, D., Miller, G., and Mittler, R. (2008). Metabolomics for plant stress response. *Physiol. Plant.* 132, 199–208. doi: 10.1111/j.1399-3054.2007.01025.x

Smyth, G. K. (2004). Linear models and empirical bayes methods for assessing differential expression in microarray experiments. *Stat. Appl. Genet. Mol. Biol.* 3:Article3. doi: 10.2202/1544-6115.1027

Stacklies, W., Redestig, H., Scholz, M., Walther, D., and Selbig, J. (2007). pcaMethods–a bioconductor package providing PCA methods for incomplete data. *Bioinformatics* 23, 1164–1167. doi: 10.1093/bioinformatics/btm069

Steinhauser, M. C., Steinhauser, D., Koehl, K., Carrari, F., Gibon, Y., Fernie, A. R., et al. (2010). Enzyme activity profiles during fruit development in tomato cultivars and *Solanum pennellii*. *Plant Physiol.* 153, 80–98. doi: 10.1104/pp.110.154336

Sweetlove, L. J., Beard, K. F., Nunes-Nesi, A., Fernie, A. R., and Ratcliffe, R. G. (2010). Not just a circle: flux modes in the plant TCA cycle. *Trends Plant Sci.* 15, 462–470. doi: 10.1016/j.tplants.2010.05.006

Thimm, O., Blasing, O., Gibon, Y., Nagel, A., Meyer, S., Kruger, P., et al. (2004). MAPMAN: a user-driven tool to display genomics data sets onto diagrams of metabolic pathways and other biological processes. *Plant J.* 37, 914–939. doi: 10.1111/j.1365-313X.2004.02016.x

Tomato Genome, C. (2012). The tomato genome sequence provides insights into fleshy fruit evolution. *Nature* 485, 635–641. doi: 10.1038/nature11119

Trouwborst, G., Oosterkamp, J., Hogewoning, S. W., Harbinson, J., and Van Ieperen, W. (2010). The responses of light interception, photosynthesis and fruit yield of cucumber to LED-lighting within the canopy. *Physiol. Plant.* 138, 289–300. doi: 10.1111/j.1399-3054.2009.01333.x

Urano, K., Kurihara, Y., Seki, M., and Shinozaki, K. (2010). 'Omics' analyses of regulatory networks in plant abiotic stress responses. *Curr. Opin. Plant Biol.* 13, 132–138. doi: 10.1016/j.pbi.2009.12.006

Usadel, B., Nagel, A., Thimm, O., Redestig, H., Blaesing, O. E., Palacios-Rojas, N., et al. (2005). Extension of the visualization tool MapMan to allow statistical analysis of arrays, display of corresponding genes, and comparison with known responses. *Plant Physiol.* 138, 1195–1204. doi: 10.1104/pp.105.060459

Wang, H., Jones, B., Li, Z., Frasse, P., Delalande, C., Regad, F., et al. (2005). The tomato *Aux*/*IAA* transcription factor *IAA9* is involved in fruit development and leaf morphogenesis. *Plant Cell* 17, 2676–2692. doi: 10.1105/tpc.105.033415

Wanner, L. A., and Gruissem, W. (1991). Expression dynamics of the tomato rbcS gene family during development. *Plant Cell* 3, 1289–1303. doi: 10.1105/tpc.3.12.1289

Wulff-Zottele, C., Gatzke, N., Kopka, J., Orellana, A., Hoefgen, R., Fisahn, J., et al. (2010). Photosynthesis and metabolism interact during acclimation of *Arabidopsis thaliana* to high irradiance and sulphur depletion. *Plant Cell Environ.* 33, 1974–1988. doi: 10.1111/j.1365-3040.2010.02199.x

Conflict of Interest Statement: The authors declare that the research was conducted in the absence of any commercial or financial relationships that could be construed as a potential conflict of interest.

frontiers in Plant Science

ORIGINAL RESEARCH
published: 04 July 2017
doi: 10.3389/fpls.2017.01188

A Non-targeted Metabolomics Approach Unravels the VOCs Associated with the Tomato Immune Response against *Pseudomonas syringae*

María Pilar López-Gresa†, Purificación Lisón†, Laura Campos, Ismael Rodrigo, José Luis Rambla, Antonio Granell, Vicente Conejero and José María Bellés*

Instituto de Biología Molecular y Celular de Plantas, Universitat Politècnica de València – Consejo Superior de Investigaciones Científicas, Ciudad Politécnica de la Innovación, Valencia, Spain

OPEN ACCESS

Edited by:
Marta Sousa Silva, Universidade de Lisboa, Portugal

Reviewed by:
Xavier Daire, Institut National de la Recherche Agronomique, France
Yonathan Asikin, University of Tsukuba, Japan

***Correspondence:**
Purificación Lisón
plison@ibmcp.upv.es

† These authors have contributed equally to this work.

Specialty section:
This article was submitted to Plant Metabolism and Chemodiversity, a section of the journal Frontiers in Plant Science

Received: *05 May 2017*
Accepted: *21 June 2017*
Published: *04 July 2017*

Citation:
López-Gresa MP, Lisón P, Campos L, Rodrigo I, Rambla JL, Granell A, Conejero V and Bellés JM (2017) A Non-targeted Metabolomics Approach Unravels the VOCs Associated with the Tomato Immune Response against Pseudomonas syringae. Front. Plant Sci. 8:1188. doi: 10.3389/fpls.2017.01188

Volatile organic compounds (VOCs) emitted by plants are secondary metabolites that mediate the plant interaction with pathogens and herbivores. These compounds may perform direct defensive functions, i.e., acting as antioxidant, antibacterial, or antifungal agents, or indirectly by signaling the activation of the plant's defensive responses. Using a non-targeted GC-MS metabolomics approach, we identified the profile of the VOCs associated with the differential immune response of the Rio Grande tomato leaves infected with either virulent or avirulent strains of *Pseudomonas syringae* DC3000 pv. *tomato*. The VOC profile of the tomato leaves infected with avirulent bacteria is characterized by esters of (Z)-3-hexenol with acetic, propionic, isobutyric or butyric acids, and several hydroxylated monoterpenes, e.g., linalool, α-terpineol, and 4-terpineol, which defines the profile of an immunized plant response. In contrast, the same tomato cultivar infected with the virulent bacteria strain produced a VOC profile characterized by monoterpenes and SA derivatives. Interestingly, the differential VOCs emission correlated statistically with the induction of the genes involved in their biosynthetic pathway. Our results extend plant defense system knowledge and suggest the possibility for generating plants engineered to over-produce these VOCs as a complementary strategy for resistance.

Keywords: metabolomics, tomato, bacteria, VOCs, defense

INTRODUCTION

Plants have developed multiple defense mechanisms to protect themselves against biotic and abiotic stresses. Accumulation of secondary metabolites, which display numerous biological properties, constitutes a major component of stress responses (Dixon, 2001; Pusztahelyi et al., 2015; Qian et al., 2015; Kalaivani et al., 2016). Among them, volatile organic compounds (VOCs) are a relevant group involved in plant protection against pathogens and herbivores, and also in attracting pollinators and seed dispersers (Dudareva et al., 2013). Plant VOCs include a wide range

of chemical structures, such as terpenoids and phenylpropanoids-benzenoids, as well as fatty and amino acid derivatives (Holopainen and Gershenzon, 2010; Granell and Rambla, 2013). They all have a low molecular weight and polarity, high vapor pressures, and possess the ability to both cross membranes freely and be released into the surrounding atmosphere (Dudareva et al., 2006).

The bacterial speck of tomato, caused by *Pseudomonas syringae* pv. *tomato* (*Pst*), is a major problem in the agricultural industry (Willis and Kinscherf, 2009). Tomato cultivar Rio Grande, which contains the *Pto* gene (RG-*Pto*), is resistant to *Pst*, which expresses effectors or avirulence genes *avrPto/avrPtoB*. Such "gene-for-gene" recognition (*Pto-avrPto/avrPtoB*) elicits Effector-Triggered Immunity (ETI) establishment in plants, which allows the control of bacterial spread, and results in an incompatible interaction (Jia et al., 1997; Dangl and Jones, 2001; Lin and Martin, 2005). In contrast, *Pst,* which bears a deletion of *avrPto* genes (Δ*avrPto*/Δ*avrPtoB*), becomes virulent to RG-*Pto* plants by causing disease in plants and the development of a compatible interaction (Salmeron et al., 1994). Therefore, this tomato pathosystem represents an excellent model to study both kinds of plant–pathogen interactions.

Different signal molecules, such as salicylic acid (SA), gentisic acid (GA), ethylene (ET), or jasmonic acid (JA), have been described to accumulate upon pathogen attacks in tomato plants. SA accumulation has been associated with avirulent infections (Block et al., 2005), while high levels of GA and ET have been found in compatible interactions in tomato (Bellés et al., 1999; Zacarés et al., 2007). JA has been associated with plant responses to herbivores or necrotrophic pathogens (Zhang et al., 2017). However, the role of these defensive molecules has not been characterized in tomato Rio Grande plants infected with virulent or avirulent *Pst* strains.

More and more studies are being conducted to understand the participation of small metabolites in plant–pathogen interactions (Allwood et al., 2008, 2012). However, the interest in VOCs has focused mainly on the plant response to herbivores and fruit quality, and studies of VOCs in the plant response to pathogens are scarce (Niinemets et al., 2013). Specifically, differential volatile emission has been described for tobacco and pepper leaves in response to both avirulent and virulent strains of *Pseudomonas* (Huang et al., 2003, 2005) and *Xanthomonas* (Cardoza and Tumlinson, 2006), respectively, but the biological meaning of this phenomenon is not well understood.

In this paper, we applied an untargeted GC-MS metabolomics approach to analyze the volatiles differentially emitted in RG-*Pto* tomato plants infected with either avirulent strain *Pst* DC3000 or virulent strain *Pst* DC3000 Δ*avrPto*/Δ*avrPtoB*. Besides, levels of classical defense hormones, such as SA, GA, ET, and JA, were characterized in both tomato interactions. Finally, the activation of a set of genes involved in the corresponding VOC biosynthesis pathways was also studied. Our results will unravel the VOC network that underlies the tomato immune response against *Pseudomonas syringae*.

MATERIALS AND METHODS

Bacterial Strains, Growth Conditions, and Inoculum Preparation

The bacterial strains used in this study were *Pseudomonas syringae* pv. *tomato* DC3000 (*Pst* DC3000), and *Pst* DC3000 that contains deletions in genes *avrPto* and *avrPtoB* (*Pst* DC3000 Δ*avrPto*/Δ*avrPtoB*) (Ntoukakis et al., 2009). Bacteria were grown overnight at 28°C in 20 mL Petri dishes with King's B agar medium supplemented with different antibiotic doses: rifampicin (10 mg/mL) and kanamicin (0.5 mg/mL) for *Pst* DC3000, and rifampicin (10 mg/mL), kanamycin (0.25 mg/mL) and spectinomycin (2.5 mg/mL) for *Pst* DC3000 Δ*avrPto*/Δ*avrPtoB*. Then bacterial colonies were transferred to 15 mL of King's B medium supplemented with rifampicin (10 mg/mL), and were grown overnight at 28°C with stirring. Bacteria were then pelleted by centrifugation and resuspended in 10 mM of $MgCl_2$, which contained 0.05% (v/v) Silwet L-77, to an optical density of 0.1 at 600 nm. Dilution plating was used to determine the final inoculum concentration, which averaged at 1×10^7 CFU/mL.

Plant Material and Bacterial Inoculation

Tomato seeds from the cultivar Rio Grande that contained resistance (*R*) gene *Pto* (RG-*Pto*) were grown under greenhouse conditions with a 16/8-h (26/30°C) light/dark photoperiod (300 μmol/m^2/s) and 65% relative humidity in 12 cm-diameter pots that contained a 1:1 mixture of peat and vermiculite.

Inoculations with compatible and incompatible bacteria were produced by immersing 28-day-old RG-*Pto* plants in *Pst* DC3000 or *Pst* DC3000 Δ*avrPto*/Δ*avrPtoB* suspension, respectively, as previously described (Martin et al., 1993). For mock inoculations, plants were dipped in 10 mM of $MgCl_2$ solution that contained Silwet L-77 (0.05%) without the bacterial inoculum. The third and fourth leaves, from bottom to top, were harvested and frozen in liquid nitrogen at the indicated times. The fifth leaf was placed freshly in a 10-mL screw cap vial and was kept for 5 h to take ET measurements. Six biological replicates were analyzed for each time and tomato–bacteria interaction.

Extraction and the HPLC Analysis of Salicylic and Gentisic Acids

Extraction of free and total SA and GA from tomato leaflets was performed according to our previously published protocol (Bellés et al., 2008). Aliquots of 30 μL were injected through a Waters 717 autosampler into a reverse-phase Sun Fire 5-μm C18 column (4.6 mm ×150 mm) equilibrated in 1% (v/v) acetic acid at room temperature. A 20-min linear gradient of 1% acetic acid to 100% methanol was applied using a 1525 Waters Binary HPLC pump at a flow rate of 1 mL/min. SA and GA were detected with a 2475 Waters Multi-λ Fluorescence detector (λ excitation 313 nm; λ emission 405 nm), and were quantified with the Waters Empower Pro software using authentic standard compounds (SA sodium salt and GA, Sigma–Aldrich, Madrid, Spain). Standard curves were performed for each compound using similar concentration ranges to those detected in the samples. Data were corrected for losses in the extraction

procedure, and recovery of metabolites ranged between 50 and 80%.

Jasmonic Acid and Ethylene Measurements

Ethylene production was measured as described by Lieberherr et al. (2003) with some modifications. Approximately 0.5 g of fresh tissue from the fifth tomato leaf, harvested at the indicated time points after bacterial inoculation, was quickly enclosed in gas-tight 10-mL glass vials fitted with a septum. After 5 h, 400 μL of the gas phase from the vial were analyzed by gas chromatography in a 4890A Hewlett Packard gas chromatograph fitted with a flame ionization detector (FID) using a Teknokroma capillary column (2 m × 1/6″ OD × 1 mm ID, Alumina F1 80/100). The carrier gas was helium, used at a pre-column pressure of 140 kPa. The injector and detector temperatures were set at 200°C, while the oven temperature was 80°C. The retention time of the ET peak under these conditions was 2.5 min. For each time point, six replicates were analyzed and the amount of ET was calculated from the data recorded and analyzed with the MassLynx Waters software by constructing a standard ET curve.

For JA quantification, 250 mg of frozen tissue from the third and fourth tomato leaves were added to 80% methanol–1% acetic acid that contained the internal standard dihydrojasmonate (OlChemIm, Czechia), and were mixed by shaking for 1 h at 4°C. The extract was kept at −20°C overnight and was then centrifuged. The supernatant was dried in a vacuum evaporator. The dry residue was dissolved in 1% acetic acid and passed through a reverse phase Oasis HLB column (Seo et al., 2011). The dried eluate was dissolved in 5% acetonitrile–1% acetic acid, and the hormone was identified using a reverse phase Ultra Performance Liquid Chromatography (UPLC) system coupled to a Q-Exactive mass spectrometer (Orbitrap detector; Thermo Fisher Scientific) by targeted Selected Ion Monitoring (SIM). Separation was performed in a 2.6 μm Accucore RP-MS column, 50 mm long × 2.1 mm i.d.; (Thermo Fisher Scientific) using a 5–50% acetonitrile gradient that contained 0.05% acetic acid as the solvent system at 400 μL/min for 14 min. The JA concentration in the extracts was determined using embedded calibration curves with the authentic standard (OlChemIm, Czechia) and the Xcalibur 2.2 SP1 build 48 and TraceFinder software.

HS-SPME Extraction and the GC-MS Analysis of Volatile Compounds

For the volatile analysis, 100 mg of frozen tomato leaf powder were weighed in a 10-mL headspace screw-cap vial. One milliliter of a saturated $CaCl_2$ solution and 100 μL of 750 mM EDTA (adjusted to 7.5 pH with NaOH) were added, mixed gently and sonicated for 5 min. Extraction of volatile compounds was performed by headspace solid-phase micro-extraction (HS-SPME) (Rambla et al., 2015). The pre-incubation and extraction periods, both at 50°C, were 10 and 20 min, respectively. Adsorption was performed by means of a 65 μm DVB/PDMS fiber (Supelco, Bellefonte, PA, United States). Desorption was done in the injection port of the gas chromatograph for 1 min at 250°C in the splitless mode. Volatile extraction and injection were performed automatically with a CombiPAL autosampler (CTC Analytics, Zwingen, Switzerland).

The chromatographic separation of compounds was performed in an Agilent 6890N gas chromatograph (Santa Clara, CA, United States) equipped with a DB-5 ms fused silica capillary column (60 m long, 0.25 mm i.d., 1 μm film thickness). The oven temperature conditions were 40°C for 2 min, 5°C/min ramp until 250°C and then held isothermally at 250°C for 5 min. Helium was used as the carrier gas at 1.2 mL/min at a constant flow. Detection was performed in an Agilent 5975B mass spectrometer (Santa Clara, CA, United States), which operated in the EI mode (ionization energy, 70 eV; source temperature 230°C). Data acquisition was performed in the scan mode (*m/z* range 35–250; six scans per second). Chromatograms and mass spectra were recorded and processed by the Enhanced ChemStation software (Agilent).

The unequivocal compound identification of the 70 volatile compounds was carried out by comparing both mass spectra and retention times with those of pure standards. All the commercial standards were purchased from Sigma–Aldrich (Madrid, Spain). Three other compounds were tentatively identified by comparing their mass spectra with those in the NIST 05 Mass Spectral library. Such tentatively identified compounds are marked with an asterisk.

RNA Extraction and the Quantitative RT-PCR Analysis

The total RNA of tomato leaves was extracted using TRIzol reagent (Invitrogen, Carlsbad, CA, United States), following the manufacturer's protocol. RNA was then precipitated by adding one volume of 6 M LiCl and keeping it on ice for 4 h. Afterward the pellet was washed using 3 M LiCl and was dissolved in RNase-free water. Finally, in order to remove any contaminating genomic DNA, 2 U of TURBO DNase (Ambion, Austin, TX, United States) were added per microliter of RNA.

For the quantitative RT-PCR (qRT-PCR) analysis, one microgram of total RNA was employed to obtain the corresponding cDNA target sequences using an oligo$(dT)_{18}$ primer and the PrimeScript RT reagent kit (Perfect Real Time, Takara Bio Inc., Otsu, Shiga, Japan), following the manufacturer's directions. Quantitative PCR was carried out as previously described (Campos et al., 2014). A housekeeping gene transcript, *Elongation Factor 1 alpha* (eEF1α), was used as the endogenous reference. The PCR primers were designed using the pcr Efficiency software (Mallona et al., 2011) and are listed in Supplementary Table S1. The primers used to amplify *TomLOXF* have been previously described (Shen et al., 2014).

Statistical Analysis

The statistical analyses of the signal compounds levels (GA, SA, ET, and JA) and the qRT-PCR of the selected genes were done by an analysis of variance (multifactor ANOVA) using Statgraphics Centurion XVI.

For the untargeted analysis of the volatile profile, the GC-MS data were processed with the MetAlign software (Wageningen,

Netherlands) for the alignment of the chromatograms and the quantitation of each MS feature. The resulting dataset was submitted to a Partial Least Square (PLS) study by the SIMCA-P software (v. 11.0, Umetrics, Umeå, Sweden) using unit variance (UV) scaling.

For the Hierarchical Cluster Analysis (HCA), the ratios for each VOC were calculated and $\log_2$-transformed for normalization. HCA was performed with the Acuity 4.0 software (Axon Instruments) with the distance metrics based on the Pearson correlation. The normalized data were represented as a heat map using the same software. The Pearson correlations between gene expression and the VOCs concentrations were performed with the SPSS 16.0 software by considering data at 10 and 18 hpi (hour post-inoculation).

RESULTS

RG-*Pto* Tomato Plants Infected Either with the Avirulent or Virulent Bacterial Strain Displayed Noticeable Symptom Differences

Symptoms development of the tomato plants infected with either avirulent strain *Pst* DC3000 or virulent *Pst* DC3000 Δ*avrPto*/Δ*avrPtoB* is shown in **Figure 1**. These symptoms ranged on a 0–4 scale as follows: symptomless (0), weak (1), moderate (2), severe (3), and very severe (4). Inoculation of the RG-*Pto* tomato plants with the virulent strain resulted in chlorotic lesions appearing by 18 hpi, which displayed a symptom degree from (0) to (1). These initial lesions increased in intensity and size, and caused significant leaf damage that ranged from (2) to (3) at 24 and 36 hpi, respectively. By 48 hpi, necrotic lesions extended to the total area, and leaves lost their firmness and completely collapsed, which was the maximum level of symptomatology (4). Strong epinasty was observed in the leaves of these symptomatic tomato plants. In contrast, no symptoms (0) were observed at any time on the RG-*Pto* tomato plants inoculated with avirulent strain *Pst* DC3000 due to *Pto-avrPto/avrPtoB* recognition and ETI establishment. Therefore, these immunized tomato leaves were similar to the mock-inoculated plants.

Levels of Salicylic Acid, Gentisic Acid, and Ethylene Were Enhanced in the RG-*Pto* Tomato Plants Infected with the Virulent Bacterial Strain, While Jasmonic Acid Drastically Lowered

The levels of the signaling defense molecules, SA, GA, ET, and JA were analyzed in the plants infected with both virulent and avirulent strains in a time-course study. **Figure 2** shows the significant GA induction that occurred in all the inoculated plants that bore both interactions. The increased amount of GA was already evident in tomato plants at 10 hpi. Leaf GA accumulation increased as bacterial infection progressed, and the highest levels peaked at 48 hpi (45 nmol/g FW) in the symptomatic tomato plant leaves. By 24 hpi, a significantly higher GA value was obtained in the compatible interaction compared to the incompatible infection. No remarkable increments in SA were observed in the *Pseudomonas*-infected tomato plants at any time point, although differences in the SA levels started to become significant in the compatible interaction by 24 hpi.

The evolution of ET from the leaves of both the compatible and incompatible tomato interactions was also measured. A dramatic increase in the production of this stress hormone was detected in the compatible interaction, which paralleled GA accumulation and appearance of symptoms (**Figure 3A**). Maximum ET production (188 nL/gFW/h) was reached at 18 hpi, which coincided with the onset of symptom development. These high levels of ET (up to 10-fold) could explain the strong epinasty observed in the tomato plants infected with the virulent bacteria. Remarkably during this compatible infection, ET biosynthesis was higher than that observed in the incompatible interaction, and was significantly elevated at any time point. Regarding infection with the avirulent bacteria, the differences in ET emission between the infected and mock-inoculated plants was only significant at 24, 36, and 48 hpi.

In contrast, the JA levels drastically lowered during virulent infection, and almost non-detectable values were displayed at 10 hpi. Regarding avirulent infection, JA production remained unaltered compared to the mock-inoculated tomato plants. A similar tendency was observed at 24 hpi (**Figure 3B**).

The Volatile Profile of Tomato Leaves Altered Differentially upon Infection with Both *Pseudomonas syringae* Strains

In order to examine the VOCs involved in the tomato–pathogen interactions, changes in the levels of these metabolites in the RG-*Pto* tomato plants, which were either mock-inoculated or infected with avirulent strain *Pst* DC3000 or virulent *Pst* DC3000 Δ*avrPto*/Δ*avrPtoB,* were analyzed by GC-MS in the leaves infected between 10 and 48 hpi (see Materials and Methods). **Table 1** lists the VOCs detected on our HS-SPME/GC-MS platform for the mock and infected RG-*Pto* tomato plants. In all, 73 compounds were identified: 11 esters (9 aliphatic and 2 aromatic), 20 aldehydes (16 aliphatic, 3 aromatic and 1 norcarotenoid), 13 alcohols (6 aliphatic, 1 norcarotenoid, 5 monoterpenic, and 1 sesquiterpenic), 9 monoterpene hydrocarbons, 8 ketones (5 aliphatic, 1 aromatic, and 2 norcarotenoid), 3 sesquiterpene hydrocarbons, 2 furans, 2 nitriles, 4 aliphatic acids, and 1 aromatic hydrocarbon. They were all unequivocally confirmed by using pure standards, except for three of them, which were tentatively identified based on their mass spectra similarity (match > 900).

To manage the large amount of mass data, a multivariate data analysis was performed that consisted in a PLS analysis, where compound abundance was assigned to the X variable, and harvesting time (10, 18, 24, 36, and 48 hpi) and type of infection (mock, compatible, and incompatible interaction) were defined as stepwise Y variables. The PLS analysis (**Figure 4**) showed that the first component (PC1) explained changes in the chemical composition during the experiment (harvesting time),

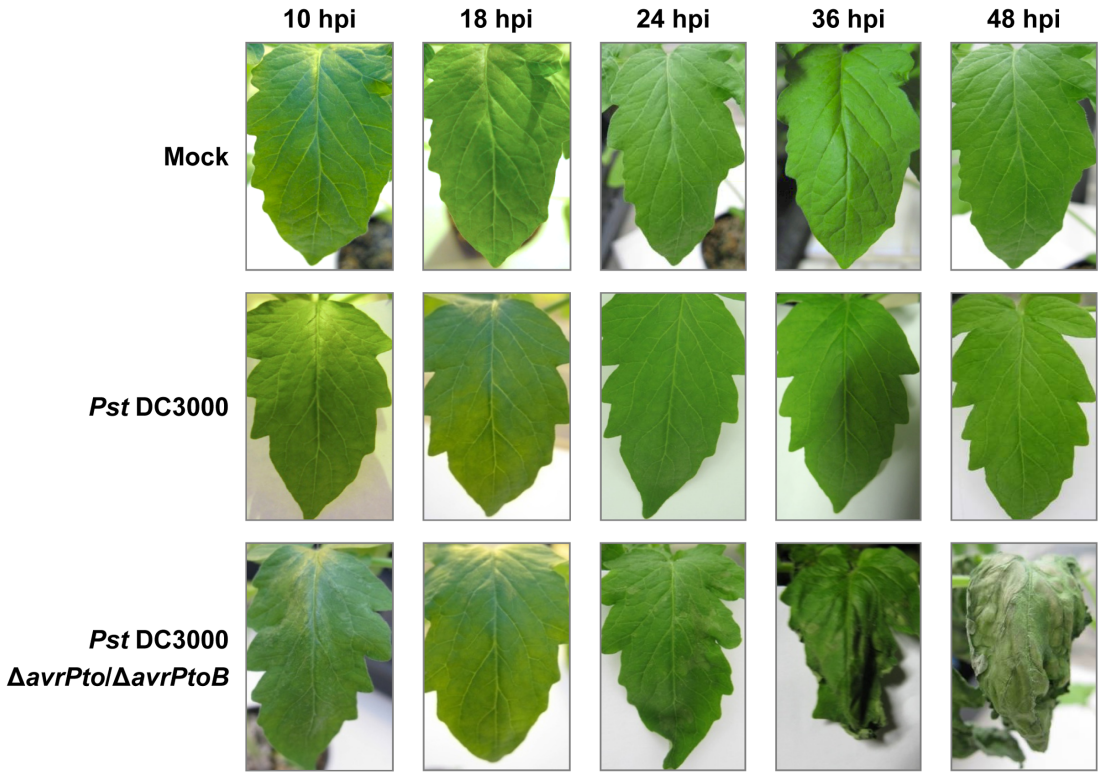

FIGURE 1 | Symptom evolution in RG-*Pto* plants at 10, 18, 34, 36, and 48 h post-inoculation (hpi) with 10 mM of $MgCl_2$ solution (mock), or either *Pst* DC3000 or *Pst* DC3000 Δ*avrPto*/Δ*avrPtoB* at 10^7 CFU/mL.

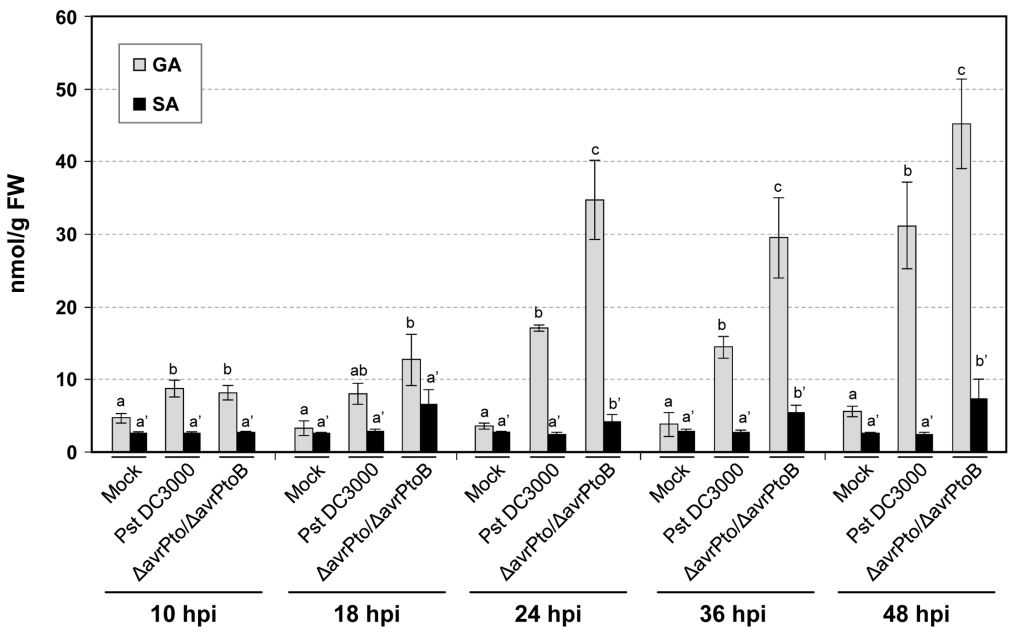

FIGURE 2 | Levels of the free and total salicylic (SA) and gentisic (GA) acids, measured in an HPLC-fluorescence detector in the mock-inoculated RG-*Pto* tomato plants (mock) and upon infection with *Pst* DC3000 or *Pst* DC3000 Δ*avrPto*/Δ*avrPtoB* at 10, 18, 24, 36, and 48 hpi. Two multifactor ANOVA analyses were performed using GA (x) or SA (x') data. Different letters indicate the statistical significances with a p-value < 0.05 compared with the mock-inoculated plants.

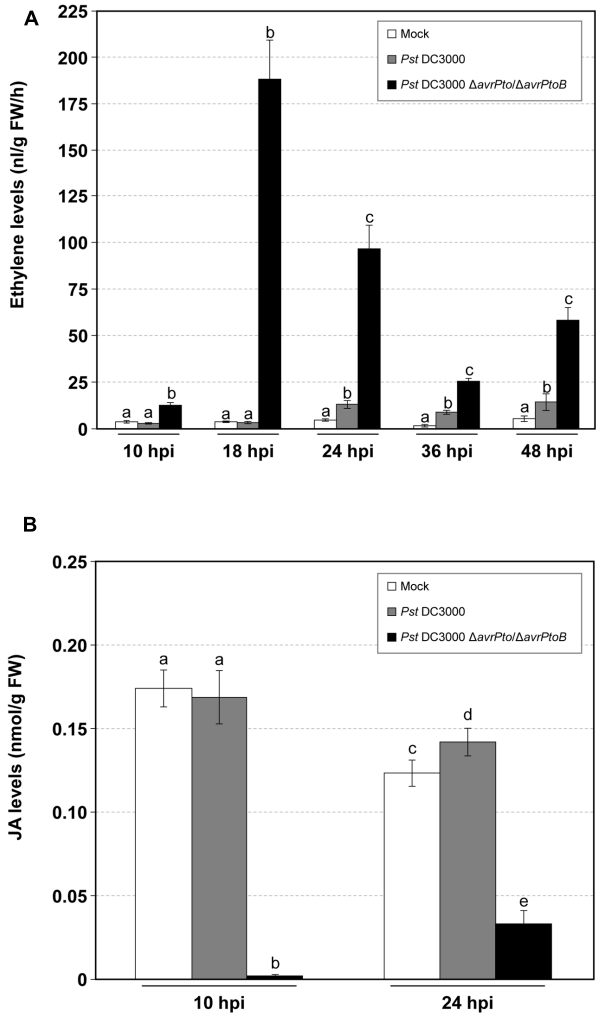

FIGURE 3 | Time-course analysis of the mock-inoculated RG-*Pto* tomato plants (mock) and upon infection with *Pst* DC3000 or *Pst* DC3000 Δ*avrPto*/Δ*avrPtoB* at 10, 18, 24, 36, and 48 hpi for ethylene production **(A)**, and at 10 and 24 hpi for jasmonic acid (JA) accumulation **(B)**. Different letters indicate the statistical significances with a p-value < 0.05 compared with the mock-inoculated plants.

while the metabolic alteration due to bacterial infection was clearly characterized by the second component (PC2). **Figure 4** also displays the over-emitted metabolites in both infected plants, which were identified by the loading plot analysis. As expected, the VOCs from the non-infected plants were chemically similar within 48 h of the experiment. However, the plants infected with both bacterial strains showed an evident variation in their metabolic profile compared to the mock plants. This indicated that VOCs emission was independent of symptomatology. However, no clear separation between the virulent and avirulent infections was observed in this PLS score plot.

In order to distinguish the defense metabolites associated with each plant–pathogen interaction, the two infections were independently analyzed. The volatile content of the mock-inoculated RG-*Pto* tomato plants was compared with that of the RG-*Pto*-infected one with either avirulent strain *Pst* DC3000 (Supplementary Figure S1) or virulent strain *Pst* DC3000 Δ*avrPto*/Δ*avrPtoB* (Supplementary Figure S2). In these PLS analyses, a marked separation between the infected and mock plants was clearly observed by PC2. In both cases, the loading plot revealed a specific set of VOCs that strongly contributed to the separation of samples according to the specific plant–bacterial infection. **Figure 5** shows a hierarchically clustered heat map, including the most discriminative compounds by comparing the volatile profile of the tomato plants infected with the avirulent or virulent Pst strains with the control plants (column 1 and column 2, respectively).

These defense compounds, induced by both infection types, derive from three important plant metabolic pathways: fatty acids, terpenoids and benzenoids. Among them, the most prominent VOCs produced upon both bacterial infections (red in columns 1 and 2) were some esters of (*Z*)-3-hexenol, such as (*Z*)-3-hexenyl acetate, (*Z*)-3-hexenyl propionate, (*Z*)-3-hexenyl isobutyrate, (*Z*)-3-hexenyl butyrate, some hydroxylated monoterpenes (HMT), such as linalool, α-terpineol, both (*Z*)- and (*E*)- isomers of linalool oxide, and an unidentified sesquiterpene. The statistical analyses showed that their differential induction was significant (Supplementary Table S2). Regarding benzenoids emission, an increase in the production of methyl salicylate (MeSA), salicylaldehyde, and ethyl salicylate was also observed in both infections. The accumulation of the VOCs that derived from salicylate was consistent with the SA accumulation detected in the compatible interaction since levels of these phenolic derivatives were also higher in this virulent infection (**Figure 2**).

Comparison of the VOCs Profiles of Tomato Leaves upon Infection with Virulent and Avirulent *Pseudomonas syringae* Strains Unraveled a Specific Volatile Response for ETI

In order to identify whether a specific set of volatile metabolites was involved in the establishment of effective defense such as ETI, another PLS analysis was performed by comparing the VOCs emitted from the tomato plants infected with avirulent strain *Pst* DC3000 and with virulent strain *Pst* DC3000 Δ*avrPto*/Δ*avrPtoB* (**Figure 6**). Once again, the second component clearly showed the different set of volatile compounds emitted by the plant that underwent either a compatible or an incompatible interaction during the 48 hpi period. This metabolomic approach allowed us to identify the differentially induced VOCs in each infection type, by using the loading plot analysis. The hierarchically clustered heat map shows the VOCs that were differentially emitted by the tomato plants infected with virulent Pst strains compared with the avirulent infection (**Figure 5**, column 3). Most VOCs, which were over-emitted by tomato plants during the establishment of the ETI triggered by the avirulent strain (green-colored), showed significant differences compared with the symptomatic infection (Supplementary Table S2).

TABLE 1 | List of the VOCs identified in tomato leaves by GC-MS.

Code	Volatile Organic Compound	Family Code/Number	Retention time (min)	Specific ion (m/z)
1	Ethanol	Alc/1	4.95	45
2	Acetone	Ket/1	5.68	58
3	Butanol	Alc/2	10.41	56
4	1-Penten-3-ol	Alc/3	11.17	57
5	1-Penten-3-one	Ket/2	11.29	55
6	2-Pentanone	Ket/3	11.31	86
7	3-Pentanone	Ket/4	11.68	86
8	Pentanal	Ald/1	11.79	44
9	2-Ethylfuran	Fur/1	11.85	81
10	3-Methylbutanenitrile	Nit/1	13.38	43
11	(*E*)-2-Methyl-2-butenal	Ald/2	13.62	84
12	(*E*)-2-Pentenal	Ald/3	14.07	83
13	1-Pentanol	Alc/4	14.36	42
14	(*Z*)-2-Penten-1-ol	Alc/5	14.48	68
15	(*Z*)-3-Hexenal	Ald/4	15.75	69
16	Hexanal	Ald/5	15.84	72
17	Butyl acetate	Est/1	16.18	43
18	Methyl pentanoate	Est/2	16.65	85
19	(*Z*)-3-Hexen-1-ol	Alc/6	18.01	82
20	(*E*)-2-Hexenal	Ald/6	18.03	83
21	Pentanoic acid	Acid/1	18.29	60
22	2-Heptanone	Ket/5	19.30	58
23	Heptanal	Ald/7	19.85	70
24	Methyl hexanoate	Est/3	20.47	74
25	(*E,E*)-2,4-Hexadienal	Ald/8	20.35	81
26	α-Pinene	Mt hd/1	21.51	93
27	Hexanoic acid	Acid/2	21.95	60
28	(*E*)-2-Heptenal	Ald/9	22.02	68
29	Benzaldehyde	Ald/10	22.66	106
30	*o*-Cymene*	Mt hd/2	22.96	119
31	Myrcene	Mt hd/3	23.11	93
32	Pseudocumene	Ar/1	23.11	105
33	2-Pentylfuran	Fur/2	23.22	81
34	(*E,Z*)-2,4-Heptadienal	Ald/11	23.52	81
35	(*Z*)-3-Hexenyl acetate	Est/4	23.53	43
36	Octanal	Ald/12	23.64	84
37	2-Carene	Mt hd/4	23.89	93
38	(*E,E*)-2,4-Heptadienal	Ald/13	24.10	81
39	α-Phellandrene	Mt hd/5	24.15	93
40	α-Terpinene	Mt hd/6	24.50	121
41	*p*-Cymene	Mt hd/7	24.77	119
42	Limonene	Mt hd/8	24.96	68
43	β-Phellandrene*	Mt hd/9	25.15	93
44	Phenylacetaldehyde	Ald/14	25.16	91
45	(*E*)-2-Octenal	Ald/15	25.48	83
46	Salicylaldehyde	Ald/16	25.77	122
47	(*Z*)-Linalool oxide[a,b]	Alc/7	26.34	59
48	Acetophenone	Ket/6	26.38	105
49	(*Z*)-3-Hexenyl propionate	Est/5	26.77	67
50	(*E*)-Linalool oxide[a,b]	Alc/8	26.90	111
51	2-Ethyl hexanoic acid	Acid/3	26.91	88
52	Linalool[a]	Alc/9	27.04	93
53	Nonanal	Ald/17	27.18	57
54	(*Z*)-3-Hexenyl isobutyrate	Est/6	28.25	82
55	Octanoic acid	Acid/4	28.84	60
56	Benzonitrile	Nit/2	28.78	117
57	(*E*)-2-Nonenal	Ald/18	28.92	70
58	Benzyl acetate	Est/7	29.30	108
59	(*Z*)-3-Hexenyl butyrate	Est/8	29.67	67
60	4 Terpineol[a]	Alc/10	30.27	71
61	α-Terpineol[a]	Alc/11	30.65	59
62	Methyl salicylate	Est/9	30.67	65
63	Decanal	Ald/19	31.18	70
64	β-Cyclocitral[c]	Ald/20	31.53	137
65	δ-Elemene*	Sqt/1	34.88	121
66	Eugenol[c]	Alc/12	35.32	164
67	Ethyl decanoate	Est/10	35.76	88
68	α-Ionone[c]	Ket/7	37.25	121
69	β-Caryophyllene	Sqt/2	37.76	133
70	α-Humulene	Sqt/3	38.73	121
71	β-Ionone[c]	Ket/8	38.80	177
72	Methyl dodecanoate	Est/11	39.30	74
73	Nerolidol[d]	Alc/13	40.55	93

*Family Code: Alc, alcohol; Ald, aldehyde; Ar, aromatic hydrocarbon; Est, ester; Fur, furane; Ket, ketone; Mt hd, monoterpene hydrocarbon; Nit, nitrile; Sqt, sesquiterpene. *Tentative identification based on mass spectrum. [a]Monoterpene-derived compound. [b]In addition to the alcohol group, it has a tetrahydrofuran group. [c]Norcarotenoid compound. [d]Sesquiterpene-derived compound.*

The specific VOCs differentially released from the symptomatic tomato plants (virulent/avirulent ratio > 1; Supplementary Table S2) were an unidentified sesquiterpene, SA derivatives methyl salicylate and salicylaldehyde, monoterpenes α-pinene, α-phellandrene, β-phellandrene and limonene, as well as two isoprenoid chlorides. The strong induction of the SA derivatives was previously observed when comparing the volatile profiles of these susceptible plants to their corresponding mock-inoculated plants (Supplementary Figure S2). This study also revealed enhanced emission of monoterpenes after infection with virulent strain *Pst* DC3000 Δ*avrPto*/Δ*avrPtoB*.

Interestingly, we identified a set of volatiles that were significantly over-emitted by tomato plants when effectively resisting disease (green-colored in column 3 of **Figure 5**). Among them, several HMT, such as linalool, α-terpineol, 4-terpineol, (*Z*) and (*E*)-linalool oxides, HMT-1, HMT-2, HMT-3, and HMT-4, as well as the esters (*Z*)-3-hexenyl propionate, (*Z*)-3-hexenyl butyrate and (*Z*)-3-hexenyl isobutyrate, were found. The induction of these compounds is mentioned above (when comparing the volatile profiles of the resistant plants with their corresponding mock-inoculated plants; Supplementary Figure S1). The specific over-emission of these green leaf volatiles (GLVs) esters and HMTs during ETI suggests that these VOCs could participate in the defense response.

As a result of these untargeted metabolomic analyses, we conclude that the infected tomato plants emitted quantitatively

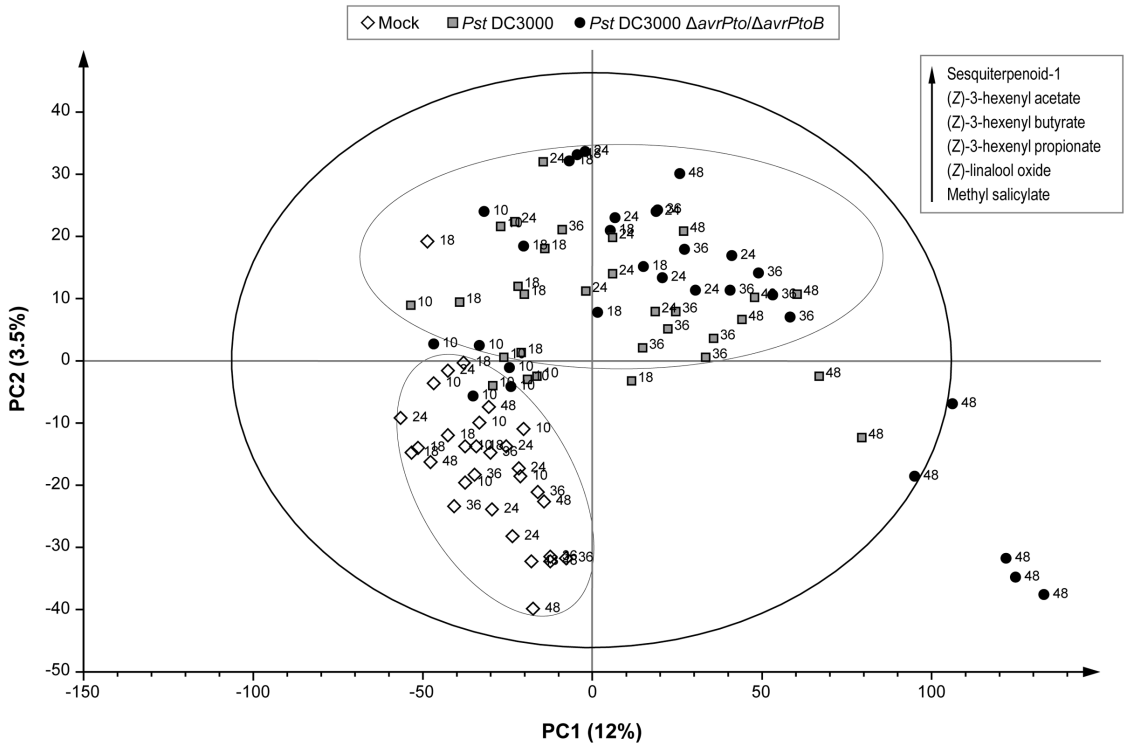

FIGURE 4 | Score plot of the PLS based on the whole array of the mass spectra within a *m/z* range from 35 to 250. (◇) Leaves of the mock-inoculated RG-*Pto* plants, (■) leaves of the RG-*Pto* plants upon infection with *Pst* DC3000, (●) leaves of the RG-*Pto* plants infected with *Pst* DC3000 Δ*avrPto*/Δ*avrPtoB*, at 10, 18, 24, 36, and 48 hpi. Metabolites displayed in the box were identified by loading plot analysis as the responsible for the observed separation.

different volatiles depending on each type of bacterial strain used in this experiment. Monoterpenes and SA derivatives were released at higher rates by the symptomatic plants upon successful bacterial infection, while HMT and hexenyl esters were differentially over-emitted during ETI establishment, which led to resistance.

Bacterial Infection Induces the Specific Expression of the Genes Involved in VOCs Biosynthesis

To study whether differential volatile production was due to transcriptional activation, we analyzed the expression levels of several key genes involved in the VOC biosynthesis by qRT-PCR. The results of the mock-inoculated RG-*Pto* tomato plants and the plants infected with *Pst* DC3000 or *Pst* DC3000 Δ*avrPto*/Δ*avrPtoB* at 10, 18, 24, 36, and 48 hpi are shown in **Figure 7**. We used the induction of the tomato Pathogenesis-Related *PR1* gene as a positive control of bacterial infection, and observed a correlation of the expression of this gene and symptom development (**Figure 7A**). GLVs esters are known to be synthesized by 13-lipoxygenases (13-LOX) via 13-hydroperoxides, which are later cleaved by 13-hydroperoxide lyases (13-HPL) into (*Z*)-3-hexenal. This last compound is reduced by alcohol dehydrogenase (ADH). Finally, ester formation is catalyzed by alcohol acyl transferases (AAT) (Scala et al., 2013a).

In tomato, six genes that encode various types of lipoxygenases (TomloxA-F) have been described (Mariutto et al., 2011). *TomloxC*, *TomloxD,* and *TomloxF* encode 13-LOX lipoxygenases, and are involved in the synthesis of oxylipins, which play an important role in the response to biotic stress. Tomlox D lipoxygenase participates in the synthesis of JA, while Tomlox C and Tomlox F are involved in the biosynthesis of GLVs. As **Figure 7B** shows, a significant induction of *TomloxF* was detected upon bacterial infection with both strains at all the studied time points, and this induction was greater when ETI had been established. Regarding alcohol acyltransferases, five *AAT* genes (SlAAT1 - 5) have been identified in tomato (Goulet et al., 2015). We observed that the induction of *AAT1* followed a similar pattern to that of *TomloxF* (**Figure 7C**). These induction patterns statistically correlated with the emission of the GLV esters (Supplementary Table S3A) in both infections, and became higher during ETI establishment. Therefore, these data are consistent with the VOCs metabolomic analysis, and suggest a possible role of the biosynthesis of GLV esters in plant defense against bacteria.

Terpene synthases (TPS) catalyze the synthesis of mono-, sesqui- and diterpenes, and are responsible for the diversity of the isoprene compounds found in nature (Degenhardt et al., 2009). There are 44 TPS genes in *Solanum lycopersicum*, 29 of which are potentially functional (Falara et al., 2011). By qRT-PCR, we observed a significant induction of *TPS5*, also known as *MTS1*

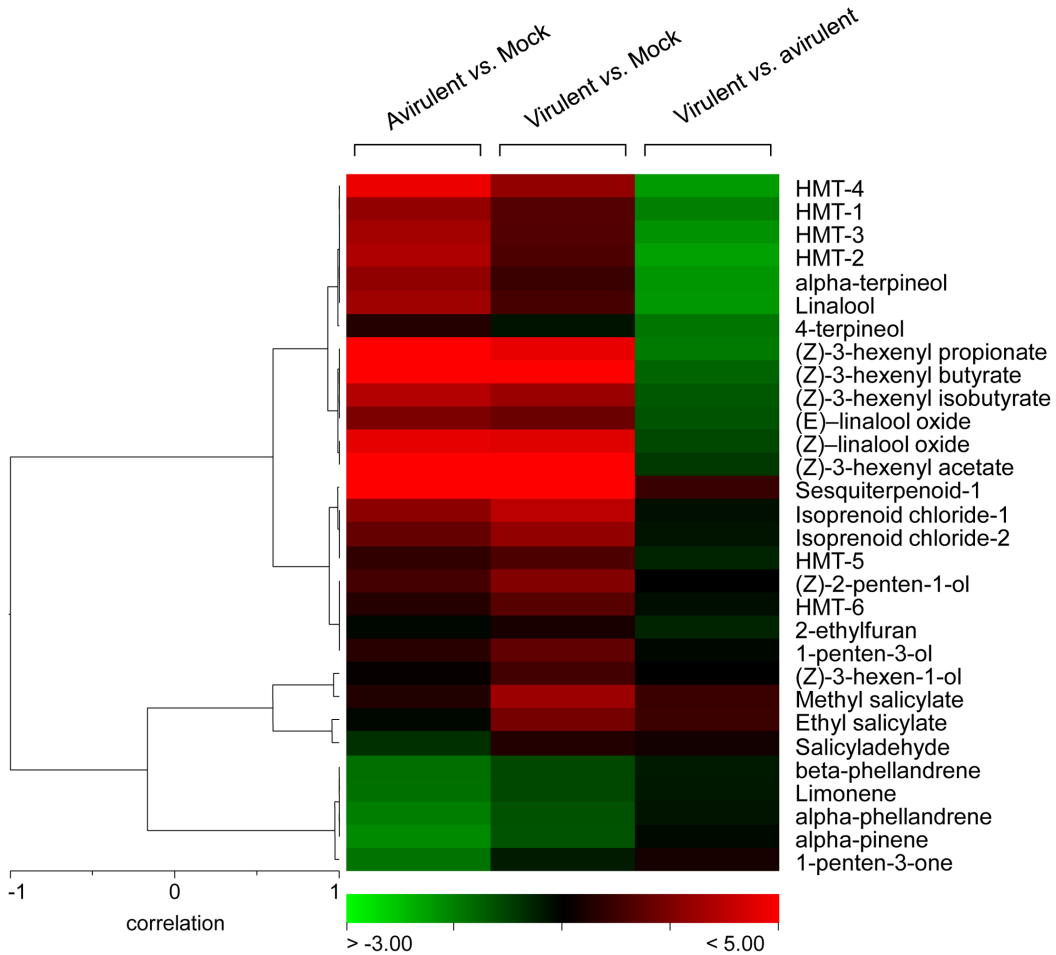

FIGURE 5 | Hierarchical cluster of the volatile compounds from infected plants. Log_2-transformed ratios are represented as a heat map according to the scale below. Red corresponds to higher values; green denotes lower values. Column 1 represents the ratios of the VOCs emitted by the tomato plants infected with avirulent strain *Pst* DC3000 *versus* the mock-inoculated tomato plants. Column 2 represents the ratios of the VOCs emitted by the tomato plants infected with virulent strain *Pst* DC3000 Δ*avrPto*/Δ*avrPtoB versus* the mock-inoculated tomato plants. Column 3 represents the ratios of the VOCs emitted by the tomato plants infected with virulent strain *Pst* DC3000 Δ*avrPto*/Δ*avrPtoB versus* the tomato plants infected with avirulent strain *Pst* DC3000.

(**Figure 7D**), in the immunized tomato plants, which peaked at 18 hpi. This gene induction correlated with the production of several HMTs, such as linalool or α-terpineol (Supplementary Table S3B).

DISCUSSION

Tomato VOCs have been associated mainly with either improved fruit quality (Rambla et al., 2014) or the response against herbivores (Wei et al., 2013). Here, we extend this knowledge to the volatile differential emission of tomato leaves infected with virulent or avirulent bacteria. We were particularly interested in studying the contribution of VOCs to the resistance mechanisms presented by tomato leaves, which display no symptoms upon bacterial infection (**Figure 1**).

To better characterize both types of compatible and incompatible interactions, the levels of the different signal molecules, e.g., SA, GA, ET, or JA, were measured at several time points (**Figures 2**, **3**). Simple natural phenolics SA and GA are fundamental components of the signal transduction pathway, which triggers defense responses against different invading pathogens in many plant species. However, the biological role of these signals depends on the plant–pathogen system (Métraux and Raskin, 1993; Bellés et al., 1999; Dempsey et al., 1999). SA accumulation is associated with incompatible interactions (Métraux et al., 1990; Rasmussen et al., 1991; Malamy et al., 1992; Silverman et al., 1993; Uknes et al., 1993; Shirasu et al., 1997), while GA is associated mainly with compatible plant–pathogen systems (Bellés et al., 2006; López-Gresa et al., 2010). GA could also constitute a signal molecule that is complementary to SA since exogenous treatments with this compound are able to induce different defense responses to those triggered by SA (Bellés et al., 1999; Campos et al., 2014). Plants also produce ET in response to most biotic and abiotic stresses (Abeles et al., 1992; Merchante et al., 2013). ET has been particularly involved

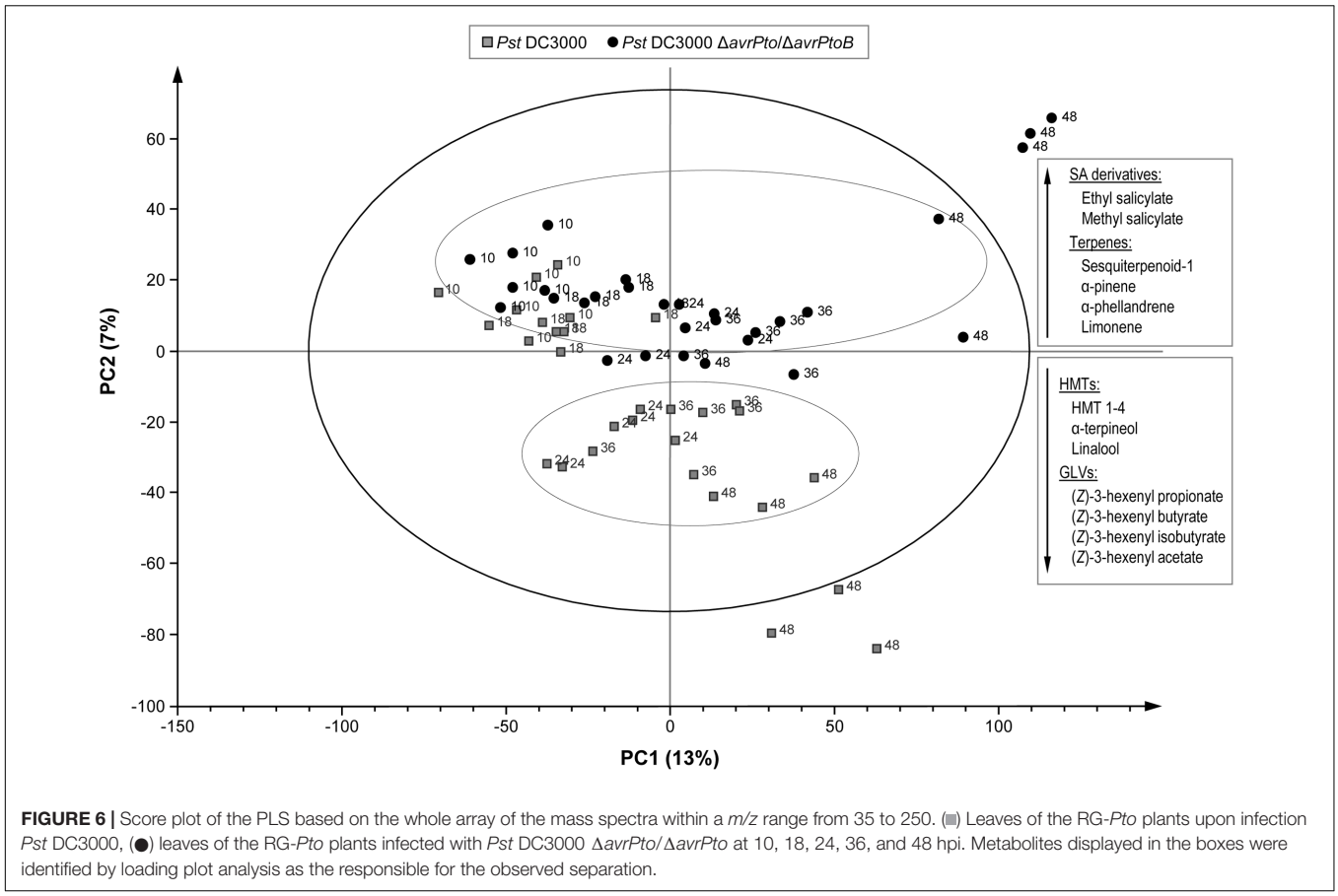

FIGURE 6 | Score plot of the PLS based on the whole array of the mass spectra within a *m/z* range from 35 to 250. (■) Leaves of the RG-*Pto* plants upon infection *Pst* DC3000, (●) leaves of the RG-*Pto* plants infected with *Pst* DC3000 Δ*avrPto*/Δ*avrPto* at 10, 18, 24, 36, and 48 hpi. Metabolites displayed in the boxes were identified by loading plot analysis as the responsible for the observed separation.

in the response of Rutgers tomato plants to bacterial pathogen *Pseudomonas syringae* when infiltrated into leaves (Bellés et al., 1989; Zacarés et al., 2007). Finally, lipid-derived hormone JA has been described as being associated with wounding response and necrotrophic infections, and produces an antagonistic effect on SA-mediated signaling (Zhang et al., 2017). Indeed JA-insensitive tomato *jai1* mutants are more resistant to virulent *Pseudomonas syringae* DC3000 (Zhao et al., 2003). However, jasmonate-deficient *def1* tomato mutants have been described as being more susceptible to *Pseudomonas syringae* and *Xanthomonas campestris* (Thaler et al., 2004), which thus indicates that the role of JA in tomato bacterial infections is still unclear.

We generally observed that SA, GA, and ET accumulated at higher levels in the tomato plants infected with the virulent bacterial strain compared to those infected with avirulent bacteria. These higher levels correlated with symptom severity. SA accumulation has been described to occur at 4 or 10 dpi in tomato plants inoculated with either avirulent or virulent *Xanthomonas,* respectively (O'Donnell et al., 2001; Block et al., 2005). Besides in these tomato interactions, an earlier increase in ET has been described in avirulent infection, while delayed ET synthesis happens in the tomato plants infected with virulent *Xanthomonas* (Ciardi et al., 2000; Block et al., 2005). These results contrast with those observed herein, where the highest ET and SA levels were detected in symptomatic bacterial infection. Several factors could be behind the different SA and ET levels described in each pathosystem, such as timing during infection progress, pathogen dose, greenhouse conditions, or the plant growth stage. Yet in all the cases, the accumulation of either SA or ET correlated with PR1 induction (**Figure 7A**), a classical marker gene that is useful for assessing disease development. The higher level of both ET and GA, detected in the RG tomato plants infected with the virulent *Pst* strain, was associated mainly with symptom development, and agrees with those previously described (Lund et al., 1998; Bellés et al., 2006). Regarding ET, the mutants and tomato genotypes impaired in ET perception or ET synthesis exhibit a significant reduction in disease symptoms *versus* the wild type upon infection with different pathogens (Lund et al., 1998). These previous results present compelling evidence that both biosynthesis and ET perception are critical for symptoms development in tomato leaves.

Unlike the accumulations of SA, GA, and ET, we observed that JA levels drastically lowered in the virulent infection in accordance with the well-known SA–JA antagonism (Zhang et al., 2017). However, in the plants infected with avirulent bacteria, JA accumulation remained comparable to the mock-inoculated plants, similarly to the detected SA levels. Very few reported studies have monitored JA levels in bacteria-infected

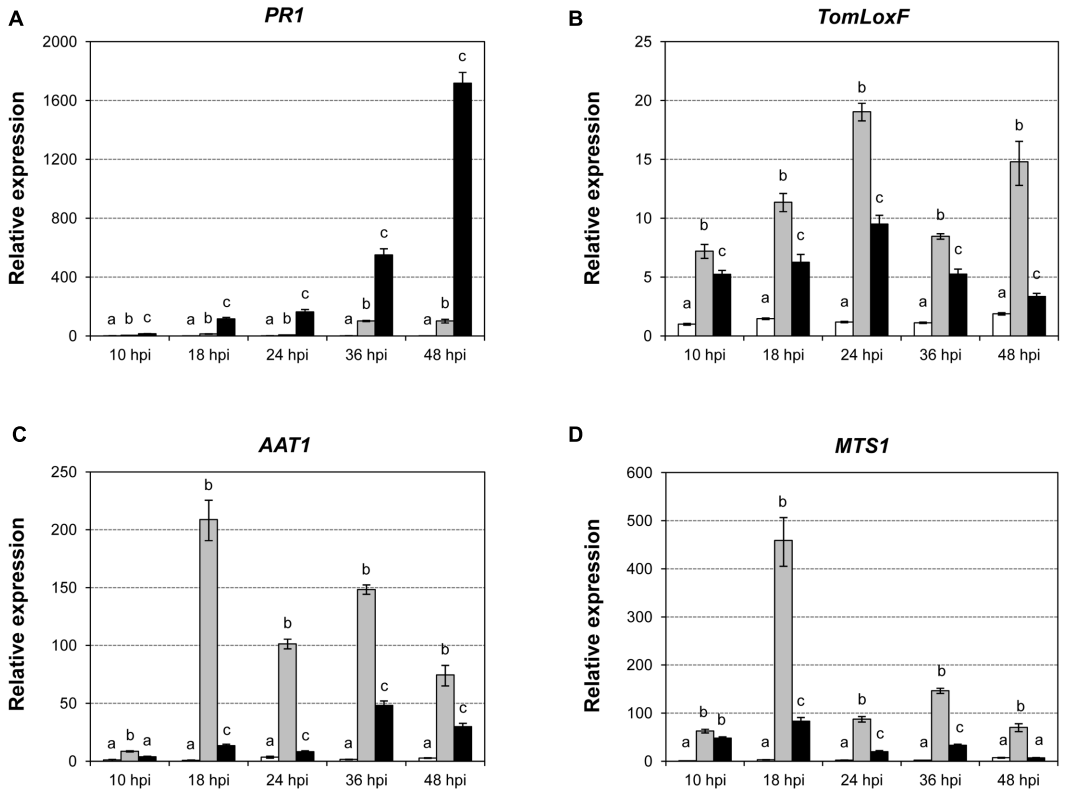

FIGURE 7 | Expression levels of the tomato *PR1* **(A)**, *TomLOXF* **(B)**, *AAT* **(C)**, and *MTS1* **(D)** genes in the mock-inoculated RG-*Pto* tomato plants (white bars) and upon infection with *Pst* DC3000 (light gray bars) or *Pst* DC3000 Δ*avrPto*/Δ*avrPtoB* (dark gray bars) at 10, 18, 24, 36, and 48 hpi, determined by a real-time qRT-PCR analysis. Values were first normalized to the *Elongation Factor 1 alpha* (*eEF1α*) expression level. Expression levels are represented as mean ± standard error of three biological repetitions. An ANOVA analysis was performed at each time point. Different letters indicate the statistical significance differences with p-value < 0.05.

plants. In Arabidopsis plants, no differences in JA levels between mock-inoculated plants and those infected with a virulent bacteria have been described at 2 and 24 hpi (Scala et al., 2013b). Unlike our dipping infection method, these authors performed inoculation with a syringe, which thus caused mechanical damage to both mock and infected leaves. This difference in the inoculation procedure could explain the divergence of our results with those previously published.

All these data indicate that the different accumulation patterns of these four signal molecules depend on the diversity of pathogens with a range of lifestyles. To our knowledge, this is the first study in which the levels of all these signal molecules have been measured in RG tomato plants infected with both *Pst* strains.

Interestingly, we observed that changes in VOCs emission were mostly independent of macroscopic symptoms since the tomato leaves infected with the avirulent strain overproduced some specific VOCs. We identified 73 emitted VOCs by the GC-MS technology. Although more than 300 VOCs have been reported in tomato fruit (Tikunov et al., 2005), very little information is available on the detailed volatile profile in tomato leaves (Buttery et al., 1987; Wang et al., 2001; Thelen et al., 2005; Zhang et al., 2008; Zhang and Chen, 2009; Proffit et al., 2011), thus our data contribute to this knowledge. The comparison of the VOCs profiles of tomato leaves upon infection with virulent and avirulent *Pseudomonas syringae* strains allowed us to identify the differentially emitted compounds associated with each interaction. The VOCs emission of a diseased leaf is enriched in monoterpenes and SA derivatives, while that of a resisting leaf is characterized mainly by esters of hexenyl GLVs and HMTs.

For the VOCs emitted by symptomatic tomato leaves, the induction of monoterpenes in tomato plants upon *Botrytis* infection has been described, where α-phellandrene and β-phellandrene, 2-carene, limonene, and α-pinene contributed to more than 95% of volatile emissions (Jansen et al., 2009). Nevertheless, the specific release of monoterpenes has been described in pepper plants exposed to the incompatible *Xanthomona*s pathogen, but not in compatible interaction (Cardoza and Tumlinson, 2006). MeSA is generally induced upon pathogen infection (Loake and Grant, 2007). In pepper plants infected with avirulent and virulent *Xanthomonas* strains, MeSA is also emitted at higher levels in the compatible interaction (Cardoza and Tumlinson, 2006). However, in tobacco plants infected with several *P. syringae* strains, MeSA levels become higher upon avirulent inoculation (Huang et al., 2003).

Biotic stresses have been described to trigger emissions of volatile molecules, which are products of the lipoxygenase (LOX) pathway, such as C_6 aldehydes, alcohols and derivatives, generally referred to as GLVs (Niinemets et al., 2013). For example, *Pst* infection provokes the emission of (*Z*)-3-hexenol and (*E*)-2-hexenal in bean and tobacco leaves, respectively (Croft et al., 1993; Heiden et al., 2003). GLVs are also emitted after fungal and virus infections (Scala et al., 2013a). In tomato plants, (*Z*)-3-hexenol, (*Z*)-3-hexenal, and (*Z*)-3-hexenyl acetate are the dominant LOX products in the volatile emission after *Botrytis cinerea* inoculation (Jansen et al., 2009). Volatile esters not only contribute to the aroma of many fruits and flowers, but are also related to plant defense and plant-to-plant signaling (Goulet et al., 2015). The ester (*Z*)-3-hexenyl acetate is one of the most abundant volatiles to be emitted from mechanically or herbivore-damaged *Arabidopsis thaliana* plants (D'Auria et al., 2007), and can prime a defense response in nearby plants (Engelberth et al., 2004; Frost et al., 2008). The emission of other (*Z*)-3-hexenyl esters has also been described in pepper plants upon *Xanthomonas* infection (Cardoza and Tumlinson, 2006). The induction of (*Z*)-3-hexenol and some of its derived esters upon both bacterial infection types in the tomato plants reported herein extend GLVs emission to other plant–pathogen interactions. Our results, together with those in which (*Z*)-3-hexenol induces defense genes in Arabidopsis and maize plants (Bate and Rothstein, 1998; Farag et al., 2005), suggest that this alcohol can act as a signaling molecule involved in plant response. Another short-chain alcohol, 3-pentanol, has been found to trigger induced resistance in Arabidopsis against *Pseudomonas syringae* (Song et al., 2015), and also in pepper against *Xanthomonas axonopodis* pv. *vesicatoria* (Choi et al., 2014), by priming the SA and JA signaling pathways. Besides, several reports have shown the antifungal (Vaughn et al., 1993) and antibacterial properties (Croft et al., 1993; Deng et al., 1993) of GLVs, which thus reinforces the role of these VOCs in plant defense. Our results also reveal the possible defensive role of GLV esterification since these GLV esters were overproduced during ETI establishment.

Some of these GLVs, including hexanal, (*Z*)-3-hexenal or (*E*)-2-hexenal, have also been described as major compounds emitted by tomato fruit (Rambla et al., 2014), where *Pseudomonas syringae* can cause damage (Xin and He, 2013). Although esterase activity in fruit is enhanced in the red-fruited species of the tomato clade (Goulet et al., 2012), it would be interesting to study whether infection with virulent or avirulent bacteria could produce the esterification of these aldehydes in fruit, which would thus extend the defensive role of these GLVs esters to other organs.

Other VOCs involved in the defense response of plants are terpenoids, which are emitted after wounding or egg deposition by insects. Terpenoids induced by herbivores act in plant defense by attracting insect predators, and by acting as repellents or toxic compounds (Turlings and Tumlinson, 1992; Wegener et al., 2001). Besides, they have been associated to resistance against downy mildew in grapevine (Alarcón et al., 2015). However, the role of terpenoids in plant-bacteria interactions is not well studied. Here, we detected different HMTs, such as (*Z*)- and (*E*)-linalool oxides, linalool, α-terpineol, 4-terpineol, and six putative HMTs emitted from both infected plant types, where induction was greater in avirulent infection. The release of linalool and β-ocimene has also been described in tobacco plants infected by an avirulent strain of *Pseudomonas* (Huang et al., 2003). Since monoterpenes are emitted mainly by symptomatic plants, and HMTs are differentially released by those displaying the immune response, terpene hydroxylation appears to be a key process in the plant defense response.

In order to study whether the increase in VOC was associated with the induction of the VOC biosynthesis machinery, the expression of several genes, e.g., *Tomlox* and *AAT,* involved in the biosynthetic pathway of the esters of GLVs, and *TPS*, implicated in the biosynthesis of terpenoids, was studied by qRT-PCR. We observed a positive correlation in the induction of *TomloxF, AAT1,* and *MTS1* with the emission of the corresponding VOCs, which were differentially released in the tomato plants that displayed ETI.

Among the six described Tomlox isoforms, the induction of the *TomloxF* gene has also been described to result from the infection caused by *Pseudomonas putida* (Mariutto et al., 2011). Our results reinforce the defensive role of this tomato LOX isoform and validate the metabolomic analysis. Regarding the different isoforms of the tomato alcohol acyltransferases, AAT1 has been correlated to the production of GLV esters in tomato fruits (Goulet et al., 2015). Accordingly, we observed the induction of the *AAT1* gene upon bacterial infection, and the corresponding GLV esters accumulation, being this induction greater in the tomato plants that exhibited ETI.

Volatile isoprenoids represent the most abundant group of volatile compounds in plants, and are common components of both their aroma and defensive response induced by herbivores and pathogens (Aharoni et al., 2005). The observed induction of *MTS1* upon bacterial infection correlates with the detected emission of monoterpenes and HMTs, and agrees with the previously described role of TPS in plant defense. Transgenic plants of *Arabidopsis thaliana,* which overexpress the *TPS (E)-β-caryophyllene synthase* gene, emit larger amounts of this sesquiterpene and are more resistant to bacterial infection, which confirms the role of this gene in defense (Huang et al., 2012). *MTS1* expression in tomato leaves has been described to be induced by spider mite-infestation, wounding and JA treatment (van Schie et al., 2007).

Terpene synthases reaction products are subsequently modified by hydroxylation, methylation, acylation, reduction, oxidation, isomerization, or glycosylation, which gives rise to more complex terpene compounds. Hydroxylation of monoterpenes, which would lead to compounds such as α-terpineol, is performed by Cytochrome P450 enzymes (CYP450) (Höfer et al., 2014). There are approximately 250 CYPs in tomato[1], which means that clarifying which CYP450 might be responsible for terpene hydroxylation and is, therefore, involved in defense through this signaling pathway, is a complex task. However, approximately 25 CYP proteins have been reported to

[1]www.solgenomics.net

be involved in the immune response of tomato plants to bacteria *Pst*, which helps limit the search of the CYP450 responsible for the hydroxylation of terpenes and confirms the importance of hydroxylation in plant defense response (Pombo et al., 2014).

Our results suggested that the esters of GLVs and HMTs could play a defensive role in the tomato plant response. Unlike SA accumulation, which is the classical signal molecule in incompatible interactions that accumulates at higher levels in virulent infections, these VOCs were differentially emitted at higher levels when plants efficiently resisted bacterial infection, which indicates that they could play a defensive role. Further studies, such as pharmacological or genetic approaches, could be conducted to test this possibility. These volatile compounds could also display interesting biological properties, such as antioxidant, antimicrobial, insecticide or resistance inducers, and could be good candidates for agrochemical and pharmaceutical industries. Besides, the generation of tomato transgenic plants over-expressing enzymes involved in the biosynthesis of these volatiles could result in a new biotechnological strategy to obtain resistance.

AUTHOR CONTRIBUTIONS

MPL-G and JMB conceived and designed the study. MPL-G, PL, and LC carried out the experiments. IR prepared the figures. MPL-G, JLR, and AG performed the GC-MS-based metabolomics approach. MPL-G and PL did the data processing and statistical analysis. MPL-G, PL, IR, VC, and JMB interpreted the results. MPL-G and PL wrote the manuscript. JMB handled the literature.

FUNDING

This work was funded by Grant BIO2012-33419 from the Spanish Ministry of Economy and Competitiveness.

ACKNOWLEDGMENTS

We would like to thank Dr. Selena Giménez-Sánchez (Centro Nacional de Biotecnología, Madrid) for kindly providing us with both strains of *Pseudomonas syringae* pv. *tomato* DC3000. We thank Dr. Isabel López-Díaz and Dr. Esther Carrera for the hormone quantification carried out at the Plant Hormone Quantification Service, IBMCP, Valencia, Spain. We are also very grateful to Teresa Caballero and Ana Ruiz for their excellent technical support.

SUPPLEMENTARY MATERIAL

The Supplementary Material for this article can be found online at: http://journal.frontiersin.org/article/10.3389/fpls.2017.01188/full#supplementary-material

REFERENCES

Abeles, F. B., Morgan, P. W., and Saltveit, M. E. Jr. (1992). "Regulation of ethylene production by internal, environmental, and stress factors," in *Ethylene in Plant Biology*, eds F. Abeles, P. Morgan, and M. Saltveit Jr. (San Diego, CA: Academic Press Inc.), 56–119.

Aharoni, A., Jongsma, M. A., and Bouwmeester, H. J. (2005). Volatile science? Metabolic engineering of terpenoids in plants. *Trends Plant Sci.* 10, 594–602. doi: 10.1016/j.tplants.2005.10.005

Alarcón, A., Lazazzara, V., Cappellin, L., Bianchedi, P. L., Schuhmacher, R., Wohlfahrt, G., et al. (2015). Emission of volatile sesquiterpenes and monoterpenes in grapevine genotypes following *Plasmopara viticola* inoculation *in vitro*. *Mass Spectrom.* 50, 1013–1022. doi: 10.1002/jms.3615

Allwood, J. W., Ellis, D. I., and Goodacre, R. (2008). Metabolomic technologies and their application to the study of plants and plant–host interactions. *Physiol. Plant.* 132, 117–135. doi: 10.1111/j.1399-3054.2007.01001.x

Allwood, J. W., Heald, J., Lloyd, A. J., Goodacre, R., and Mur, L. A. J. (2012). Separating the inseparable: the metabolomic analysis of plant-pathogen interactions. *Methods Mol. Biol.* 860, 31–49. doi: 10.1007/978-1-61779-594-7_3

Bate, N. J., and Rothstein, S. J. (1998). C6-volatiles derived from the lipoxygenase pathway induce a subset of defense-related genes. *Plant J.* 16, 561–569. doi: 10.1046/j.1365-313x.1998.00324.x

Bellés, J. M., Garro, R., Fayos, J., Navarro, P., Primo, J., and Conejero, V. (1999). Gentisic acid as a pathogen-inducible signal, additional to salicylic acid for activation of plant defenses in tomato. *Mol. Plant Microbe Interact.* 12, 227–235. doi: 10.1094/MPMI.1999.12.3.227

Bellés, J. M., Garro, R., Pallás, V., Fayos, J., Rodrigo, I., and Conejero, V. (2006). Accumulation of gentisic acid as associated with systemic infections but not with the hypersensitive response in plant-pathogen interactions. *Planta* 223, 500–511. doi: 10.1007/s00425-005-0109-8

Bellés, J. M., Granell, A., Durán-Vila, N., and Conejero, V. (1989). ACC synthesis as the activated step responsible for the rise of ethylene production accompanying Citrus Exocortis Viroid infection in tomato plants. *J. Phytopathol.* 125, 198–208. doi: 10.1111/j.1439-0434.1989.tb01061.x

Bellés, J. M., López-Gresa, M. P., Fayos, J., Pallás, V., Rodrigo, I., and Conejero, V. (2008). Induction of cinnamate 4-hydroxylase and phenylpropanoids in virus-infected cucumber and melon plants. *Plant Sci.* 174, 524–533. doi: 10.1016/j.plantsci.2008.02.008

Block, A., Schmelz, E., O'Donnell, P. J., Jones, J. B., and Klee, H. J. (2005). Systemic acquired tolerance to virulent bacterial pathogens in tomato. *Plant Physiol.* 138, 1481–1490. doi: 10.1104/pp.105.059246

Buttery, R. G., Ling, L. C., and Light, D. M. (1987). Tomato leaf volatile aroma components. *J. Agric. Food Chem.* 35, 1039–1042. doi: 10.1021/jf00078a043

Campos, L., Granell, P., Tárraga, S., López-Gresa, P., Conejero, V., Bellés, J. M., et al. (2014). Salicylic acid and gentisic acid induce RNA silencing-related genes and plant resistance to RNA pathogens. *Plant Physiol. Biochem.* 77, 35–43. doi: 10.1016/j.plaphy.2014.01.016

Cardoza, Y. J., and Tumlinson, J. H. (2006). Compatible and incompatible *Xanthomonas* infections differentially affect herbivore-induced volatile emission by pepper plants. *J. Chem. Ecol.* 32, 1755–1768. doi: 10.1007/s10886-006-9107-y

Choi, H. K., Song, G. C., Yi, H. S., and Ryu, C. M. (2014). Field evaluation of the bacterial volatile derivative 3-pentanol in priming for induced resistance in pepper. *J. Chem. Ecol.* 40, 882–892. doi: 10.1007/s10886-014-0488-z

Ciardi, J. A., Tieman, D. M., Lund, S. T., Jones, J. B., Stall, R. E., and Klee, H. J. (2000). Response to *Xanthomonas campestris* pv. *vesicatoria* in tomato involves regulation of ethylene receptor gene expression. *Plant Physiol.* 123, 81–92. doi: 10.1104/pp.123.1.81

Croft, K. P. C., Juttner, F., and Slusarenko, A. J. (1993). Volatile products of the lipoxygenase pathway evolved from *Phaseolus vulgaris* (L.) leaves inoculated with *Pseudomonas syringae* pv *phaseolicola*. *Plant Physiol.* 101, 13–24. doi: 10.1104/pp.101.1.13

Dangl, J. L., and Jones, J. D. G. (2001). Plant pathogens and integrated defence responses to infection. *Nature* 411, 826–833. doi: 10.1038/35081161

D'Auria, J. C., Pichersky, E., Schaub, A., Hansel, A., and Gershenzon, J. (2007). Characterization of a BAHD acyltransferase responsible for producing the green leaf volatile (*Z*)-3-hexen-1-yl acetate in *Arabidopsis thaliana*. *Plant J.* 49, 194–207. doi: 10.1111/j.1365-313X.2006.02946.x

Degenhardt, J., Koellner, T. G., and Gershenzon, J. (2009). Monoterpene and sesquiterpene synthases and the origin of terpene skeletal diversity in plants. *Phytochemistry* 70, 1621–1637. doi: 10.1016/j.phytochem.2009.07.030

Dempsey, D. M. A., Shah, J., and Klessig, D. F. (1999). Salicylic acid and disease resistance in plants. *Crit. Rev. Plant Sci.* 18, 547–575. doi: 10.1080/07352689991309397

Deng, W., Hamilton-Kemp, T. R., Nielsen, M. T., Andersen, R. A., Collins, G. B., and Hildebrand, D. F. (1993). Effects of six-carbon aldehydes and alcohols on bacterial proliferation. *J. Agric. Food Chem.* 41, 506–510. doi: 10.1021/jf00027a030

Dixon, R. A. (2001). Natural products and plant disease resistance. *Nature* 411, 843–847. doi: 10.1038/35081178

Dudareva, N., Klempien, A., Muhlemann, J. K., and Kaplan, I. (2013). Biosynthesis, function and metabolic engineering of plant volatile organic compounds. *New Phytol.* 198, 16–32. doi: 10.1111/nph.12145

Dudareva, N., Negre, F., Nagegowda, D. A., and Orlova, I. (2006). Plant volatiles: recent advances and future perspectives. *Crit. Rev. Plant Sci.* 25, 417–440. doi: 10.1080/07352680600899973

Engelberth, J., Alborn, H. T., Schmelz, E. A., and Tumlinson, J. H. (2004). Airborne signals prime plants against insect herbivore attack. *Proc. Natl. Acad. Sci. U.S.A* 101, 1781–1785. doi: 10.1073/pnas.0308037100

Falara, V., Akhtar, T. A., Nguyen, T. T. H., Spyropoulou, E. A., Bleeker, P. M., Schauvinhold, I., et al. (2011). The tomato terpene synthase gene family. *Plant Physiol.* 157, 770–789. doi: 10.1104/pp.111.179648

Farag, M. A., Fokar, M., Abd, H., Zhang, H., Allen, R. D., and Pare, P. W. (2005). (*Z*)-3-Hexenol induces defense genes and downstream metabolites in maize. *Planta* 220, 900–909. doi: 10.1007/s00425-004-1404-5

Frost, C. J., Mescher, M. C., Dervinis, C., Davis, J. M., Carlson, J. E., and De Moraes, C. M. (2008). Priming defense genes and metabolites in hybrid poplar by the green leaf volatile *cis*-3-hexenyl acetate. *New Phytol.* 180, 722–734. doi: 10.1111/j.1469-8137.2008.02599.x

Goulet, C., Kamiyoshihara, Y., Lam, N. B., Richard, T., Taylor, M. G., Tieman, D. M., et al. (2015). Divergence in the enzymatic activities of a tomato and *Solanum pennellii* alcohol acyltransferase impacts fruit volatile ester composition. *Mol. Plant* 8, 153–162. doi: 10.1016/j.molp.2014.11.007

Goulet, C., Mageroy, M. H., Lam, N. B., Floystad, A., Tieman, D. M., and Klee, H. J. (2012). Role of an esterase in flavor volatile variation within the tomato clade. *Proc. Natl. Acad. Sci. U.S.A.* 109, 19009–19014. doi: 10.1073/pnas.1216515109

Granell, A., and Rambla, J. L. (2013). "Biosynthesis of Volatile Compounds," in *The Molecular Biology and Biochemistry of Fruit Ripening*, eds G. B. Seymour, M. Poole, J. J. Giovannoni, and G. A. Tucker (Hoboken, NJ: Blackwell Publishing Ltd.), 135–161. doi: 10.1002/9781118593714.ch6

Heiden, A. C., Kobel, K., Langebartels, C., Schuh-Thomas, G., and Wildt, J. (2003). Emissions of oxygenated volatile organic compounds from plants. Part I: emissions from lipoxygenase activity. *J. Atmos. Chem.* 45, 143–172. doi: 10.1023/A:1024069605420

Höfer, R., Boachon, B., Renault, H., Gavira, C., Miesch, L., Iglesias, J., et al. (2014). Dual function of the cytochrome P450 CYP76 family from *Arabidopsis thaliana* in the metabolism of monoterpenols and phenylurea herbicides. *Plant Physiol.* 166, 1149–1161. doi: 10.1104/pp.114.244814

Holopainen, J. K., and Gershenzon, J. (2010). Multiple stress factors and the emission of plant VOCs. *Trends Plant Sci.* 15, 176–184. doi: 10.1016/j.tplants.2010.01.006

Huang, J., Cardoza, Y. J., Schmelz, E. A., Raina, R., Engelberth, J., and Tumlinson, J. H. (2003). Differential volatile emissions and salicylic acid levels from tobacco plants in response to different strains of *Pseudomonas syringae*. *Planta* 217, 767–775. doi: 10.1007/s00425-003-1039-y

Huang, J., Schmelz, E. A., Alborn, H., Engelberth, J., and Tumlinson, J. H. (2005). Phytohormones mediate volatile emissions during the interaction of compatible and incompatible pathogens: the role of ethylene in *Pseudomonas syringae* infected tobacco. *J. Chem. Ecol.* 31, 439–459. doi: 10.1007/s10886-005-2018-5

Huang, M., Sanchez-Moreiras, A. M., Abel, C., Sohrabi, R., Lee, S., Gershenzon, J., et al. (2012). The major volatile organic compound emitted from *Arabidopsis thaliana* flowers, the sesquiterpene (*E*)-β-caryophyllene, is a defense against a bacterial pathogen. *New Phytol.* 193, 997–1008. doi: 10.1111/j.1469-8137.2011.04001.x

Jansen, R. M. C., Miebach, M., Kleist, E., Van Henten, E. J., and Wildt, J. (2009). Release of lipoxygenase products and monoterpenes by tomato plants as an indicator of *Botrytis cinerea*-induced stress. *Plant Biol.* 11, 859–868. doi: 10.1111/j.1438-8677.2008.00183.x

Jia, Y. L., Loh, Y. T., Zhou, J. M., and Martin, G. B. (1997). Alleles of *Pto* and *Fen* occur in bacterial speck-susceptible and fenthion-insensitive tomato cultivars and encode active protein kinases. *Plant Cell* 9, 61–73. doi: 10.1105/tpc.9.1.61

Kalaivani, K., Kalaiselvi, M. M., and Senthil-Nathan, S. (2016). Effect of methyl salicylate (MeSA), an elicitor on growth, physiology and pathology of resistant and susceptible rice varieties. *Sci. Rep.* 6:34498. doi: 10.1038/srep34498

Lieberherr, D., Wagner, U., Dubuis, P.-H., Métraux, J.-P., and Mauch, F. (2003). The rapid induction of glutathione S-transferases AtGSTF2 and AtGSTF6 by avirulent *Pseudomonas syringae* is the result of combined salicylic acid and ethylene signaling. *Plant Cell Physiol.* 44, 750–757. doi: 10.1093/pcp/pcg093

Lin, N. C., and Martin, G. B. (2005). An *avrPto/avrPtoB* mutant of *Pseudomonas syringae* pv. *tomato* DC3000 does not elicit Pto-mediated resistance and is less virulent on tomato. *Mol. Plant Microbe Interact.* 18, 43–51. doi: 10.1094/MPMI-18-0043

Loake, G., and Grant, M. (2007). Salicylic acid in plant defence—the players and protagonists. *Curr. Opin. Plant Biol.* 10, 466–472. doi: 10.1016/j.pbi.2007.08.008

López-Gresa, M. P., Maltese, F., Bellés, J. M., Conejero, V., Kim, H. K., Choi, Y. H., et al. (2010). Metabolic response of tomato leaves upon different plant–pathogen interactions. *Phytochem. Anal.* 21, 89–94. doi: 10.1002/pca.1179

Lund, S. T., Stall, R. E., and Klee, H. J. (1998). Ethylene regulates the susceptible response to pathogen infection in tomato. *Plant Cell* 10, 371–382. doi: 10.1105/tpc.10.3.371

Malamy, J., Hennig, J., and Klessig, D. F. (1992). Temperature dependent induction of salicylic acid and its conjugates during the resistance response to tobacco mosaic virus infection. *Plant Cell* 4, 359–366. doi: 10.1105/tpc.4.3.359

Mallona, I., Weiss, J., and Egea-Cortines, M. (2011). pcrEfficiency: a Web tool for PCR amplification efficiency prediction. *BMC Bioinformatics* 12:404. doi: 10.1186/1471-2105-12-404

Mariutto, M., Duby, F., Adam, A., Bureau, C., Fauconnier, M.-L., Ongena, M., et al. (2011). The elicitation of a systemic resistance by *Pseudomonas putida* BTP1 in tomato involves the stimulation of two lipoxygenase isoforms. *BMC Plant Biol.* 11:29. doi: 10.1186/1471-2229-11-29

Martin, G. B., Brommonschenkel, S. H., Chunwongse, J., Frary, A., Ganal, M. W., Spivey, R., et al. (1993). Map-based cloning of a protein kinase gene conferring disease resistance in tomato. *Science* 262, 1432–1436. doi: 10.1126/science.7902614

Merchante, C., Alonso, J. M., and Stepanova, A. N. (2013). Ethylene signaling: simple ligand, complex regulation. *Curr. Opin. Plant Biol.* 16, 554–560. doi: 10.1016/j.pbi.2013.08.001

Métraux, J. P., and Raskin, I. (1993). "Role of phenolics in plant disease resistance," in *Application on Biotechnology in Plant Pathology*, ed. I. Che (New York, NY: Willey), 191–209.

Métraux, J. P., Signer, H., Ryals, J., Ward, E., Wyssbenz, M., Gaudin, J., et al. (1990). Increase in salicylic-acid at the onset of systemic acquired-resistance in cucumber. *Science* 250, 1004–1006. doi: 10.1126/science.250.4983.1004

Niinemets, U., Kaennaste, A., and Copolovici, L. (2013). Quantitative patterns between plant volatile emissions induced by biotic stresses and the degree of damage. *Front. Plant Sci.* 4:262. doi: 10.3389/fpls.2013.00262

Ntoukakis, V., Mucyn, T. S., Gimenez-lbanez, S., Chapman, H. C., Gutierrez, J. R., Balmuth, A. L., et al. (2009). Host inhibition of a bacterial virulence effector triggers immunity to infection. *Science* 324, 784–787. doi: 10.1126/science.1169430

O'Donnell, P. J., Jones, J. B., Antoine, F. R., Ciardi, J., and Klee, H. J. (2001). Ethylene-dependent salicylic acid regulates an expanded cell death response to a plant pathogen. *Plant J.* 25, 315–323. doi: 10.1046/j.1365-313x.2001.00968.x

Pombo, M. A., Zheng, Y., Fernández-Pozo, N., Dunham, D. M., Fei, Z., and Martin, G. B. (2014). Transcriptomic analysis reveals tomato genes whose expression is induced specifically during effector-triggered immunity and identifies the Epk1 protein kinase which is required for the host response to three bacterial effector proteins. *Genome Biol.* 15:492. doi: 10.1186/s13059-014-0492-1

Proffit, M., Birgersson, G., Bengtsson, M., Reis, R. Jr., Witzgall, P., and Lima, E. (2011). Attraction and oviposition of *Tuta absoluta* females in response to

tomato leaf volatiles. *J. Chem. Ecol.* 37, 565–574. doi: 10.1007/s10886-011-9961-0

Pusztahelyi, T., Holb, I., and Pócsi, I. (2015). Secondary metabolites in fungus-plant interactions. *Front. Plant Sci.* 6:573. doi: 10.3389/fpls.2015.00573

Qian, Y., Tan, D.-X., Reiter, R. J., and Shi, H. (2015). Comparative metabolomic analysis highlights the involvement of sugars and glycerol in melatonin-mediated innate immunity against bacterial pathogen in *Arabidopsis*. *Sci. Rep.* 5:15815. doi: 10.1038/srep15815

Rambla, J. L., López-Gresa, M. P., Bellés, J. M., and Granell, A. (2015). "Metabolomic profiling of plant tissues," in *Plant Functional Genomics. Methods and Protocols*, eds J. M. Alonso and N. A. Stepanova (New York, NY: Humana Press), 221–235.

Rambla, J. L., Tikunov, Y. M., Monforte, A. J., Bovy, A. G., and Granell, A. (2014). The expanded tomato fruit volatile landscape. *J. Exp. Bot.* 65, 4613–4623. doi: 10.1093/jxb/eru128

Rasmussen, J. B., Hammerschmidt, R., and Zook, M. N. (1991). Systemic induction of salicylic acid accumulation in cucumber after inoculation with *Pseudomonas syringae* pv *syringae*. *Plant Physiol.* 97, 1342–1347. doi: 10.1104/pp.97.4.1342

Salmeron, J. M., Barker, S. J., Carland, F. M., Mehta, A. Y., and Staskawicz, B. J. (1994). Tomato mutants altered in bacterial disease resistance provide evidence for a new locus controlling pathogen recognition. *Plant Cell* 6, 511–520. doi: 10.1105/tpc.6.4.511

Scala, A., Allmann, S., Mirabella, R., Haring, A. M., and Schuurink, C. R. (2013a). Green leaf volatiles: a plant's multifunctional weapon against herbivores and pathogens. *Int. J. Mol. Sci.* 14, 17781–17811. doi: 10.3390/ijms140917781

Scala, A., Mirabella, R., Mugo, C., Matsui, K., Haring, M., and Schuurink, R. (2013b). *E*-2-hexenal promotes susceptibility to *Pseudomonas syringae* by activating jasmonic acid pathways in *Arabidopsis*. *Front. Plant Sci.* 4:74. doi: 10.3389/fpls.2013.00074

Seo, M., Jikumaru, Y., and Kamiya, Y. (2011). "Profiling of hormones and related metabolites in seed dormancy and germination studies," in *Seed Dormancy. Methods and Protocols*, ed. A. R. Kermode (Totowa, NJ: Humana Press), 99–111.

Shen, J., Tieman, D., Jones, J. B., Taylor, M. G., Schmelz, E., Huffaker, A., et al. (2014). A 13-lipoxygenase, TomloxC, is essential for synthesis of C5 flavour volatiles in tomato. *J. Exp. Bot.* 65, 419–428. doi: 10.1093/jxb/ert382

Shirasu, K., Nakajima, H., Rajasekhar, V. K., Dixon, R. A., and Lamb, C. (1997). Salicylic acid potentiates an agonist-dependent gain control that amplifies pathogen signals in the activation of defense mechanisms. *Plant Cell* 9, 261–270. doi: 10.1105/tpc.9.2.261

Silverman, P., Nuckles, E., Ye, X. S., Kuc, J., and Raskin, I. (1993). Salicylic acid, ethylene, and pathogen resistance in tobacco. *Mol. Plant Microbe Interact.* 6, 775–781. doi: 10.1094/MPMI-6-775

Song, G. C., Choi, H. K., and Ryu, C. M. (2015). Gaseous 3-pentanol primes plant immunity against a bacterial speck pathogen, *Pseudomonas syringae* pv. *tomato* via salicylic acid and jasmonic acid-dependent signaling pathways in *Arabidopsis*. *Front. Plant Sci.* 6:821. doi: 10.3389/fpls.2015.00821

Thaler, J. S., Owen, B., and Higgins, V. J. (2004). The role of the jasmonate response in plant susceptibility to diverse pathogens with a range of lifestyles. *Plant Physiol.* 135, 530–538. doi: 10.1104/pp.104.041566

Thelen, J., Harbinson, J., Jansen, R., Van Straten, G., Posthumus, M. A., Woltering, E. J., et al. (2005). The sesquiterpene α-copaene is induced in tomato leaves infected by *Botrytis cinerea*. *J. Plant Interact.* 1, 163–170. doi: 10.1080/17429140600968177

Tikunov, Y., Lommen, A., de Vos, C. H. R., Verhoeven, H. A., Bino, R. J., Hall, R. D., et al. (2005). A novel approach for nontargeted data analysis for metabolomics. Large-scale profiling of tomato fruit volatiles. *Plant Physiol.* 139, 1125–1137. doi: 10.1104/pp.105.068130

Turlings, T. C., and Tumlinson, J. H. (1992). Systemic release of chemical signals by herbivore-injured corn. *Proc. Natl. Acad. Sci. U.S.A.* 89, 8399–8402. doi: 10.1073/pnas.89.17.8399

Uknes, S., Winter, A. M., Delaney, T., Vernooij, B., Morse, A., Friedrich, L., et al. (1993). Biological induction of systemic acquired resistance in *Arabidopsis*. *Mol. Plant Microbe Interact.* 6, 692–698. doi: 10.1094/MPMI-6-692

van Schie, C. C., Haring, M. A., and Schuurink, R. C. (2007). Tomato linalool synthase is induced in trichomes by jasmonic acid. *Plant Mol. Biol.* 64, 251–263. doi: 10.1007/s11103-007-9149-8

Vaughn, S. F., Spencer, G. F., and Shasha, B. S. (1993). Volatile compounds from raspberry and strawberry fruit inhibit postharvest decay fungi. *J. Food Sci.* 58, 793–796. doi: 10.1111/j.1365-2621.1993.tb09360.x

Wang, C., Xing, J., Chin, C. K., Ho, C. T., and Martin, C. E. (2001). Modification of fatty acids changes the flavor volatiles in tomato leaves. *Phytochemistry* 58, 227–232. doi: 10.1016/S0031-9422(01)00233-3

Wegener, R., Schulz, S., Meiners, T., Hadwich, K., and Hilker, M. (2001). Analysis of volatiles induced by oviposition of elm leaf beetle *Xanthogaleruca luteola* on Ulmus minor. *J. Chem. Ecol.* 27, 499–515. doi: 10.1023/A:1010397107740

Wei, J., Yan, L., Ren, Q., Li, C., Ge, F., and Kang, L. (2013). Antagonism between herbivore-induced plant volatiles and trichomes affects tritrophic interactions. *Plant Cell Environ.* 36, 315–327. doi: 10.1111/j.1365-3040.2012.02575.x

Willis, D. K., and Kinscherf, T. G. (2009). Population dynamics of *Pseudomonas syringae* pv. *tomato* strains on tomato cultivars Rio Grande and Rio Grande-*Pto* under field conditions. *J. Phytopathol.* 157, 219–227. doi: 10.1111/j.1439-0434.2008.01481.x

Xin, X. F., and He, S. Y. (2013). *Pseudomonas syringae* pv. *tomato* DC3000: a model pathogen for probing disease susceptibility and hormone signaling in plants. *Annu. Rev. Phytopathol.* 51, 473–498. doi: 10.1146/annurev-phyto-082712-102321

Zacarés, L., López-Gresa, M. P., Fayos, J., Primo, J., Bellés, J. M., and Conejero, V. (2007). Induction of p-coumaroyldopamine and feruloyldopamine, two novel metabolites, in tomato by the bacterial pathogen *Pseudomonas syringae*. *Mol. Plant Microbe Interact.* 20, 1439–1448. doi: 10.1094/MPMI-20-11-1439

Zhang, L., Zhang, F., Melotto, M., Yao, J., and He, S. Y. (2017). Jasmonate signaling and manipulation by pathogens and insects. *J. Exp. Bot.* 68, 1371–1385. doi: 10.1093/jxb/erw478

Zhang, P., and Chen, K. (2009). Age-dependent variations of volatile emissions and inhibitory activity toward *Botrytis cinerea* and *Fusarium oxysporum* in tomato leaves treated with chitosan oligosaccharide. *J. Plant Biol.* 52, 332–339. doi: 10.1007/s12374-009-9043-9

Zhang, P.-Y., Chen, K.-S., He, P.-Q., Liu, S.-H., and Jiang, W.-F. (2008). Effects of crop development on the emission of volatiles in leaves of Lycopersicon esculentum and its inhibitory activity to *Botrytis cinerea* and *Fusarium oxysporum*. *J. Integr. Plant Biol.* 50, 84–91. doi: 10.1111/j.1744-7909.2007.00597.x

Zhao, Y., Thilmony, R., Bender, C. L., Schaller, A., He, S. Y., and Howe, G. A. (2003). Virulence systems of *Pseudomonas syringae* pv. *tomato* promote bacterial speck disease in tomato by targeting the jasmonate signaling pathway. *Plant J.* 36, 485–499. doi: 10.1046/j.1365-313X.2003.01895.x

Conflict of Interest Statement: The authors declare that the research was conducted in the absence of any commercial or financial relationships that could be construed as a potential conflict of interest.

frontiers in Plant Science

ORIGINAL RESEARCH
published: 28 February 2019
doi: 10.3389/fpls.2019.00188

Untargeted Metabolomics Approach Reveals Differences in Host Plant Chemistry Before and After Infestation With Different Pea Aphid Host Races

*Carlos Sanchez-Arcos[1†], Marco Kai[2†], Aleš Svatoš[2], Jonathan Gershenzon[1] and Grit Kunert[1]**

[1]*Department of Biochemistry, Max-Planck Institute for Chemical Ecology, Jena, Germany,* [2]*Research Group Mass Spectrometry/Proteomics, Max-Planck Institute for Chemical Ecology, Jena, Germany*

OPEN ACCESS

Edited by:
Andreia Figueiredo, Universidade de Lisboa, Portugal

Reviewed by:
Anna-Maria Botha-Oberholster, Stellenbosch University, South Africa
Javier Sanchez, University of Zurich, Switzerland

***Correspondence:**
Grit Kunert
gkunert@ice.mpg.de

†Present address:
Carlos Sanchez-Arcos, Institute for Inorganic and Analytical Chemistry, Friedrich Schiller University Jena, Jena, Germany
Marco Kai, Department of Biochemistry, University Rostock, Rostock, Germany

Specialty section:
This article was submitted to Plant Metabolism and Chemodiversity, a section of the journal Frontiers in Plant Science

Received: *15 March 2018*
Accepted: *05 February 2019*
Published: *28 February 2019*

Citation:
Sanchez-Arcos C, Kai M, Svatoš A, Gershenzon J and Kunert G (2019) Untargeted Metabolomics Approach Reveals Differences in Host Plant Chemistry Before and After Infestation With Different Pea Aphid Host Races. Front. Plant Sci. 10:188. doi: 10.3389/fpls.2019.00188

The pea aphid (*Acyrthosiphon pisum*), a phloem-sucking insect, has undergone a rapid radiation together with the domestication and anthropogenic range expansion of several of its legume host plants. This insect species is a complex of at least 15 genetically different host races that can all develop on the universal host plant *Vicia faba*. However, each host race is specialized on a particular plant species, such as *Medicago sativa*, *Trifolium pratense*, or *Pisum sativum*, which makes it an attractive model insect to study ecological speciation. Previous work revealed that pea aphid host plants produce a specific phytohormone profile depending on the host plant – host race combination. Native aphid races induce lower defense hormone levels in their host plant than non-native pea aphid races. Whether these changes in hormone levels also lead to changes in other metabolites is still unknown. We used a mass spectrometry-based untargeted metabolomic approach to identify plant chemical compounds that vary among different host plant-host race combinations and might therefore, be involved in pea aphid host race specialization. We found significant differences among the metabolic fingerprints of the four legume species studied prior to aphid infestation, which correlated with aphid performance. After infestation, the metabolic profiles of *M. sativa* and *T. pratense* plants infested with their respective native aphid host race were consistently different from profiles after infestation with non-native host races and from uninfested control plants. The metabolic profiles of *P. sativum* plants infested with their native aphid host race were also different from plants infested with non-native host races, but not different from uninfested control plants. The compounds responsible for these differences were putatively identified as flavonoids, saponins, non-proteinogenic amino acids and peptides among others. As members of these compound classes are known for their activity against insects and aphids in particular, they may be responsible for the differential performance of host races on native vs. non-native host plants. We conclude that the untargeted metabolomic approach is suitable to identify candidate compounds involved in the specificity of pea aphid – host plant interactions.

Keywords: ***Acyrthosiphon pisum*, pea aphid host races, legume metabolome, saponins, flavonoids, *Medicago sativa*, *Trifolium pratense*, *Pisum sativum***

INTRODUCTION

Insects are the most diverse group of eukaryotic species on earth (Stork, 1993), and herbivorous species constitute a major group of insects (Strong et al., 1984; Mitter et al., 1988). Many herbivorous insect species are specialized on certain plant species (Bernays and Graham, 1988). Even within a single insect species, specialization can occur with different populations feeding preferentially on different plant taxa (Drès and Mallet, 2002). Adaptation to multiple plant species can lead to the formation of host races or biotypes within a species of an insect herbivore and might therefore play an important role in insect speciation. Nevertheless, the mechanisms behind these adaptations are hardly understood so far. Why is a certain host race able to feed on one plant but not another one? To some extent, differences in the constitutive chemical profiles of the plant species might be crucial (Hegnauer, 2001). However, various plants can also react differently to a specific insect herbivore (Arimura et al., 2005; Wu and Baldwin, 2010; Hogenhout and Bos, 2011; Sanchez-Arcos et al., 2016). Such differential plant responses can become apparent in changes in i.e., the plant metabolome (Jansen et al., 2009; Tzin et al., 2015).

Secondary metabolites used by plants as defenses against herbivores can act directly as feeding deterrents or toxins that decrease food intake or food-utilization efficiency (Gabrys and Tjallingii, 2002; Kim et al., 2008), decrease survival (Behmer et al., 2011), or indirectly as attractants for natural enemies of herbivores (reviewed in Unsicker et al., 2009). Chemical compounds involved in direct and indirect plant defense include terpenoids, phenolics, cyanogenic glycosides, glucosinolates, and alkaloids (Dreyer et al., 1985; Avé et al., 1987; Zagrobelny et al., 2004; Unsicker et al., 2009; Mithöfer and Boland, 2012; Maag et al., 2015; Züst and Agrawal, 2016). Specialized insect herbivores have to somehow cope with the presence of defensive secondary metabolites in their host plants, and have evolved specific adaptations to enable feeding (Ehrlich and Raven, 1964; Berenbaum and Zangerl, 1998).

To evaluate the potential defensive effects of plant metabolites on insect herbivores, the identity and concentration of these substances must be measured. Targeted analyses can be used for such studies if previous knowledge suggests that a specific metabolite or metabolite class like flavonoids or glucosinolates might be important. However, in some cases previous knowledge about the chemical composition of the plants involved or compounds relevant to herbivores is not available. In these cases the untargeted investigation of the whole metabolome by the use of metabolomics, might be a good tool to reveal candidate chemicals that are the cause of different plant-insect interactions (Fiehn, 2002; Krastanov, 2010; Nakabayashi and Saito, 2013).

One especially interesting plant-insect herbivore system to study the role of plant metabolites for speciation is the interaction between the pea aphid complex (*Acyrthosiphon pisum* Harris, Homoptera, Aphididae) and its legume (Fabaceae) host plants. The pea aphid underwent a rapid diversification about 6500–9500 years ago (Peccoud et al., 2009b) that led to the development of at least 15 different sympatric host races or biotypes each specialized on one or a few legume host plants (called native host plants) on which they perform well and prefer for feeding (Peccoud et al., 2009a, 2015). Such host plant preferences lead to assortative mating and reproductive isolation among populations (Caillaud and Via, 2000; Peccoud et al., 2009a). However, all pea aphid host races can perform well on *Vicia faba*, which is considered to be the universal host plant for all pea aphid host races characterized to date. The existence of the different host races and the fact that the pea aphid genome is entirely sequenced (The International Aphid Genomics Consortium, 2010) has made the pea aphid a model for studying ecological speciation (Brisson and Stern, 2006; Peccoud and Simon, 2010) and provides the opportunity to investigate the mechanisms underlying host plant adaptation.

Pea aphids like all aphids feed on phloem sap. With their sucking mouthparts called stylets they navigate through the epidermis and mesophyll to reach the phloem. During this penetration process they pierce many plant cells, salivate into the cells and also suck tiny amounts of cell contents (Tjallingii and Esch, 1993; Martin et al., 1997). It is assumed that aphid salivary proteins are involved in the adaptation of pea aphid host races to host plants (Jaquiery et al., 2012). Recent studies with other aphid species have revealed a close relation between proteins secreted with the saliva into the plant and host plant reactions (Rodriguez and Bos, 2013; Kaloshian and Walling, 2016). While several aphid proteins were found to facilitate aphid feeding (Will et al., 2007; Bos et al., 2010; Atamian et al., 2013; Elzinga et al., 2014; Naessens et al., 2015); other aphid proteins induce defense reactions in the plant and could lead to an incompatible aphid – plant interaction (Chaudhary et al., 2014; Elzinga et al., 2014). Concerning the pea aphid host races and their adaptation to their native hosts, despite the efforts made to investigate the role of candidate saliva proteins on host plant adaptation (Jaquiery et al., 2012; Guy et al., 2016; Boulain et al., 2018; Nouhaud et al., 2018) saliva proteins important for host plant specialization are not yet known. However, it is known that legumes differ in their production of defense hormones depending on whether native or non-native pea aphid host races are feeding on plants (Sanchez-Arcos et al., 2016). These hormone differences might lead to changes in plant metabolomes, especially for compounds having a deterrent or toxic impact on aphids.

Several studies show that plant secondary compounds have detrimental effects on pea aphids (Züst and Agrawal, 2016). For example, higher levels of saponins and phenolic compounds led to a reduction of aphid population growth (Golawska et al., 2006; Golawska and Lukasik, 2009) and increased mortality (De Geyter et al., 2012). Diverse flavonoid glycosides reduced aphid fecundity (Golawska and Lukasik, 2012; Golawska et al., 2012a), while nitrogen-containing compounds caused a rejection of a potential host plant by pea aphids (Kordan et al., 2012). Although these targeted approaches revealed that some secondary metabolites affect pea aphid performance, in most of these studies just one plant species was used and often the pea aphid host race was unknown. Thus, the contribution of plant compounds to the maintenance and performance of pea aphid host races on legume plants is still largely unknown. Only one study (Hopkins et al., 2017) combined a metabolomic profiling approach with behavioral tests to understand the chemical signatures that underlie host preferences by *A. pisum*. This study investigated

the metabolome of uninfested plants of different plant species belonging to the genera *Medicago* and *Trifolium*, but was limited to constitutive defense compounds or other compounds important for initial acceptance.

To pave the way for later targeted analyses in which the contribution of plant metabolites to the maintenance and performance of pea aphid host races on different legume plants could be analyzed, we applied an untargeted mass spectrometry-based metabolomic approach. Polar and semi-polar fractions of three native host plants of the pea aphid, *Medicago sativa*, *Pisum sativum*, *Trifolium pratense*, and the universal host *Vicia faba*, each infested with their native or one of two non-native aphid host races were analyzed and compared to fractions of uninfested control plants. These data made it possible to evaluate the use of metabolomics in identifying plant metabolites potentially involved in determining host race-host plant interactions in pea aphids.

MATERIALS AND METHODS

Plant Material

Four legume plant species, *Medicago sativa* (alfalfa) cultivar (cv.) "Giulia," *Trifolium pratense* (red clover) cv. "Dajana," *Pisum sativum* (pea) cv. "Baccara," and *Vicia faba* (broad bean) cv. "The Sutton," were grown in 10 cm diameter plastic pots with a standardized soil mixture (7:20 mixture of Klasmann Tonsubstrat and Klasmann Kultursubstrat TS1, Klasmann-Deilmann GmbH, Geeste, Germany), in climate chambers at 20°C, 70 ± 10% relative humidity, and under a 16 h light/8 h dark photoperiod. The plants were watered twice a week. To have a sufficient amount of plant material for the extraction of metabolites, *M. sativa* and *T. pratense* plants were used 4 weeks after sowing, while *P. sativum* and *V. faba* were used 3 weeks after sowing.

Aphids

Three pea aphid (*Acyrthosiphon pisum* Harris) clones, each representing one pea aphid host race, were used in the experiments: the clone L84 representing the Medicago race (here called MR), the clone T3-8V1 representing the Trifolium race (TR), and the clone Colmar representing the Pisum race (PR). Aphids were initially collected from their native host plants *T. pratense*, *M. sativa*, and *P. sativum*, respectively, and genotypically assigned to their respective host race (for detailed information see Table S1 in Peccoud et al., 2009b). All aphids were reared on 4 week old broad bean plants. To synchronize the age of the aphids for the experiments, five apterous female adults were placed on a broad bean plant and were allowed to reproduce for 48 h and were then removed from the plants. Nymphs were kept on the plants for 9 days until they reached adulthood. Then they were transferred to new plants were they reproduced. This procedure was repeated until enough synchronized young adult aphids were available for the experiment. To avoid escape of aphids, all aphid-containing plants were covered with air permeable cellophane bags (18.8 × 39 cm, Armin Zeller, Nachf. Schütz & Co, Langenthal, Switzerland), and placed in a climate chamber under the same conditions described for the plant material.

Experimental Design

Five adult apterous female aphids of each host race were placed in magnetic clip-cages (Ø 3.5 cm), on leaves of each plant species (two leaves for *M. sativa* and *T. pratense*, one leaf for *P. sativum* and *V. faba* plants). Leaves from all four plant species enclosed in magnetic clip cages but without aphids served as controls (**Supplementary Figure 1**). Ten replicates of each combination were employed. All the infested and control plants were placed in climate chambers at 20°C, 70 ± 10% relative humidity, and under a 16 h light/8 h dark photoperiod. Plant material was sampled after 48 h, a period which allowed the aphids to settle and the plant to react to the aphid infestation (Sanchez-Arcos et al., 2016).

Plant Material Sampling and Metabolite Extraction

For plant material sampling, the clip cages were carefully opened, and aphids were removed using a paintbrush. Control plants without aphids were brushed in the same way as aphid-infested plants to control for possible induction of metabolic changes due to contact with the paintbrush. Leaves enclosed in the clip cages were harvested and rapidly frozen in liquid nitrogen. Frozen samples were stored overnight in Eppendorf tubes (2 ml) at −80°C and then freeze-dried for 48 h. Dried plant material was homogenized into a fine powder by adding three stainless steel beads (3 mm Ø) in each tube and vigorous shaking for 4 min on a paint shaker (Skandex shaker SO-10m, Fast & Fluid Management, Sassenheim, The Netherlands). Portions of 10 mg dried plant material were extracted with 1 ml ice-cold extraction solution containing 80% methanol acidified with 0.1% formic acid and 0.1 μg/ml of L-(+)-α-phenylglycine (as a lock mass internal standard). Samples were immediately vortexed for 10 s and continuously sonicated in a water bath at room temperature (20°C) for 15 min at a maximum frequency of 35 kHz. After centrifugation (10 min at 4,500 g and −10°C), supernatants were filtered using 0.45 μm PTFE AcroPrep^{TM} 96-well filtration plates (Pall Corporation, Port Washington, NY, United States) and a vacuum filtration unit. All filtered plant extracts were stored at −80°C until LC-Orbitrap-MS analysis.

Plant Extract Analysis

From each plant extract 10 μl were analyzed using a UHPLC system of the Ultimate 3000 series RSLC (Dionex, Sunnyvale, CA, United States) connected to an LTQ-Orbitrap XL mass spectrometer (Thermo Fisher Scientific, Bremen, Germany). UHPLC was performed on an Acclaim^{TM} C18 column (150 × 2.1 mm, 2.2 μm, Dionex) pre-fitted with a C-18, 3.5 μm guard column (2.1 × 10 mm, Waters, Dublin, Ireland). Separation was accomplished using a gradient of 0.1% (v/v) formic acid in water (solvent A) and 0.1% formic acid in acetonitrile (solvent B) as follows: 0–5 min isocratic 100% (v/v) A, 5–32 min gradient phase to 100% B, 32–42 min isocratic 100% B, 42–42.1 min gradient phase to 100% (v/v) A, 42.1–47 min isocratic 100% A. The flow rate was set to 300 μl min^{-1}.

The electrospray ionization (ESI) source parameters were set to 4.5 kV spray voltage, and 35 V capillary transfer voltage at a capillary temperature of 275°C. The samples were measured in the negative (NI) and positive (PI) ionization modes in separate runs using 30,000 m/Δm resolving power (mass range of *m/z* 150–2000) in the Orbitrap mass analyzer. Xcalibur™ software (Thermo Fisher Scientific™, Waltham, MA, United States) was used for data acquisition and visualization.

UHPLC-MS^2 analysis of selected compounds was carried out by injecting l µl of each extract into a UHPLC system (Dionex UltiMate 3000, Thermo Fisher Scientific, Dreieich, Germany) coupled to a Q-Exactive Plus mass spectrometer (Thermo Fisher Scientific). Separation was performed on a Accucore™ C18 column (2.1 × 100 mm, 2.6 µm, Thermo Fisher Scientific), using a gradient of 0.1% (v/v) formic acid in water (solvent A) and 0.1% formic acid in acetonitrile (solvent B) as follows: 0–0.2 min isocratic 100% (v/v) A, 0.2–8 min gradient phase to 100% B, 8–11 min isocratic 100% B, 11.1–12 min isocratic 100% (v/v) A. A constant flow rate of 400 µl min^{-1} was set. For the parallel reaction monitoring, selective ion scanning in the negative ionization mode was used with the following parameters: target ions $[M\text{-}H]^-$ (*m/z* 1085.55 and *m/z* 605.19); resolution: 17,500; AGC target: 2×10^5; maximum IT: 100 ms; sheath gas flow rate: 60; aux gas flow rate: 20; sweep gas flow rate: 5; spray voltage: 3.3 kV; capillary temperature: 360°C; S-lens RF level: 50; aux gas heater temperature: 400°C; acquisition time frame: 3.75–5.88 min.

Data Preprocessing

Raw data files were converted to mzXML format files using the MSconvert tool (ProteoWizard 3.0x software) and uploaded to the interactive XCMS online platform (Tautenhahn et al., 2012). Parameter settings for XCMS data processing were as follows: A multigroup analysis was run in the centWave mode for feature detection (Δ *m/z* = 2.5 ppm, minimum peak width = 10 s, and maximum peak width = 60 s); correction of the retention time was performed with an obiwarp method (profStep = 1); and for chromatogram alignment: minfrac = 0.5, bw = 5, mzwid = 0.015, max = 100, minsamp = 1. Tables with the intensities of the detected features were obtained as output. Features that were missing in 3 or more out of the 10 samples for each treatment combination were classified as sporadic features and were discarded from the data set. This resulted in 5735 features in the negative ionization mode and 9057 features in the positive ionization mode.

Data Analysis

For the initial colonization of plants by aphids, constitutive compounds that are uniquely characteristic of a plant species might play a crucial role. A feature was classified as unique to a certain plant species when it fulfilled the following criteria: It appeared in at least eight of ten samples of the plant species of interest, and was absent in the other plant species or appeared in not more than two out of ten samples per plant species. In the same way features were selected that appeared in two or more plant species. Thus 3132 features (NI) and 5323 features (PI) were analyzed. Unique features (1081 NI; 1013 PI) were filtered again to remove adducts or isotopes which resulted in 280 (NI) and 289 (PI) possible metabolites.

To determine how the metabolic profiles differed between uninfested control plants, principal component analyses (PCAs) were performed with the web-based tool MetaboAnalyst (Xia et al., 2009; Xia and Wishart, 2011). Due to technical reasons (limited number of features which can be processed in the program) 40% of the features that were near constant throughout the plant species based on the interquartile range were filtered out prior to analyses. Thus 3441 features out of 5735 features (NI) and 5434 features out of 9057 features (PI) were analyzed in the PCA. Features were then mean-centered and divided by the standard deviation of each feature (equivalent to auto scaling) to make them comparable. In order to support the results of the PCA and to check which compound classes contribute most to the separation of the different host plants, partial least squares discriminant analyses (PLS-DA) with unique features only were performed (**Supplementary Figure 3**).

To determine how metabolic profiles changed within a given host plant species after pea aphid infestation, several PCAs were performed. Since it was assumed that most features would not differ among plants of the same species infested with different aphid host races and uninfested control plants, PCA analyses were carried out on the 5% of metabolomic features that changed most in each species. To identify the 5% most differently regulated host race features, all features were compared by a non-parametric one-way ANOVA on ranks and sorted by their false discovery rate (FDR). Before PCA these 5% most differently regulated features were normalized by log-transformation and scaled by mean centering and division by the standard deviation of each feature (auto-scaling) to make them comparable.

To detect chemical compounds that might be involved in plant defense, we looked for features that were down regulated in plants when a native aphid race was feeding but up regulated when non-native aphid races were applied using the pattern hunter tool in the MetabolAnalyst tool. A Spearman rank correlation analysis was performed against given patterns. A pattern was specified as a series of numbers, where each number corresponded to the concentration levels of the features in the corresponding group. For instance, the pattern "2-1-2-2" corresponding to the groups "uninfested control plants – plants infested with the native aphid race – plants infested with non-native aphid race A – plants infested with non-adapted aphid race B" searched for features down regulated (positive correlation) or up regulated (negative correlation) exclusively by the native aphid race. To test whether intensities of selected features differed among the four treatments, one-way analyses of variance (one-way ANOVA) were performed. In case of significant differences, Tukey HSD tests were executed to reveal which groups were different from each other. These univariate analyses were conducted using R software version 3.2.0 (R Development Core Team, 2015).

Selected features were assigned to chemical groups through putative identifications by performing library mass searches allowing a mass deviation in all databases of 5 ppm, and checked for spectrum matches in METLIN, Human Metabolome Database (HMDB), MetFrag, MassBank, KEGG, and LipidMaps.

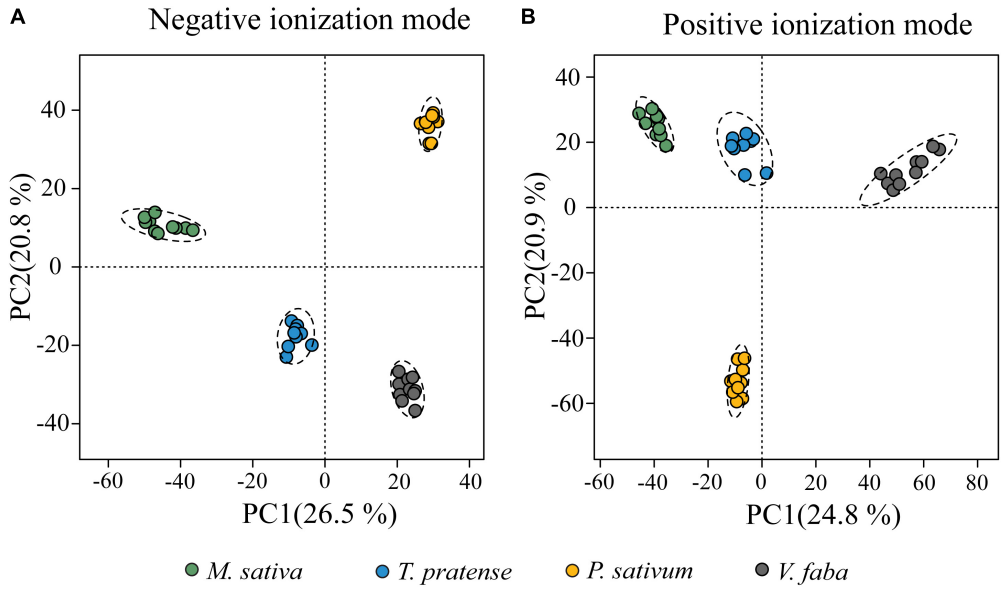

FIGURE 1 | PCA plots of metabolic features of leaves of pea aphid host plant species harvested prior to infestation by aphids. Features derived from UHPLC-Orbitrap mass spectrometry of aqueous methanol were analyzed in **(A)** negative and **(B)** positive ionization modes. Colored circles represent the metabolic profiles of individual plants. Dotted ellipses represent the 95% confidence regions for each group.

Features not found in these libraries or databases were considered as "unknown."

RESULTS

Pea Aphid Host Plant Species Differ in Their Constitutive Metabolic Profiles

To evaluate how the metabolic profiles of the four uninfested plant species, *M. sativa, T. pratense, P. sativum* and *V. faba*, differed, PCA were conducted. PCA plots showed a clear separation of all four plant species in both ionization modes (**Figure 1**). Biological replicates of each plant species always grouped together with small confidence intervals. The first principal components (PC1) explained 26.5 and 24.8% of the total variability for negative ionization mode (NI) and positive ionization mode (PI) datasets, respectively, whereas the second principal components (PC2) accounted for 20.8 and 20.9% (for NI and PI modes, respectively) of the total variability of the data set. For both ionization modes, the metabolic profiles of *M. sativa*, *T. pratense,* and *V. faba* were separated mainly along PC1. *P. sativum* metabolic profiles were separated from those of the other plant species along PC2.

To visualize the characteristic features shared among plant species, Venn diagrams were used (**Figure 2**). In both ionization modes, most features were shared between all four plants species (1676 out of 3132 features or 53.5% and 3865 out of 5323 features or 72.6% of all features for NI and PI, respectively), while features unique to a certain plant species were much less common. Only 34.5% (1081 features; NI) and 19% (1013 features; PI) of all features were assigned to only one plant species. *M. sativa* and *T. pratense* plants possessed a higher number of unique features in comparison to *P. sativum* and *V. faba* plants, while *V. faba* displayed the lowest number of unique features. Additionally, *M. sativa* and *T. pratense* plants shared more common features, with 149 and 109 features for NI and PI modes, respectively, than any other pair of plant species (**Figure 2**).

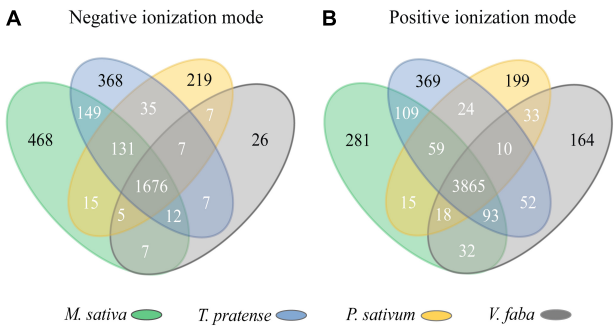

FIGURE 2 | Venn diagrams depicting the metabolic features of uninfested pea aphid host plant species in **(A)** negative and **(B)** positive ionization modes. Highlighted are the features unique to each species (black numbers) and shared with others (white numbers). Colored areas enclose the values for each plant species.

Metabolites unique to a pea aphid host plant could serve as host identification cues responsible for the acceptance or rejection of a potential host by the different host races, and might even function as defenses against non-native races. To obtain an overview of the unique compounds of each plant

species, we assigned putative identifications to the unique features and organized them by chemical classes (**Table 1** and **Supplementary Table 1**). *M. sativa* displayed the highest number of unique metabolites with 107 and 86 in NI and PI mode, respectively, followed by *T. pratense* with 103 and 83 metabolites, *P. sativum* with 57 (NI) and 53 (PI) metabolites, and *V. faba* with 13 (NI) and 67 (PI) metabolites. From all these compounds 55% (156 out of 280 compounds; NI) and 40% (115 out of 289 compounds; PI) were putatively identified. The most common class of putatively identified unique compounds among all plant species was the flavonoids. Steroidal and triterpene saponins were not only specific but also the most abundant classes in *M. sativa* (**Table 1**, **Supplementary Table 1** and **Supplementary Figure 3**).

TABLE 1 | Numbers of unique metabolites in uninfested *M. sativa*, *T. pratense*, *P. sativum* and *V. faba* plants and their putative chemical classification.

	Negative ionization mode		Positive ionization mode	
Plant species	**Number of unique metabolites**	**Putative chemical class**	**Number of unique metabolites**	**Putative chemical class**
Medicago sativa	47	Triterpene saponins	24	Triterpene saponins
	2	Steroidal saponins	14	Flavonoids
	9	Flavonoids	4	Peptides
	4	Peptides	1	Non-proteinogenic amino acid
	1	Benzoic acid ester	43	Unknowns
	1	Prostaglandin-like compound		
	1	Diterpene		
	1	Lignan glycoside		
	41	Unknowns		
	Σ 107		Σ 86	
Trifolium pratense	48	Flavonoids	31	Flavonoids
	6	Peptides	1	Phenolic glycoside
	2	Hydroxycinnamic acid esters	51	Unknowns
	2	Triterpene saponins		
	45	Unknowns		
	Σ 103		Σ 83	
Pisum sativum	22	Flavonoids	20	Flavonoids
	3	Peptides	2	Peptides
	32	Unknowns	31	Unknowns
	Σ 57		Σ 53	
Vicia faba	6	Flavonoids	12	Flavonoids
	1	Peptide	6	Peptides
	6	Unknowns	49	Unknowns
	Σ 13		Σ 67	

Retention times, m/z values and putative chemical class of the compounds can be found in ***Supplementary Table 1****.*

Metabolic Profiles of Host Plant Species Are Modified Differently by the Various Pea Aphid Host Races

To find out how plant metabolic profiles were modified after infestation by the various pea aphid host races, PCAs were performed based on the 5% of metabolomic features that changed most among plants infested with different pea aphid host races and uninfested control plants. In general, the metabolic profiles of uninfested control plants were separated from the profiles of aphid-infested plants, and thus plant metabolomes changed significantly upon aphid infestation. The degree of separation among profiles of plants infested with different host races depended on the plant species. Whereas the metabolic profiles of *V. faba* and *M. sativa* changed substantially depending on the attacking host race, profiles of *T. pratense* and *P. sativum* changed to a smaller extent (**Figure 3**).

The metabolic profiles of aphid-infested *M. sativa* plants were separated from the profiles of uninfested control plants along the first principal component (**Figures 3A,B**). The first PC explained 29% (NI) and 23.4% (PI) of the total variability. Among the infested plants, the metabolic profiles of those infested with the native MR host race were separated from those infested with the non-native TR and PR host races mainly along the second principal component. This explained 17.5% (NI) and 12.3% (PI) of the total variability.

The metabolic profiles of aphid-infested *T. pratense* plants also separated from those of uninfested control plants, but only in the positive ionization mode (**Figure 3D**) and not the negative ionization mode (**Figure 3C**). Furthermore, those plants infested with the native TR host race were grouped apart from those of the non-native MR and PR host races, especially in the positive ionization mode (**Figure 3D**). Of the total variability in the metabolic profiles of *T. pratense,* 62.5% (NI) and 49.8% (PI), was explained by the first two principal components.

The proportion of variability in the metabolic profiles of *P. sativum* that could be explained by the first two principal components was slightly lower than in the other plant species, 39.5% (NI) and 39.1% (PI). In contrast to the other three plant species where metabolic profiles of uninfested plants separated well from profiles of aphid-infested plants, in *P. sativum* the metabolic profiles of uninfested plants overlapped to some extent with those of plants infested with the native PR host race (**Figures 3E,F**). However, in the negative ionization mode, the metabolic profiles of plants infested with the non-native MR and TR host races were separated from those of uninfested control plants along the first principal component (**Figure 3E**). In

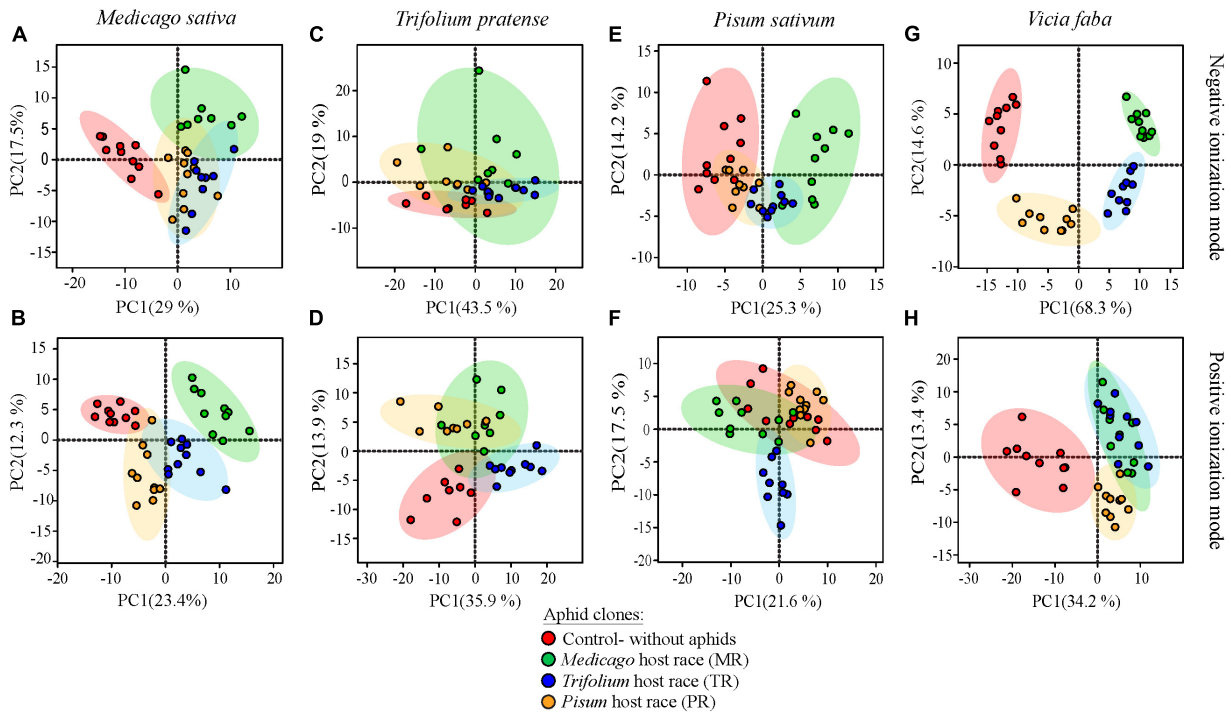

FIGURE 3 | PCA plots of metabolic features of leaves of pea aphid host plant species before and after infestation by three different aphid host races. Features are derived from UHPLC-Orbitrap mass spectrometry of aqueous methanol extracts conducted in negative (top row: **A,C,E,G**) and positive (bottom row: **B,D,F,H**) ionization modes for *M. sativa* **(A,B)**, *T. pratense* **(C,D)**, *P. sativum* **(E,F)**, and *V. faba* **(G,H)**. Only the 5% of metabolomic features that changed most are plotted. Small colored circles represent individual plant metabolic profiles after infestation with the MR (green), TR (blue), or PR (yellow) host race or of uninfested control plants (red). Colored ellipses represent the 95% confidence regions for each group.

the positive ionization mode, the metabolic profiles of plants infested with non-native TR race separated from the metabolic profiles of the other treatments along the second principal component (**Figure 3F**).

A large proportion of the variability in metabolic profiles of the universal host plant *V. faba* could be explained by the first two principal components (82.9% for NI and 47.6% for PI). Metabolic profiles changed drastically between the differently treated plants, especially in the negative ionization mode. There was a clear separation between infested and uninfested plants in both ionization modes along the first principal component (**Figures 3G,H**). The second principal component separated MR host race-infested and uninfested plants from PR and TR host race-infested plants in the negative ionization mode (**Figure 3G**).

Some Metabolites Are Reduced by Native Pea Aphid Host Races, but Induced by Non-native Races

Pea aphid host races perform much better on their native host plants than on other species (Ferrari et al., 2006, 2008; Peccoud et al., 2009a, 2015; Schwarzkopf et al., 2013). This difference may be a consequence of the ability of each race to suppress defense signaling processes on its native plant and reduce the levels of defenses (Sanchez-Arcos et al., 2016). When feeding on a non-native host plant, on the other hand, aphid feeding may trigger signaling that leads to the induction of defenses like toxic or deterrent compounds. To test these ideas, we searched for metabolites that showed (1) significantly reduced levels only after infestation with native aphid host races, or (2) significantly increased levels only after infestation with non-native aphid host races (**Table 2** and **Supplementary Table 2**).

M. sativa plants contained the highest number of metabolites that fit with these patterns, with 4 and 13 metabolites detected in the NI and PI modes, respectively, followed by *T. pratense* with 4 (NI) and 10 (PI) metabolites and *P. sativum* with 2 (NI) and 3 (PI) metabolites. A number of compounds showing these patterns could be assigned to chemical classes including several flavonoids, a triterpene saponin, a sterol and a jasmonate derivate in *M. sativa*, a flavonoid and a non-proteinogenic amino acid in *T. pratense* and a flavonoid in *P. sativum*. The abundance of two of the *M. sativa* compounds in different pea aphid treatments is illustrated in **Figure 4**. The levels of a putatively identified triterpene saponin (MS: with $[M\text{-}H]^-$ ion at *m/z* 1085.55, $[M+FA\ (formic\ acid)\text{-}H]^-$ adduct ion at *m/z* 1131.56, and $[M\text{-}shikimic\ acid\text{-}H]^-$ ion at *m/z* 911.46; **Supplementary Figures 2A,B**) were decreased by aphid infestation only with the native MR host race. On the other hand, the amount of a compound, putatively classified as a glycosylated flavonoid (MS: with $[M\text{-}H]^-$ ion at *m/z* 605.19, MS^2: fragment ions at *m/z*: 577.16 and 561.20, **Supplementary Figures 2C,D**), was significantly increased upon infestation with the non-native

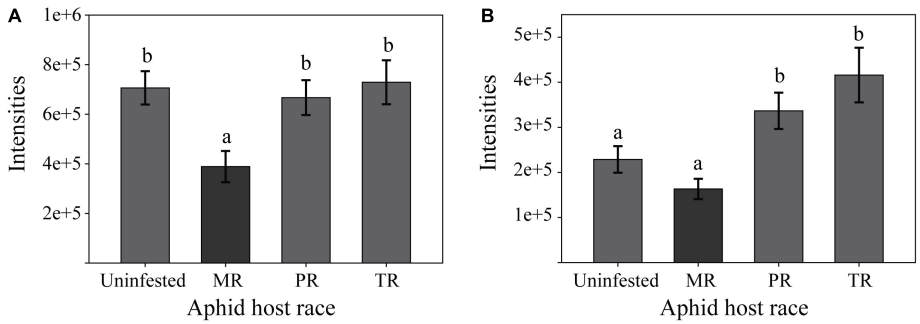

FIGURE 4 | Examples of pea aphid host plant metabolites from *M. sativa* that are decreased only after infestation with the native aphid host race **(A)** or that are significantly increased only after infestation with non-native aphid host races **(B)**. **(A)** Metabolite with [M-H] $^-$ *m/z* 1085.55, was decreased only by the native MR host race. **(B)** Metabolite with [M-H]$^-$ *m/z* 605.19 was induced only by the non-native PR and TR host races. Both metabolites were detected in negative ionization mode. Bars represent means ± SE. MR, Medicago race; TR, Trifolium race; PR, Pisum race; Uninfested, uninfested control plants. Different letters indicate significant differences ($P \leq 0.05$) based on One-way ANOVA followed by Tukey HSD test. MS and MS^2 spectra of these two compounds can be seen in **Supplementary Figure 2**.

TR and PR host races, but remained at similar levels as in uninfested control plants when the native MR host race infested the plant (**Figure 4B**).

TABLE 2 | Numbers of compounds down-regulated only after infestation with native, but not non-native aphid host races or up-regulated only after infestation with non-native, but not native host races, and their putative chemical classification.

	Negative ionization mode		Positive ionization mode	
Plant species	**Number of metabolites**	**Putative chemical class**	**Number of metabolites**	**Putative chemical class**
Medicago sativa	1	Triterpene saponin	1	Triterpene saponin
	1	Isoflavonoid	1	Flavonoid
	1	Chalcone	1	Sterol
	1	Unknown	1	Jasmonate derivative
			9	Unknowns
	Σ 4		Σ 13	
Trifolium pratense	1	Flavonoid	1	Non-proteinogenic amino acid
	3	Unknowns	9	Unknowns
	Σ 4		Σ 10	
Pisum sativum	2	Unknowns	1	Flavonoid
			2	Unknowns
	Σ 2		Σ 3	

Retention times, m/z values and putative formulas of the compounds can be found in ***Supplementary Table 2****.*

DISCUSSION

Chemical Differences Among Pea Aphid Host Plants Prior to Infestation Are Correlated With Subsequent Aphid Performance

Untargeted mass spectrometry-based analysis of the metabolites of four legume host plants of the pea aphid showed significant differences among these plants prior to aphid feeding (**Figure 1**). These differences might help explain the differential performance of the various pea aphid host races on specific host plants since individual metabolites could stimulate or deter feeding in disparate ways. Interestingly, the chemical complexity of the four plant species (the number of unique features found in our mass spectrometry analysis) is correlated with the performance of pea aphid host races on the various plants. *Medicago sativa*, which contained the highest number of unique chemical features (**Figure 2**), was previously found to be completely unsuitable for feeding by all other host races except the Medicago host race (Peccoud et al., 2009a; Schwarzkopf et al., 2013; Sanchez-Arcos et al., 2016). *Trifolium pratense*, which contained the second highest number of unique chemical features, was found to be unsuitable for other host races (Peccoud et al., 2009a), but did support some growth and reproduction of the Medicago host race (Peccoud et al., 2009a; Sanchez-Arcos et al., 2016).

The exceptional behavior of the Medicago race on *T. pratense* might be ascribed to the many chemical features shared between *M. sativa* and *T. pratense* (**Figure 2**), which also parallels their close phylogenetic relationship as members of the Tribe Trifolieae of the Fabaceae (Wojciechowski et al., 2004; The Legume Phylogeny Working Group et al., 2013). On the other hand, *V. faba* and *P. sativum*, both belonging to the Tribe Vicieae (Wojciechowski et al., 2004), had a much lower number of unique features, and can therefore be considered less chemically complex than *M. sativa* and *T. pratense*. This might be the reason for the good performance of all pea aphid host races on *V. faba* and their

intermediate performance on *P. sativum* (Peccoud et al., 2009a; Schwarzkopf et al., 2013; Sanchez-Arcos et al., 2016).

The negative correlations between host plant chemical complexity and pea aphid performance suggest that the unique metabolites of each host might play a role in limiting aphid feeding. The most abundant class of unique chemical compounds found in *M. sativa*, and also responsible for the separation of *M. sativa* from other plant species were putatively identified as steroidal and triterpene saponins (**Supplementary Figure 3**). Saponins originate from the mevalonate pathway (**Supplementary Figure 4**), and although saponins are distributed in many plant families, they are frequently found in legumes (Vincken et al., 2007), especially the genus *Medicago,* which is well known for containing a complex mixture of triterpene saponins with a broad spectrum of biological properties (Carelli et al., 2015). Saponins are reported to be defenses against aphids (De Geyter et al., 2012; Golawska et al., 2012b, 2014) as well as other insect herbivores (De Geyter et al., 2007; Chaieb, 2010), pathogens (Oleszek et al., 1990; Abbruscato et al., 2014), and nematodes (D'Addabbo et al., 2011). Saponins exhibit strong detergent properties, and can interact with membranes disturbing permeability and leading to cell death and necrosis (Wink, 2008).

The most frequent class of unique chemical compounds putatively identified in the other pea aphid host plants studied was the flavonoids. They are synthesized by the phenylpropanoid pathway (**Supplementary Figure 4**) and are widely distributed in all plants (Iwashina, 2000), but flavonoids, particularly isoflavonoids, are especially abundant in legumes (Velázques et al., 2010; Wink, 2013). Flavonoids can be deterrent or toxic for insects (Brignolas et al., 1998; Widstrom and Snook, 2001; Haribal and Feeny, 2003) including phloem feeders such as aphids (Montgomery and Arn, 1974; Lattanzio et al., 2000), and also have activity against microbes (Grayer and Harborne, 1994; Rauha et al., 2000). Interestingly, in a previous metabolomics investigation of host plant choice in pea aphids, L-phenylalanine and L-tyrosine were found to be associated with differential acceptability of species of *Medicago* and *Trifolium* by the Medicago and Trifolium host races (Hopkins et al., 2017). Since L-phenylalanine is one of the major precursors of flavonoids, its correlation with pea aphid host choice may be due to the flavonoids formed from this amino acid. Thus untargeted chemical analysis of pea aphid host plants has revealed several candidate groups of compounds that may play a role in host race specificity. Future studies on these compounds are warranted to determine how they are involved in defining pea aphid-host plant interactions.

Host Plant Compounds Induced or Suppressed by Pea Aphid Host Races May Influence Their Performance

Pea aphids may be affected not only by the constitutive chemistry of their host plants, but also by the changes induced upon aphid feeding. Thus in this study we compared the metabolic composition of host plants after feeding by the different host races with the composition of uninfested plants. Our results showed that host plant metabolomes were indeed modified by aphid feeding with modification occurring in a host race-dependent manner. The metabolic profiles of *M. sativa* and *T. pratense* plants after aphid infestation were consistently different from those of their respective uninfested control plants, and the metabolic profiles measured after feeding by the Medicago and Trifolium native host races were different from those after feeding by non-native host races (**Figures 3A–D**). In contrast, the metabolic profile of *P. sativum* after infestation by the native Pisum host race was not different from that of the control plants, but infestation with the non-native host races generated distinct changes in metabolic profiles. These patterns of metabolic change correspond well with changes in defense hormone levels found in a previous study after pea aphid feeding (Sanchez-Arcos et al., 2016). The salicylic and jasmonate levels of *M. sativa* and *T. pratense* were substantially altered by aphid infestation. Native host races caused slight induction or reduction of hormone levels, and non-native host races caused significant increases. In *P. sativum*, the native host race did not modify defense hormone levels compared to those found in uninfested control plants.

The metabolic changes measured after aphid feeding may result from a series of aphid behaviors that occur during the establishment of phloem feeding. En route to the phloem, aphids pierce many plant cells and secrete watery saliva into these cells (Martin et al., 1997; Powell, 2005). They also secrete gelling saliva into the apoplast to form a sheath around the stylet. Interestingly, even in incompatible interactions (such as those resulting from non-native host races) when aphids are not able to feed on the sieve elements, they insert their stylets and salivate into the plant (Schwarzkopf et al., 2013). The saliva contains proteins some of which may function as herbivore associated molecular patterns that bind to plant recognition receptors leading to the activation of plant defense responses (Hogenhout and Bos, 2011). For instance, a proteinaceous elicitor from *M. persicae* saliva induced resistance against this aphid in Arabidopsis, and pre-treatment of the host plant with aphid saliva decreased aphid fecundity (De Vos and Jander, 2009). Some of the metabolic changes observed after pea aphid infestation in this study might be a direct consequence of the defense responses induced by salivary proteins.

Aphids that are able to feed on a plant, such as native host races, may prevent the induction of defense responses by secreting effector proteins into the plant (Hogenhout and Bos, 2011; Elzinga and Jander, 2013; Van Bel and Will, 2016). For example, the effector molecule C002 from the pea aphid was shown to be essential for feeding on its universal host plant *V. faba*, and silencing of the *C002* gene reduced aphid fecundity (Mutti et al., 2008). However, plants have developed mechanisms to recognize such effector molecules and consequently activate their defense. Thus the chemical changes occurring after pea aphid infestation may reflect the outcome of the plant-aphid interaction.

The specificity of host race performance on different host plants may well be due to chemical differences among plants induced by infestation. Plants commonly synthesize new chemical compounds after herbivore attack, but this phenomenon has been studied for phloem feeding insects in only a few cases (Züst and Agrawal, 2016). Thus, in this study we sought compounds that were either induced by non-native host races but not native races, or suppressed by native host races but not non-native races. Such substances might be critical in facilitating the good performance of native host races and poor performance on non-native races. Interestingly, the number of compounds that were up or down regulated in this manner was again higher in *M. sativa* and *T. pratense* than in *P. sativum* (**Table 2**).

One of the compounds with these characteristics, putatively classed as a triterpene saponin, was unique to *M. sativa* and down regulated only by the native MR host race (**Figure 4A**). Saponins in plants have been reported to play a widespread role in resistance against insect herbivores (Applebaum et al., 1969; Fields et al., 2010; Nielsen et al., 2010), including in *M. sativa* (Nozzolillo et al., 1997; Adel et al., 2000), and in resistance against aphids in particular (Soulé et al., 2000; Golawska et al., 2012b). The adverse effects of saponins against the pea aphid have been observed in several studies (Golawska, 2007; De Geyter et al., 2012). These results suggest that the down regulation of the *M. sativa* saponin by the native Medicago host race, as described above, could be responsible for the increased performance on its native host plant. At the same time, the inability of non-native host races to down regulate this saponin may contribute to their poor performance due to the potential deterrent or toxic effects of this compound.

Another compound whose levels varied in a host race-specific manner was putatively classed as a sterol. Plant sterols are essential dietary requirements for insects, which cannot produce their own *de novo*, but need sterols as structural components of cell membranes and precursors in the formation of ecdysteroids (molting and sex hormones) (Clark and Bloch, 1959; Behmer and Nes, 2003; Behmer, 2017). However, sterols can also have negative effects on insects (Behmer, 2017). For instance the sterol stigmasterol suppressed the lifetime reproductive output of pea aphids when added to an artificial diet (Bouvaine et al., 2012). The aphid *M. persicae* had a reduced reproduction and a higher mortality when feeding on tobacco plants with high levels of atypical steroids (Behmer et al., 2011). Thus the sterol identified in this study may also represent a good candidate to be tested further with different pea aphid host races to deduce its role in determining patterns of host plant specificity.

Another compound that was induced in *M. sativa* after infestation with non-native, but not native host races was putatively classified as a flavonoid (**Figure 4B**). Increased levels of flavonoids in legumes after pea aphid infestation were previously reported to cause detrimental effects on the pea aphid (Golawska and Lukasik, 2012). Host race-specific regulation of flavonoids also occurred in *T. pratense*. Thus flavonoids are also good candidates to explain the differential performance of pea aphid host races.

CONCLUSION

An untargeted metabolomics approach allowed the detection of a number of candidate compounds that could be responsible for the disparate performance of various pea aphid host races on leguminous plant species. Some of these candidates are constitutive substances that are unique to one of the host plants. Other candidates were differentially induced or suppressed following infestation by the various host races. The most abundant chemical classes represented were saponins and flavonoids. Based on these results, untargeted metabolomics should be more widely considered as a valuable technique to discover plant metabolites of potential importance in plant interactions with herbivores and pathogens. When related plant species differ in their susceptibility or resistance, metabolomic comparison before and after enemy attack may reveal the chemical compounds responsible.

AUTHOR CONTRIBUTIONS

CS-A and GK conceived and designed the experiments. CS-A performed the experiments. MK measured the metabolic profiles. CS-A and GK analyzed the data. CS-A, GK, and JG interpreted the results and wrote the manuscript. All authors critically revised and consented to the final version of the manuscript.

FUNDING

This project was supported by the Max Planck Society, Germany, and the German Academic Exchange Service (DAAD) within the framework of the PPP – Procope German-French collaboration program (Project Code 57049694).

ACKNOWLEDGMENTS

We thank Jean-Christophe Simon (INRA, Le Rheu, France) for providing the aphid clones, Kerstin Zipfel, Christoph Scheck, Lindsey Roark, and Kristina Schädel for experimental help, Andreas Weber and Elke Goschala for plant cultivation, Tim Baumeister for his help with the visualization of PLS-DA results, and Ilka Vosteen, Elizabeth Pringle, and Maria Paulmann for helpful comments on previous versions of the manuscript.

SUPPLEMENTARY MATERIAL

The Supplementary Material for this article can be found online at: https://www.frontiersin.org/articles/10.3389/fpls.2019.00188/full#supplementary-material

REFERENCES

Abbruscato, P., Tosi, S., Crispino, L., Biazzi, E., Menin, B., Picco, A. M., et al. (2014). Triterpenoid glycosides from 'as antifungal agents against *Pyricularia oryzae*. *J. Agric. Food Chem.* 62, 11030–11036. doi: 10.1021/jf5049063

Adel, M. M., Sehnal, F., and Jurzysta, M. (2000). Effects of alfalfa saponins on the moth *Spodoptera littoralis*. *J. Chem. Ecol.* 26, 1065–1078. doi: 10.1023/A:1005445217004

Applebaum, S. W., Marco, S., and Birk, Y. (1969). Saponins as possible factors of resistance of legume seeds to attack of insects. *J. Agric. Food Chem.* 17:618. doi: 10.1021/jf60163a020

Arimura, G., Kost, C., and Boland, W. (2005). Herbivore-induced, indirect plant defences. *Biochim. Biophys. Acta* 1734, 91–111. doi: 10.1016/j.bbalip.2005.03.001

Atamian, H. S., Chaudhary, R., Dal Cin, V., Bao, E., Girke, T., and Kaloshian, I. (2013). In planta expression or delivery of potato aphid *Macrosiphum euphorbiae* effectors Me10 and Me23 enhances aphid fecundity. *Mol. Plant Microbe Interact.* 26, 67–74. doi: 10.1094/MPMI-06-12-0144-FI

Avé, D. A., Gregory, P., and Tingey, W. M. (1987). Aphid repellent sesquiterpenes in glandular trichomes of *Solanum berthaultii* and *Solanum tuberosum*. *Entomol. Exp. Appl.* 44, 131–138. doi: 10.1111/j.1570-7458.1987.tb01057.x

Behmer, S. T. (2017). Overturning dogma: tolerance of insects to mixed-sterol diets is not universal. *Curr. Opin. Insect Sci.* 23, 89–95. doi: 10.1016/j.cois.2017.08.001

Behmer, S. T., Grebenok, R. J., and Douglas, A. E. (2011). Plant sterols and host plant suitability for a phloem-feeding insect. *Funct. Ecol.* 25, 484–491. doi: 10.1111/j.1365-2435.2010.01810.x

Behmer, S. T., and Nes, W. D. (2003). Insect sterol nutrition and physiology: a global overview. *Adv. Insect Physiol.* 31, 1–72. doi: 10.1016/S0065-2806(03)31001-X

Berenbaum, M. R., and Zangerl, A. R. (1998). "Population-level adaptation to host-plant chemicals: the role of cytochrome P450 monooxygenases," in *Genetic Structure and Local Adaptation in Natural Insect Populations*, eds S. Mopper and S. Y. Strauss (Boston, MA: Springer-Science+Business Media, B.V), 91–112. doi: 10.1007/978-1-4757-0902-5_5

Bernays, E., and Graham, M. (1988). On the evolution of host speificity in phytophagous arthropods. *Ecology* 69, 886–892. doi: 10.2307/1941237

Bos, J. I. B., Prince, D., Pitino, M., Maffei, M. E., Win, J., and Hogenhout, S. A. (2010). A functional genomics approach identifies candidate effectors from the aphid species *Myzus persicae* (green peach aphid). *PLoS Genetics* 6:e1001216. doi: 10.1371/journal.pgen.1001216

Boulain, H., Legeai, F., Guy, E., Morliere, S., Douglas, N. E., Oh, J., et al. (2018). Fast evolution and lineage-specific gene family expansions of aphid salivary effectors driven by interactions with host-plants. *Genome Biol. Evol.* 10, 1554–1572. doi: 10.1093/gbe/evy097

Bouvaine, S., Behmer, S. T., Lin, G. G., Faure, M.-L., Grebenok, R. J., and Douglas, A. E. (2012). The physiology of sterol nutrition in the pea aphid *Acyrthosiphon pisum*. *J. Insect Physiol.* 58, 1383–1389. doi: 10.1016/j.jinsphys.2012.07.014

Brignolas, F., Lieutier, F., Sauvard, D., Christiansen, E., and Berryman, A. A. (1998). Phenolic predictors for Norway spruce resistance to the bark beetle *Ips typographus* (Coleoptera: Scolytidae) and an associated fungus, *Ceratocystis polonica*. *Can. J. Forest Res.* 28, 720–728. doi: 10.1139/x98-037

Brisson, J. A., and Stern, D. L. (2006). The pea aphid, *Acyrthosiphon pisum*: an emerging genomic model system for ecological, developmental and evolutionary studies. *Bioessays* 28, 747–755. doi: 10.1002/bies.20436

Caillaud, M. C., and Via, S. (2000). Specialized feeding behavior influences both ecological specialization and assortative mating in sympatric host races of pea aphids. *Am. Nat.* 156, 606–621. doi: 10.1086/316991

Carelli, M., Biazzi, E., Tava, A., Losini, I., Abbruscato, P., Depedro, C., et al. (2015). Sapogenin content variation in Medicago inter-specific hybrid derivatives highlights some aspects of saponin synthesis and control. *New Phytol.* 206, 303–314. doi: 10.1111/nph.13162

Chaieb, I. (2010). Saponins as insecticides: a review. *Tunis. J. Plant Protect.* 5, 39–50.

Chaudhary, R., Atamian, H. S., Shen, Z., Briggs, S. P., and Kaloshian, I. (2014). GroEL from the endosymbiont *Buchnera aphidicola* betrays the aphid by triggering plant defense. *Proc. Natl. Acad. Sci.* 111, 8919–8924. doi: 10.1073/pnas.1407687111

Clark, A. J., and Bloch, K. (1959). Conversion of ergosterol to 22-dehydrocholesterol in *Blattella germancia*. *J. Biol. Chem.* 234, 2589–2594.

D'Addabbo, T., Carbonara, T., Leonetti, P., Radicci, V., Tava, A., and Avato, P. (2011). Control of plant parasitic nematodes with active saponins and biomass from *Medicago sativa*. *Phytochem. Rev.* 10, 503–519. doi: 10.1007/s11101-010-9180-2

De Geyter, E., Lambert, E., Geelen, D., and Smagghe, G. (2007). Novel advances with plant saponins as natural insecticides to control pest insects. *Pest Technol.* 1, 96–105.

De Geyter, E., Smagghe, G., Rahbe, Y., and Geelen, D. (2012). Triterpene saponins of *Quillaja saponaria* show strong aphicidal and deterrent activity against the pea aphid *Acyrthosiphon pisum*. *Pest Manag. Sci.* 68, 164–169. doi: 10.1002/ps.2235

De Vos, M., and Jander, G. (2009). *Myzus persicae* (green peach aphid) salivary components induce defence responses in *Arabidopsis thaliana*. *Plant Cell Environ.* 32, 1548–1560. doi: 10.1111/j.1365-3040.2009.02019.x

Drès, M., and Mallet, J. (2002). Host races in plant-feeding insects and their importance in sympatric speciation. *Philos. Trans. R. Soc. London Ser. B Biol. Sci.* 357, 471–492. doi: 10.1098/rstb.2002.1059

Dreyer, D. L., Jones, K. C., and Molyneux, R. J. (1985). Feeding deterrency of some pyrrolizidine, indolizidine, and quinolizidine alkaloids towards pea aphid (*Acyrthosipon pisum*) and evidence for phloem transport of indolizidine alkaloid swainsonine. *J. Chem. Ecol.* 11, 1045–1051. doi: 10.1007/BF01020674

Ehrlich, P. R., and Raven, P. H. (1964). Butterflies and plants: a study in coevoltion. *J. Ecol.* 18, 586–608.

Elzinga, D. A., De Vos, M., and Jander, G. (2014). Suppression of plant defenses by a *Myzus persicae* (Green peach aphid) salivary effector protein. *Mol. Plant Microbe Interact.* 27, 747–756. doi: 10.1094/MPMI-01-14-0018-R

Elzinga, D. A., and Jander, G. (2013). The role of protein effectors in plant-aphid interactions. *Curr. Opin. Plant Biol.* 16, 451–456. doi: 10.1016/j.pbi.2013.06.018

Ferrari, J., Godfray, H. C. J., Faulconbridge, A. S., Prior, K., and Via, S. (2006). Population differentiation and genetic variation in host choice among pea aphids from eight host plant genera. *Evolution* 60, 1574–1584. doi: 10.1111/j.0014-3820.2006.tb00502.x

Ferrari, J., Via, S., and Godfray, H. C. J. (2008). Population differentiation and genetic variation in performance on eight hosts in the pea aphid complex. *Evolution* 62, 2508–2524. doi: 10.1111/j.1558-5646.2008.00468.x

Fiehn, O. (2002). Metabolomics - the link between genotypes and phenotypes. *Plant Mol. Biol.* 48, 155–171. doi: 10.1023/A:1013713905833

Fields, P. G., Woods, S., and Taylor, W. G. (2010). Triterpenoid saponins synergize insecticidal pea peptides: effect on feeding and survival of *Sitophilus oryzae* (Coleoptera: Curculionidae). *Can. Entomol.* 142, 501–512. doi: 10.4039/n10-024

Gabrys, B., and Tjallingii, W. F. (2002). The role of sinigrin in host plant recognition by aphids during initial plant penetration. *Entomol. Exp. Appl.* 104, 89–93. doi: 10.1046/j.1570-7458.2002.00994.x

Golawska, S. (2007). Deterrence and toxicity of plant saponins for the pea aphid *Acyrthosiphon pisum* Harris. *J. Chem. Ecol.* 33, 1598–1606. doi: 10.1007/s10886-007-9333-y

Golawska, S., Bogumil, L., and Wieslaw, O. (2006). Effect of low and high-saponin lines of alfalfa on pea aphid. *J. Insect Physiol.* 52, 737–743. doi: 10.1016/j.jinsphys.2006.04.001

Golawska, S., and Lukasik, I. (2009). Acceptance of low-saponin lines of alfalfa with varied phenolic concentrations by pea aphid (Homoptera: Aphididae). *Biologia* 64, 377–382. doi: 10.2478/s11756-009-0051-5

Golawska, S., and Lukasik, I. (2012). Antifeedant activity of luteolin and genistein against the pea aphid, *Acyrthosiphon pisum*. *J. Pest Sci.* 85, 443–450. doi: 10.1007/s10340-012-0452-z

Golawska, S., Lukasik, I., Kapusta, I., and Janda, B. (2012a). Do the contents of luteolin, tricin, and chrysoeriol glycosides in alfalfa (*Medicago sativa* L.) affect the behavior of pea aphid (*Acyrthosiphon pisum*)? *Pol. J. Environ. Stud.* 21, 1613–1619.

Golawska, S., Lukasik, I., Wojcicka, A., and Sytykiewicz, H. (2012b). Relationship between saponin content in alfalfa and aphid development. *Acta Biol. Cracov. Ser. Bot.* 54, 39–46. doi: 10.2478/v10182-012-0022-y

Golawska, S., Sprawka, I., and Lukasik, I. (2014). Effect of saponins and apigenin mixtures on feeding behavior of the pea aphid, *Acyrthosiphon pisum* Harris. *Biochem. Syst. Ecol.* 55, 137–144. doi: 10.1016/j.bse.2014.03.010

Grayer, R. J., and Harborne, J. B. (1994). A survey of antifungal compounds from higher plants, 1982-1993. *Phytochemistry* 37, 19–42. doi: 10.1016/0031-9422(94)85005-4

Guy, E., Boulain, H., Aigu, Y., Le Pennec, C., Chawki, K., Morliere, S., et al. (2016). Optimization of agroinfiltration in *Pisum sativum* provides a new tool for studying the salivary protein functions in the pea aphid complex. *Front. Plant Sci.* 7:1171. doi: 10.3389/fpls.2016.01171

Haribal, M., and Feeny, P. (2003). Combined roles of contact stimulant and deterrents in assessment of host-plant quality by ovipositing zebra swallowtail butterflies. *J. Chem. Ecol.* 29, 653–670. doi: 10.1023/A:1022820719946

Hegnauer, R. (2001). *Chemotaxonomie der Pflanzen*. Basel: Birkhäuser Verlag. doi: 10.1007/978-3-0348-7986-6

Hogenhout, S. A., and Bos, J. I. B. (2011). Effector proteins that modulate plant-insect interactions. *Curr. Opin. Plant Biol.* 14, 422–428. doi: 10.1016/j.pbi.2011.05.003

Hopkins, D. P., Cameron, D. D., and Butlin, R. K. (2017). The chemical signatures underlying host plant discrimination by aphids. *Sci. Rep.* 7:8498. doi: 10.1038/s41598-017-07729-0

Iwashina, T. (2000). The structure and distribution of the flavonoids in plants. *J. Plant Res.* 113, 287–299. doi: 10.1007/PL00013940

Jansen, J. J., Allwood, J. W., Marsden-Edwards, E., Van Der Putten, W. H., Goodacre, R., and Van Dam, N. M. (2009). Metabolomic analysis of the interaction between plants and herbivores. *Metabolomics* 5, 150–161. doi: 10.1007/s11306-008-0124-4

Jaquiery, J., Stoeckel, S., Nouhaud, P., Mieuzet, L., Maheo, F., Legeai, F., et al. (2012). Genome scans reveal candidate regions involved in the adaptation to host plant in the pea aphid complex. *Mol. Ecol.* 21, 5251–5264. doi: 10.1111/mec.12048

Kaloshian, I., and Walling, L. L. (2016). Hemipteran and dipteran pests: effectors and plant host immune regulators. *J. Integr. Plant Biol.* 58, 350–361. doi: 10.1111/jipb.12438

Kim, J. H., Lee, B. W., Schroeder, F. C., and Jander, G. (2008). Identification of indole glucosinolate breakdown products with antifeedant effects on *Myzus persicae* (green peach aphid). *Plant J.* 54, 1015–1026. doi: 10.1111/j.1365-313X.2008.03476.x

Kordan, B., Dancewicz, K., Wroblewska, A., and Gabrys, B. (2012). Intraspecific variation in alkaloid profile of four lupine species with implications for the pea aphid probing behaviour. *Phytochem. Lett.* 5, 71–77. doi: 10.1016/j.phytol.2011.10.003

Krastanov, A. (2010). Metabolomics - the state of art. *Biotechnol. Biotechnol. Equip.* 24, 1537–1543. doi: 10.2478/V10133-010-0001-Y

Lattanzio, V., Arpaia, S., Cardinali, A., Di Venere, D., and Linsalata, V. (2000). Role of endogenous flavonoids in resistance mechanism of Vigna to aphids. *J. Agric. Food Chem.* 48, 5316–5320. doi: 10.1021/jf000229y

Maag, D., Erb, M., Köllner, T. G., and Gershenzon, J. (2015). Defensive weapons and defense signals in plants: some metabolites serve both roles. *Bioessays* 37, 167–174. doi: 10.1002/bies.201400124

Martin, B., Collar, J. L., Tjallingii, W. F., and Fereres, A. (1997). Intracellular ingestion and salivation by aphids may cause the acquisition and inoculation of non-persistently transmitted plant viruses. *J. Gen. Virol.* 78, 2701–2705. doi: 10.1099/0022-1317-78-10-2701

Mithöfer, A., and Boland, W. (2012). Plant defense against herbivores: chemical aspects. *Ann. Rev. Plant Biol.* 63, 431–450. doi: 10.1146/annurev-arplant-042110-103854

Mitter, C., Farrell, B., and Wiegmann, B. (1988). The phylogenetic study of adaptive zones: has phytophagy promoted insect diversification? *Am. Nat.* 132, 107–128. doi: 10.1086/284840

Montgomery, M. E., and Arn, H. (1974). Feeding response of *Aphis pomi*, *Myzus persicae*, and *Amphorophora agathonica* to phlorizin. *J. Insect Physiol.* 20, 413–421. doi: 10.1016/0022-1910(74)90071-7

Mutti, N. S., Louis, J., Pappan, L. K., Pappan, K., Begum, K., Chen, M. S., et al. (2008). A protein from the salivary glands of the pea aphid, *Acyrthosiphon pisum*, is essential in feeding on a host plant. *Proc. Natl. Acad. Sci. U.S.A.* 105, 9965–9969. doi: 10.1073/pnas.0708958105

Naessens, E., Dubreuil, G., Giordanengo, P., Baron, O. L., Minet-Kebdani, N., Keller, H., et al. (2015). A secreted MIF cytokine enables aphid feeding and represses plant immune responses. *Curr. Biol.* 25, 1898–1903. doi: 10.1016/j.cub.2015.05.047

Nakabayashi, R., and Saito, K. (2013). Metabolomics for unknown plant metabolites. *Anal. Bioanal. Chem.* 405, 5005–5011. doi: 10.1007/s00216-013-6869-2

Nielsen, N. J., Nielsen, J., and Staerk, D. (2010). New resistance-correlated saponins from the insect-resistant crucifer *Barbarea vulgaris*. *J. Agric. Food Chem.* 58, 5509–5514. doi: 10.1021/jf903988f

Nouhaud, P., Gautier, M., Gouin, A., Jaquiery, J., Peccoud, J., Legeai, F., et al. (2018). Identifying genomic hotspots of differentiation and candidate genes involved in the adaptive divergence of pea aphid host races. *Mol. Ecol.* 27, 3287–3300. doi: 10.1111/mec.14799

Nozzolillo, C., Arnason, J. T., Campos, F., Donskov, N., and Jurzysta, M. (1997). Alfalfa leaf saponins and insect resistance. *J. Chem. Ecol.* 23, 995–1002. doi: 10.1023/B:JOEC.0000006384.60488.94

Oleszek, W., Price, K. R., Colquhoun, I. J., Jurzysta, M., Ploszynski, M., and Fenwick, G. R. (1990). Isolation and identification of alfalfa (*Medicago sativa* L) root saponins - their activity in relation to a fungal bioassay. *J. Agric. Food Chem.* 38, 1810–1817. doi: 10.1021/jf00099a006

Peccoud, J., Maheo, F., De La Huerta, M., Laurence, C., and Simon, J.-C. (2015). Genetic characterisation of new host-specialised biotypes and novel associations with bacterial symbionts in the pea aphid complex. *Insect Conserv. Div.* 8, 484–492. doi: 10.1111/icad.12131

Peccoud, J., Ollivier, A., Plantegenest, M., and Simon, J. C. (2009a). A continuum of genetic divergence from sympatric host races to species in the pea aphid complex. *Proc. Natl. Acad. Sci. U.S.A.* 106, 7495–7500. doi: 10.1073/pnas.0811117106

Peccoud, J., Simon, J. C., Mclaughlin, H. J., and Moran, N. A. (2009b). Post-Pleistocene radiation of the pea aphid complex revealed by rapidly evolving endosymbionts. *Proc. Natl. Acad. Sci. U.S.A.* 106, 16315–16320. doi: 10.1073/pnas.0905129106

Peccoud, J., and Simon, J. C. (2010). The pea aphid complex as a model of ecological speciation. *Ecol. Entomol.* 35, 119–130. doi: 10.1111/j.1365-2311.2009.01147.x

Powell, G. (2005). Intracellular salivation is the aphid activity associated with inoculation of non-persistently transmitted viruses. *J. Gen. Virol.* 86, 469–472. doi: 10.1099/vir.0.80632-0

R Development Core Team (2015). *R: A Language and Environment for Statistical Computing*. Vienna: R Foundation for Statistical Computing.

Rauha, J. P., Remes, S., Heinonen, M., Hopia, A., Kahkonen, M., Kujala, T., et al. (2000). Antimicrobial effects of Finnish plant extracts containing flavonoids and other phenolic compounds. *Int. J. Food Microbiol.* 56, 3–12. doi: 10.1016/S0168-1605(00)00218-X

Rodriguez, P. A., and Bos, J. I. B. (2013). Toward understanding the role of aphid effectors in plant infestation. *Mol. Plant Microbe Interact.* 26, 25–30. doi: 10.1094/MPMI-05-12-0119-FI

Sanchez-Arcos, C., Reichelt, M., Gershenzon, J., and Kunert, G. (2016). Modulation of legume defense signaling pathways by native and non-native pea aphid clones. *Front. Plant Sci.* 7:1872. doi: 10.3389/fpls.2016.01872

Schwarzkopf, A., Rosenberger, D., Niebergall, M., Gershenzon, J., and Kunert, G. (2013). To feed or not to feed: plant factors located in the epidermis, mesophyll, and sieve elements influence pea aphid's ability to feed on legume species. *PLoS One* 8:e75298. doi: 10.1371/journal.pone.0075298

Soulé, S., Guntner, C., Vazquez, A., Argandona, V., Moyna, P., and Ferreira, F. (2000). An aphid repellent glycoside from *Solanum laxum*. *Phytochemistry* 55, 217–222. doi: 10.1016/S0031-9422(00)00273-9

Stork, N. E. (1993). How many species are there? *Biodivers. Conserv.* 2, 215–232. doi: 10.1007/BF00056669

Strong, D. R., Lawton, J. H., Southwood, T. R. E., Strong, D. R., Lawton, J. H., and Southwood, T. R. E. (1984). *Insects on Plants; Community Patterns and Mechanisms*. London: Blackwell Scientific Publications.

Tautenhahn, R., Patti, G. J., Rinehart, D., and Siuzdak, G. (2012). XCMS Online: a web-based platform to process untargeted metabolomic data. *Anal. Chem.* 84, 5035–5039. doi: 10.1021/ac300698c

The International Aphid Genomics Consortium (2010). Genome sequence of the pea aphid *Acyrthosiphon pisum*. *PLoS Biol.* 8:e1000313. doi: 10.1371/journal.pbio.1000313

The Legume Phylogeny Working Group, Bruneau, A., Doyle, J. J., Herendeen, P., Hughes, C., Kenicer, G., et al. (2013). Legume phylogeny and classification in the 21st century: progress, prospects and lessons for other species-rich clades. *Taxon* 62, 217–248. doi: 10.12705/622.8

Tjallingii, W. F., and Esch, T. H. (1993). Fine-structure of aphid stylet routes in plant-tissues in correlation with EPG signals. *Physiol. Entomol.* 18, 317–328. doi: 10.1111/j.1365-3032.1993.tb00604.x

Tzin, V., Fernandez-Pozo, N., Richter, A., Schmelz, E. A., Schoettner, M., Schafer, M., et al. (2015). Dynamic maize responses to aphid feeding are revealed by a time series of transcriptomic and metabolomic assays. *Plant Physiol.* 169, 1727–1743. doi: 10.1104/pp.15.01039

Unsicker, S. B., Kunert, G., and Gershenzon, J. (2009). Protective perfumes: the role of vegetative volatiles in plant defense against herbivores. *Curr. Opin. Plant Biol.* 12, 479–485. doi: 10.1016/j.pbi.2009.04.001

Van Bel, A. J. E., and Will, T. (2016). Functional evaluation of proteins in watery and gel saliva of aphids. *Front. Plant Sci.* 7:1840. doi: 10.3389/fpls.2016.01840

Velázques, E., Silva, L. R., and Peix, Á (2010). Legumes: a healthy and ecological source of flavonoids. *Curr. Nutr. Food Sci.* 6, 109–144. doi: 10.2174/157340110791233247

Vincken, J. P., Heng, L., De Groot, A., and Gruppen, H. (2007). Saponins, classification and occurrence in the plant kingdom. *Phytochemistry* 68, 275–297. doi: 10.1016/j.phytochem.2006.10.008

Widstrom, N. W., and Snook, M. E. (2001). Recurrent selection for maysin, a compound in maize silks, antibiotic to earworm. *Plant Breed.* 120, 357–359. doi: 10.1046/j.1439-0523.2001.00610.x

Will, T., Tjallingii, W. F., Thonnessen, A., and Van Bel, A. J. E. (2007). Molecular sabotage of plant defense by aphid saliva. *Proc. Natl. Acad. Sci. U.S.A.* 104, 10536–10541. doi: 10.1073/pnas.0703535104

Wink, M. (2008). Evolutionary advantage and molecular modes of action of multi-component mixtures used in phytomedicine. *Curr. Drug Metabol.* 9, 996–1009. doi: 10.2174/138920008786927794

Wink, M. (2013). Evolution of secondary metabolites in legumes (Fabaceae). *S. Afr. J. Bot.* 89, 164–175. doi: 10.1016/j.sajb.2013.06.006

Wojciechowski, M. F., Lavin, M., and Sanderson, M. J. (2004). A phylogeny of legumes (Leguminosae) based on analyses of the plastid matK gene resolves many well-supported subclades within the family. *Am. J. Bot.* 91, 1846–1862. doi: 10.3732/ajb.91.11.1846

Wu, J., and Baldwin, I. T. (2010). New insights into plant responses to the attack from insect herbivores. *Ann. Rev. Genet.* 44, 1–24. doi: 10.1146/annurev-genet-102209-163500

Xia, J., and Wishart, D. S. (2011). Web-based inference of biological patterns, functions and pathways from metabolomic data using MetaboAnalyst. *Nat. Protoc.* 6, 743–760. doi: 10.1038/nprot.2011.319

Xia, J. G., Psychogios, N., Young, N., and Wishart, D. S. (2009). MetaboAnalyst: a web server for metabolomic data analysis and interpretation. *Nucleic Acids Res.* 37, W652–W660. doi: 10.1093/nar/gkp356

Zagrobelny, M., Bak, S., Rasmussen, A. V., Jorgensen, B., Naumann, C. M., and Moller, B. L. (2004). Cyanogenic glucosides and plant-insect interactions. *Phytochemistry* 65, 293–306. doi: 10.1016/j.phytochem.2003.10.016

Züst, T., and Agrawal, A. A. (2016). Mechanisms and evolution of plant resistance to aphids. *Nat. Plants* 2:15206. doi: 10.1038/nplants.2015.206

Conflict of Interest Statement: The authors declare that the research was conducted in the absence of any commercial or financial relationships that could be construed as a potential conflict of interest.

frontiers in Plant Science

ORIGINAL RESEARCH
published: 03 August 2018
doi: 10.3389/fpls.2018.01131

Polyphenolic Composition of Lentil Roots in Response to Infection by *Aphanomyces euteiches*

Navid Bazghaleh, Pratibha Prashar, Randy W. Purves and Albert Vandenberg*

Department of Plant Sciences, University of Saskatchewan, Saskatoon, SK, Canada

Polyphenols comprise the largest group of plant secondary metabolites and have critical roles in plant physiology and response to the biotic and abiotic environment. Changes in the content of polyphenols in the root extracts and root tissues of wild (*Lens ervoides*) and cultivated (*Lens culinaris*) lentil genotypes were examined in response to infection by *Aphanomyces euteiches* using liquid chromatography mass spectrometry (LC-MS). Genotype, infection and their interaction determined the composition of polyphenols in lentil roots. The levels of several polyphenols were lower in the root extract of the low-tannin genotype *L. culinaris* ZT-4 compared to *L. ervoides* L01-827A. Kaempferol derivatives including kaempferol dirutinoside and kaempferol 3-robinoside 7-rhamnoside were more concentrated in the healthy root tissues of *L. ervoides* L01-827A than in *L. culinaris* genotypes. Infection increased the concentration of kaempferol, apigenin, and naringenin in the root tissues of all genotypes, but had no effect on some polyphenols in the low-tannin genotype *L. culinaris* ZT-4. The concentrations of apigenin, naringenin, apigenin 4-glucoside, naringenin7-rutinoside, diosmetin, and hesperetin 7-rutinoside were higher in the infected root tissues of *L. ervoides* L01-827A compared with the *L. culinaris* genotypes. Organic acids including coumaric acid, vanillic acid, 4-aminosalicylic acid, 4-hydroxybenzoic acid, and 3,4-dihydroxybenzoic acid effectively suppressed the *in-vitro* hyphal growth of *A. euteiches*. Some of these bioactive polyphenols were more concentrated in roots of *L. ervoides* L01-827A but were low to undetectable in ZT-4. This study shows that genotypic differences exist in the composition of root polyphenols in lentil, and is related to the response to infection caused by *A. euteiches*. Polyphenols, particularly the organic acid content could be useful for selection and breeding of lentil genotypes that are resistant to Aphanomyces root rot (ARR) disease.

Keywords: lentil, *Lens ervoides*, *Lens culinaris*, polyphenols, *Aphanomyces euteiches*, root rot, liquid chromatography, mass spectrometry

OPEN ACCESS

Edited by:
Andreia Figueiredo, Universidade de Lisboa, Portugal

Reviewed by:
Alessandra Durazzo, Consiglio per la Ricerca in Agricoltura e l'Analisi dell'Economia Agraria (CREA), Italy
Galina Suvorova, All-Russia Research Institute of Legumes and Groat Crops, Russia
Marisa Porrini, Università degli Studi di Milano, Italy

***Correspondence:**
Navid Bazghaleh
navid.bazghaleh@usask.ca

Specialty section:
This article was submitted to Plant Metabolism and Chemodiversity, a section of the journal Frontiers in Plant Science

Received: *13 April 2018*
Accepted: *13 July 2018*
Published: *03 August 2018*

Citation:
Bazghaleh N, Prashar P, Purves RW and Vandenberg A (2018) Polyphenolic Composition of Lentil Roots in Response to Infection by Aphanomyces euteiches. Front. Plant Sci. 9:1131. doi: 10.3389/fpls.2018.01131

INTRODUCTION

Lentil (*Lens culinaris* Medik.) is an important cool season legume, grown in more than 70 countries around the world. Canada is the largest lentil producer, contributing nearly 41% of the global production (FAO, 2017). Lentil seeds are a rich source of proteins, carbohydrates, vitamins, minerals, fibers and antioxidants (Roy et al., 2010). They also contain non-nutritional compounds

such as tannins and phytic acid that serve as a defense mechanism against pathogens, insects and parasites (Urbano et al., 2007; Constabel et al., 2014; Sánchez-Chino et al., 2015). *Lens* species differ in the size of seeds (5–90 mg per seed) and the color and pattern of seed coats, which vary from yellow or gray to dark brown (Ladizinsky, 1979a,b; Ferguson et al., 2000). As a legume crop, lentil provides agro-ecological services by incorporating atmospheric nitrogen into the soil through biological fixation, and promoting the diversity of soil microbial communities (Borrell et al., 2016).

Aphanomyces euteiches is a soil-borne oomycete that causes Aphanomyces root rot (ARR) in many legume crops such as lentil, pea (*Pisum sativum* L.), alfalfa (*Medicago sativa* L.), common bean (*Phaseolus vulgaris* L.), and red clover (*Trifolium pratense*; Wicker et al., 2001; Chatterton et al., 2016). This pathogen has recently been reported in western Canada (Armstrong-Cho et al., 2014; Chatterton et al., 2016). ARR can cause major crop losses especially under environmental conditions that are conducive to pathogen growth and disease development (McPhee, 2003; Gossen et al., 2016). Susceptible crop plants generally have a limited range of genetic resistance. No effective seed treatment is available for protection against *A. euteiches,* and its spores are long-lived in soil (Gossen et al., 2016). These characteristics make ARR the most difficult and serious root pathogen of susceptible legumes. Crop rotation and the use of cultivars with partial resistance are the only efficient ways to control ARR (Wicker et al., 2001; Moussart et al., 2013).

Polyphenols are the largest group of secondary metabolites and have very diverse structures (Cheynier, 2012) that make them unique and multifunctional natural products in plants (Quideau et al., 2011). They often have important ecological roles and are involved in a range of functions in plant growth, development, and defense. Polyphenols can attract, repel or protect plants against insects, fungi, bacteria, and viruses (Bennett and Wallsgrove, 1994; Daayf et al., 2012; Olivoto et al., 2017). Synthesis of polyphenols is a complex process that is associated with the shikimate, malonate, and phenylpropanoid pathways (Lattanzio, 2013) and is encoded by multiple genes (Vermerris and Nicholson, 2008; Olivoto et al., 2017). A detailed understanding of how these polyphenols fit into the biochemical pathways for disease resistance is necessary to develop strategies to control plant diseases.

The roots of plants are able to produce a diversity of compounds that directly or indirectly influence microbial species (Lanoue et al., 2010; Baetz and Martinoia, 2014; Bazghaleh et al., 2016). The production of antimicrobial polyphenols have been reported in various plant species (Puupponen-Pimiä et al., 2001; Deng et al., 2015; Shalaby and Horwitz, 2015; Pagliarulo et al., 2016) which could be independent or part of a plant's response to infection. Some polyphenols accumulate in plant tissues even prior to an active defense response (Nicholson and Hammerschmidt, 1992; Balmer et al., 2015). Knowledge of the components of the range of polyphenols in the root tissues and root extracts of crop plants and the potential effect of those compounds on pathogenic microbial species could be used as a first step for identifying plant genotypes that are more resistant to plant diseases (Wink, 1988; Reuveni et al., 1991; Wille et al., 2018).

Polyphenols have been detected in plants roots and their effects on soil pathogens described (Evidente et al., 2010), however, little is known about the composition of these metabolites, particularly in legume plants. This study tested the hypothesis that lentil genotypes have different compositions of polyphenols in their root tissues and root extracts. We also hypothesized that infection by *A. euteiches* alters the accumulation of specific polyphenols in the root tissues of lentil, and that some of these might inhibit the hyphal growth of *A. euteiches*. We compared the polyphenol profiles found in root tissues and root extracts of selected genotypes of cultivated (*L. culinaris*) and wild (*Lens ervoides*) lentil, including a low-tannin cultivar, using liquid chromatography-mass spectrometry. The effect of the individual polyphenols on the growth of *A. euteiches* was investigated *in vitro*. The aim of this study was to identify potential polyphenols that could be involved in providing resistance to ARR in lentil.

MATERIALS AND METHODS

Composition of Polyphenols in Root Extracts of Lentil

Experimental Design and Plant Growth Conditions

Seeds of the *L. culinaris* cultivars ZT-4 (low-tannin), CDC Maxim (gray seed coat), Eston (green seed coat), and *L. ervoides* genotype L01-827A (wild type seed coat) were obtained from the Crop Development Centre at the University of Saskatchewan (Saskatoon, SK, Canada). The lentil genotypes were selected based on differences in the color and polyphenolic profile of their seed coats (Mirali et al., 2016a,b, 2017). The seeds were scarified by puncturing the seed coats using a small blade. The seeds were surface sterilized by successive immersion in 95% ethanol for 30 s, in sterile distilled water for 30 s, in 2.5% Javex® bleach solution (sodium hypochlorite) for 2 min, and then in distilled water for 5 min. The seeds were germinated on moist, sterile filter paper in Petri dishes in the dark at 25°C for 72 h prior to use. Eight germinated seeds of each genotype were transplanted into a 10 cm plastic pot filled with porous ceramic media (Profile® Greens Grade™, BrettYoung, Edmonton, AB). The planting holes in the media were treated with a peat-based *Rhizobium leguminosarum* inoculant (Nitragin Nitrastick GC®, Nitragin Inc., Brookfield, WI, USA). The pots were arranged as a randomized complete block design in four replicates. Plants were grown under 22/16°C d/night temperatures and 16/8 h d/night length for 30 d in a growth room (GR48, Conviron, Winnipeg, MB) located in the controlled environment facilities of the College of Agriculture and Bioresources at the University of Saskatchewan. Distilled water was added to pots as needed, and plants fertilized weekly with 100 mL of the half strength modified Hoagland's nutrient solution.

Abbreviations: ARR, Aphanomyces Root Rot; CDC, Crop Development Centre; LC, Liquid Chromatography; MS, Mass Spectrometry; SRM, Single Reaction Monitoring; ZT, Zero Tannin.

Collection of Roots and Extraction of Polyphenols

All plants in each pot were gently removed 30 d after transplanting. The intact roots were collected, weighed, and transferred into 50 mL tubes containing 10 mL 80% MeOH. Polyphenols that had been released from root tissues were extracted by soaking roots in 80% MeOH for 72 h. The tubes were stored at −20°C until further use. After 3 d, the tube was thawed at room temperature, vortexed, and 1.5 mL was transferred into a 2 mL centrifuge tube, which was centrifuged for 5 min at 12,000 rpm. Then 1 mL of the supernatant was removed and dried using a benchtop centrifugal vacuum concentrator (Labconco, Kansas City, Mo) for approximately 2 h and immediately reconstituted in 200 μL of the recon solution (90:10 H_2O:MeOH v/v) to reconstitute the extract.

Composition of Polyphenols in Root Tissues of Healthy and Diseased Lentil Plants

Experimental Design and Plant Growth Conditions

A factorial pot experiment with four lentil genotypes and two infection levels was conducted in a controlled temperature environment. Seeds of the lentil genotypes ZT-4, CDC Maxim, Eston, and *L. ervoides* L01-827A were scarified, surface sterilized, and germinated as described for experiment 1. Eight germinated seeds of each genotype were transplanted into 10 cm plastic pots filled with peat and vermiculite-based media, Sunshine Mix 3® (Sun Gro Horticulture Canada Ltd.). The planting holes in the media were treated with a peat-based *R. leguminosarum* inoculant (Nitragin Nitrastick GC®, Nitragin Inc., Brookfield, WI, USA). The pots were arranged in four replicates. Plants were grown under 22/16°C d/night temperatures and 16/8 h d/night length for 30 d in the growth room (GR48, Conviron, Winnipeg, MB). Distilled water was added to pots as needed, and plants were fertilized weekly with 100 mL of the half strength modified Hoagland's nutrient solution. Roots of the infected plants were inoculated with zoospores of *A. euteiches*. The experiment was repeated two times.

Preparation of Inoculum of *Aphanomyces euteiches* and Root Infection

Zoospores of *A. euteiches* were produced following a protocol developed in the Plant Pathology Laboratory, University of Saskatchewan, Canada (Banniza, pers. comm.). After counting the zoospores using a haemocytometer, the final concentration was adjusted to 5×10^3 zoospores mL^{-1} with sterile deionized water. Ten days after planting, a 5-mL aliquot of the zoospore suspension was injected into the soil near the base of the lentil plants.

Collection of Roots and Extraction of Root Polyphenols

Fourteen days after inoculation, the plants were uprooted and the adhering media (Profile® Greens Grade™, Winnipeg, MB) were removed from the roots by soaking the roots in the tap water. The roots were then visually evaluated for infection on the basis of discoloration and root decay. The roots were stored at −80°C until use.

Polyphenols were extracted from roots of healthy and diseased plants using a procedure similar to that of Mirali et al. (2014) with a few modifications. One hundred fifty milligram of fresh root tissue was placed in 2 mL Sarstedt microtube and then freeze dried over 24 h. The freeze-dried samples were weighed, and then one ¼- inch ceramic bead (MP Bio, Cat. No. 6540-412) was placed in each tube along with 1 mL of an extraction solvent containing 70:30 v/v acetone:water plus internal standards. The root tissues were pulverized using a Mini-Beadbeater-16 (BioSpec Products, Inc. US) for 2 × 2.5 min followed by shaking using an Eppendorf mixer for 1 h at 1,400 rpm and 23°C. After centrifuging the tubes at 12,000 rpm for 5 min, 500 μL of the supernatant was pipetted into 1.5 mL Eppendorf tubes and centrifuged again at 12,000 rpm for 5 min. From the Eppendorf tube, 200 μL of the supernatant was pipetted into a new 1.5 mL Eppendorf tube and dried down for approximately 2 h using a benchtop centrifugal vacuum concentrator (Labconco, Kansas City, MO). The supernatant was then reconstituted by adding 200 μL of 90:10 MiliQ-water:MeOH to each tube followed by vortexing for 20 sec and shaking on an Eppendorf mixer for 30 min at 1,400 rpm at 23°C. The tubes were centrifuged at 12,000 rpm for 5 min and then 150 μL of the supernatant was transferred into LC vials and used for LC-MS analysis.

LC-MS Analysis

Polyphenols were purchased from Sigma-Aldrich (Missouri, USA), and Extrasynthese (Genay, France) except for the deuterated compounds, which were purchased from Toronto Research Compounds (Toronto, Canada).

Root tissues and root extracts of the lentil plants were analyzed for polyphenols using a diode-array detector (DAD) for UV-vis detection and a targeted LC-MS method. Since all polyphenols absorb UV-vis, the DAD detector detects all polyphenols in the sample and the MS gives the *m/z* of the ion(s) within each peak. The targeted method (list of polyphenols analyzed is given in **Table 1**) uses LC-selective reaction monitoring (SRM) and is based on the method initially developed by Mirali et al. (2014), that has been more recently updated (Mirali et al., 2016a; Purves et al., 2016). Note that catechin-$^{13}C_3$, 4-hydroxybenzoic acid-$^{13}C_7$, ferulic acid-d_3, resveratrol 4-hydroxyphenyl-$^{13}C_6$, vanillin ring-$^{13}C_3$, and quercetin-d_3 were used as internal standards. The *m/z* values used for the parent and fragment ions for each of the polyphenols are given in **Table 1**.

Previous chromatographic conditions optimized by Mirali et al. (2016a) were applied with some modifications. An Agilent 1290 UPLC (Agilent Technologies, Santa Clara, CA) equipped with an auto sampler (G4226A), a binary pump (G4220), a thermostatted column compartment (G1316), and a diode array detector (G4212) was used. Compounds were separated using a Phenomenex (Torrance, CA) core-shell Kinetex pentafluorophenyl (PFP) column (100 mm × 2.1 mm, 2.6 μm particle size). The mobile phase employed a 30 min binary gradient shown in **Table 2**; solvent A consisted of H_2O: CH_2O_2 99:1, and solvent B was ACN:H2O: CH_2O_2 90:9:1 (v/v). The injection volume was 5 μL and the flow rate was 0.35 mL/min. Polyphenols exiting the column were detected by the DAD and then subsequently with a Thermo Fisher TSQ Vantage

TABLE 1 | Polyphenols analyzed in the root extracts and root tissues of cultivated lentil genotypes ZT-4, CDC Maxim, Eston, and *Lens ervoides* L01-827A using liquid chromatography-mass spectrometry.

Compound	Retention time (min)	Mode	Molecular ion (*m/z*)	Fragment ion (*m/z*)
Gallic acid	2.1	NEG[a]	169	125
Salicin	3.3	NEG	285	123
3,4-dihydroxybenzoic acid	3.5	NEG	153	109
4-aminosalicylic acid	3.5	NEG	152	108
Vanillic acid 4-glucoside	4.1	NEG	329	167
Gallocatechin	4.5	NEG	305	125
4-hydroxybenzoic acid	4.8	NEG	137	93
4-hydroxybenzoic acid-13C7*	4.8	NEG	144	99
Delphinidin 3,5-diglucoside	5.5	NEG	625	299
Procyanidin B1	5.8	NEG	577	289
Cyanidin 3,5-diglucoside	6.1	NEG	609	447
Catechin 3-glucoside	6.1	NEG	451	137
Vanillic acid	6.2	NEG	167	108
Epigallocatechin	6.3	NEG	305	125
Catechin	6.4	NEG	289	203
Catechin 13C3*	6.4	NEG	292	206
Chlorogenic acid	6.8	NEG	353	191
Caffeic acid	6.8	NEG	179	135
Delphinidin 3-glucoside	6.9	NEG	463	300
Quercetin 3-galactoside	11.0	NEG	463	300
Quercetin 3-glucoside	11.2	NEG	463	300
Procyanidin B2	6.9	NEG	577	289
Malvidin 3,5-diglucoside	7.3	NEG	653	329
Vanillin ring 13C6*	7.5	NEG	157	142
Epicatechin	7.8	NEG	289	203
Dihydromyricetin	8.0	NEG	319	193
p-Coumaric acid	8.4	NEG	163	119
Kaempferol 3-rhamnoside	14.6	NEG	431	285
Kaempferol dirutinoside	8.7	NEG	901	755
Cyanidin 3-rhamnoside	8.7	NEG	431	285
Malvidin 3-galactoside	8.7	NEG	491	313
Malvidin 3-glucoside	9.1	NEG	491	313
3-hydroxycinnamic acid	9.3	NEG	163	119
3-hydroxy-4-methoxycinnamic acid	9.6	NEG	193	134
Ferulic acid	9.6	NEG	193	134
Ferulic acid-d3*	9.6	NEG	196	134
Kaempferol 3-rutinoside 4′-glucoside	9.6	NEG	755	593
Quercetin 3,4′-diglucoside	9.7	NEG	625	463
Luteolin 8′-glucoside	9.7	NEG	447	327
Kaempferol 3-robinoside 7-rhamnoside	10.2	NEG	739	593
Taxifolin	10.2	NEG	303	125
Resveratrol 3-glucoside	10.5	NEG	389	227
Luteolin 3′,7-diglucoside	10.5	NEG	609	285
Naringenin 7-rutinoside	11.6	NEG	597	271
Epicatechin gallate	10.6	NEG	441	169
Myricetin 3-rhamnoside	10.8	NEG	463	316
Quercetin 3-rutinoside	10.8	NEG	609	300
Luteolin 7-rutinoside	11.4	NEG	593	285
Luteolin 7-glucoside	11.6	NEG	447	285
Kaempferol 3-galactoside	11.7	NEG	447	255
Kaempferol 3-rutinoside	11.8	NEG	593	285
Dihydrokaempferol	11.9	NEG	287	125
Kaempferol 3-glucoside	12.1	NEG	447	285
Quercetin 3-rhamnoside	12.2	NEG	447	300
Hesperetin 7-rutinoside	12.3	NEG	609	301
Kaempferol 7-neohesperidoside	12.3	NEG	593	285
Apigenin 7-rutinoside	12.4	NEG	577	269
Kaempferol 7-glucoside	12.4	NEG	447	285
Apigenin 7-neohesperidoside	12.6	NEG	577	269
Apigenin 7-glucoside	12.8	NEG	431	268
Diosmetin 7-rutinoside	12.8	NEG	607	299
Quercetin 4′-glucoside	13.0	NEG	463	301
Myricetin	13.2	NEG	317	151
Luteolin 4′-glucoside	13.3	NEG	447	285
Resveratrol 4-hydroxyphenyl 13C6*	13.5	NEG	233	149
Resveratrol	13.5	NEG	227	143
4-hydroxy-6-methylcoumarin	13.8	NEG	175	131
Eriodicytol	14.6	NEG	287	151
Quercetin	15.4	NEG	301	151
Quercetin-d3*	15.4	NEG	304	151
Luteolin	15.8	NEG	285	133
Naringenin	16.6	NEG	271	151
Genistein	16.7	NEG	269	133
Hesperetin	17.2	NEG	301	164
Phloretin	17.5	NEG	273	167
Kaempferol	17.5	NEG	285	187
Apigenin	17.6	NEG	269	117
Isorhamnetin	17.8	NEG	315	300
Diosmetin	17.9	NEG	299	284
Flavone	20.0	POS[b]	223	77
5,7-dimethoxyflavone	20.8	POS	283	239
Flavanone	21.8	POS	225	121
Xanthohumol	25.1	POS	355	179

(Continued)

TABLE 1 | Continued

**Internal standard.*
[a] Negative ionization mode.
[b] Positive ionization mode.

triple quadrupole mass spectrometer equipped with a heated electrospray ionization (HESI) interface.

Data were processed by comparing peak areas of polyphenols normalized to the peak area of an internal standard (IS) using Thermo Xcalibur 2.2 software. Each compound (**Table 1**) was quantified using a 4-point calibration curve that was obtained using serial dilutions. Kaempferol dirutinoside and

catechin-3-glucoside were not commercially available, however, their presence has been reported in lentil seeds, and they were examined here based on previous reports (Aguilera et al., 2010; Mirali et al., 2016a). The standard curves of kaempferol 3-rutinoside and catechin were used to estimate the quantities of these compounds, respectively. Concentration values were converted to ng/g based on dry sample weight.

Bioassay of the Effect of Polyphenols on Mycelial Growth of *Aphanomyces euteiches*

The polyphenols found in the root tissues and root extracts were evaluated for their effect on mycelial growth of the pathogen *A. euteiches* (AE1) isolated from Saskatchewan soils.

TABLE 2 | Binary gradient used in this study.

Time (min)	A%	B%	Flow (mL/min)
0	99	1	0.35
1	99	1	0.35
21	59	41	0.35
24	40	60	0.35
24.1	20	80	0.35
26	20	80	0.35
26.1	99	1	0.35
30	99	1	0.35

Solvent A consists of water: formic acid (99;1, v/v), and solvent B consists of water: acetonitrile: formic acid (9:90:1, v/v/v).

Commercially available polyphenols were used to prepare the stock solutions. A 1 mm well was created in the center of 5% corn meal agar (CMA) plates. An aliquot of 20 μL of 1 g L^{-1} of each polyphenol was added to the well.

Control plates received 20 μL of sterilized deionized water and a 1 mm plug of *A. euteiches* was cut from the margins of an actively growing culture plate and placed in the well. Inoculated plates were incubated in the dark at 22°C and radial growth was measured daily for up to 5 d. Percentage inhibition or stimulation of radial growth was calculated using the formula:

$$\%\text{age growth inhibition/stimulation} = (C - T)/C \times 100$$

Where C = growth in the control plate and T = growth in the treated plate (Dickinson and Skidmore, 1976). The experiment was repeated three times with three replicated plates per treatment.

Polyphenols found to be active against the pathogen *A. euteiches* were selected for further examination of their minimum inhibitory concentration. Using the same protocol described above, three concentrations of the selected polyphenols were examined for their effect on radial growth of the pathogen. Each concentration included a 10 times dilution level. We used a wide range of concentrations for each polyphenol to detect the possible inhibitory effects. The experiment was repeated three times with three replicated plates per treatment.

Statistical Analysis

Analysis of variance (ANOVA) was performed to test the significance of the effect of genotype, treatments and the interactions between genotype and treatment on the

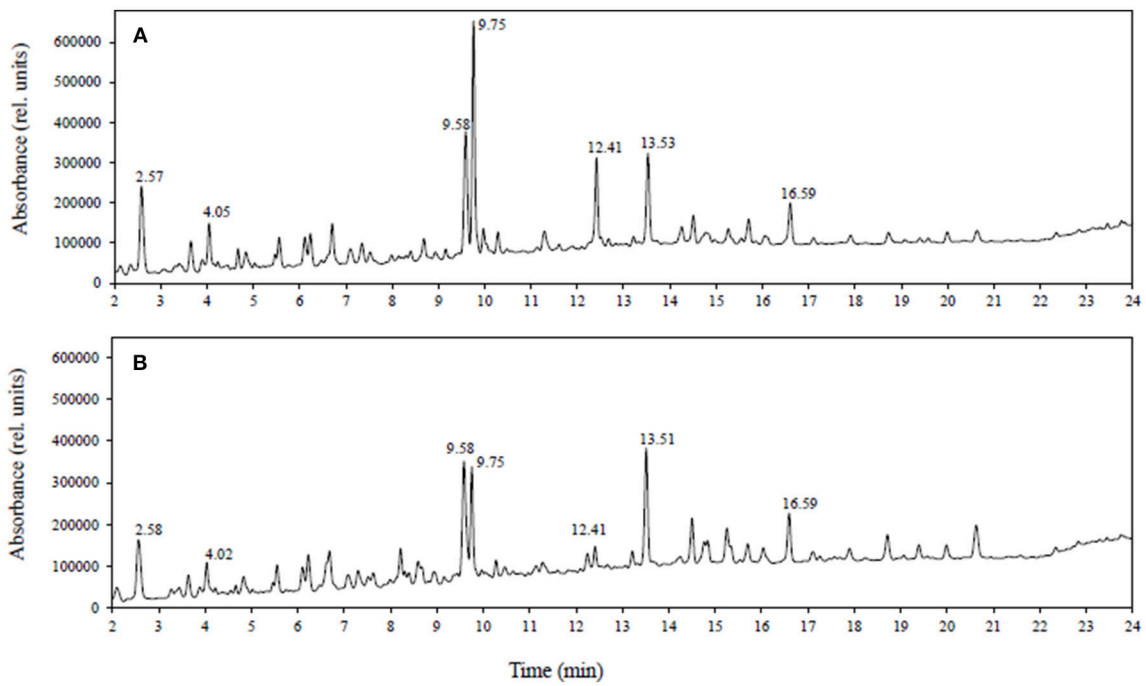

FIGURE 1 | LC-DAD spectra (UV-vis: 250–600 nm) obtained from tissue extracts of **(A)** healthy roots and **(B)** diseased roots of lentil genotype ZT-4.

concentration of polyphenols in roots tissues. The least significant difference (LSD) test was used to determine differences in the concentration of the compounds among genotypes and between the treatments. LSD was also used to test differences among genotypes in the concentration of the compounds in the root extract. A p-value of 0.05 was used as the threshold below which the null hypothesis was rejected. Comparisons of mean values and principal component analysis (PCA) were completed using R package (R, v.3.3.2) (www.r-project.org). A Dunnett's test was used to compare the *A. euteiches* mycelial inhibition of each polyphenol/concentration with control ($P < 0.05$).

RESULTS

Since all polyphenols absorb in the UV-vis region, the combination of LC-DAD with LC-MS is a powerful approach for investigating polyphenols. **Figure 1** shows a comparison of LC-DAD spectra (UV-vis 250–600 nm) obtained using extracts of (A) healthy roots and (B) diseased root tissues of lentil genotype ZT-4. The figure shows that the most significant changes in the spectra are observed at 9.75 and 12.41 min, with less significant changes being observed at other retention times. The compound at 9.75 min has an *m/z* of 755 (negative mode MS) and no standard has this *m/z* and retention time in our targeted LC-SRM method. This compound was observed to have a similar product ion spectrum compared with kaempferol 3-O-rutinoside-4′-glucoside (*m/z* 755, tr = 9.6 min included in the targeted method) and therefore is consistent with being a structural isomer of kaempferol 3-O-rutinoside-4′-glucoside. Similarly, the compound at 12.41 min has an *m/z* of 901 (negative mode) and no standard has this *m/z* and retention time in our targeted method. This unknown compound was observed to have many of the same product ions as kaempferol dirutinoside (*m/z* 901, tr = 8.69 min,

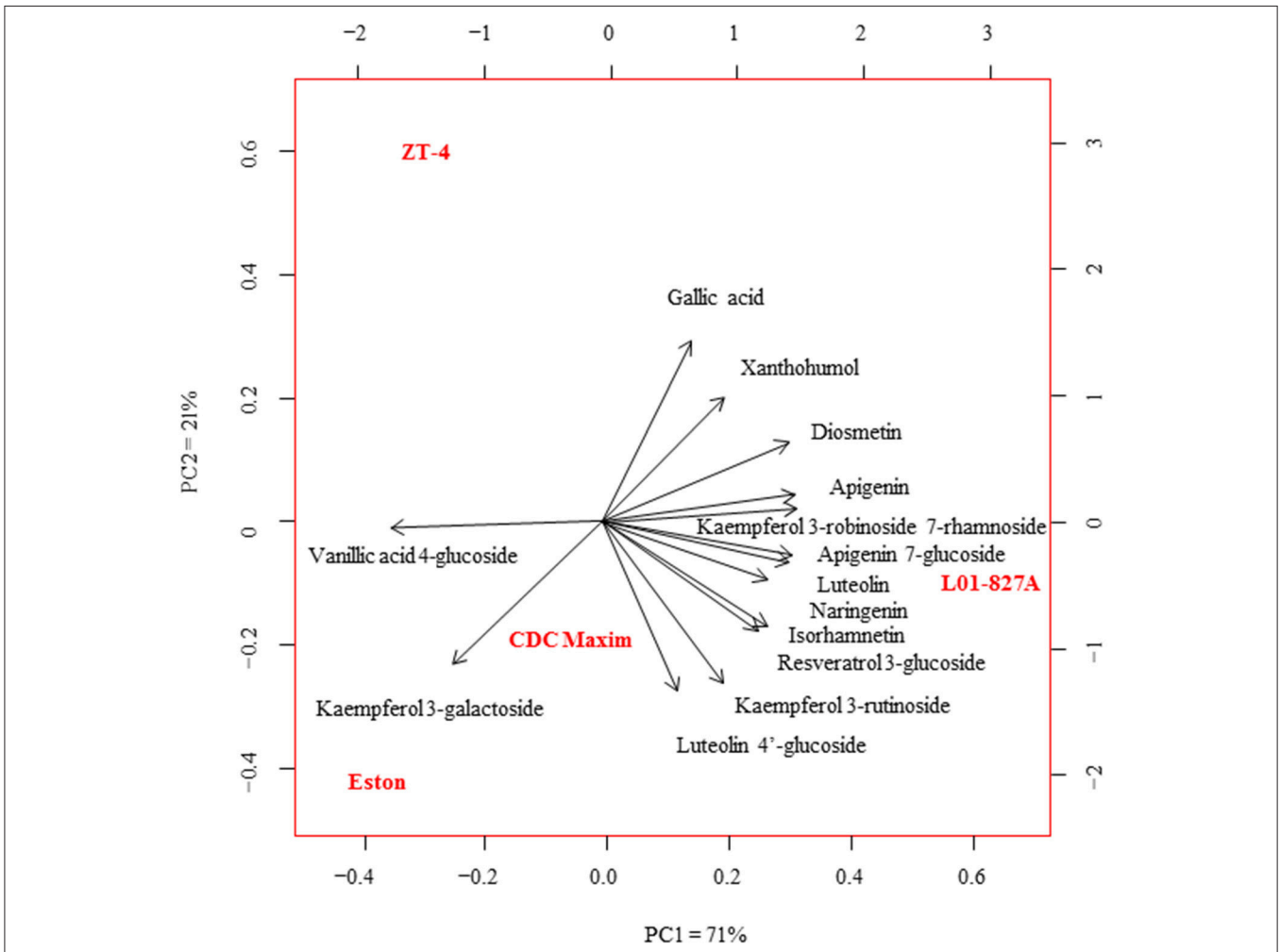

FIGURE 2 | Principal component analysis of the concentration of phenolic compounds in the root extracts of cultivated lentil genotypes ZT-4, CDC Maxim and Eston and *Lens ervoides* L01-827A using liquid chromatography-mass spectrometry ($n = 4$). Phenolic compounds were extracted from root extracts using 80% MeOH, and analyzed using LC-SRM.

included in the targeted method) and therefore is consistent with being a structural isomer of kaempferol dirutinoside. Thus, the UV-vis spectra not only detected large changes in the profile but also the presence of polyphenols not included in the targeted SRM method. For this study, we are focusing on quantifying polyphenols already present in our library.

Biochemical Analysis of Root Extracts

Fourteen polyphenols detected by LC-SRM were common to the root extracts of all 4 genotypes of lentil. Variation in the level of these polyphenols among the 4 genotypes of lentil was shown in **Figure 2**. *Lens ervoides* L01-827A had elevated amounts of most of the polyphenols in its root extract (**Table 3**).

Biochemical Analysis of Healthy and Diseased Root Tissues

The LC-SRM analysis detected 17 polyphenols in the root tissues of all 4 lentil genotypes. The effect of genotype, infection and the interactions between genotype and infection on the concentration of each of these polyphenols was described in **Table 4**. Concentrations of some of the polyphenols varied among the genotypes in healthy plants, whereas in diseased plants, the concentration of most of the polyphenols varied among the genotypes (**Table 5**). Concentration of several compounds varied between diseased and healthy root tissues of the same genotype. The variation observed in the concentration of polyphenols between healthy and diseased roots was larger in *L. ervoides* L01-827A whereas it was smaller in ZT-4 and CDC Maxim (**Figure 3**). The concentration of apigenin, kaempferol, and naringenin was higher in diseased root tissues for all four lentil genotypes (**Table S1**). Diosmetin, hesperetin 7-rutinoside, kaempferol 3-galactoside, kaempferol 3-rutinoside, naringenin 7-rutinoside, and vanillic acid were only significantly more abundant in diseased roots of *L. ervoides* L01-827A (**Table S1**). Coumaric acid was only detected in diseased roots of *L. ervoides* L01-827A and Eston. 3,4-dihydroxybenzoic acid was detected in

TABLE 4 | Statistical significance of the effect[a] of genotype and infection on the composition of some phenolic compounds in the root tissues of cultivated lentil genotypes ZT-4, CDC Maxim, Eston, and *Lens ervoides* L01-827A determined by liquid chromatography-mass spectrometry ($n = 4$).

Compound	Genotype	Infection	Genotype × Infection
Apigenin	0.01	< 0.0001	< 0.0001
Apigenin 7-glucoside	0.01	0.002	0.04
Dihydrokaempferol	0.51	0.008	0.88
Diosmetin	< 0.0001	< 0.0001	0.003
Eriodictyol	0.39	0.001	0.25
Hesperetin 7-rutinoside	0.04	0.74	0.001
Isorhamnetin	0.91	0.008	0.92
Kaempferol 3 galactoside	0.39	0.03	0.23
Kaempferol 3-robinoside 7-rhamnoside	0.001	0.006	0.06
Kaempferol 3-rutinoside	0.02	0.04	0.2
Kaempferol dirutinoside	0.001	0.005	0.003
Kaempferol	0.94	< 0.0001	0.97
Luteolin	0.03	0.001	0.22
Naringenin 7-rutinoside	0.54	0.48	0.009
Naringenin	0.01	< 0.0001	0.001
Vanillic acid 4-glucoside	0.14	0.03	0.28
Vanillic acid	0.09	< 0.0001	0.10

[a] *Significant effects were detected using analysis of variance (ANOVA) (n = 4).*

TABLE 3 | Concentration of phenolic compounds (ng/g root) detected in the root extracts of cultivated lentil genotypes ZT-4, CDC Maxim and Eston and *Lens ervoides* L01-827A using liquid chromatography-mass spectrometry.

Compound	Genotype			
	ZT-4	Eston	CDC Maxim	L01-827A
Vanillic acid 4-glucoside	5886 ± 2123[1] a	7166 ± 2947 a[2]	3433 ± 1782 ab	2302 ± 1143 b
Diosmetin	436 ± 89 b	180 ± 61 c	310 ± 204 bc	888 ± 72 a
Apigenin	43.7 ± 13.4 b	33.5 ± 20.6 b	56.2 ± 29.6 ab	87.6 ± 27.8 a
Naringenin	24.4 ± 3.5 b	29.3 ± 9.4 b	24.4 ± 12.4 b	62.1 ± 15.4 a
Kaempferol 3-robinoside 7-rhamnoside	2.08 ± 0.98 b	1.74 ± 1.19 b	2.46 ± 2.24 b	9.85 ± 4.36 a
Gallic acid	1.72 ± 0.01 a	1.11 ± 0.73 a	1.20 ± 1.04 a	1.61 ± 0.52 a
Kaempferol 3-galactoside	1.58 ± 1.17 ab	3.67 ± 1.52 a	3.48 ± 3.31 ab	1.05 ± 0.75 b
Apigenin 7-glucoside	0.68 ± 0.32 b	0.63 ± 0.44 b	1.02 ± 0.83 ab	2.88 ± 2.36 a
Luteolin	0.64 ± 0.18 b	0.20 ± 0.15 b	1.33 ± 1.19 b	15.57 ± 0.62 a
Kaempferol 3-rutinoside	0.22 ± 0.2 a	0.28 ± 0.1 a	0.29 ± 0.2 a	0.37 ± 0.2 a
Isorhamnetin	0.23 ± 0.09 b	0.35 ± 0.3 ab	0.31 ± 0.2 b	0.69 ± 0.2 a
Xanthohumol	0.03 ± 0.03 a	0.02 ± 0.02 a	0.03 ± 0.03 a	0.03 ± 0.03 a
Luteolin 4′-glucoside	0.02 ± 0.02 b	0.07 ± 0.07 ab	0.11 ± 0.06 ab	0.15 ± 0.08 a
Resveratrol 3-glucoside	0.05 ± 0.05 b	0.09 ± 0.09 b	0.37 ± 0.3 ab	0.86 ± 0.7 a

[1] *Standard deviation.*

[2] *Significant differences were detected using a Least Significant Difference (LSD) test (n = 4) ($p < 0.05$). Different letters indicate significant differences between means.*

TABLE 5 | Concentration of phenolic compounds ($\mu g\ g^{-1}$ root) detected in the root tissues of cultivated lentil genotypes ZT-4, CDC Maxim and Eston and *Lens ervoides* L01-827A using liquid chromatography-mass spectrometry.

Compound	Treatment	Genotype			
		ZT-4	Eston	CDC Maxim	L01-827A
Apigenin	Healthy	1.02 a[1]	0.44 a	0.21 a	0.77 a
	Infected	3.19 b	1.99 b	1.67 b	6.67 a
Apigenin 7-glucoside	Healthy	0.06 a	0.01 a	0.002 a	0.07 a
	Infected	0.07 b	0.12 b	0.05 b	0.32 a
Dihydrokaempferol	Healthy	0.34 a	0.04 a	0.03 a	0.11 a
	Infected	0.69 a	0.21 a	0.35 a	0.75 a
Diosmetin	Healthy	24.3 b	25.5 b	28.6 ab	39.9 a
	Infected	34.4 b	36.9 b	43.6 b	100.7 a
Eriodictyol	Healthy	0.03 a	0.03 a	0.02 a	0.03 a
	Infected	0.05 a	0.05 a	0.05 a	0.08 a
Hesperetin 7-runtinoside	Healthy	0.41 a	0.16 a	0.15 a	0.14 a
	Infected	0.17 b	0.20 b	0.15 b	0.42 a
Isorhamnetin	Healthy	0.61 a	0.44 a	0.27 a	0.76 a
	Infected	1.37 a	1.85 a	1.43 a	1.73 a
Kaempferol 3-galactoside	Healthy	0.20 a	0.12 a	0.09 a	0.09 a
	Infected	0.17 a	0.32 a	0.13 a	0.28 a
Kaempferol 3-robinoside 7-rhamnoside	Healthy	0.99 b	0.68 b	0.74 b	3.28 a
	Infected	1.47 bc	4.73 ab	0.64 c	7.72 a
Kaempferol 3-rutinoside	Healthy	0.19 a	0.15 a	0.03 a	0.11 a
	Infected	0.11 b	0.24 ab	0.04 b	0.41 a
Kaempferol dirutinoside	Healthy	2.21 b	7.04 b	1.73 b	26.9 a
	Infected	3.88 b	78.9 a	0.75 b	42.8 ab
Kaempferol	Healthy	0.39 a	0.46 a	0.22 a	0.18 a
	Infected	4.80 a	4.15 a	3.56 a	4.57 a
Luteolin	Healthy	1.05 a	0.98 a	0.15 a	1.13 a
	Infected	1.86 b	4.40 a	0.86 b	2.86 ab
Naringenin 7-rutinoside	Healthy	0.09 a	0.04 ab	0.05 ab	0.03 b
	Infected	0.04 b	0.04 b	0.05 b	0.08 a
Naringenin	Healthy	0.29 a	0.07 b	0.08 ab	0.11 ab
	Infected	0.66 b	0.57 b	0.85 b	1.85 a
Vanillic acid 4-glucoside	Healthy	32.9 a	32.2 a	21.8 a	21.4 a
	Infected	45.3 ab	94.5 a	35.5 b	41.1 ab
Vanillic acid[2]	Healthy	20.7 a	13.9 a	21.5 a	18.1 a
	Infected	35.8 ab	26.0 b	34.1 ab	54.5 a

[1] *Significant differences were detected using a Least Significant Difference (LSD) test ($n = 4$) ($p < 0.05$). Different letters indicate significant differences between means.*
[2] *Due to a co-eluting interference in the SRM channel, the value of vanillic acid was estimated by LC-UV.*

diseased roots of all and in healthy roots of *L. ervoides* L01-827A (**Table S2**).

In vitro Assay Testing the Effect of Polyphenols on Mycelial Growth of *Aphanomyces euteiches*

Seven polyphenols including vanillic acid, 4-hydroxybenzoic acid, 3,4-dihydroxybenzoic acid, 4-aminosalicylic acid, coumaric acid, delphinidin 3-glucoside and phloretin inhibited the mycelial growth of *A. euteiches* at 1 mg mL^{-1} *in vitro* ($p < 0.0001$). Coumaric acid and phloretin also inhibited *A. euteiches* at 0.1 g L^{-1} (10x dilution). No inhibition was observed for other compounds at 0.1 g L^{-1} (10x dilution), or at lower concentrations of any of these polyphenols (**Table 6**).

DISCUSSION

We used semi-quantitative mass spectrometry to investigate genotypic variations within the composition of polyphenols that naturally exist in the root tissues and root extracts of lentil. We analyzed a wide range of polyphenols and demonstrated that the qualitative and quantitative composition of polyphenols not only differs among the lentil genotypes, but also between the healthy and *A. euteiches* infected roots.

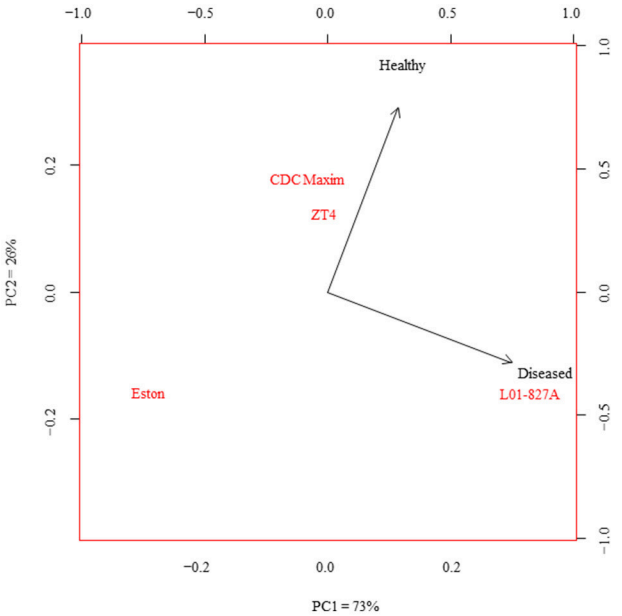

FIGURE 3 | Principal component analysis of the concentration of phenolic compounds in the healthy and diseased root tissues of cultivated lentil genotypes ZT-4, CDC Maxim and Eston and *Lens ervoides* L01-827A using liquid chromatography-mass spectrometry ($n = 4$). Phenolic compounds were extracted from root tissues, and analyzed using LC-SRM.

TABLE 6 | Inhibitory effect of bioactive polyphenols[a] detected in lentil root tissues on the *in vitro*[b] radial growth of *Aphanomyces euteiches*[c].

Polyphenol	Concentration		
	1 g L^{-1} (%)	0.1 g L^{-1} (%)	0.05 g L^{-1} (%)
4-hydroxybenzoic acid	100***[d,e]	10.50[nsf]	2.60[ns]
4-aminosalicylic acid	100***	6.60[ns]	5.60[ns]
Vanillic acid	100***	8.50[ns]	4.60[ns]
Coumaric acid	100***	44.90*	12.50[ns]
3,4-dihydroxybenzoic acid	100***	12.50[ns]	11.50[ns]
Phloretin	61.70*	31.10*	13.40[ns]
Delphinidin 3-glucoside	21.50*	14.50[ns]	11.40[ns]

[a] *20 μL of phenolic compound was applied.*
[b] *Corn meal agar (CMA) medium (5%).*
[c] *Mycelial growth was measured 5 d after inoculation.*
[d] *Values represent percent inhibition of radial growth of Aphanomyces euteiches compared to control.*
[e] *Significant differences between treatments and control were detected using Dunnett's test ($n = 3$) (***$p < 0.001$, *$p < 0.05$).*
[f] *Not significant.*

The higher concentration of polyphenols in the root extracts of the *L. ervoides* genotype (tertiary gene pool) compared to the cultivated *L. culinaris* genotypes (primary gene pool) could be an evolutionary divergence or a consequence of selection for larger plants and seeds during the domestication process (Alo et al., 2011; Wong et al., 2015). It was shown that the selection of new cultivars for specific traits or under optimal growth conditions may inadvertently lead to the loss of specific genes and phytochemicals (Hättenschwiler and Vitousek, 2000; Dixon, 2001) including those involved in the synthesis of polyphenols.

Lentil genotype ZT-4 is characterized by the expression of the single recessive gene, *tan,* that affects the color and thickness of the seed coat (Vaillancourt et al., 1986). The seed coats of low-tannin lentils lack many of the polyphenols found in normal seed coats, causing them to be thinner and more fragile compared to the seed coat of normal genotypes (Matus et al., 1993; Mirali et al., 2016a). This study shows that the *tan* gene is also expressed in the root tissues and results in a lower concentration of most of the polyphenols.

Variations observed in the levels of specific polyphenols between healthy and diseased root tissues may be due to defensive responses through the inactivation of microbial enzymes, reinforcement of plant structural components or creation of strategic barriers at points of entry (Sylvia and Sinclair, 1983; Beckman, 2000; Vermerris and Nicholson, 2008). In this study, the elevated concentration of apigenin, kaempferol, and naringenin in the diseased roots of all four lentil genotypes (**Table S1**) may suggest that these three polyphenols are associated with a general response against *A. euteiches*. Support for this hypothesis can be found in previous studies in which naringenin and apigenin were shown to have inhibitory effects on the bacterial pathogens and nematodes (Baidez et al., 2006; Treutter, 2006). Since such inhibitory effect was not detected against *A. euteiches* in our bioassay, these polyphenols might have other potential roles in a response against *A. euteiches*. Similar levels of several compounds in healthy and diseased roots of the low-tannin genotype ZT-4 may suggest that the expression of the gene *tan* is one of the factors influencing the composition of polyphenols in responses to phytopathogens. The differences observed in the concentration of polyphenols between healthy and diseased roots in different genotypes (**Tables 3**, **4**) may indicate that the synthesis of defensive metabolites is genotype dependent. The variation was larger in *L. ervoides* L01-827A (**Figure 3**), suggesting that this wild genotype might have a wider capacity for a defensive response to plant pathogens.

In this study, the lentil genotypes were treated by the endosymbiont *R. leguminosarum*. It is notable that some polyphenols act as chemoattractants for rhizobium, improving the root colonization (Fisher and Long, 1992; Begum et al., 2001; Cooper, 2004) and, rhizobium may aid the plant to resist against pathogen by mediating the polyphenolic content of root tissues (Mishra et al., 2006). However, rhizobium may interact differently with the lentil genotypes resulting in different degrees of root colonization, and different responses to plant pathogens.

Certain phytochemicals were shown to attract the zoospores or inhibit the hyphal growth of *A. euteiches* (Yokosawa et al., 1986; Smolinska et al., 1997; Cannesan et al., 2012). In our study, the first involving lentil, some of the root polyphenols that inhibited the hyphal growth of the *A. euteiches* were more concentrated in specific lentil genotypes. For instance, the concentration of vanillic acid and 3,4-dihydroxybenzoic acid were higher in *L. ervoides* L01-827A which has a marbled gray seed coat. Coumaric acid was detected only in diseased roots of *L. ervoides* L01-827A, and in the green seed coat of the cultivar Eston (Mirali et al., 2016b). Differences in the quantity and

quality of the phenylpropanoid metabolites in different genotypes of lentil suggests there could be useful genotypic variation in the level of resistance to *A. euteiches* in lentil. Since the majority of these *A. euteiches* inhibitors were organic acids, the organic acid content of root tissues and extracts appears to be associated with some level of resistance to ARR. Organic acids comprise a major portion of root extracts in most plant species (Neumann and Römheld, 2001; Cawthray, 2003; Sandnes et al., 2005). Organic acids and their derivatives were detected in both root tissue and root extracts of lentil. The observation that some organic acids, including caffeic acid, gallic acid, and 3-hydroxy-4-methoxycinnamic acid, did not affect the hyphal growth of *A. euteiches* suggests that the inhibitory effect on *A. euteiches* is limited to specific organic acids. The concentrations of root polyphenols could be variable in real conditions depending on various factors. However, an accumulative concentration of the bioactive polyphenols could be achieved and be effective to inhibit the root rot pathogen. Polyphenols, particularly those released from roots, are involved in a wide range of agro-ecological processes, and could affect specific ecological niches in the rhizosphere (Aira et al., 2010; Doornbos et al., 2012). The selective release of organic acids and other polyphenols that inhibit *A. euteiches* may improve soil health by reducing the abundance of the pathogen in soil, and the severity of ARR in subsequent susceptible crops in rotation.

To date there is no report of detection of effective resistance to *A. euteiches* in lentil. Among the genotypes used in this study, ZT4 was more susceptible to *A. euteiches* (Knowpulse Report, 2015), while L01-827A and Eston have shown a moderate level of resistance to *A. euteiches* (Banniza, pers. comm.; Saskpulse, 2015). One reason for their better tolerance to *A. euteiches* could be the elevated levels of specific of polyphenols. Such variations could increase the understanding of pathways of biochemical resistance to plant diseases and could be used as a starting point for identification of lentil genotypes that are resistant to root rot diseases in breeding programs.

Our study revealed that genotypic variations for the composition of polyphenols exist in lentil, and that there is a relationship between the composition of polyphenols and tolerance to *A. euteiches*. The *tan* gene in lentil influences the composition of polyphenols in root extracts. A number of studies have described the potential role of polyphenols in providing resistance against root rot diseases in different plant species (Farkas and Kiraaly, 1962; Lagrimini et al., 1993; Daayf et al., 2012; Aksoya et al., 2017). Such studies usually focus on a small number of compounds and thus cannot provide a clear image of the function of polyphenols. Here, we analyzed a wide range of polyphenols in response to root rot disease. Understanding of the role of polyphenols in providing resistance against root rot diseases, and their potential application in breeding programs is still not well defined. In lentil breeding programs, the exploitation of polyphenol content has mainly targeted the seed coats in order to improve seed quality, storage, marketability and nutritional values (Vaillancourt et al., 1986; Mirali et al., 2016b, 2017; Ganesan and Xu, 2017). Further research is required to identify and quantify all the polyphenols that are differentially expressed in uninfected and infected root tissues of lentil species. It is necessary to detect correlations between the concentration of specific polyphenols and other metabolites in the root tissues in order to identify mechanisms of resistance to *A. euteiches*. The induction of resistance in host plants can be influenced by a number of factors, including plant genotype, nutrition and environmental conditions (Walters et al., 2013). Therefore, it is necessary to understand the influence of plant nutrition on the polyphenolic content of roots, since this may override the influence of plant genetics on the composition of polyphenols. We are currently investigating unknown peaks in the UV spectra to identify new compounds of importance for roots that will be added to the polyphenol library in future studies.

AUTHOR CONTRIBUTIONS

NB grew plants and collected the root materials. NB and RP contributed to LCMS analyses. PP prepared the inoculum and conducted the *in-vitro* plate assay. All authors contributed to experimental design and to preparation of the manuscript.

ACKNOWLEDGMENTS

The authors acknowledge financial assistance from the NSERC Industrial Research Chair program, and Saskatchewan Pulse Growers. We also acknowledge the assistance provided by Thermo Fisher Scientific (San Jose, CA) through instrumentation made available as part of a collaboration between Thermo Fisher and the University of Saskatchewan. Additional support was provided by the University of Saskatchewan Health Sciences core mass spectrometry facility, and by the Pulse Research Crew at the Crop Development Centre, University of Saskatchewan.

SUPPLEMENTARY MATERIAL

The Supplementary Material for this article can be found online at: https://www.frontiersin.org/articles/10.3389/fpls.2018.01131/full#supplementary-material

REFERENCES

Aguilera, Y., Dueñas, M., Estrella, I., Hernández, T., Benitez, V., Esteban, R. M., et al. (2010). Evaluation of phenolic profile and antioxidant properties of Pardina lentil as affected by industrial dehydration. *J. Agric. Food Chem.* 58, 10101–10108. doi: 10.1021/jf102222t

Aira, M., Gomez-Brandon, M., Lazcano, C., Baath, E., and Domínguez, J. (2010). Plant genotype strongly modifies the structure and growth of maize rhizosphere microbial communities. *Soil Biol. Biochem.* 42, 2276–2281. doi: 10.1016/j.soilbio.2010.08.029

Aksoya, H. M., Kaya, Y., Ozturk, M., Secgin, Z., Onder, H., and Okumus, A. (2017). Pseudomonas putida – Induced response in phenolic profile of tomato seedlings (*Solanum lycopersicum* L.) infected by *Clavibacter michiganensis* subsp. michiganensis. *Biol. Control* 105, 6–12. doi: 10.1016/j.biocontrol.2016.11.001

Alo, F., Furman, B. J., Akhunov, E., Dvorak, J., and Gepts, P. (2011). Leveraging genomic resources of model species for the assessment of diversity

and phylogeny in wild and domesticated lentil. *J Hered.* 102, 315–329. doi: 10.1093/jhered/esr015

Armstrong-Cho, C., Tetreault, M., Banniza, S., Bhadauria, V., and Morrall, R. A. A. (2014). *Reports of Aphanomyces euteiches in Saskatchewan.* The Canadian Phytopathological Society. Canadian Plant Disease Survey. Disease Highlights.

Baetz, U., and Martinoia, E. (2014). Root exudates: the hidden part of plant defense. *Trends Plant Sci.* 19, 90–98. doi: 10.1016/j.tplants.2013.11.006

Baidez, A. G., Gomez, P., Del Rio, J. A., and Ortuno, A. (2006). Antifungal capacity of major phenolic compounds of *Olea europaea* L. against *Phytophthora megasperma* Drechsler and *Cylindrocarpon destructans* (Zinssm.) Scholten. *Physiol. Mol. Plant Pathol.* 69, 224–229. doi: 10.1016/j.pmpp.2007.05.001

Balmer, A., Pastor, V., Gamir, J., Flors, V., and Mauch-Mani, B. (2015). The "prime-ome": towards a holistic approach to priming. *Trends Plant Sci.* 20, 443–452. doi: 10.1016/j.tplants.2015.04.002

Banniza, S. (2015). *BRE1519: Developing Rapid Generation Technology Involving Wild Lentil Crosses to Produce Aphanomyces-Resistant Lentil Varieties–Proof of Concept.* Saskpulse Report. Available online at: http://saskpulse.com/files/general/BRE1519_%28Banniza%29.pdf

Bazghaleh, N., Hamel, C., Gan, Y., Knight, J. D., Vujanovic, V., Cruz, A. F., et al. (2016). Phytochemicals induced in chickpea roots selectively and non-selectively stimulate and suppress fungal endophytes and pathogens. *Plant Soil* 409, 479–493. doi: 10.1007/s11104-016-2977-z

Beckman, C. H. (2000). Phenolic-storing cells: keys to programmed cell death and periderm formation in wilt disease resistance and in general defence responses in plants? *Physiol. Mol. Plant Pathol.* 57, 101–110. doi: 10.1006/pmpp.2000.0287

Begum, A. A., Leibovitch, S., Migner, P., and Zhang, F. (2001). Specific flavonoids induced nod gene expression and pre-activated nod genes of *Rhizobium leguminosarum* increased pea (*Pisum sativum* L.) and lentil (*Lens culinaris* L.) nodulation in controlled growth chamber environments. *J. Exp. Bot.* 52, 1537–1543. doi: 10.1093/jexbot/52.360.1537

Bennett, R., and Wallsgrove, R. (1994). Secondary metabolites in plant defence mechanisms. *New Phytol.* 127, 617–633. doi: 10.1111/j.1469-8137.1994.tb02968.x

Borrell, A. N., Shi, Y., Gan, Y., Bainard, L. D., Germida, J. J., and Hamel, C. (2016). Fungal diversity associated with pulses and its influence on the subsequent wheat crop in the Canadian prairies. *Plant Soil* 414, 13–31. doi: 10.1007/s11104-016-3075-y

Cannesan, M. A., Durand, C., Burel, C., Gangneux, C., Lerouge, P., Ishii, T., et al. (2012). Effect of arabinogalactan proteins from the root caps of pea and brassica napus on *Aphanomyces euteiches* zoospore chemotaxis and germination. *Plant Physiol.* 159, 1658–1670. doi: 10.1104/pp.112.198507

Cawthray, G. R. (2003). An improved reversed-phase liquid chromatographic method for the analysis of low-molecular mass organic acids in plant root exudates. *J. Chromatogr. A* 1011, 233–240. doi: 10.1016/S0021-9673(03)01129-4

Chatterton, S., Bowness, R., and Harding, M. W. (2016). First report of root rot of field pea caused by *Aphanomyces euteiches* in Alberta, Canada. *Plant Dis.* 99:288. doi: 10.1094/PDIS-09-14-0905-PDN

Cheynier, V. (2012). Phenolic compounds: from plants to foods. *Phytochem. Rev.* 11, 153–177. doi: 10.1007/s11101-012-9242-8

Constabel, C. P., Yoshida, K., and Walker, V. (2014). Diverse ecological roles of plant tannins: plant defense and beyond. *Recent Adv. Polyphen. Res.* 4, 115–142. doi: 10.1002/9781118329634.ch5

Cooper, J. E. (2004). Multiple responses of rhizobia to flavonoids during legume root infection. *Adv. Bot. Res.* 41, 1–62. doi: 10.1016/S0065-2296(04)41001-5

Daayf, F., El Hadrami, A., El-Bebany, A. F., Henriquez, M. A., Yao, Z., Derksen, H., et al. (2012). Phenolic compounds in plant defense and pathogen counter-defense mechanisms. *Recent Adv. Polyphen. Res.* 3, 191–208. doi: 10.1002/9781118299753.ch8

Deng, Y., Zhao, Y., Padilla-Zakour, O., and Yang, G. (2015). Polyphenols, antioxidant and antimicrobial activities of leaf and bark extracts of *Solidago canadensis* L. *Ind. Crops Prod.* 74, 803–809. doi: 10.1016/j.indcrop.2015.06.014

Dickinson, C. H., and Skidmore, A. M. (1976). Interactions between germinating spores of Septoria nodorum and phylloplane fungi. *Trans. Br. Mycol. Soc.* 66, 45–56. doi: 10.1016/S0007-1536(76)80091-5

Dixon, R. A. (2001). Natural products and plant disease resistance. *Nature* 411, 843–847. doi: 10.1038/35081178

Doornbos, R. F., Van Loon, L. C., and Bakker, P. A. H. M. (2012). Impact of root exudates and plant defense signaling on bacterial communities in the rhizosphere. A review. *Agron. Sustain. Dev.* 32, 227–243. doi: 10.1007/s13593-011-0028-y

Evidente, A., Cimmino, A., Fernandez-Aparicio, M., Andolfi, A., Rubiales, D., and Motta, A. (2010). Polyphenols, including the new peapolyphenols A–C, from pea root exudates stimulate *Orobanche foetida* seed germination. *J. Agric. Food Chem.* 58, 2902–2907. doi: 10.1021/jf904247k

FAO (2017). *FAOSTAT. Food and Agriculture Organization of the United Nations.* Rome. Available online at: http://faostat.fao.org

Farkas, G. L., and Kiraaly, Z. (1962). Role of phenolic compounds in the physiology of plant diseases and disease resistance. *J. Phytopathol.* 44, 105–150. doi: 10.1111/j.1439-0434.1962.tb02005.x

Ferguson, M. E., Maxted, N., Van Slageren, M., and Robertson, L. D. (2000). A re-assessment of the taxonomy of *Lens* Mill. (Leguminosae, Papilionaceae, Vicieae). *Bot. J. Linn. Soc.* 133, 41–59. doi: 10.1111/j.1095-8339.2000.tb01536.x

Fisher, R. F., and Long, S. R. (1992). Rhizobium–plant signal exchange. *Nature* 357, 655–660. doi: 10.1038/357655a0

Ganesan, K., and Xu, B. (2017). Polyphenol-rich lentils and their health promoting effects. *Int. J. Mol. Sci.* 18, 1–23. doi: 10.3390/ijms18112390

Gossen, B. D., Conner, R. L., Chang, K. F., Pasche, J. S., McLaren, D. L., Henriquez, M. A., et al. (2016). Identifying and managing root rot of pulses on the northern great plains. *Plant Dis.* 100, 1965–1978. doi: 10.1094/PDIS-02-16-0184-FE

Hättenschwiler, S., and Vitousek, P. M. (2000). The role of polyphenols in terrestrial ecosystems nutrient cycling. *Trends Ecol. Evol.* 15, 238–243. doi: 10.1016/S0169-5347(00)01861-9

Knowpulse Report (2015). *Trichoderma: A Possible Solution for Aphanomyces?* Root rot report. Available online at: http://knowpulse.usask.ca/portal/sites/default/files/NAPIARootRot_Prashar.pdf

Ladizinsky, G. (1979a). The genetics of several morphological traits in the lentil. *J. Hered.* 70, 135–137.

Ladizinsky, G. (1979b). The origin of lentil and its wild genepool. *Euphytica* 28, 179–187.

Lagrimini, L. M., Vaughn, J., Erb, W. A., and Miller, S. A. (1993). Peroxidase overproduction in tomato: wound-induced polyphenol deposition and disease resistance. *Hortscience* 28, 218–221.

Lanoue, A., Burlat, V., Henkes, G. J., Koch, I., Schurr, U., and Röse, U. S. R. (2010). *De novo* biosynthesis of defense root exudates in response to fusarium attack in barley. *New Phytol.* 185, 577–588. doi: 10.1111/j.1469-8137.2009.03066.x

Lattanzio, V. (2013). "Phenolic compounds," in *Natural Products*, eds K. G. Ramawat and J. M. Merillon (Berlin; Heidelberg: Springer-Verlag), 1543–1580.

Matus, A., Slinkard, A. E., and Vandenberg, A. (1993). "The potential of zero tannin lentil," in *New Crops*, eds J. Janick and J. E. Simon (New York, NY: Wiley), 279–282.

McPhee, K. (2003). Dry pea production and breeding: A minireview. *J. Food Agric. Environ.* 1, 64–69.

Mirali, M., Ambrose, S. J., Wood, S. A., Vandenberg, A., and Purves, R. W. (2014). Development of a fast extraction method and optimization of liquid chromatography-mass spectrometry for the analysis of phenolic compounds in lentil seed coats. *J. Chromatogr. B* 969, 149–161. doi: 10.1016/j.jchromb.2014.08.007

Mirali, M., Purves, R. W., Stonehouse, R., Song, R., Bett, K., and Vandenberg, A. (2016a). Genetics and biochemistry of zero-tannin lentils. *PLoS ONE* 11:e0164624. doi: 10.1371/journal.pone.0164624

Mirali, M., Purves, R. W., and Vandenberg, A. (2016b). Phenolic profiling of green lentil (*Lens culinaris* Medic.) seeds subjected to long-term storage. *Eur. Food Res. Technol.* 242, 2161–2170. doi: 10.1007/s00217-016-2713-1

Mirali, M., Purves, R. W., and Vandenberg, A. (2017). Profiling the phenolic compounds of the four major seed coat types and their relation to color genes in lentil. *J. Nat. Prod.* 80, 1310–1317. doi: 10.1021/acs.jnatprod.6b00872

Mishra, R. P., Singh, R. K., Jaiswal, H. K., Kumar, V., and Maurya, S. (2006). Rhizobium-mediated induction of phenolics and plant growth promotion in rice (*Oryza sativa* L.). *Curr. Microbiol.* 52, 383–389. doi: 10.1007/s00284-005-0296-3

Moussart, A., Even, M. N., Lesne, A., and Tivoli, B. (2013). Successive legumes tested in a greenhouse crop rotation experiment modify the inoculum potential of soils naturally infested by *Aphanomyces euteiches*. *Plant Pathol.* 62, 545–551. doi: 10.1111/j.1365-3059.2012.02679.x

Neumann, G., and Römheld, V. (2001). "The release of root exudates as affected by the plant's physiological status," in *The Rhizosphere: Biochemistry and Organic*

Substances at the Soil–Plant Interface, eds R. Pinton, Z. Varanini, and P. Nannipieri (New York, NY: Dekker), 23–72.

Nicholson, R. L., and Hammerschmidt, R. (1992). Phenolic compounds and their role in disease resistance. *Annu. Rev. Phytopathol.* 30, 369–389. doi: 10.1146/annurev.py.30.090192.002101

Olivoto, T., Nardino, M., Carvalho, I. R., Follmann, D. N., Szareski, V. J., Ferrari, M., et al. (2017). Plant secondary metabolites and its dynamical systems of induction in response to environmental factors: a review. *Afr. J. Agric. Res.* 12, 71–84. doi: 10.5897/AJAR2016.11677

Pagliarulo, C., De Vito, V., Picariello, G., Colicchio, R., Pastore, G., Salvatore, P., et al. (2016). Inhibitory effect of pomegranate (*Punica granatum* L.) polyphenol extracts on the bacterial growth and survival of clinical isolates of pathogenic *Staphylococcus aureus* and *Escherichia coli*. *Food chem.* 190, 824–831. doi: 10.1016/j.foodchem.2015.06.028

Purves, R. W., Mirali, M., Bazghaleh, N., and Vandenberg, A. (2016). "Semi quantitative LC-MRM workflow for the analysis of over 100 polyphenols in lentil crops," in *29th Workshop on Tandem Mass Spectrometry* (Lake Louise, AB), 1.

Puupponen-Pimiä, R., Nohynek, L., Meier, C., Kähkönen, M., Heinonen, M., Hopia, A., et al. (2001). Antimicrobial properties of phenolic compounds from berries. *J. Appl. Microbiol.* 90, 494–507. doi: 10.1046/j.1365-2672.2001.01271.x

Quideau, S., Deffieux, D., Douat-Casassus, C., and Pouységu, L. (2011). Plant polyphenols: chemical properties, biological activities, and synthesis. *Angew. Chemie. Int. Ed.* 50, 586–621. doi: 10.1002/anie.201000044

Reuveni, R., Shimoni, M., Karchi, Z., and Kuc, J. (1991). Peroxidase activity as a biochemical marker for resistance of muskmelon (*Cucumis melo*) to *Pseudoperonospora cubensis*. *Resistance* 82, 749–753.

Roy, F., Boye, J. I., and Simpson, B. K. (2010). Bioactive proteins and peptides in pulse crops: pea, chickpea and lentil. *Food Res. Int.* 43, 432–442. doi: 10.1016/j.foodres.2009.09.002

Sánchez-Chino, X., Jiménez-Martínez, C., Dávila-Ortiz, G., Álvarez-González, I., and Madrigal-Bujaidar, E. (2015). Nutrient and nonnutrient components of legumes, and its chemopreventive activity: a review. *Nutr. Cancer* 67, 401–410. doi: 10.1080/01635581.2015.1004729

Sandnes, A., Eldhuset, T. D., and Wollebaek, G. (2005). Organic acids in root exudates and soil solution of Norway spruce and silver birch. *Soil Biol. Biochem.* 37, 259–269. doi: 10.1016/j.soilbio.2004.07.036

Shalaby, S., and Horwitz, B. A. (2015). Plant phenolic compounds and oxidative stress: integrated signals in fungal–plant interactions. *Curr. Genet.* 61, 347–357. doi: 10.1007/s00294-014-0458-6

Smolinska, U., Knudsen, G. R., Morra, M. J., Borek, V. (1997). Inhibition of *Aphanomyces euteiches* f. sp. *pisi* by volatiles produced by hydrolysis of *Brassica napus* seed meal. *Plant Dis*. 81, 288–292.

Sylvia, D. M., and Sinclair, W. A. (1983). Phenolic compounds and resistance to fungal pathogens induced in primary roots of douglas fir seedlings by the ectomycorrhizal fungus *Laccaria laccata*. *Phytopathology* 73, 390–397. doi: 10.1094/Phyto-73-390

Treutter, D. (2006). Significance of flavonoids in plant resistance: a review. *Environ. Chem. Lett.* 4, 147–157. doi: 10.1007/s10311-006-0068-8

Urbano, G., Porres, J. M., Frías, J., and Vidal-valverde, C. (2007). "Nutritional value," in *Lentil: An Ancient Crop for Modern Times,* eds S. S. Yadav, D. McNeil, and P. C. Stevenson (Dordrecht: Springer), 47–93.

Vaillancourt, R., Slinkard, A. E., and Reichert, R. D. (1986). The inheritance of condensed tannin concentration in lentil. *Can. J. Plant Sci.* 66, 241–246. doi: 10.4141/cjps86-038

Vermerris, W., and Nicholson, R. (eds.). (2008). "The role of phenols in plant defense," in *Phenolic Compound Biochemistry* (Dordrecht: Springer), 211–234.

Walters, D. R., Ratsep, J., and Havis, N. D. (2013). Controlling crop diseases using induced resistance: challenges for the future. *J. Exp. Bot.* 64, 1263–1280. doi: 10.1093/jxb/ert026

Wicker, E., Hullé, M., Rouxel, F. (2001). Pathogenic characteristics of isolates of *Aphanomyces euteiches* from pea in France. *Plant Pathol.* 50, 433–442. doi: 10.1046/j.1365-3059.2001.00590.x

Wille, L., Messmer, M. M., Studer, B., and Hohmann, P. (2018). Insights to plant-microbe interactions provide opportunities to improve resistance breeding against root diseases in grain legumes. *Plant Cell Environ.* doi: 10.1111/pce.13214. [Epub ahead of print].

Wink, M. (1988). Plant breeding: importance of plant secondary metabolites for protection against pathogens and herbivores. *Theor. Appl. Genet.* 75, 225–233. doi: 10.1007/BF00303957

Wong, M. M., Gujaria-Verma, N., Ramsay, L., Yuan, H. Y., Caron, C., Diapari, M., et al. (2015). Classification and characterization of species within the genus lens using genotyping-by-sequencing (GBS). *PLoS ONE* 10:e0122025. doi: 10.1371/journal.pone.0122025

Yokosawa, R., Kuninaga, S., and Sekizaki, H. (1986). *Aphanomyces euteiches* zoospore Attractant isolated from pea root; prunetin. *Ann. Phytopath. Soc. Jpn.* 52, 809–816. doi: 10.3186/jjphytopath.52.809

Conflict of Interest Statement: The authors declare that the research was conducted in the absence of any commercial or financial relationships that could be construed as a potential conflict of interest.

frontiers in Plant Science

ORIGINAL RESEARCH
published: 14 August 2018
doi: 10.3389/fpls.2018.01189

Phenolic Profile and Susceptibility to *Fusarium* Infection of Pigmented Maize Cultivars

Jamila Bernardi[1], Lorenzo Stagnati[1], Luigi Lucini[2,3], Gabriele Rocchetti[4], Alessandra Lanubile[1], Carolina Cortellini[5], Giovanni De Poli[5], Matteo Busconi[1,3] and Adriano Marocco[1,3]**

[1] Department of Sustainable Crop Production, Università Cattolica del Sacro Cuore, Piacenza, Italy, [2] Department for Sustainable Food Process, Università Cattolica del Sacro Cuore, Piacenza, Italy, [3] Research Centre for Biodiversity and Ancient DNA, Università Cattolica del Sacro Cuore, Piacenza, Italy, [4] Department of Animal Science, Food and Nutrition, Università Cattolica del Sacro Cuore, Piacenza, Italy, [5] Terra Srl, Cremona, Italy

OPEN ACCESS

Edited by:
Andreia Figueiredo, Universidade de Lisboa, Portugal

Reviewed by:
Paula Branquinho Andrade, Universidade do Porto, Portugal
Wieslaw Wiczkowski, Institute of Animal Reproduction and Food Research (PAN), Poland
Andrei Mocan, Iuliu Haţieganu University of Medicine and Pharmacy, Romania

***Correspondence:**
Luigi Lucini
luigi.lucini@unicatt.it
Adriano Marocco
adriano.marocco@unicatt.it

Specialty section:
This article was submitted to Plant Metabolism and Chemodiversity, a section of the journal Frontiers in Plant Science

Received: *19 February 2018*
Accepted: *25 July 2018*
Published: *14 August 2018*

Citation:
Bernardi J, Stagnati L, Lucini L, Rocchetti G, Lanubile A, Cortellini C, De Poli G, Busconi M and Marocco A (2018) Phenolic Profile and Susceptibility to Fusarium Infection of Pigmented Maize Cultivars. Front. Plant Sci. 9:1189. doi: 10.3389/fpls.2018.01189

Maize is a staple food source in the world, whose ancient varieties or landraces are receiving a growing attention. In this work, two Italian maize cultivars with pigmented kernels and one inbred line were investigated for untargeted phenolic profile, *in vitro* antioxidant capacity and resistance to *Fusarium verticillioides* infection. "Rostrato Rosso" was the richest in anthocyanins whilst phenolic acids were the second class in abundance, with comparable values detected between cultivars. Tyrosol equivalents were also the highest in "Rostrato Rosso" (822.4 mg kg^{-1}). Coherently, "Rostrato Rosso" was highly resistant to fungal penetration and diffusion. These preliminary findings might help in breeding programs, aiming to develop maize lines more resistant to infections and with improved nutraceutical value.

Keywords: flavonoids, *Fusarium*, metabolomics, anthocyanins, FER, phytoalexins

INTRODUCTION

Maize is the most cultivated cereal grain throughout the world, considering both yield and harvested area (Organization for Economic Cooperation and Development-OECD and FAO, 2015). Maize is a staple crop in the African region and South America, while in developed countries is used mainly to feed livestock as forage, silage and grain rather than as biofuel and for industrial uses. A new study by FAO and OECD estimates that global consumption of cereals will increase by 390 million tons between 2014 and 2024. The core driver of the increase will be the rising demand for animal feed, of which about 70% is maize, accounting for more than half of the total (FAO, 2014).

Endosperm is the main storage tissue in maize kernel, accumulating carbohydrates, such as starch (90–95%), and storage proteins, such as prolamins (10–12%) (Wu and Messing, 2014). Considering its nutritional value, other important components in maize kernels are: carotenoids, flavonoids and hydroxycinnamic acids. Carotenoids are the common pigments in maize, insoluble compounds that accumulate in the endosperm and confer the typical orange color. Most of the cultivated maize has yellow kernels, but some varieties possess the ability to pigment different tissues (i.e., anthers and roots), especially in response to stresses. Phenolic compounds such as flavonoids, are responsible for the red, purple, blue and black coloration of kernels and other parts of the plant. In maize seed, accumulation of pigments can occur in two tissues, namely the pericarp, the maternal-derived tissue, rather than the aleurone that is the peripheral part of

the endosperm. Anthocyanins are water-soluble flavonoids that accumulate in vacuoles of the aleurone. Other colored flavonoids in maize are the red pigments phlobaphenes, polymers of the flavan-4-ols apiforol and luteoforol that accumulate in the seed pericarp and cob glumes of maize (Sharma et al., 2012). Flavonoids, like other phenolics, have the power to protect the kernel from biotic and abiotic stresses, and have been associated with the beneficial effects of the Mediterranean diet, given their potent antiangiogenic, anti-inflammatory, and anticarcinogenic activities (Petroni and Tonelli, 2011). In rats fed with anthocyanin-rich maize, the amount of cardiac tissue that was damaged following ischemic conditions was reduced by approximately 30% compared to rats fed with anthocyanin-free maize (Toufektsian et al., 2011). Anthocyanins from purple corn also prevent weight gain and obesity in mice under high fat diet, and they can reduce severe diabetic complications (Tsuda, 2012). Phenolic compounds that accumulate in the maize endosperm and pericarp may contribute to resistance against insect damages, Fusarium ear rot (FER) and fumonisin contamination (Sharma et al., 2012; Atanasova-Penichon et al., 2016). Indeed, flavonoids could act as physical impediment against fungal attack (in particular when accumulated in the pericarp) by hardening maize kernel thus reducing the spread of mycelium in the inner parts of the seeds (Atanasova-Penichon et al., 2016). Other flavonoids are known to reduce insect attack like the flavone maysin (a *C*-glycosyl luteolin derivative) that can decrease the growth of earworm larvae in maize (Sharma et al., 2012).

In the last years, there was a growing demand of consumers in increasing the phenolic content of vegetables by rediscovering ancient cultivars that possess a natural pigmentation, because they are expected to have higher nutritional value (Falcone Ferreyra et al., 2012; Casas et al., 2014). With this regard, metabolomics has been proposed as a powerful tool to achieve a comprehensive picture of the phenolic signature in crop foods (Rocchetti et al., 2017, 2018a). Nonetheless, the actual phenolic profile is also supposed to play a range of physiological roles in plant, including protection toward both abiotic (e.g., UV radiation or oxidative stress via radical scavenging) and biotic stresses (Nakabayashi and Saito, 2015; Talhaoui et al., 2015). Extensive literature can be found on phenolics in non-pigmented maize, whereas most of the work on pigmented maize referred to blue genotypes from Mexico. However, red-purple genotypes received limited attention to date, although they have been recently reported to possess a favorable nutritional profile (Rocchetti et al., 2018b). Furthermore, previous works investigated phenolic profile of maize through targeted approaches, and therefore they might have not comprehensively screened the whole profile, including eventual conjugates and glycosylated compounds.

Therefore, the aim of this work was to study some maize genotypes featured by red-purple kernel pigmentation, according to their field performance, phenolic profile, *in vitro* antioxidant capacity and resistance to *Fusarium* infection. Assumed that phenolics alone are not the unique component in the resistance to *Fusarium* infection, it becomes relevant to test to which extent these compounds can interfere with fungal spread. On these bases, the phenolic profiles and resistance to *Fusarium* of three genotypes were compared to a non-pigmented commercial maize hybrid. In fact, these genotypes received less attention than other pigmented maize genotypes, even they might have a double attitude both in disease resistance and functional ingredients. A recent study on starch digestibility after cooking highlighted that the three genotypes "Nostrano della Val di Non" and "Rostrato Rosso," and a "Purple B73" possessed distinctive and diverse pigmentation patterns that could be linked to the modulation of starch digestibility (Rocchetti et al., 2018b). On these bases, the ultimate aim of this work was to investigate the potential exploitation of the above-mentioned cultivars in breeding programs rather than gaining information on their viability as functional foods.

MATERIALS AND METHODS

Maize Germplasm

Two pigmented cultivars "Nostrano della Val di Non" and "Rostrato Rosso", and a "Purple B73" line, were provided by ISTA, Agroalimentare Sud S.p.A. (Lodi, Italy). The yellow maize hybrid Agrister (Limagrain, Saint-Beauzire- France) and the B73 inbred line (available as our stock) were used as non-pigmented control (**Figures 1Aa–Dd**). The former non-pigmented genotype was used as reference for field evaluation, phenolic profile and antioxidant capacity investigations. However, the latter was a fungicide-free inbred line to be used as control for both *in vitro* and field infection assays.

Field Evaluation

The maize genotypes were sown on April 2015 in randomized blocks, with four replicates per genotype, including the commercial hybrid Agrister, in the experimental field located in San Damiano (PC), Italy (44°54′10.7′′N, 9°41′25.6′′E). Plots consisted of six rows 5 m long and spaced 0.75 m apart, planting 25 seeds per row. Each plot was spaced apart by four rows of the commercial hybrid Agrister and by a 5 m block of hybrid on the edge. Standard agricultural practices were followed. Phenotypic evaluation was performed according to the UPOV characters (ASFIS, 1992). Ears were harvested at maturity, kernels were sampled and kept at −20°C for further analyses on phenolic profile and antioxidant capacity.

A further experiment was carried out on April 2017, using the same genotypes, to investigate resistance to *Fusarium*. The field trials were located at CERZOO "Centro Di Ricerche Per La Zootecnia E L′Ambiente S.C.R.L." facilities (San Bonico 45.003624N, 9.705179E, Piacenza, Italy). Plot scheme and agricultural practices were the same as for previous trials. The "Rostrato Rosso" and "Nostrano della Val di Non" plants derived from a second-cycle of selfing.

Resistance to Artificial Infection

In the field trial, plants were hand self-pollinated and at 15 days after pollination ears were artificially inoculated with a spore suspension of *F. verticillioides* ITEM10027 (MPVP 294, 1×10^6 spores per mL) according to the pin-bar method (Maschietto et al., 2017). Ears were harvested at maturity and phenotypically

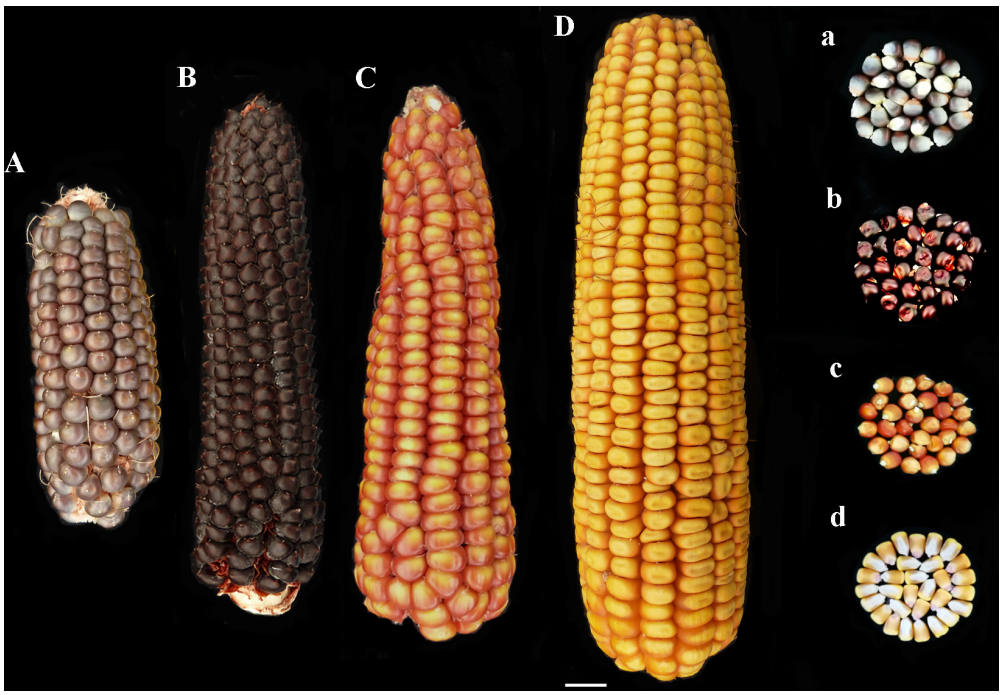

FIGURE 1 | Phenotype of ears and kernels of "Purple B73" **(Aa)**, "Rostrato Rosso" **(Bb)**, "Nostrano della Val di Non" **(Cc)**, and control **(Dd)**.

evaluated for FER severity using a seven-point scale (Maschietto et al., 2017). Ears not inoculated were harvested at maturity and kernels used for the further investigation through *in vitro* infection, according to the rolled towel assay (RTA) (Lanubile et al., 2015). With this aim, seeds with similar size and shape, preferably flattened and without visible damage, were selected from each maize genotype. To minimize at most the presence of contaminating fungi, the seeds were surface-sterilized by shaking them in 50-mL tubes at room temperature with 70% ethanol for 5 min, washed by sterilized bi-distilled water for 1 min, then with commercial bleach solution for 10 min, and finally rinsed three times with sterile distilled water for 5 min each time (Lanubile et al., 2015). Two towels of germination paper (Anchor Paper, Saint Paul, MN, United States) were moistened with sterilized distilled water. For each genotype, 20 seeds were placed on the germination paper about 10 cm from the top of the towel with the embryo side facing out. Kernels were inoculated on the embryo side near the pedicel with 100 μL of a 1×10^6 spores per ml suspension of *F. verticillioides* ITEM10027 (MPVP 294) and covered with another moistened towel. Towels were rolled up and arranged vertically in a 25-L bucket covered with a black plastic bag and kept for 7 days at 25°C in the dark. For each genotype, a control RTA was prepared as previously described, but avoiding the inoculation step.

Seedlings were rated using a five-point severity scale adapted from previous research on soybean seedlings (Lanubile et al., 2015). According to this scale, the scores were as follows: 1 = healthy, germinated seedlings with no visible signs of colonization; 2 = germination and colonization of the kernel near the pedicel; 3 = germination with widespread colonization of the kernel and browning of the coleoptile; 4 = germination with reduced seedling development, complete colonization of the kernel, and lesions and abundant mold on the shoot, 5 = no germination due to complete rotting of the kernel. Severity after inoculation (SEV_I) and in the control assays (SEV_C) were recorded for each genotype.

Extraction of Phenolic Compounds

The maize samples were randomly collected from four ears within each plot of the same genotype, obtaining six replicates. Kernels were grinded in a laboratory mill equipped with a 1-mm screen. Thereafter, 10 ml of a hydro-alcoholic solution (80% methanol, acidified with 0.1% formic acid, v/v) was used to extract phenolic compounds from 1 g of each replicate, by means of an Ultra-Turrax (25,000 rpm for 3 min). Suspensions were centrifuged 6,000 × *g*, and then 5% trichoroacetic acid (TCA) was added to the liquid phase to precipitate proteins. The solutions were stored overnight in freezer, at −18°C, filtered by means of a 0.22 μm syringe cellulose filter, and stored in dark vials at −18°C until further analyses. Six individual replicates were extracted from each genotype.

UHPLC-ESI/QTOF Screening of Phenolic Compounds

The comprehensive phenolic profile of maize samples was investigated through an untargeted metabolomic approach, using ultra-high-pressure liquid chromatography (UHPLC) in combination to a quadrupole-time-of-flight (QTOF) mass spectrometer. In more detail, the instrumentation consisted of a

1290 UHPLC coupled to a G6550 mass spectrometer (all from Agilent Technologies, Santa Clara, CA, United States) via a JetStream dual electrospray ionization source. Chromatographic and mass spectrometric instrumental conditions to screen phenolic compounds in the samples were optimized in previous works (Borgognone et al., 2016; Rocchetti et al., 2017). Briefly, a Knauer BlueOrchid C18 column (100 mm × 2 mm, 1.8 μm) was used for chromatographic separation, using a binary mixture of methanol and water as mobile phase (LCMS grade, VWR, Milan, Italy). The gradient elution was designed to increase methanol from 5 to 95% within 34 min with a flow rate of 220 μL min^{-1} and a 3.5 μL injection volume. The mass spectrometer was set up to positive SCAN mode, detecting masses in the range 100–1000 m/z. Each extract was injected once, as single instrumental replicate.

The software Profinder B.07 (from Agilent Technologies) was used to elaborate raw data, and polyphenols annotation was carried out using the database Phenol-Explorer 3.6 (Rothwell et al., 2013), considering the whole isotopic pattern. The "find-by-formula" algorithm, that includes monoisotopic mass, isotopes spacing and ratio, was used for annotation (mass accuracy tolerance < 5 ppm). Thereafter, mass and retention time alignment and filter-by-frequency (features not present in at least one treatment in 100% of replications were discarded) were applied.

In order to provide quantitative information, phenolic compounds were firstly ascribed into classes and sub-classes, and then cumulative intensity for each phenolic sub-class were converted in mg kg^{-1} equivalents, by means of calibration curves from nine polyphenol standards (from Extrasynthese, Lyon, France). Furofuran lignans were quantified as sesamin, dibenzylbutyrolactone lignans as matairesinol, phenolic acids as ferulic acid, anthocyanins as cyanidin, tyrosols and low-molecular-weight phenolics as tyrosol, alkylresorcinols as 5-pentadecylresorcinol (also known as cardol), stilbenes as resveratrol, flavanols and flavonols as catechin, and flavones as luteolin equivalents. Calibration curves were built using a linear fitting (un-weighted and not forced to axis-origin) in the range 0.05–500 mg L^{-1}; a coefficient of determination $R^2 > 0.97$ was used as acceptability threshold for calibration purposes.

In vitro Antioxidant Capacity Assays

Antioxidant capacity assays were carried out on the same extracts used for phenolic profiling. The *in vitro* antioxidant capacity of each maize sample was evaluated as radical scavenging ability (DPPH assay) and ferric reducing power (FRAP assay), as previously described (Ghisoni et al., 2017). Briefly, 1.5 mL of maize extract was combined to the same volume of an ethanol solution of DPPH (1.0 mM). The absorbance was recorded at 5-min intervals (until the steady state) to 517 nm using a Perkin Elmer Lambda 12 spectrophotometer (Ontario, Canada). The results were finally expressed as gallic acid equivalents (GAE).

The FRAP antioxidant assay was carried out by means of a clinical analyzer ILAB 600 (Instrumentation Laboratory, Lexington, MA, United States). The FRAP working reagent consist of acetate buffer (300 mM, pH 3.6), TPTZ (10 mM) in 40 mM HCl and FeCl3 (20 mM), in the ratio 10:1:1 (v/v). Each extract (100 μL) was combined to 3 ml of FRAP working reagent, and the absorbance was recorded at λ = 600 nm, after 243 s of incubation at 37°C. The FRAP results were expressed as GAE.

Statistical Analysis

The analysis of variance for the agronomic traits and the statistical analysis of artificially infected samples was performed using the R software. Phenotypic values collected in the RTA experiment were square-root transformed and mean values of severity were calculated. FER phenotypes, scored as percentages, were arccosine transformed before performing statistical analysis. The Kruskal–Wallis one-way analysis of variance and the Kruskal–Dunn *post hoc* test, available in the R package PMCMR (Pohlert, 2014) were applied to detect significant differences between maize accessions tested in the RTA experiment; the Welch one-way ANOVA and the Games–Howell *post hoc* test, available in the R packages one waytes (Dag et al., 2017) and user friendly science (Peters, 2017) were applied for FER field evaluation.

Analysis of variance for *in vitro* antioxidant capacity (one-way ANOVA, $P < 0.05$) and correlations between antioxidant capacity and concentration of different phenolic classes (Pearson, two-tails) were carried out in IBM SPSS statistics 24.

Metabolomics data were elaborated by means of Agilent Mass Profiler Professional B.12.06 software, as previously described (Rocchetti et al., 2017). Abundance of phenolic compounds was normalized at the 75th percentile and corrected for the corresponding median in all samples. Volcano plots, carried out combining ANOVA ($p < 0.01$, Bonferroni multiple testing correction) and fold-change (FC) analysis (cut-off = 5), and Venn diagrams were also generated. The not-supervised statistical approach Hierarchical Cluster Analysis was then carried out as previously described (Rocchetti et al., 2017). Finally, the raw data were elaborated into SIMCA 13 (Umetrics, Malmo, Sweden) for the supervised statistical approach orthogonal projection to latent structures discriminant analysis (OPLS-DA). A confidence limit of 95 and 99% was used to investigate the presence of outliers in the model (according to Hotelling's T2 approach), while cross validation (CV-ANOVA, $p < 0.01$) together with a permutation test ($N = 100$) to exclude overfitting, were then carried out. The goodness-of-fit and prediction ability of the model (i.e., R^2Y and Q^2Y, respectively) were also investigated, adopting cut-off values provided in literature (Rombouts et al., 2017). Finally, the VIP analysis was carried out to investigate the variable's importance in projection, i.e., considering those phenolic metabolites with the highest discrimination potential (VIP score > 1.2).

RESULTS

Phenotyping of Pigmented Maize Genotypes

Three colored genotypes ("Nostrano della Val di Non," "Rostrato Rosso" and "Purple B73") and a yellow hybrid used as reference ("Agrister"), were characterized both for vegetative and reproductive traits. Agronomic measurements of the main traits

are summarized in **Table 1** whereas all the parameters are listed in **Table 2**.

"Purple B73"

"Purple B73" is a medium-short inbred line; given this, plants are phenotypically uniform, with a very strong purple pigmentation of the stalk, leaves, glumes, bracts and tassel while silks and anthers are white (**Table 2**). Ears are classified as short of 15–18 cm with violet – deep-gray kernels arranged in 16 rows (**Figure 1Aa**). This inbred line reached silking at 804 GDD and physiological maturity at 1327 GDD (**Table 2**). The purple corn is resistant to stalk lodging and the percentage of barren plants was around 30%.

"Rostrato Rosso"

The "Rostrato Rosso" plants are medium-high tall with a short cycle, silking was at 709 GDD and physiological maturity at 1291 GDD. The variety is variable for anthocyanin pigmentation of the leaf sheath that can be deep green or with purple strikes, also the tassel attitude may vary between erect or pendulous (**Table 2**). Ears are morphologically uniform with flint violet–black kernels with a pronounced rostrum (**Figure 1Bb**). The ear is slightly conical and longer than 20 cm, kernels are arranged in 12–14 rows. Forty-one percent of plants were earless and lodging was noted for this variety. Lodging can be a consequence of the very high ratio of ear insertion related to plant height (**Table 2**).

"Nostrano della Val di Non"

The "Nostrano della Val di Non," hereafter called "Val di Non" has a low-medium height and reached mid silk 1 week before the other genotypes getting the physiological maturity at 1234 growing-degree days (GDD; **Table 2**). Neither leaves nor the stem are pigmented while silks and kernels are pigmented (**Table 2**). The kernel pigmentation can vary from deep orange to dark red (**Figure 1Cc**). Variability has been observed in the anthocyanin pigmentation of tassel glumes that could be violet, red or intermediate colors. Nonetheless the number of barren plants was quite high (62%) the production was good since this plant did not present lodging symptoms (**Table 1**).

Phenolic Profile of Pigmented and Yellow Genotypes

The phenolic profile in pigmented genotypes (i.e., "Purple B73," "Rostrato Rosso," and "Val di Non") and in non-pigmented references (i.e., "Agrister" and "B73 line") was investigated using an untargeted metabolomics approach based on UHPLC-ESI/QTOF mass spectrometry. Overall, phenolic profile was diverse, with flavonoids being the most frequently detected class detected (152 annotated compounds: 46 anthocyanins, 48 flavanols and 58 flavones), followed by phenolic acids (55 compounds), tyrosols (43 compounds), alkylphenols (14 compounds) and other phenolics (20 lignans and 6 stilbenes). All the comprehensive information regarding phenolic compounds identified across the different maize samples are provided as supporting information (**Supplementary Tables S2**, **S3**), including annotations (raw formula, identification scores) and composite spectra (masses and abundances).

The Agrister yellow maize was used as control for both phenolic profiling and related antioxidant capacity, since this former was grown together with pigmented genotypes, i.e., under the same pedoclimatic conditions. Unsupervised hierarchical cluster analysis was then produced considering the fold-change heat map, highlighting a substantial change of the phenolic profile moving from the Agrister yellow maize (control) toward the pigmented genotypes (**Figure 2**). The output of the heat map showed two main clusters; the first one was represented by the line "Purple B73," while the second cluster included "Rostrato Rosso" and "Val di Non," together with the control. However, this latter showed a distinct phenolic profile, when compared to pigmented varieties, being in a separate sub-cluster. Nevertheless, the heat map of the hierarchical cluster analysis clearly showed that the abundance of several phenolics tends to disappear moving from yellow to pigmented varieties.

Subsequently, the Venn diagrams were carried out in order to shed light on differentially and common phenolic compounds, considering pigmented varieties and Agrister yellow maize (**Figure 3**). Overall, the output of Venn diagrams showed that the three pigmented genotypes had 30 common phenolic compounds. Nevertheless, "Val di Non" possessed 8 exclusive compounds (**Supplementary Table S1**), being above all phenolic acids (coumaric acid, coumaric acid 4-*O*-glucoside, and hydroxycaffeic acid), while "Rostrato Rosso" and "Purple B73" reported 22 and 17 exclusive phenolics, respectively. Interestingly, among phenolic compounds characterizing the "Rostrato Rosso," several cyanidin-derivatives forms were detected, i.e., pelargonidin 3-*O*-glucosyl-rutinoside/sophoroside,

TABLE 1 | Main agronomic traits of the four maize genotypes.

Agronomic traits	Agrister	Val di Non	Purple B73	Rostrato Rosso
Plant height (cm)	190–200^{d}	130–170^{b}	140–150^{a}	170–180^{c}
Ear height (cm)	80–90^{c}	70–80^{a}	70–80^{a}	100–110^{b}
Number of rows per ear	18–20^{a}	10–14^{b}	16^{a}	12–14^{c}
Number of plants per plot	116.2^{c}	105.5^{b}	93.5^{a}	95.2^{a}
Number of ears per plot	111.7^{c}	43.2^{a}	63.2^{b}	54.5^{ab}
Grain weight per plot (g)	13660.6^{a}	1172.1^{b}	1032.9^{b}	1247.3^{b}
% of barren plants	1.5^{c}	62.2^{b}	30.2^{a}	40.7^{a}

Within the same column, means followed by the same letter are not significantly different at $P \leq 0.05$ according to Fisher's test.

TABLE 2 | Morphological and physiological traits of all the genotypes according to the UPOV characters.

Trait	VdN[a]	RR[b]	Purple B73	Agrister
First leaf: anthocyanin coloration of sheath	1	1	3	1
Leaf: angle between leaf and stem	1	3	1	1
Leaf: attitude of leaf	1–3	3	1	1
Stem: zig-zag attitude	1	5	2	1
Stem: anthocyanin coloration of secondary roots	5	5	3	3
Tassel: time of male flowering (days after sowing)	20–06	30–06	08–07	28–07
Tassel: time of male flowering (GDD)	535	636	775	1063
Tassel: anthocyanin coloration of ring of the glume	3–5	3	3	1
Tassel: anthocyanin coloration of the glumes	3–5	1	9	1
Tassel: anthocyanin coloration of the anthers	3	3	1	5
Tassel: density of main axis	5	3	5	5
Tassel: angle between main axis and lateral branches	1	1–7	3	1
Tassel: attitude of lateral branches	3	1–7	1	5
Tassel: number of lateral branches	7–9	7–9	3-5	5–6
Ear: silking time (days after sowing)	23–06	04–07	10–07	01–08
Ear: silking time (GDD)	535	109	804	1120
Ear: anthocyanin coloration of the silks	1	1	1	1
Leaf: anthocyanin coloration of sheat	1–3	1–3	9	1
Tassel: length of main axis above lowest side branch	5	5–7	3	7
Tassel: length of main axis above highest side branch	5	3–5	3	7
Tassel: length of lowest lateral branch	1	1–3	1	7
Plant: height (upper-leaf)	130–170	170–180	140–150	190–200
Plant: ear height (upper-ear)	70–80	100–110	70–80	80–90
Plant: height of ear relative to plant length	5	9	7	3
Leaf: width of blade	1	1	1	1
Ear: length of peduncle	3	7	3	3
Ear: length of ear	5	9	3	9
Ear: diameter of ear	3	3	3	7
Ear: shape of ear	2	2	2	2
Ear: number of rows	3	3	5	7
Ear: type of grain	2	3	2	5
Ear: color of the tip of grain	6	9	8	3
Ear: color of the dorsal side of grain	4	9	1	1
Ear: anthocyanin pigmentation of the glumes of cob	5	9	7	3
Physiological maturity (days after sowing)	10–08	15–08	18–08	15–09
Physiological maturity (GDD)	1234	1291	1327	1666
Stem: anthocyanin pigmentation of nodes	1	7	7	3
Stem: anthocyanin pigmentation of internodes	1	5	5	3

[a]*VdN, Nostrano della Val di Non;* [b]*RR, Rostrato Rosso.*

cyanidin 3,5-*O*-diglucoside and cyanidin 3-*O*-sambubioside, delphinidin 3-*O*-xyloside, and malvidin 3-*O*-(6″-acetyl-galactoside). "Purple B73" showed an abundance of flavonoids as exclusive compounds, being characterized by flavones, flavonols and anthocyanins.

Considering specific compounds, apiforol that is a precursor of phlobaphenes was up accumulated in "Val di Non" and "Rostrato Rosso" respect to both "Purple B73" and yellow maize. This evidence suggests that these two cultivars could accumulate also phlobaphenes in kernels, additionally to the other phenolics detected. Furthermore, the compound maysin was up accumulated in "Rostrato Rosso" respect to other pigmented genotypes.

Starting from these differences, the relative abundance of each phenolic subclass was investigated according to the curves from the respective phenolic standards (**Figure 4A** and **Table 3**). Remarkably, the flavonoid profile was very explicative, allowing to clearly discriminate among the four maize genotypes; "Rostrato Rosso" and "Purple B73" were the richest in anthocyanins, being 4399.4 and 3167.9 mg kg^{-1}, respectively, while "Val di Non" and the yellow maize (used as control) showed the lowest values in anthocyanin equivalents (752.5 and 205.4 mg kg^{-1}, respectively). The second phenolic class recorded in abundance was that of phenolic acids, with comparable values detected for "Purple B73" (1305.9 mg kg^{-1}), "Rostrato Rosso" (1149.7 mg kg^{-1}), and the control sample (979.6 mg kg^{-1}), while

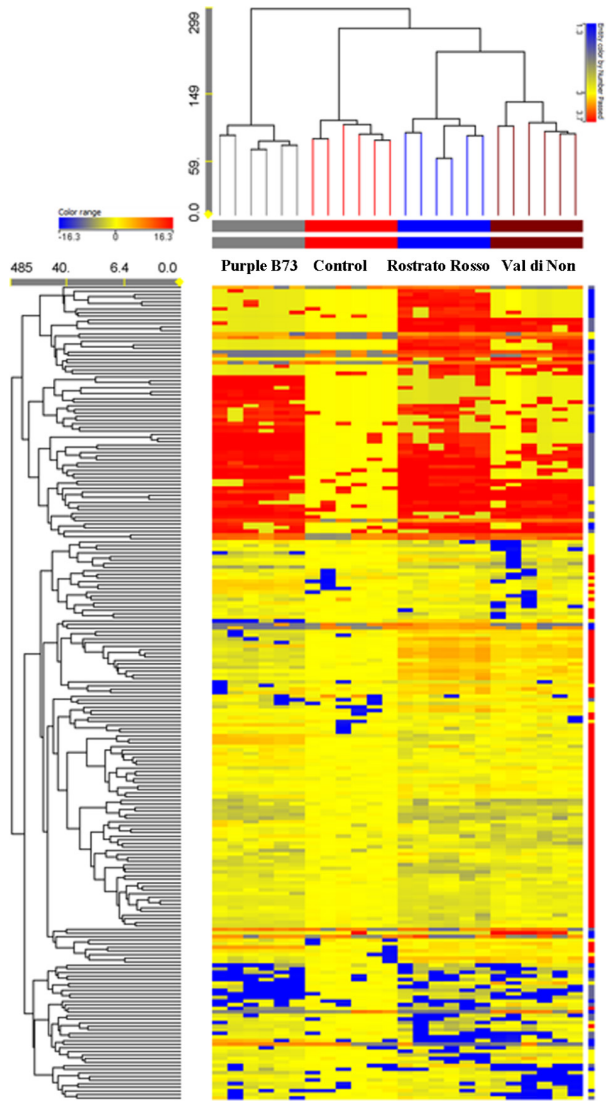

FIGURE 2 | Not averaged unsupervised hierarchical clustering on the phenolic profile of maize samples (similarity: Euclidean; linkage rule: Ward). Compounds' intensity was used to build up fold-change based heat map, on the bases of which clusters analysis was done. Agrister was used as a non-pigmented kernel control.

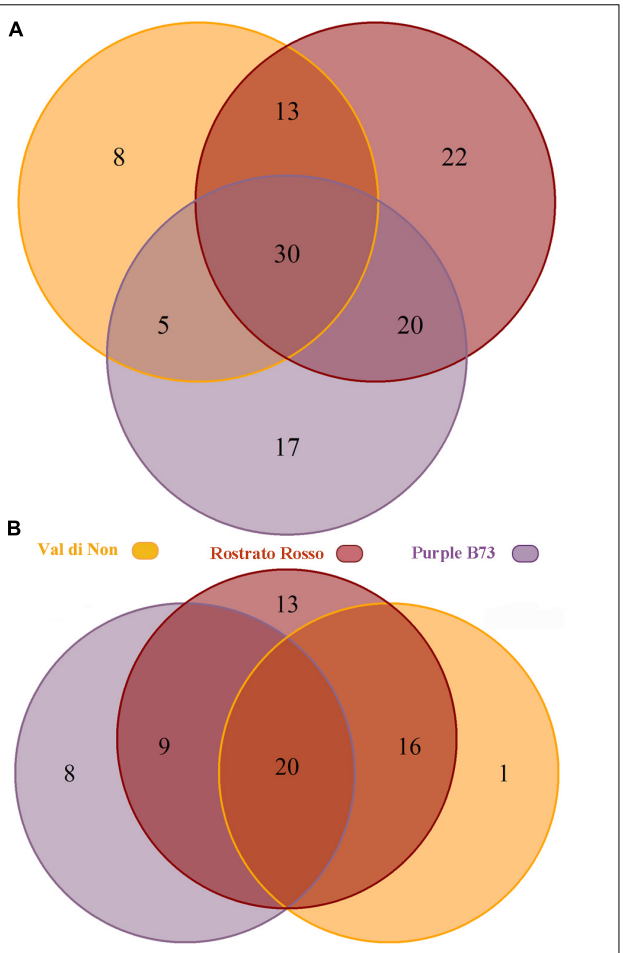

FIGURE 3 | Venn diagram of differentially accumulated compounds (Volcano plot analysis, $P < 0.01$, fold-change > 5), comparing each of the three genotypes against Agrister. The upper diagram **(A)** represents all the differential phenolic compounds, while the lower one **(B)** only the up-regulated compounds.

the lowest values were recorded in "Val di Non" (589.2 mg kg^{-1}). Furthermore, "Rostrato Rosso" showed the highest content of tyrosol equivalents (822.4 mg kg^{-1}) when compared to the other maize samples.

Subsequently, the OPLS-DA analysis was performed in order to better account for markers of the differences observed in phenolic profile. The predictive model clearly discriminated among maize cultivars (**Figure 4B**), showing that the pigmented genotypes, i.e., "Rostrato Rosso" and "Purple B73" samples possessed a completely differentiated phenolic profile when compared to the other samples, the latter clustering together onto the OPLS-DA hyperspace. The characteristics of the OPLS-DA model were excellent, with R^2Y and Q^2Y being 0.97 and 0.88, respectively. No outliers could be identified using Hotelling's T2, whereas OPLS-DA over fitting could be excluded by both CV-ANOVA (correlation p 6.2 10^{-17}) and permutation testing (**Supplementary Figure S1**). Afterwards, the variable's importance in the OPLS-DA model was evaluated using the VIP analysis and exporting the VIP scores for each phenolic compound detected through the untargeted UHPLC-ESI/QTOF-MS approach. The VIP score summarizes the contribution that a variable makes to the OPLS-DA model. The phenolic compounds with the highest recorded VIP scores (>1.2) are reported in **Table 4**; the 42 phenolic compounds detected could be considered the most important and contributing variables in class discrimination. In line with the previously reported evaluations from unsupervised multivariate statistics and Volcano analysis, the most abundant phenolics identified by the VIP analysis could be ascribed to flavonoids (i.e., anthocyanins and flavones) and phenolic acids (above all, hydroxycinnamics), thus confirming that these two phenolic

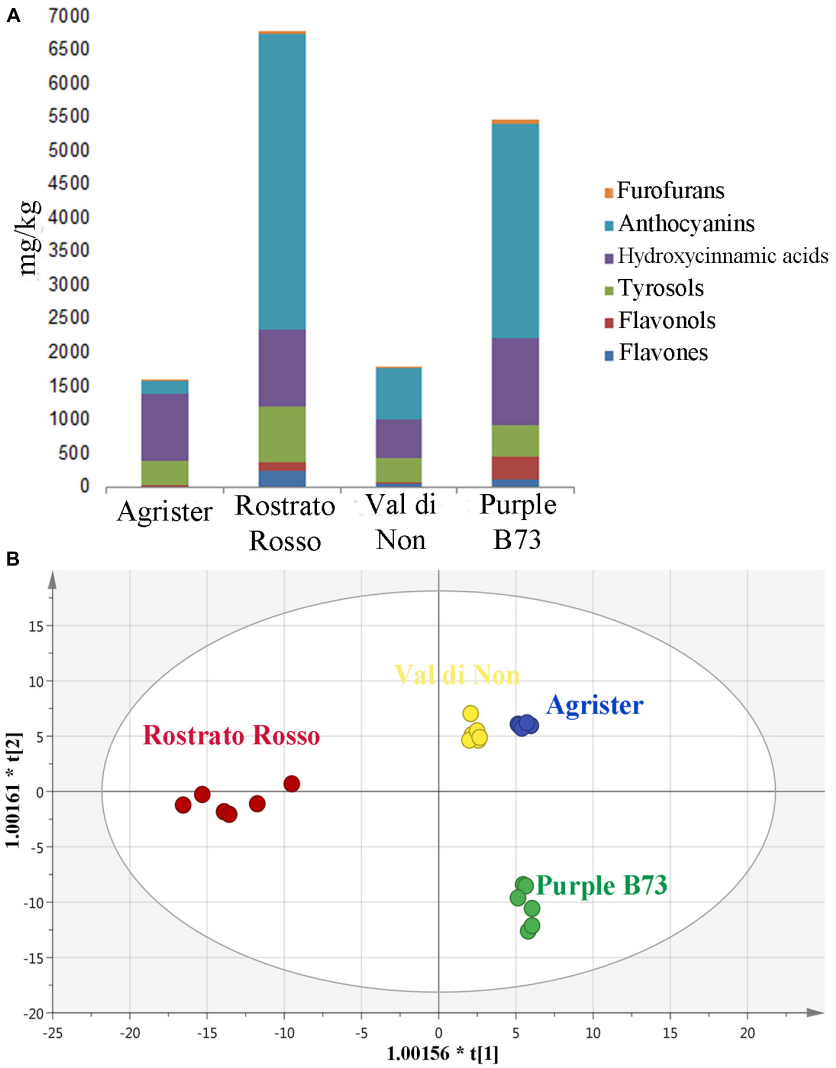

FIGURE 4 | (A) Cumulative abundance, expressed as mg kg^{-1} equivalents, of the different phenolic subclasses in the analyzed maize genotypes, as gained from UHPLC-ESI/QTOF-MS screening analysis. **(B)** Orthogonal Projections to Latent Structures Discriminant Analysis (OPLS-DA) on maize genotypes according to their phenolic profile. Individual replications are given in the class prediction model score plot.

TABLE 3 | Semi-quantitative data for the different phenolic classes, as phenolic equivalents (±standard deviation) following UHPLC/QTOF profiling in each of the four maize genotypes.

Phenolic class	Phenolic equivalents (mg kg^{-1})			
	Agrister	Rostrato Rosso	Val di Non	Purple B73
Anthocyanins	205.39 ± 36.69	4399.42 ± 1862.37	752.54 ± 399.19	3167.94 ± 526.02
Flavones	16.52 ± 3.70	242.64 ± 87.97	40.68 ± 19.96	112.85 ± 14.85
Flavonols	17.86 ± 10.80	131.65 ± 59.63	33.73 ± 15.60	342.74 ± 66.88
Tyrosols	365.35 ± 58	822.35 ± 177.51	352.60 ± 78.40	464.15 ± 63.21
Hydroxycinnamic acids	979.64 ± 282.22	1149.68 ± 272.21	589.15 ± 262.26	1305.92 ± 480.18
Furofurans	24.02 ± 6.64	40.44 ± 15.74	16.65 ± 4.41	60.14 ± 29.31
Alkylphenols	42.21 ± 24.10	33.75 ± 7.03	53.42 ± 18.78	30.36 ± 4.02
Stilbenes	5.87 ± 1.77	2.41 ± 1.79	4.05 ± 3.34	1.39 ± 0.51

TABLE 4 | Compounds better discriminating between different maize genotypes, as selected by VIP analysis following OPLS-DA.

Phenolic class	Phenolic subclass	Compound	VIP score
Flavonoids	Anthocyanins	Pelargonidin 3-*O*-(6″-malonyl-glucoside)	1.34 ± 0.14
		Cyanidin 3-*O*-(6″-malonyl-glucoside)	1.33 ± 0.15
		Peonidin 3-*O*-(6″-malonyl-glucoside)	1.32 ± 0.17
		Malvidin 3-*O*-(6″-caffeoyl-glucoside)	1.32 ± 0.19
		Cyanidin 3-*O*-galactoside	1.30 ± 0.31
		Malvidin 3-*O*-glucoside	1.28 ± 0.37
		Cyanidin	1.22 ± 0.33
		Petunidin 3,5-*O*-diglucoside	1.20 ± 0.41
	Dihydroflavonols	Dihydromyricetin 3-*O*-rhamnoside	1.30 ± 0.31
		Dihydroquercetin	1.25 ± 0.29
	Flavanones	2 Hydroxy-eriodictyol	1.20 ± 0.34
	Flavones	Luteolin 7-*O*-diglucuronide	1.33 ± 0.18
		Chrysoeriol 7-*O*-(6″-malonyl-glucoside)	1.32 ± 0.19
		Apigenin 7-*O*-diglucuronide	1.32 ± 0.23
		6-Hydroxyluteolin 7-*O*-rhamnoside	1.30 ± 0.31
		Apigenin 7-*O*-apiosyl-glucoside	1.21 ± 0.24
	Flavonols	Kaempferol 3-*O*-glucosyl-rhamnosyl-galactoside	1.58 ± 0.24
		Jaceidin 4′-*O*-glucuronide	1.34 ± 0.11
		5,4′-Dihydroxy-3,3′-dimethoxy-6:7-methylenedioxyflavone 4′-*O*-glucuronide	1.33 ± 0.16
		Kaempferol 3-*O*-(2′′-rhamnosyl-galactoside) 7-*O*-rhamnoside	1.32 ± 0.48
		Kaempferol 3,7,4′-*O*-triglucoside	1.29 ± 0.31
		Myricetin 3-*O*-rhamnoside	1.27 ± 0.19
		Kaempferol 3-*O*-xylosyl-rutinoside	1.26 ± 0.54
		Kaempferol	1.24 ± 0.34
		Quercetin 3-*O*-glucosyl-xyloside	1.22 ± 0.25
		Quercetin 3-*O*-arabinoside	1.20 ± 0.29
	Isoflavonoids	6′′-*O*-Malonylgenistin	1.34 ± 0.10
		6′′′-*O*-Acetylgenistin	1.20 ± 0.46
Phenolic acids	Hydroxycinnamics	24-Methylcholestanol ferulate	1.52 ± 0.43
		Isoferulic acid	1.34 ± 0.90
		1-Caffeoylquinic acid	1.30 ± 0.88
		3-Feruloylquinic acid	1.23 ± 0.30
		3-Sinapoylquinic acid	1.22 ± 0.59
		1,3-Dicaffeoylquinic acid	1.22 ± 0.19
	Hydroxyphenylacetics	Methoxyphenylacetic acid	1.37 ± 0.70
Others	Lignans	7-Hydroxysecoisolariciresinol	1.59 ± 0.17
		Episesaminol	1.44 ± 0.68
		Medioresinol	1.35 ± 0.23
		Episesamin	1.21 ± 0.32
	Alkylresorcinols	5-Tricosenylresorcinol	1.26 ± 0.90
		5-Nonadecenylresorcinol	1.20 ± 0.89
	Tyrosols	Hydroxytyrosol	1.35 ± 0.80

Compounds are provided together with VIP scores ± standard error (measure of variable's importance in the OPLS-DA model).

classes are the most explicative in determining the differences observed in phenolic profile.

In vitro Antioxidant Capacity of the Maize Kernels

In this work, the *in vitro* antioxidant capacity of different maize genotypes was evaluated by means of two different methods, being the DPPH radical scavenging and the FRAP reducing power, since the aforementioned methods are based on different reaction kinetics, i.e., a hydrogen atom transfer (DPPH method) and a single electron transfer (FRAP). The results for antioxidant capacity are reported in **Table 5**. Remarkably, both assays provided essentially the same information, when compared to the cumulative abundances by UHPLC-ESI/QTOF-MS for each phenolic class equivalent. DPPH values were in the range 18.8 – 150.1 mg kg^{-1} GAE, whereas FRAP values were comprised between 4364.6 and 18616.2 mg kg^{-1} GAE. The FRAP results were consistent with the semi-quantitative values, recording the highest values in "Rostrato Rosso" followed by "Purple B73," "Val di Non" and the Agrister yellow maize samples.

TABLE 5 | *In vitro* antioxidant capacity values in the selected maize genotypes, as obtained through DPPH radical scavenging and FRAP reducing power assays.

	mg kg^{-1} gallic acid equivalents	
	DPPH	**FRAP**
Agrister	19.9 ± 7[a]	4364.6 ± 242.4[a]
Val di Non	21.4 ± 4.1[a]	5567.2 ± 258.6[a]
Purple B73	18.8 ± 1.5[a]	6139.1 ± 396.6[a]
Rostrato Rosso	150.1 ± 86.8[b]	18616.2 ± 6060[b]

Within the same column, means followed by the same letter are not significantly different at P ≤ 0.05 according to Fisher's test.

Response to Artificial Infection With *F. verticillioides*

The inbred line B73 was chosen as a yellow kernel reference because of its common use in association panels to screen for FER resistance (Zila et al., 2013). Previous literature on the concentration of beneficial phytochemicals in harvested grains of yellow maize highlighted a moderate variability of phenolic profile, mainly ascribable to a year × genotype interaction (Butts-Wilmsmeyer et al., 2017). Our UHPLC-ESI/QTOF-MS phenolic profiling of the B73 non-pigmented maize, followed by quantification as phenolic sub-classes, resulted in a substantially comparable profile, as compared to the Agrister genotype used as reference for antioxidant activity (**Supplementary Tables S2**, **S3**). The modest differences we observed between the two yellow maize samples could be likely ascribed to the above-mentioned year × genotype interaction. Nonetheless, the use of a commercial hybrid such as Agrister (i.e., the genotype used as reference in phenolic profiling) would not have been suitable for *in vitro* infection assays, because these seeds were commercialized as fungicide-coated kernels. All maize genotypes in the control RTA were free from *F. verticillioides* presence, with the exception of "Purple B73" and "Val di Non" (mean value of 1.25). After artificial inoculation different responses could be observed: "Rostrato Rosso" was the less infected with SEV_I means of 2.1 while "Val di Non" and "Purple B73" were the most favorable for fungal development (3.3 and 4.2 of mean values, respectively) (**Figures 5A,B**). Analysis of variance of SEV_I phenotypic values, performed according to the Kruskal–Wallis test, resulted in a p-value = 4.196×10^{-9}. Therefore, samples were compared each other to shed light to significant variations between genotypes (Kruskal–Dunn *post hoc* test). "Purple B73" was significantly different with respect to the other pigmented and not pigmented varieties. Likewise, "Rostrato Rosso" was found to be significantly different from all other maize genotypes, while "Val di Non" response to infection was not different from that of the control. These results suggest that within colored maize cultivars different levels of resistance can be evidenced: "Rostrato Rosso" was the most resistant and "Purple B73" was the most susceptible (**Table 6** and **Figures 5A,B**).

Field Evaluation for FER Resistance

Field-grown maize genotypes were visually scored for FER severity following artificial inoculation, and variation between accessions is shown in **Figures 5C,D**. Because ears of the cultivar "Val di Non" were poorly pollinated, they were not used for *Fusarium* infection analysis in order to prevent an incorrect FER evaluation (Walker and White, 2001).

ANOVA after Welch test resulted in significant differences (p = 0.00102) and thus the Games–Howell *post hoc* test was applied to check for homogenous classes (**Table 6**). All the genotypes were significantly different each other, with the highest significance values considering comparisons to "Rostrato Rosso" (**Table 6**).

DISCUSSION

Pigmented maize genotypes were characterized by different contents in anthocyanins, and in other not pigmented phenolic compounds. Even though anthocyanins were the highest in "Rostrato Rosso" and "Purple B73," phenolic acids were the second class in abundance, having the highest content in "Rostrato Rosso," "Purple B73" and control. Tyrosols and flavones were highest in "Rostrato Rosso," whereas "Purple B73" showed the highest flavonols content. Therefore, the difference in phenolic profile among the considered genotypes was far beyond what observed at phenotype level. With this regard, an untargeted metabolomic profiling approach appears to be more appropriate in describing the actual phenolic profile from a holistic perspective. Indeed, VIP analysis from OPLS-DA multivariate statistics highlighted that compounds belonging to flavonoids such as flavones and flavonols, rather than hydroxycinnamic acids, were also responsible of differences in phenolic profile between cultivars, together with anthocyanins. Previous literature on phenolics in pigmented maize mainly focused on anthocyanins profile, highlighting as the malonyl and succinyl derivatives are the predominant one (Carmelo-Méndez et al., 2016). The results obtained confirm the importance of acylated anthocyanins, whereas total anthocyanins in our samples were in the same range of other pigmented maize (Lopez-Martinez et al., 2009) and one order higher than values reported for Mexican blue maize (Mora-Rochín et al., 2016). However, to the best of our knowledge, no comparative information has been reported regarding the phenolic content of other classes of phenolic compounds.

A confirmation on the relevance of colorless phenolics also in pigmented maize can be gained looking at Pearson's correlation values (**Table 7**) between the *in vitro* antioxidant capacity and the phenolic classes content. Tyrosols and anthocyanins were highly correlated to FRAP reducing power (0.87 and 0.86, respectively, $p < 0.01$) whereas DPPH radical scavenging capacity correlated with flavones, tyrosols and anthocyanins (0.85, 0.80, and 0.70, respectively, $p < 0.01$). A significant but weak correlation was observed between DPPH and FRAP values (0.47, $p < 0.01$); this result is not surprising, considering that the different antioxidant tests rely on different mechanisms and should be better considered as complementary rather than alternative (Przygodzka et al., 2014). Indeed, the *in vitro* antioxidant capacity should not be determined based on a single antioxidant test

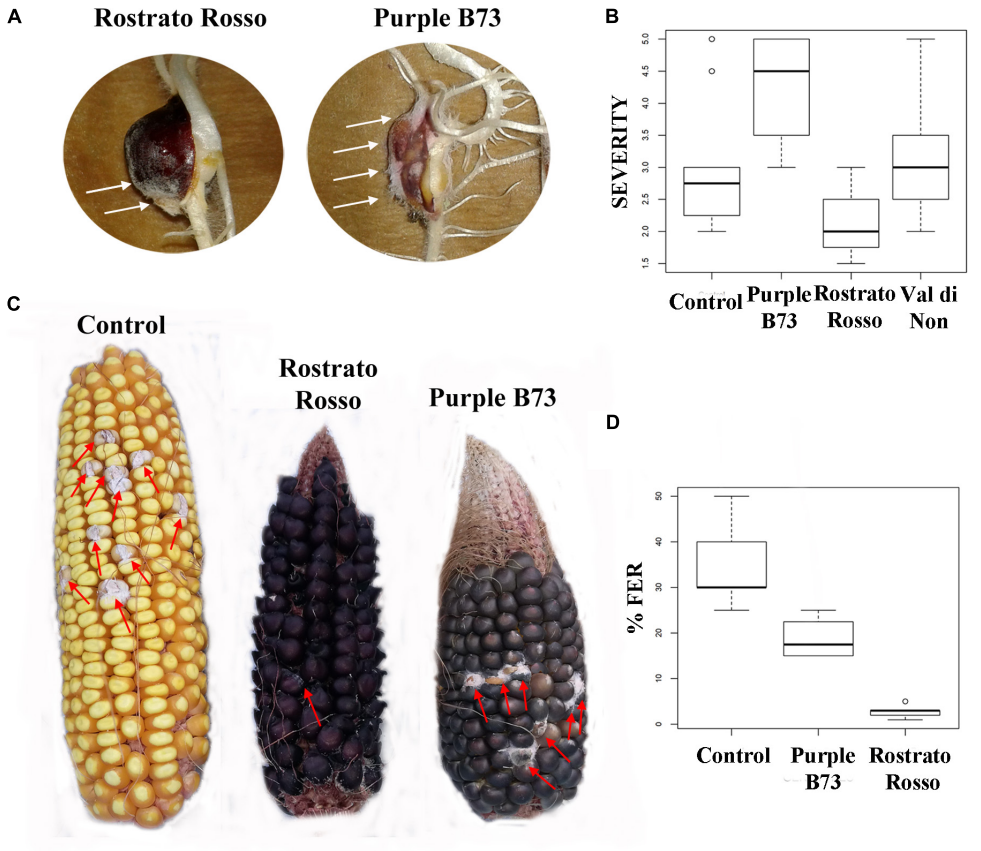

FIGURE 5 | Pictures and box-plots of maize kernels artificially inoculated with *F. verticillioides*. Examples of treated seedling after RTA assay **(A)**; the same genotypes after ear inoculation in field **(C)**. Box plots representing severity after inoculation in RTA **(B)** and percentage of FER after field inoculation **(D)**.

TABLE 6 | *P-values* after Kruskal–Dunn *post hoc* test on severity of infection phenotypic values following RTA inoculation with *F. verticillioides* (SEV_I) and *in field* inoculation (FER).

SEV_I	B73	Purple B73	Val di Non	FER	B73	Purple B73
Purple B73	0.002*	#	#	Purple B73	0.05*	#
Val di Non	0.2919	0.0483*	#	Rostrato Rosso	<0.01*	0.01*
Rostrato Rosso	0.0136*	1×10^{-9}*	0.0008*			

Significant comparisons are marked by an asterisk.

TABLE 7 | Two-tails Pearson correlation between *in vitro* antioxidant capacity assays and content of the main phenolic classes.

	FRAP	DPPH	Anthocyanins	Flavonols	Flavones	Tyrosols	Hydroxycinnamics
FRAP	–	0.47*	0.86**	n.s.	0.75**	0.87**	n.s.
DPPH	0.47*	–	0.70*	n.s.	0.85**	0.80**	n.s.
Anthocyanins	0.86**	0.70**	–	n.s.	0.96**	0.97**	0.58**
Flavonols	n.s.	n.s.	n.s.	–	n.s.	n.s.	0.79**
Flavones	0.75**	0.85**	0.96**	n.s.	–	0.97**	0.47*
Tyrosols	0.87**	0.80**	0.97**	n.s.	0.97**	–	0.48*
Hydroxycinnamics	n.s.	n.s.	0.58**	0.79**	0.47*	0.48*	–
RTA infection	−0.60**	−0.57**	−0.52*	n.s.	−0.57**	−0.61**	n.s.
Field infection	−0.64**	−0.54*	−0.80**	−0.46*	−0.73**	−0.78**	−0.79**

Significant correlations are indicated by asterisks ($p < 0.05$, **$p < 0.01$).*

model (Alam et al., 2013). Interestingly, the spread of DPPH values was much narrower than FRAP reducing power values, suggesting that DPPH assay might be less informative for the description of antioxidant capacity in the maize samples analyzed. Nonetheless, our results regarding antioxidant capacity values were consistent with previous studies. In particular, the antioxidant capacity of pigmented maize samples and by-products has been previously studied (Bello-Pérez et al., 2015), with anthocyanins giving the most important contribution to the FRAP, DPPH, and ABTS recorded values (Bello-Pérez et al., 2015; Carmelo-Méndez et al., 2017). However, most of the available studies in literature investigated the use pigmented maize varieties as potential ingredient for the development of functional foods, but focusing the attention above all on blue maize.

Moving toward the involvement of phenolic profiles in resistance toward *Fusarium* infection, interesting differences could be pointed out from both RTA and field inoculation experiments. The genotype "Rostrato Rosso" was the most resistant after *F. verticillioides* infection, both *in vitro* and in field conditions. Interestingly, this cultivar was featured by a significantly higher phenolic content. "Purple B73" presented a more severe infection following *in vitro* and field inoculation with *Fusarium*, as compared to pigmented genotypes.

With this regard, it is important to highlight that plants use a complex and interconnected defense system against pests and pathogens; the production of low molecular weight secondary metabolites having antimicrobial activity, collectively known as phytoalexins, is part of these defense mechanisms (Ahuja et al., 2012). Previous literature reported that the kernel color can be associated to *Fusarium* resistance and that the accumulation of flavonoids pigments in kernel is able to reduce the accumulation of fumonisin B1 (Pilu et al., 2011). Nonetheless, the localization of pigments in maize kernel might have a prominent role in the actual degree of resistance to *Fusarium* infection. Recently, it was reported that flavonoids can inhibit fumonisin accumulation in *Fusarium*-inoculated maize ears, even though pigmented pericarp alone was ineffective in preventing the accumulation of the mycotoxin (Venturini et al., 2016).

CONCLUSION

The different pigmented maize cultivars selected in this work appear to be interesting both in terms of phenolic profile and antioxidant capacity. Therefore, the findings support further studies in order to formulate food matrices enriched in phenolic compounds, and thus with beneficial health-promoting effects.

Given the fact that the highest resistance to *Fusarium* infection was observed in the cultivar having the highest phenolic content, further studies should be made to confirm the association between specific phenolic compounds or classes of phenolics, and fungal resistance. Undeniably, pigmented maize cultivars could be important both in finding breeding strategies in the framework of sustainable agriculture as well as in developing foods/food ingredients with higher nutraceutical value.

AUTHOR CONTRIBUTIONS

All authors contributed to revise work critically, gave the final approval of the version to be published and agreed on all aspects of the work. In particular, AM designed the study, in cooperation with JB and LL. JB, LS, and MB carried out the field experiments and the artificial infections, contributed to interpretation of data, drafted and revised the manuscript. LL and GR developed the mass spectrometric method, performed statistics, and drafted the manuscript. AL, MB, CC, and GDP drafted and critically revised the manuscript.

FUNDING

This work is a part of the Italian project "Pasta e Nuovi Prodotti Alimentari ad Alta Qualità" (PAQ) funded by the Italian Ministry of Economic Development. GR was recipient of a Ph.D. fellowship from the AgriSystem School at Università Cattolica del Sacro Cuore. The authors acknowledge Fondazione Invernizzi for the contribution to the funding of the metabolomics platform, Paola Battilani and Paola Giorni for kindly providing *F. verticillioides* strain.

SUPPLEMENTARY MATERIAL

The Supplementary Material for this article can be found online at: https://www.frontiersin.org/articles/10.3389/fpls.2018.01189/full#supplementary-material

REFERENCES

Ahuja, I., Kissen, R., and Bones, A. M. (2012). Phytoalexins in defense against pathogens. *Trends Plant Sci.* 17, 73–90. doi: 10.1016/j.tplants.2011.11.002

Alam, M. N., Bristi, N. J., and Rafiquzzaman, M. (2013). Review on *in vivo* and *in vitro* methods evaluation of antioxidant activity. *Saudi Pharm. J.* 21, 143–152. doi: 10.1016/j.jsps.2012.05.002

ASFIS (1992). *Association Pour la Formation Professionelle de l'Interprofession Semences, Description of Components and Varieties of Maize*. Paris: *ASFIS*.

Atanasova-Penichon, V., Barreau, C., and Richard-Forget, F. (2016). Antioxidant secondary metabolites in cereals: potential involvement in resistance to *Fusarium* and mycotoxin accumulation. *Front. Microbiol.* 7:566. doi: 10.3389/fmicb.2016.00566

Bello-Pérez, L. A., Carmelo-Méndez, G. A., Agama-Acevedo, E., and Utrilla-Coello, R. G. (2015). Effect of nixtamalization process on dietary fiber content, starch digestibility, and antioxidant capacity of blue maize tortilla. *Cereal Chem.* 92, 265–270. doi: 10.1094/CCHEM-06-14-0139-R

Borgognone, D., Rouphael, Y., Cardarelli, M., Lucini, L., and Colla, G. (2016). Changes in biomass, mineral composition, and quality of cardoon in response to NO3:Cl ratio and nitrate deprivation from the nutrient solution. *Front. Plant Sci.* 7:978. doi: 10.3389/fpls.2016.00978

Butts-Wilmsmeyer, C. J., Mumm, R. H., and Bohn, M. O. (2017). Concentration of beneficial phytochemicals in harvested grain of U.S. yellow dent maize (*Zea mais* L.) germoplasm. *J. Agric. Food Chem.* 65, 8311–8318. doi: 10.1021/acs.jafc.7b02034

Carmelo-Méndez, G. A., Agama-Acevedo, E., Sanchez-Rivera, M. M., and Bello-Pérez, L. A. (2016). Effect on *in vitro* starch digestibility of Mexican blue maize anthocyanins. *Food Chem.* 211, 281–284. doi: 10.1016/j.foodchem.2016.05.024

Carmelo-Méndez, G. A., Agama-Acevedo, E., Tovar, J., and Bello-Pérez, L. A. (2017). Functional study of raw and cooked blue maize flour: starch digestibility, total phenolic content and antioxidant activity. *J. Cereal Sci.* 76, 179–185. doi: 10.1016/j.jcs.2017.06.009

Casas, M., Duarte, S., Doseff, A., and Grotewold, E. (2014). Flavone-rich maize: an opportunity to improve the nutritional value of an important commodity crop. *Front. Plant Sci.* 5:440. doi: 10.3389/fpls.2014.00440

Dag, O., Dolgun, A., and Konar, N. M. (2017). *Onewaytests: One-Way Tests in Independent Groups Designs. R package version 1.5*.

Falcone Ferreyra, M. L., Rius, S. P., and Casati, P. (2012). Flavonoids: biosynthesis, biological functions, and biotechnological applications. *Front. Plant Sci.* 3:222. doi: 10.3389/fpls.2012.00222

FAO (2014). *Food and Agriculture Organization of the United Nations, Crops Production*. Available at: http://www.fao.org/faostat/en/#data/QC

Ghisoni, S., Chiodelli, G., Rocchetti, G., Kane, D., and Lucini, L. (2017). UHPLC-ESI-QTOF-MS screening of lignans and other phenolics in dry seeds for human consumption. *J. Funct. Foods* 34, 229–236. doi: 10.1016/j.jff.2017.04.037

Lanubile, A., Muppirala, U. K., Severin, A. J., Marocco, A., and Munkvold, G. P. (2015). Transcriptome profiling of soybean (*Glycine max*) roots challenged with pathogenic and non-pathogenic isolates of *Fusarium oxysporum*. *BMC Genomics* 16:1089. doi: 10.1186/s12864-015-2318-2

Lopez-Martinez, L. X., Oliart-Ros, R. M., Valerio-Alfaro, G., Lee, C. H., Parkin, K. L., and Garcia, H. S. (2009). Antioxidant activity, phenolic compounds and anthocyanins content of eighteen strains of Mexican maize. *LWT Food Sci. Technol.* 42, 1187–1192. doi: 10.1016/j.lwt.2008.10.010

Maschietto, V., Colombi, C., Pirona, R., Pea, G., Strozzi, F., Marocco, A., et al. (2017). QTL mapping and candidate genes for resistance to Fusarium ear rot and fumonisin contamination in maize. *BMC Plant Biol.* 17:20. doi: 10.1186/s12870-017-0970-1

Mora-Rochín, S., Gaxiola-Cuevas, N., Gutiérrez-Uribe, J. A., Milán-Carrillo, J., Milán-Noris, E. A., Reyes-Moreno, C., et al. (2016). Effect of traditional nixtamalization on anthocyanin content and profile in Mexican blue maize (*Zea mays* L.) landraces. *LWT Food Sci. Technol.* 68, 563–569. doi: 10.1007/s13197-014-1307-9

Nakabayashi, R., and Saito, K. (2015). Integrated metabolomics for abiotic stress responses in plants. *Curr. Opin. Plant Biol.* 24, 10–16. doi: 10.1016/j.pbi.2015.01.003

Organization for Economic Cooperation and Development-OECD and FAO (2015). OECD Publishing, Paris.

Peters, G. (2017). *Userfriendlyscience: Quantitative analysis Made Accessible*. Available at: http://userfriendlyscience.com

Petroni, K., and Tonelli, C. (2011). Recent advances on the regulation of anthocyanin synthesis in reproductive organs. *Plant Sci.* 181, 219–229. doi: 10.1016/j.plantsci.2011.05.009

Pilu, R., Cassani, E., Sirizzotti, A., Petroni, K., and Tonelli, C. (2011). Effect of flavonoid pigments on the accumulation of fumonisin B1 in the maize kernel. *J. Appl. Genet.* 52, 145–152. doi: 10.1007/s13353-010-0014-0

Pohlert, T. (2014). *PMCMR: Calculate Pairwise Multiple Comparisons of Mean Rank Sums*. Available at: https://cran.r-project.org/web/packages/PMCMR/index.html

Przygodzka, M., Zielińska, D., Ciesarová, Z., Kukurová, K., and Zieliński, H. (2014). Comparison of methods for evaluation of the antioxidant capacity and phenolic compounds in common spices. *LWT Food Sci. Technol.* 58, 321–326. doi: 10.1016/j.lwt.2013.09.019

Rocchetti, G., Chiodelli, G., Giuberti, G., Ghisoni, S., Baccolo, G., Blasi, F., et al. (2018a). UHPLC-ESI-QTOF-MS profile of polyphenols in Goji berries (*Lycium barbarum* L.) and its dynamics during *in vitro* gastrointestinal digestion and fermentation. *J. Funct. Foods* 40, 564–572. doi: 10.1016/j.jff.2017.11.042

Rocchetti, G., Giuberti, G., Gallo, A., Bernardi, J., Marocco, A., and Lucini, L. (2018b). Effect of dietary polyphenols on the *in vitro* starch digestibility of pigmented maize varieties under cooking conditions. *Food Res. Int.* 108, 183–191. doi: 10.1016/j.foodres.2018.03.049

Rocchetti, G., Chiodelli, G., Giuberti, G., Masoero, F., Trevisan, M., and Lucini, L. (2017). Evaluation of phenolic profile and antioxidant capacity in gluten-free flours. *Food Chem.* 228, 367–373. doi: 10.1016/j.foodchem.2017.01.142

Rombouts, C., Hemeryck, L. Y., Van Hecke, T., De Smet, S., De Vos, W. H., and Vanhaecke, L. (2017). Untargeted metabolomics of colonic digests reveals kynurenine pathway metabolites, dityrosine and 3-dehydroxycarnitine as red versus white meat discriminating metabolites. *Sci. Rep.* 7:42514. doi: 10.1038/srep42514

Rothwell, J. A., Pérez-Jiménez, J., Neveu, V., Medina-Ramon, A., M'Hiri, N., Garcia Lobato, P., et al. (2013). Phenol-Explorer 3.0: a major update of the Phenol-Explorer database to incorporate data on the effects of food processing on polyphenol content. *Database* 2013:bat070. doi: 10.1093/database/bat070

Sharma, M., Chai, C., Morohashi, K., Grotewold, E., Snook, M. E., and Chopra, S. (2012). Expression of flavonoid 3′-hydroxylase is controlled by P1, the regulator of 3-deoxyflavonoid biosynthesis in maize. *BMC Plant Biol.* 12:196. doi: 10.1186/1471-2229-12-196

Talhaoui, N., Taamalli, A., Gómez-Caravaca, A. M., Fernández-Gutiérrez, A., and Segura-Carretero, A. (2015). Phenolic compounds in olive leaves: analytical determination, biotic and abiotic influence, and health benefits. *Food Res. Int.* 77, 92–108. doi: 10.1016/j.foodres.2015.09.011

Toufektsian, M. C. C., Salen, P., Laporte, F., Tonelli, C., and de Lorgeril, M. (2011). Dietary flavonoids increase plasma very long-chain (n-3) fatty acids in rats. *J. Nutr.* 141, 37–41. doi: 10.3945/jn.110.127225

Tsuda, T. (2012). Dietary anthocyanin-rich plants: biochemical basis and recent progress in health benefits studies. *Mol. Nutr. Food Res.* 56, 159–170. doi: 10.1002/mnfr.201100526

Venturini, G., Babazadeh, L., Casati, P., Pilu, R., Salomoni, D., and Toffolatti, S. L. (2016). Assessing pigmented pericarp of maize kernels as possible source of resistance to Fusarium ear rot, *Fusarium* spp. infection and fumonisin accumulation. *Int. J. Food Microbiol.* 227, 56–62. doi: 10.1016/j.ijfoodmicro.2016.03.022

Walker, R. D., and White, D. G. (2001). Inheritance of resistance to Aspergillus ear rot and aflatoxin production of corn from CI2. *Plant Dis.* 85, 322–327. doi: 10.1094/PDIS.2001.85.3.322

Wu, Y., and Messing, J. (2014). Proteome balancing of the maize seed for higher nutritional value. *Front. Plant Sci.* 5:240. doi: 10.3389/fpls.2014.00240

Zila, C. T., Samayoa, L. F., Santiago, R., Butrón, A., and Holland, J. B. (2013). A genome-wide association study reveals genes associated with Fusarium ear rot resistance in a maize core diversity panel. *G3* 3, 2095–2104. doi: 10.1534/g3.113.007328

Conflict of Interest Statement: The authors declare that the research was conducted in the absence of any commercial or financial relationships that could be construed as a potential conflict of interest.

frontiers in Plant Science

ORIGINAL RESEARCH
published: 05 September 2017
doi: 10.3389/fpls.2017.01524

Identification of Biomarkers for Defense Response to *Plasmopara viticola* in a Resistant Grape Variety

*Giulia Chitarrini[1,2], Evelyn Soini[1], Samantha Riccadonna[3], Pietro Franceschi[3], Luca Zulini[4], Domenico Masuero[1], Antonella Vecchione[4], Marco Stefanini[4], Gabriele Di Gaspero[5], Fulvio Mattivi[1,6] and Urska Vrhovsek[1]**

[1] Food Quality and Nutrition Department, Fondazione Edmund Mach, San Michele all'Adige, Italy, [2] Department of Agricultural and Environmental Sciences, University of Udine, Udine, Italy, [3] Computational Biology Unit, Fondazione Edmund Mach, San Michele all'Adige, Italy, [4] Genomics and Biology of Fruit Crop Department, Fondazione Edmund Mach, San Michele all'Adige, Italy, [5] Istituto di Genomica Applicata, Udine, Italy, [6] Center Agriculture Food Environment, University of Trento, Trento, Italy

OPEN ACCESS

Edited by:
Marta Sousa Silva, Universidade de Lisboa, Portugal

Reviewed by:
Michaela Griesser, University of Natural Resources and Life Sciences, Vienna, Austria
Luigi Bavaresco, Università Cattolica del Sacro Cuore, Italy

***Correspondence:**
Urska Vrhovsek
urska.vrhovsek@fmach.it

Specialty section:
This article was submitted to Plant Metabolism and Chemodiversity, a section of the journal Frontiers in Plant Science

Received: *03 July 2017*
Accepted: *21 August 2017*
Published: *05 September 2017*

Citation:
Chitarrini G, Soini E, Riccadonna S, Franceschi P, Zulini L, Masuero D, Vecchione A, Stefanini M, Di Gaspero G, Mattivi F and Vrhovsek U (2017) Identification of Biomarkers for Defense Response to Plasmopara viticola in a Resistant Grape Variety. Front. Plant Sci. 8:1524. doi: 10.3389/fpls.2017.01524

Downy mildew (*Plasmopara viticola*) is one of the most destructive diseases of the cultivated species *Vitis vinifera*. The use of resistant varieties, originally derived from backcrosses of North American *Vitis* spp., is a promising solution to reduce disease damage in the vineyards. To shed light on the type and the timing of pathogen-triggered resistance, this work aimed at discovering biomarkers for the defense response in the resistant variety Bianca, using leaf discs after inoculation with a suspension of *P. viticola*. We investigated primary and secondary metabolism at 12, 24, 48, and 96 h post-inoculation (hpi). We used methods of identification and quantification for lipids (LC-MS/MS), phenols (LC-MS/MS), primary compounds (GC-MS), and semi-quantification for volatile compounds (GC-MS). We were able to identify and quantify or semi-quantify 176 metabolites, among which 53 were modulated in response to pathogen infection. The earliest changes occurred in primary metabolism at 24–48 hpi and involved lipid compounds, specifically unsaturated fatty acid and ceramide; amino acids, in particular proline; and some acids and sugars. At 48 hpi, we also found changes in volatile compounds and accumulation of benzaldehyde, a promoter of salicylic acid-mediated defense. Secondary metabolism was strongly induced only at later stages. The classes of compounds that increased at 96 hpi included phenylpropanoids, flavonols, stilbenes, and stilbenoids. Among stilbenoids we found an accumulation of ampelopsin H + vaticanol C, pallidol, ampelopsin D + quadrangularin A, *Z*-miyabenol C, and α-viniferin in inoculated samples. Some of these compounds are known as phytoalexins, while others are novel biomarkers for the defense response in Bianca. This work highlighted some important aspects of the host response to *P. viticola* in a commercial variety under controlled conditions, providing biomarkers for a better understanding of the mechanism of plant defense and a potential application in field studies of resistant varieties.

Keywords: biomarkers, *Plasmopara viticola*, hybrid, plant pathogen, Bianca, grapevine, resistance, metabolomics

INTRODUCTION

Downy mildew is one of the most destructive diseases of the grapevine caused by the biotrophic oomycete *Plasmopara viticola* (Berk. and Curt.) Berl. & de Toni. This pathogen was introduced from North America into Europe in the second half of the nineteenth century. The cultivated species *Vitis vinifera* is susceptible to *P. viticola*. Disease management strategies rely on the use of fungicides potentially harmful to humans and the environment (Negatu et al., 2016; Christen et al., 2017; Rortais et al., 2017). In some situations, chemical protection is also economically challenging, due to the costs of synthetic fungicides and the labor involved in spraying.

The pathogen is able to infect green tissues and establish biotrophism widely across the *Vitis* genus. Unlike the European *V. vinifera*, some accessions in North American wild species have evolved host resistance. Resistant accessions are able to activate defense responses upon pathogen infection, which culminate in localized necrosis, resulting into lower rates of sporangia release compared to susceptible accessions (Bellin et al., 2009; Polesani et al., 2010).

Resistant accessions of wild species have been crossed with cultivated varieties to introgress resistance. The use of resistant varieties is a promising strategy for viticulture to cope with downy mildew (Bisson et al., 2002). Among these, the variety Bianca is widely cultivated in Hungary, Moldova, and Russia and is one of the few resistant accessions in which the genetic basis of resistance has been elucidated (Bellin et al., 2009). Bianca is an hybrid between Bouvier and the resistant grapevine Villard Blanc. It was obtained in 1963 (Csizmazia and Bereznai, 1968), and officially registered for use in wine production in 1982 (Kozma and Dula, 2003). A large part of the resistance phenotype of Bianca is explained by the *Rpv3* locus, located in chromosome 18. In Bianca and in all known resistant descendants of the Villard Blanc the *Rpv3* locus controls the ability to trigger a localized hypersensitive response (HR) soon after the initiation of the infection (Bellin et al., 2009; Di Gaspero et al., 2012). HR in the proximity of infection sites confines biotrophic pathogens, restricting their endophytic growth (Jones and Dangl, 2006). Early inducible responses include cell wall deposition, release of reactive oxygen species and hypersensitive cell death (HR) at the infection site, controlled by interactions between avirulence gene products and plant receptors, and it can be the result of multiple signaling pathways (Heath, 2000).

Plant defense responses require energy and activation of signaling molecules, primarily supplied by primary metabolism of carbohydrates, organic acids, amines, amino acids, and lipids (Bolton, 2009; Rojas et al., 2014). HR also stimulates the expression of defense responses near the infected area and the onset of systemic acquired resistance (Greenberg and Yao, 2004). Several studies have shown the importance of secondary metabolites for expressing plant defense, often related to specific functions such as toxicity against pathogens, or acting as signal molecules after stress (Bennett and Wallsgrove, 1994; Gershenzon and Dudareva, 2007). The induction of stress-related metabolites known as phytoalexins contributed to the inhibition of biotrophic pathogens in resistant grapevines (Dercks and Creasy, 1989; Derckel et al., 1999; Slaughter et al., 2008; Godard et al., 2009; Ferri et al., 2011; Gessler et al., 2011). Stilbenes is a class of phytoalexins that provided active compounds with antifungal activity against various pathogens, including *P. viticola* (Dercks and Creasy, 1989). The pattern of stilbene accumulation upon *P. viticola* infection differs among *Vitis* species. Stilbene concentration showed earlier and higher increase in resistant varieties as compared to susceptible ones. In other cases, downy mildew resistance was observed in the absence of stilbene accumulation (Keller, 2015). This suggests the necessity to investigate which secondary metabolites play a key role in resistance and which of them are reliable biomarkers of the defense response in resistant varieties.

We expect that several classes of primary and secondary metabolites are modulated in Bianca during the defense response to *P. viticola*. In this scenario, metabolomics is the most suitable approach for monitoring a wide range of molecules. Indeed, several metabolomics studies have been already reported in grapevine. Some of them aimed at highlighting intervarietal variation in berry composition (Mulas et al., 2011; Gika et al., 2012; Degu et al., 2014; Teixeira et al., 2014; Bavaresco et al., 2016). Other studies aimed at identifying metabolite changes in infected leaves (Batovska et al., 2009; Ali et al., 2012; Becker et al., 2013; Algarra Alarcon et al., 2015). However, the metabolite changes that are brought about by the resistance mechanism have not yet been fully described.

In this work, we monitored metabolite changes in leaf discs of the resistant variety Bianca after infection with a suspension of *P. viticola*, with the aim of discovering biomarkers for specific stages of the host defense. In particular, we evaluated both primary and secondary metabolism at 12, 24, 48, and 96 h post-inoculation (hpi). We used existing protocols of LC-MS/MS for identification and quantification of lipids and phenols, and GC-MS for identification and semi-quantification of volatile organic compounds (VOCs). Moreover, we validated a new GC-MS protocol for the identification and quantification of primary compounds, including organic acids, amino acids, amines, sugars, and lipids, which yielded 48 metabolites in Bianca leaf discs.

MATERIALS AND METHODS

Plant Material

Metabolite analyses were performed using leaves from two-node cuttings of the cultivar Bianca. The mother plants were held at Fondazione Edmund Mach grape collection, San Michele all'Adige, Italy (46°12′0″N, 11°8′0″E). Own-rooted vines ($n = 45$) were grown in potted soil in controlled greenhouse conditions. Water was supplied by drip irrigation in order to avoid premature infections of downy mildew on leaves. At the stage of 12-leaf shoots, the plants were sorted into three homogenous groups; each group represented a biological replicate. At the time of the experiment plants were healthy, with no evidence of foliar diseases.

Artificial Inoculation of Leaf Discs and Incubation under Controlled Conditions

The third, fourth, and fifth fully expanded leaves beneath the apex were detached from each plant, rinsed with ultrapure water. From each leaf, 1.1 cm diameter discs were excised with a cork borer and placed randomly onto wet paper in Petri dishes with the abaxial side up. Around 100 discs per condition per time point (i.e., 12 hpi, inoculated, biological replicate 1 = 100 discs) were used. Leaf discs were left to equilibrate at 21°C for 12 h after punching and prior to inoculation. *P. viticola* spores were collected from natural infected leaves in an untreated vineyard in 2014 and immediately frozen at −20°C. They were propagated by infecting a susceptible variety and collecting fresh sporulation. After sporulation, the fresh spores were immediately used to prepare the experiment suspension. Discs were sprayed with *P. viticola* inoculum suspension at 1×10^6 sporangia/mL. Sealed Petri dishes were incubated in a growth chamber at 21°C until sampling. Mock inoculated control were prepared with ultrapure water. Leaf discs were sampled at 12, 24, 48, and 96 hpi/mock, then ground under liquid nitrogen to obtain a frozen powder. Three biological replicates were sampled at each time point.

Targeted Primary Compound Analysis and Method Validation

Sample Preparation

The extraction of primary metabolites was carried out according to Fiehn et al. (2008) with some modifications. Briefly, 0.1 g of fresh leaf powder was subjected to extraction by adding 1 mL of cool (−20°C) extraction solvent, composed of isopropanol/acetonitrile/water (3:3:2 v/v/v). A 20 μL aliquot of a solution containing palmitic-D3, nicotinic-D4, and glucose-D7 (1000 mg/L) was added as an internal standard. The extraction mixture was vortexed for 10 s, shaken at 4°C for 5 min and centrifuged at 12,000 *g* for 2 min at 5°C. A second round of extraction was carried out following the same procedure. The two supernatants were merged and re-suspended in a final volume of 5 mL using the extraction solvent. A total of 250 μL of supernatant was placed in a 1.5 mL Eppendorf tube and evaporated to dryness under N_2. The residue was re-suspended in 500 μL of acetonitrile/water (50:50 v/v), vortexed for 10 s, sonicated and centrifuged at 12,000 *g* for 2 min. The supernatant was then transferred into a 1.5 mL Eppendorf tube and dried out under N_2. The dried extract was subject to derivatization, first by adding 20 μL of methoxamine hydrochloride in pyridine (20 mg/mL) to inhibit cyclization of reducing sugars and shaken at 30°C for 1 h; then by adding 80 μL of *N*-methyl-*N*-trimethylsilyl-trifluoroacetamide with 1% trimethylchlorosilane for trimethylsilylation of acidic protons and shaken at 37°C for 30 min. Finally, 5 μL of a solution containing decane and heptadecane (1000 mg/L) were added in order to monitor the chromatographic analysis and the instrumental conditions. The derivatized extract was then transferred into vials for analysis. One microliter of derivatized extract was injected for GC/MS analysis.

Instrumental Conditions

Analyses were performed using a Trace GC Ultra combined with a mass spectrometer TSQ Quantum GC and an autosampler Triplus (Thermo Electron Corporation, Waltham, MA, United States). A RXI-5-Sil MS w/Integra-Guard®(fused silica) (30 m × 0.25 mm × 0.25 μm) column was used for compound separation. Helium was used as the carrier gas at 1.2 mL/min and the injector split ratio was set to 1:10. The injector, transfer line and source temperature were set to 250°C. The initial oven temperature was kept at 65°C for 2 min, increased by 5.2°C/min to 270°C and held at 270°C for 4 min. These conditions were shown to represent a good compromise in order to obtain a not excessively long chromatographic run, a high number of compounds and good peak separation. The mass spectrometer was operated in electron ionization mode. Data acquisition was performed in full scan mode from 50 to 700 *m/z*. Data processing was performed using XCALIBUR™ 2.2 SOFTWARE.

Method Validation

The method for primary metabolites was validated according to the currently accepted US Food and Drug Administration (FDA) bio-analytical method validation guide (US Department of Health and Human Services, 2001). Validation assays were established on calibration standards and quality control (QC) samples prepared as a pool of grape samples, extracted and derivatized according to the procedure described above. QC samples were used to evaluate the recovery of each compound and the stability of sample, intra- and inter-day variability, and to evaluate the efficiency of the extraction procedure. The standard mix was used to determine the limit of detection (LOD), limit of quantification (LOQ), and linearity range for each compound. Matrix calibration curves built using QC samples were compared with solvent calibration curves. Matrix effect (ME) values were determined using the slope ratios: ME% = 100 × (1 − slope solvent calibration curve/slope matrix calibration curve) (Kwon et al., 2012). LOQ and LOD were evaluated at the concentration in which the quantifier transition presented a signal-to-noise (S/N) ratio of >10 and >3, respectively. Intra- and inter-day variability were evaluated using the coefficient of variation (CV%) of QC samples injected 10 times on 1 day and then for 5 consecutive days. The recovery test was estimated on 10 spiked grape samples and calculated as the average of the "measured value/expected value" ratio (%). Each compound was identified and quantified against the standard, using one, or in the case of a few compounds, two specific *m/z* characteristics for the individual metabolite (extracted ion monitoring) and excluding saturated fragments. The fragments used for quantitation and the linear retention index (RI) are reported in Supplementary Table S1. Compounds were expressed as mg/kg of fresh leaves.

Targeted Lipid Compound Analysis

Lipid analysis was carried out according to Della Corte et al. (2015), using Folch's extraction method (Folch et al., 1957; Della Corte et al., 2015) with some modifications. Briefly, 0.3 mL of methanol were added to 0.1 g of fresh leaf powder and vortexed for 30 s, then 0.6 mL of chloroform containing butylated hydroxyl

toluene (500 mg/L) were added, followed by the addition of 10 μL of internal standard (docosahexaenoic acid 100 μg/mL). Samples were placed in an orbital shaker for 60 min. After the addition of 0.25 mL of water, samples were centrifuged at 3600 rpm for 10 min. The total lower lipid-rich layer was collected and re-extracted by adding 0.4 mL of chloroform/methanol/water 86:14:1 v/v/v. The samples were centrifuged at 3600 rpm for 10 min, the total lower lipid-rich layer was collected. Both chloroform fractions were merged and evaporated to dryness under N_2. Samples were re-suspended in 300 μL of acetonitrile/2-propanol/water (65:30:5 v/v/v) containing the internal standard cholesterol at a concentration of 1 μg/mL and transferred into a HPLC vial. Separation was performed using a UHPLC Dionex 3000 (Thermo Fisher Scientific, Germany), with a RP Ascentis Express column (15 cm × 2.1 mm; 2.7 μm C18) purchased from Sigma, following a 30 min multistep linear gradient following Della Corte et al. (2015). The UHPLC system was coupled with an API 5500 triple-quadrupole mass spectrometer (Applied Biosystems/MDS Sciex) equipped with an electrospray ionization (ESI) source. Compounds were identified using Analyst Software based on their true reference standard, retention time and qualifier and quantifier ion, and were quantified using their calibration curves and expressed as mg/kg of fresh leaves.

Targeted Phenolic Compound Analysis

Phenolic compounds were determined according to Vrhovsek et al. (2012), with some modifications. Briefly, 0.4 mL of chloroform and 0.6 mL of methanol:water (2:1) were added to 0.1 g of fresh leaf powder. A 20 μL aliquot of gentisic acid (50 mg/L) and rosmarinic acid (50 mg/L) were added as internal standards. The extraction mixture was shaken for 15 min in an orbital shaker, then centrifuged for 5 min at 15,000 *g* at 4°C. The upper aqueous-methanolic phase was collected. The extraction was repeated by adding 0.6 mL of methanol and water (2:1 v/v) and 0.2 mL of chloroform; the samples were centrifuged for 5 min at 15,000 *g* at 4°C. The aqueous-methanolic phase was collected and combined with the previous one. Both fractions were merged and evaporated to dryness under N_2. Samples were re-suspended in 500 μL of methanol and water (1:1 v/v), centrifuged and transferred carefully into an HPLC vial. Chromatographic analysis was performed using a Waters Acquity UPLC system (Milford) with a Waters Acquity HSS T3 column (100 mm × 2.1 mm; 1.8 μm) following Vrhovsek et al. (2012). Mass spectrometry detection was performed on a Waters Xevo triple-quadrupole mass spectrometer detector (Milford) with an electrospray ionization (ESI) source (Vrhovsek et al., 2012). Compounds were identified based on their reference standard, retention time and qualifier and quantifier ion, and were quantified using their calibration curves and expressed as mg/kg of fresh leaves. Data processing was performed using Waters MassLynx V4.1 software.

Volatile Compound Analysis

Volatile compounds were extracted with solid phase microextraction, using a method adapted from Matarese et al. (2014) and Salvagnin et al. (2016). The extraction was carried out with some modifications; briefly, 0.1 g of fresh leaves were placed in 10 mL glass vials with 2 mL of buffer (0.1 m Na_2HPO_4 and 50 mM citric acid; pH 5), 0.2 g of NaCl, and 5 μL of 1-heptanol (25 mg/L) as internal standard. Samples were kept at 60°C for 20 min and compounds in the headspace were captured for 35 min at 60°C. A Trace GC Ultra gas chromatograph coupled to a Quantum XLS mass spectrometer (Thermo Electron Corporation, Waltham, MA, United States) was used to separate the compounds with a fused silica Stabilwax®-DA column (30 m × 0.25 mm i.d. × 0.25 μm) (Restek Corporation, Bellefonte, United States). The headspace was sampled using 2-cm DVB/CAR/PDMS 50/30 μm fiber from Supelco (Bellefonte, PA, United States). The compounds were desorbed in the GC inlet at 250°C for 4 min. The GC oven parameters were set following Salvagnin et al. (2016). The MS detector was operated in scan mode (mass range 40–450 *m/z*) with a 0.2 s scan time and the transfer line to the MS system was maintained at 250°C. Data processing was performed using XCALIBUR™ 2.2 SOFTWARE. For the identification of volatile compounds we used letter "A" for compounds with comparable mass spectra and retention time to those of the pure standard, "B" for those with a RI match on a similar phase column with the database NIST MS Search 2.0, and "C" for those identified in the mass spectral database NIST MS Search 2.0 (Sumner et al., 2007). The experimental linear temperature RI of each compound was calculated using a series of *n*-alkanes (C10-C30) in the same experimental conditions as the samples. The results were expressed in a semi-quantitative manner and expressed in μg/kg using 1-heptanol as the internal standard.

Data Analysis

Statistical analysis and data visualization were performed with custom R scripts (R Core Team, 2017). Missing values were imputed with a random value between zero and LOQ. The concentrations were transformed using the base 10 logarithm, in order to make data distribution more normal-like (van den Berg et al., 2006). Principal component analysis (PCA) was performed on the obtained multidimensional dataset, after mean centering and unit scaling, using the FactoMineR and Factoextra R packages (Lê et al., 2008; Kassambara and Mundt, 2017). The *t*-statistic was computed using the Stats package (R Core Team, 2017), while network visualization exploited the ggraph package (Pedersen, 2017).

RESULTS

In leaf discs inoculated with *P. viticola* and in mock-inoculated controls, we identified 176 compounds (Supplementary Table S2) belonging to acids (18), amino acids (13), amines and others (3), sugars (14), carnitines (1), sterols (3), fatty acids (14), glycerolipids (4), glycerophospholipids (4), sphingolipids (1) prenols (1), benzoic acid derivates (4), coumarins (2), phenylpropanoids (6), dihydrochalcones (1), flavones (1), flavan-3-ols (9), flavonols (11), stilbenes and stilbenoids (14), and other phenolics (2). All these metabolites were annotated with identification level 1 (with standards) and their concentration was expressed as mg/kg of fresh leaves. The volatile acids

(3), alcohols (7), aldehydes (9), benzenoids (4), ketones (4), terpenoids (14), other VOCs (5), and unknown VOCs (5) were semi-quantified as the equivalent of the internal standard (1-heptanol) and their concentration was expressed as μg/kg of fresh leaves (Supplementary Table S2). The concentration reported represents the average value of three biological replicates ± standard error. For the identification of VOCs, we reported the confidence levels for metabolite identification defined by the Metabolomics Standards Initiative (Sumner et al., 2007): level A is assigned to compound for which the mass spectrum and the retention time match with the one of the pure standard; level B indicates that the RI of the compound and of the reference standard matches on a similar phase column; level C is assigned when the compounds mass spectrum is available into mass spectra databases (Supplementary Table S2).

Validation Results of the Primary Compound Method

Unlike for lipid, phenolic, and volatile compounds, a validated protocol for identification and quantification of primary metabolites in grapevine leaves was missing at the beginning of this study. We thus adopted a method established by Fiehn et al. (2008) on grape berries and performed a validation step to confirm the identity of each compound in a leaf matrix. All the standards were injected to obtain their fragmentation patterns and to calculate their retention indices. The calculated retention indices and mass spectra were compared with the NIST MS Search 2.0 database. The method was validated with the injection of relative standards for 96 compounds: 29 acids, 17 amino acids, 12 amines and others, 24 sugars and 14 fatty acids (Supplementary Figure S1). All the validation results are summarized in Supplementary Table S1. The ME values evaluated by comparing the calibration curves (matrix and solvent) were in the range between −20 and 20%, except for salicylic acid, citric acid, glycine, beta-alanine, tyrosine, fructose, and *myo*-inositol, which slightly exceeded the limit of ±20% established by the validation method guide; this value can be considered as insignificant, because it is close to the relative standard deviation values of repeatability (European Commission, 2011). Intra- and inter-day repeatability were evaluated for each compound and expressed as CV%. The value should not exceed 15% for intra-day and 20% for inter-day; again in this case we had very good results, except for oxalic acid (intra-day 18.2%; inter-day 26.4) and malonic acid (intra-day 15.2%; inter-day 44.6%). The recovery ranges were over 90% for 74 compounds, between 80 and 90% for 13 compounds, between 70 and 80% for four compounds, and between 50 and 70% for five compounds. Using solvent calibration curves we evaluated the linearity ranges and the LOD and LOQ limits for each compound reported in Supplementary Table S1. In general, we obtained good validation results for the method, which make us confident about the possibility of applying the method for accurate quantification of primary compounds in different matrices.

The fatty acid derivatization step can modify the profile, with the formation of oxidation or isomerization products (Rigano et al., 2016) and as previously reported, the best option is to use trimethylsilyl diazomethane, with the production of methyl esters (FAMEs), avoiding the poor separation of fatty acid compounds and substantial interference (Topolewska et al., 2015). In our method, we validated all the compounds following the derivatization used by Fiehn et al. (2008), but we found a consistent residue in blank injections of some compounds, such as palmitic acid, stearic acid, and arachidic acid in particular during the sample runs. Due to this interference, we were not able to correctly quantify fatty acid compounds in our matrix using the GC-MS method therefore their quantification was performed using LC-MS/MS.

Metabolite Changes during the Defense Response

Global metabolite changes in the resistant host upon pathogen inoculation were first visualized by using PCA (**Figure 1**). In the plot, the position of the three biological replicates and their average is reported for each time point (12, 24, 48, and 96 h) for inoculated and not inoculated leaves. PCA of all compounds revealed good separation between the factors of the study and the temporal evolution was clearly captured by the first PCA component (Dim 1), accounting for 35.8% of total variance. The second component (Dim 2), accounting for 13.4% of total variance, discriminated leaf discs undergoing a defense response to *P. viticola* from mock inoculated controls (**Figure 1**).

In order to identify which class of metabolites was responsible for this separation, we performed PCA (**Figure 2**) separately for primary metabolites (**Figure 2A**), lipids (**Figure 2B**), phenolic compounds (**Figure 2C**), and VOCs (**Figure 2D**). Again the time trend was clearly distinguishable (captured by the first component), and also a good separation between the two conditions can be noticed for specific time points for the different classes of compounds. Indeed, we observed for primary compounds a clear separation between the two conditions along the second dimension (which captured 24.1% of the total variance) at 48 hpi and, looking at the two components (explaining a total of 55.3% of the variance), possibly at 24 hpi (**Figure 2A**). Lipids showed the greatest differences at 24 hpi, where the inoculated and control samples are separated mainly along the second component, explaining 16.4% of the total variance (**Figure 2B**). Phenols were involved in the plant response only later, at 96 hpi, with the first component capturing 52.3% of the variance and possibly explaining both the time course and the differences between the two conditions (**Figure 2C**). Finally, PCA of VOCs separated inoculated and not inoculated samples at 48 hpi, and at 96 hpi, mainly along the first component, which explains 51.5% of the variance due to both the time trend and the differences between the two conditions in the last two time points (**Figure 2D**).

In order to select biomarkers for each specific stage of the defense response, we computed the *t*-statistic for all the metabolites for each time point, since it takes into account both the difference between the means and the estimate of the biological variability. To concentrate on the compounds most different between inoculated and control samples, we focused on a subset of metabolites (176) and time points (4) having an arbitrary absolute value for the *t*-statistic greater than 3 ($|t| > 3$): 64 values of the *t*-statistic satisfied our constraint.

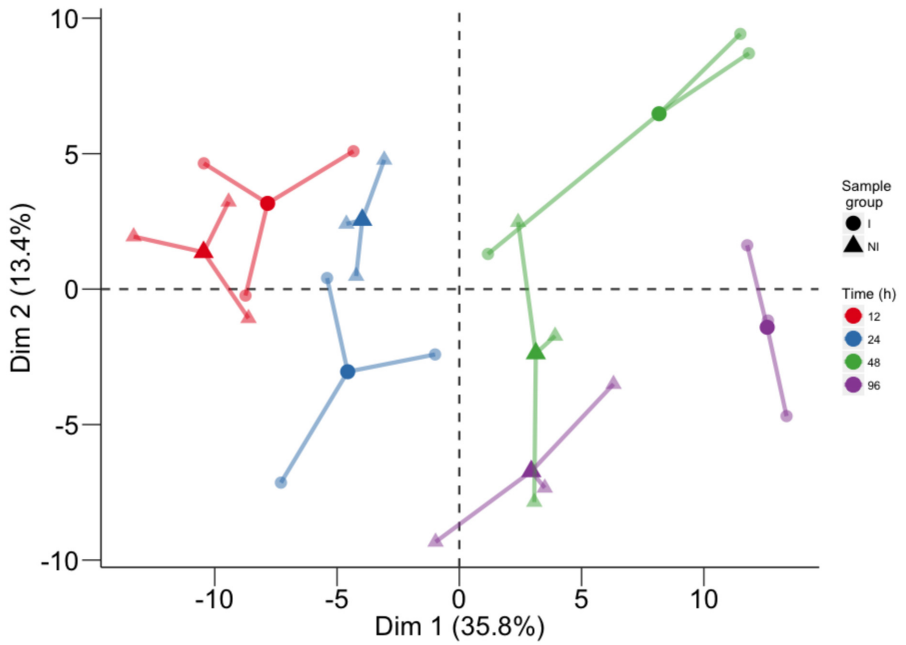

FIGURE 1 | Principal component analysis performed on the log10 of the concentration of all analyzed compounds. For each time point, three biological replicates (smaller dots) are represented for each condition (circle: inoculated samples; triangle: not inoculated) and linked with their means (larger dots). Each time point is represented with a different color: red for samples collected at 12 hpi, blue for 24 hpi samples, green for 48 hpi samples, and violet for 96 hpi samples.

In terms of compounds we identified 53 metabolites, which were different between inoculated and control samples in at least one time point (Supplementary Figure S2 and Table S3). The results of this analysis are represented in the network of **Figure 3**. The network contains 53 nodes, each one representing one metabolite. A link is drawn between two metabolites only if both metabolites have $|t| > 3$ at the same time point. In the same visualization the class of the compound is highlighted by the color of the node and the time course information by the color of the link (**Figure 3**). Time point specific cliques are characterizing the structure of the network: the metabolites shown in one of these cliques show differences between the two conditions at that specific time point. The smaller number of nodes in the network at 12 hpi indicates that metabolic changes were minimal at this time point, only involving a small group of volatile compounds, glycine, ampelopsin D + quadrangularin A, *trans*-resveratrol, kaempferol-3-*O*-rutinoside, and pallidol. Several lipids and primary metabolites were highly modulated at 24 hpi, as already shown in **Figure 2**. No lipids were highly modulated at 48 hpi, and many polyphenols were highly modulated at 96 hpi. Moreover, it is apparent that ceramide and *trans*-piceid show a central position in the network, meaning that these compounds were highly modulated at all the time points. Some interesting results are represented by metabolites connected with two different colored links; these were different at two time points, as exemplified by *trans*-resveratrol (**Figure 3**).

To further investigate this interesting subset of compounds and as further check for both the selection criterion and the visualization proposed, we explored the trends of log10 concentration over time for some key metabolites. These plots show results consistent with the network representation (Supplementary Figure S3). Ceramide concentration in inoculated leaves was already higher at 12 hpi compared with controls and reached the highest concentration at 96 hpi (0.32 mg/kg; Supplementary Table S2). *Trans*-piceid concentration was already high at 12 hpi and reached the highest concentration at 48 hpi (5.29 mg/kg) (Supplementary Table S2). Among the polyphenols, *trans*-ε-viniferin was the compound that was modulated earliest at 48 hpi, while other trimeric and tetrameric stilbenoids, such as ampelopsin H + vaticanol C, pallidol, ampelopsin D + quadrangularin A, *Z*-miyabenol C and α-viniferin for example, were modulated at 96 hpi (Supplementary Figure S3). Accumulation of *trans*-resveratrol occurred early after infection (12 hpi), and was followed by a decrease in concentration at 24 and 48 hpi, and a resumption of accumulation at 96 hpi (Supplementary Figure S3).

A considerable number of compounds belonging to each class increased in concentration over time in both inoculated and not inoculated samples (Supplementary Table S2); this would explain the high variance in the first dimension of PCA, which is associated with the time course (**Figure 1**). The progressive accumulation of stress-related compounds in leaf discs, regardless pathogen inoculation, can be explained by other stresses affecting the tissues as a consequence of leaf removal, punching of the leaf lamina, and artificial conditions of leaf disc incubation. We found accumulation of some lipid compounds, such as arachidic acid, oleanolic acid, and uvaol, in inoculated

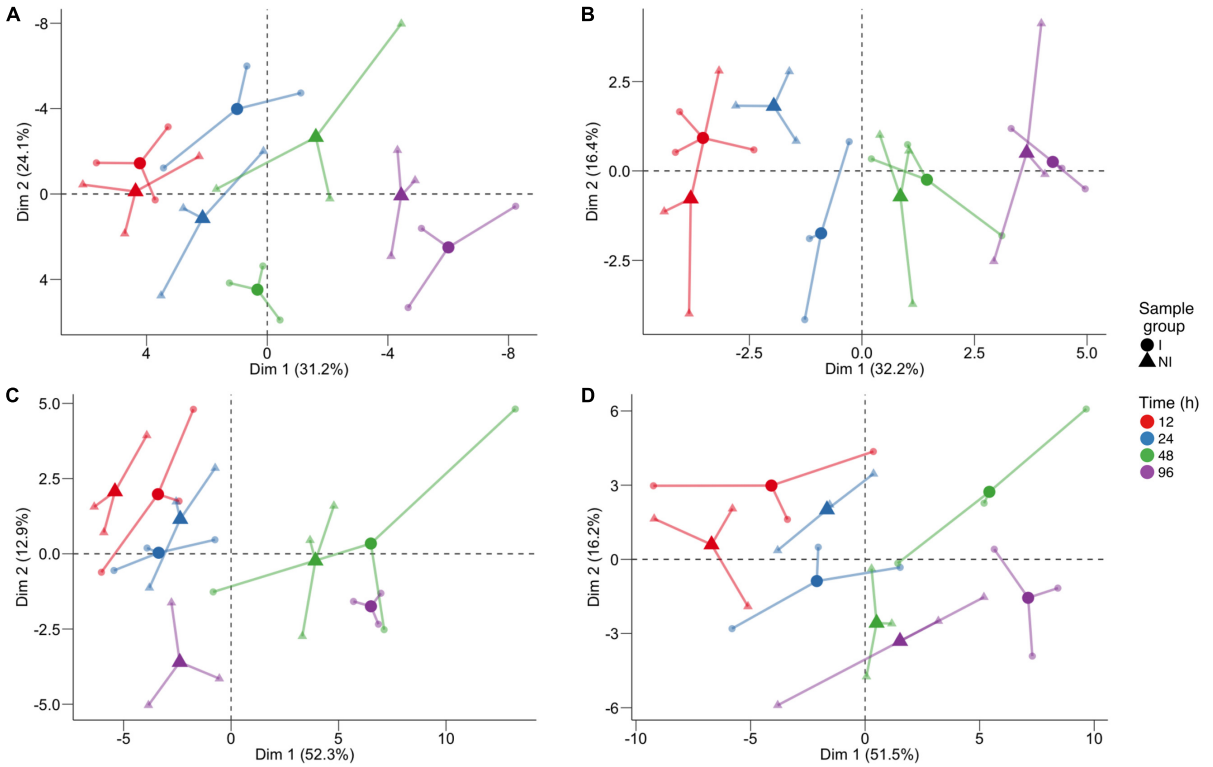

FIGURE 2 | Principal component analysis of the log10-transformed metabolite concentration of individual classes: **(A)** primary compounds, **(B)** lipids, **(C)** phenol compounds, and **(D)** volatile compounds. The analysis was performed on the log10 of the concentration. For each time point, three biological replicates (smaller dots) are represented for each condition (circle: inoculated samples; triangle: not inoculated) and are linked with their means (larger dots). Each time point is represented with a different color: red for samples collected 12 h post-infection (hpi), blue for 24 hpi samples, green for 48 hpi samples, and violet for 96 hpi samples.

and control samples (Supplementary Table S2). In polyphenols we also observed an accumulation of flavonols and some trimers and tetramers belonging to the stilbene and stilbenoid class during the first 48 h, irrespective of pathogen infection, and then differentiation at 96 hpi (Supplementary Table S2). These results are consistent with previous reports of metabolite changes caused by mechanical wounding (Chitarrini et al., 2017).

DISCUSSION

Grapevine and *P. viticola* interaction is still poorly understood in terms of metabolites: there is the need to improve the knowledge about how the plant system is perturbed after stress. In this study, a metabolomic approach has revealed major changes in primary and secondary metabolism of a resistant grape variety during the defense response to *P. viticola*. The identification of biomarkers, specific of four stages of the defense response, from 12 to 96 hpi, reflected a progression of physiological events that bring about resistance.

In addition to the importance of secondary metabolites in the fight against pathogens, the role of primary metabolism needs to be taken into account, since it is not only an energy provider but also regulates defense responses in plants in the presence of potential pathogens or pathogen-derived elicitors (Rojas et al., 2014). We expected that a defense response against an endophytic biotroph could be triggered only after the establishment of intimate contact between pathogen haustoria and host plasma membranes. In fact, we observed minimal metabolite changes in the host within 12 hpi, compatibly with a scenario in which *P. viticola* oospores/zoospores take several hours to germinate on the leaf lamina, target the stomata, form appressoria, break through the cell wall of mesophyll cells and develop functional haustoria. We identified a few biomarkers for this very early stage of host–pathogen interaction. Most of them were volatile compounds, which may interfere with the pathogen endophytic invasion of mesophyll air spaces.

The classes of biomarkers specific to 24 and 48 hpi suggested that early host responses to *P. viticola* were being set in place during those stages. We detected a sharp shift in primary metabolism. Leaf discs undergoing the defense response showed a cumulative amount of sugars, organic acids, and amino acids 6.7% higher than controls at 12 hpi, 9.4% higher at 24 hpi, 14.1% higher at 48 dpi, and 11% lower at 96 dpi. These data suggest that most of the metabolic effort for containing pathogen infection was carried out by 48 hpi and the metabolic cost for this effort was paid at 96 hpi. In leaf discs undergoing the defense response, organic acids were 13.3% higher than controls at 12 hpi and 24.6% higher at 24 hpi. Vice versa, sugars and amino acids were consistently lower at the same time points in leaf discs

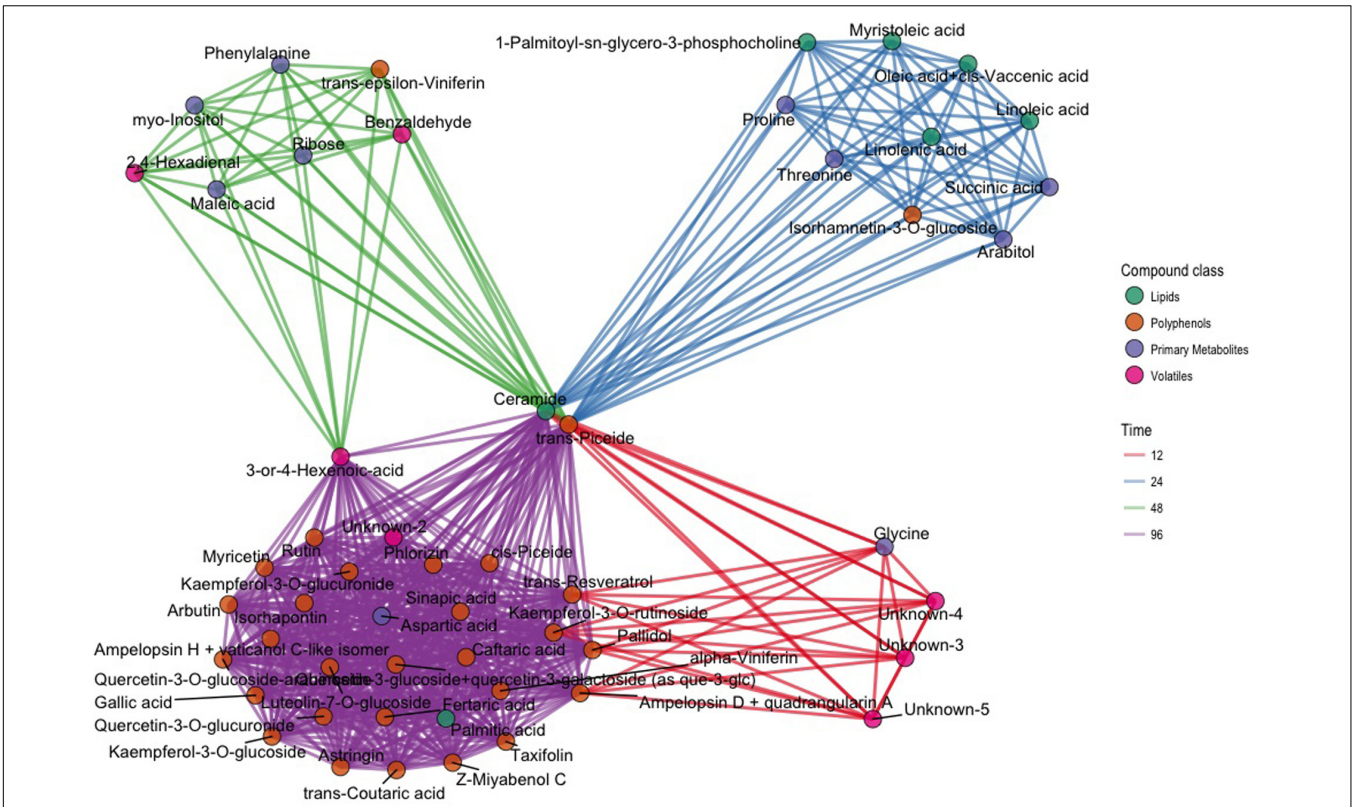

FIGURE 3 | Network plot representing the 64 most different metabolites in inoculated and not inoculated samples, corresponding to compounds having an absolute value of the *t*-statistic greater than 3 ($|t| > 3$). Each of the 64 compounds is represented with a dot; dots belonging to different classes are in different colors (green: lipids; brown: polyphenols; violet: primary compounds; pink: volatile compounds). Metabolites with differences after infection modulated at the same time point are linked using the color link of the specific time point (red: 12 hpi; blue: 24 hpi; green: 48 hpi; violet: 96 hpi).

undergoing the defense response (−2.3 and −12.1% sugars at 12 and 24 hpi, respectively; −8.9 and −19.9% amino acids at 12 and 24 hpi, respectively). At 48 hpi sugars and amino acids were 33.9 and 42.3% higher in leaf discs undergoing the defense response compared to controls. The cost of expressing defense has been shown in barley as a peak of respiration rate during the expression of host resistance to *Blumeria graminis* (Brown and Rant, 2013).

Primary metabolism is important for energy supply but it also has a role providing precursors of secondary metabolites, building blocks of PR proteins, and components of the defense signaling cascade (Rojas et al., 2014). Less et al. (2011) found different regulation of specific genes in *Arabidopsis* related to primary metabolism, due to abiotic and biotic stress response; in particular, up-regulation of genes involved in energy production processes and down-regulation of genes associated with assimilatory processes was found (Less et al., 2011). We found changes in primary compounds at 24 and 48 hpi, in particular we observed an interesting modulation for proline. In *Arabidopsis*, both supply and catabolism of proline are components of salicylic acid-mediated resistance, contributing to cell death in response to *Pseudomonas* (Deuschle et al., 2004; Cecchini et al., 2011). The role of proline in the Bianca grapevine variety after *P. viticola* infection should be elucidated with further experiments, however, for the moment we can identify this molecule as a putative biomarker.

Lipids represent a class of compounds with structural diversity and complexity. They are critical components of plant cell membranes and provide energy for metabolic activities. We found changes at 24 hpi in particular with a faster decrease in some unsaturated fatty acids after *P. viticola* infection. Ceramide started accumulating very early in infected samples compared to the control, and continued to accumulate after biotic stress up to 96 hpi; it was previously reported that ceramides can be essential as signaling molecules in the activation of defense-related plant programmed cell death (Kachroo and Kachroo, 2009; Berkey et al., 2012).

Subsequently, secondary metabolism was affected more strongly by the pathogen, with changes in the volatile compounds at 48–96 hpi and at the latest at 96 hpi in phenolic compounds. Some phenolic compounds, such as phenylpropanoids and flavonoids, have previously been identified and considered responsible for distinguishing the resistant cultivar Regent from the susceptible Trincadeira (Ali et al., 2012). We found higher concentrations of these compounds in our infected samples compared with the control at 96 hpi (Supplementary Table S2); this result suggests their involvement as biomarkers of

resistance to the pathogen in the Bianca grapevine. *Trans*-resveratrol production in grapevine leaves after pathogen infection was identified by Langcake and Pryce (1977). It has been demonstrated that *trans*-resveratrol is a precursor of fungal toxicity compounds identified as phytoalexins; these compounds can be produced by grapevine leaves after abiotic and biotic stress and can be used in the grapevine as a marker of resistance against pathogens (Jeandet et al., 2002). The accumulation of *trans*-resveratrol at 12 hpi in our infected samples can reflect the role of this molecule as a precursor of other toxic molecules, and the very early *trans*-resveratrol accumulation in Bianca is probably due to a rapid response to the pathogen. In our study we found a major increase in some molecules deriving from resveratrol, such as *trans*-ε-viniferin at 48 hpi and subsequently *trans*- and *cis*-piceid, isorhapontin, ampelopsin H + vaticanol C-like isomer, α-viniferin and pallidol at 96 hpi. During the first hpi, a low accumulation of viniferins (grapevine specific stress related metabolites) was found after pathogen infection, probably due to their accumulation at a later stage (4–7 days after inoculation), as previously described (Pezet et al., 2004; Jean-Denis et al., 2006; Slaughter et al., 2008). The time course of accumulation of these viniferins is in full agreement with several experiments reviewed by Bavaresco et al. (2012), beginning with the synthesis of resveratrol and progressing with the formation of dimers and then the higher oligomers. Such a path requires growth through the subsequent addition of one resveratrol unit to an existing dimer, leaving one part of the initial structure unchanged. The biosynthesis of dimers and higher oligomers appears to be important for resistance, in agreement with the observations of Malacarne et al. (2011) in a segregating population of Merzling × Teroldego. This paper indeed highlighted a negative correlation between the content of different oligomers and the percentage of sporulation upon infection, while this was not the case for the monomers *trans*-resveratrol and *trans*-piceid, which were also found in sensitive genotypes with high sporulation. Moreover, the importance of viniferin oligomers is further confirmed by the concentration values required to induce inhibition of mildew development recently reported by Gabaston et al. (2017).

In our study, the peak of accumulation of phenolic compounds at 96 hpi was anticipated at 48 h by the accumulation of phenylalanine in inoculated samples (**Figure 3** and Supplementary Table S2). Phenylalanine is the precursor of the phenylpropanoid pathway, leading to the synthesis of flavonoids and stilbenes by stilbenes, two classes of compounds that increased at 96 (Sparvoli et al., 1994; Flamini et al., 2013).

Among the volatile compounds, we found an increase in benzaldehyde production at 48 and 96 hpi in inoculated samples (Supplementary Figure S2) Benzaldehyde is considered as a growth suppressor and spore inhibitor, with activity against *Botrytis cinerea*, also at a low concentration (Martínez, 2012). Benzaldehyde also promotes salicylic acid accumulation, induces expression of PR proteins and increases TMV resistance in tobacco (Ribnicky et al., 1998). The higher concentration we found in infected Bianca samples at 48 and 96 hpi (around 1.5 times higher compared to the control) suggests its involvement as a putative biomarker against *P. viticola* growth or diffusion.

Based on our results, we can argue that all the compounds significantly differentiated in infected samples have a role in Bianca-*P. viticola* interaction. In particular, 53 metabolites have been identified as putative biomarkers in hybrid Bianca grapevine leaves after *P. viticola* infection. Some of them are known biomarkers of resistance (viniferins). Among the others, some are likely to be putative biomarkers of resistance in Bianca leaf discs after *P. viticola* infection, such as benzaldehyde and proline.

To the best of our knowledge, this is the first time that an extensive metabolomic study has been undertaken using a resistant grape variety to better understand metabolic perturbation after *P. viticola* infection, finding early stage biomarkers for different chemical classes of metabolites. These results can represent a starting point for better understanding grapevine resistance and can lead to discoveries regarding new mechanisms for plant–pathogen interaction between the grapevine and *P. viticola*.

We also obtained good results for method validation in relation to the identification and quantification of 97 primary compounds belonging to different chemical classes: acids, amino acids, amines, sugars, and fatty acids, using a GC-MS method for separation and identification. The method can easily be applied to further analysis for the identification and quantification of primary compounds in different matrices.

AUTHOR CONTRIBUTIONS

GC, LZ, AV, MS, GD, FM, and UV designed the experiment. GC, GD, LZ, and AV performed the experiment. GC, ES, and DM did the extractions, analytical analysis, and data treatment. GC, ES, and DM developed and validated the method. SR and PF conducted all the statistical analyses. All authors discussed the results and implications and commented on the manuscript at all stages.

FUNDING

This research was supported by the FIRST International Ph.D. program and ADP 2016 project founded by the Autonomous Province of Trento.

ACKNOWLEDGMENT

Cesare Lotti is acknowledged for his assistance in GC-MS analysis.

SUPPLEMENTARY MATERIAL

The Supplementary Material for this article can be found online at: http://journal.frontiersin.org/article/10.3389/fpls.2017.01524/full#supplementary-material

REFERENCES

Algarra Alarcon, A., Lazazzara, V., Cappellin, L., Bianchedi, P. L., Schuhmacher, R., Wohlfahrt, G., et al. (2015). Emission of volatile sesquiterpenes and monoterpenes in grapevine genotypes following *Plasmopara viticola* inoculation in vitro. *J. Mass Spectrom.* 50, 1013–1022. doi: 10.1002/jms.3615

Ali, K., Maltese, F., Figueiredo, A., Rex, M., Fortes, A. M., Zyprian, E., et al. (2012). Alterations in grapevine leaf metabolism upon inoculation with *Plasmopara viticola* in different time-points. *Plant Sci. Int. J. Exp. Plant Biol.* 19, 100–107. doi: 10.1016/j.plantsci.2012.04.014

Batovska, D. I., Todorova, I. T., Parushev, S. P., Nedelcheva, D. V., Bankova, V. S., Popov, S. S., et al. (2009). Biomarkers for the prediction of the resistance and susceptibility of grapevine leaves to downy mildew. *J. Plant Physiol.* 166, 781–785. doi: 10.1016/j.jplph.2008.08.008

Bavaresco, L., De Rosso, M., Gardiman, M., Morreale, G., and Flamini, R. (2016). Polyphenol metabolomics of twenty Italian red grape varieties. *BIO Web Conf.* 7:01022. doi: 10.1051/bioconf/20160701022

Bavaresco, L., Mattivi, F., De Rosso, M., and Flamini, R. (2012). Effects of elicitors, viticultural factors, and enological practices on resveratrol and stilbenes in grapevine and wine. *Mini Rev. Med. Chem.* 12, 1366–1381. doi: 10.2174/13895575112091366

Becker, L., Poutaraud, A., Hamm, G., Muller, J.-F., Merdinoglu, D., Carré, V., et al. (2013). Metabolic study of grapevine leaves infected by downy mildew using negative ion electrospray–Fourier transform ion cyclotron resonance mass spectrometry. *Anal. Chim. Acta* 795, 44–51. doi: 10.1016/j.aca.2013.07.068

Bellin, D., Peressotti, E., Merdinoglu, D., Wiedemann-Merdinoglu, S., Adam-Blondon, A.-F., Cipriani, G., et al. (2009). Resistance to *Plasmopara viticola* in grapevine "Bianca" is controlled by a major dominant gene causing localised necrosis at the infection site. *Theor. Appl. Genet.* 120, 163–176. doi: 10.1007/s00122-009-1167-2

Bennett, R. N., and Wallsgrove, R. M. (1994). Secondary metabolites in plant defence mechanisms. *New Phytol.* 127, 617–633. doi: 10.1111/j.1469-8137.1994.tb02968.x

Berkey, R., Bendigeri, D., and Xiao, S. (2012). Sphingolipids and Plant Defense/Disease: The "Death" connection and beyond. *Front. Plant Sci.* 3:68. doi: 10.3389/fpls.2012.00068

Bisson, L. F., Waterhouse, A. L., Ebeler, S. E., Walker, M. A., and Lapsley, J. T. (2002). The present and future of the international wine industry. *Nature* 418, 696–699. doi: 10.1038/nature01018

Bolton, M. D. (2009). Primary metabolism and plant defense—fuel for the fire. *Mol. Plant. Microbe Interact.* 22, 487–497. doi: 10.1094/MPMI-22-5-0487

Brown, J. K. M., and Rant, J. C. (2013). Fitness costs and trade-offs of disease resistance and their consequences for breeding arable crops. *Plant Pathol.* 62, 83–95. doi: 10.1111/ppa.12163

Cecchini, N. M., Monteoliva, M. I., and Alvarez, M. E. (2011). Proline dehydrogenase contributes to pathogen defense in Arabidopsis[1,[C][W][OA]]. *Plant Physiol.* 155, 1947–1959. doi: 10.1104/pp.110.167163

Chitarrini, G., Zulini, L., Masuero, D., and Vrhovsek, U. (2017). Lipid, phenol and carotenoid changes in "Bianca" grapevine leaves after mechanical wounding: a case study. *Protoplasma* doi: 10.1007/s00709-017-1100-5 [Epub ahead of print].

Christen, V., Rusconi, M., Crettaz, P., and Fent, K. (2017). Developmental neurotoxicity of different pesticides in PC-12 cells in vitro. *Toxicol. Appl. Pharmacol.* 325, 25–36. doi: 10.1016/j.taap.2017.03.027

Csizmazia, J., and Bereznai, L. (1968). A szőlő *Plasmopara viticola* és a Viteus vitifolii elleni rezisztencia nemesités eredményei. *Dans Orszől Bor Kut Int Evönyve* 191–200.

Degu, A., Hochberg, U., Sikron, N., Venturini, L., Buson, G., Ghan, R., et al. (2014). Metabolite and transcript profiling of berry skin during fruit development elucidates differential regulation between Cabernet Sauvignon and Shiraz cultivars at branching points in the polyphenol pathway. *BMC Plant Biol.* 14:188. doi: 10.1186/s12870-014-0188-4

Della Corte, A., Chitarrini, G., Di Gangi, I. M., Masuero, D., Soini, E., Mattivi, F., et al. (2015). A rapid LC–MS/MS method for quantitative profiling of fatty acids, sterols, glycerolipids, glycerophospholipids and sphingolipids in grapes. *Talanta* 140, 52–61. doi: 10.1016/j.talanta.2015.03.003

Derckel, J. P., Baillieul, F., Manteau, S., Audran, J. C., Haye, B., Lambert, B., et al. (1999). Differential induction of grapevine defenses by two strains of *Botrytis cinerea*. *Phytopathology* 89, 197–203. doi: 10.1094/PHYTO.1999.89.3.197

Dercks, W., and Creasy, L. L. (1989). The significance of stilbene phytoalexins in the *Plasmopara viticola*-grapevine interaction. *Physiol. Mol. Plant Pathol.* 34, 189–202. doi: 10.1016/0885-5765(89)90043-X

Deuschle, K., Funck, D., Forlani, G., Stransky, H., Biehl, A., Leister, D., et al. (2004). The role of [Delta]1-pyrroline-5-carboxylate dehydrogenase in proline degradation. *Plant Cell* 16, 3413–3425. doi: 10.1105/tpc.104.023622

Di Gaspero, G., Copetti, D., Coleman, C., Castellarin, S. D., Eibach, R., Kozma, P., et al. (2012). Selective sweep at the *Rpv3* locus during grapevine breeding for downy mildew resistance. *Theor. Appl. Genet.* 124, 277–286. doi: 10.1007/s00122-011-1703-8

European Commission (2011). *Method Validation and Quality Control Procedures for Pesticide Residues Analysis in Food and Feed.* Doc.SANCO/12495/2011. Brussels: European Commission.

Ferri, M., Righetti, L., and Tassoni, A. (2011). Increasing sucrose concentrations promote phenylpropanoid biosynthesis in grapevine cell cultures. *J. Plant Physiol.* 168, 189–195. doi: 10.1016/j.jplph.2010.06.027

Fiehn, O., Wohlgemuth, G., Scholz, M., Kind, T., Lee, D. Y., Lu, Y., et al. (2008). Quality control for plant metabolomics: reporting MSI-compliant studies. *Plant J. Cell Mol. Biol.* 53, 691–704. doi: 10.1111/j.1365-313X.2007.03387.x

Flamini, R., Mattivi, F., De Rosso, M., Arapitsas, P., and Bavaresco, L. (2013). Advanced knowledge of three important classes of grape phenolics: anthocyanins, stilbenes and flavonols. *Int. J. Mol. Sci.* 14, 19651–19669. doi: 10.3390/ijms141019651

Folch, J., Lees, M., and Stanley, G. H. S. (1957). A simple method for the isolation and purification of total lipides from animal tissues. *J. Biol. Chem.* 226, 497–509.

Gabaston, J., Cantos-Villar, E., Biais, B., Waffo-Teguo, P., Renouf, E., Corio-Costet, M. F., et al. (2017). Stilbenes from *Vitis vinifera* L. waste: a sustainable tool for controlling plasmopara viticola. *J. Agric. Food Chem.* 65, 2711–2718. doi: 10.1021/acs.jafc.7b00241

Gershenzon, J., and Dudareva, N. (2007). The function of terpene natural products in the natural world. *Nat. Chem. Biol.* 3, 408–414. doi: 10.1038/nchembio.2007.5

Gessler, C., Pertot, I., and Perazzolli, M. (2011). *Plasmopara viticola*: a review of knowledge on downy mildew of grapevine and effective disease management. *Phytopathol. Mediterr.* 50, 3–44. doi: 10.14601/Phytopathol_Mediterr-9360

Gika, H. G., Theodoridis, G. A., Vrhovsek, U., and Mattivi, F. (2012). Quantitative profiling of polar primary metabolites using hydrophilic interaction ultrahigh performance liquid chromatography–tandem mass spectrometry. *J. Chromatogr. A* 1259, 121–127. doi: 10.1016/j.chroma.2012.02.010

Godard, S., Slacanin, I., Viret, O., and Gindro, K. (2009). Induction of defence mechanisms in grapevine leaves by emodin- and anthraquinone-rich plant extracts and their conferred resistance to downy mildew. *Plant Physiol. Biochem.* 47, 827–837. doi: 10.1016/j.plaphy.2009.04.003

Greenberg, J. T., and Yao, N. (2004). The role and regulation of programmed cell death in plant-pathogen interactions. *Cell. Microbiol.* 6, 201–211. doi: 10.1111/j.1462-5822.2004.00361.x

Heath, M. C. (2000). "Hypersensitive response-related death," in *Programmed Cell Death in Higher Plants*, eds E. Lam, H. Fukuda, and J. Greenberg (Berlin: Springer), 77–90. doi: 10.1007/978-94-010-0934-8_6

Jean-Denis, J. B., Pezet, R., and Tabacchi, R. (2006). Rapid analysis of stilbenes and derivatives from downy mildew-infected grapevine leaves by liquid chromatography–atmospheric pressure photoionisation mass spectrometry. *J. Chromatogr. A* 1112, 263–268. doi: 10.1016/j.chroma.2006.01.060

Jeandet, P., Douillet-Breuil, A.-C., Bessis, R., Debord, S., Sbaghi, M., and Adrian, M. (2002). Phytoalexins from the Vitaceae: biosynthesis, phytoalexin gene expression in transgenic plants, antifungal activity, and metabolism. *J. Agric. Food Chem.* 50, 2731–2741. doi: 10.1021/jf011429s

Jones, J. D. G., and Dangl, J. L. (2006). The plant immune system. *Nature* 444, 323–329. doi: 10.1038/nature05286

Kachroo, A., and Kachroo, P. (2009). Fatty Acid–Derived Signals in Plant Defense. *Annu. Rev. Phytopathol.* 47, 153–176. doi: 10.1146/annurev-phyto-080508-081820

Kassambara, A., and Mundt, F. (2017). *factoextra: Extract and Visualize the Results of Multivariate Data Analyses*. R package version 1.0.3.

Keller, M. (2015). *The Science of Grapevines: Anatomy and Physiology*. Burlington, MA: Academic Press.

Kozma, P., and Dula, T. (2003). Inheritance of resistance to downy mildew and powdery mildew of hybrid family Muscadinia x V. *vinifera x V. amurensis x*

Franco-American hybrid. *Acta Hortic* 603, 457–463. doi: 10.17660/ActaHortic.2003.603.58

Kwon, H., Lehotay, S. J., and Geis-Asteggiante, L. (2012). Variability of matrix effects in liquid and gas chromatography–mass spectrometry analysis of pesticide residues after QuEChERS sample preparation of different food crops. *J. Chromatogr. A* 1270, 235–245. doi: 10.1016/j.chroma.2012.10.059

Langcake, P., and Pryce, R. J. (1977). A new class of phytoalexins from grapevines. *Experientia* 33, 151–152. doi: 10.1007/BF02124034

Lê, S., Josse, J., and Husson, F. (2008). FactoMineR: an R package for multivariate analysis. *J. Stat. Softw.* 25, 1–18. doi: 10.18637/jss.v025.i01

Less, H., Angelovici, R., Tzin, V., and Galili, G. (2011). Coordinated gene networks regulating arabidopsis plant metabolism in response to various stresses and nutritional Cues[W]. *Plant Cell* 23, 1264–1271. doi: 10.1105/tpc.110.082867

Malacarne, G., Vrhovsek, U., Zulini, L., Cestaro, A., Stefanini, M., Mattivi, F., et al. (2011). Resistance to *Plasmopara viticola* in a grapevine segregating population is associated with stilbenoid accumulation and with specific host transcriptional responses. *BMC Plant Biol.* 11:114. doi: 10.1186/1471-2229-11-114

Martínez, J. A. (2012). *Natural Fungicides Obtained from Plants*. Rijeka: InTech, doi: 10.5772/26336

Matarese, F., Cuzzola, A., Scalabrelli, G., and D'Onofrio, C. (2014). Expression of terpene synthase genes associated with the formation of volatiles in different organs of *Vitis vinifera*. *Phytochemistry* 105, 12–24. doi: 10.1016/j.phytochem.2014.06.007

Mulas, G., Galaffu, M. G., Pretti, L., Nieddu, G., Mercenaro, L., Tonelli, R., et al. (2011). NMR analysis of seven selections of vermentino grape berry: metabolites composition and development. *J. Agric. Food Chem.* 59, 793–802. doi: 10.1021/jf103285f

Negatu, B., Kromhout, H., Mekonnen, Y., and Vermeulen, R. (2016). O04-2 Occupational pesticide exposure and respiratory health of famers and farm workers: a study in three commercial farming systems in ethiopia. *Occup. Environ. Med.* 73, A7–A8. doi: 10.1136/oemed-2016-103951.19

Pedersen, T. L. (2017). *ggraph: An Implementation of Grammar of Graphics for Graphs and Networks version 1.0.0 from CRAN*. Available at: https://CRAN.R-project.org/package=ggraph [accessed June 21, 2017].

Pezet, R., Gindro, K., Viret, O., and Spring, J.-L. (2004). Glycosylation and oxidative dimerization of resveratrol are respectively associated to sensitivity and resistance of grapevine cultivars to downy mildew. *Physiol. Mol. Plant Pathol.* 65, 297–303. doi: 10.1016/j.pmpp.2005.03.002

Polesani, M., Bortesi, L., Ferrarini, A., Zamboni, A., Fasoli, M., Zadra, C., et al. (2010). General and species-specific transcriptional responses to downy mildew infection in a susceptible (*Vitis vinifera*) and a resistant (*V. riparia*) grapevine species. *BMC Genom.* 11:117. doi: 10.1186/1471-2164-11-117

R Core Team (2017). *R: A Language and Environment for Statistical Computing*. Available at: http://www.gbif.org/resource/81287 [accessed June 21, 2017].

Ribnicky, D. M., Shulaev, V., and Raskin, I. (1998). Intermediates of salicylic acid biosynthesis in tobacco. *Plant Physiol.* 118, 565–572. doi: 10.1104/pp.118.2.565

Rigano, F., Albergamo, A., Sciarrone, D., Beccaria, M., Purcaro, G., and Mondello, L. (2016). Nano liquid chromatography directly coupled to electron ionization mass spectrometry for free fatty acid elucidation in mussel. *Anal. Chem.* 88, 4021–4028. doi: 10.1021/acs.analchem.6b00328

Rojas, C. M., Senthil-Kumar, M., Tzin, V., and Mysore, K. S. (2014). Regulation of primary plant metabolism during plant-pathogen interactions and its contribution to plant defense. *Front. Plant Sci.* 5:17. doi: 10.3389/fpls.2014.00017

Rortais, A., Arnold, G., Dorne, J.-L., More, S. J., Sperandio, G., Streissl, F., et al. (2017). Risk assessment of pesticides and other stressors in bees: principles, data gaps and perspectives from the European Food Safety Authority. *Sci. Total Environ.* 58, 524–537. doi: 10.1016/j.scitotenv.2016.09.127

Salvagnin, U., Carlin, S., Angeli, S., Vrhovsek, U., Anfora, G., Malnoy, M., et al. (2016). Homologous and heterologous expression of grapevine E-(β)-caryophyllene synthase (VvGwECar2). *Phytochemistry* 131, 76–83. doi: 10.1016/j.phytochem.2016.08.002

Slaughter, A. R., Hamiduzzaman, M. M., Gindro, K., Neuhaus, J.-M., and Mauch-Mani, B. (2008). Beta-aminobutyric acid-induced resistance in grapevine against downy mildew: involvement of pterostilbene. *Eur. J. Plant Pathol.* 122, 185–195. doi: 10.1007/s10658-008-9285-2

Sparvoli, F., Martin, C., Scienza, A., Gavazzi, G., and Tonelli, C. (1994). Cloning and molecular analysis of structural genes involved in flavonoid and stilbene biosynthesis in grape (*Vitis vinifera* L.). *Plant Mol. Biol.* 24, 743–755. doi: 10.1007/BF00029856

Sumner, L. W., Amberg, A., Barrett, D., Beale, M. H., Beger, R., Daykin, C. A., et al. (2007). Proposed minimum reporting standards for chemical analysis Chemical Analysis Working Group (CAWG) Metabolomics Standards Initiative (MSI). *Metabolomics* 3, 211–221. doi: 10.1007/s11306-007-0082-2

Teixeira, A., Martins, V., Noronha, H., Eiras-Dias, J., and Gerós, H. (2014). The first insight into the metabolite profiling of grapes from three *Vitis vinifera* L. cultivars of two controlled appellation (DOC) regions. *Int. J. Mol. Sci.* 15, 4237–4254. doi: 10.3390/ijms15034237

Topolewska, A., Czarnowska, K., Haliński, Ł.P., and Stepnowski, P. (2015). Evaluation of four derivatization methods for the analysis of fatty acids from green leafy vegetables by gas chromatography. *J. Chromatogr. B* 990, 150–157. doi: 10.1016/j.jchromb.2015.03.020

US Department of Health and Human Services (2001). *Guidance for Industry, Bioanalytical Method Validation*. Rockville, MD: US Department of Health and Human Services.

van den Berg, R. A., Hoefsloot, H. C. J., Westerhuis, J. A., Smilde, A. K., and van der Werf, M. J. (2006). Centering, scaling, and transformations: improving the biological information content of metabolomics data. *BMC Genomics* 7:142. doi: 10.1186/1471-2164-7-142

Vrhovsek, U., Masuero, D., Gasperotti, M., Franceschi, P., Caputi, L., Viola, R., et al. (2012). A versatile targeted metabolomics method for the rapid quantification of multiple classes of phenolics in fruits and beverages. *J. Agric. Food Chem.* 60, 8831–8840. doi: 10.1021/jf2051569.ref

Conflict of Interest Statement: The authors declare that the research was conducted in the absence of any commercial or financial relationships that could be construed as a potential conflict of interest.

frontiers in Plant Science

ORIGINAL RESEARCH
published: 21 March 2018
doi: 10.3389/fpls.2018.00360

Identification of Lipid Markers of *Plasmopara viticola* Infection in Grapevine Using a Non-targeted Metabolomic Approach

*Lise Negrel, David Halter, Sabine Wiedemann-Merdinoglu, Camille Rustenholz, Didier Merdinoglu, Philippe Hugueney and Raymonde Baltenweck**

SVQV, Institut National de la Recherche Agronomique, Université de Strasbourg, Colmar, France

The Oomycete *Plasmopara viticola* is responsible for downy mildew, which is one of the most damaging grapevine diseases. Due to the strictly biotrophic way of life of *P. viticola,* its metabolome is relatively poorly characterized. In this work, we have used a mass spectrometry-based non-targeted metabolomic approach to identify potential *Plasmopara*-specific metabolites. This has led to the characterization and structural elucidation of compounds belonging to three families of atypical lipids, which are not detected in healthy grapevine tissues. These lipids include ceramides and derivatives of arachidonic and eicosapentaenoic acid, most of which had not been previously described in Oomycetes. Furthermore, we show that these lipids can be detected in *Plasmopara*-infected tissues at very early stages of the infection process, long before the appearance the first visible symptoms of the disease. Therefore, the potential use of these specific lipids as markers to monitor the development of *P. viticola* is discussed.

Keywords: grapevine, downy mildew, metabolomics, lipids, biomarkers

OPEN ACCESS

Edited by:
Andreia Figueiredo, Universidade de Lisboa, Portugal

Reviewed by:
Luigi Bavaresco, Università Cattolica del Sacro Cuore, Italy
Michele Perazzolli, Fondazione Edmund Mach, Italy

****Correspondence:***
Raymonde Baltenweck
raymonde.baltenweck@inra.fr

Specialty section:
This article was submitted to Plant Metabolism and Chemodiversity, a section of the journal Frontiers in Plant Science

Received: *12 November 2017*
Accepted: *05 March 2018*
Published: *21 March 2018*

Citation:
Negrel L, Halter D, Wiedemann-Merdinoglu S, Rustenholz C, Merdinoglu D, Hugueney P and Baltenweck R (2018) Identification of Lipid Markers of Plasmopara viticola Infection in Grapevine Using a Non-targeted Metabolomic Approach. Front. Plant Sci. 9:360. doi: 10.3389/fpls.2018.00360

INTRODUCTION

Plasmopara viticola is an obligate biotrophic Oomycete responsible for downy mildew, which is one of the most damaging grapevine diseases. As downy mildew outbreaks may result in significant economic losses, control of the disease is most often achieved by fungicide treatments, whose impacts on environment and health raise more and more concerns. The relationships between grapevine and *P. viticola* have therefore been subjected to thorough investigations in order to better understand the infection process and to identify potential targets for alternative control strategies (Gessler et al., 2011). Grapevine responses to downy mildew infection have been characterized in both compatible and incompatible situations, through the study of susceptible *Vitis vinifera* cultivars and resistant species such as *Vitis riparia*, *V. rupestris,* or *Muscadinia rotundifolia*. Transcriptomic analyses have shown that downy mildew infection induces a strong and rapid transcriptional reprogramming in host tissues, including the induction of pathogenesis-related proteins and enzymes required for the synthesis of phenylpropanoid-derived compounds (Kortekamp, 2006; Polesani et al., 2008, 2010; Wu et al., 2010; Gessler et al., 2011; Legay et al., 2011; Lenzi et al., 2016). Similarly, metabolomic profiling experiments have revealed profound changes in grapevine tissues upon downy mildew infection, which affect both the primary and the secondary metabolism (Figueiredo et al., 2008; Ali et al., 2009; Buonassisi et al., 2017). One of the most prominent metabolic change is the biosynthesis of large amounts of stilbene phytoalexins

in both compatible and incompatible interactions (Pezet et al., 2003; Alonso-Villaverde et al., 2011), specific patterns of stilbene accumulation being associated with increased resistance to the pathogen (Malacarne et al., 2011; Duan et al., 2015; Chitarrini et al., 2017). However, metabolomic analyses of grapevine-downy mildew interactions have mostly resulted in the characterization of metabolites from grapevine, the metabolome of *P. viticola* being paradoxically relatively poorly characterized. This is probably partly due to the strictly biotrophic way of life of *P. viticola,* which thus cannot be obtained in pure culture, making the characterization of its metabolome difficult.

In this work, we have used a high-resolution mass spectrometry-based non-targeted metabolomic approach to characterize metabolites differentially accumulated in grapevine and in *P. viticola.* The rationale behind this strategy was to look for prominent ions present in *P. viticola* and absent in grapevine healthy tissues, which may be derived from *Plasmopara*-specific molecules. This has led to the characterization and structural elucidation of compounds belonging to three families of atypical lipids, which are not detected in healthy grapevine tissues. Furthermore, we show that these lipids can be detected in *Plasmopara*-infected tissues from very early stages of the infection process. Therefore, the potential use of these specific lipids as markers to monitor the development of *P. viticola* is discussed.

MATERIALS AND METHODS

Chemicals and Standards

LC-MS grade methanol and chloroform were from Roth Sochiel (Lauterbourg, France), water was provided by a Millipore water purification system. Arachidonic acid, eicosapentaenoic acid and N-Arachidoyl-D-sphingosine Cer(d18:1/20:0) were purchased from Sigma–Aldrich (Saint-Quentin Fallavier, France). N-Hexadecanoyl-D-erythro-C16-sphingosine Cer(d16:1/16:0) was from Abcam (Paris, France). Triarachidonoyl-glycerol and trieicosapentaenoyl-glycerol were purchased from Larodan Fine Chemicals (Malmö, Sweden). AG, DAG, EPG, and DEPG were obtained from AA and EPA by $ZnCl_2$-catalyzed esterification of glycerol (Spring and Haas, 2004; Mostafa et al., 2013).

Plant Material and Downy Mildew Inoculation

The isolate SC of *P. viticola* used in this work and the leaf disc bioassay were described previously (Peressotti et al., 2010). Inoculum (sporangia) was prepared from infected leaves of *V. vinifera* cv Muscat Ottonel treated with Topsin 70 WG fungicide (50 mg/L) (Nisso Chemical, Germany), in order to avoid fungal contamination (Peressotti et al., 2010). Before inoculation leaves were surface-sterilized with bleach (2% active chlorine) for 2 min, followed by three washes with sterile water. In this work, the leaf disc bioassay was conducted with the following grapevine varieties and species: *V. vinifera* cv Cabernet-Sauvignon, cv Syrah, cv Cinsault, *V. rupestris*, *V. riparia*, and *V. rotundifolia*, using 15 leaf discs for each variety. Kinetic analysis of *Plasmopara*-specific lipids accumulation was performed on green cuttings of *V. vinifera* cv Syrah, the hybrid variety Bianca and *V. riparia*, grown in a greenhouse. The sixth leaf counted from the apex of 3.5 months old plants, were harvested, surface-sterilized, and washed with sterile water. Leaves were infected by flotation of their abaxial surface on a suspension of sporangia (10^5 sporangia mL^{-1}) for 5 h. Control leaves were floated on sterile water. Three leaves were used for each treatment. The leaves were then transferred to wet paper with the abaxial surface up and closed in transparent plastic bags. Leaves were stored in a growth chamber at 21°C, with 16 h of light per day. 0, 24, 48, 72 h, and 6 days following inoculation, discs (diameter 1.5 cm) were punched from infected and control leaves, weighed, placed in a 2 mL tube, frozen into liquid nitrogen and stored at −80°C until analysis.

Preparation of Sporangia Extracts From *P. viticola*

The abaxial faces of the leaves of 2 month-old Muscat Ottonel plants were sprayed with a suspension of sporangia (10^5 sporangia mL^{-1} in water). Mock-inoculated leaves were sprayed with sterile water. Three inoculated and three control plants were then placed separately in growth chambers at 21°C, with 16 h of light per day. Seven days later, two leaves per plant were carefully cut and randomly distributed in three groups. Sporulating leaves were shaken in 35 mL ultrapure water to recover sporangia. The three suspensions of sporangia were adjusted to 10^5 sporangia mL^{-1} and 30 mL of each suspension was centrifuged at 30,000 g for 20 min. Pellets of sporangia were extracted with 2 mL of MeOH/$CHCl_3$ (1/1, v/v), by sonicating for 15 min in an ultrasound bath. Two mL of ultrapure water was added to allow phase separation. After centrifugation at 15,000 g for 10 min, the chloroform phase was concentrated to 100 µL and diluted with 100 µL of MeOH. Final extracts corresponded to $1.5.10^7$ sporangia mL^{-1}. Mock inoculated leaves were extracted as described below.

Metabolite Extraction From Grapevine Leaves

Leaf discs were freeze-dried and weighed. After grinding the discs using a bead mill (TissueLyser II, Qiagen, Courtaboeuf, France), metabolites were extracted with MeOH/$CHCl_3$ (1/1, v/v) using 15 µL per mg dry weight. The suspension of leaf powder in MeOH/$CHCl_3$ was then sonicated for 15 min in an ultrasound bath. Two milliliters of ultrapure water was added to allow phase separation. After centrifugation at 15,000 g for 10 min, 100 µL of the chloroform phase was recovered, diluted with 100 µL of MeOH and analyzed by UHPLC-MS.

UHPLC-HRMS

Analyses were performed using a Dionex Ultimate 3000 UHPLC system (Thermo Fisher Scientific, San Jose, USA). The chromatographic separation was performed on a Nucleodur C18 HTec column (50 × 2 mm, 1.8 µm particle size; Macherey-Nagel, Düren, Germany) maintained at 20°C. The mobile phase consisted of methanol with formic acid (0.1%, v/v) in isocratic elution at a flow rate of 0.30 mL/min. The sample volume injected was 1 µL. The UHPLC system was coupled to an Exactive Orbitrap mass spectrometer (Thermo Fischer Scientific)

equipped with an atmospheric pressure chemical ionization (APCI) source operating in positive mode. Parameters were set at 300°C for ion transfer capillary temperature and the corona discharge current was set at 5 μA. Nebulization with nitrogen sheath gas and auxiliary gas were maintained at 15 and 10 arbitrary units, respectively, and the nebulizer temperature was maintained at 400°C. The spectra were acquired within the *m/z* mass range of 100–1,200 atomic mass units (amu), using a resolution of 50,000 at *m/z* 200 amu. The system was calibrated internally using dibutylphthalate as lock mass at *m/z* 279.1591, giving a mass accuracy lower than 1 ppm. The instruments were controlled using the Xcalibur software and data was processed using the XCMS software package (Smith et al., 2006). Raw data were converted to the mzXML format using MSconvert before analysis. Settings of the xcmsSet function of XCMS were as follows: method = "centWave", ppm = 2, noise = 50,000, mzdiff = 0.001, prefilter = c(5,15,000), snthresh = 6, peakwidth = c(6,35). Peaks were aligned using the obiwarp function using the followings settings of the function group.density: bw = 10, mzwid = 0.0025. This allowed the alignment of 2,156 peaks in the positive mode. Ion identifiers were generated automatically by XCMS as MxxxTyyy, where xxx is the *m/z* and yyy the retention time in seconds. Selection of major differential ions (peak area $> 10^6$, fold > 15) between sporangia and leaf extracts led to a final set of 123 major ions. The integration of each peak was checked manually before validation. *T*-tests were performed in R with the *t.test* function. Differential ions with $p \leq 0.05$ were considered for further characterization. The exact *m/z* and retention time of each metabolite were used for targeted metabolomic analyses using the Excalibur software. For kinetic analysis of *P. viticola* development, seven major *Plasmopara*-specific lipids [AA, DAG, EPA, DEPG, TEPG, Cer(d16:1/18:0), Cer(d16:1/20:0)] were selected.

RESULTS

Characterization of Candidate *Plasmopara*-Specific Metabolites Using Non-targeted Metabolomics

As an obligate biotrophic pathogen, *P. viticola* cannot be grown in pure culture. However, sporangia can easily be collected from infected grapevine leaves. In order to characterize potential *Plasmopara*-specific metabolites, we compared extracts of sporangia and uninfected grapevine leaves using ultra high-performance liquid chromatography coupled to high-resolution mass spectrometry (UHPLC-HRMS). This differential metabolomic approach has led to the selection of a set of 123 major ions (peak area $> 10^6$, $p \leq 0.05$), which are at least 15 times more abundant in sporangia extracts than in leaf extracts (Supplementary Table 1). The level of contamination of sporangia extracts by leaf-derived material was estimated by quantifying chlorophyll *a*. Chlorophyll *a* content in sporangia extracts ($1.7.10^4 \pm 1.2.10^4$ arbitrary units) was 4,000 times lower than in leaf extracts ($6.8.10^7 \pm 4.1.10^7$ arbitrary units), indicating very low levels of contamination. Submission of these 123 ions to the Metlin database (Smith et al., 2005) led to the putative identification of two compounds of particular interest. Indeed, one of the proposed structures for compounds giving the ion n°10 (M303T44) with the mass-to-charge ratio (*m/z*) 303.2316 was eicosapentaenoic acid (EPA). Similarly, ion n°12 (M305T48) with *m/z* 305.2473 was potentially associated to arachidonic acid (AA) (**Table 1**). Both EPA and AA had previously been identified in mycelial extracts of *Phytophthora infestans*, another phytopathogenic Oomycete causing the late blight of potato (Bostock et al., 1981). Commercial EPA and AA standards were therefore analyzed by UHPLC-HRMS using the same conditions as those used for *P. viticola* extracts. The retention times (RTs) and fragment patterns of the standards were identical to those of M303T44 (n°10) and M305T48 (n°12) (Supplementary Figure 1), confirming their identities as EPA and AA, respectively.

Structural Elucidation of EPA-Containing Lipids

In both the *P. viticola* extracts and the commercial standard, in source fragmentation of EPA produced a characteristic ion with *m/z 285*.2212 ($C_{20}H_{29}O$) corresponding to a loss of water. Extracted ion chromatogram (EIC) for *m/z* 285.2212 showed that other metabolites gave rise to this particular ion in *P. viticola* sporangia extracts (**Figure 1**), indicating that these molecules may contain EPA. A more detailed analysis of the mass spectra of some of these metabolites showed that they were actually present in our list of major *Plasmopara*-specific ions (**Figure 1**, **Table 1**). This prompted us to characterize these putative EPA-containing compounds further. The mass and the formula of some of these compounds indicated that they may correspond to glycerides, constituted by glycerol ($C_3H_8O_3$) partially or totally esterified by EPA. For example, the ion M377T39 (n°5) with *m/z* 377.2683, corresponding to the formula $C_{23}H_{37}O_4$ (average mass error, AME 0.8 ppm), was putatively identified as eicosapentaenoyl-glycerol (EPG). Indeed, it gave rise to a first dehydration fragment with *m/z* 359.2579 ($C_{23}H_{35}O_3$), as well as to the characteristic dehydration fragment of EPA (*m/z* 285.2210). The first fragment corresponded to the ion M359T39 (n°4). The same reasoning could be applied to the ions M661T85 (n°16) and M946T474 (n°117), which where therefore putatively identified as dieicosapentaenoyl-glycerol (DEPG) and trieicosapentaenoyl-glycerol (TEPG), respectively. The identification of EPA glycerides was confirmed by comparing their characteristics to those of the corresponding synthetic standards (see below). Altogether, EPA and EPA glycerides give rise to 15 of 123 the major *Plasmopara*-specific ions selected in Supplementary Table 2.

Structural Elucidation of AA-Containing Lipids

In source fragmentation of the AA standard gave rise to a characteristic ion with *m/z* 287.2369 ($C_{20}H_{31}O$, AME 0.1 ppm) corresponding to a loss of water. Using the same strategy as with EPA, EIC for *m/z* 287.2369 revealed several potential AA-containing molecules in *P. viticola* sporangia extracts (Supplementary Figure 2), some of them being listed among the *Plasmopara*-specific compounds (**Table 1**). Similarly, the formula

TABLE 1 | *Plasmopara*-specific ions identified by non-targeted metabolomics, which are referred to in the text.

Ion n°	Identifier	m/z	RT(s)	Ion formula	Identification
10	**M303T44**	**303.2316**	**43.87**	**$C_{20}H_{30}O_2$**	**eicosapentaenoic acid (EPA)**
5	**M377T39**	**377.2683**	**38.81**	**$C_{23}H_{37}O_4$**	**eicosapentaenoyl-glycerol (EPG)**
4	M359T39	359.2577	38.81	**$C_{23}H_{35}O_3$**	fragment from EPG $[M\text{-}H_2O+H]^+$
16	**M661T85**	**661.4825**	**84.66**	**$C_{43}H_{65}O_5$**	**dieicosapentaenoyl-glycerol (DEPG)**
117	**M946T474**	**945.6964**	**473.78**	**$C_{63}H_{93}O_6$**	**trieicosapentaenoyl-glycerol (TEPG)**
12	**M305T48**	**305.2474**	**47.97**	**$C_{20}H_{32}O_2$**	**arachidonic acid (AA)**
8	**M379T42**	**379.2839**	**41.59**	**$C_{23}H_{39}O_4$**	**arachidonoyl-glycerol (AG)**
30	**M666T124**	**665.5134**	**123.80**	**$C_{43}H_{69}O_5$**	**diarachidonoyl-glycerol (DAG)**
19	**M492T96**	**492.4773**	**96.14**	**$C_{32}H_{64}NO_3$**	**Cer(d16:1/16:0)**
40	**M539T125**	**538.5189**	**125.15**	**$C_{34}H_{68}NO_3$**	***Cer(d16:1/18:0)***
33	M236T125	236.2371	125.15	$C_{16}H_{30}N$	*fragment N from Cer(d16:1/18:0)*
34	M254T125	254.2477	125.15	$C_{16}H_{32}NO$	*fragment N′ from Cer(d16:1/18:0)*
37	M521T125	520.5084	125.15	$C_{34}H_{66}NO_2$	*fragment $[M\text{-}H_2O+H]^+$ from Cer(d16:1/18:O)*
42	M356T126	356.3156	125.61	$C_{21}H_{42}NO_3$	*fragment C from Cer(d16:1/18:0)*
43	M284T126	284.2945	126.06	$C_{18}H_{38}NO$	*fragment A from Cer(d16:1/18:0)*
73	**M567T166**	**566.5502**	**165.80**	**$C_{36}H_{72}NO_3$**	***Cer(d16:1/20:0)***
66	M236T165	236.2371	164.83	$C_{16}H_{30}N$	*fragment N from Cer(d16:1/20:0)*
67	M254T165	254.2476	164.83	$C_{16}H_{32}NO$	*fragment N′ from Cer(d16:1/20:0)*
71	M549T166	548.5399	165.69	$C_{36}H_{70}NO_2$	*fragment $[M\text{-}H_2O+H]^+$ from Cer(d16:1/20:0)*
97	**M595T223**	**594.5818**	**223.18**	**$C_{38}H_{76}NO_3$**	***Cer(d16:1/22:0)***
93	M236T223	236.2372	223.18	$C_{16}H_{30}N$	*fragment N from Cer(d16:1/22:0)*
94	M412T223	412.3784	223.18	$C_{25}H_{50}NO_3$	*fragment C from Cer(d16:1/22:0)*
95	M577T223	576.5713	223.18	$C_{38}H_{74}NO_2$	*fragment $[M\text{-}H_2O+H]^+$ from Cer(d16:1/22:0)*
13	M281T50	281.2473	50.26	$C_{18}H_{32}O_2$	*$C_{18:2}$ acid*
46	**M642T142**	**641.5134**	**141.80**	**$C_{41}H_{69}O_5$**	***diglyceride 20:5/18:1***

Major compounds are indicated in bold. Identifications confirmed using the corresponding standards are marked by a gray background. Ions are numbered according to their retention time and are organized as derivatives of EPA, AA, and ceramides, indicated in green, blue, and red, respectively. Putative identifications are indicated with italics. For all ions, the identifier, the m/z, and retention time (RT) are indicated. For fragment nomenclature, see Supplementary Figure 3. The original list of ions identified by non-targeted metabolomics on one experiment including three biological replicates of extracts of P. viticola sporangia and of mock-inoculated leaves is presented in Supplementary Table 1 and the full list of 51 ions identified in this work is presented in Supplementary Table 2.

and the fragmentation pattern of some of them indicate that they may be AA glycerides. For example, the ion M379T42 (n°8, **Table 1**) with *m/z* 379.2839 ($C_{23}H_{39}O_4$, AME 1 ppm) could be putatively identified as arachidonoyl-glycerol (AG), as it produced a dehydration product with *m/z* 361.2736 ($C_{23}H_{37}O_3$, AME 0.1 ppm) together with the characteristic dehydration ion of AA (*m/z* 287.2369, $C_{20}H_{31}O$). Applying the same reasoning, the ion M666T124 (n°30) was putatively identified as diarachidonoyl-glycerol (DAG). As TEPG was abundant in *P. viticola* sporangia, we logically looked for triarachidonoyl-glycerol (TAG), although no ion potentially derived from this compound was found in **Table 1**. TAG was indeed detected, albeit with a retention time of 21.81 min, exceeding the 10 min limit originally set for the XCMS analysis, and therefore explaining its absence in **Table 1**. In order to confirm the identity of the fatty acid glycerides detected in *P. viticola* extracts, the corresponding standards were synthesized by $ZnCl_2$-catalyzed esterification of glycerol (Mostafa et al., 2013). Using EPA and AA, mixtures of glycerides of the corresponding fatty acids were obtained and analyzed by UHPLC-HRMS using the same conditions as those used for sporangia extracts. The synthetic AG, DAG, EPG, and DEPG exhibited the same RT and fragment patterns as the corresponding compounds detected *P. viticola* extracts, therefore confirming their identity. The identities of the triglycerides were confirmed using the corresponding commercial TAG and TEPG standards.

Characterization and Structural Elucidation of Further *Plasmopara*-Specific Lipids

Among putative *Plasmopara*-specific metabolites, the ion with *m/z* 236.2371 (putative formula $C_{16}H_{30}N$) appeared three times at different RTs (ions n°33, 66, and 93, at RT 125, 165, and 223 s, respectively; **Table 1**). For all RTs, this ion seemed to belong to a group of ions corresponding to fragments of larger metabolites. Indeed, EIC for *m/z* 236.2371 revealed four different peaks at RTs 96, 125, 165, and 223 s (**Figure 2A**). Analysis of the major ions present at these RTs revealed four compounds, which are also present in **Table 1**, namely M492T96, M521T125, M549T166, M577T223 (n°19, n°37, n°71, n°95). Each of these ions exhibited a mass difference of 28.031 atomic mass units (amu) with the

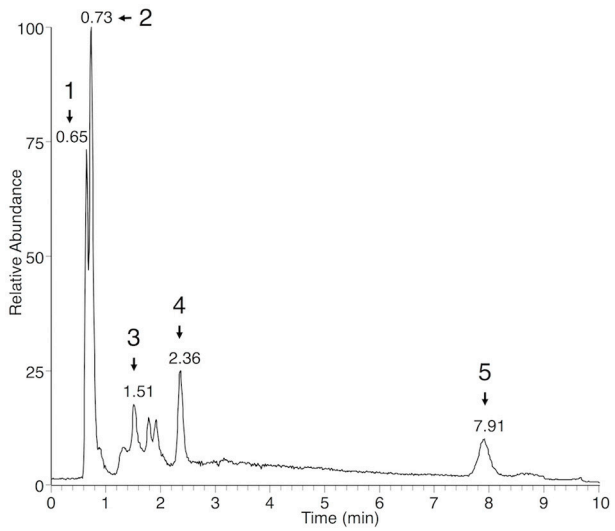

FIGURE 1 | Extracted ion chromatogram of sporangia extracts showing putative EPA-containing lipids. EIC of sporangia extracts for *m/z* 285.2212 (±2 ppm), a characteristic ion of EPA, is presented. Peaks corresponding to EPA-containing ions (**Table 1**) are numbered from 1 to 5 and retention times are indicated. Peak 1: M377T39 = EPG; peak 2: M303T44 = EPA; peak 3: M661T85 = DEPG; peak 4: M642T142 = diglyceride 20:5/18:1; peak 5: M946T474 = TEPG. Identity of EPA, EPG, DEPG, and TEPG have been confirmed by using the corresponding standards.

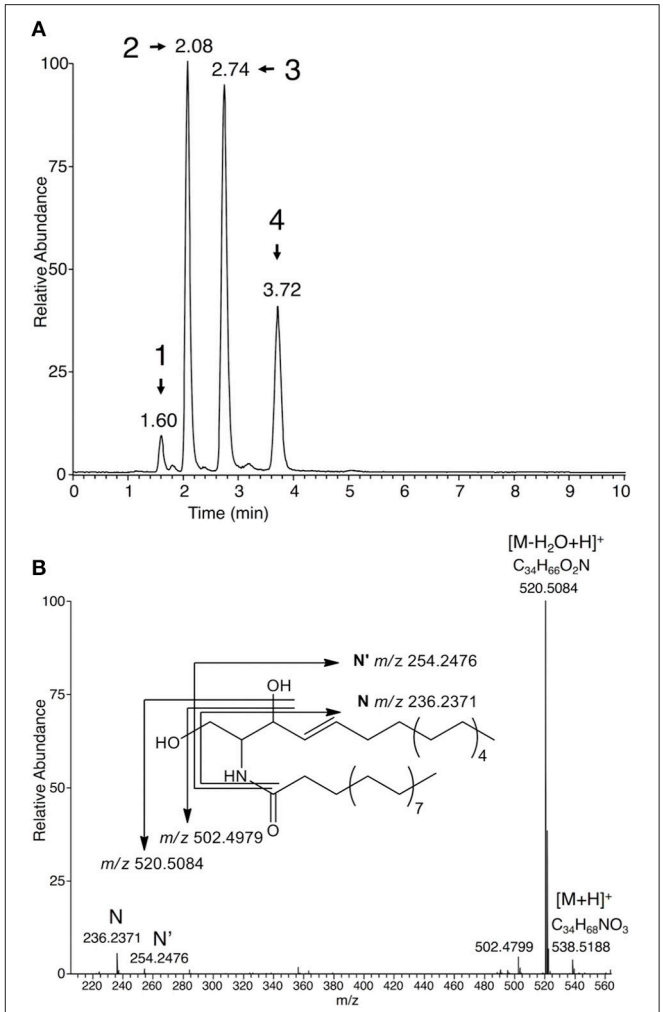

FIGURE 2 | Characterization of ceramides in sporangia extracts. **(A)** EIC of sporangia extracts for *m/z* 236.2371 (±2 ppm), a characteristic ion of C16:1 ceramides. Peaks corresponding to *Plasmopara*-specific ions (**Table 1**) are numbered from 1 to 4 and retention times are indicated. Peak 1: M492T96 = Cer(d16:1/16:0); peak 2: M521T125 = Cer(d16:1/18:0); peak 3: M549T166 = Cer(d16:1/20:0); peak 4: Cer(d16:1/22:0). Identity of Cer(d16:1/16:0) was confirmed by using the corresponding standard. **(B)** Mass spectrum of putative Cer(d16:1/18:0) (M521T125) from *P. viticola*. The fragmentation giving rise to the main fragments is indicated. A detailed fragmentation is given in Supplementary Figure 3.

following one, this mass increase being compatible with their belonging to a family of compounds that differentiate themselves by an increasing number of ethylene (C_2H_4) groups. Therefore, the putative formula of M492T96 (n°19) was $C_{32}H_{62}O_2N$, and the following metabolites corresponded to the putative formulas $C_{34}H_{66}O_2N$, $C_{36}H_{70}O_2N$, $C_{38}H_{74}O_2N$, respectively. Further analysis of the mass spectra revealed that, alongside the major ions listed above, we could detect minor ions corresponding to the same formula with either a loss of water or one additional water molecule (H_2O). The latter ions corresponded to *m/z* 510.4877, 538.5189, 566.5502, and 594.5818, respectively. Search of the Metlin database for compounds possibly corresponding to these ions (with 1 ppm AME) retrieved candidates belonging to the ceramide family, composed of a C16:1 or C18:1 sphingosine, linked to a C14, C16, C18, C20, or C22 saturated fatty acid (Supplementary Table 3). In order to validate these potential candidates, a commercial standard of the ceramide N-arachidoyl-D-sphingosine Cer(d18:1/20:0), which may correspond to the ion M577T223 (n°95), was analyzed by UHPLC-HRMS using the same conditions as those used for *P. viticola* extracts. Its mass spectrum showed a $[M+H]^+$ pseudo molecular ion with *m/z* 594.5814 corresponding to $C_{38}H_{76}O_3N$, together with several fragments with *m/z* 264.2683 ($C_{18}H_{36}N$), *m/z* 282.2791 ($C_{18}H_{38}ON$) and *m/z* 576.5713 ($C_{38}H_{74}O_2N$), which was the major fragment. Ions coming from the fatty acid part were detected too (*m/z* 312.3258, $C_{20}H_{42}ON$ and *m/z* 354.3363, $C_{22}H_{44}O_2N$), in agreement with the fragmentation of ceramides described previously in several studies (Levery et al., 2000; Hsu and Turk, 2002; Murphy, 2015) and obtained with this standard (Supplementary Table 3). However, neither its RT nor its fragmentation corresponded to any of the ions found in *P. viticola*, excluding the hypothesis that some of these ions may be derived from C18:1 sphingosines.

A second set of candidates retrieved from the Metlin database contained C16:1 sphingosine. Indeed, the four compounds present in *P. viticola* extracts shared the same specific fragments with *m/z* 236.2371 ($C_{16}H_{30}N$) and 254.2476 ($C_{16}H_{32}ON$) (**Figure 2B**). The formulas of these fragments could be compatible with their being derived from a C16:1 sphingosine (Lhomme et al., 1990; Pivot et al., 1994). Therefore, a commercial standard of the ceramide Cer(d16:1/16:0) was analyzed by UHPLC-HRMS. Both its RT and its fragmentation pattern

corresponded to that of the ion M492RT96 (n°19) found in *P. viticola* (Supplementary Table 3). Furthermore, M492RT96 and Cer(d16:1/16:0) exhibited the same RT in three different chromatographic conditions (data not shown), showing that the ion M492RT96 (n°19) is indeed derived from Cer(d16:1/16:0) present in *P. viticola* extracts (**Figures 2A**, **3**). The ions M492T96, M521T125, M549T166, and M577T223 (n°19, n°37, n°71, n°95) all share common fragments with *m/z* 236.2373 and 254.2476, corresponding to $C_{16}H_{30}N$ et $C_{16}H_{32}ON$, respectively, which are derived from the C16:1 sphingosine. As for the commercial standards Cer(d16:1/16:0) and Cer(d18:1/20:0), three ions coming from the fatty acid part are detected for all four ceramides (Supplementary Table 3). For Cer(d16:1/18:0) (n°37), these characteristic fragments termed A, B, and C are indicated in Supplementary Figure 3. Therefore, the ions M521T125, M549T166, and M577T223 (n°37, n°71, n°95) are very likely to be derived from a family or ceramides with a C16:1 sphingosyl group bound to a saturated fatty acid with 18–22 carbon atoms, namely Cer(d16:1/18:0), Cer(d16:1/20:0), and Cer(d16:1/22:0), respectively (**Figures 2A**, **3**). Detailed analysis of the fragments derived from these compounds is presented in Supplementary Table 3.

Altogether, we could propose an identification for 51 (Supplementary Table 2) of the final set of 123 major ions, which are at least 15 times more abundant in sporangia extracts than in leaf extracts (with $p \leq 0.05$, Supplementary Table 1).

Plasmopara-Specific Lipids Can Be Used for Phenotyping Resistance to Downy Mildew

The accurate quantification of pathogen development is important for a better understanding of plant-pathogen interactions. In the case of *P. viticola*, methods based on cell counting or image analysis are routinely used to quantify sporulation, especially as a phenotyping tool to characterize resistance sources in the *Vitis* genus (Peressotti et al., 2011; Divilov et al., 2017). Our differential metabolomic approach has led to the characterization of lipids, which are abundant in the sporangia of *P. viticola* and not detected in healthy grapevine leaf tissues. In order to evaluate the possibility to use these compounds for phenotyping resistance to *P. viticola*, analysis of lipid markers was compared to image analysis for quantifying sporulation in a leaf disc assay routinely used to assess resistance to *P. viticola* (**Figure 4A**; Peressotti et al., 2011). Correlations between sporulation and quantification of all individual lipid markers were very good (**Figure 4B**), all associated *p*-values being lower than 10^{-9}. This demonstrates the specificity of the lipid markers and confirms that they are perfectly suited for phenotyping resistance to *P. viticola*. In particular, EPA and AA are giving the best correlation coefficients, meaning that they are very valuable markers for phenotyping resistance.

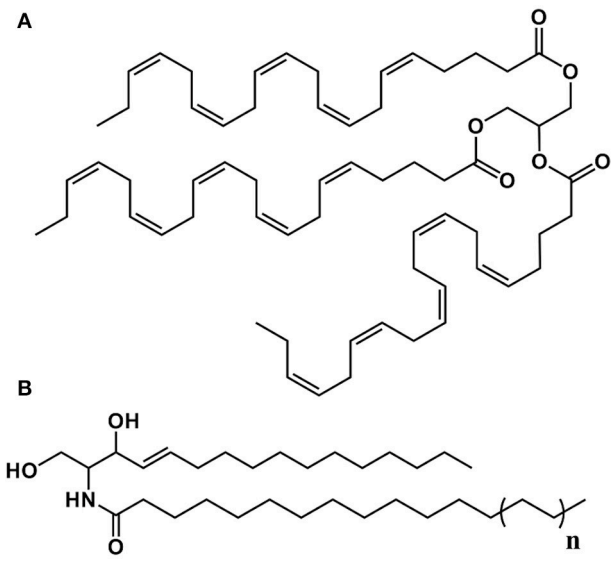

FIGURE 3 | Structure of some of the lipids characterized in *P. viticola*. **(A)** Trieicosapentaenoyl-glycerol (TEPG). **(B)** $n = 1$: Cer(d16:1/16:0); $n = 2$: Cer(d16:1/18:0); $n = 3$: Cer(d16:1/20:0); $n = 4$: Cer(d16:1/22:0).

Early Detection and Kinetic Analysis of *Plasmopara*-Specific Lipids Accumulation During Downy Mildew Infection

Beside end-point quantification of sporulation, an accurate monitoring of disease progression is important for precise description of disease susceptibility phenotypes. Therefore, we evaluated the possibility to use *Plasmopara*-specific lipids to quantify *P. viticola* in grapevine tissues before sporulation, i.e., as early and dynamic markers of downy mildew infection. Comparison of infected and mock-inoculated leaves showed that all ceramides and fatty acid derivatives described above were easily detected in the extract of infected leaves before sporulation, all these compounds being absent in control leaves (**Figure 5**). This prompted us to evaluate the potential of the *Plasmopara*-specific lipids to monitor the kinetic of *P. viticola* infection in three grapevines genotypes, which differ in their susceptibility to downy mildew: Syrah, Bianca, and *V. riparia*. Lipid analysis at different times post-inoculation allowed effective monitoring of disease development throughout the infection process, all lipids being efficiently detected even at early infection stages (24 h post-inoculation; **Figure 6**, Supplementary Figure 4, Supplementary Table 4). Different patterns and timings of *Plasmopara*-specific lipids accumulation were obtained in grapevine varieties with different susceptibility to downy mildew. However, patterns of *Plasmopara*-specific lipid accumulated in infected grapevine leaves differed significantly from that of isolated sporangia.

DISCUSSION

P. viticola Contains Unusual Lipids, Which Are Not Detected in Healthy Grapevine Leaf Tissues

Looking for potential markers of downy mildew infection using a non-targeted metabolomic approach, we could identify derivatives of *Plasmopara*-specific lipids, which include EPA and AA-containing lipids, in addition to ceramides. Both

EPA and AA have previously been isolated from extracts of *P. infestans*, as elicitors of the accumulation of antimicrobial stress metabolites in potato tubers (Bostock et al., 1981). EPA and AA have been detected in a number of other Oomycetes (Gandhi and Weete, 1991; Spring and Haas, 2002; Pang et al., 2015), and more recently, the role of EPA and AA as microbial associated molecular patterns (MAMPs) has been extended to other plant-Oomycete interactions (Savchenko et al., 2010; Bostock et al., 2011). Due its remarkable abundance in *Plasmopara halstedii*, EPA has been proposed as a marker for downy mildew contamination in sunflower seeds (Spring and Haas, 2004). Similarly, fatty acids, including AA, have been used to detect *Phytophthora sojae* in soybean fields (Yousef et al., 2012). However, lipid analysis in Oomycetes has mostly targeted fatty acids released after total lipid hydrolysis and the information on complex lipids is very scarce. Here, we have used UHPLC-HRMS to directly characterize complex lipids without the modification usually needed for GC-MS analysis (hydrolysis, derivatization). In particular, optimized mild atmospheric pressure chemical ionization (APCI) has allowed the identification of ions corresponding to the whole molecules, as well as characteristic fragments. The use of APCI for the characterization of complex lipids has been reported very recently (Mutemberezi et al., 2016), and this approach is likely to gain in popularity in the current context of the development of lipidomics.

UHPLC-HRMS has led to the characterization of two families of glycerides derived, respectively, from EPA and AA, which had not been formally identified in Oomycetes to date. Furthermore, occurrence of TAG and TEPG is poorly documented and very few natural sources of these triglycerides have been described. TAG has been reported in the red algae *Gracilaria verrucosa* (Kinoshita et al., 1986). Several organisms such as *Mortierella* sp. (Shimizu et al., 1988) and the Oomycetes *Pythium* sp. (Gandhi and Weete, 1991; O'Brien et al., 1993) and *Saprolegnia* sp. (Shirasaka and Shimizu, 1995) have been reported to produce EPA-containing triglycerides. However, to our knowledge, TEPG has not been formally identified in these organisms.

In addition to EPA and AA derivatives, sporangia of *P. viticola* contain a family of C16:1 ceramides including Cer(d16:1/16:0), whose identification could be confirmed using a commercial standard. Although we could not identify them formally due to the lack of standards, other major C16:1 ceramides of *P. viticola* are very likely to include Cer(d16:1/18:0), Cer(d16:1/20:0), and Cer(d16:1/22:0) (**Figure 3**). Several shingophospholipids containing a C16:1 sphingosine have been detected in different plant Oomycete pathogens (Lhomme et al., 1990; Kim et al., 1998; Moreau et al., 1998). However, Cer(d16:1/16:0), Cer(d16:1/18:0), Cer(d16:1/20:0), and Cer(d16:1/22:0) had never been reported in Oomycetes before this work.

None of the lipids characterized above were detected in significant amounts in healthy grapevine leaf tissues. In addition, using an array of grapevine varieties, hybrids, and *Vitis* species with different susceptibility to downy mildew, correlation between sporulation and quantification of individual lipid markers was excellent (**Figure 4**), thus demonstrating that, in the context of grapevine-downy mildew interaction, these lipids can be considered as *Plasmopara*-specific. Their potential use as markers of downy mildew infection was therefore investigated.

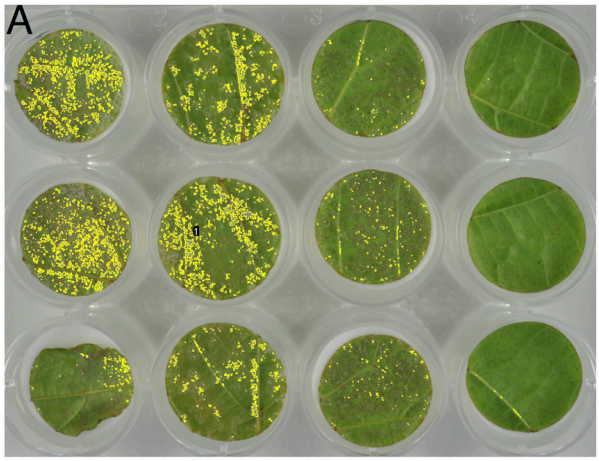

Metabolite	Pearson's correlation coefficient	P-value
EPA	0.849	1.37 e-18
AA	0.848	1.91 e-18
Cer(d16:1/18:0)	0.840	7.56 e-18
Cer(d16:1/22:0)	0.775	8.82 e-14
DAG	0.741	3.71 e-12
Cer(d16:1/16:0)	0.728	1.38 e-11
Cer(d16:1/20:0)	0.709	8.17 e-11
TEPG	0.702	1.47 e-10
AG	0.693	3.02 e-10
EPG	0.691	3.58 e-10
DEPG	0.689	4.18 e-10

FIGURE 4 | Correlation between image analysis-based quantification of sporulation and quantification of lipid markers of *P. viticola*. Leaf disc bioassay was performed with Cabernet-Sauvignon, Syrah, Cinsault, *V. rupestris*, *V. riparia*, and *V. rotundifolia*, using 15 leaf discs for each variety. **(A)** Typical quantification of sporulating area 6 days post inoculation using image analysis (Peressotti et al., 2011). **(B)** Correlation and associated *p*-value of individual lipid marker quantification with sporulating area, using Pearson's correlation test.

Lipids of *P. viticola* Can Be Used as Early Markers of Downy Mildew Infection in Grapevine Leaves

Most of the lipids characterized in sporangia extracts could be detected at early stages of downy mildew infection, indicating that these lipids are also present in the mycelium of *P. viticola* (**Figure 5**). The presence of seven major *Plasmopara*-specific lipids could easily be detected 24 h post-inoculation (**Figure 6**), long before the first external symptoms, which usually start to appear 4 days post-inoculation on susceptible grapevine varieties (Smith et al., 2006; Unger et al., 2007; Peressotti et al., 2011). The patterns of lipid accumulation were different in susceptible and resistant grapevine varieties. The accumulation of *Plasmopara*-specific lipids was unexpectedly higher 24 h post-inoculation in *V. riparia* than in the more susceptible varieties, suggesting

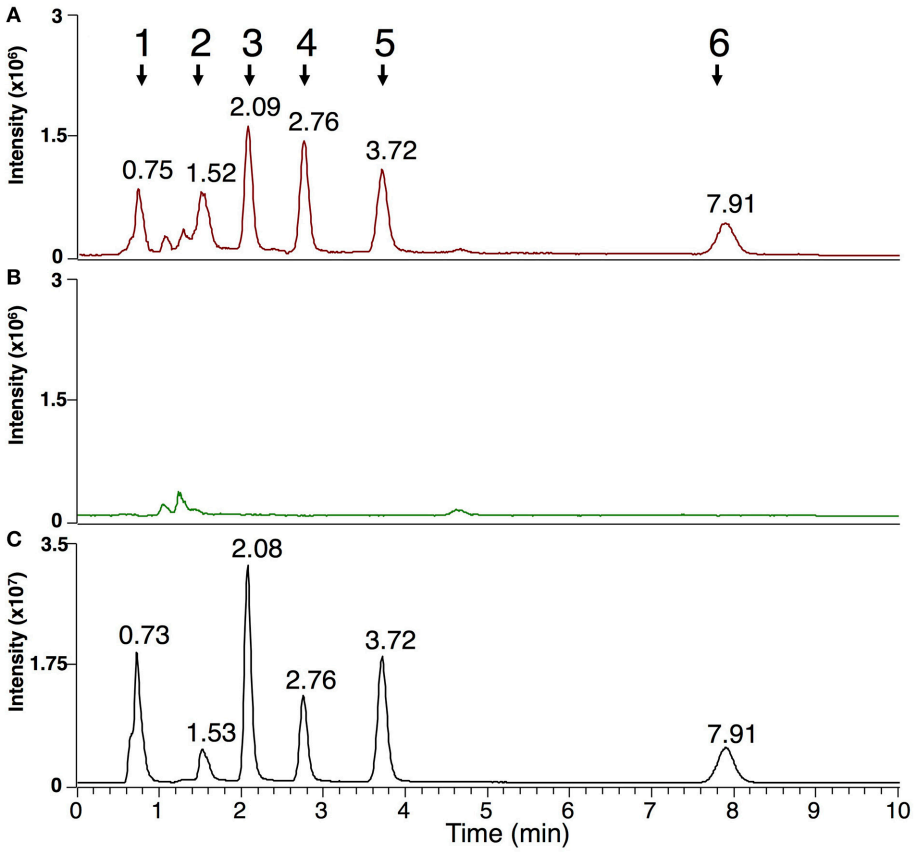

FIGURE 5 | Markers of *P. viticola* in downy mildew-infected grapevine leaves before sporulation. Analysis of MeOH/$CHCl_3$ extracts presenting the sum of the EIC for *m/z* of the characterized lipids of *P. viticola* (±2 ppm): 303.2316 + 305.2474 + 377.2683 + 379.2839 + 492.4773 + 520.5084 + 548.5399 + 576.5713 + 661.4825 + 665.5134 + 945.6964. **(A)** Typical pattern obtained from downy mildew-infected leaves (Muscat Ottonel) 4 days post infection; **(B)** control leaves; **(C)** sporangia of *P. viticola*. For easier comparison, infected **(A)** and control leaves **(B)** are presented at the same intensity scale (3.10^6 arbitrary units). Peaks corresponding to lipids of *P. viticola* are numbered from 1 to 6 and the corresponding retention times are indicated. Peak 1: AA, EPA, AG, EPG; peak 2: DAG, DEPG, Cer(d16:1/16:0); peak 3: Cer(d16:1/18:0); peak 4: Cer(d16:1/20:0); peak 5: Cer(d16:1/22:0); peak 6: TEPG.

a rapid development of hyphae from zoospores, even on the resistant variety (**Figure 6**). This is consistent with previous studies showing that *P. viticola* can form primary hyphae in the context of compatible, incompatible, and even non-host interactions (Díez-Navajas et al., 2008). However, the infection process was quickly stopped presumably as the result of plant defense reactions, the amount of detectable lipids reaching a plateau 24 h post-inoculation. Lipid accumulation in the fully susceptible variety Syrah was significantly higher than in Bianca, consistent with the partial resistance of this variety (Bellin et al., 2009).

Interestingly, the pattern of lipid accumulation was modified along the infection process. At early stages, AA and EPA were rather accumulated as fatty acids, whereas at late stages, the corresponding triacylglycerols, and especially TEPG, were massively accumulated (**Figure 6**), suggesting that the lipid pattern may be used as an indicator of infection developmental step. Indeed, the pattern of *Plasmopara*-specific lipids observed on Syrah leaves at late infection stage (6 days post inoculation) differed substantially from that of sporangia (**Figure 6**), although, at this stage, leaves were covered with an intense downy sporulation. This suggests that, even at the sporulation stage, the major part of *Plasmopara*-specific lipids comes from mycelial material localized inside grapevine leaves, this material being characterized by its high TEPG content. Altogether, these results show that *Plasmopara*-specific lipids may be used to monitor the development of downy mildew throughout the infection process, in both susceptible and resistant grapevine varieties.

Future Development of Mass Spectrometry-Based Methods for Monitoring Early Steps of Grapevine-Downy Mildew Interaction

In this work, we have used a non-targeted metabolomic approach to characterize unusual *P. viticola*-specific lipids. Although AA, EPA, and shingophospholipids have been found in Oomycetes before (Bostock et al., 1981; Lhomme et al., 1990; Pivot et al., 1994; Judelson, 2017), the major triglycerides TAG and TEPG and the ceramide family characterized in this

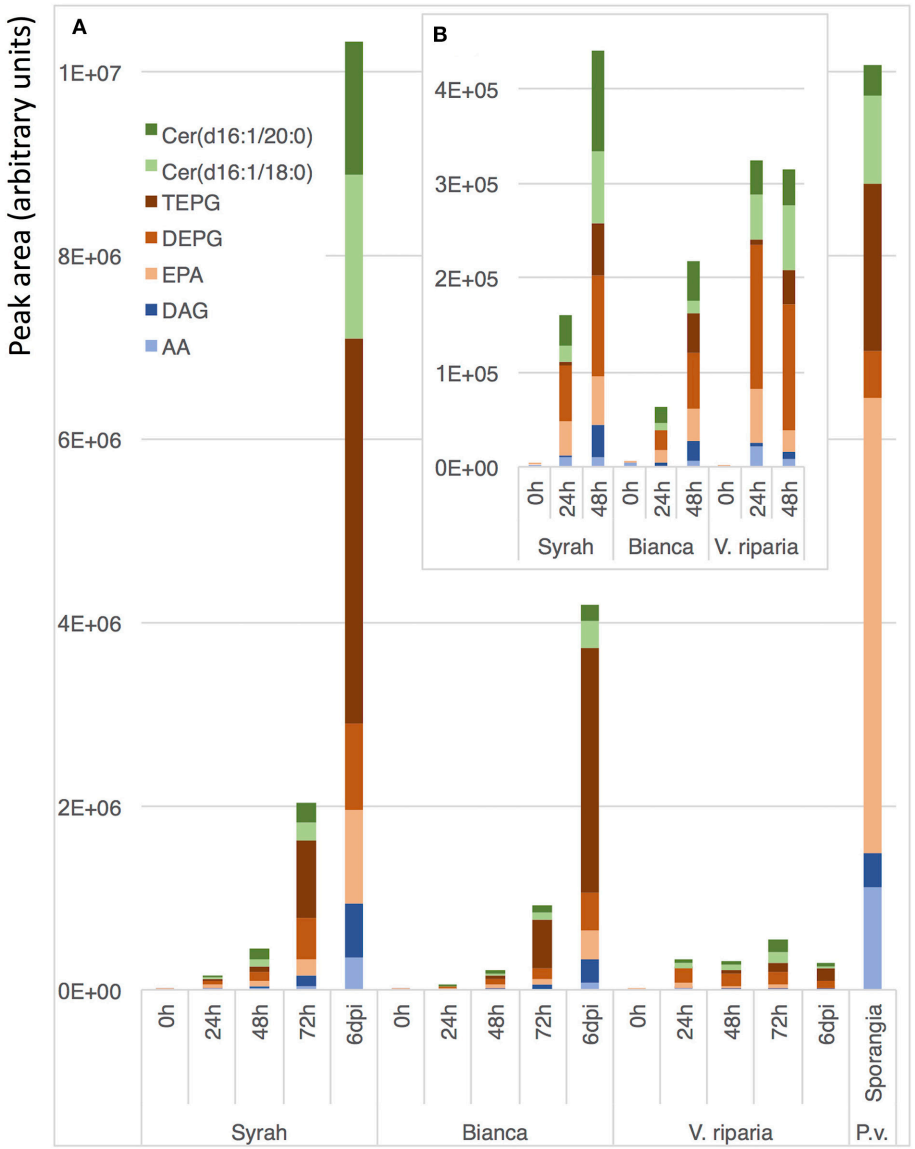

FIGURE 6 | Kinetic analysis of *Plasmopara*-specific lipids accumulation. Genotypes with different susceptibility to downy mildew were used: Syrah (susceptible), Bianca (partially resistant) and *V. riparia* (resistant). **(A)** Quantification of the 7 major lipids 0, 24, 48, 72 h, and 6 days post inoculation (dpi) with *P. viticola*. As a comparison, a typical lipid profile of sporangia of *P. viticola* is indicated. **(B)** Enlargement for early infection times (0–48 h). Three biological replicates were analyzed for each condition and means are presented. A detailed analysis of *Plasmopara*-specific lipids in these samples is presented in Supplementary Figure 4 and the associated statistics are presented in Supplementary Table 4.

work had not been unambiguously identified in Oomycetes. Beyond the identification of new lipids from *P. viticola*, we show that some of these compounds can be used to efficiently monitor the infection process of downy mildew, long before the appearance of any external symptom of the disease. The availability of reliable methods for analysis of early steps of pathogen development contributes to a better understanding of plant–pathogen interactions. Genetic analysis of quantitative resistance to plant pathogens require methods allowing a precise quantification of pathogen development for a reliable detection of the genomic regions involved in resistance. Assessment of resistance to grapevine downy mildew has been traditionally performed by visually scoring disease symptoms or by measuring sporulation using a cell counter (Bellin et al., 2009). More recently, high-throughput imaging-based methods to quantify sporulation have been developed (Peressotti et al., 2011; Divilov et al., 2017). Although such high-throughput methods are very useful to screen breeding populations, they do not allow monitoring of disease progression. Pathogen growth can be monitored by quantitative PCR-based methods (Brouwer et al., 2003; Anderson and McDowell, 2015). These methods are sensitive, however, they require costly reagents and rather

complicated sample preparation. Pre-symptomatic detection of downy mildew can be achieved using chlorophyll fluorescence imaging (Cséfalvay et al., 2009), but this approach is not quantitative. Through the characterization of lipid markers of *P. viticola*, we provide targets for the development of LC-MS-based methods allowing a sensitive, continuous and quantitative monitoring of downy mildew progression inside infected leaves. These methods will be likely to been successfully applied to a wide range of grapevine genotypes, including varieties and *Vitis* species. Optimization of chromatographic conditions will allow the development of fast (5 min or less) separation methods targeting the most relevant compounds, compatible with medium to high-throughput quantification. Finally, the same strategy could be applied to other important Oomycete or fungal plant pathogens, in order to develop high-sensitivity LC-MS-based methods for quantification of pathogen growth and disease progression. These methods could be used for accurate analysis of host-pathogen interaction and for the assessment of resistance to fungicides.

AUTHOR CONTRIBUTIONS

DM and PH: conceived the original research plans and raised the funding; RB: supervised experiments and identifications of unknown compounds; LN: performed most of the experiments; DH and CR: participated in data and statistical analyses; SW-M: supervised the experiments with downy mildew; LN, DM, PH, and RB: wrote the article with contributions of all the authors.

FUNDING

LN was supported by a doctoral fellowship from the Conseil Interprofessionnel des Vins d'Alsace, the Conseil Interprofessionnel du Vin de Bordeaux, and the Comité Interprofessionnel du Vin de Champagne and from the Région Alsace. This work was co-funded by the European Regional Development Fund (ERDF) in the framework of the INTERREG IV and V Upper Rhine programs (BACCHUS and VITIFUTUR projects), and by the Fondation Jean Poupelain (Javrezac, France) through the HealthyGrape2 program.

ACKNOWLEDGMENTS

We thank the staff of UE0871 Service d'Expérimentation Agronomique et Viticole (SEAV, INRA, Colmar) for maintenance of plant material. We are grateful to Marie-Annick Dorne and Marie-Céline Lacombe (INRA, Colmar) for help with downy mildew infections and to Andy Schneider (INRA, Colmar) for help with lipid extraction and analysis. We thank Patrick Schaub, Florian Wüst, and Peter Beyer (University Freiburg, Germany) for MS2 analyses.

SUPPLEMENTARY MATERIAL

The Supplementary Material for this article can be found online at: https://www.frontiersin.org/articles/10.3389/fpls.2018.00360/full#supplementary-material

REFERENCES

Ali, K., Maltese, F., Zyprian, E., Rex, M., Choi, Y. H., and Verpoorte, R. (2009). NMR metabolic fingerprinting based identification of grapevine metabolites associated with downy mildew resistance. *J. Agric. Food Chem.* 57, 9599–9606. doi: 10.1021/jf902069f

Alonso-Villaverde, V., Voinesco, F., Viret, O., Spring, J. L., and Gindro, K. (2011). The effectiveness of stilbenes in resistant vitaceae: ultrastructural and biochemical events during *Plasmopara viticola* infection process. *Plant Physiol. Biochem.* 49, 265–274. doi: 10.1016/j.plaphy.2010.12.010

Anderson, R. G., and McDowell, J. M. (2015). A PCR assay for the quantification of growth of the oomycete pathogen *Hyaloperonospora arabidopsidis* in *Arabidopsis thaliana*. *Mol. Plant Pathol.* 16, 893–898. doi: 10.1111/mpp.12247

Bellin, D., Peressotti, E., Merdinoglu, D., Wiedemann-Merdinoglu, S., Adam-Blondon, A. F., Cipriani, G., et al. (2009). Resistance to *Plasmopara viticola* in grapevine "Bianca" is controlled by a major dominant gene causing localised necrosis at the infection site. *Theor. Appl. Genet.* 120, 163–176. doi: 10.1007/s00122-009-1167-2

Bostock, R. M., Kuc, J. A., and Laine, R. A. (1981). Eicosapentaenoic and arachidonic acids from *Phytophthora infestans* elicit fungitoxic sesquiterpenes in the potato. *Science* 212, 67–69. doi: 10.1126/science.212.4490.67

Bostock, R. M., Savchenko, T., Lazarus, C., and Dehesh, K. (2011). Eicosapolyenoic acids: novel MAMPs with reciprocal effect on oomycete-plant defense signaling networks. *Plant Signal. Behav.* 6, 531–533. doi: 10.4161/psb.6.4.14782

Brouwer, M., Lievens, B., Van Hemelrijck, W., van den Ackerveken, G., Cammue, B. P., and Thomma, B. P. (2003). Quantification of disease progression of several microbial pathogens on *Arabidopsis thaliana* using real-time fluorescence PCR. *FEMS Microbiol. Lett.* 228, 241–248. doi: 10.1016/S0378-1097(03)00759-6

Buonassisi, D., Colombo, M., Migliaro, D., Dolzani, C., Peressotti, E., Mizzotti, C., et al. (2017). Breeding for grapevine downy mildew resistance: a review of "omics" approaches. *Euphytica* 213:103. doi: 10.1007/s10681-017-1882-8

Chitarrini, G., Soini, E., Riccadonna, S., Franceschi, P., Zulini, L., Masuero, D., et al. (2017). Identification of biomarkers for defense response to *Plasmopara viticola* in a resistant grape variety. *Front. Plant Sci.* 8:1524. doi: 10.3389/fpls.2017.01524

Cséfalvay, L., Di Gaspero, G., Matouš, K., and Bellin, D. (2009). Pre-symptomatic detection of *Plasmopara viticola* infection in grapevine leaves using chlorophyll fluorescence imaging. *Eur. J. Plant Pathol.* 125, 291–302. doi: 10.1007/s10658-009-9482-7

Díez-Navajas, A. M., Wiedemann-Merdinoglu, S., Greif, C., and Merdinoglu, D. (2008). Nonhost versus host resistance to the grapevine downy mildew, *Plasmopara viticola*, studied at the tissue level. *Phytopathology* 98, 776–780. doi: 10.1094/PHYTO-98-7-0776

Divilov, K., Wiesner-Hanks, T., Barba, P., Cadle-Davidson, L., and Reisch, B. I. (2017). Computer vision for high-throughput quantitative phenotyping: a case study of grapevine downy mildew sporulation and leaf trichomes. *Phytopathology* 107, 1549–1555. doi: 10.1094/PHYTO-04-17-0137-R

Duan, D., Halter, D., Baltenweck, R., Tisch, C., Tröster, V., Kortekamp, A., et al. (2015). Genetic diversity of stilbene metabolism in Vitis sylvestris. *J. Exp. Bot.* 66, 3243–3257. doi: 10.1093/jxb/erv137

Figueiredo, A., Fortes, A. M., Ferreira, S., Sebastiana, M., Choi, Y. H., Sousa, L., et al. (2008). Transcriptional and metabolic profiling of grape (*Vitis vinifera L.*) leaves unravel possible innate resistance against pathogenic fungi. *J. Exp. Bot.* 59, 3371–3381. doi: 10.1093/jxb/ern187

Gandhi, S. R., and Weete, J. D. (1991). Production of the polyunsaturated fatty acids arachidonic acid and eicosapentaenoic acid by the fungus *Pythium ultimum*. *J. Gen. Microbiol.* 137, 1825–1830. doi: 10.1099/00221287-137-8-1825

Gessler, C., Pertot, I., and Perazzolli, M. (2011). *Plasmopara viticola*: a review of knowledge on downy mildew of grapevine and effective disease management. *Phytopathol. Mediterr.* 50, 3–44. doi: 10.14601/Phytopathol_Mediterr-9360

Hsu, F. F., and Turk, J. (2002). Characterization of ceramides by low energy collisional-activated dissociation tandem mass spectrometry with negative-ion electrospray ionization. *J. Am. Soc. Mass Spectrom.* 13, 558–570. doi: 10.1016/S1044-0305(02)00358-6

Judelson, H. S. (2017). Metabolic diversity and novelties in the Oomycetes. *Annu. Rev. Microbiol.* 71, 21–39. doi: 10.1146/annurev-micro-090816-093609

Kim, H., Gandhi, S. R., Moreau, R. A., and Weete, J. D. (1998). Lipids of Haliphthoros philippinensis: an Oomycetous marine microbe. *J. Am. Oil Chem. Soc.* 75, 1657–1665. doi: 10.1007/s11746-998-0108-6

Kinoshita, K., Takahashi, K., and Zama, K. (1986). Triarachidonin and diarachidonylphosphatidylcholine in "ogonori" *Gracilaria verrucosa*. *Bull. Jpn. Soc. Sci. Fish* 52:757.

Kortekamp, A. (2006). Expression analysis of defence-related genes in grapevine leaves after inoculation with a host and a non-host pathogen. *Plant Physiol. Biochem.* 44, 58–67. doi: 10.1016/j.plaphy.2006.01.008

Legay, G., Marouf, E., Berger, D., and Neuhaus, J. M. (2011). Identification of genes expressed during the compatible interaction of grapevine with through suppression subtractive hybridization (SSH). *Eur. J. Plant Pathol.* 129, 281–301. doi: 10.1007/s10658-010-9676-z

Lenzi, L., Caruso, C., Bianchedi, P. L., Pertot, I., and Perazzolli, M. (2016). Laser microdissection of grapevine leaves reveals site-specific regulation of transcriptional response to *Plasmopara viticola*. *Plant Cell Physiol.* 57, 69–81. doi: 10.1093/pcp/pcv166

Levery, S. B., Toledo, M. S., Doong, R. L., Straus, A. H., and Takahashi, H. K. (2000). Comparative analysis of ceramide structural modification found in fungal cerebrosides by electrospray tandem mass spectrometry with low energy collision-induced dissociation of Li+ adduct ions. *Rapid Commun. Mass Spectrom.* 14, 551–563. doi: 10.1002/(SICI)1097-0231(20000415)14:7<551::AID-RCM909>3.0.CO;2-L

Lhomme, O., Bruneteau, M., Costello, C. E., Mas, P., Molot, P. M., Dell, A., et al. (1990). Structural investigations and biological activity of inositol sphingophospholipids from *Phytophthora capsici*. *Eur. J. Biochem.* 191, 203–209. doi: 10.1111/j.1432-1033.1990.tb19111.x

Malacarne, G., Vrhovsek, U., Zulini, L., Cestaro, A., Stefanini, M., Mattivi, F., et al. (2011). Resistance to *Plasmopara viticola* in a grapevine segregating population is associated with stilbenoid accumulation and with specific host transcriptional responses. *BMC Plant Biol.* 11:114. doi: 10.1186/1471-2229-11-114

Moreau, R. A., Young, D. H., Danis, P. O., and Powell, M. J. (1998). Identification of ceramide-phosphorylethanolamine in oomycete plant pathogens: *Pythium ultimum*, *Phytophthora infestans*, and *Phytophthora capsici*. *Lipids* 33, 307–317. doi: 10.1007/s11745-998-0210-1

Mostafa, N. A., Maher, A., and Abdelmoez, W. (2013). Production of mono-, di-, and triglycerides from waste fatty acids through esterification with glycerol. *Adv. Biosci. Biotechnol.* 4, 900–907. doi: 10.4236/abb.2013.49118

Murphy, R. C. (2015)*Tandem Mass Spectrometry of Lipids: Molecular Analysis of Complex Lipids*. London: Royal Society of Chemistry.

Mutemberezi, V., Masquelier, J., Guillemot-Legris, O., and Muccioli, G. G. (2016). Development and validation of an HPLC-MS method for the simultaneous quantification of key oxysterols, endocannabinoids, and ceramides: variations in metabolic syndrome. *Anal. Bioanal. Chem.* 408, 733–745. doi: 10.1007/s00216-015-9150-z

O'Brien, D. J., Kurantz, M. J., and Kwoczak, R. (1993). Production of eicosapentaenoic acid by the filamentous fungus *Pythium irregulare*. *Appl. Microbiol. Biotechnol.* 40, 211–214. doi: 10.1007/BF00170368

Pang, K. L., Lin, H. J., Lin, H. Y., Huang, Y. F., and Chen, Y. M. (2015). Production of arachidonic and eicosapentaenoic acids by the marine oomycete Halophytophthora. *Mar. Biotechnol.* 17, 121–129. doi: 10.1007/s10126-014-9600-1

Peressotti, E., Duchêne, E., Merdinoglu, D., and Mestre, P. (2011). A semi-automatic non-destructive method to quantify grapevine downy mildew sporulation. *J. Microbiol. Methods* 84, 265–271. doi: 10.1016/j.mimet.2010.12.009

Peressotti, E., Wiedemann-Merdinoglu, S., Delmotte, F., Bellin, D., Di Gaspero, G., Testolin, R., et al. (2010). Breakdown of resistance to grapevine downy mildew upon limited deployment of a resistant variety. *BMC Plant Biol.* 10:147. doi: 10.1186/1471-2229-10-147

Pezet, R., Perret, C., Jean-Denis, J. B., Tabacchi, R., Gindro, K., and Viret, O. (2003). δ-Viniferin, a resveratrol dehydrodimer: one of the major stilbenes synthesized by stressed grapevine leaves. *J. Agric. Food Chem.* 51, 5488–5492. doi: 10.1021/jf030227o

Pivot, V., Bruneteau, M., Más, P., Bompeix, G., and Michel, G. (1994). Isolation, characterization and biological activity of inositol sphingophospholipids from *Phytophthora Capsici*. *Lipids* 29, 21–25. doi: 10.1007/BF02537086

Polesani, M., Bortesi, L., Ferrarini, A., Zamboni, A., Fasoli, M., Zadra, C., et al. (2010). General and species-specific transcriptional responses to downy mildew infection in a susceptible (*Vitis vinifera*) and a resistant (*V. riparia)* grapevine species. *BMC Genomics* 11:117. doi: 10.1186/1471-2164-11-117

Polesani, M., Desario, F., Ferrarini, A., Zamboni, A., Pezzotti, M., Kortekamp, A., et al. (2008). cDNA-AFLP analysis of plant and pathogen genes expressed in grapevine infected with *Plasmopara viticola*. *BMC Genomics* 9:142. doi: 10.1186/1471-2164-9-142

Savchenko, T., Walley, J. W., Chehab, E. W., Xiao, Y., Kaspi, R., Pye, M. F., et al. (2010). Arachidonic acid: an evolutionarily conserved signaling molecule modulates plant stress signaling networks. *Plant Cell* 22, 3193–3205. doi: 10.1105/tpc.110.073858

Shimizu, S., Shinmen, Y., Kawashima, H., Akimoto, K., and Yamada, H. (1988). Fungal mycelia as a novel source of eicosapentaenoic acid. Activation of enzyme(s) involved in eicosapentaenoic acid production at low temperature. *Biochem. Biophys. Res. Commun.* 150, 335–341. doi: 10.1016/0006-291X(88)90525-6

Shirasaka, N., and Shimizu, S. (1995). Production of eicosapentaenoic acid by *Saprolegnia* sp. 28YTF-1. *J. Am. Oil Chem. Soc.* 72, 1545–1549. doi: 10.1007/BF02577852

Smith, C. A., O'Maille, G., Want, E. J., Qin, C., Trauger, S. A., Brandon, T. R., et al. (2005). METLIN: a metabolite mass spectral database. *Ther. Drug Monit.* 27, 747–751. doi: 10.1097/01.ftd.0000179845.53213.39

Smith, C. A., Want, E. J., O'Maille, G., Abagyan, R., and Siuzdak, G. (2006). XCMS: processing mass spectrometry data for metabolite profiling using nonlinear peak alignment, matching, and identification. *Anal. Chem.* 78, 779–787. doi: 10.1021/ac051437y

Spring, O., and Haas, K. (2002). The fatty acid composition of *Plasmopara halstedii* and its taxonomic significance. *Eur. J. Plant Pathol.* 108, 263–267. doi: 10.1023/A:1015173900047

Spring, O., and Haas, K. (2004). Eicosapentaenoic acid, a possible marker for downy mildew contamination in sunflower seeds. *Adv. Downy Mildew Res.* 2, 241–248. doi: 10.1007/978-1-4020-2658-4_16

Unger, S., Büche, C., Boso, S., and Kassemeyer, H. H. (2007). The course of colonization of two different vitis genotypes by *Plasmopara viticola* Indicates compatible and incompatible host-pathogen interactions. *Phytopathology* 97, 780–786. doi: 10.1094/PHYTO-97-7-0780

Wu, J., Zhang, Y., Zhang, H., Huang, H., Folta, K. M., and Lu, J. (2010). Whole genome wide expression profiles of *Vitis amurensis* grape responding to downy mildew by using Solexa sequencing technology. *BMC Plant Biol.* 10:234. doi: 10.1186/1471-2229-10-234

Yousef, L. F., Wojno, M., Dick, W. A., and Dick, R. P. (2012). Lipid profiling of the soybean pathogen *Phytophthora sojae* using fatty acid methyl esters (FAMEs). *Fungal Biol.* 116, 613–619. doi: 10.1016/j.funbio.2012.02.009

Conflict of Interest Statement: The authors declare that the research was conducted in the absence of any commercial or financial relationships that could be construed as a potential conflict of interest.

Advantages of publishing in Frontiers

OPEN ACCESS
Articles are free to read for greatest visibility and readership

FAST PUBLICATION
Around 90 days from submission to decision

HIGH QUALITY PEER-REVIEW
Rigorous, collaborative, and constructive peer-review

TRANSPARENT PEER-REVIEW
Editors and reviewers acknowledged by name on published articles

Frontiers
Avenue du Tribunal-Fédéral 34
1005 Lausanne | Switzerland

Visit us: www.frontiersin.org
Contact us: info@frontiersin.org | +41 21 510 17 00

REPRODUCIBILITY OF RESEARCH
Support open data and methods to enhance research reproducibility

DIGITAL PUBLISHING
Articles designed for optimal readership across devices

FOLLOW US
@frontiersin

IMPACT METRICS
Advanced article metrics track visibility across digital media

EXTENSIVE PROMOTION
Marketing and promotion of impactful research

LOOP RESEARCH NETWORK
Our network increases your article's readership